Freeze-Thaw Experiments on Some British Soils

Volume 1 of 2

By

Fiona Mhairi Thomson

A thesis submitted to the University of Warwick

for the degree of Doctor of Philosophy

School of Engineering, University of Warwick

December 2002

Table of Contents

List of Figures vii

List of Tables xii

List of Equations xiii

Acknowledgements xv

Notation xvi

Summary xviii

Chapter 1 - Introduction 1

1.1 Statement of Research Problem 1

1.2 Background to the Research 1

1.3 Justification for the Research 2

1.4 Outline of the Thesis 2

1.5 Key Assumptions 4

Chapter 2 – Literature Review 5

2.1 Periglacial Phenomena 5
2.1.1 Periglacial Conditions 5
2.1.2 Permafrost and the Active Layer 8
2.1.3 Thaw-Consolidation Theory 10
2.1.4 Processes of Periglacial Mass Wasting 12
2.1.5 Periglacial Slope Deposits in Lowland Britain 16
2.1.6 Periglacial Slope Evolution in Lowland Britain 17

2.2 Theory Related to Low-Angled Slope Failures 18
2.2.1 Residual Strength 18
2.2.2 Semi-Infinite Slope Analysis 21

2.3 Field Observations of Low-Angled Slope Failures 25
2.3.1 Sevenoaks – An Example of Re-activated Relic Slip Surfaces 25
2.3.2 Further Examination of Re-activated Relic Slip Surfaces 29
2.3.3 Vestspitsbergen – An Example of an Active Slide 34

2.4 Freeze-Thaw Experiments on Small Specimens 37
2.4.1 The Development of the Permode Apparatus 37
2.4.2 Freeze-Thaw Tests Concerning Moisture Migration and Ice Lens Formation 39
2.4.3 Freeze-Thaw Tests Concerned with Permeability 41

2.5 Freeze-Thaw Experiments on Model Slopes 45

2.6 Freeze-Thaw Experiments using Centrifuge Technology 51

Chapter 3 - Test Methodology 53

3.1 Introduction 53
3.1.1 The Apparatus and Tests Required 53
3.1.2 Research at Warwick 53

3.2 Development of Apparatus 55
3.2.1 The Apparatus Set-Up 55
3.2.2 The Origin of the Permode 56
3.2.3 Description of Permode Mark I 57
3.2.3.1 The Main Cell 59
3.2.3.2 The Base Plate 60
3.2.3.3 The Loading Piston 63
3.2.4 Limitations of Permode Mark I 63
3.2.4.1 Leakage 63
3.2.4.2 Material Failure 64
3.2.5 Modifications leading to Permode Mark II 64
3.2.5.1 Dealing with Leakage 64
3.2.5.2 Dealing With Material Failure 68
3.2.5.3 Overview 68
3.2.6 Cooling system 69
3.2.6.1 Method of Cooling 69
3.2.6.2 Method of Circulation 70
3.2.6.3 Circulation Fluid 71
3.2.6.4 Test Environment 73
3.2.7 Instrumentation 74
3.2.7.1 Displacement 74
3.2.7.2 Pore Water Pressure 75
3.2.7.3 Temperature 76
3.2.8 Data-Logging System 77
3.2.8.1 The Data-Logger 77
3.2.8.2 Use of PC 77

3.3 Soil Index Properties 78
3.3.1 Sample Description and Preparation 78
3.3.2 Index Tests 78
3.3.2.1 Liquid and Plastic Limits 78
3.3.2.2 Particle Size Distribution 80
3.3.2.3 Ring Shear Tests 82
3.3.2.4 Results of Consolidation Tests 83

3.4 Permode Test Procedure 91
3.4.1 Specimen Preparation 91
3.4.2 Test Programme 92
3.4.3 Test Procedure and Conditions 93
3.4.3.1 Basic Procedure 93
3.4.3.2 Temperature Control 94
3.4.3.3 Test Environment 95
3.4.3.4 Permode Apparatus and Instrumentation 96
3.4.3.5 Definitive Procedure (Tests 14-28) 96

Chapter 4 – Presentation of Results – Tests 1-13 98

4.1 Summary of Results for Tests 1-13 98

4.2 Individual Test Results 98
4.2.1 Test 1 98
4.2.2 Test 2 104
4.2.3 Test 3 109
4.2.4 Test 4 109
4.2.5 Test 5 115
4.2.6 Test 6 120
4.2.7 Test 7 125
4.2.8 Test 8 131
4.2.9 Test 9 139
4.2.10 Test 10 140
4.2.11 Test 11 141
4.2.12 Test 12 142
4.2.13 Test 13 147

Chapter 5 – Analysis of Results – Tests 1-13 153

5.1 Analysis of results 153
5.1.1 Patterns of Results 153
5.1.2 Temperature Control 154
5.1.2 The Consideration of Moisture Migration 156

5.2 Consideration of Zero Curtain Behaviour 157

5.3 Summary of Analyses 168

5.4 Revised Purpose of Experimentation 169

Chapter 6 – Presentation of Results – Tests 14-28 171

6.1 Results of Consolidation Tests 171

6.2 Summary of Results for Tests 14-28 171

6.3 Individual Test Results 172
6.3.1 Test 14 172
6.3.2 Test 15 179
6.3.3 Test 16 180
6.3.4 Test 17 181
6.3.5 Test 18 186
6.3.6 Test 19 191
6.3.7 Test 20 192
6.3.8 Test 21 193
6.3.9 Test 22 198
6.3.10 Test 23 203
6.3.11 Test 24 207
6.3.12 Test 25 208
6.3.13 Test 26 209
6.3.14 Test 27 213
6.3.15 Test 28 213

Chapter 7 – Analysis of Results – Tests 14-28 219

7.1 General Points 219

7.2 Application of the Semi-Infinite Slope Model 219
7.2.1 Model Definition 219
7.2.2 Consideration of Permode Test Results 225
7.2.3 Reference to Existing Knowledge Base 229

7.3 The Consideration of Moisture Migration 232
7.3.1 Moisture Migration Observed 232
7.3.2 The Significance of Leakage 233
7.3.3 Reference to Existing Knowledge Base 234

7.4 Frost Heave 235
7.4.1 Observed Frost Heave 235
7.4.2 Predicting Frost Heave 238
7.4.3 Frost Heave and the 0°C Isotherm 244
7.4.4 Possible Effects of a Closed System 255

7.5 The Consideration of Zero Curtain Behaviour 256
7.5.1 Comparison of Permode Testing to Model Slope Simulation 256
7.5.2 Initial Indications of Zero Curtain Behaviour 257
7.5.3 Examples of Zero Curtain Behaviour 260
7.5.3.1 Lias Clay 260
7.5.3.2 Weald Clay 261
7.5.3.3 Oxford Clay 261
7.5.4 Summary 261

7.6 Initial Decreases in Pore Water Pressure with Temperature 268

7.7 Summary of Analyses 273

Chapter 8 – Conclusions 274

8.1 Increases in Pore Water Pressure due to Freezing and Thawing 274

8.2 Slope Failure Due to Increases in Pore Water Pressure 274

8.3 Patterns of Moisture Migration 275

8.4 Frost Heave 276

8.5 Zero Curtain Behaviour 276

8.6 The Efficiency of the Test Methodology 277
8.6.1 Validity of the Test Set-Up 277
8.6.2 Prevention of Leakage 278
8.6.3 Initial Drop in Pore Water Pressure with Temperature 278
8.6.4 Direction of Thaw 278
8.6.5 Overall Performance of the Apparatus 279

8.7 Implications for Theory and Practice 279

Chapter 9 – Scope for Further Work 280

9.1 Scope for Further Modifications to the Apparatus 280
9.1.1 Upgrading of Temperature Sensors 280
9.1.2 Increased Number and Optimisation of Temperature Sensors 281
9.1.3 Provision of Large-Scale Controlled Temperature Environment 282
9.1.4 Upgrading of Pressure Transducers 282
9.1.5 Optimisation of Permode Cell Construction 282
9.1.6 Development of an Integrated Data-Logging and Post-Processing System 283

9.2 Scope for Further Research 284
9.2.1 Investigation of Different Soil Types 284
9.2.2 Investigation of Moisture Migration and Frost Heave 284
9.2.3 Introduction of a Freezing Zero Curtain 284
9.2.4 Investigation of Drained tests and In-Cell Consolidation 285
9.2.5 Investigation of Varying Levels of Saturation 285
9.2.6 Consideration of Varying Modes of Slope Failure 285

References 287

Bibliography 294

Appendix A – Photographs of Apparatus 296

Appendix B – Instrumentation Calibration Data 300

B.1 The Instrumentation to be Calibrated 300

B.2 The 'Least Squares' Method of Regression Analysis 300

B.3 Summary of Calibrations 301

Appendix C – Computer Analysis Techniques 311

C.1 Turbo-Pascal Program 311

C.2 The Use of Microsoft Excel 313

C.3 The Use of Matlab 314

Appendix D – Permode Test Results – All Tests 315

List of Figures

Figure 2.1 - The Extent of Glaciation In Great Britain and Ireland (reproduced from Figure 2.1, Ballantyne & Harris, 1994, who acknowledge the figure as modified from Bowen et al., 1986) 6

Figure 2.2 - Reconstruction of Probable Values of Mean Temperatures for the Warmest and Coldest Months of the Year (reproduced from Figure 2.2, Ballantyne & Harris, 1994, after Atkinson et al., 1987) 7

Figure 2.3 - Frost Creep (after Figure 7.2, Ballantyne & Harris, 1994) 12

Figure 2.4 - Cambering and Valley Bulging (after Figure 7.31, Ballantyne & Harris, 1994, after Figure 2, Parks, 1991) 14

Figure 2.5 - Decrease in ϕ'_r with Increasing Clay Fraction (reproduced from Figure 7, Skempton, 1964) 19

Figure 2.6 - Semi-infinite Slope Analysis 21

Figure 2.7 - Hydraulic Conductivity of Various Frozen Soils, (after Burt & Williams, (1976), from Williams & Smith, (1989) 50

Figure 3.1 - Basic Test Programme 55

Figure 3.2 - Apparatus Set-Up 56

Figure 3.3 - Drawing No. ES919 Sheet 1 62a

Figure 3.4 - Drawing No. ES919 Sheet 2 62b

Figure 3.5 - Cross-section and Plan of Membrane Holder 65

Figure 3.6 - Drawing No. ES919 Sheet 3 67

Figure 3.7 - Peristaltic Action 70

Figure 3.8 - Results of Index Tests Plotted on A-Line Graph 79

Figure 3.9 - PSD Results for Lias Clay 80

Figure 3.10 - PSD Results for Weald Clay 81

Figure 3.11 - PSD Results for Oxford Clay 81

Figure 3.12 - Ring Shear Envelope for Lias Clay 82

Figure 3.13 - Ring Shear Envelope for Weald Clay 83

Figure 3.14 - Ring Shear Envelope for Oxford Clay 83

Figure 3.15 - Rowe Cell Consolidation Test - Lias Clay 86

Figure 3.16 - Rowe Cell Consolidation Tests - Weald Clay 87

Figure 3.17 - Rowe Cell Consolidation Tests - Oxford Clay 88

Figure 3.18 - Position of Soil Elements in Test Model 89

Figure 4.1 - Results for Test 1 100

Figure 4.2 - Temperature Profiles for Test 1 Cycle 1 101

Figure 4.3 - Test 1 Cycle 1 102

Figure 4.4 - Test 1 Cycle 2 103

Figure 4.5 - Test 1 Cycle 5 103

Figure 4.6 - Test 1 Cycle 6 104

Figure 4.7 - Results for Test 2 105

Figure 4.8 - Temperature Profiles for Test 2 Cycle 1 106

Figure 4.9 - Test 2 Cycle 2 107

Figure 4.10 - Test 2 Cycle 3 107

Figure 4.11 - Test 2 Cycle 4 108

Figure 4.12 - Test 2 Cycle 8 108

Figure 4.13 - Results for Test 4 110

Figure 4.14 - Temperature Profiles for Test 4 Cycle 3 111

Figure 4.15 - Temperature Profiles for Test 4 Cycle 4 111
Figure 4.16 - Test 4 Cycle 3 Base 113
Figure 4.17 - Test 4 Cycle 3 Top 113
Figure 4.18 - Test 4 Cycle 4 Base 114
Figure 4.19 - Test 4 Cycle 4 Top 114
Figure 4.20 - Results for Test 5 115
Figure 4.21 - Temperature Profiles for Test 5 Cycle 2 116
Figure 4.22 - Test 5 Cycle 1 Base 117
Figure 4.23 - Test 5 Cycle 1 Top 117
Figure 4.24 - Test 5 Cycle 2 Base 118
Figure 4.25 - Test 5 Cycle 2 Top 118
Figure 4.26 - Test 5 Cycle 10 Base 119
Figure 4.27 - Test 5 Cycle 10 Top 119
Figure 4.28 - Results for Test 6 121
Figure 4.29 - Temperature Profiles for Test 6 Cycle 1 121
Figure 4.30 - Test 6 Cycle 1 Base 123
Figure 4.31 - Test 6 Cycle 1 Top 123
Figure 4.32 - Test 6 Cycle 2 Base 124
Figure 4.33 - Test 6 Cycle 2 Top 124
Figure 4.34 - Results for Test 7 125
Figure 4.35 - Temperature Profiles for Test 7 Cycle 1 126
Figure 4.36 - Test 7 Cycle 1 Base 127
Figure 4.37 - Test 7 Cycle 1 Top 127
Figure 4.38 - Test 7 Cycle 2 Base 128
Figure 4.39 - Test 7 Cycle 2 Top 128
Figure 4.40 - Test 7 Cycle 3 Base 129
Figure 4.41 - Test 7 Cycle 3 Top 129
Figure 4.42 - Test 7 Cycle 4 Base 130
Figure 4.43 - Test 7 Cycle 4 Top 130
Figure 4.44 - Results for Test 8 132
Figure 4.45 - Temperature Profiles for Test 8 Cycle 1 132
Figure 4.46 - Test 8 Cycle 2 Base 134
Figure 4.47 - Test 8 Cycle 2 Top 134
Figure 4.48 - Test 8 Cycle 3 Base 135
Figure 4.49 - Test 8 Cycle 3 Top 135
Figure 4.50 - Test 8 Cycle 5 Base 136
Figure 4.51 - Test 8 Cycle 5 Top 136
Figure 4.52 - Test 8 Cycle 6 Base 137
Figure 4.53 - Test 8 Cycle 6 Top 137
Figure 4.54 - Test 8 Cycle 7 Base 138
Figure 4.55 - Test 8 Cycle 7 Top 138
Figure 4.56 - Results for Test 12 143
Figure 4.57 - Temperature Profiles for Test 12 Cycle 1 144
Figure 4.58 - Test 12 Cycle 3 Base 145
Figure 4.59 - Test 12 Cycle 3 Top 145
Figure 4.60 - Test 12 Cycle 4 Base 146
Figure 4.61 - Test 12 Cycle 4 Top 146
Figure 4.62 - Results for Test 13 148
Figure 4.63 - Temperature Profiles for Test 13 Cycle 2 148
Figure 4.64 - Test 13 Cycle 2 Base 150

Figure 4.65 - Test 13 Cycle 2 Top 150
Figure 4.66 - Test 13 Cycle 5 Base 151
Figure 4.67 - Test 13 Cycle 5 Top 151

Figure 5.1 - Test 7 Cycle 1 Pore Water Pressure & Temperatures 160
Figure 5.2 - Test 7 Cycle 1 Pore Water Pressure & Temperature at Base 160
Figure 5.3 - Test 7 Cycle 2 Pore Water Pressure & Temperatures 161
Figure 5.4 - Test 7 Cycle 2 Pore Water Pressure & Temperature at Base 161
Figure 5.5 - Test 7 Cycle 3 Pore Water Pressure & Temperatures 162
Figure 5.6 - Test 7 Cycle 3 Pore Water Pressure & Temperature at Base 162
Figure 5.7 - Test 7 Cycle 4 Pore Water Pressure & Temperatures 163
Figure 5.8 - Test 7 Cycle 4 Pore Water Pressure & Temperature at Base 163
Figure 5.9 - Test 8 Cycle 2 Pore Water Pressure & Temperatures 164
Figure 5.10 - Test 8 Cycle 2 Pore Water Pressure & Temperature at Base 164
Figure 5.11 - Test 8 Cycle 3 Pore Water Pressure & Temperatures 165
Figure 5.12 - Test 8 Cycle 3 Pore Water Pressure & Temperature at Base 165
Figure 5.13 - Test 8 Cycle 5 Pore Water Pressure & Temperatures 166
Figure 5.14 - Test 8 Cycle 5 Pore Water Pressure & Temperature at Base 166
Figure 5.15 - Test 8 Cycle 6 Pore Water Pressure & Temperatures 167
Figure 5.16 - Test 8 Cycle 6 Pore Water Pressure & Temperature at Base 167

Figure 6.1 - Results for Test 14 173
Figure 6.2 - Temperature Profiles for Test 14 Cycle 1 174
Figure 6.3 - Temperature Profiles for Test 14 Cycle 5 174
Figure 6.4 - Temperature Profiles for Test 14 Cycle 7 175
Figure 6.5 - Test 14 Cycle 1 Pore Water Pressure & Temperature at Base 176
Figure 6.6 - Test 14 Cycle 1 Pore Water Pressure & Temperature at Top 176
Figure 6.7 - Test 14 Cycle 5 Pore Water Pressure & Temperature at Base 177
Figure 6.8 - Test 14 Cycle 5 Pore Water Pressure & Temperature at Top 177
Figure 6.9 - Test 14 Cycle 7 Pore Water Pressure & Temperature at Base 178
Figure 6.10 - Test 14 Cycle 7 Pore Water Pressure & Temperature at Top 178
Figure 6.11 - Results for Test 17 181
Figure 6.12 - Temperature Profiles for Test 17 Cycle 1 182
Figure 6.13 - Test 17 Cycle 1 Pore Water Pressure & Temperature at Base 183
Figure 6.14 - Test 17 Cycle 1 Pore Water Pressure & Temperature at Top 183
Figure 6.15 - Test 17 Cycle 2 Pore Water Pressure & Temperature at Base 184
Figure 6.16 - Test 17 Cycle 2 Pore Water Pressure & Temperature at Top 184
Figure 6.17 - Test 17 Cycle 3 Pore Water Pressure & Temperature at Base 185
Figure 6.18 - Test 17 Cycle 3 Pore Water Pressure & Temperature at Top 185
Figure 6.19 - Test 17 Cycle 4 Pore Water Pressure & Temperature at Base 186
Figure 6.20 - Test 17 Cycle 4 Pore Water Pressure & Temperature at Top 186
Figure 6.21 - Results for Test 18 187
Figure 6.22 - Temperature Profiles for Test 18 Cycle 1 188
Figure 6.23 - Test 18 Cycle 1 Pore Water Pressure & Temperature at Base 189
Figure 6.24 - Test 18 Cycle 1 Pore Water Pressure & Temperature at Top 189
Figure 6.25 - Test 18 Cycle 2 Pore Water Pressure & Temperature at Base 190
Figure 6.26 - Test 18 Cycle 2 Pore Water Pressure & Temperature at Top 190
Figure 6.27 - Results for Test 21 193
Figure 6.28 - Temperature Profiles for Test 21 Cycle 1 194
Figure 6.29 - Test 21 Cycle 1 Pore Water Pressure & Temperature at Base 195

Figure 6.30 - Test 21 Cycle 1 Pore Water Pressure & Temperature at Top 195
Figure 6.31 - Test 21 Cycle 2 Pore Water Pressure & Temperature at Base 196
Figure 6.32 - Test 21 Cycle 2 Pore Water Pressure & Temperature at Top 196
Figure 6.33 - Test 21 Cycle 3 Pore Water Pressure & Temperature at Base 197
Figure 6.34 - Test 21 Cycle 3 Pore Water Pressure & Temperature at Top 197
Figure 6.35 - Results for Test 22 198
Figure 6.36 - Temperature Profiles for Test 22 Cycle 1 199
Figure 6.37 - Test 22 Cycle 1 Pore Water Pressure & Temperature at Base 200
Figure 6.38 - Test 22 Cycle 1 Pore Water Pressure & Temperature at Top 200
Figure 6.39 - Test 22 Cycle 2 Pore Water Pressure & Temperature at Base 201
Figure 6.40 - Test 22 Cycle 2 Pore Water Pressure & Temperature at Top 201
Figure 6.41 - Test 22 Cycle 3 Pore Water Pressure & Temperature at Base 202
Figure 6.42 - Test 22 Cycle 3 Pore Water Pressure & Temperature at Top 202
Figure 6.43 - Results for Test 23 203
Figure 6.44 - Temperature Profiles for Test 23 Cycle 1 204
Figure 6.45 - Test 23 Cycle 1 Pore Water Pressure & Temperature at Base 205
Figure 6.46 - Test 23 Cycle 1 Pore Water Pressure & Temperature at Top 205
Figure 6.47 - Test 23 Cycle 2 Pore Water Pressure & Temperature at Base 206
Figure 6.48 - Test 23 Cycle 2 Pore Water Pressure & Temperature at Top 206
Figure 6.49 - Results for Test 26 209
Figure 6.50 - Temperature Profiles for Test 26 Cycle 2 210
Figure 6.51 - Test 26 Cycle 2 Pore Water Pressure & Temperature at Base 211
Figure 6.52 - Test 26 Cycle 2 Pore Water Pressure & Temperature at Top 211
Figure 6.53 - Test 26 Cycle 5 Pore Water Pressure & Temperature at Base 212
Figure 6.54 - Test 26 Cycle 5 Pore Water Pressure & Temperature at Top 212
Figure 6.55 - Results for Test 28 214
Figure 6.56 - Temperature Profiles for Test 28 Cycle 1 215
Figure 6.57 - Test 28 Cycle 1 Pore Water Pressure & Temperature at Base 216
Figure 6.58 - Test 28 Cycle 1 Pore Water Pressure & Temperature at Top 216
Figure 6.59 - Test 28 Cycle 2 Pore Water Pressure & Temperature at Base 217
Figure 6.60 - Test 28 Cycle 2 Pore Water Pressure & Temperature at Top 217
Figure 6.61 - Test 28 Cycle 3 Pore Water Pressure & Temperature at Base 218
Figure 6.62 - Test 28 Cycle 3 Pore Water Pressure & Temperature at Top 218

Figure 7.1 - The Effect of $+\Delta u$ on the Stability of Slopes 224
Figure 7.2 - Numerical Solution for R and r_u, after Morgenstern & Nixon, (1971); Nixon, (1973). 231
Figure 7.3 - Measured Frost Heave 236
Figure 7.4 - Percentage Increase in Volume for Different Saturation Levels 243
Figure 7.5 - Plotting the Zero Isotherm for Freeze Phase of Test 14 Cycle 5 246
Figure 7.6 - Plotting the Zero Isotherm for Thaw Phase of Test 14 Cycle 5 247
Figure 7.7 - Comparing Heave with Progression of Zero Isotherm for Test 14 Cycle 5 248
Figure 7.8 - Plotting the Zero Isotherm for Freeze Phase of Test 25 Cycle 5 249
Figure 7.9 - Plotting the Zero Isotherm for Thaw Phase of Test 25 Cycle 5 250
Figure 7.10 - Comparing Heave with Progression of Zero Isotherm for Test 25 Cycle 5 251
Figure 7.11 - Plotting the Zero Isotherm for Freeze Phase of Test 20 Cycle 5 252
Figure 7.12 - Plotting the Zero Isotherm for Thaw Phase of Test 20 Cycle 5 253
Figure 7.13 - Comparing Heave with Progression of Zero Isotherm for Test 20 Cycle 5 254

Figure 7.14 - Position of Minimum Pore Water Pressure – Top 258
Figure 7.15 - Position of Minimum Pore Water Pressure – Base 258
Figure 7.16 - Test 15 Cycle 1 262
Figure 7.17 - Test 15 Cycle 2 262
Figure 7.18 - Test 15 Cycle 3 263
Figure 7.19 - Test 15 Cycle 4 263
Figure 7.20 - Test 17 Cycle 1 264
Figure 7.21 - Test 17 Cycle 2 264
Figure 7.22 - Test 17 Cycle 3 265
Figure 7.23 - Test 17 Cycle 4 265
Figure 7.24 - Test 26 Cycle 2 266
Figure 7.25 - Test 26 Cycle 5 266
Figure 7.26 - Test 19 Cycle 2 267
Figure 7.27 - Test 19 Cycle 5 267
Figure 7.28 - Pressure Transducer Behaviour 270
Figure 7.29 - Pressure Transducer Behaviour for Time Period 25 – 90.5 Hours 271

Figure 9.1 - Retrogressive Slope Failure, after Petley & Hutchinson, (2001) 286

Figure A.1 - The Permode Cell (usually inside refrigerated cabinet) 296
Figure A.2 - Permode Barrel and Liner 297
Figure A.3 - Thermocouple and Washer Assembly 297
Figure A.4 - Pressure and Displacement Transducers 298
Figure A.5 - Baseplate Assembly 298
Figure A.6 - Piston and Porous Plate 299

Figure B.1 - Excel Regression Analysis for SGDT Displacement Transducer – 1 308
Figure B.2 - Excel Regression Analysis for SGDT Displacement Transducer – 2 308
Figure B.3 - Excel regression Analysis for PWP Base Transducer - 1 309
Figure B.4 - Excel Regression Analysis for PWP Base Transducer – 2 309
Figure B.5 - Excel Regression Analysis for PWP Top Transducer - 1 310
Figure B.6 - Excel Regression Analysis for PWP Top Transducer – 2 310

Figure D.1 - Test 1 - Lias clay - σ = 29 kPa, m.c. = 29% 315
Figure D.2 - Test 2 - Lias clay - σ = 104 kPa, m.c. = 32% 316
Figure D.3 - Test 3 - Lias clay - σ = 104 kPa, m.c. = 30% 316
Figure D.4 - Test 4 - Lias clay - σ = 104 kPa, m.c. = 32% 317
Figure D.5 - Test 5 - Lias clay - σ = 104 kPa, m.c. = 30% 317
Figure D.6 - Test 6 - Lias clay - σ = 104 kPa, m.c. = 35% 318
Figure D.7 - Test 7 - Lias clay - σ = 104 kPa, m.c. = 33% 318
Figure D.8 - Test 8 - Lias clay - σ = 80 kPa, m.c. = 30% 319
Figure D.9 - Test 9 - Lias clay - σ = 104 kPa, m.c. = 29% 319
Figure D.10 - Test 10 - Lias clay - σ = 80 kPa, m.c. = 32% 320
Figure D.11 - Test 11 - Lias clay - σ = 80 kPa, m.c. = 31% 320
Figure D.12 - Test 12 - Lias clay - σ = 80 kPa, m.c. = 30% 321
Figure D.13 - Test 13 - Lias clay - σ = 80 kPa, m.c. = 32% 321
Figure D.14 - Test 14 - Lias clay - σ = 80 kPa, m.c. = 27% 322
Figure D.15 - Test 15 - Lias clay - σ = 55 kPa, m.c. = 27% 322
Figure D.16 - Test 16 - Lias clay - σ = 80 kPa, m.c. = 31% 323

Figure D.17 - Test 17 - Lias clay - σ = 55 kPa, m.c. = 31% 323
Figure D.18 - Test 18 - Lias clay - σ = 120 kPa, m.c. = 31% 324
Figure D.19 - Test 19 - Oxford clay - σ = 55 kPa, m.c. = 49% 324
Figure D.20 - Test 20 - Oxford clay - σ = 80 kPa, m.c. = 49% 325
Figure D.21 - Test 21 - Oxford clay - σ = 55 kPa, m.c. = 50% 325
Figure D.22 - Test 22 - Oxford clay - σ = 55 kPa, m.c. = 50%, Freezing from base upwards 326
Figure D.23 - Test 23 - Oxford clay - σ = 80 kPa, m.c. = 50%, Freezing from base upwards 326
Figure D.24 - Test 24 - Weald clay - σ = 55 kPa, m.c. = 39% 327
Figure D.25 - Test 25 - Weald clay - σ = 80 kPa, m.c. = 39% 327
Figure D.26 - Test 26 - Weald clay - σ = 55 kPa, m.c. = 38% 328
Figure D.27 - Test 27 - Weald clay - σ = 80 kPa, m.c. = 38% 328
Figure D.28 - Test 28 - Weald clay - σ = 67.5 kPa, m.c. = 38% 329

List of Tables

Table 2.1 - Data from Ring Shear Tests of Brecciated Weald Clay (Skempton & Weeks, 1976) 28
Table 2.2 - Calculated Values of β for Brecciated Weald Clay (Skempton & Weeks, 1976) 28
Table 2.3 - Comparison of Predicted and Actual β (after Chandler, 1970b) 29
Table 2.4 - Pore Water Pressures Required for Initiation of Mudslides (after Table 1, Chandler, 1972) 35
Table 2.5 - A Comparison of Freeze-Thaw Permeameter Testing Methods (after Table 2, Othman et al., 1994) 44

Table 3.1 - Description of Apparatus 58
Table 3.2 - Properties of Antifreeze (after Munro, 1964) 72
Table 3.3 - Index Properties 80
Table 3.4 - Consolidation Characteristics and Permeability Coefficients 85
Table 3.5 - Values of z Corresponding to the Various Applied Stresses 89
Table 3.6 - Estimated Values of t90 in the Field – 2 Way Drainage 90
Table 3.7 - Estimated Values of t90 in the Field – 1 Way Drainage 90
Table 3.8 - Programme for Tests 1-13 92
Table 3.9 - Programme for Tests 14-28 93
Table 3.10 - Temperature Control 94
Table 3.11 - Test Environment 95
Table 3.12 - Permode Apparatus and Instrumentation 96

Table 4.1 - Summary of Results for Tests 1-13, All on Lias Clay 98
Table 4.2 - Values of Pore Water Pressure Recorded at End of Cycle – Test 1 100
Table 4.3 - Values of Pore Water Pressure Recorded at End of Cycle – Test 2 105

Table 6.1 - Consolidation Characteristics and Permeability Coefficients 171
Table 6.2 - Summary of Results for Tests 14-28 172

Table 7.1 - Comparisons Between the Soil Types 220
Table 7.2 - Values of z Corresponding to the Various Applied Stresses 221
Table 7.3 - Values of β Found using Conventional Analysis, ($r_u = 0.5$) 223
Table 7.4 - The Effect on Slope Stability of +Δu Found in Permode Tests – Top of Specimen 225
Table 7.5 - The Effect on Slope Stability of +Δu Found in Permode Tests – Base of Specimen 226
Table 7.6 - Summary of Minimum Values of β Found 228
Table 7.7 - Values of R for Each Soil Type 230
Table 7.8 - Values of r_u found from Nixon & Morgenstern, (1971), Solution. 231
Table 7.9 - Moisture Migration in Tests 14-28 232
Table 7.10 - Mean Values of Frost Heave for Cycles 1-5, $\sigma = 80$ kPa 237
Table 7.11 - Lias Clay Test 14 Expected and Actual Heave 241
Table 7.12 - Weald Clay Test 25 Expected and Actual Heave 241
Table 7.13 - Oxford Clay Test 20 Expected and Actual Heave 242
Table 7.14 - Position of Minimum Pore Water Pressures Recorded at the Top of the Specimen 257
Table 7.15 - Position of Minimum Pore Water Pressures Recorded at the Base of the Specimen 257

Table 8.1 - Comparison of Rates of Thaw, (using Equations 2.1 & 2.2 and Figure 7.2) 277

Table B.1 - Summary of Calibrations 301
Table B.2 - Calibration Table for SGDT Displacement Transducer – 1 302
Table B.3 - Calibration Table for SGDT Displacement Transducer – 2 303
Table B.4 - Calibration Table for PWP Base Transducer – 1 304
Table B.5 - Calibration Table for PWP Base Transducer - 2 305
Table B.6 - Calibration Table for PWP Top Transducer - 1 306
Table B.7 - Calibration Table for PWP Top Transducer - 2 307

List of Equations

Equation 2.1 - The Thaw-Consolidation Ratio 11
Equation 2.2 - The Rate of Thaw, Neumann Solution 11
Equation 2.3 - Movement of the Thaw Front (Nixon & Morgenstern, 1973a) 11
Equation 2.4 - Factor of Safety against Sliding in Basic Terms 21
Equation 2.5 - Shear Stress Developed Along a Potential Slip Surface 22
Equation 2.6 - Effective Stress 22
Equation 2.7 - Mobilised Shear Resistance 22
Equation 2.8 - Factor of Safety against Sliding 22
Equation 2.9 - An Equation to find the Angle of Slope Failure, β, (Skempton & DeLory, 1957) 22
Equation 2.10 - An Equation to find β for the Full Hydrostatic Case (Skempton & DeLory, 1957) 23
Equation 2.11 - Factor of Safety against Sliding using Residual Strength Parameters 23
Equation 2.12 - A General Equation to Find β 23
Equation 2.13 - A Simplified Equation to Find β for the Full Hydrostatic Case 24

Equation 2.14 - Conditions of Limiting Equilibrium for Solifluction (Skempton & Hutchinson, 1969) 24
Equation 2.15 - Semi-infinite Slope Analysis Solution (McRoberts & Morgenstern, 1974) 25
Equation 2.16 - Factor of Safety against Sliding used for Vestspitsbergen (Chandler, 1972) 35

Equation 3.1 - Terzaghi's Theory of Consolidation 84
Equation 3.2 - An Equation to Find mv 85
Equation 3.3 - An Equation to Find k 85

Equation 7.1 - $r_{u(1)}$, the Full Hydrostatic Component of r_u 221
Equation 7.2 - $r_{u(2)}$, the Additional Pore Water Pressure Component of r_u 221
Equation 7.3 - The Combined Value of r_u 222
Equation 7.4 - An Equation to Find β Using the Combined Value of r_u 222
Equation 7.5 - The Limiting Value of $+\Delta u$ 222
Equation 7.6 - Void Ratio 238
Equation 7.7 - Water Content 238
Equation 7.8 - Density Relationships 239
Equation 7.9 - Volume of Solids 239
Equation 7.10 - Volume of Water 239
Equation 7.11 - Volume of Specimen After Freezing 239
Equation 7.12 - Percentage Increase in Volume from Freezing 240
Equation 7.13 - Moving Average Calculation performed by Microsoft Excel 268

Equation B.1 - x against y 300
Equation B.2 - m found using the 'Least Squares' method 300
Equation B.3 - Conversion factor for datalogger 300
Equation B.4 - Correlation coefficient, r 301

Acknowledgements

I have been lucky enough to have received a great deal of support from a large number of people during the course of my research, but would like to thank the following especially:

My supervisor, Dr Derek Petley, for all his guidance and help over the past four years.

Mr Dickon Woods, for his interesting questions.

Dr David Sego and Mr Gerry Cyre of the Department of Geotechnical Engineering, University of Alberta, for their kind assistance and advice during my visit in 1998.

Mr Colin Banks for his invaluable part in getting, (and keeping), the apparatus up and running.

Mr John Roe from the drafting office, for producing the construction drawings and advising on the design of the permode.

Mr Malcolm Farrow for constructing the permode and everybody else from the workshops and labs who became involved in the process.

Notation

Symbol	Units	Definition
n/a	°C	Degrees Celsius
n/a	dgC	Degrees Celsius in graphics packages
α	as required	Rate of thaw in time *t*
β	°	Slope angle of failure
BP	ka	Before Present
c'	p.s.i./kPa	Apparent drained cohesion
c_r'	p.s.i./kPa	Apparent drained cohesion - residual
Cu	p.s.i./kPa	Undrained compression strength
c_v	m^2/year	Coefficient of Consolidation
e	n/a	Void ratio
e_g	n/a	Granular void ratio (Lupini *et al.*, 1981)
F_s	n/a	Factor of safety against sliding
G_s	n/a	Specific gravity
ϕ'	°	Angle of internal shearing resistance
ϕ_r'	°	Angle of internal shearing resistance – residual strength
γ	kN/m^3	Saturated unit weight
γ_w	kN/m^3	Unit weight of water
γ'	kN/m^3	$\gamma - \gamma_w$: Buoyant unit weight
h	m	The height of the water table above a potential slip surface
k	m/s	Permeability
M	g	Total mass
M_s	g	Mass of solids
M_w	g	Mass of water
m	n/a	Gradient
m.c.	%	Moisture Content
m_v	m^2/MN	Coefficient of Compressibility
PI	%	Plasticity Index
PWP	kPa	Pore water pressure
r	n/a	Correlation coefficient
R	n/a	Thaw Consolidation Ratio
r_u	n/a	Pore water pressure ratio
ρ	g/cm^3	Bulk density
ρ_w	g/cm^3	Density of water
σ	kPa	Applied stress
σ'	kPa	Effective Stress
S_r	n/a	Degree of saturation
s	p.s.i.	Shear resistance that can be mobilised by a soil
t	as required	Time
τ	p.s.i.	Shear stress developed along a potential failure surface
$\tau/\sigma'n$	n/a	Residual friction coefficient (Lupini *et al.*, 1981)
$+\Delta u$	kPa	Increase in pore water pressure
$+\Delta u_L$	kPa	Limiting increase in pore water pressure
V	cm^3	Volume

Symbol	Units	Definition
V_s	cm^3	Volume of solids
V_w	cm^3	Volume of water
V_f	cm^3	Volume of specimen after freezing
w	% or ratio	Water content
w_L	%	Liquid Limit
w_P	%	Plastic Limit
X	m	Depth of thaw in time t
z	m	The depth below ground surface to a potential slip surface

Summary

Relic periglacial solifluction features cover most of Britain, particularly the Midlands and the South, causing serious and continuing earthwork and construction problems. Although the engineering significance of the presence of periglacial solifluction deposits is widely appreciated, the mechanics of emplacement of these deposits has received surprisingly little attention.

The principal objective of the research has been to investigate the freeze-thaw behaviour of some clay soils in Britain which have been exposed to periglacial conditions. The behaviour was examined using a Permafrost Oedometer or Permode, based on the apparatus used by Morgenstern and Smith, (1973).

Tests have been carried out on Lias Clay, Weald Clay and Oxford Clay. In each test, a specimen was placed under an applied stress and subjected to 24 hour cycles of freezing and thawing. Freezing was mainly imposed from the top of the specimen downwards. The tests were carried out undrained.

The pore water pressures were found to increase as a result of cyclic freeze-thaw conditions. Greater pore water pressures were generally recorded at the top than at the base of the specimen. This was considered to be due to moisture migration towards the freezing front during freezing, and impeded filtration, (due to underlying frozen material), during thaw.

The significance of the additional pore water pressures in terms of slope stability was considered. A semi-infinite slope analysis model was used primarily, but reference was made to other, similar research.

The analysis found that the predicted slope angle of failure is reduced significantly by relatively low increases in pore water pressure. Greater increases in pore water pressure are gained for soils of lower residual shear strength/higher plasticity.

It was determined that the generation of excess pore water pressure and corresponding decrease in residual strength have considerable implications for the stability of slopes previously exposed to periglacial conditions.

Chapter 1 - Introduction

1.1 Statement of Research Problem

Immediately prior to the Pleistocene period, Britain experienced a semi-tropical climate. During the glaciation of the Pleistocene, ice sheets covered much of the country, extending as far south as Watford and North Devon. To the south of the ice sheets, the remaining country was subjected to a cold climate similar to that currently existing in the tundra areas of North America and Northern Europe. As the ice sheets receded, these tundra conditions followed. The ground was subjected to alternate periods of intense freezing and thawing, which has had a profound effect on the engineering properties and behaviour of the ground (Blyth and de Freitas, 1984).

Although the engineering significance of the presence of periglacial solifluction deposits is widely appreciated, the mechanics of emplacement of these deposits has received surprisingly little attention. Consequently, the resultant relic slip surfaces, along which the shear strength has reduced to residual values, are not always considered when investigating contemporary slope stability. Safe slope angles have been predicted using r_u between 0 and 0.5 combined with peak values of shear strength, which are inappropriate. Prior conditions are thus not being taken into account. A greater understanding of the effects of periglacial activity is required for engineering design and planning.

1.2 Background to the Research

Research on the engineering aspects of fossil periglacial solifluction has been conducted at the University of Warwick for several years. Recently, attention has also been directed towards the scientific understanding of the mechanisms involved. To this end, a 'Permode' has been constructed, based on the design of the originators at the University of Alberta in Edmonton, Canada. The Permode is a test cell equipped with freezing and thawing capabilities and associated pore water pressure measurement devices. The apparatus in use at the University of Warwick tests specimens 100mm in diameter and 100mm long. The samples are subjected to axial (vertical) loading and pore pressure measurements can be made at top and/or bottom of the sample. The top loading cap and

lower platen each contain a convoluted channel through which antifreeze solution can be circulated.

Thermocouples situated at various positions along the length of the apparatus monitor the temperature profile through the sample.

During the author's research the permode was used to investigate the pore pressure response of soils under applied stress being subjected to cycles of freezing and thawing under undrained conditions. Tests were carried out on 3 British soils – Lias, Weald and Oxford clays – taken from sites where shear surfaces developed under periglacial conditions have been recognised. Changes in pore water pressure during the tests were closely monitored, and their significance to slope stability investigated.

1.3 Justification for the Research

Seasonal freezing and thawing during previous periglacial activity has caused high enough pore water pressures to allow solifluction to take place, and failure surfaces to be formed. These relic or fossil slip surfaces may be reactivated by new engineering work. Therefore, there is a need for a more precise understanding of periglacial behaviour in order to avoid unnecessary, costly slope failures.

1.4 Outline of the Thesis

The thesis is composed of 9 chapters and 5 appendices. The appendices comprise material not essential to the main body of the thesis, but which is still of interest.

Chapter 1 introduces the research problem, giving some basic background information and a guide to the remaining chapters.

Chapter 2 comprises the literature review. Here, relevant background literature is collated and discussed. The papers reviewed are considered to form an ' existing knowledge base' which is referred to in later chapters.

Chapter 3 describes the test methodology. This includes both the design and commissioning of the test apparatus, and the development of the definitive test procedure.

Chapter 4 presents the results obtained from Tests 1-13. These tests primarily served as commissioning tests but also yielded some interesting data. Tests were carried out on one soil type only, in order to aid the commissioning process. The results are then discussed individually.

Chapter 5 presents the analysis of Tests 1-13 with respect to patterns of pore water pressure response, temperature control and moisture migration. Some comparisons are also drawn with results from the existing knowledge base. Finally, a statement of 'Revised Purpose of Experimentation' is given. This statement summarises how the experimental model – both physical and theoretical - was modified as a result of the first tranche of tests. The 'Revised Purpose' was incorporated into the remaining experimental work.

Chapter 6 presents the results obtained from Tests 14-28. The results are discussed individually in a similar fashion to Chapter 4.

Chapter 7 presents the analysis of Tests 14-28. More points of comparison, (e.g. maxima and minima), are established due to the common test methodology but variable soil type and initial conditions. The results are initially analysed for 'general trends' demonstrated by the soil specimens. Further analysis follows, examining selected aspects of the research in depth, including application of a slope stability model. Some comparisons are also drawn with results from the existing knowledge base.

Chapter 8 details the conclusions reached following analysis of the results, and considers the implications for theory and practice.

Chapter 9 sets out the scope of further work in the research area. Modifications to the test apparatus are discussed, and future research topics suggested.

Appendix A presents photographs of the permode and associated test apparatus.

Appendix B presents calibration data for the instrumentation used during the test programme.

Appendix C describes the computer analysis techniques used to examine the test results.

Appendix D presents plots of pore water pressure response, average temperature and displacement against time for the whole permode test programme, Tests 1-28.

1.5 Key Assumptions

The soils examined were Upper Lias clay, Weald clay and Oxford clay. In the experimental model, drainage has not been allowed for. The assumption behind this decision is that the low permeability of the soils would mean that the drainage of excess pore water, (meltwater on thaw), would be negligible through the specimen length.

The experimental model was designed to investigate the effect of increases in pore water pressure on slope stability, in particular planar shear surfaces developing at 2-5 m below the ground surface, within the active layer. Water was not allowed to enter through the base of the permode at any stage of the tests. Freezing of the specimens under an applied total stress was induced from the top downwards in order to simulate the advance of the freezing front through an element of soil, at a depth equivalent to the self-weight expressed as the applied stress. Upwards freezing from the permafrost layer was not induced as this would have caused 'flash' freezing due to the size of the specimen, not allowing detailed understanding of the soil behaviour to be achieved.

Chapter 2 – Literature Review

2.1 Periglacial Phenomena

2.1.1 Periglacial Conditions

Harris *et al.*, (1988), defined the term *periglacial* as referring to 'the conditions, processes and landforms associated with cold, non-glacial environments'. Ballantyne & Harris, (1994), extended this definition to give two further terms – *periglacial geomorphology*: concerning the understanding of landforms, deposits and processes of cold non-glacial environments; *periglacial environments*: past or present environments in which cold non-glacial processes have produced distinctive landforms and deposits. Such features are considered to be often a result of ground freezing.

The landscape of Great Britain evolved under climatic conditions much colder than those today, (Ballantyne & Harris, 1994). Glaciers developed in the upland areas expanded into the lowlands, but always left a *periglacial zone* of land not covered by the ice sheets. Williams *et al.*, (1993), determined that during the coldest part of the last glaciation the total land area covered by snow and ice increased from 10 % to more than 30 %. Of this zone known as the cryosphere, the periglacial component is estimated to take up 25 % of the planet's land surface, rising to 50 % during the last glaciation, (French, 1996). In southern Britain, successive glacial episodes caused a relic periglacial landscape to be developed. Figure 2.1 shows the extent of various glaciation stages. Blyth & de Freitas, (1984), indicated that areas below the extent of the ice sheet were subject to permafrost.

Ballantyne & Harris, (1994), described periglacial conditions in Great Britain as evidenced to have occurred during the Quaternary Period. This period is divided into 2 epochs, the Pleistocene, (2.4 Ma – 10 ka BP) and the Holocene, (after 10 ka BP). Ballantyne & Harris, (1994), stated that most relic periglacial features were formed in the Middle or Late Pleistocene age, (c. 810 - 10 ka BP).

The 'cold' temperatures experienced in periglacial environments varied substantially over the complete glaciation or 'ice age' period. Sparks & West, (1972), found that the use of such a general term could be misleading. Considering the glaciation in greater detail, cold periods known as glacials were separated by warmer interglacials, with shorter

milder periods called interstadials during the glacial periods. Ballantyne & Harris, (1994), presented a detailed review of the glacial stages, split into 'cold' stadials and warmer interstadials, and also the interglacial stages.

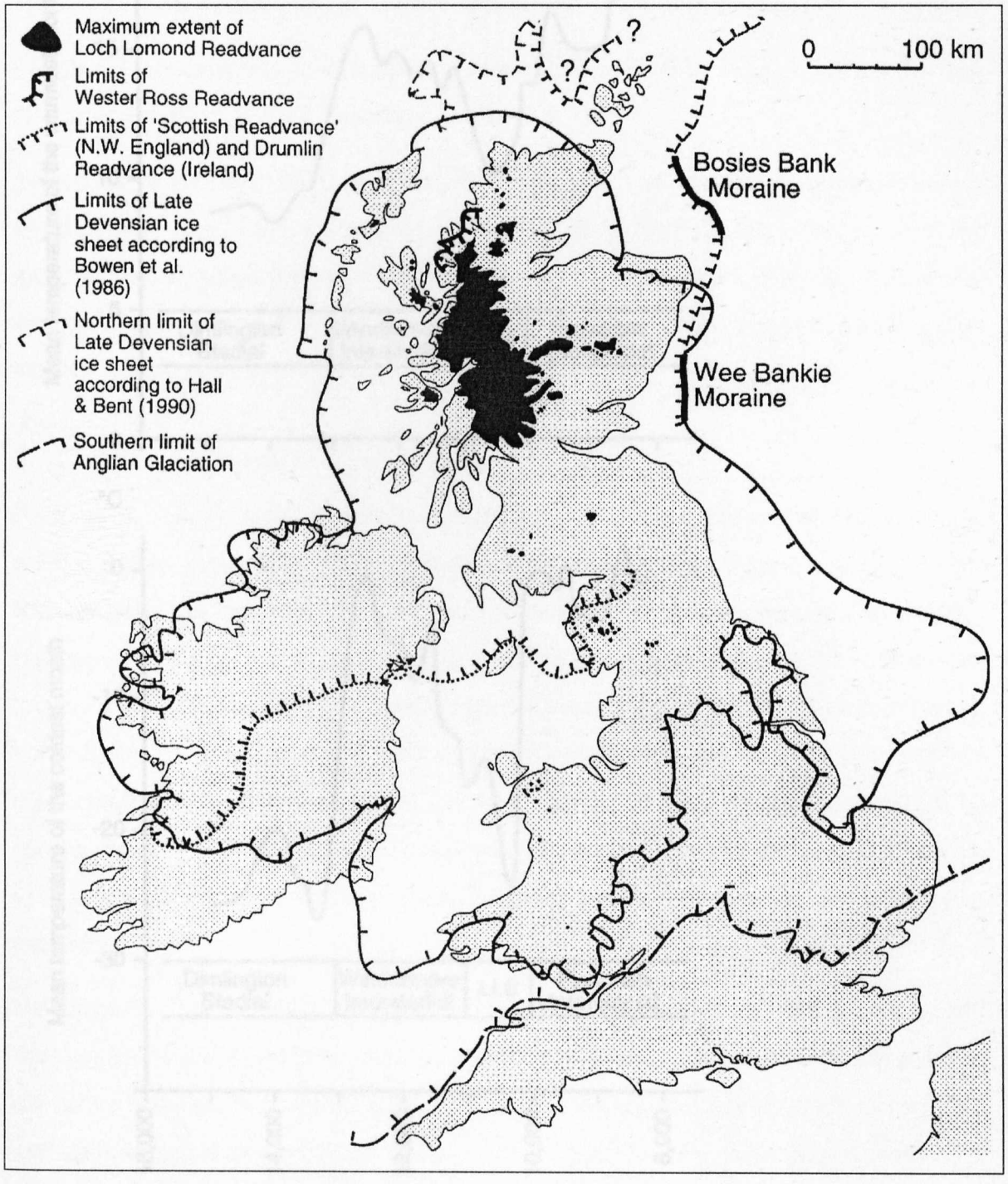

Figure 2.1 – The Extent of Glaciation In Great Britain and Ireland (reproduced from Figure 2.1, Ballantyne & Harris, 1994, who acknowledge the figure as modified from Bowen et al., 1986)

Figure 2.2 indicates the variation in temperatures over the Late Devensian Glacial and Flandrian Interglacial. The temperatures were reconstructed from the radiocarbon dating of coleoptera assemblages (Atkinson *et al.*, 1987).

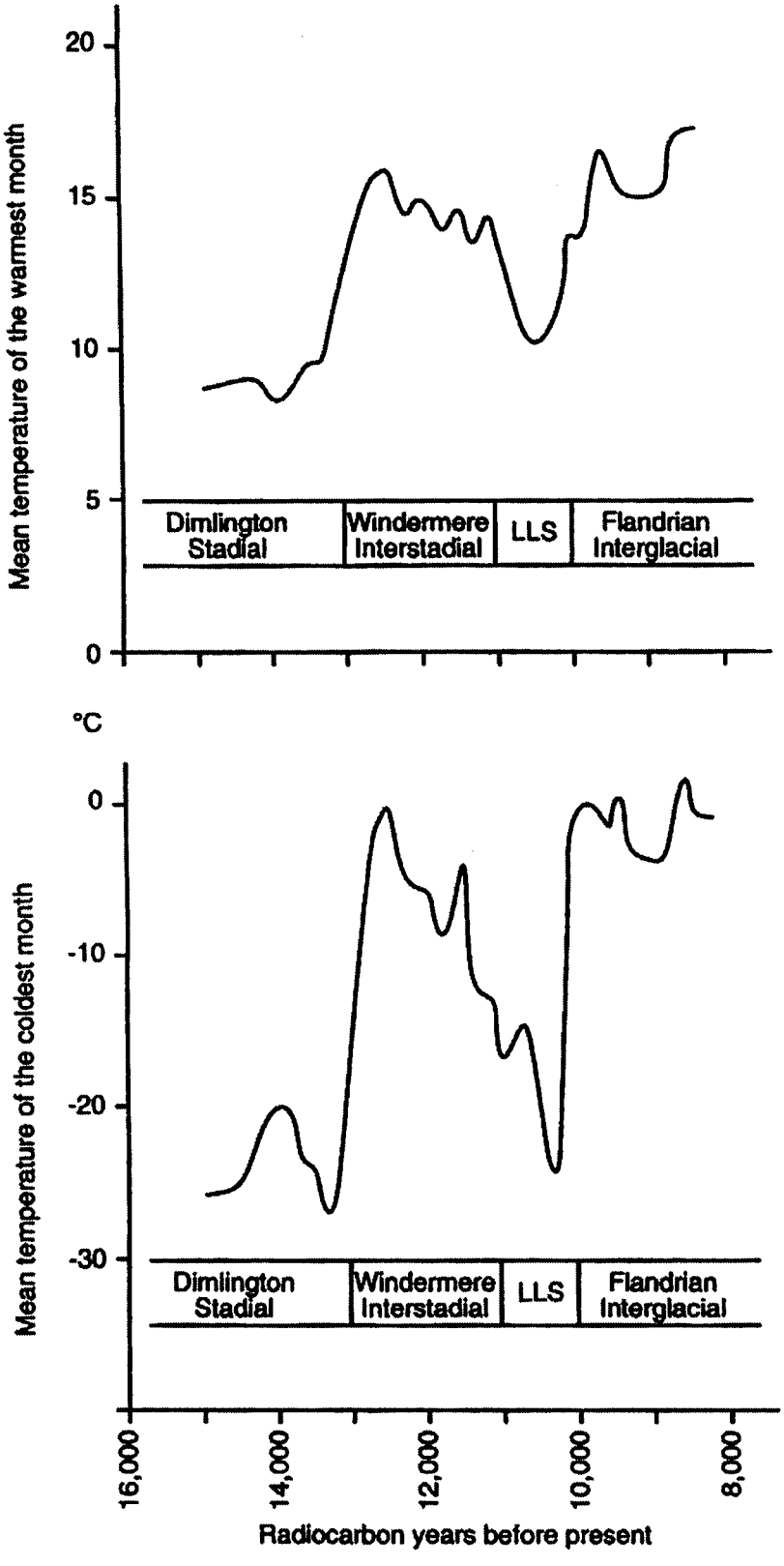

Figure 2.2 – Reconstruction of Probable Values of Mean Temperatures for the Warmest and Coldest Months of the Year (reproduced from Figure 2.2, Ballantyne & Harris, 1994, after Atkinson et al., 1987)

Ballantyne & Harris, (1994), differentiated between lowland and upland periglacial phenomena. A more refined sense of timescale can be gained from considering whether

upland or lowland periglacial features are being investigated. In the uplands, periglacial processes and features are active and are essentially post-glacial, and therefore likely to date from the end of the last ice age, (c. 10 ka BP). In lowland Britain, however, relic features have the potential to have been formed from up to a million years ago.

Periglacial processes and conditions have been well described by Higginbottom & Fookes, (1971); Hutchinson, (1991); Ballantyne & Harris, (1994).

Ballantyne & Harris, (1994), reviewed the development of research of periglaciation in Great Britain. One of the recent themes, (from c. 1965), has been the investigation of the geotechnical significance of periglacial deposits. A particular area of this is the understanding of periglacial mudslides, and their implications for slope stability. The author's research lies within this theme.

2.1.2 Permafrost and the Active Layer

Harris *et al.*, (1988), defined *permafrost* as ground in which the temperature lies below 0°C for at least two consecutive years. They also introduced the terms *cryotic* referring to soils with temperatures less than 0°C, and *non-cryotic* for soils with temperatures above 0°C. Ballantyne & Harris, (1994), explained that the use of these terms avoids the confusion of 'frozen' and 'unfrozen' as ground may or may not contain ice and water, (frozen/unfrozen), but will still be cryotic or non-cryotic. A further specification can be made as to whether the permafrost is 'warm', (over c. -5°C), or 'cold', (under c. -5°C). Permafrost zones can be considered to be *continuous,* usual in very cold climates of high latitude, or *discontinuous*, in less severe climates where surface insulation has caused gaps in the under-lying permafrost layer.

Ballantyne & Harris, (1994), defined the *active layer* as the zone of annual freezing and thawing above the permafrost layer. In current permafrost environments the thickness of the active layer has been found to be $\approx$ 0.5 m, but this increases southwards as increased surface heating occurs over longer summers. In areas of 'warm' permafrost, the active layer is seasonally frozen from the top downwards only. If the active layer is underlain by 'cold' permafrost, then two-sided freezing of the active layer may result.

Hutchinson, (1991), stated that negative pore water pressures are set up at a freezing front as it progresses downwards through the soil. Water migrates to this freezing zone, forming lenses of *segregation ice.*

Ballantyne & Harris, (1994), further described the formation of segregation ice. When cooling of the ground surface occurs, soil freezing commences as soil temperatures drop below 0°C. The 0°C isotherm moves slowly downwards through the soil, with the soil water behind it undergoing progressive freezing. Latent heat is released during the phase change from water to ice and is conducted up to the ground surface. Ice segregation is the process by which water migrates upwards to the freezing front. Ice segregation does not occur at the freezing front but at some distance behind it. Between the freezing front and the ice segregation level lies the 'frozen fringe', (Miller, 1980). This fringe consists of unfrozen soil water occupying smaller pores surrounding ice-filled larger pores. The upwards-migrating water passes through the frozen fringe to join ice lenses forming at the upper limit. Ice lenses grow for as long as the water migrating upwards releases enough latent heat to maintain the heat flow. If the supply of water is reduced, the fringe cools and builds up more ice, reducing permeability (Konrad & Morgenstern, 1982). This in turn closes down the water supply to the ice lenses. The frozen fringe advances down through the soil until equilibrium is established between the water entering the frozen fringe, ice formation above the fringe and the latent heat flow to the ground surface. When this point is reached, ice lens growth begins again.

The amount of ice segregation experienced by a soil layer depends on its granulometry, (Williams & Smith, 1989; Ballantyne & Harris, 1994). In coarse-grained soils water has little tendency to migrate upwards to the frozen fringe. Fine-grained soils, however, have smaller pores and there is a strong tendency for water migration to occur. Soils which exhibit this tendency are called *frost susceptible.*

Ballantyne & Harris, (1994), stated that clay-rich soils, while classed as frost susceptible in terms of granulometry, have low permeability which may restrict water migration and hence ice lens growth.

As a result of segregation ice formation, *frost heave* occurs, (Hutchinson, 1991; Ballantyne & Harris, 1994). This process entails the expansion of the soil structure and produces heave (i.e. upward displacement) of the ground surface. Hutchinson, (1991), states that the soil structure is dilated by amounts far greater than the 9% expansion of the original water content turning to ice. Hutchinson, (1991), noted that silts were particularly prone to frost heaving as they have the optimum balance between suction potential at the freezing front and permeability, but that other soil types were also affected.

Ballantyne & Harris, (1994), further described the processes involved in thaw-induced instability, which is primarily responsible for periglacial mass wasting. After upwards frost heaving of the soil surface, thaw occurs from the ground surface downwards with drainage impeded by the still-frozen soil underneath. As thaw takes place more meltwater is produced than can be taken by the available pore space. The voids left from the melting of the ice lenses can only be closed by the expulsion of this excess meltwater. The meltwater leaves the soil at a rate limited by the permeability of the thawed soil. During the time period over which drainage takes place, part or all of the overburden weight is supported by pore water pressures. As stress is transferred from the soil grain structure to the porewater, the direct stress on the soil grains reduces, reducing frictional forces between them and hence resistance. If gravity induced forces now exceed the shear strength of thawing soil, slope failure results.

Ballantyne & Harris, (1994), also described the 2-way freezing effect seen in winter in areas of continuous, 'cold' permafrost. In this case, freezing occurs as usual from the ground surface downwards, and also from the permafrost table upwards, as heat is lost to the colder permafrost below.

2.1.3 Thaw-Consolidation Theory

Ballantyne & Harris, (1994), stated that the generation of pore water pressures during thaw depends on the ratio between the rate of thaw and the rate of consolidation. This ratio is known as the thaw-consolidation ratio, *R*.

Morgenstern & Nixon, (1971), defined the thaw-consolidation ratio, R, as:

$$R = \frac{1}{2}\alpha c_v^{-\frac{1}{2}}$$

Equation 2.1 – The Thaw-Consolidation Ratio

c_v = the coefficient of consolidation

α = the rate of thaw, found from the Neumann equation

$$\alpha = Xt^{-\frac{1}{2}}$$

Equation 2.2 – The Rate of Thaw, Neumann Solution

X = depth of thaw in time t.

Morgenstern & Nixon, (1971), reported that as a first approximation, a value of R greater than unity would predict the danger of pore water pressures being sustained at the thaw line, giving the possibility of instability. The one-dimensional consolidation of thawing soils is discussed in further detail in Nixon, (1973).

Nixon & Morgenstern, (1973a), extended the Morgenstern & Nixon, (1971), thaw-consolidation theory in order to consider a more general thaw rate, where X is not proportional to $\sqrt{t}$. The movement of the thaw front could then be expressed as:

$$X(t) = Bt^n$$

Equation 2.3 – Movement of the Thaw Front (Nixon & Morgenstern, 1973a)

B and n being constants specified for individual cases.

Nixon & Morgenstern, (1973a), found that the substitution of $\sqrt{t}$ for a more complex thaw depth-time function gave reasonable average pore pressure predictions, but did not predict the extremes that might be encountered.

Ballantyne & Harris, (1994), stated that the texture of a thawing soil, and in particular its clay content, controlled its geotechnical properties and also its response to thaw-induced high water contents. Sandy and silty soils have low plastic and liquid limits, and low plasticity. Such soils derive most of their strength from intergranular friction, and have little cohesion. Clay soils, with higher plastic and liquid limits, and much greater plasticity, have lower intergranular friction but are highly cohesive. Sandy/silty soils consequently

have much lower void ratios and so lower saturation moisture contents than clay soils. Therefore less water is required for the sandy/silty soils to reach saturation point. Due to the low plastic and liquid limits, the soils are sensitive to changes in moisture content, and will reach a flow condition if the moisture content is greater than the liquid limit. Clay soils, in response to the high pore water pressures induced by thaw consolidation, often fail along clearly-defined slip surfaces.

2.1.4 Processes of Periglacial Mass Wasting

Periglacial mass wasting can result from rapid mass movements or gradual downslope displacement (Ballantyne & Harris, 1994).

The gradual downslope displacement of material is termed solifluction and is due to repeated freezing and thawing of soil. Solifluction is generally taken to consist of two processes in combination, frost creep and gelifluction, as the two processes are often impossible to differentiate from field measurements (Ballantyne & Harris, 1994).

Both frost creep and gelifluction result from frost heaving in soil, which together with the thaw-consolidation process and gravity, enable this form of periglacial mass wasting to take place (Hutchinson, 1991).

Frost creep occurs during thawing of ground. The heave process pushes soil particles outwards normal to the surface while particle resettlement during thawing tends to the vertical. The interparticle attraction between soil grains prevents true vertical resettlement, but a net downslope movement known as *creep* is achieved, (see Figure 2.1). Frost creep is thought to dominate solifluction in drier areas where mass wasting is relatively slow (Ballantyne & Harris, 1994).

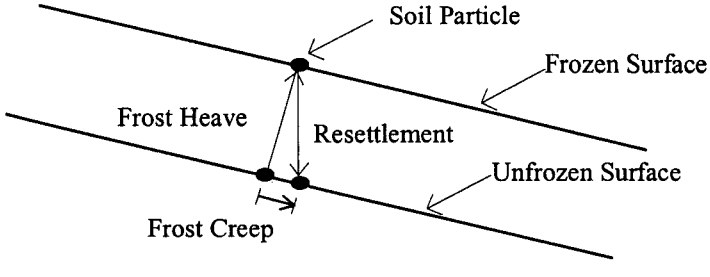

Figure 2.3 - Frost Creep (after Figure 7.2, Ballantyne & Harris, 1994)

Gelifluction occurs when soil loses strength during thaw consolidation. When moisture content exceeds the liquid limit the soil becomes fluidised and moves slowly downslope

(Ballantyne & Harris, 1994). Gelifluction therefore depends on moisture content, the granulometry and also the distribution of segregation ice.

Gallop, (1991), conducted research under Professor Charles Harris concerning laboratory simulated periglacial mass movements with respect to geological conditions in South West England. The origins of relic periglacial sediments were determined by examining the following critical geotechnical parameters: Atterberg limits, permeability, consolidation characteristics and shear strength. The experimental work consisted of developing and monitoring a model slope under freezing and thawing conditions, with 4 soil types, derived from granite, slate, mudstone and limestone. The experiments showed displacement of the granite and limestone soils to be mainly due to frost creep, but the displacement of the slate and mudstone soils, (which was greater), required additional thaw-induced gelifluction. These experiments demonstrated the relative influence of the two processes in solifluction, depending on the slope soil types. Ballantyne &| Harris, (1994), reviewed Gallop's findings and explained the differing mass wasting processes in terms of permeability. The granite and limestone soils were of high permeability, and contained little excess ice. Therefore, pore water pressures failed to develop as thawing progressed down through the soils. However, the mudstone and slate soils experienced extensive segregation ice formation throughout, and the melting of this excess ice meant the development of high pore water pressures. This resulted in a loss of frictional strength, and as water contents exceeded the liquid limit a viscous flow occurred. The pore water pressures subsequently dissipated gradually, leading to stabilisation.

Rapid mass movements are summarised by Ballantyne & Harris, (1994), as being either flow-dominated or slide-dominated.

Flow-dominated slides have been termed *skinflows* by McRoberts & Morgenstern, (1974), and described as involving the detachment of a thin layer of vegetation plus topsoil, followed by movement over a planar inclined surface. Ballantyne & Harris, (1994), also note the use of the terms *mudflow* and *earthflow* for this type of failure. According to Ballantyne & Harris, (1994), skinflows are caused by the moisture content being greater than the liquid limit during thaw consolidation, leading to a flow situation. They are common in cohesionless, frost susceptible silty soils with low liquid limits (Ballantyne & Harris, 1994).

Slide-dominated failures have been termed *active-layer detachment slides* by Lewkowicz, (1990), and are discussed by Harris & Lewkowicz, (1993). The alternative terms *mudslide* and *slab slide* are noted by Ballantyne & Harris, (1994). Failure occurs by sliding due to the soils being clay-rich, (i.e. cohesive), or because upwards freezing from the permafrost table has left the middle of the active layer desiccated and hardened (Ballantyne & Harris, 1994). The former case, active-layer detachment slides in clay-rich soils, is of particular interest to the author's research.

Two other mass wasting processes should be mentioned; *cambering* and *valley bulging,* although they can be considered as two aspects of the same phenomenon (Higginbottom & Fookes, 1971).

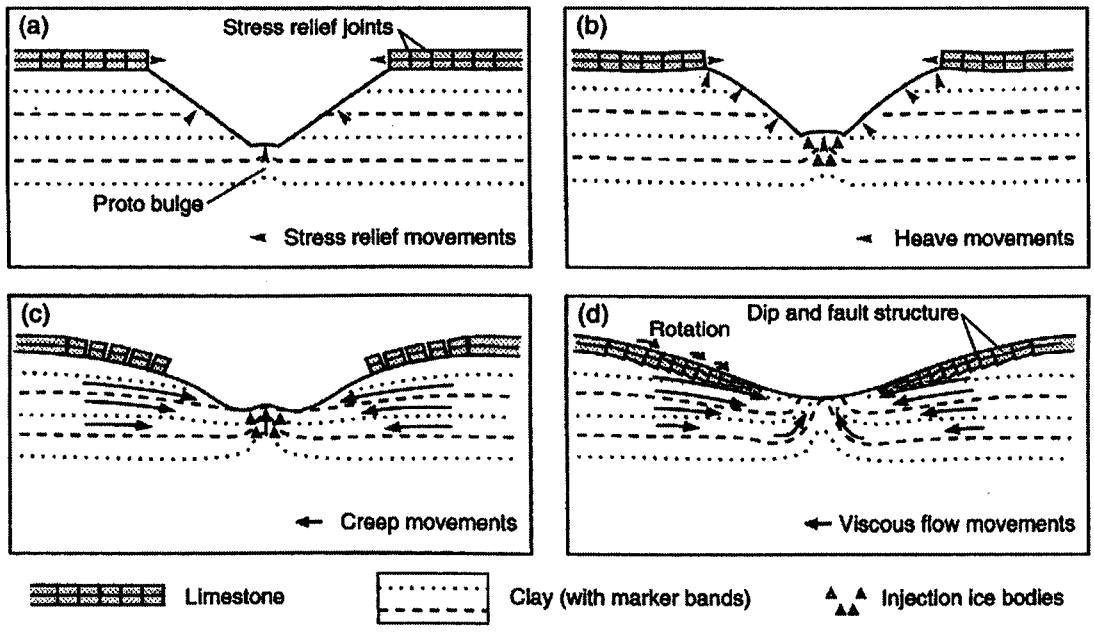

(a) Valley erosion creates a proto valley bulge and joints due to stress release.

(b) Frost heave increases the size of the bulge and the effects of stress relief in the caprocks.

(c) Erosion of the valley and creep of the ice-rich strata cause cambering and increase the size of the bulge.

(d) Thaw of the strata creates high pore water pressure and consequent viscous flow, enhancing the effects of cambering and valley bulging. Rotation of caprock blocks gives rise to dip-and-fault structures.

Figure 2.4 – Cambering and Valley Bulging (after Figure 7.31, Ballantyne & Harris, 1994, after Figure 2, Parks, 1991)

Ballantyne & Harris, (1994), defined cambering as the large-scale flexing and stretching of competent caprocks over the upper parts of valley-side slopes. This process occurs where valleys have been cut through a caprock into softer strata underneath, which then deforms under the weight of the caprock. This deformation causes the caprock to extend down the valley sides as a 'drape' (Ballantyne & Harris, 1994). The bending and extension of the

caprock leads to the development of deep fissures known as *gulls* (Higginbottom & Fookes, 1971; Ballantyne & Harris, 1994). These features run parallel to the valley line, forming separate coherent blocks of (Ballantyne & Harris, 1994), and may be infilled with debris (Higginbottom & Fookes, 1971). Valley bulging takes the form of anticlinal deformation of the argillaceous strata underlying the valley floor, having a fold axis approximately parallel to the valley axis (Ballantyne & Harris, 1994).

Parks, (1991), proposed a mechanism for cambering and valley bulging based on the premise that the processes occurred during a period of periglaciation, partly at the start of the cold period but mainly during the frozen and thawing states. The example used was of a valley with sides comprising a sandstone or limestone overlying Upper Lias Clay. Reviewing the findings of Vaughan, (1976), Parks, (1991), stated that the stress relief from the valley excavation would result in a small, proto valley bulge developing, and probably a basal shear plane some distance below the valley floor. During ground freezing, (from the surface downwards), the formation of segregation ice and subsequent frost heave increases the size of the bulge and may stress the valley sides, affecting the caprocks above. The research continued with an examination of the valley in its frozen state, when the processes of creep and erosion would be taking place. The creep of the ice-rich strata causes cambering. Erosion due to seasonal meltwater steepens the valley sides, (without causing failure), and increases the size of the bulge. At the onset of thaw, it was found that if the rate of thaw of the segregation ice was sufficiently rapid in soils of low permeability, very high pore water pressures could be generated. Consequent viscous flow enhances the effects of cambering and valley bulging, as well as allowing the cambered blocks to settle and rotate downslope.

Parks, (1991), also carried out experimental work to support the cambering/valley bulging mechanism. Speeton Clay specimens were triaxially loaded and subjected to cyclic freeze-thaw conditions. The specimens were overconsolidated, being subject to the equivalent of 20 m maximum overburden. Differential and all-round pressures were in the range 0–400 kPa. Considerable ice lens formation was observed. The moisture contents of all the specimens increased significantly as a result of testing, and the vertical heave generated exceeded that which would have been found from freezing the original specimen moisture. In all cases the specimens failed on thawing due to the decrease in shear strength caused by the increase in pore water pressure.

Hutchinson, (1991), also considered cambering and valley bulging, adding that permafrost thawing could have occurred from the base upwards as well as from the top downwards.

This may have resulted in sideways movement of thaw-softened clay towards the valley floor, increasing the amount of valley bulging.

2.1.5 Periglacial Slope Deposits in Lowland Britain

Harris, (1987), defined the term *head* as 'slope deposits accumulated through various periglacial mass movement processes'. Ballantyne & Harris, (1994), stated that the general effect of periglacial mass wasting in lowland Britain involved the downslope movement of material and accumulation of head on lower slopes and valley floors. Hutchinson, (1991), considering the engineering significance of periglacial slope deposits, identified 2 main types of head: *relic granular solifluction deposits* resulting from gelifluction and frost creep; *relic clayey solifluction deposits*, resulting from shallow periglacial landsliding above the former permafrost layer. This second type of head is of particular interest to the author's research.

Hutchinson, (1967), noted that many slopes developed in stiff clays had achieved their present form due to periglacial processes, and stated that such slopes have undergone little modification during the temperate Holocene. These slopes were described as being mantled by 2-3 m of head, (rock fragments in clay or silty clay matrix). Planar slip surfaces roughly parallel to the ground surface could be found within and underlying the head mantle. Periglacially weathered clay underlies the head, and may contain slip surfaces at its upper boundary. The weathered clay is often *brecciated* - consisting of small nodules of intact clay in a matrix of reworked clay - and softer than the lower, undisturbed clay.

Ballantyne & Harris, (1994), observed that there has been a consistent pattern of shallow translational landslides in lowland areas of Britain where slopes of modest gradient are mantled by clay-rich soils. Stability analyses have found slope failures to have required higher pore water pressures than those likely under temperate conditions, and it is widely believed that such pore water pressures were produced by thaw consolidation during periglaciation. Ballantyne & Harris, (1994), reported that these relic shallow clay slides resemble active-layer detachment slides found in arctic environments, implying that the relic slides indicate former permafrost in these areas.

2.1.6 Periglacial Slope Evolution in Lowland Britain

Hutchinson, (1967), while investigating free degradation of London clay cliffs, also considered inland London clay slopes. These were found to be more mature than the coastal cliffs and therefore more complex in terms of landslide behaviour. Most of the slopes examined were situated away from streams and rivers and were unlikely to have experienced significant post-glacial erosion. Hutchinson, (1967), therefore considered it probable that the slopes were mantled by solifluction deposits and hillwash. In support of this, augering revealed the slopes to be mantled to depths of at least 4 m by reworked London clay mixed with coarser material, (up to gravel size). The unstable inland slopes were split into 2 groups. The smaller group comprised slopes apparently showing late stage free degradation of slopes once steepened by marine or fluvial erosion. These were termed *fossil abandoned cliffs*, and exhibited successive rotational slips or well-developed undulations. However, the larger group of slopes had experienced more recent landsliding of the non-circular or slab types. The slides were found to occur in the steepest part of otherwise smooth and stable slopes, seemingly without external cause, although their shallow nature was thought to derive from the presence of the solifluction mantle. The shallow slab slides were found to occur on slopes of 8-10° inclination. Hutchinson, (1967), observed that surface features of landslide activity, such as undulations, could be obscured by ploughing.

Chandler, (1970a), carried out a survey of slopes in the Rutland valleys of Northamptonshire formed of Upper Lias Clay capped with the Inferior Oolite. The objective of the survey was to compare the pattern of degradation observed by Hutchinson, (1967), in London Clay with that observed for the quite different Upper Lias Clay. In addition, observations were to be made on the common situation of a rigid layer capping an incompetent clay stratum (Chandler, 1970a).

Chandler, (1970a), reported that cambering and valley bulging had taken place in the area, and that Pleistocene deposits were present. It seemed likely that much of the current topography had been subject to periglacial conditions during the Weichselian Glaciation. Many of the more mature slopes were found to be mantled by hillwash or solifluction material, comprising fragments of the Inferior Oolite and Upper Lias Clay.

A sequence of slope degradation was observed similar to that found for the coastal slopes of London Clay by Hutchinson, (1967). Where direct comparisons were made between the

two cases, slopes for a given type of slide were found to be slightly steeper in the Upper Lias Clay, in keeping with its lower plasticity. The capping effect of the Inferior Oolite was associated with relatively steep slopes in the Upper Lias Clay, causing shallow rotational slides which were rare for inland London Clay. Some slab or translational slides were observed, (although they were relatively uncommon). Chandler, (1970a), supported the suggestion of Hutchinson, (1967), that slides of this type were local re-activations of movement in the solifluction mantle. In addition, Chandler, (1970a), also reported the obscuring effect of farming activity on the landslide topography of the area.

2.2 Theory Related to Low-Angled Slope Failures

2.2.1 Residual Strength

In the 4th Rankine Lecture, Skempton, (1964), outlined the consideration of peak and residual shear strengths, together with their significance for the analysis of long term slope stability in clays.

Skempton, (1964), considered the shear behaviour of some over-consolidated clays, (mostly containing fissures and joints). In general, as the clay is strained, an increasing amount of resistance is offered by the soil, culminating in a *peak* strength. After this point, as displacement increases, resistance decreases in a process known as *strain softening*, eventually reaching a lower limit or *residual* strength.

Various clays from sites of slope failure were examined, (and re-analysed in the case of sites previously investigated). The residual shear strength parameters were determined using a reversible shear box since the ring shear test apparatus, (see Bishop *et al.*, 1971 for details), had not yet been completed. The angle of residual shearing resistance, ϕ_r', was found to decrease as the clay fraction increased.

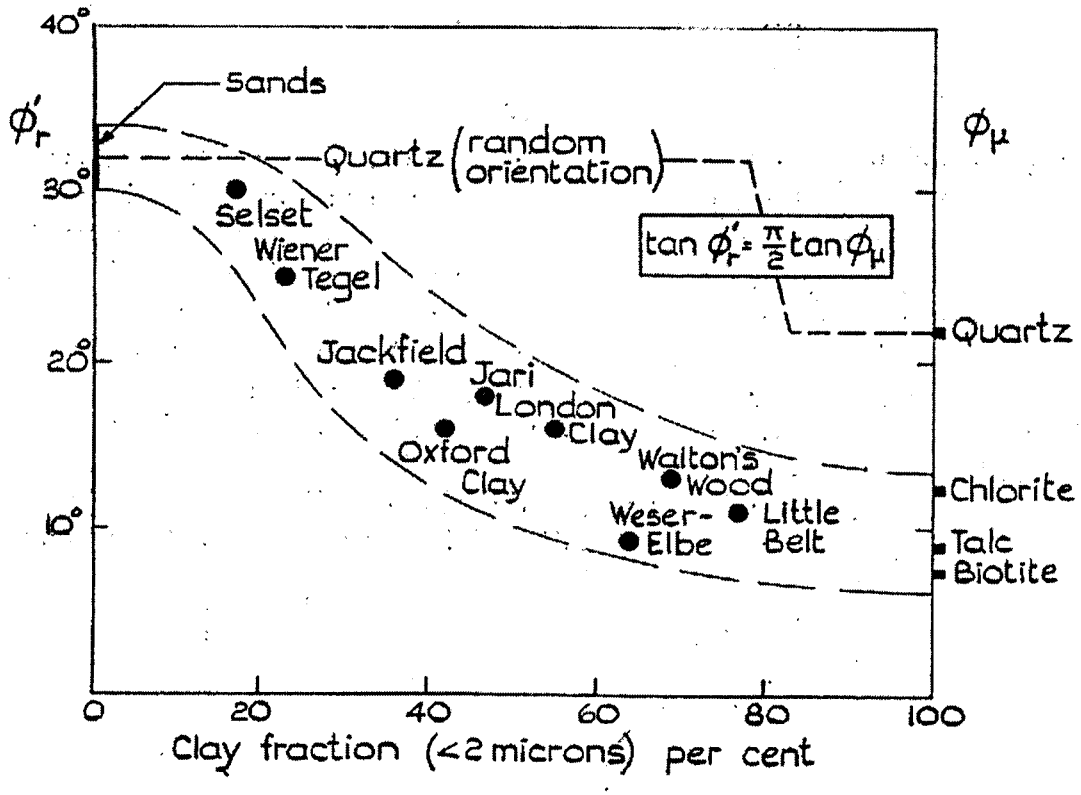

Figure 2.5 – Decrease in ϕ_r' with Increasing Clay Fraction (reproduced from Figure 7, Skempton, 1964)

Skempton, (1964), then explored the significance of whether peak or residual shear strengths are used in slope stability analysis. Clay taken from a landslide at Walton's Wood, Staffordshire, was found to have $\phi' = 21°$, $c' = 320$ lb/ft^2 and $\phi_r' = 13°$, $c_r' = 0$ assumed. Laboratory tests showed that the strength at the slip plane was comparable to the residual strength of the soil. Skempton, (1964), stated that the peak factor of safety as calculated on the slip surface was about three times that determined using ϕ_r'.

After outlining other examples of landslides, Skempton, (1964), stated that if a failure had occurred on a slope, any subsequent movements on the existing slip surface would be controlled by residual strength, irrespective of the clay type.

The Walton's Wood landslide was also considered by Skempton & Petley, (1967). Assuming a factor of safety of 1.0 at the time of the landslide, the average shear strength and effective normal pressure were estimated. These indicated strengths only a little higher than those corresponding to $\phi_r' = 13°$, $c_r' = 0$.

Skempton & Petley, (1967), summarised their study of landslide examples as follows:

- The strength along a principal slip surface is at or very close to its residual value.
- The residual strength may be much lower than the peak strength of the intact clay.
- After displacements of several centimetres in laboratory tests, the strength of the intact clay falls to about the residual value.
- The clay particles are strongly orientated along the slip surface, practically in the direction of movement.

Lupini *et al.*, (1981), presented a review of previous studies of residual strength and in particular correlations between ϕ_r' and index properties. The mechanisms causing shear were then considered and experimental work reported on. The experimental work consisted of testing artificially graded soils, with regard to the proportion of platy particles to rotound particles and the coefficient of interparticle friction of the platy particles. A residual friction coefficient, τ/σ'_n was defined in the presentation of the results. Three modes of residual shear failure were found to exist:

1. Turbulent shear mode in soils with a high proportion of rotound particles or with platy particles of high interparticle friction and no preferred platy particle orientation.
2. Sliding shear mode featuring low strength shear surfaces with strongly orientated low friction platy particles.
3. Transitional mode involving both turbulent and sliding shear modes.

Lupini *et al.*, (1981), reported that the type of shear mode correlated best with the granular void ratio, e_g, which is the ratio of the volume of platy particles plus voids to the volume of rotound particles. The shape of the clay mineral particles is therefore highly significant. The correlation outlined above was not effective for the sliding shear mode, and it was also considered that high friction platy particles, (if present), could behave as rotound particles. The paper closed by noting that correlations between residual strength and soil properties and gradings could not be generalised, although they might be useful in studying the residual strength of a particular variable soil deposit, so long as the correlation properly reflected changes in fundamental soil properties.

Hawkins & Privett, (1986), reviewed BS 5930, (1981), drawing attention to the simplified straight line envelope assumed for residual shear strength. Hawkins & Privett, (1986), rejected the use of a single angle of residual shear strength for a soil, taking it instead to be dependant on the effective applied pressure.

2.2.2 Semi-Infinite Slope Analysis

The problem of re-activation of relic slip surfaces can be considered in terms of semi-infinite slope analysis. This analysis method was outlined by Skempton & DeLory, (1957), for investigation of slope failures in London clay in several sites north of the River Thames. The slip surfaces considered were found in relatively gentle clay slopes at shallow depths. The movements generally took place as sheets of material sliding down hill on a slip surface parallel to the ground surface. The length of the slipping mass was usually great relative to the depth, allowing a semi-infinite slope analysis to be used.

This method is described below, with adaptations of the terms used by Skempton & DeLory, (1957), for the purposes of the author's research. Figure 2.2 shows a layer of material of depth z to a potential slip surface, at inclination β. the water table is at height h above the potential slip surface.

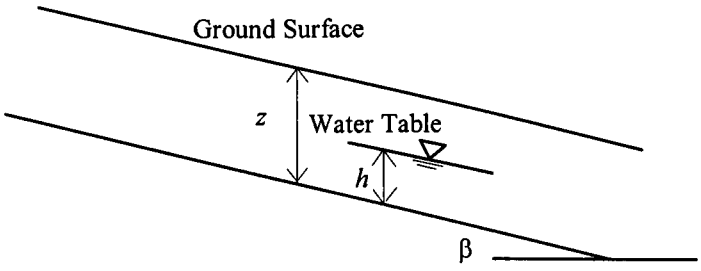

Figure 2.6 – Semi-infinite Slope Analysis

The factor of safety against sliding can be defined as

$$F_s = s/\tau$$

Equation 2.4 - Factor of Safety against Sliding in Basic Terms

s = shear resistance that can be mobilised by the soil.

τ = shear stress developed along a potential failure surface.

The shear stress, τ, is defined as:

$$\tau = \gamma z \sin\beta \cos\beta$$

Equation 2.5 – Shear Stress Developed Along a Potential Slip Surface

γ = saturated unit weight of the clay.

In order to define *s*, the mobilised shear resistance, σ', the effective stress is first defined:

$$\sigma' = \left(\gamma - \frac{h}{z}\gamma_w\right) z\cos^2\beta$$

Equation 2.6 – Effective Stress

γ_w = unit weight of water

The shear strength parameters c′ and ϕ' can be combined to give s.

$$s = c' + \left(\gamma - \frac{h}{z}\gamma_w\right) z\cos^2\beta \tan\phi'$$

Equation 2.7 – Mobilised Shear Resistance

$c' = 0$ is assumed for the failure condition, so, for $0 \le h \le z$,

$$F_s = \frac{\left(\gamma - \frac{h}{z}\gamma_w\right) z\cos^2\beta \tan\phi'}{\gamma z \sin\beta \cos\beta}$$

$$= \left(1 - \frac{\gamma_w h}{\gamma z}\right)\frac{\tan\phi'}{\tan\beta}$$

$$F_s = \left(1 - \frac{\gamma_w h}{\gamma z}\right)\frac{\tan\phi'}{\tan\beta}$$

Equation 2.8 – Factor of Safety against Sliding

At the point of failure, $F_s = 1.0$,

$$\tan\beta = \left(1 - \frac{\gamma_w h}{\gamma z}\right)\tan\phi'$$

Equation 2.9 – An Equation to find the Angle of Slope Failure, β, (Skempton & DeLory, 1957)

When the groundwater surface is at ground level (i.e. the full hydrostatic case) :

$h = z$, or $h/z = 1$, so:

$$\tan\beta = \left(1 - \frac{\gamma_w}{\gamma}\right)\tan\phi'$$

Equation 2.10 – An Equation to find β for the Full Hydrostatic Case (Skempton & DeLory, 1957)

When investigating the London clay slopes, Skempton & DeLory, (1957), found that for $h = z$, β was predicted to be 9.75°. This coincided well with the observations taken. All slopes with a slope angle less than 10° were found to be stable. All unstable slopes located had inclinations of 10-12°. No slopes were found with angles greater than 12°. Skempton & DeLory, (1957), noted that 10° appeared to be a critical value for the London clay. However, residual shear strength parameters as later defined by Skempton, (1964), were not considered.

In light of the introduction of residual shear strength, the factor of safety against sliding, (semi-infinite slope model), can be revised. The pore water pressure ratio is also identified below.

$c_r' = 0$ is assumed for residual conditions, so, for $0 \leq h \leq z$,

$$F_s = \left(1 - \frac{\gamma_w h}{\gamma z}\right)\frac{\tan\phi_r'}{\tan\beta}$$

$\gamma_w h/\gamma z = r_u$, the pore water pressure ratio, so

$$F_s = (1 - r_u)\frac{\tan\phi_r'}{\tan\beta}$$

Equation 2.11 – Factor of Safety against Sliding using Residual Strength Parameters

It can be seen that the larger the value of r_u, the smaller the value of F_s.

At the point of failure, $F_s = 1.0$,

$$\tan\beta = (1 - r_u)\tan\phi_r'$$

Equation 2.12 – A General Equation to Find β

When the groundwater surface is at ground level (i.e. the full hydrostatic case) :

$h = z$, $r_u = \gamma_w h/\gamma z = \gamma_w/\gamma$

Typically, $\gamma_w/\gamma \approx 0.5$, giving $r_u \approx 0.5$, so $\tan\beta \approx 0.5\tan\phi'_r$, and therefore:

$$\beta \approx \frac{\phi'_r}{2}$$

Equation 2.13 – A Simplified Equation to Find β for the Full Hydrostatic Case

The form of the equation above has also been presented by Weeks, (1969), who refers to the work carried out by Skempton & DeLory, (1957), Skempton, (1964) and Hutchinson, (1967) as support. However, there are many examples in the literature of shear surfaces being found on much shallower slopes than predicted using the above method, (see, for example, Skempton and Petley, 1967).

Hutchinson, (1974), proposed an approximate mechanism for the periglacial solifluction of clayey soils; where the rate of thaw is sufficiently rapid relative to the rate of consolidation of the soil, and where shear strength is sufficiently low, the active layer would tend to slide downslope in a translational mode. The conditions for this slide could be taken as undrained. The following variant of the semi-infinite slope model, considering the problem in total stress terms, was presented, (derived from an equation given by Skempton & Hutchinson, 1969):

$$z = \frac{2c_u}{\gamma} \text{cosec} 2\beta$$

Equation 2.14 – Conditions of Limiting Equilibrium for Solifluction (Skempton & Hutchinson, 1969)

c_u = undrained cohesive strength.

Hutchinson, (1974), observed that the validity of the approximate mechanism should be tested against field evidence from contemporary clayey solifluction sites. However, such sites are uncommon in present-day periglacial environments. Some preliminary analyses were made using data from relic periglacial sheets in South East England. The total strength approach was found to broadly account for the field data obtained, although it was tentatively concluded that the proposed mechanism did not operate on very flat slopes.

Hutchinson, (1974), therefore stated that in principle, periglacial mudsliding on low-angled slopes could also be explained using the effective stress approach.

McRoberts & Morgenstern, (1974), gave an expression for semi-infinite slope analysis using the thaw-consolidation ratio, *R*:

$$\beta = \tan^{-1}\left[\frac{\gamma'}{\gamma}\left(1-\frac{1}{1+\frac{1}{2R^2}}\right)\tan\phi'_r\right]$$

Equation 2.15 – Semi-infinite Slope Analysis Solution (McRoberts & Morgenstern, 1974)

$\gamma' = \gamma - \gamma_w$

McRoberts & Morgenstern, (1974), used the above expression to examine a soil with ϕ'_r assumed as 25°. The value of β, (required for $F_s = 1.0$), was plotted against water content of the soil for different values of R. For example, for the model soil at water content 40%, if $R = 0$, $\beta \approx 12°$, but if $R = 0.5$, $\beta \approx 8°$. It was determined that when R values were low in a thawing soil no excess pore water pressures were generated, while if R was high, effective stress levels approached zero. McRoberts & Morgenstern, (1974), therefore showed, (by means of their expression and also a graphical solution), that for a given moisture content the value of β, (required for $F_s = 1.0$), decreases as R increases.

2.3 Field Observations of Low-Angled Slope Failures

2.3.1 Sevenoaks – An Example of Re-activated Relic Slip Surfaces

Re-activation of relic clayey slip surfaces has serious civil engineering implications. Hutchinson, (1991), stated that such reactivation due to ill-advised earthworks was probably the most frequent and costly type of periglaciation-linked failure in Britain. Hutchinson, (1991), also stated that although the existence of clayey solifluction mantles was known, their engineering significance was not realised until the investigation of the failures at the Sevenoaks bypass, Kent, in 1965.

The new road, the A21, was designed to bypass the town of Sevenoaks. The road crossed the Hythe Beds escarpment. The beds are of thickness c. 45 m below the escarpment crest, consisting of sands and sandstone (Skempton & Weeks, 1976), and overlie Atherfield Clay and Weald Clay. These strata are all of the Lower Cretaceous age (Skempton & Petley, 1967). At the base of the escarpment a solifluction sheet extends for over 500 m onto gentle slopes of gradient 3-4° with solifluction lobes of lesser extent overlying. The lower solifluction sheet dates from the Weichselian glaciation, and the solifluction lobes are considered to date from Zone III of the Late-Glacial sequence (Skempton & Petley, 1967). Ingold, (1975), stated that a large proportion of pre-existing slip surfaces encountered in

highway construction were formed during the Pleistocene, and specifically during the Weichselian Glaciation.

The Hythe Beds were found to be cambered, and corresponding valley bulging was seen in the Weald Clay and Atherfield Clay. The solifluction sheets contained chert fragments up to 20 cm in size, brought down from the Hythe beds together with pieces of sandstone. These were set in a highly variable matrix containing silt, sand and clay (Skempton & Petley, 1967). When construction commenced, cuts and fills of only a few metres triggered retrogressive and progressive failures (Symons & Booth, 1971).

There was difficulty dealing with the lower solifluction sheet as it had no topographical expression (Skempton & Petley, 1967; Skempton & Weeks, 1976; Hutchinson, 1991). During the Sevenoaks investigation, (post-failures), shear surfaces in the solifluction sheets were found at depth 2-3 m by trial pitting (Hutchinson, 1991). One trial pit showed that the soliflucted lobe material had moved downhill, on a slope of about 7°, over reworked clay taken to be the Atherfield (Skempton & Petley, 1967). A fossil soil was found in the pit, between the 2 solifluction sheets, (immediately beneath the layer of reworked clay). Carbon dating showed the organic matter of the fossil soil to date back about 12,200 years BP (Skempton & Petley, 1967).

Site investigation is clearly important in cases like Sevenoaks, as inadequate studies may miss vital evidence of periglacial activity. For example, some site investigation specifications have boreholes only to a required depth, not to a specific geological surface (Higginbottom & Fookes, 1971). Greater use of trial pits and trenches is advocated by Higginbottom & Fookes, (1971), and Jones & Derbyshire, (1983).

At Sevenoaks the lower solifluction sheet was found to overlie weathered Weald Clay, with slopes of 3-4°, (Higginbottom & Fookes, 1971). The weathered clay was in a brecciated state. This effect is thought to be caused by the melting of ice lenses in the soil (Skempton & Weeks, 1976).

At one trial pit the slip surface was found to have a gradient of only 4°, assumed stable at present day conditions. Well-defined slip surfaces were found to depths of 3 m in the brecciated Weald Clay, indicating that mass wasting occurred along these surfaces by shear. This also indicates that under periglacial conditions the 'active layer' of the permafrost penetrated to 3m below ground level (Skempton & Weeks, 1976).

Weeks, (1969), used the semi-infinite slope model, (see Section 2.2.2), to demonstrate that the 7° slip surface under the solifluction lobes was in keeping with $\beta \approx 0.5\phi'_r$, as ϕ'_r was found to be about 7°. However, for the 4° slip surfaces found, an excess pore water pressure would be required. This excess value was estimated by Weeks, (1969), to be equivalent to a piezometric level $0.31z$ above the ground surface, where z is the depth to the slip surface. From Sevenoaks and other examples, Weeks, (1969), concluded that the maximum natural slope-angle for stiff fissured clays in areas of periglacial activity is controlled by the presence of pre-existing slip surfaces resulting from these periods. In addition, he concluded that slip surfaces could be found in slopes flatter than the predicted value of β, (full hydrostatic case assumed).

Skempton and Weeks, (1976), described the process of solifluction at Sevenoaks as clayey gravels moving downslope by shearing on a slip surface at or near the top of the Weald Clay. In current, temperate conditions this mechanism was not expected possible on slopes of less than 8° in gradient, compared with the slip surfaces found at inclinations of 3-4°. However, during periglacial activity seasonal thawing of the active layer above the permafrost would have provided high enough pore water pressures at the base of the layer to allow solifluction to take place, at slopes down to 2° and less. Skempton & Weeks, (1976), reviewed the semi-infinite slope model, (see Section 2.2.2), outlining the full hydrostatic case of $r_u = 0.5$, and also the geostatic case. The latter case is the extreme upper limit of $r_u = 1.0$, corresponding to a piezometric level of z above the ground surface, where z is the depth below the ground surface to the slip surface. Although impossible under ordinary conditions, this indicated that such excess pore water pressures could theoretically be generated if frozen soil thawed rapidly enough to transfer all the overburden to the pore water before any dissipation took place. This line of reasoning was continued by considering that at Sevenoaks slip surfaces were found mainly within the brecciated Weald Clay, which has a low consolidation rate, which could prevent substantial dissipation of the pore water pressures from the slip surfaces.

Skempton & Weeks, (1976), then applied the thaw-consolidation ratio analysis (Morgenstern & Nixon, 1971; see also Sections 2.1.3, 2.2.2), to the results of laboratory tests on the brecciated Weald Clay and overlying chert gravel matrix. Almost identical values of c_v were found for each, giving an accepted value of about 2.5 m^2/year. A depth of thaw of 2 m was assumed, this being the typical depth of slip surfaces beneath the lower

solifluction sheet. The time for thaw was taken as 3 months. Having made these assumptions, the thaw consolidation ratio, *R*, was found as 1.3. Skempton & Weeks, (1976), then determined the corresponding r_u value to be 0.89. In order to allow for changes in c_v and the approximation of time of thaw, t, R was varied by ± 25%. This in turn gave upper and lower values of r_u as 0.93 and 0.83 respectively.

The assembled ring shear test data is given in Table 2.1 below:

Table 2.1 – Data from Ring Shear Tests of Brecciated Weald Clay (Skempton & Weeks, 1976)

σ′ (kPa)	c′ (kPa)	ϕ'_r (°)
20-50	1	14
5-20	0.2	16
< 5	0	18

The Terzaghi effective stress equation, ($\sigma' = \sigma - u$), and semi-infinite slope model, (with c′ not always equal to 0), were used to find β for various values of r_u. The thickness of the soil layer considered was z = 2 m, and γ = 20 kN/m^3 was assumed. The findings are given below in Table 2.2.

Table 2.2 – Calculated Values of β for Brecciated Weald Clay (Skempton & Weeks, 1976)

r_u	σ′ (kPa)	c′ (kPa)	ϕ'_r (°)	β(°)
0.50	≥ 20	1	14	~8
0.93	~ 3	0	18	1.3
		0.2	16	1.4
0.89	4.5	0	18	2.0
		0.2	16	2.0
0.83	~ 7	0.2	16	3.0

Some uncertainty was expressed over the shear strength parameters determined at effective stresses less than 5 kN/m^2. Therefore, where applicable the analyses were carried out using the parameters for both effective stresses above and below 5 kN/m^2.

Skempton & Weeks, (1976), estimated the water contents of the clays at the time of movement. For a 2° slope in the Weald Clay, the water content was determined to be about 55 %. The water content of the chert gravel clay matrix was estimated to be about 50 %. These were noted to be much higher than the present values, (27 % and 28 % respectively), as they referred to the state of the clays immediately after thawing, when the effective stresses were very small. Ballantyne & Harris, (1994), observed that as the liquid limit for

Weald Clay ranges from 60-80 % it is likely that failure by sliding during active layer thaw commenced at water contents below the liquid limit, i.e. before the soil could fail through fluid flow.

In the Transport Research Laboratory report on the original investigation, Symons & Booth, (1971), reported that the most economic solution to the Sevenoaks stability problem was determined to be the re-siting of the affected sections of the bypass. An alternative might have been to excavate the affected sites and construct retaining walls, but this solution could well have been more costly and time-consuming.

2.3.2 Further Examination of Re-activated Relic Slip Surfaces

Chandler, (1970b), contributed a technical note in response to Weeks, (1969), detailing two examples of solifluction in low-angled slopes. In both cases, slip surfaces had been found on slopes where the angle of slope was less than the angle of ultimate stability against sliding.

The note described two sites, Wellingborough and Isham, both in Northamptonshire. The sites were situated on the edge of cambered slopes of Northampton Sand overlying Upper Lias Clay. Wellingborough was the site of a temporary section in a cutting slope, and Isham the site of a road improvement scheme. At both sites, slip surfaces were found at about an inch below the junction between the Northampton Sand and the Lias Clay. The slip surfaces were observed to be undulatory but roughly parallel to the ground surface. No morphological expression of recent movement was detected.

Using the semi-infinite analysis technique outlined by Skempton & DeLory, (1957), (see Section 2.2.2), Chandler, (1970b), obtained the following results:

Table 2.3 – Comparison of Predicted and Actual β (after Chandler, 1970b)

Site:	β predicted (°)	β actual (°)
Wellingborough	12	6.75
Isham	8.75	4

Chandler, (1970b), noted that as the slopes were clearly stable under current conditions, it was probable that the slip surfaces were relic surfaces developed during prior periglaciation. Two possible explanations were offered. Firstly, the angle of slope failure, β, could have been lower if the soil above the slip surface were very wet, as its bulk density

would then be reduced. Secondly, the development of artesian pore water pressures at the slip surface. According to Chandler, (1970b), the latter explanation would in fact have a far greater reductive effect on β.

Biczysko, (1976), described the geology and geological processes responsible for the formation for the present Jurassic outcrop environment in the East Midlands, and especially in Northamptonshire. Five case histories were presented in order to show some of the difficulties of working in Jurassic soils. The processes of cambering, valley bulging and re-activation of relic clayey slip surfaces were discussed. The planning of site investigations was also considered. Biczysko, (1976), stated that careful examination was required at the time of the route investigation and soil survey stages in order to minimise geotechnical problems during construction. In particular, Biczysko, (1976), identified a need for flexibility when carrying out an investigation. Experienced engineering supervision of the investigation was also highlighted as a requirement, together with regional knowledge of the soils and geological structures. Biczysko, (1976), closed by stating the need to continue the investigation past the initial soil survey through to the completion of construction and perhaps beyond; as well as identifying any soils problems, the findings could be appraised and referred to in future works.

Biczysko & Starzewski, (1977a), discussed slope stability problems experienced on the A45 Daventry Bypass. During construction, earthworks failure occurred at the Fox Hill location, causing a mass movement, (covering approximately 2000m^2 in area), into the road cutting.

The cutting through Fox Hill is within Upper Lias Clay capped by Northampton Sand Ironstone. Biczysko & Starzewski, (1977a), described the Upper Lias Clay as a stiff, blue-grey fissured silty clay, marking the closing stages of the Lower Jurassic. The Northampton Sand Ironstone was described as being rusty brown in colour and varying in composition between silty clay and clayey sand. It dated from the start of the Middle Jurassic. Cambering had taken place and solifluction sheets formed. An additional complication was that Daventry exists in a gap in the Jurassic escarpment generated by meltwater from the glacial Lake Harrison. Due to weathering processes, little topographical evidence of periglacial activity remained.

Biczysko & Starzewski, (1977a), gave slopes for Fox Hill of 20° for the Northampton Sand Ironstone, and 9° for the Upper Lias Clay solifluction sheet, reducing to 4° as the hillside

approaches the valley floor. The road cutting was contained within the solifluction sheet for a depth of 2.5 m, and then within the Upper Lias Clay to a total depth of 9 m.

The failure was reported to have taken place after the cutting had been excavated to a depth of 3 m only. The slip surface therefore lay approximately 0.5 m into the Upper Lias Clay. A slab of soil slipped as a unit and moved about 2 m into the cutting. The slip surface was found to be undulating, but roughly parallel to the ground surface. Subsequent laboratory analysis found additional slip surfaces. After slope monitoring was fully established, excavation recommenced down to the full 9 m depth below ground surface. A further set of slip surfaces was found at approximately 5 m depth, between the Lias Clay and a green silty clay. This green silty clay was considered to be glacial in origin, possibly 'trapped' by a glacial landslip in the Lias Clay.

Biczysko & Starzewski, (1977a), concluded that excavations in gentle hillsides, (< 10°), of Jurassic origin were liable to induce slope failures, even if there had been no apparent previous movement. Investigation of relic slip surfaces in trial pits was found to be difficult and often inconclusive, and detection of the slip surfaces required skill on the part of the investigator. This suggested that the residual strength parameters may vary with locality, citing a value of $\phi'_r = 15°$ from Chandler & Skempton, (1974), in comparison to their own value of $\phi'_r = 13°$.

Biczysko & Starzewski, (1977a), noted the cost of the investigation to be considerable, but also commented on the possible disastrous effects that could have occurred, e.g. if existing structures had been in the path of the landslip. The eventual solution was to alter the road alignment and acquire the land beyond the roadworks, accepting slip debris as an on-going maintenance operation.

Chandler, (1977), responded to Biczysko & Starzewski, (1977a), with two observations.

Firstly, the conclusion that excavations in gentle hillsides, (< 10°), of Jurassic origin was accepted by Chandler, but considered too restrictive, and hence misleading. Chandler, (1977), cited the works of Skempton & DeLory, (1957), showing slopes in London Clay as low as 10° might have been subjected to landsliding.; Hutchinson, (1967), referring to a modification of the Skempton & DeLory, (1957), conclusion in that evidence of landsliding in London Clay slopes as flat as 8°; Chandler, (1970a), referring to similar conclusions applied to the Upper Lias Clay in the Midlands, (slopes at least as gentle as 9°). Chandler,

(1977), also drew attention to the obscuring of landslide topography by agricultural work, as observed by Chandler, (1970a). The work of Weeks, (1969), was then discussed, showing that landslides could occur on inclinations as low as 3° due to high pore water pressures developed during periglacial periods. Chandler, (1977), concluded his first observation by broadening Biczysko & Starzewski's conclusion to read 'excavations and embankments on any clay slope are liable to induce slope failures'.

Chandler's second observation on the Biczysko & Starzewski, (1977a), paper concerned the residual shear strength value chosen for the Upper Lias Clay. Chandler, (1977), considered that the pore water pressure data obtained was less than satisfactory due to the monitoring methods employed, (only 2 piezometers in the slip mass), and also the lowering effect that would have been caused by stress relief during the excavation. Chandler, (1977), therefore considered the average effective stresses on the slip surface to be in doubt, and hence the value of $\phi'_r = 13°$. Chandler, (1977), continued by stating the value of ϕ'_r to be stress-dependant, and the failure envelope curved. Relatively high values of ϕ'_r would apply at low effective stresses, but would fall as the effective stress increased. Chandler, (1977), estimated an average effective stress of 45 kN/m^2 and determined that the value of $\phi'_r = 13°$ gained agreed with his own Lias clay landslides investigations. Chandler, (1977), considered the Biczysko & Starzewski conclusion of ϕ'_r varying with locality to probably be incorrect. The value of $\phi'_r = 15°$ quoted from Chandler & Skempton, (1974), had actually been a typical value related to relatively low stresses.

Biczysko & Starzewski, (1977b), responded to the observations made by Chandler, (1977), expressing interest in the additional gentle slope failures quoted. However, in laboratory tests on the Daventry Bypass samples, ϕ'_r was not found to decrease at higher effective stresses. Some residual strength tests carried out at Aston University indicated difficulty in obtaining consistent results at normal stresses lower than 30kN/m^2.

Biczysko, (1981), returned to the Daventry Bypass case, reviewing the findings of Biczysko & Starzewski, (1977a), and extending the study to consider a second site of failure at Newnham Hill. The geometry of the Fox Hill landslip (Biczysko & Starzewski, 1977a), was applied to the design of stabilisation works at Newnham Hill ~1 km away, as a bridge for a side road was to be installed at this location. The geology and slope angles were in the same category as Fox Hill (Biczysko, 1981).

The 10 m cutting at Newnham Hill remained stable for 2 years until a large 'lozenge-shaped slab' slide took place. The slide extended 80 m upslope from the crest of the cutting, with the soil moving downslope as an intact mass. A well-developed, polished and striated slip surface was found about 50 m away from the slipped mass on an area of non-moved ground. The slip surface was at a depth of 4.5 m on the interface of the Upper Lias Clay over glacial clay. The principal plane at Newnham Hill was found to have a more undulatory shape than Fox Hill, and was located at depths varying between 4.3 and 5.5 m below ground surface (Biczysko, 1981). The slip surface at Newnham was at a comparable depth to those found at Fox Hill, but the shallower, solifluction slip experienced at Fox Hill was absent from Newnham Hill (Biczysko, 1981). According to Biczysko, (1981), the reasons for this were not clear.

Biczysko, (1981), concluded that hillsides that had the potential for re-activation of relic landslip presented a difficult problem, where avoidance and relocation is preferred to interference. He also concluded that the detection of relic shear surfaces required care and skill, and an open mind concerning the geometry of the relic landslip. Finally, Biczysko, (1981), concluded that if landslips were reactivated during construction, the cost of remedial measures would probably be high.

Penn, Royce & Evans, (1983), related another example of clayey head deposits underlain by slip surfaces in their paper concerning the periglacial modification of the Lincoln Scarp. The crest of the scarp comprises Northampton Ironstone and Lincolnshire Limestone of the Middle Jurassic, with the Lincolnshire Limestone resting directly upon the Northampton Ironstone. Underneath the crest lies 38 m of overconsolidated Upper Lias Clay, a thin limestone band and Middle Lias Clays. The scarp rises from gently from the valley floor to a steepening slope of maximum angle 16° just below the caprock. The Upper Lias scarp face is covered by mudslide and solifluction deposits.

Detailed topographical profiles of the scarp face showed small scars and toes from recent failure on the upper slopes, and the lower slopes having a smooth convex profile of an apparently stable landslide toe. The mean natural slope angle for the upper section of the slope was 14.7°, and for the lower slopes 8°.

The profiles indicated shallow rotational slides with mudflow toes on the upper slopes. The data obtained was judged to be compatible with the interpretation of the slips as taking

place within the soliflucted material and being at least in part the re-activation of existing planar slip surfaces.

Penn, Royce & Evans, (1983), concluded that periglacial weathering and mass wasting had had a major effect on the slope evolution of the Lincoln Scarp. It was determined that the strata on the crest had been weakened by weathering and gulls formation, as well as modification by cambering. It was also concluded that the scarp morphology may have been determined by early solifluction mudslides creating deposits on the lower slopes. A second phase of mudslide activity was considered to have overlapped earlier deposits and was still susceptible to re-activation. The paper closed by stating that complex earlier failures might still be concealed by a mantle of colluvial material and not have been detected during site investigation.

2.3.3 Vestspitsbergen – An Example of an Active Slide

Chandler, (1972), stated that the shear surfaces found in low-angle clay slopes in Britain are generally assumed to be relic forms developed during former, periglacial conditions. Such conditions, last occurring during the late-Glacial, might have allowed excess, artesian pore water pressures to be developed. These artesian pore water pressures would be required to explain low-gradient landsliding. He presented slope stability data from sites experiencing a current periglacial climate, in order to consider how low-gradient shear surfaces could have been developed under similar conditions in Britain.

The basis of the research was the investigation of mudslides at Vestspitsbergen, Norway, during the 1971 'Cambridge-Norwich' expedition. The bedrock material at the sites investigated was Tertiary grey micaceous siltstone, interbedded with conglomerate. A number of small scale, very silty mudslides were observed on apparently low-gradient slopes. At one site, mudslides were observed to be particularly active, on slopes of gradient 8.5-12°, considered to be very low for a silt soil. The site was investigated using peg lines to track surface movement, and piezometers to monitor pore water pressure. The piezometers recorded consistent artesian pore water pressures, and piezometers inserted at different depths indicated an upward flow of water. Soil temperatures were also measured, and trial pits dug for examination purposes.

Shear box tests were carried out on samples taken from the site and also on a remoulded slurry of the silt soil, with a water content of 50 %, approaching twice the soil's liquid limit. The slurry was prepared in order to obtain the residual strength of the soil. A curved failure envelope was obtained, and values of ϕ'_r found for use in subsequent slope stability analysis. For example, the value of ϕ'_r corresponding to very low effective stresses of less than 4 kN/m^2, applicable to mudslides less than 0.4 m thick, was found to be 36° or greater. It was assumed that there was no cohesion intercept.

According to Chandler, the looseness of the soil fabric arising from the melting ground ice made it necessary to carry out shear box tests on samples formed as loosely as possible. He considered that the maximum strength of the slurried samples corresponded to the critical state condition and that the continued shearing would show little or no drop in strength. This suggests that consolidation could be anticipated as a result of shearing rather than dilation.

As part of the investigation, a semi-infinite slope analysis, (Skempton & DeLory, 1957; see Section 2.2.2 and Equation 2.11), was undertaken. In order to account for lateral stresses on the sides of mudslide channels, extra terms were incorporated into a second equation for factor of safety against sliding, F_s. The channel sides were taken as vertical, and the width expressed as *b*. K_L, the coefficient of lateral pressure on the channel sides, was also added as shown below:

$$F_s = \frac{\tan\phi'_r\left[b\left(\cos^2\beta - r_u\right) + K_L z\left(1 - r_u\right)\right]}{b\sin\beta\cos\beta}$$

Equation 2.16 – Factor of Safety against Sliding used for Vestspitsbergen (Chandler, 1972)

Assuming a width:depth ratio of 4:1, then for movement to be initiated, $F_s = 1$, and pore water pressures must be as great as, or greater than the values shown below.

Table 2.4 – Pore Water Pressures Required for Initiation of Mudslides (after Table 1, Chandler, 1972)

	Minimum r_u required for initiation of mudslide	
β(°)	Equation 2.11	Equation 2.16
6	0.84	0.86
8.5	0.78	0.80
12	0.68	0.72

Therefore, it could be noted that pore water pressures must have been significantly greater than the full hydrostatic case $r_u = 0.5$. With a value of $r_u = 0.5$, failure slopes of at least 18° and 20° respectively were determined for the two semi-infinite slope models used. It was observed in the field that mudslides did not occur at points where artesian pressures were recorded, and further examination showed the values of r_u to be greater than the full hydrostatic case, but not as great as the values required for initiation of movement. In one case the artesian value of r_u was greater than that required by the first semi-infinite slope model, but not as great as the value required by the second, width:depth modified model.

Chandler, (1972), concluded that the observation that artesian pore water pressures were necessary to generate movement on low-angle slopes was strongly supported by values of r_u recorded at the same location. Calculations of the stability of the slope at the points of artesian pressure show that the slope is just stable, as found by observation in the field. The origin of the artesian pressures is believed to be the contrasting permeability of the soil layers parallel to the ground surface. Underlying permafrost prevents downwards movement of water, allowing it to move upwards or parallel to the ground surface only. The blanketing effect of lower permeability soil layers then causes the generation of artesian pore water pressures. The development of artesian pore water pressures was considered to be localised, except if resulting form freezing of the ground surface, whereupon the effect would be more widespread.

The paper proceeded to discuss the implications of the Vestspitsbergen observations on the origin of shear surfaces in lowland Britain. First, criticisms of the analogue of present day arctic climates to periglacial processes in Britain were outlined. The climatic differences due to high latitude of Vestspitsbergen mean that a very different thermal regime is experienced than would have been in Britain in periglacial periods. Also, the soil types affected are different, thought to be due to the relative lack of suitable clays in the Vestspitsbergen area. Chandler, (1972), advises caution in interpreting Pleistocene deposits in Britain with respect to current Arctic conditions.

With this in mind, the types of failure observed in low-gradient clayey slopes in Britain were then discussed. In the case of cohesive sheet movements, for slopes greater than 7-8° non-artesian pore water pressures were considered to be required for failure. These would be obtained by having a high groundwater table, (the maximum pore water pressure being the full hydrostatic case when the water table reaches the ground surface). Sheet

movements in cohesive soil slopes gentler than this were considered to require artesian pore water pressures, but a mechanism for pore water pressure generation could not be offered.

Chandler, (1972), closed by offering the explanation of 'blanketing' of soils overlying permafrost at a relatively shallow depth, and the presence of a frozen surface or varying permeability as an explanation for at least some of the relic mudslides found on low-gradient slopes in Britain.

2.4 Freeze-Thaw Experiments on Small Specimens

2.4.1 The Development of the Permode Apparatus

The first Permode was devised by Professor N.R. Morgenstern at the University of Alberta, Edmonton, Canada. This first design is described in Smith, (1972), and Morgenstern and Smith, (1972). The Permode was originally used to examine thaw-consolidation of remoulded clays from permafrost regions. The results gained were compared to the solution to the one-dimensional consolidation theory put forward by Morgenstern and Nixon, (1971).

The Morgenstern and Smith permode consisted of a cylindrical Lucite ring inside a stainless steel outer ring. The Lucite cylinder had an internal diameter of 63.5 mm (2.5 inches), and an inside height of 88.9 mm (3.5 inches). The inner walls were lined with Teflon and fitted with a rubber membrane. The loading piston fitted inside the membrane and liner as loosely as possible without allowing soil to extrude. Use of the apparatus as a conventional oedometer (Smith, 1972), found that the frictionless Teflon allowed smooth travel of the load piston without tilting or other distortion.

Temperatures could be measured at the top, base and two intermediate points along the tested specimens. Vertical displacement was measured by dial gauge or LVDT. Drainage was one-way through the top of the apparatus, allowing consolidation to take place. The base of the apparatus was seated on a refrigerated heat sink. Temperatures at each end of the specimen were controlled using thermoelectric elements. At the base, the element was in contact with the heat sink, and at the top, a heat sink was provided during freezing by packing dry ice against the load cap.

Pore water pressure was measured at the base of the specimen only, through a transducer and porous stone assembly. This measuring system was filled with a 50% antifreeze solution. An arrangement of valves permitted the re-zeroing of the pressure transducer during tests without affecting pressure within the permode itself. During freezing phases the pressure transducer was isolated from the permode.

Each soil specimen was prepared as a de-aired slurry and vacuum-stored until required. With the permode set up, the slurry was deposited into the cell under a head of water. Freezing of the specimen was attained by packing the load cap with dry ice, and removing it for the thaw phase.

The tests carried out by Smith, (1972), essentially examined consolidation behaviour over consecutive freeze and thaw periods, (approximately 4 hours for each complete cycle).

Nixon & Morgenstern, (1973b), used a permode apparatus to investigate residual stresses by thawing remoulded soils in undrained conditions. This permode measured pore water pressure at both the top and the base, through a valve system leading to the same transducer. During the test, the pressure at the top was monitored continuously. The cylinder used was split into two halves, so that the permode could be assembled around a pre-frozen specimen of remoulded soil. Temperature measurement was possible, but not considered necessary for the tests undertaken, which were to consider the final, residual stress and post-thaw consolidation behaviour. The basic test procedure comprised cutting a frozen core to size, placing it inside the permode and thawing from the top down, by circulation of warm water around the load cap. After thawing, the specimen could then be tested for permeability, compressibility and consolidation coefficients in standard fashion. At the end of the test, the specimen was removed, and water content determined.

Roggensack, (1977), conducted research at the University of Alberta concerning the geotechnical properties of fine-grained permafrost soils. A permode-type apparatus, termed a *frost cell*, was used to examine residual stresses and thaw-consolidation behaviour. In this case, the thermoelectric elements used by Smith, (1972), were replaced by a fluid circulation system. The fluid used is quoted as 'automotive antifreeze in 50% solution'. The change in temperature control method was possible as a more relaxed method of thaw was allowed.

Pore water pressures were recorded at the base and top of the specimen, using a de-aired system filled with 50% antifreeze as before. Roggensack was concerned that leakage of

antifreeze was causing erosion of the soil surfaces, and used a lower concentration of ethylene glycol as a reagent in contact with the soil. Another precaution utilised was to wait until just before the test to attach the pressure transducer. This was intended to avoid exposing the transducer to large temperature changes. The transducer was zeroed to atmospheric pressure before the start of each test.

2.4.2 Freeze-Thaw Tests Concerning Moisture Migration and Ice Lens Formation

McRoberts & Morgenstern, (1975), stated that when a freezing front advances through a saturated soil water can be attracted to or expelled away from the freezing front depending on the soil type, stress level and rate of freezing. McRoberts & Morgenstern, (1975), considered experimental evidence which showed that in an open system, (i.e. drainage allowed), coarse-grained soils expel water under most conditions while fine-grained soils only expel water at higher overburden pressures.

Arvidson & Morgenstern, (1977), investigated the effects of overburden on the freezing behaviour of saturated soils in an open system. Arvidson & Morgenstern, (1977), established a value of pressure termed the *shut-off pressure*. At applied pressures less than this value water migrated towards the freezing front and formed segregation ice and thus frost heave. Water was also drawn into the specimen. At the shut-off pressure, no flow occurred towards the freezing front. When the applied pressure was greater than the shut-off pressure water was expelled from the freezing front, and out of the specimen. As the volume of in situ water was now decreased, only a relatively small amount of heave was observed. The shut-off pressure, P_o, was thus defined as the overburden pressure at which no flow of water into or out of the frozen soil occurred during an open system test.

Specimens were tested by being placed as a slurry in the permode and subjected to a backpressure to achieve 100 % saturation. A constant backpressure was maintained during the freezing stage. Before freezing, consolidation took place. Once this stage was completed, freezing was initiated from the top down. The freezing stage took between 3-5 hours. A set of tests were carried out at various pressures in order to form a relationship between the net change in pore water volume and the applied pressure. This procedure was repeated for changes in the other parameters, soil type and freezing temperature.

Arvidson & Morgenstern, (1977), reported the results of tests on different soils: a granular soil, Ottawa sand; fine-grained Devon silt, (Liquid Limit 30.2 %, Plasticity Index 7.7 %); modified Devon silt, (Liquid Limit 36 %, Plasticity Index 15.1 %). Each of the tests produced only one P_o value. Approximate values found were zero for the Ottawa sand, 69 kN/m^2 for the Devon silt, and 215 kN/m^2 for the modified Devon silt. The results also showed P_o to depend on stress history and freezing temperature, but Arvidson & Morgenstern, (1977), stated that further investigation was required in this area.

Mageau & Morgenstern, (1979), prepared specimens of Devon silt, (Liquid Limit 41 %, Plasticity Index 20 %), by consolidation and then immersion in liquid nitrogen. This was done in an attempt to obtain a homogeneous sample. The frozen sample was trimmed to size and placed in a frost cell, modified from that used by Roggensack, (1977), in order to study frost heave in completely frozen soils. Both open and closed system tests were carried out. The frost cell allowed water intake through the porous base plate in open system tests, but in closed tests the plate was replaced with an impervious copper disc. Temperature in the specimen was controlled by circulation of antifreeze-water solution as in the Roggensack, (1977), tests. The temperature gradient was set up as 0.0°C at the base and –4.0°C at the top of the specimen, and kept constant throughout the test. In open system tests water intake started immediately after the temperature gradient was set up and continued at a decreasing rate throughout the test, which ranged from 5-22 days length. In two open system tests overburden pressures were applied, of 50 kPa and 75 kPa. In the closed system tests the frozen specimen was placed in the cell and the temperature gradient applied.

It was subsequently found that for closed system tests, moisture near the bottom of the soil was found to migrate towards the upper, colder portion of the soil as a result of the temperature gradient induced. Moisture migration was found to be negligible at -2.0°C. In one open system test a 1.0 cm thick ice lens was found to form near the bottom of the specimen after 4.3 days. A sharp increase in water content was observed above this lens. The amount of increase dropped off with distance above the lens. Moisture migration again became negligible at a soil temperature of around -2.0°C. further open system tests were carried out with a pre-made ice lens at the base of the specimen. These test showed that, while some moisture migration did occur above the pre-made ice lens, the increase was very small compared with that seen in the tests without pre-made ice lenses. In addition, a new ice lens formed near the bottom of the sample, with a corresponding increase in

moisture in the thin soil layer below the pre-made lens. The presence of ice lenses was shown to greatly reduce the amount of moisture migration in the soil.

Mageau & Morgenstern, (1979), stated that substantial amounts of water could be taken into frozen soils in open system tests. If ice lenses were present, the increase in water content was found to be greater on the warm side than the cold side of the lens. The rate of flow was determined to be governed by the apparent permeability of the frozen soil and the suction force from the frozen fringe. Permeabilty and suction were considered as functions of soil temperature. For the clayey silt tested, moisture migration was negligible at temperatures around -2.0°C. Mageau & Morgenstern, (1979), continued by stating that at a certain temperature, the apparent permeability decreases to a limiting value at which an ice lens forms. The paper concluded by observing that the process outlined appeared to represent an important mechanism in the formation of ice lenses during freezing of a saturated soil. Also, apart from self-weight, the frozen soil above the most recent ice lens had little effect on the heave rate of the specimen. Instead, this was dependent on the frozen fringe of soil between the most recent ice lens and the freezing front.

2.4.3 Freeze-Thaw Tests Concerned with Permeability

The permeability of soils subjected to freezing and thawing has been a subject of interest to many researchers. The apparatus used has sometimes developed along similar lines to the permode. In Section 2.1.4 the work of Parks, (1991), was reviewed, which included experiments carried out using a triaxial cell apparatus and cycles of freeze-thaw. Other researchers have also adopted the triaxial form of test apparatus for cyclic freeze-thaw tests.

Chamberlain & Gow, (1979), of the United States Army Cold Regions Research and Engineering Laboratory, (CRREL), describe a thaw consolidation cell used to examine the effect of freezing and thawing on the permeability and structure of fine-grained soils. Fine-grained soils with varied plasticity indexes were formed into slurries with water contents of twice the appropriate liquid limit, and then degassed before testing. The slurry was then poured into the thaw consolidation cell. A drainage line ran from the base of the cell to a volume change burette and pore pressure transducer, while a line from the piston was connected to a constant head device. Specimens were frozen from the base upwards with free access to water at the top. After freezing was completed, the sample thawed in an uncontrolled manner to approximately 22°C, with free access to water at both ends. On

completion of the thaw-consolidation stage, falling head permeability tests were undertaken. This process was repeated until little or no change in permeability or void ratio occurred. After this the specimen was frozen in order to examine thin sections. Further information on the test apparatus is noted to be given by Chamberlain & Blouin, (1977).

Chamberlain & Gow, (1979), found that freeze-thaw cycles caused structural changes in consolidated clay slurries and therefore large increases in permeability. The greatest increase was observed in the soil with the largest plasticity index, and in general, the increase was smaller at higher applied stresses.

Graham & Au, (1985), investigated weathering processes on the medium to highly plastic Lake Agassiz clay from Winnipeg, Canada. Block samples were obtained and carefully trimmed to 76 mm diameter to be tested in triaxial cells. Some of the samples were subjected to freeze-thaw cycles before being placed in the triaxial cell. The samples were enclosed in membranes with no access to water allowed, and subjected to all-round freezing. Graham & Au, (1985), found that the tests showed freeze-thaw cycling to produce higher pore water pressures at failure, lower consolidation stiffnesses, higher relative stiffnesses and lower strengths compared with values obtained for samples tested 'undisturbed'. The freeze-thaw cycles were also found to produce a strongly defined fissure structure in the clay.

Wong & Haug, (1991), investigated the permeability of soil liner and cover materials, namely clay, till and sand-bentonite mixtures. Test specimens were prepared by dry mixing, moisture conditioning and compaction. The specimens were then trimmed to size and placed in a triaxial permeameter and initial permeability established. Low confining stresses and hydraulic gradients were applied. Changes in volume were also noted at this stage in the test. After the initial permeability was established, the specimen was frozen with no access to water. The freezing of the specimen was achieved by lowering a hood over the triaxial cell. The test specimens were then subjected to all-round freezing, with no drainage allowed. After freezing, the specimens were permitted to thaw, and then another permeability test performed. This process continued until the change in permeability between freeze-thaw cycles became insignificant. The results obtained from the tests showed that the permeabilities of both the clay and till specimens increased due to freeze-thaw cycles, but that the sand-bentonite specimens showed no such increase.

Ono & Mitachi, (1997), introduced a computer-controlled triaxial freeze-thaw-shear apparatus. Ono & Mitachi, (1997), stated the need for laboratory tests to be simulate the in-situ condition as well as possible in order to obtain engineering design parameters. Details of a newly-developed triaxial cell and control system were then presented. Brine circulation baths control the temperature of the top and base of the specimen independently. During tests the specimen is frozen from the top downwards, with the base temperature kept constant. Load is applied to the specimen through an air cylinder, which is kept in adjustment by a computer program. Confining cell pressure is also controlled by computer. Various instrumentation, (e.g. pressure, volume change, displacement), is monitored by the computer system. Some examples of tests and results were also presented, finding that the undrained shear strength of frozen-thawed clay specimens was about 20 % greater than that of unfrozen specimens, but that little difference was seen in terms of effective stress parameters.

Othman *et al.*, (1994), reviewed methods of testing compacted clay soils, with regard to evaluating changes in permeability, (here termed *hydraulic conductivity*), caused by freeze-thaw. As part of this review, methods of freeze-thaw within a permeameter apparatus were considered.

Othman *et al.*, (1994), described the apparatus used by Chamberlain & Gow, (1979), terming it a consolidometer. Further to the specification given in Chamberlain & Gow, (1979), detail is given on the control of ambient temperature around the test cell b eing achieved by circulating ~1°C ethylene glycol solution through a freezing jacket around the cell. Top and base boundary temperatures are read using precision thermistors at the contact points between the porous plates and the specimen. A computer system monitors temperatures and adjusts the thermoelectric devices supplying the freezing as necessary.

The paper went on to describe a flexible wall permeameter, an adapted triaxial apparatus. This apparatus is widely used for permeability testing, and is commercially available with standard procedures developed for its use. Freezing of the soil is achieved by filling the cell with a 50 % solution of ethylene glycol. First, pressure is applied and the specimen allowed to consolidate. After consolidation is complete, the specimen is placed in a cold environment. The specimen freezes, but the ethylene glycol does not, so the total stress on

the specimen does not alter. Thawing is achieved by removal to a warm environment. After a specified number of freeze-thaw cycles a permeability test is carried out.

Advantages and disadvantages of the two methods are given in Table 2.5. Othman *et al.*, (1994), also considered the different test conditions possible, and summarised principal findings from various research studies, including Bowders & McClelland, (1994); Wong & Haug, (1991). It was shown that freeze-thaw cycles may increase permeability by up to three orders of magnitude. During freeze-thaw larger pores and crack networks appeared in the soil, thus increasing its permeability. The increase in permeability was inversely proportional to the initial magnitude of the permeability, i.e. if the initial Permeabilty was low, the subsequent increase was greater. Studies also showed that the permeability increased as the rate of freezing and number of freeze-thaw cycles increased, and as the overburden pressure decreased. Other factors such as dimensionality of freezing and availability of external water supply did not appear to have a significant effect.

Table 2.5 – A Comparison of Freeze-Thaw Permeameter Testing Methods (after Table 2, Othman et al., 1994)

Apparatus	Advantages	Disadvantages
CRREL consolidometer	• minimal specimen disturbance • simulates overburden pressure • closed/open system of freezing • Precise control of temperature gradient • 1-D freeze-thaw	• possible side-wall leakage at low overburden pressure due to rigid walls • expensive • complicated
Flexible wall permeameter	• minimal specimen disturbance • simulates overburden pressure • no side-wall leakage • inexpensive • commercially available	• difficult to control temperature gradient • 3-D freeze-thaw • closed system of freezing

According the Othman *et al.*, (1994), changes in permeability for a variety of soils were similar to each other. Bowders & McClelland, (1994), obtained results indicating that the magnitude of the change in permeability increased with plasticity, (as did Chamberlain & Gow, 1979). However, Bowders & McClelland, (1994), suggested that the magnitude of the increase was in fact a function of the volume of water available during freezing.

2.5 Freeze-Thaw Experiments on Model Slopes

A great deal of research in this area has been carried out at the University of Cardiff, Wales, and CNRS, Caen, France, as described by Harris *et al.*, (1995); Harris & Davies, (1996); Harris, (1996); Harris *et al.*, (1997); Harris & Davies, (1998).

Harris *et al.*, (1995), described a 12° slope constructed in a 5m square chamber. Freezing and thawing took place from the top downwards, with an open hydraulic system. Two parallel slopes were formed, one of a sandy silt, (Vire), the other a gravelly silty sand, (Feuguerolles), from Normandy, France. The soils were wetted slowly by introducing water through a base sand drainage layer. Freezing was imposed by dropping the air temperature to -10°C and maintaining this level until the soils were frozen to base depth. Thawing was allowed by raising the temperature to +5°C in winter and +15°C in summer. Freeze-Thaw cycles were of length 30-60 days, with approximately equal freezing and thawing times. The slope was subjected to 7 freeze-thaw cycles.

The objective of the model slope simulation was to investigate soil movement in relation to freeze-thaw cycles, considering the effects of thermal regime and ice segregation on pore water pressure and total stress.

Instrumentation included thermistors to track temperature; Druck mini-transducers to measure the pore water pressure response; LVDTs mounted on special frames to track downslope and vertical displacement, reading off footplates embedded in the soil to 20mm. A column of ceramic tiles was placed in each soil to enable tracking of downslope displacement above the LVDT footplate level. All instrumentation was scanned by a PC datalogger at half-hourly intervals. Moisture contents were sampled during the thaw phase of Cycle 4, and a shear vane used to find *in situ* undrained shear strengths.

The Vire soil was the more frost susceptible of the two, and accordingly experienced greater frost heave. The amount of heave is related to ice segregation and hence the excess ice content, which was greater in the Vire soil than in the coarser Feuguerolles soil. Due to this, it was found that the progress of both the freezing and thawing fronts was slower in the Vire soil, as more ice required to be changed into water, leading to a longer 'zero curtain' period of latent heat flux.

The zero curtain is defined by Harris *et al.*, (1995) as the period when rapid phase change and latent heat flux takes place. It is further refined by Harris & Davies, (1996), as 'at or

immediately below 0°C, marking the period of latent heat flow during phase change,'. This effect was seen in both the freezing and thawing stages, but most clearly in the latter. Considering the zero curtain during the thaw phase only, latent heat flux is the process by which ice changes to water. An example is provided by Benson, (1991), where a 1 kg block of ice at 1 atm is quoted as requiring 80 kcal of heat to convert all the ice into water. This adsorbed heat does not manifest as an increase in temperature, which remains at 0°C until all the ice is melted, but is 'hidden', i.e. latent.

Surface downslope movements were also found to be greater in the Vire soil. Solifluction was found to occur in both soils during the thaw period.

Pore water pressures dropped to negative values during the thaw zero curtain period. Towards the end of this period, pore water pressures were found to rise rapidly. This effect was also discussed in Harris & Davies, (1996), Harris *et al.*, (1997), and Harris & Davies, (1998).

According to Harris *et al.*, (1995), The positive pore water pressures immediately after thaw indicated fully saturated conditions. The pressures then fell to below hydrostatic conditions and upward hydraulic gradients were established. After the thaw stages the soils, in particular the Vire soil, were found to be very soft consistency near the slope surface, but increasing in strength with depth.

Moisture contents determined during thaw were found to be greater than the liquid limit for all but one of the Vire samples, but only in one case for the Feuguerolles samples. When the moisture content exceeded the liquid limit, (i.e. liquidity index > 1), then viscous flow is likely to have occurred. Moisture contents remained high for several days after the end of thawing, but longer for the Vire than for the Fueguerolles soil.

The results gained from the simulation were analysed with respect to slope stability. Harris *et al.*, (1995), considered thaw consolidation theory, (Morgenstern & Nixon, 1971), suggesting that excess pore water pressures could be induced in ice-rich soils, e.g. Vire, leading to loss of frictional strength and failure of relatively low-angle slopes. A total and effective stress analysis were carried out for both soils. However, both analyses give safe conditions in the most part. A factor of safety below unity was found in one case for the Vire soil, but no evidence of a slip surface was found.

It was proposed that the slope movements observed did not result from slip surfaces caused by excess pore water pressures. A gelifluction-type movement was put forward instead, with the soils having properties in between those of a viscous fluid and a plastic creeping solid. This thaw-strain behaviour was not predicted using conventional slope stability analysis. Harris *et al.*, (1995), suggested that thawing soil probably displayed both viscous properties, (such as those found in the simulation), and frictional properties, (as would be found in slope stability analysis). The relative importance of the two sets of properties would change through time, and with drainage.

Harris *et al.*, (1997), stated that the profiles of soil movement gained from the simulation resembled those measured in field studies of periglacial activity in mountainous regions. The timescale of monthly freeze-thaw cycles for the simulation were considered to be equivalent to annual cycles in the field.

The link between post-thaw moisture contents and shear strain behaviour was explained further. The coarser, sandy Fueguerolles had lower frost susceptibility and higher permeability than the finer, silt-rich Vire. This meant that the Fueguerolles experienced less frost heave, lower moisture contents and faster post-thaw drainage than the Vire. In keeping with the fact that soil viscosity has been shown to fall as moisture contents rise, the amount of shear strain was found to be somewhat greater for the Vire than for the Fueguerolles. Harris *et al.*, (1997), went on to identify the derivation of viscosity/moisture content data as the next stage in the research. A predictive understanding of shear strain behaviour under different soil thermal and moisture conditions could be developed.

Harris *et al.*, (1997), closed by considering the equivalence of full-scale slope models to field situations. Current field equivalents were identified as being areas subject to deep seasonal frost penetration, with surface-downwards freezing employed. Typical locations quoted were the Alps, the Scandinavian mountains and the Rocky Mountains of North America. Two-sided freezing was also considered. This process can take place where cold permafrost is present, one example being given as the Mackenzie Delta of Canada. The distribution of soil ice on commencement of the thaw phase would be different from one-sided freezing, although the processes responsible for thaw-induced soil strain would be likely to occur in any case of ice-rich soil thawing. Two-sided freezing of model slopes was another area identified for further research.

Harris & Davies, (1998), presented further results for the Vire soil, with reference to the pore water pressures recorded during freezing and thawing. The pore water pressure transducers were considered to be acting intermittently for the Fueguerolles, and so the results were not considered. The data was presented for 150 and 250 mm depths for selected cycles. Temperature and pore water pressure were plotted against the common time axis. Pore water pressure against corresponding temperature was also plotted.

The zero curtain effect was examined once more, during both freezing and thawing. During freezing of the slope, pressures gradually dropped to negative values of the region –5 to –15 kPa. Towards the end of the freezing zero curtain period, pressures rose rapidly to 15-40 kPa, with pressures being higher at lower depths. These pressures were maintained until soil thawing began. Warming was found to progress through the soil ahead of the thaw front leading to a rapid fall in pressure. Pressures became substantially negative at the start of the thawing zero curtain, becoming positive by the end of this period.

Harris & Davies, (1998), argued that the quick transition from negative to positive pore water pressures during freezing was due to the pressure transducer becoming sealed within the frozen slope, which became an effectively closed hydraulic system. As the transducer became isolated from pore water films it became influenced instead by positive ice pressures developed during frost heave. In the thaw stage the soil warming caused a progressive thickening of unfrozen water films and a reduction in ice pressures. At the start of the thawing zero curtain the pressures drop sharply to negative values as unfrozen water was subject to suction in the still partially-frozen soil. Towards the end of the thawing zero curtain period ice lenses melted, causing the unfrozen water films to thicken and soil water tension to fall. Pore water pressure rose to positive values once again. By the end of the zero curtain period hydraulic continuity was re-established with the pressure transducer.

The process was also considered in terms of ice segregation. Harris & Davies, (1998), outlined the generally accepted view that ice segregation occurs at some point behind the freezing front at a temperature lower than 0°C. The 'frozen fringe' lies between the level of ice segregation and the 0°C isotherm, containing both ice and unfrozen, mobile water.

Harris & Davies, (1998), cited Williams and Smith, (1989), who describe the processes above in detail, finding ice segregation commencing at temperatures of typically –0.1°C

to –0.2°C. Williams and Smith, (1989), also discuss phase transition between ice and water as considered using the property of Gibbs free energy. It is explained that two phases co-exist, e.g. at freezing point of water, when the free energies of the phases are equal. Furthermore, the two phases cannot coexist indefinitely. Instead, the substance with lower free energy, i.e. ice, increases in quantity as the substance with higher free energy, i.e. water, converts to ice. Therefore, if pure water was subject to a progressive 0°C isotherm, all the water would be converted to ice. However, when considering soils, the water contains impurities from the soil itself. The resultant solution has a lower free energy than pure water, and so ice to be formed from this solution also requires a lower free energy. This results in *freezing point depression*, where at some temperature below 0°C the free energy of ice is lower than that of the water in solution, so that ice forms from the solution. It is therefore due to this freezing point depression that water migrates towards the freezing fringe. However, as the temperature of the frozen fringe falls, permeability decreases towards the 'cold' side of the frozen fringe/unfrozen soil boundary, as the ratio of ice to unfrozen soil increases, (as stated also in Harris & Davies, 1998).

Williams & Smith, (1989), discussed further the effect of soil type and other variables on permeability, citing Burt & Williams, (1976), who showed that permeability, (or hydraulic conductivity - being the term used), decreased with temperature, as well as being related to soil type. Figure 2.7 below shows the results of Burt & Williams', (1976), permeameter tests. It can be seen that the silts maintain the highest permeability with drop in temperature, followed by the Leda Clay, and then the fine sand. This correlates with frost heave behaviour as described in Section 2.1.2.

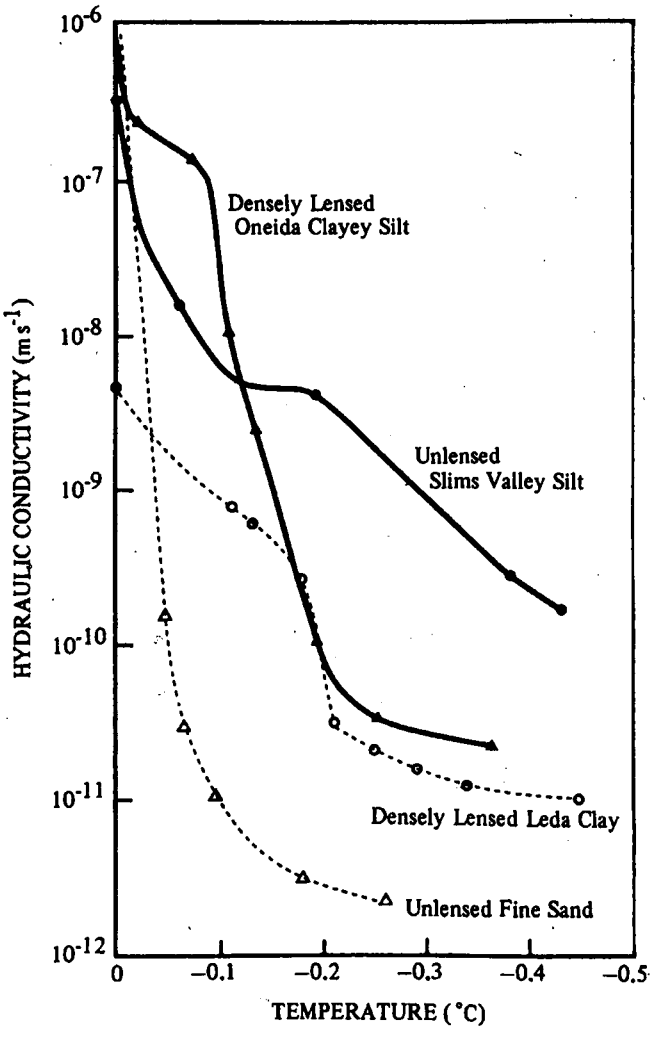

Figure 2.7 - Hydraulic Conductivity of Various Frozen Soils, after Burt & Williams, (1976), from Williams & Smith, (1989)

In the experiments undertaken by Harris & Davies, (1998), negative pore water pressures recorded at the transducers marked the arrival of the frozen fringe. The change to positive values occurred when the transducers became isolated in the frozen soil behind the fringe, away from the mobile unfrozen water. At this stage the transducers were subjected to ice heave pressures. During thaw, the transducers came back into hydraulic continuity with the soil water, recording suction within the partially-frozen soil, due to the reduction in volume as ice melts. As ice pressures fell, water pressures rose. Pore water pressures above the hydrostatic condition were then created as overburden stress was transferred from the ice/soil structure to the soil water. It was at this point that the slow, viscous downslope flow was noted in the slope simulation.

Harris & Davies, (1998), concluded that the pressures recorded correctly modelled pore water suction in the partially frozen fringe and heaving pressures in the frozen soil.

2.6 Freeze-Thaw Experiments using Centrifuge Technology

Harris, (1996), reviewed physical modelling techniques in general and discussed the emergence of centrifuge technology. In the area of model slope simulation, full-size models have been employed to date. However, difficulties arise in terms of size of model required. If a full-size model is not practicable for reasons of space, then a scaled model could be constructed instead. The scaled model must be *similar* to the actual situation, known as the 'prototype'. That is to say, each significant variable in the model must be related proportionally to the same variable in the prototype.

The rotating action of a centrifuge allows a controlled, increased gravitational field to be set up. Harris, (1996), gives the following example: For a gravitational field N =50 times 'normal' for the prototype, 1 m at model scale = 50 m at prototype scale. Therefore, a 50 m x 25 m x 5 m slope section could be modelled as a 1 m x 0.5 m x 0.1 m section. Mass density would be scaled at 1/1, force at $1/N^2$ and seepage rates at $1/N^2$. Time for force similarity is scaled at $1/N$ and time for seepage force similarity at $1/N^2$. This means that the stresses experienced in the model would be equivalent to those experienced in the prototype. The time scaling factors allow tests to take place at an accelerated rate, thus adding a further benefit to centrifuge modelling. The modelling of thaw consolidation processes in particular is also attractive, as both heat transfer and seepage rates can be modelled in the centrifuge. The scaling factor for conductive and convective heat transfer has been found to be $1/N^2$, as for seepage rates.

Harris closed by highlighting the continuing need for field monitoring. This has the twofold purpose of giving validation for laboratory data, and providing information on the variability of geomorphological processes.

Harris *et al.*, (2000), presented results of centrifuge modelling of thaw-related mass movements on frozen slopes due to global climate change.

The objectives of the research were to investigate the transition from slow annual gelifluction to rapid, thaw-induced mudflow, and also to assess the effectiveness of the modelling technique. Slope models were created for centrifuge modelling at 1/10 scale, and subjected to 10 gravities during the test. 3 gradients, 12°, 18° and 24° were tested successively, with all other variables kept constant. Monitoring of mass movement rates and changes in pore water pressure took place continuously throughout the test.

The test slopes were created within a steel strongbox of dimensions 750 mm x 550 mm x 500 mm, with transparent perspex sides. The basic planar test slope was formed from a 70 mm thick layer of fine sandy silt overlying a base sand layer. During the preparatory stage of the tests water was supplied to the slope via this base layer, (during the centrifuge test drainage ports were opened). Following saturation from the base upwards, the slope was consolidated for 24 hours under a pressure of 3.8 kPa. This pressure was equivalent to an overlying self-weight of soil of 20 mm depth at model scale, and therefore 200 mm in the prototype. A confining pressure of 3.8 kPa was maintained throughout the test.

Instrumentation consisted of two strings of sensors running through the centre line of the model. Each string comprised 5 thermocouples and 3 Druck mini pore water pressure transducers. Surface displacement was tracked by special markers, and slope movement could be measured in comparison to plastic columns placed down the slope profile.

The strongbox was insulated, allowing freezing to take place from the top downwards. A hollow metal plate was placed in contact with the soil surface and cold compressed air circulated within.

The thaw stage took place within the centrifuge under an acceleration of 10 gravities. The sensors continued to take measurements. Mini video cameras at the top and side of the strongbox were used to follow the movement of surface markers and thaw consolidation to an accuracy of ± 1 mm.

During the tests on the, 12° and 18° slopes gelifluction only was observed, although the 18° slope came close to the transition point to mudflow. Displacement patterns observed in the 12° slope were found to be of the type observed in the field and in full-scale slope simulations, as presented in Harris *et al.*, (1996). The pore water pressure response was also found to replicate what had been experienced in full-scale tests, as presented in Harris & Davies, (1998).

Two tests were carried out on 24° slopes, which did experience rapid mudflow. The duplication of the test enabled monitoring of the development of the mudflow.

Harris *et al.*, (2000), found the centrifuge modelling technique to be effective, with the potential for controlled, repeatable experiments.

Chapter 3 - Test Methodology

3.1 Introduction

3.1.1 The Apparatus and Tests Required

Previous research into freezing and thawing of soils can be split into two broad approaches:

1. The Engineer's approach: Permafrost Oedometer experiments, as reviewed in Chapter 2, Section 2.4.1.

2. The Earth Scientist's approach: Physical modelling of periglacial solifluction processes, as reviewed in Chapter 2, Section 2.5/6

The author's research is unusual in that it combines the two traditions. The first approach has mainly been the concern of the permafrost engineering community, while in the second approach physical modelling has often been approached from an earth science viewpoint.

3.1.2 Research at Warwick

The design of the Warwick test apparatus was a highly iterative process, dependant on both source information and empirical testing, (i.e. commissioning). Access to the information detailed in Chapter 2, Section 2.4.1 was not available until after commencement of manufacture and experimental usage. For example, the necessity for an internal rubber membrane was not realised at the beginning of the author's research. This alteration was made to the apparatus at a later stage, as described in Section 3.2.5. Other improvements came in the light of a visit to the University of Alberta undertaken in 1998.

The experimental programme embarked upon at the University of Warwick was original and is complementary to the Cardiff or the Alberta research programmes, useful elements from each have been adopted in its assembly. Therefore, where differences have arisen in the design of apparatus or test programme, they have not necessarily caused problems.

Considering the relevance of whole slope models to the author's permode research, the results gained for periglacial soils are certainly of interest. The cycles adopted by the author, (24 hours), were substantially shorter than those used in the slope models, (typically 30-60 days). The Druck transducers were judged to be over-sensitive for the author's research and difficult to implement. Harris and Davies, (1998), had felt concern that the antifreeze may have affected behaviour of the soil at the transducer tips. The antifreeze was therefore replaced with silicon oil, but no change was noticed in soil behaviour, so it was considered that the antifreeze was not causing inaccurate representation.

The investigation of antifreeze versus silicon oil by Harris and Davies, (1998), supports the author's visual inspection of tested specimens, which did not show end deterioration. It is possible that the ethylene glycol-based antifreeze adopted at Warwick was less harmful than that used by Roggensack, (1977), who also had concern over antifreeze intrusion.

The major difference in approach from the University of Alberta research is the fact that consolidation behaviour has not been investigated as part of the author's research programme. Pore water pressures developed as a result of repeated freeze-thaw cycles were the main concern, and their effects on the stability of low angle slopes. The test specimens were consolidated, but outside of the permode.

The test programme at Warwick required that soil samples be obtained from sites affected by periglaciation, and most usefully, solifluction. These samples first required description, and then remoulding for index testing. Each sample then required consolidation to produce near-saturated conditions, and then freezing ready for testing.

The permode testing itself was undrained, being concerned primarily with pore water pressure response. The basic plan was to produce specimens of at least three different soil types and test under a range of applied stresses, at various moisture contents providing comparable consistency between each soil type. For example, a target moisture content could be half-way between the plastic and liquid limits for each soil type.

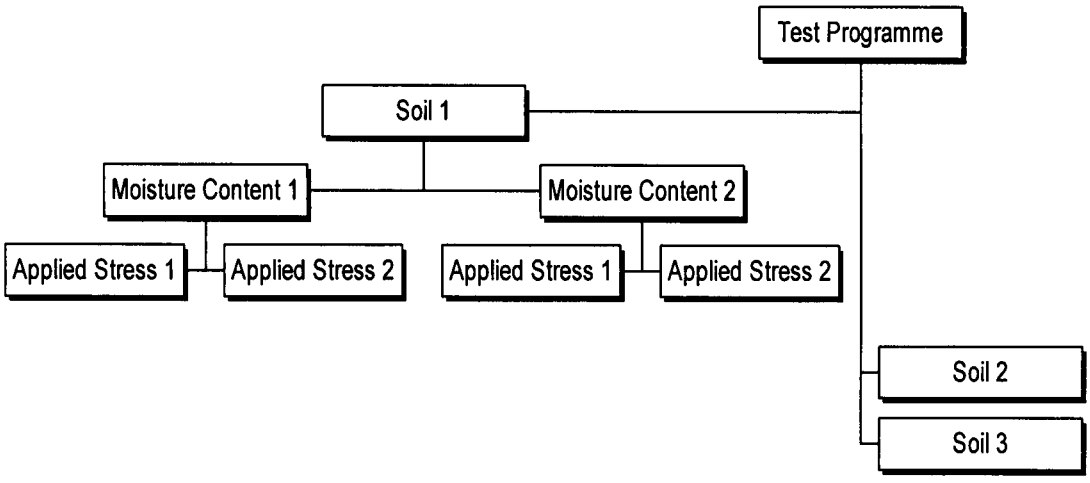

Figure 3.1 – Basic Test Programme

This programme would then allow comparison of pore water pressure response on several different levels, both within each soil type, and between the different soil types.

3.2 Development of Apparatus

3.2.1 The Apparatus Set-Up

The permode and associated apparatus are used to monitor the pore water pressure response and volume change of a soil to induced cycles of freeze-thaw. The apparatus comprises the permode, cooling system, instrumentation and datalogging system as shown in Figure 3.2 below.

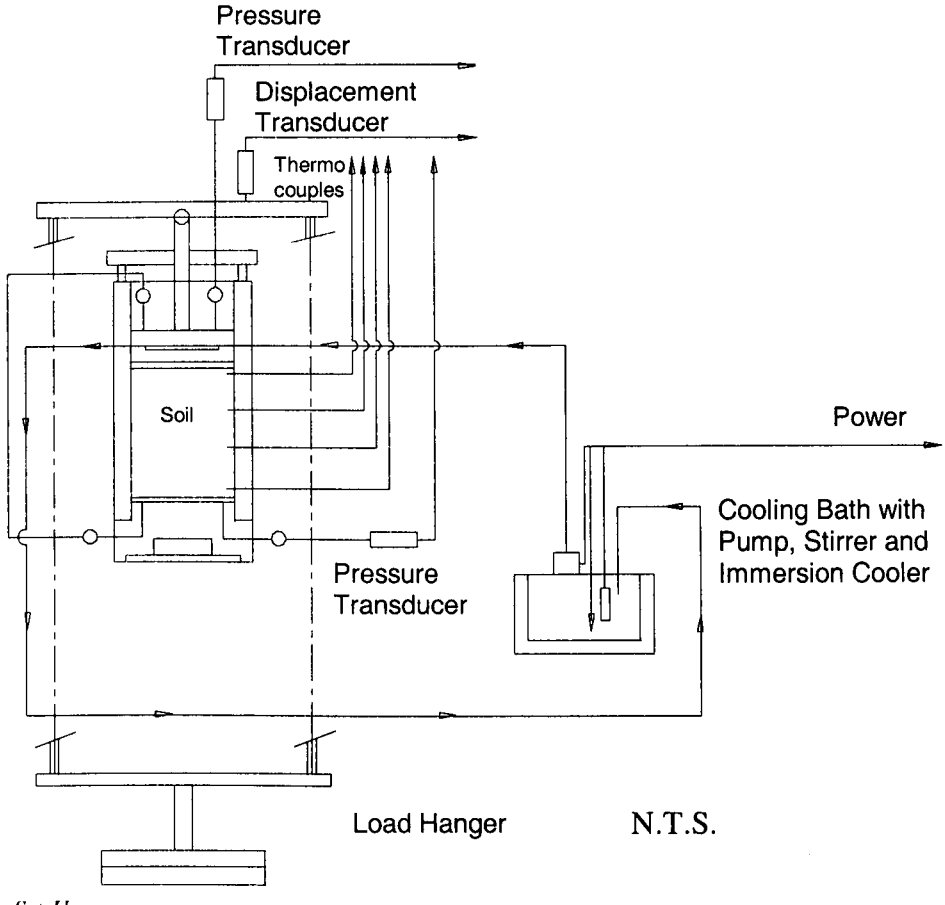

Figure 3.2 - Apparatus Set-Up

3.2.2 The Origin of the Permode

The permode or 'permafrost oedometer' was devised originally by Professor Norbert Morgenstern of the University of Alberta, Canada. Professor Morgenstern kindly made his original drawings available to the researcher, from which the Warwick permode was developed. Various other researchers in North American permafrost regions (Roggensack, 1977; Chamberlain & Gow, 1979), have used similar apparatus, generally for investigation of frost heave.

Early in the research programme, (June 1998), the author visited the University of Alberta to discuss the Warwick permode with Dr. Dave Sego. This visit showed that permodes in Canada have been used and revised over the past 30 years, as befitting state-of-the-art equipment. The Warwick permode was developed in relative isolation, without the benefit of an established research group. A steep learning curve was therefore experienced in its construction and commissioning period. However, the Warwick permode performs satisfactorily as research apparatus. The Alberta visit suggested ways of improving performance, (e.g. producing multiple samples from consolidation in a large Rowe Cell and pre-freezing), which were implemented. Possible future refinements were also considered, and are dealt with in Chapter 9. Henceforth, the term 'permode' applies to the Warwick permode unless otherwise stated.

3.2.3 Description of Permode Mark I

The original 'Mark I' permode is shown in Drawing No. ES919, Sheets 1-2, (Figures 3.3 and 3.4). Sheet 1 depicts the assembled permode with sections AA-EE plus details of barrel and end top end cap. Sheet 2 depicts other details, as shown below:

Table 3.1 - Description of Apparatus

ITEM NO.	SHEET	DESCRIPTION
1	1	Barrel
2	1	Liner
3	2	Load ram
4	2	Load bar
5	2	Clamp nut
6	1	Clamp stud (not drawn to detail)
7	2	Spacer
8	2	Load cap
9	1	End cap (top)
10	2	Baffle plate (top)
11	2	Baffle plate (base)
12	2	End cap (base)
13	2	End cap (base)
14	2	Bush

3.2.3.1 The Main Cell

The main cylindrical cell comprises a split barrel, (PVC), and liner, (PTFE). The cell height is 178 mm, with an internal diameter of 100 mm. The liner is 20 mm thick, and the barrel 40 mm, giving a total wall thickness of 60 mm. The barrel serves as insulation and stiffening of the cell wall, and the smooth liner minimises side-wall friction, allowing passage of the loading piston. Each barrel-and-liner half-cylinder is held together with locating pins at quarter-points normal to the cell wall. The two half-cylinders are joined by locating dowels fixed within the barrel, and then pulled together by means of a clamping screw through the barrel 32 mm from each end of the cylinder, for each side of the join. The cell can be assembled one way only, and is marked accordingly.

The main cell is attached to the base plate, (items 12,13), by two clamp studs, (item 6). The studs are stainless steel and threaded at each end. The studs can only be fitted one way, shown by delineation of diameter. At the base of the cell the studs extend to meet the lower, PVC end cap. At the top of the main cell, the studs pass through aluminium spacers and are clamped above the load bar.

Four ports for thermocouples are located in the barrel wall, (see Appendix 1, Photo 1), at 30 mm centres, the first at 5 mm above the lower baffle plate, i.e. 21 mm from lower end of main cell. The thermocouples pass through the centres of threaded nuts and rubber washers against the barrel recess, with their tips flush with the inside liner wall. The apertures in the liner wall are of diameter 0.8 mm only, to ensure that the thermocouple lead does not pass through onto the specimen. The length of lead passing through the nut is governed by a grub screw.

3.2.3.2 The Base Plate

The base plate comprises three sections: the lower baffle plate, (item 11), the aluminium end cap, (item 12), and the lower, PVC end cap, (item 13).

The baffle plate is a sintered bronze disc 30 mm thick by 95 mm diameter which acts as a porous plate allowing pore water pressure to be measured at the end of the specimen. The plate fits into the aluminium end cap, facing onto section DD, a radial network of troughs leading to two channels: from the centre to the pore water pressure transducer, and from the side to the drainage port. Section EE shows a convoluted channel through which cooling liquid can be circulated. The cooling and pressure/drainage paths do not intersect. Freezing of the soil from the base upwards (when required) takes place by conduction upwards through the end cap and porous plate.

The aluminium end cap has a central section standing proud of the rest of the base by 16 mm. An o-ring of 97 mm inner diameter by 2 mm thickness is positioned on the upstanding portion, in order to effect a seal with the liner.

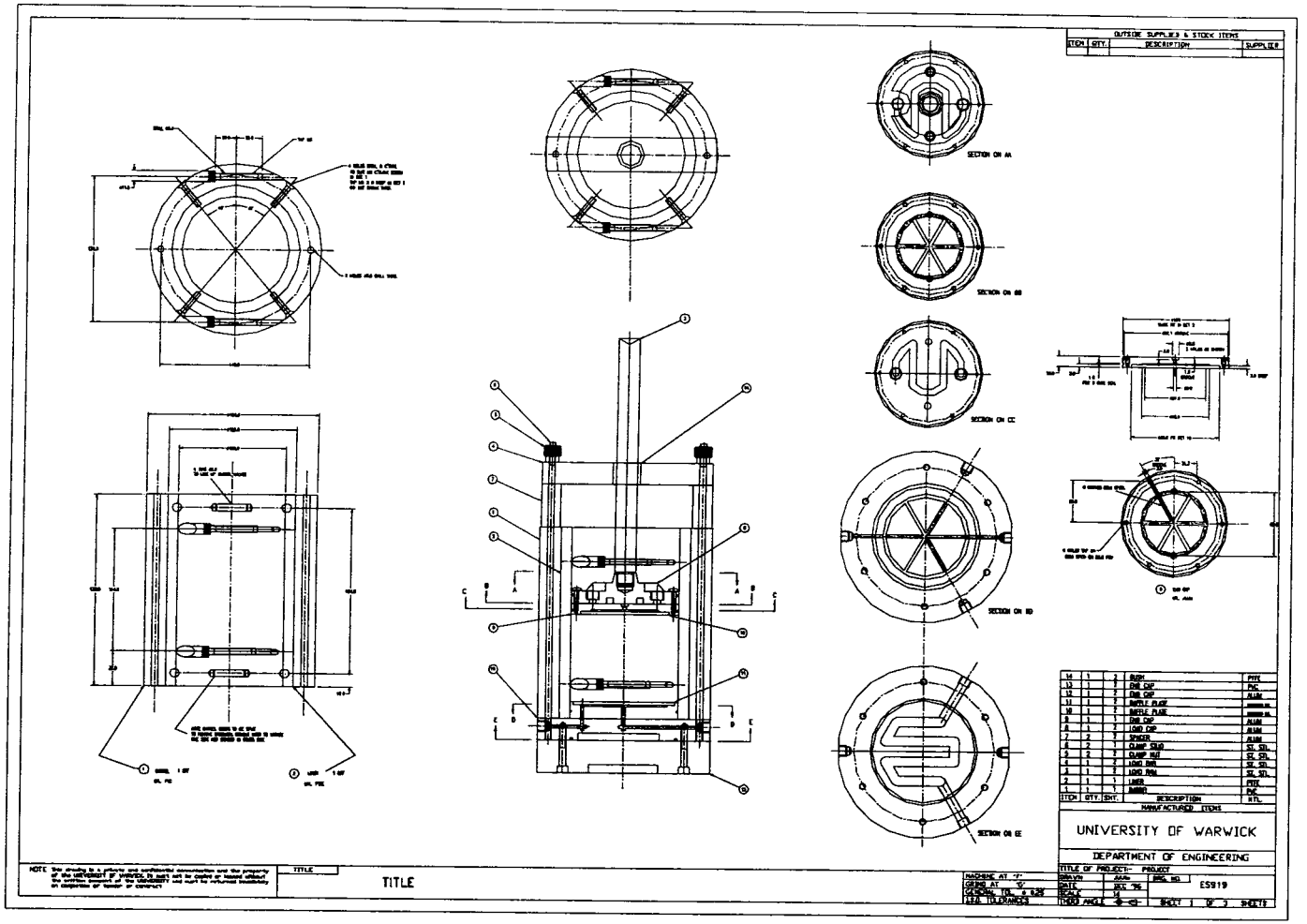

Figure 3.3 - Drawing No. ES919 Sheet 1

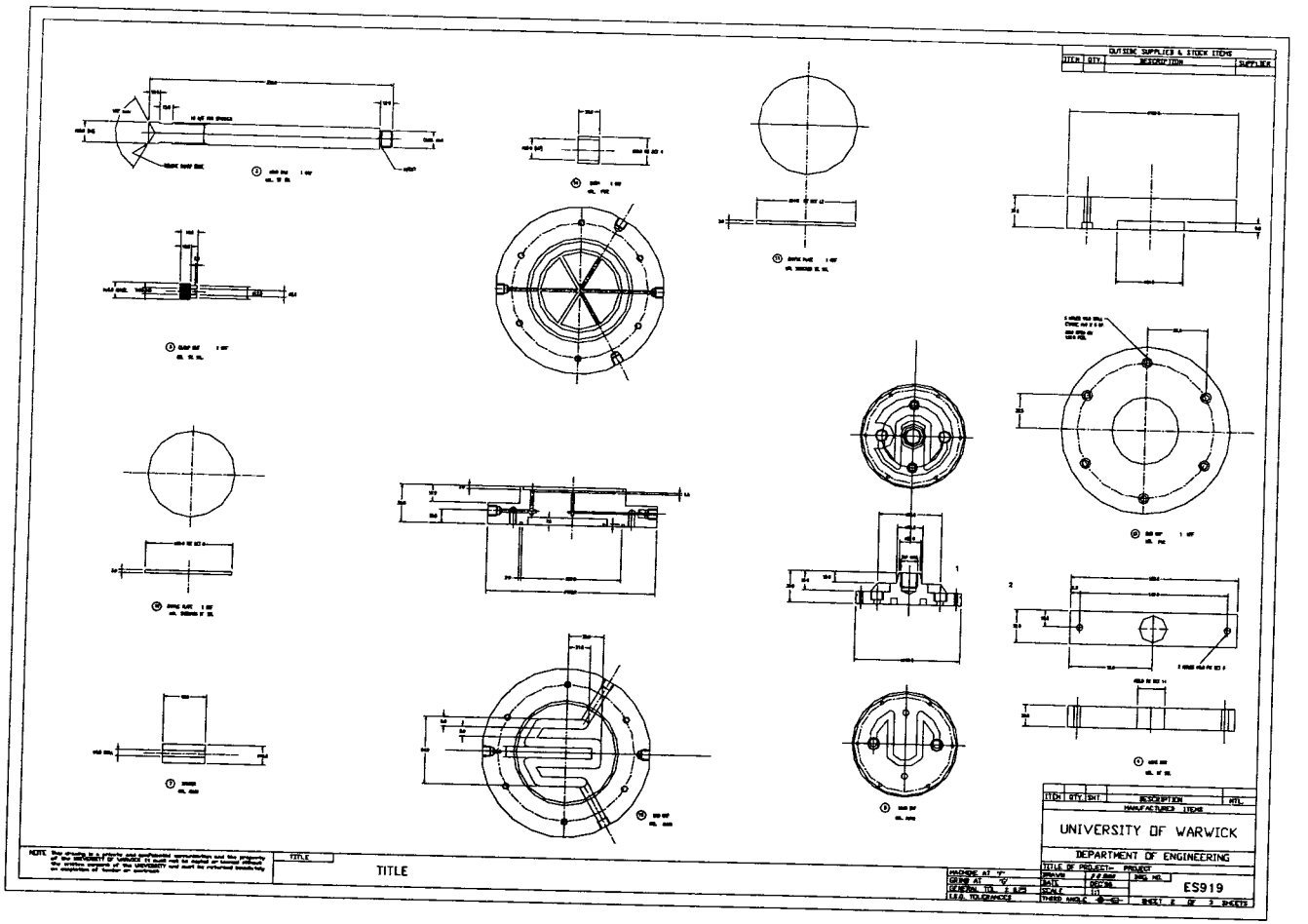

Figure 3.4 - Drawing No. ES919 Sheet 2

3.2.3.3 The Loading Piston

The loading piston comprises four parts: the stainless steel load ram, (item 3), aluminium load cap and end cap, (items 8, 9), and baffle plate, (item 10).

The load ram passes through the load bar, (item 4), and PTFE bush, (item 14). The load bar is clamped to the spacers, (item 7), by the studs connecting the main cell to the base plate. The PTFE bush acts as a bearing, allowing downwards transmission of load, i.e. to the specimen surface rather than the side walls. The bush is greased to reduce friction. Load is applied to the ram via a hanger bar and ball bearing. Loading is direct, using metal weights. This method was judged to be more reliable than air pressure, and more practicable than a lever arm.

Sections AA, BB, CC and details for the load cap, (item 8), and end cap, (item 9), show the piston components in more detail. The load ram screws into the top of the load cap. The load cap is screwed to the end cap, having a total depth of 40 mm. An o-ring of 97 mm inner diameter by 1.5 mm thickness is positioned at 18 mm depth. Section AA shows the arrangement of ports on the load cap. Two firtree vertical shunts connect to a convoluted channel for circulation of cooling fluid, (as for the base plate), as shown in section CC. Two threaded ports connect through to the end cap and a radial network of channels as shown in section BB, and thence to a 60 mm diameter, (3 mm thick), sintered bronze porous plate. Another 97 mm by 1.5 mm o-ring is positioned 3 mm above the base of the end cap. The two o-rings are designed to prevent upwards leakage of water from the specimen. When assembling the permode, all moving contacts are greased to allow ease of movement.

3.2.4 Limitations of Permode Mark I

3.2.4.1 Leakage

The main limitation of the Permode Mark I was the matter of water leaking out of the permode. This leakage was seen to occur primarily through the base o-ring and through the side walls. During freezing and thawing operations the liner halves contracted from their join, causing water ingress. Sudden leaks occurred through the top of the permode, due to the piston o-rings de-sealing from the side walls, particularly at the cylinder joins. Slower,

seeping leakage occurred through the thermocouple ports. In each case, the leaks were expressed as spiked decreases in pore water pressure recorded.

3.2.4.2 Material Failure

The outer PVC barrel had a tendency to buckle in the longitudinal direction, warping the barrel and exerting stress on the inner liner.

The PVC thermocouple ports began warping early on in the test programme. Any misplacement of the thermocouple nut resulted in jamming, and necessitated re-threading of the ports.

The inside walls of the liner cracked and warped in response to the movement of the piston. In addition, the contraction/expansion of the liner within the outer barrel caused buckling from the true cylinder shape to occur.

3.2.5 Modifications leading to Permode Mark II

3.2.5.1 Dealing with Leakage

Various methods were tried in order to combat the leakage problem, as detailed below:

1. Paper Gasket.

A paper gasket was cut to fit over the base plate. The objective was to fill any cracks between the cylinder end and the metal base plate caused by surface roughness. This method was ineffective.

2. Rubber Gasket.

Blue Hylomar paste was spread around the base and up the side wall joins. The objective was to build a flexible seal, taking account of the contraction/expansion of the various permode materials due to freezing and thawing. This method was partially successful, but not very repeatable, as placement of Hylomar varied with each application. There was concern that intrusion of the Hylomar into the cell could contaminate soil and impede the piston. In addition, the permode became very hard to disassemble, and required extensive cleaning with cellulose thinners after each test. This slowed down the turn-around time for the next test starting, and also made the laboratory area subject to fumes despite precautions being taken.

3. Membranes.

Membranes were introduced for two reasons - to stop damage being done to the side-walls of the cell due to piston travel and subsequent soil intrusion; to control water path through the specimen. Originally, 100 mm diameter latex membranes were fitted over frozen soil specimens and the specimens then placed in the permode. The top and base of the membrane were pulled in by draw-threads in an attempt to control flow of water through the ends. However, it was not possible to anchor the draw-threads without splitting the membrane, so this approach was abandoned. Next, the membrane ends were anchored over flat plastic annuli, but this approach also failed. A development of this basic idea was that the membrane ends would pass over a troughed annulus, and a large diameter o-ring placed in the trough over the o-ring, held in place by pressure. This method proved to be

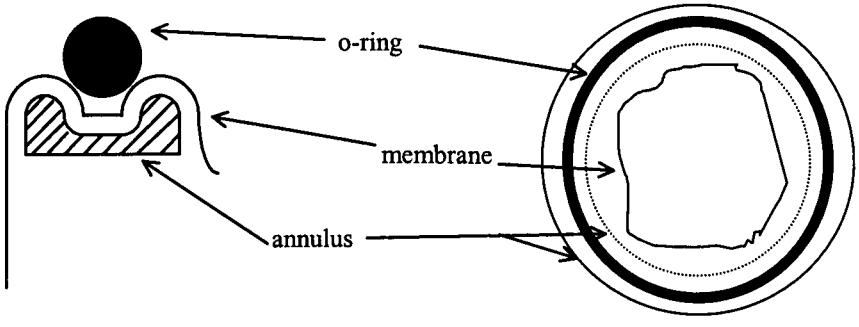

Figure 3.5 - Cross-section and Plan of Membrane Holder

partially successful. While the top o-ring plus annulus held in position quite well, the base was difficult to set up initially, and was prone to jamming and distorting the specimen within the permode. In practice, only the top o-ring-membrane-annulus assembly was used as intended. At the base of the permode the annulus and o-ring were placed facing downwards with the specimen above. The ends of the membrane were still guided into the middle of the base porous plate as was desirable.

After the introduction of the new base o-rings and one-piece liner, (see 4. and 5. below), a new system of membrane-holding was devised. Drawing no. ES919 sheet 3, (Figure 3.6), shows how two concentric stainless steel rings meet at a taper, trapping a membrane layer between the two rings. This design was originally intended for use at both the top and base of the apparatus, but the base assembly proved to be too heavy, impeding travel of the piston and causing membrane rupture. Therefore, the previous o-ring plus annulus assembly was maintained at the base. At the top of the specimen, however, for the

membrane to fit the double tapered ring, a smaller diameter (80 mm) had to be stretched over the frozen specimen and then over the tapered lip of the lower ring. The larger diameter membranes overlapped themselves and failed to cling to the metal. Once the membrane is in place, the upper ring is positioned and attached using six countersunk screws. The piston can then be positioned using two dowels on the surface of the upper ring, and then screwed into place. After this the whole piston+specimen assembly is lowered into the permode.

4. Additional O-rings.

Grooves were cut in the base to accommodate 1 no. 100 mm inner diameter by 3 mm thickness and 1 no. 120mm inner diameter by 3 mm thickness o-rings, to supplement the 97 mm by 2 mm o-ring on the proud-standing base section. All three o-rings were made from silicon-60, a softer type of rubber. The objective was to remove the need for gasket being spread on the base. The soft o-rings compressed well under load from the clamp nuts at the top of the specimen. This anti-leakage strategy worked well, except for the silicon-60 o-rings tending to fail after one or two tests. This was found to be due to the extent of the cold temperatures experienced. The base o-rings were replaced by piton rubber o-rings, which have greater resistance to cold and also to 'rolling' effects across the o-rings during assembly and disassembly of the permode.

5. One-Piece Liner.

As well as introducing additional o-rings, it was decided that a single piece liner would be more efficient than the split liner. This one-piece liner is still separate from the split barrel, but fixed in place using locator pins as before and then screwing the barrel together along the longitudinal joins. The new liner is far more efficient in terms of preventing leakage, although specimen handling, (i.e. emplacement and removal), is now slightly more difficult. As an experiment, a split liner was used at a 90° split to the barrel split, but leakage was again a problem, so the one-piece liner was retained instead.

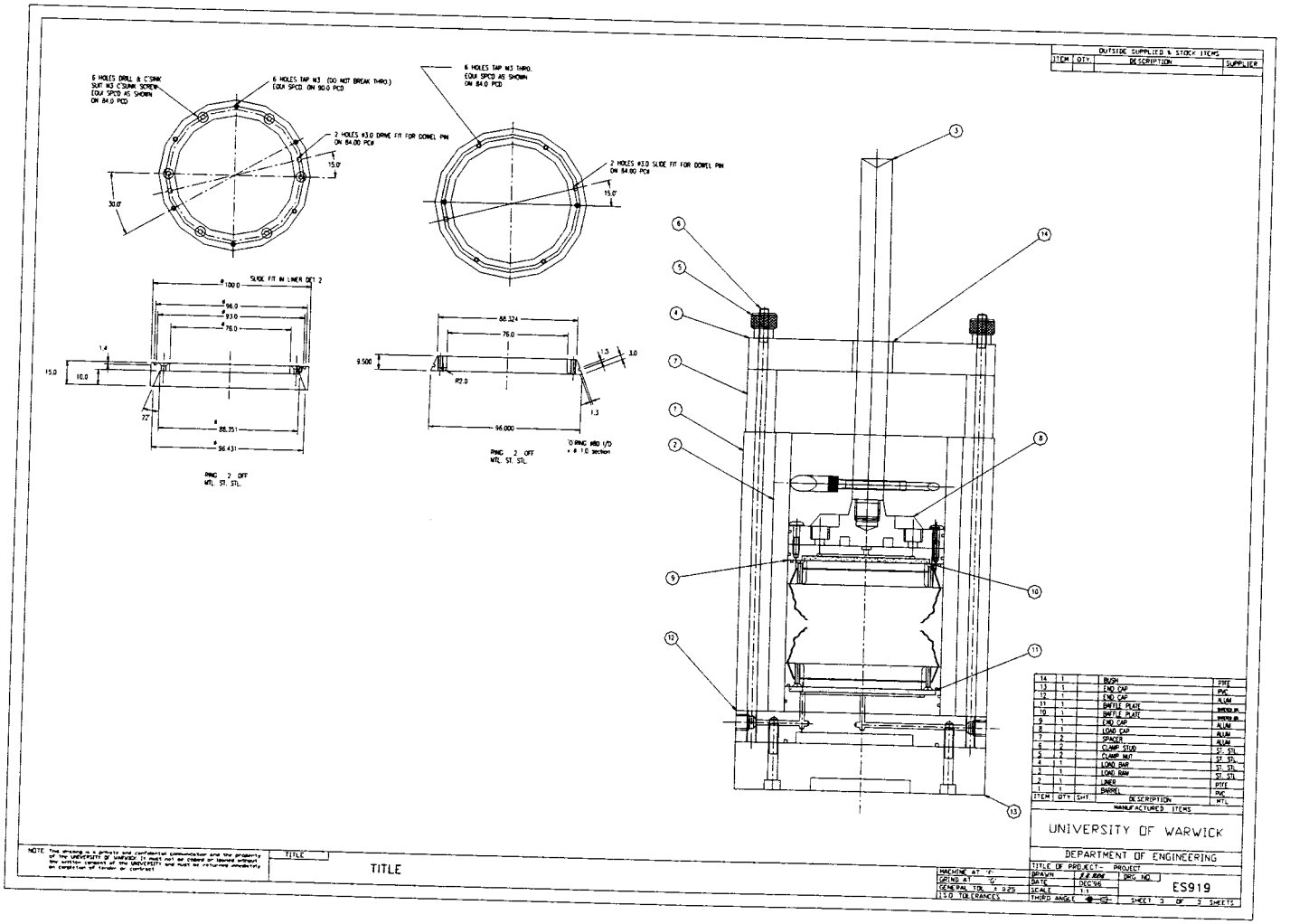

Figure 3.6 - Drawing No. ES919 Sheet 3

6. Thermocouple Wires.

The original thermocouples used were glass-fibre insulated. Although the leads at the thermocouple ports were wrapped in PTFE tape, water was being absorbed at gaps in the PTFE and seeping out along the insulation. These thermocouple leads were replaced with PTFE insulated thermocouple leads. PTFE tape is still used to wrap the leads at the ports, but now simply to ensure a close fit is obtained.

3.2.5.2 Dealing With Material Failure

Various methods were tried in order to combat material failure, as detailed below:

1. Additional Cross-Clamping Screws.

Two additional cross-clamping screws were placed along the length of the barrel on each side of the join (see Appendix 1, Photo 2). This makes the joining stresses along the barrel more evenly distributed, and reduces the risk of over-tightening to achieve maximum closure.

2. Re-Tapped Thermocouple Ports.

The thermocouple ports in the PVC barrel were re-tapped specifically so that immediately on turning the thermocouple nut in the port it was apparent whether or not the fit was correct. This was effected by having the nut turn into the tapped port with a 'jiggle' rather than a tight-threaded socket.

3. Warping Of Liner.

This problem was overcome by introduction of the one-piece liner, (negligible warping), and membranes (no soil content abrading the liner).

3.2.5.3 Overview

Leakage has been vastly reduced by the measures detailed above. Some leakage still occurs, but this is considered minor and tolerable in comparison to the earlier situation. The aim of the experiments was to perform tests in an undrained state, (i.e. no overall change in water content). Clearly, when any leakage occurs this condition is not met. Therefore, considerable effort was expended to prevent leakage.

The risk of material failure has also been reduced in the Mark II permode. The main consumables are membranes, silicon grease and occasional o-ring replacement costs.

3.2.6 Cooling system

3.2.6.1 Method of Cooling

In order to freeze a specimen, a liquid must be circulated through the end caps which are in turn in contact with the specimen ends. It is essential that the circulating fluid does not contaminate the soil. The choice of such a fluid is dealt with in Section 3.2.6.3. The method of cooling the circulation fluid down to low temperatures required careful consideration. The options were to have an 'all in one' bath and circulator taking the form of a closed cooling tank, or an immersion probe cooler, with the probe placed in a tank with separate pumps to circulate the fluid around the permode system.

After receiving quotes for the various systems available it was decided that the immersion cooler with separate tank was the best option, both in terms of economic viability and flexibility. The separate tank system was more adaptable for future work, for example with more than one permode being fed at a time. A Neslab IBC-4 unit was selected. This is a portable immersion cooler capable of cooling fluids down to -25°C. This type of unit is designed for long-term operation - essential for the research. The unit comprises a sealed refrigeration compressor and nickel-plated bronze cooling probe. The probe is placed in a suitably insulated tank, (reservoir), of the fluid to be cooled. The temperature of the fluid is controlled by a Neslab accessory, the Cryotrol Temperature Controller. This analogue unit acts as a thermostat for the IBC-4, providing accuracy to ± 0.5°C. A probe is placed in the reservoir, and at the required temperature threshold the cooler cuts out or restarts as required.

The tank for the reservoir was chosen after a visit to a building and plumbing supplier. A standard plastic cold water tank, (capacity 4 gallons), was selected, together with insulation jacket cover and lid. The insulation provided proved to be too thin, so the plastic tank was set in a custom-made wooden box with additional insulation. A aluminium lid with apertures for probes, stirring and pumping devices was also custom-made for the research.

To optimise fluid cooling, an overhead stirrer is used to ensure mixing takes place. This has the dual purpose of cooling the fluid quicker, and preventing water segregation ice

formation at the cooling probe. The stirrer has a heavy-duty brush motor and electronic feedback control to maintain set speed.

Early on in the test programme, a warming bath was included in the set-up. The objective was to provide a controlled rate of thaw by circulating warm water. However, this was discarded as the soil became prone to overheating. Also, it was extremely difficult to operate the system which required manual switching of pump source and destination twice each daily cycle. The lack of repeatability led to spurious results. The eventual test set-up therefore included only the cooling reservoir.

3.2.6.2 Method of Circulation

The cooled fluid is pumped through silicon tubing and the permode using a peristaltic pump. This type of pump uses the principle of positive displacement. The pump consists of a pumphead with three rollers around a central shaft connecting to a drive motor. As the shaft turns, the rollers push in turn against the silicone tubing. The tubing is pulled tightly over the rollers and held in place above by a fitted housing box. Each advancing roller occludes the flexible tube before releasing it to recover its' normal diameter, hence drawing in fluid which is trapped in turn, thus starting the cycle anew. The advantages afforded to the research are that the pump workings and the antifreeze do not come into contact, and that the peristaltic action is suitable for lengthy periods of use. The tube sections inside the pump housing do need periodic replacement, but this is a simple procedure. The pump is regulated by a d.c. power supply unit.

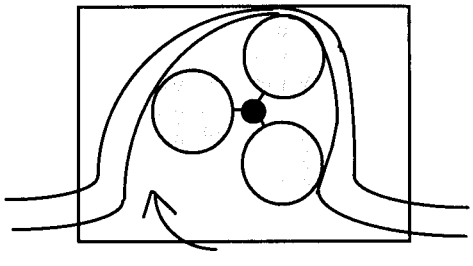

Figure 3.7 - Peristaltic Action

The power supply and pump are activated and halted using a digital plug-in timer socket. This unit can be programmed to activate the circulation procedure on a daily cycle, thus standardising the test procedure.

The silicon tubing is attached by jubilee clips to the entry and exit ports of either the top or base end cap. The tubing is insulated with pipe-lagging between the permode and the reservoir in order to reduce heat gain. The majority of the testing programme involved freezing from the top downward, but with some tests freezing upwards from the base and, in some early tests, freezing from both ends. A full review of conditions for each test is given in Section 3.3.

3.2.6.3 Circulation Fluid

Two fluids were considered for circulation, automatic transmission fluid oil and antifreeze.

Automatic transmission fluid was considered as it is a relatively 'thin' oil, and can be present and working in cars at low temperatures. However, on testing a specimen with the peristaltic pumps it proved to be unsuitable. The lowest temperature at which the oil could be pumped was only -7°C, before becoming too viscous. This was judged to be too warm to transmit much cooling to the specimen ends, particularly as the oil would regain heat during the circulation process.

'Antifreeze' is the generic name given to chemical substances which when added to water lower the freezing point of the solution. The first type of antifreeze used was a blend, containing methanol, glycols and corrosion inhibitors. This first antifreeze was selected primarily on the basis of low cost and convenience, as it was available within the university. Table 3.2 below shows various criteria by which antifreeze mixtures can be judged.

Table 3.2 - Properties of Antifreeze (after Munro, 1964)

Property #	1	2	3	4	5	6	7	8
Methanol	E	P	G	E	P	E	G	P
Ethylene Glycol	F	F	G	F	F	G	P	G

E, Excellent G, Good F, Fair P, Poor

1. Low cost
2. Low volatility
3. Good heat conductance
4. Low viscosity at low temperatures
5. Non-corrosive to metal
6. Inert to rubber
7. Resistance to leakage
8. Non-toxic vapours

After experimentation and further research, it became apparent that the methanol component made the chosen antifreeze unsuitable. Vapour was given off even at low temperatures. The laboratory area had been well ventilated, but the concentration of vapour still gave off an unpleasant odour. Also, methanol is quite volatile at relatively low temperatures (flash point 21°C). While the antifreeze was kept at low temperatures during the tests, and sealed away when not in use, this high volatility was considered a potential hazard. In the case of a power-cut, for example, temperatures could rise.

The next antifreeze mixture was selected with regard to these difficulties, and also in further consideration of criteria given in Table 3.2. An ethylene glycol was selected. Compared with the methanol/glycol blend the cost is higher, viscosity is slightly higher at lower temperatures and resistance to leakage is low. However, the advantages outweigh the disadvantages, with the glycol having lower volatility (e.g. flash point 120°C), being naturally less corrosive to metals and having no toxic vapours. As no vapours are produced at room temperature, the antifreeze can be left in the reservoir between testing periods. This greatly reduces the test preparation time. Corrosion inhibitors are included in the antifreeze mixture, increasing the level of protection to the cooling probe and permode. The increased viscosity of the low temperature solution has not made any perceived difference to pump performance and circulation. All connections are checked before and during testing to monitor any antifreeze leakage, but this has not been found to be a significant problem.

3.2.6.4 Test Environment

The basic test environment comprises a small room adjacent to the main soils laboratory. Two fans are mounted in the wall of the test environment, and serve to ventilate the area by pulling in air from outside. The air then circulates round the area. A door to the main laboratory is left open for further ventilation. The provision of adequate ventilation is important as it prevents the build-up of any fumes and helps to lower the area temperature slightly. Unfortunately, heating pipes run through the area.

Initially, the permode tests took place without further insulation of the permode. This had the disadvantages that the specimens took a long time to freeze, and that they thawed to room temperature. Also the necessary ventilation decreased ambient stability. Although the tests carried out were still of interest, it was decided that a low ambient temperature environment had to be established. This would solve the problems detailed above, and allow tests to be carried out over a narrower, more relevant temperature range, (-5°C to +5°C).

The first attempt at a controlled environment was to construct a box out of insulation panels. The permode sat within, and the box was cooled using a cooling element, fed by the cold reservoir using a peristaltic pump. This general arrangement was developed over several permode tests with a view to optimisation. However, the reservoir gained so much heat from the cooling element's return flow that the freezing process in the permode was inhibited. This problem was tackled in two ways. Firstly, by trying to provide an efficient seal on the box. This was only partially successful, as apertures were needed for instrumentation and access to the permode. Secondly, by introducing small 12 v fans to circulate the cold air within the box and stop the cooling element icing up. Unfortunately, although some progress was made, these measures failed to make a significant contribution towards a reliable, repeatable test environment.

The second, successful attempt was to replace the sealed box with a refrigerator. This meant that the test environment could be controlled independently of the permode. Also, the level of ambient stability would be drastically improved. An upright second-hand refrigerator was obtained for this purpose. Its dimensions are 1.54 m height by 0.55 m by 0.55 m. The refrigerator is attached to a side bench through a metal loading plate and side bolts. Holes are drilled through the base of the refrigerator to allow the load hanger rods to

pass through. The holes were drilled at the smallest diameter possible to permit the rods to be free-hanging. On one side of the refrigerator two holes were drilled to give an entry and exit port for antifreeze circulation. After drilling, two short lengths of flexible plastic pipe were threaded through and fixed in position with silica gel. The silicon tubing attaches on each side of the refrigerator wall with jubilee clips. On the other side of the refrigerator three larger bore holes were drilled and ~15 mm diameter pipe lengths pushed through. The instrumentation wiring then passes through the pipes, which are then filled with packing beads to avoid heat loss. The permode sits inside the refrigerator on a raised level platform.

In summary, the introduction of the refrigerator has proved to be most beneficial to the testing programme.

3.2.7 Instrumentation

3.2.7.1 Displacement

The permode allows only one-dimensional, vertical movement to take place. During the cycles of freezing and thawing, therefore, the expansion and contraction of the specimen can be measured by considering vertical displacement. This is measured using a strain gauge displacement transducer or SGDT. The SGDT works by having a cylinder housing a spindle. As the spindle extends or retracts from the housing, strain is measured by a strain gauge. These strain readings are recorded by the data-logger and so the SGDT can be calibrated with known displacements.

The calibration is carried out by fixing the SGDT into a vice and imposing known displacements by means of thin metal slip gauges. Displacements are created in series from zero to 25 mm, and then from 25 mm down to zero. This set of readings constitutes a 'run' of results. Three runs of readings were taken for each calibration exercise. Regression analysis was then carried out by the 'least squares' method, and a correlation coefficient found for dispersion of data from the resulting straight line. When a satisfactory calibration is achieved, a value of gradient is programmed into the data-logger, along with a forced value of intercept being equal to zero. This is acceptable as the SGDT is initialised to start reading from zero, rather than the intercept value.

Detailed results for calibrations can be found in Appendix B. Calibrations were carried out in the case of a set-up change. For example, when the refrigerator was installed, wiring to

the transducers was altered. Extra lengths of wire were connected to the data-logger and connected to the displacement and pressure transducers at an intermediary junction. This meant that the transducer wires could be passed back and forth through the shunt pipes in the refrigerator wall without disconnecting from the data-logger each time. The transducers were re-calibrated as a check on the extended wiring.

Consultation with the manufacturer was necessary in order to determine that the transducer was suitable for use in sub-zero temperatures. However, a true 'cold' calibration with all the slip gauges and equipment at test environment temperature would be interesting, but would require an actual cold room set-up.

3.2.7.2 Pore Water Pressure

Pore water pressure was measured at the top and base of the specimen using pressure transducers. As with the SGDT, these transducers measure strain, but this time related to fluid pressure on a diaphragm. Calibration was carried out on the same theoretical basis as the SGDT. Pressures were imposed by connecting the transducer to a water head system. A Bourdon Gauge measures the pressure set up. Each calibration run was carried out from zero to three bars and back from three bars to zero again. As for the SGDT, three runs were carried out, and further details are given in Appendix B.

Early on in the test programme, a transducer was placed at the base only. However, a top transducer was later added so that pressure distribution down the specimen could be judged.

As experience was gained with the apparatus, improvements were made to the pressure measuring system. Originally, when just the base transducer was being used, the porous plate and channels connecting down to the transducer were inadequately de-aired. This was solved by use of a de-airing block, and saturation of the porous plate. Filter paper was placed on top of the porous plate to prevent soil ingress and clogging. Also, the fluid medium became antifreeze and water 50% solution. This meant that the pressure readings would not be affected by freezing within the channels. Working in the cold test environment entailed extra consideration of how well the pressure measuring system would perform. For example, the valves to the transducer and the de-airing block had to withstand unusually low temperatures. This was catered for by using spring-loaded valves with internal packing which can expand or contract in order to keep flow area constant.

When the top transducer was added, it was not feasible to fit a de-airing block. In order to avoid difficulties with air bubbles, the transducer is connected to the permode while under load. A stub extends upwards from the load-cap. This is filled with the antifreeze solution, and the transducer then connected. The transducer has also been filled with the solution and its valve closed before connection by split-thread to the stub.

3.2.7.3 Temperature

Temperature is measured down the side of the specimen using thermocouples. Extra thermocouples are employed to check ambient temperature of the test environment.

Thermocouples measure a temperature difference due to the Seebeck effect. Two different metals are used to form a circuit with two junctions. If one junction is heated or cooled down, (but not the other), then a voltage is generated. A thermocouple works by having one end as an external tip, and the other end as a 'reference junction'. In this apparatus set-up, the reference junction is provided by the data-logger at its ambient temperature. The voltage difference caused by the tip being colder/warmer is calibrated within the data-logger to correspond to temperature change. The data-logger then records the final measured temperature.

The thermocouples used were of Type K, which consist of nickel and chromium/aluminium. Type K was selected for economy and convenience. The temperature range is certainly sufficient, (-50°C to 200°C), Accuracy is quoted by manufacturers to ±2.5°C. However, when the thermocouples were tested at water-to-steam, normal room and ice-to-water temperatures, the thermocouples agreed to ±1°C with separate digital thermometer readings. The Type K thermocouples were therefore accepted for use in the apparatus set-up. The insulation type was originally glass-fibre, but was replaced by PTFE to stop water loss as detailed in 3.2.5.1.

3.2.8 Data-Logging System

3.2.8.1 The Data-Logger

The data-logger used was a 3531D Orion data acquisition system. The unit can be programmed with up to eight 'tasks', each of which consist of commands to record various data either to floppy disk or print-roll. In the test programme, data was recorded from all transducers and permode thermocouples at 10 minute intervals to disk, and at four-hourly intervals to printer as back up. After short power-cuts the unit can restart and recommence logging. Unfortunately, long breaks causes data-wiping to occur on start-up. However, in general the data-logger proved to be reliable.

3.2.8.2 Use of PC

The test results were transferred from disk to personal computer for processing. First, a Turbo-Pascal program, (listing given in Appendix 3), is used to 'read' the data-logger's .dat format, and re-organise data into columns in a .txt file. This text file can then be imported into Excel for further processing by macro, e.g. time indexing, calculating average temperatures. Graphs can be produced in Excel, but tend to be quite time consuming to produce, and basic in format. For more detailed graphical analysis, Matlab 5.3 has been used.

3.3 Soil Index Properties

3.3.1 Sample Description and Preparation

Three soil types were prepared for permode testing:

1. Upper Lias clay from Nailsworth, Gloucestershire.

   This soil was a firm to stiff orange/green/brown clayey silt with a little fine sand, and occasional fine-medium gravel (iron-stained siltstone).

2. Weald Clay from Hailsham, Sussex.

   This soil was a stiff to hard grey to mid-brown silty clay with orange mottling and black iron-stained jointing. Some organic content was present in form of roots, but was removed before testing.

3. Weathered Oxford Clay from Peterborough, Cambridgeshire.

   This soil was a firm grey/brown clay containing selenite deposits. Evidence of solifluction having taken place was seen in the form of banding and clumps of selenite, honeycombing of the clay and peds of cohesive yellow clay.

For each of the above soils, samples were inspected and descriptions assigned as given. Following this, the samples were remoulded by a combination of mortar-and-pestle crushing, air-drying and sieving. Coarse material, (i.e. material retained on a 5mm sieve), was discarded at this point.

3.3.2 Index Tests

3.3.2.1 Liquid and Plastic Limits

The liquid and plastic limits of the soils were found using the methods described in BS 1377: Part 2: 1990, (Casagrande method for the liquid limit). With the limits and hence the Plasticity Index known, the soils were then classified using the British Classification System, (BS 5930: Part 8: 1981). The soils can be plotted onto an A-Line plot as shown in Figure 3.8.

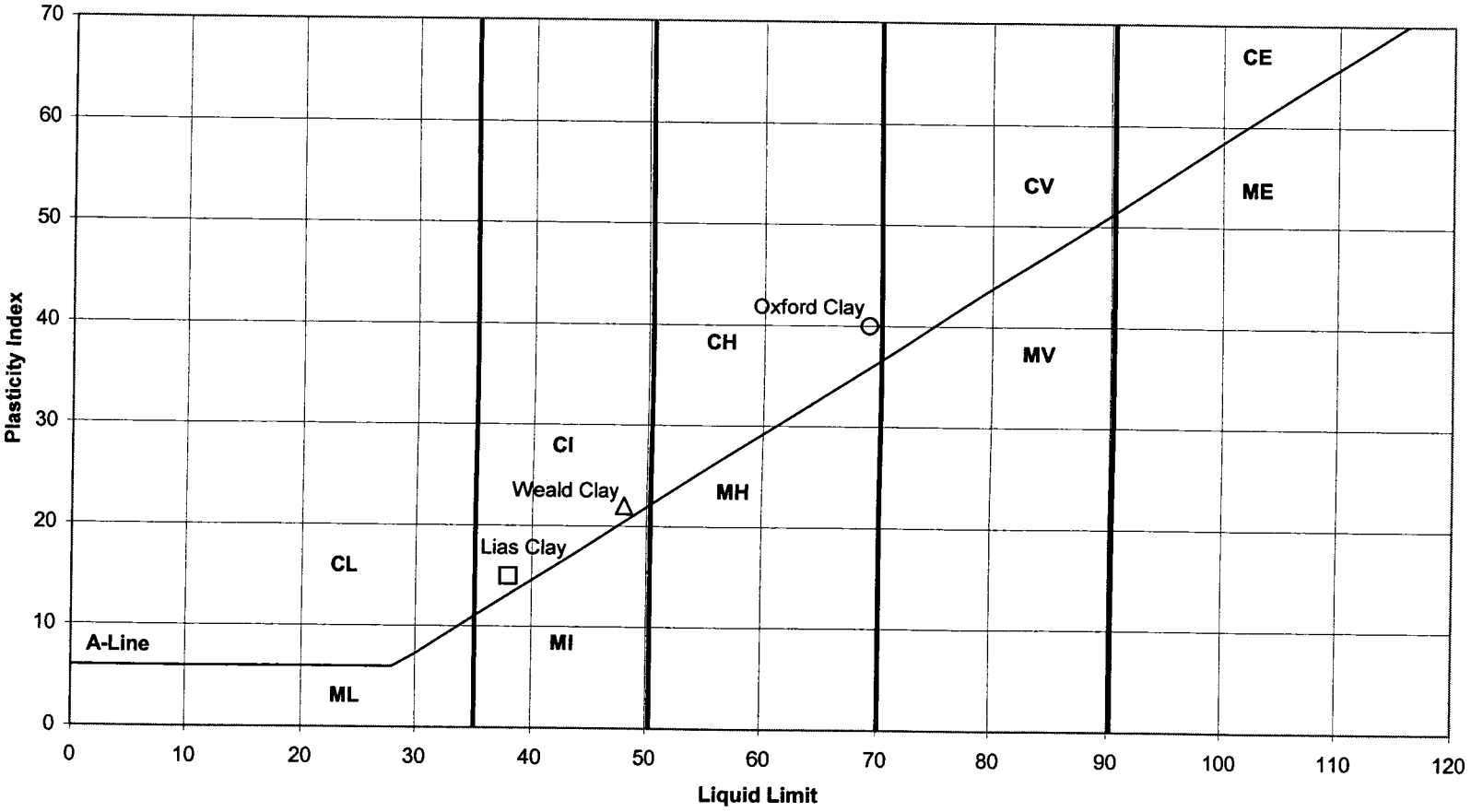

Figure 3.8 - Results of Index Tests Plotted on A-Line Graph

The summary index properties of the soils tested are given below.

Table 3.3 – Index Properties

Soil	W_L	W_P	PI	Classification (BS 5930, 1981)	% Clay Size Particles	$\phi'r$ (°)
Lias Clay	38	23	15	Low CI	16	24
Weald Clay	48	26	22	High CI	39	18
Oxford Clay	69	29	40	High CH	41	17

3.3.2.2 Particle Size Distribution

Particle Size Distribution tests were carried out primarily in order to determine the clay fraction of each soil. The tests comprised wet sieving and sedimentation analysis via the hydrometer method, and were carried out in accordance with BS 1377: Part 2: 1990. Figures 3.9-3.11 below show the resulting curves:

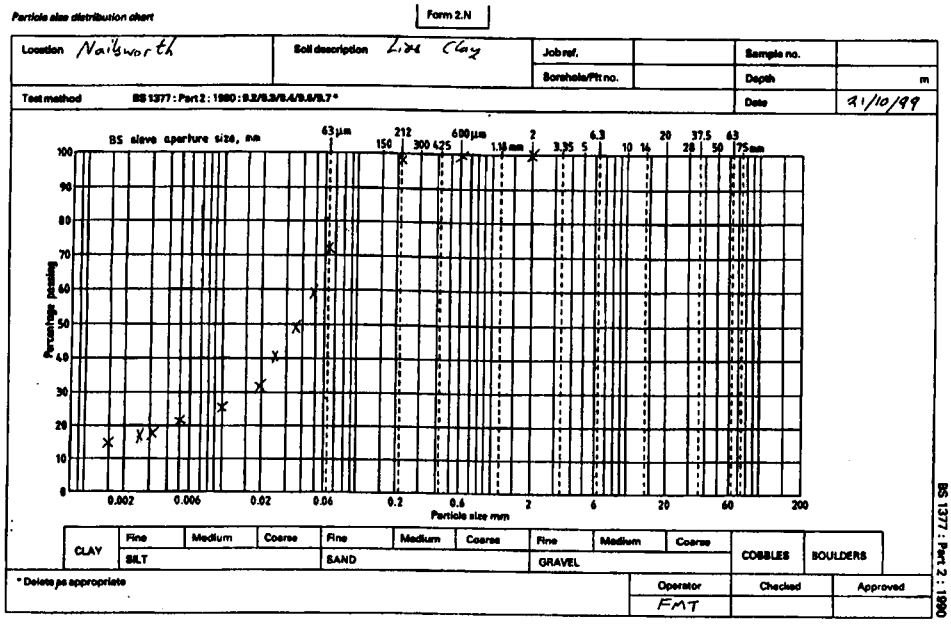

Figure 3.9 - PSD Results for Lias Clay

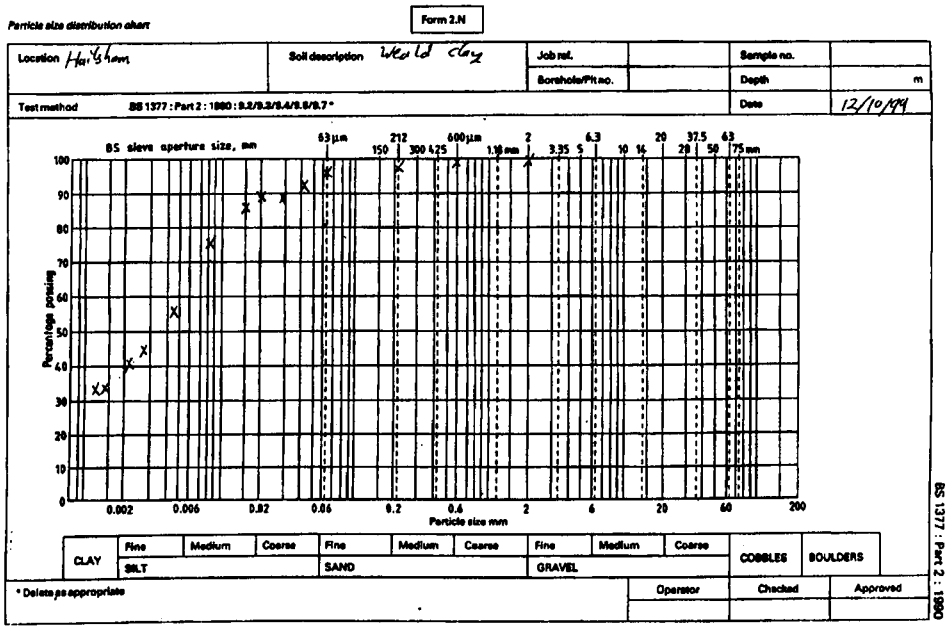

Figure 3.10 - PSD Results for Weald Clay

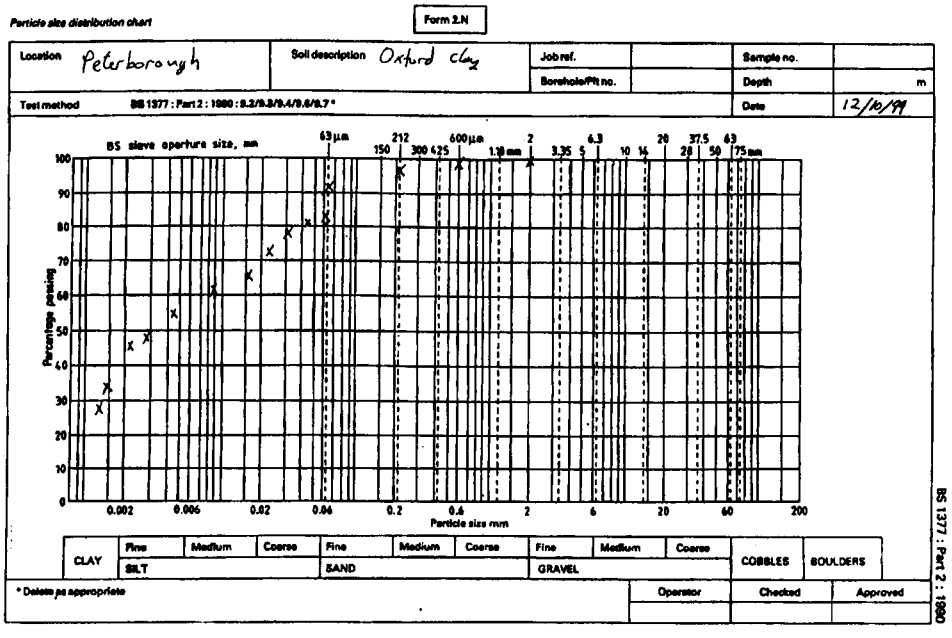

Figure 3.11 - PSD Results for Oxford Clay

3.3.2.3 Ring Shear Tests

Values of ϕ'_r were determined using a small ring shear apparatus in accordance with BS 1377: Part 7: 1990. Specimens were tested over 3 increments, 52.705 kPa, 102.630 kPa and 152.555 kPa. Hysteresis was considered by testing at the lowest increment at the end of the tests. Summary graphs of the ring shear envelopes are given below, with best-fit straight lines added. This assumes the simple case of ϕ' found from the gradient of the best-fit line, rather than the curved envelope discussed by Hawkins & Privett, (1986). This is based on the response recorded to the particular range of effective applied pressure.

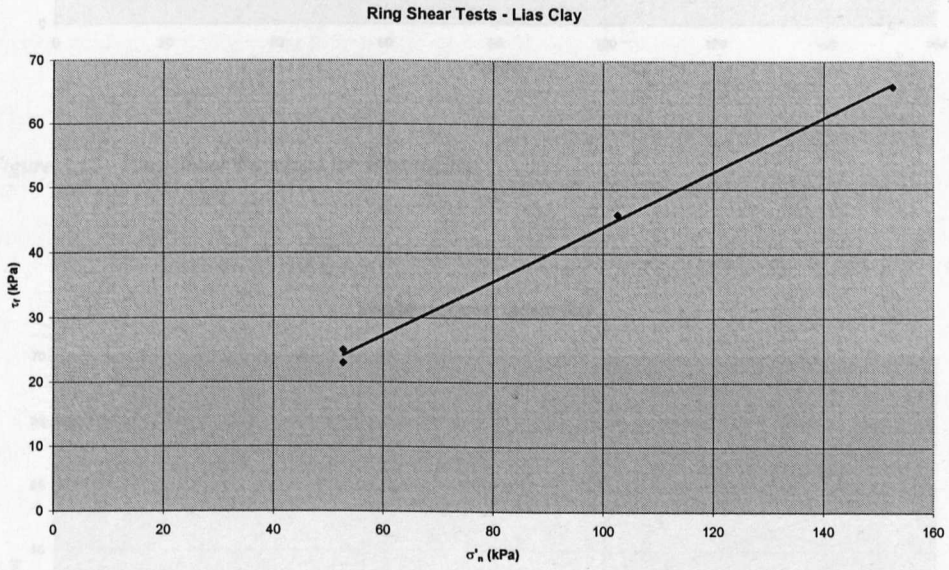

Figure 3.12 - Ring Shear Envelope for Lias Clay

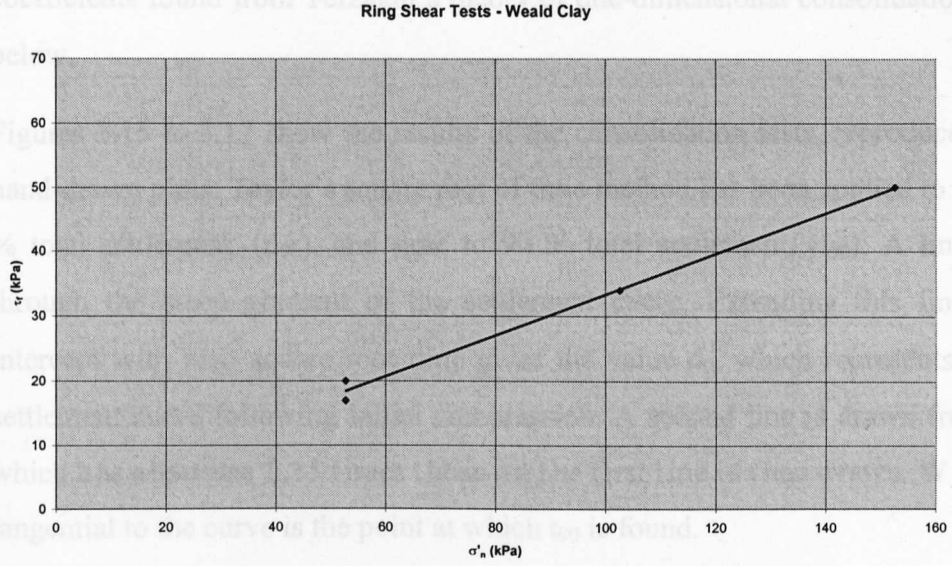

Figure 3.13 - Ring Shear Envelope for Weald Clay

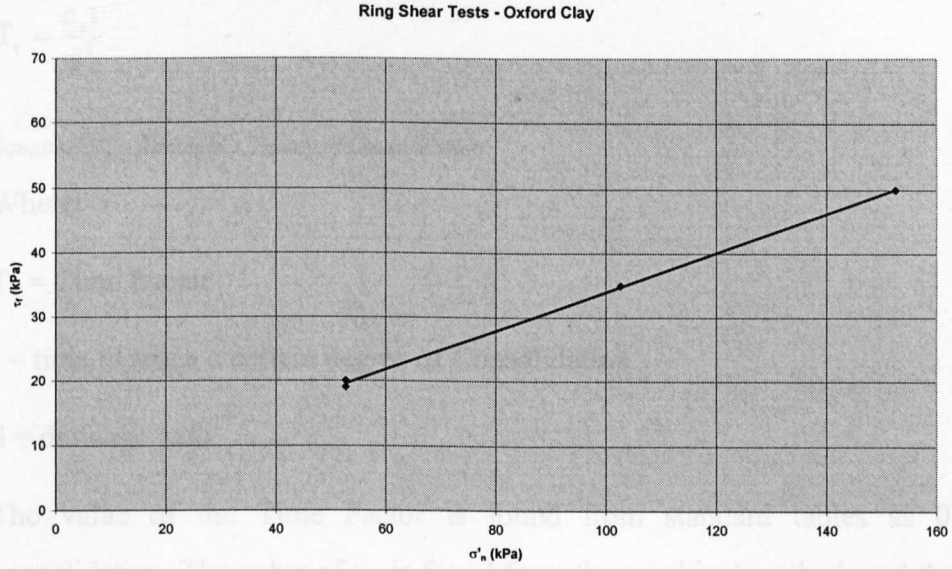

Figure 3.14 - Ring Shear Envelope for Oxford Clay

3.3.2.4 Results of Consolidation Tests

Table 3.2 below shows the consolidation characteristics determined through the preparative Rowe Cell tests. The tests were carried out over one pressure increment, of 50 kPa. Drainage was permitted from the top and the base of the specimens. The permeability

coefficients found from Terzaghi's theory of one-dimensional consolidation are also given below.

Figures 3.15 to 3.17 show the results of the consolidation tests, reproduced from original hand-drawn plots. Taylor's square root of time method has been applied to find depth of 90 % total settlement, (d_{90}), and time to 90 % total settlement, (t_{90}). A line can be drawn through the steep gradient of the settlement curve. Extending this line backwards to intercept with zero square root time gives the value d_0, which represents the start of the settlement curve following initial compression. A second line is drawn from the point d_0, which has abscissae 1.15 times those on the first line is then drawn. Where this line is tangential to the curve is the point at which t_{90} is found.

The coefficient of consolidation, c_v, represents the rate of consolidation and was derived mathematically by Terzaghi to describe the reduction in pore water pressure with time. The basic expression is as follows:

$$T_v = \frac{c_v t}{d^2}$$

Equation 3.1 – Terzaghi's Theory of Consolidation

Where:

T_v = Time Factor

t = time to reach a certain degree of Consolidation

d = drainage path

The value of the Time Factor is found from standard tables as 0.848 for 90 % consolidation. The value of t_{90} is found from the graphical method, and the drainage path d can be calculated from knowing the drainage conditions and initial and final heights of the test specimen.

For example, for Lias Clay, t_{90} was found to be $(11)^2 = 121$ minutes. The initial height of the specimen was 87.00 mm and the final height 79.34 mm. This gave the average height to be 83.17 mm. Two-way drainage means that the drainage path d is half the height, i.e. 41.59 mm.

Therefore,

c_v =[0.848 x $(41.59)^2$] / 121 = 12.0 mm^2/min x (10^{-6} x 60 x 24 x 365) = **6.31 m^2/year**

m_v is the coefficient of volume change, and has been determined using

$$m_v = \left[\frac{H_i - H_f}{H_i}\right] \times \left[\frac{1000}{P_2 - P_1}\right]$$

Equation 3.2 – An Equation to Find m_v

Where:

H_i = 87.00 mm, and H_f = 79.34 mm

$P_2 - P_1$ is the pressure difference, 50 kPa

Therefore,

m_v = [(87-79.34) / 87] x [1000 / 50] = **1.76 m^2/MN**

k is the coefficient of permeability, and has been determined using

$$k = c_v \times m_v \times \gamma_w$$

Equation 3.3 - An Equation to Find k

Where γ_w is taken as 9.81 kN/m^3 = 0.00981 MN/m^3,

k = 6.31 x 1.76 x 0.00981 = 0.11 m/year = **3.0 x 10^{-9} m/s**

The consolidation characteristics and coefficients of permeability derived from the Rowe Cell Tests are summarised in Table 3.4.

Table 3.4 – Consolidation Characteristics and Permeability Coefficients

Soil	c_v (m^2/year)	m_v (m^2/MN)	k (m/s)
Lias Clay	6.31	1.76	3.0 x 10^{-9}
Weald Clay	0.61	5.21	9.8 x 10^{-10}
Oxford Clay	0.37	5.32	6.0 x 10^{-10}

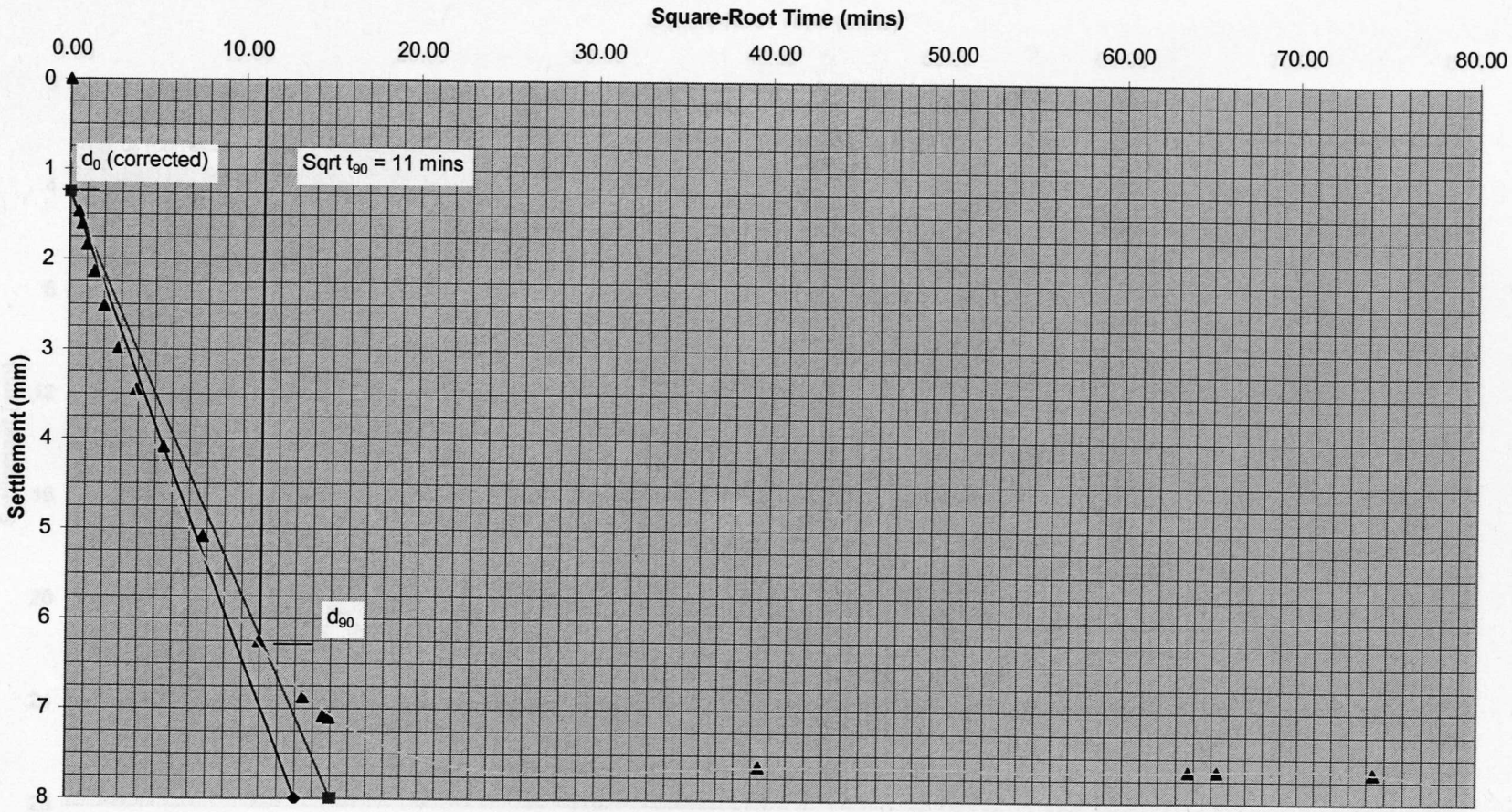

Figure 3.15 - Rowe Cell Consolidation Test - Lias Clay

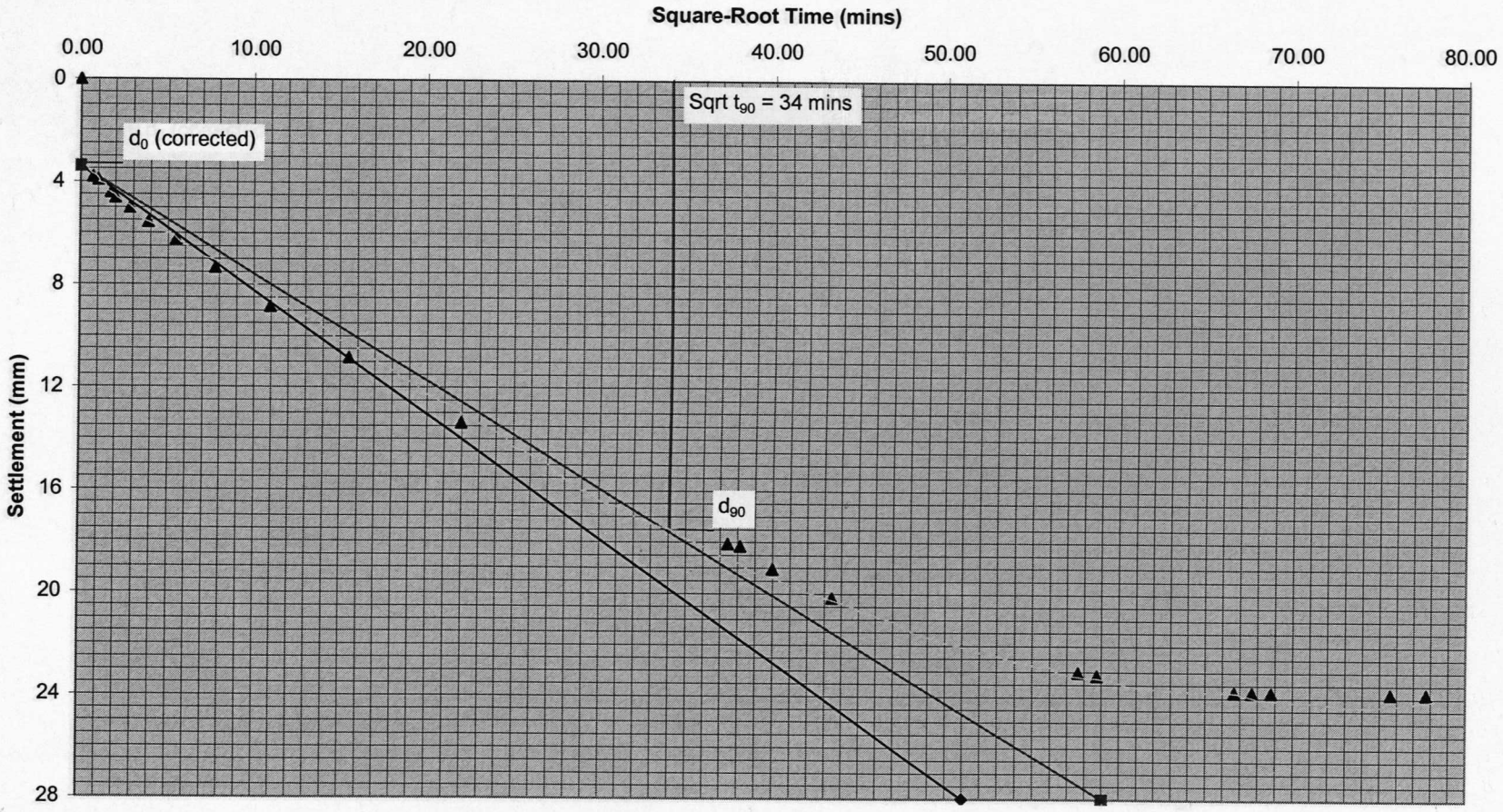

Figure 3.16 - Rowe Cell Consolidation Tests - Weald Clay

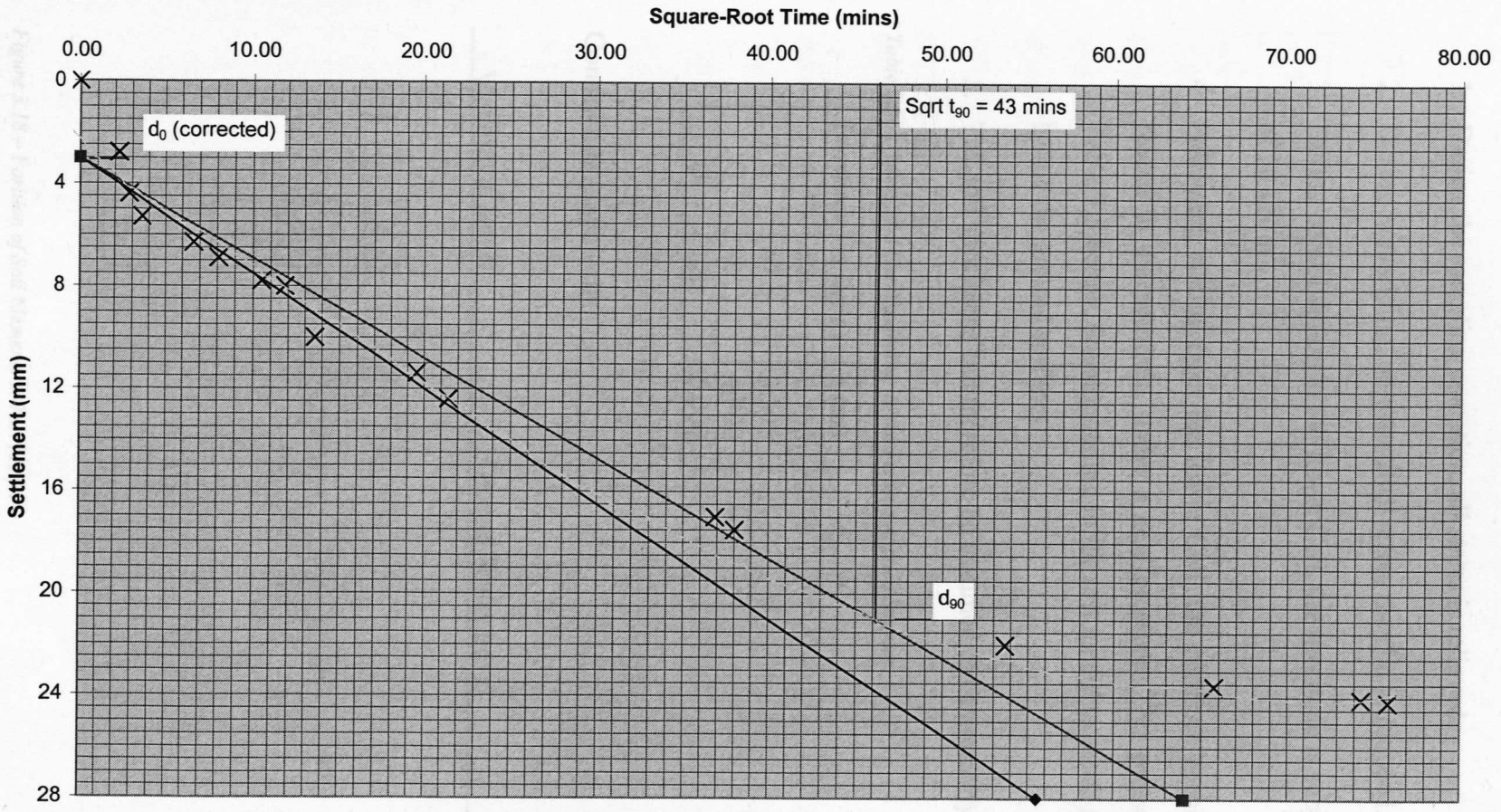

Figure 3.17 - Rowe Cell Consolidation Tests - Oxford Clay

It is now necessary to consider the consolidation test results with respect to the laboratory test programme and the field conditions.

A typical specimen in the laboratory will experience the following stress history:

1. During the sampling operation, all stress is relieved.
2. During remoulding, un-quantified stress may be introduced.
3. During consolidation in the Rowe Cell, the specimen is subjected to a vertical stress of 50 kN/m^2.
4. Following cutting from the Rowe Cell, the permode specimen is frozen and later placed in the permode, under a new pressure. This pressure ranges as shown in Table 3.5 below, (corresponding in the test model to depth z of a tested soil element below the ground surface).
5. The soil specimens can therefore be assumed to be normally consolidated.

Table 3.5 – Values of z Corresponding to the Various Applied Stresses

Position	σ (kPa)	z (m)
A	55	2.750
B	67.5	3.375
C	80	4.000
D	120	6.000

Considering graphically:

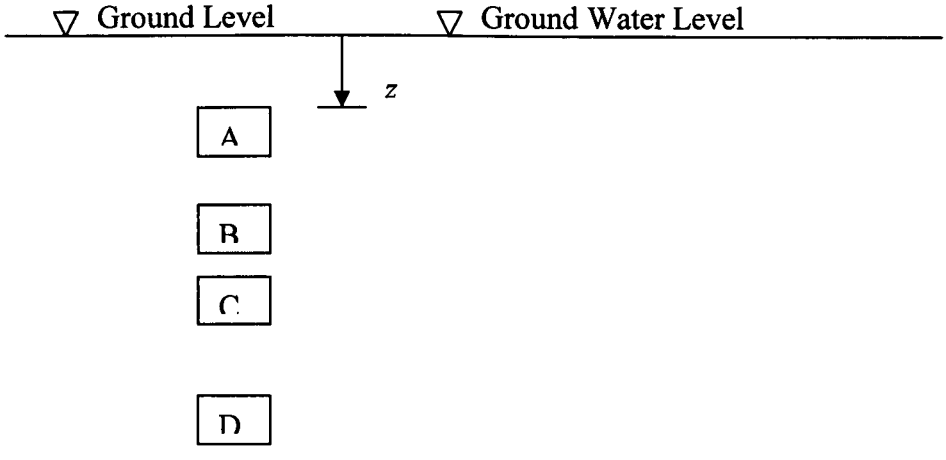

Figure 3.18 – Position of Soil Elements in Test Model

Adapting Equation 3.1 above, values of t_{90} can be found for the two way drainage condition in the field, i.e. assuming the ground surface to be free-draining and downwards drainage also permitted. The drainage path d is therefore equal to half *z*.

Table 3.6 – Estimated Values of t_{90} in the Field – 2 Way Drainage

			t_{90} (years)		
Position	**σ (kPa)**	***z* (m)**	**Lias Clay**	**Weald Clay**	**Oxford Clay**
A	55	2.750	0.25	2.63	4.33
B	67.5	3.375	0.38	3.96	6.53
C	80	4.000	0.54	5.56	9.17
D	120	6.000	1.21	12.51	20.63

From Table 3.6 above, it is possible to consider the likely accuracy of the test model. As explained in Section 1.5, drainage has not been allowed for in the model. Thus, consolidation has not been incorporated as part of the permode test procedure. The estimated values of t_{90} above demonstrate that for annual seasonal cyclical freezing and thawing, the decision not to allow drainage can be justified for the Weald Clay and Oxford Clay, but only at high values of applied pressure for the Lias Clay.

However, if drainage were considered to be obstructed by frozen ground, then the time to consolidate to a particular percentage may be greater, e.g. as shown below in Table 3.7, where the maximum drainage path *z* is utilised. This would tend to justify the decision not to allow drainage in the test model for all 3 soils.

Table 3.7 – Estimated Values of t_{90} in the Field – 1 Way Drainage

			t_{90} (years)		
Position	**σ (kPa)**	***z* (m)**	**Lias Clay**	**Weald Clay**	**Oxford Clay**
A	55	2.750	1.02	10.51	17.33
B	67.5	3.375	1.53	15.83	26.11
C	80	4.000	2.15	22.24	36.67
D	120	6.000	4.84	50.05	82.51

3.4 Permode Test Procedure

Twenty-eight tests were carried out. Tests 1-13 yielded interesting data, and also served to record the development of the test apparatus towards its final, optimum form. However, Tests 14-28 can then be considered to have produced the most informative results, as they were carried out using the definitive test apparatus and procedure. This final method of testing came about as a result of modifications made to preparation of specimens, test conditions and procedure. These modifications are detailed below.

3.4.1 Specimen Preparation

The first stage in preparation was the same for all tests. Distilled water was added to a sample, mixed and left for 24 hours to allow the sample to achieve homogeneity. For the earlier tests, (which used non-saturated specimens), samples were mixed by weight to produce the nearest value to the desired moisture content of half-way between the plastic and liquid limits. For the later experiments, (which used saturated specimens), moisture contents of up to 30% above this desired moisture content were obtained, as consolidation was then carried out, removing water, (and air), from the samples, in order to achieve as much saturation as possible.

Specimens were then created by packing the soil into the permode to a level 100 mm above the base plate. This process did not result in satisfactory specimens as uneven stresses were created due to the packing process, and soil tended to be forced up the sidewalls. From Test 4 onwards, a membrane and stretching cylinder were used to contain the specimen. The membrane-covered specimen was then allowed to slide into the permode. This modification allowed a standard size of specimen to be produced. The introduction of a membrane also stopped the inner side-walls being scored and filled by travelling soil particles. However, it was found that the specimens produced were not satisfactory with respect to degree of saturation, (i.e. not known), and pressures built up from forming the specimen in either the permode or the stretching cylinder.

From Test 14 onwards, saturated specimens were prepared using a 254 mm diameter Rowe cell oedometer (Rowe & Barden, 1966). A confining pressure of 50 kPa was applied, and vertical drainage allowed to both ends. Once consolidation was complete, (a process taking up to 7 days), 100 mm internal diameter plastic pipe lengths were pushed through the cell

to extrude and contain a specimen. Samples were taken from the remaining material in the Rowe cell for moisture content determination. Three specimens were produced from each Rowe cell operation. The specimens were then contained within plastic bags and placed in a freezer until required. Subsequently, the specimens were removed from their sleeves initially by hand extrusion, but later by the expedient of including a disposable membrane within the sleeve. The frozen specimens were then allowed to drop into a partially-stretched 80 mm diameter membrane which was then attached to a modified piston, (refer to Section 3.2.5.1 for details), ready for placing in the permode.

3.4.2 Test Programme

Tables 3.8 and 3.9 show the programme of tests carried out. Each test is assigned a number, soil type, applied stress and initial moisture content.

Table 3.8 - Programme for Tests 1-13

Test No.	Soil	σ (kPa)	m.c. (%)
1	Lias Clay	29	29
2	Lias Clay	104	32
3	Lias Clay	104	30
4	Lias Clay	104	32
5	Lias Clay	104	30
6	Lias Clay	104	35
7	Lias Clay	104	33
8	Lias Clay	80	30
9	Lias Clay	104	29
10	Lias Clay	80	32
11	Lias Clay	80	31
12	Lias Clay	80	30
13	Lias Clay	80	32

Table 3.9 - Programme for Tests 14-28

Test No.	Soil	σ (kPa)	m.c. (%)
14	Lias Clay	80	27
15	Lias Clay	55	27
16	Lias Clay	55	27
17	Lias Clay	80	31
18	Lias Clay	55	31
19	Oxford Clay	55	49
20	Oxford Clay	80	49
21	Oxford Clay	55	50
22	Oxford Clay	55	50
23	Oxford Clay	80	50
24	Weald Clay	55	39
25	Weald Clay	80	39
26	Weald Clay	55	38
27	Weald Clay	80	38
28	Weald Clay	67.5	38

3.4.3 Test Procedure and Conditions

3.4.3.1 Basic Procedure

All tests were carried out as undrained, thus providing a closed system for purposes of analysis. The basic test procedure was to place a specimen in the assembled permode, apply the vertical stress and then induce cycles of freezing and thawing. The datalogger recorded readings of temperature, pore water pressure response and vertical displacement. After a varying number of freeze-thaw cycles, the specimen was left under the applied stress for a time to allow temperatures to stabilise. The apparatus was then dismantled, and the top and base moisture contents determined.

3.4.3.2 Temperature Control

The changing procedures are illustrated in Table 3.10 below.

Table 3.10 - Temperature Control

Test No./ Procedure No.	1	2	3	4	5	6	7	8	9	10	11	12	13	14	15	→ 28
1.	■	■	■	■	■	■	■	■	■	■						
2.	▒	▒									▒	▒	▒	▒	▒	▒
3.			■	■	■	■	■	■	■	■						
4.	▒	▒	▒	▒	▒	▒	▒	▒	▒	▒	▒	▒	▒			
5.														■	■	■

1. The specimen was frozen from both ends.
2. The thaw cycle was achieved by stopping the freezing action.
3. Warm water was circulated for part of the thawing cycle in order to increase the rate of thaw.
4. Cycles of temperature change took place over the range of room temperature - freezing.
5. Cycles of temperature change took place over the range of just thawed - just frozen.

The original method of freezing the specimen from both ends was discarded as not being of interest to the test programme. Instead, the specimens were all frozen from the top down with the exception of Tests 22-23 where specimens were frozen from the base upwards as a test of the experimental set-up.

The initial freezing from both ends meant that the specimen took a long time to thaw naturally. This led to the introduction of the circulation of warm water from the top downwards, (Test 3), and later from both ends, (Tests 4-10), for all or part of a thawing stage. This was also discarded, however, as it led to undesirable effects such as soil overheating.

The initial temperature range of +20°C to -20°C was found to be unlikely and impracticable, and was replaced by the 'just thawed/frozen' range of +5°C to -5°C (approximately). The eventual pattern was to freeze from the top down for 10 hours, and allow to thaw naturally for 14 hours. The length of the thaw period was found through

experimentation as being the amount of time required for the specimen to reach its' starting temperature of the previous cycle.

3.4.3.3 Test Environment

The changing conditions are illustrated in Table 3.11 below.

Table 3.11 - Test Environment

Test No./ Condition No.	1	2	3	4	5	6	7	8	9	10	11	12	13	14	15	→ 28
1.	■	■	■	■	■	■	■	■	■	■						
2.											■	■	■			
3.														■	■	■

1.The permode stood at room temperature

2. The permode stood in a polystyrene insulated box

3. The permode stood inside a refrigerator

With the permode standing at room temperature, it proved impossible to operate over the desired temperature range of +5°C to -5°C. Attempts were therefore made to provide insulation to the permode apparatus as described in Section 3.2.6.4. The refrigerator proved successful.

3.4.3.4 Permode Apparatus and Instrumentation

The varying modifications are illustrated in Table 3.12 below.

Table 3.12 - Permode Apparatus and Instrumentation

Test No./ Mod. No.	1	2	3	4	5	6	7	8	9	10	11	12	13	14	15	→ 28
1.				■	■	■	■	■	■	■	■	■	■			
2.														▒	▒	▒
3.								■	■	■	■	■	■	■	■	■
4.								▒	▒	▒	▒	▒	▒	▒	▒	▒
5.				■	■	■	■	■	■	■	■	■	■	■	■	■
6.				▒	▒	▒	▒	▒	▒	▒	▒	▒	▒	▒	▒	▒
7.														■	■	■

1. 100 mm diameter membranes used.
2. Stretch membrane and special holding piece used.
3. One-piece liner used.
4. Base o-rings used.
5. Top pressure transducer used.
6. De-airing blocks used at base.
7. Antifreeze solution and pressure transducer system judged to be fully functional.

The technical advances listed above are described in Section 3.2.5.

3.4.3.5 Definitive Procedure (Tests 14-28)

All tests were carried out undrained. A saturated, frozen specimen was put into a stretched membrane and attached to the piston. The porous plate inside the piston was saturated in a 50% antifreeze solution. This allowed pore water pressures to be recorded throughout the freezing stage without damage to the instrumentation. Filter paper was placed over the plate. This assembly was placed in the de-aired permode (with similar plate and filter paper arrangement) and transferred to the refrigerator.

Instrumentation leads passed through the refrigerator walls and into the appropriate ports in the permode. An initial stress was applied in order to draw down the piston and to allow the upper pressure transducer connector line to be filled. After this the transducer was

attached by a split-thread joint. The initial stress was then removed, and the whole assembly left in the refrigerator to stabilise temperature. After 2 hours, the ambient temperature around the permode and specimen was at 5-8°C. The metal clamp studs became quite cold by this time, and expanded away from the PVC barrel. The clamp nuts were therefore re-tightened to maintain the base o-ring seal. At this stage, vertical stress was applied, and cycles of freezing and thawing induced.

The datalogger recorded readings of temperature, pore water pressure response and vertical displacement at 10 minute intervals. These readings, together with ambient refrigerator temperature, were printed once per minute for the first 10 minutes of testing, and then once every 4 hours. After a varying number of freeze-thaw cycles, (dependent on whether pore water pressure was continuing to increase), the specimen was left under the applied stress for a time to allow temperatures to stabilise. The apparatus was then dismantled, and the top and base moisture contents determined.

Chapter 4 – Presentation of Results – Tests 1-13

4.1 Summary of Results for Tests 1-13

A summarised set of results is not provided within the chapter for every test, but is available in Appendix D. Table 4.1 contains summary results for Tests 1-13, which were all carried out on Lias Clay. Each test is discussed below.

Table 4.1 – Summary of Results for Tests 1-13, All on Lias Clay

Test No.	σ (kPa)	m.c. (%)	Length of Test (hrs)	No. of Cycles	No. of Rest Phases	Max. PWP (kPa)		Min. PWP (kPa)	
						Top	Base	Top	Base
1	29	29	237.70	7	1	N/A	10.25	N/A	-5.76
2	104	32	362.33	11	2	N/A	8.80	N/A	-10.22
3	104	30	95.83	8	4	N/A	2.03	N/A	-7.80
4	104	32	72.50	6	3	82.78	51.25	0.55	-8.40
5	104	30	254.17	12	7	90.53	61.25	1.65	-1.22
6	104	35	144.00	8	5	118.95	96.22	1.44	0.03
7	104	33	210.83	4	5	110.86	106.2	1.65	0.02
8	80	30	309.33	7	7	117.26	114.34	0.67	0.08
9	104	29	190.82	4	5	38.21	78.81	-0.33	0.03
10	80	32	230.50	4	5	68.72	71.23	-2.90	0.06
11	80	31	160.67	4	5	87.54	129.22	1.66	0.05
12	80	30	139.82	4	5	88.16	112.3	1.65	0.04
13	80	32	494.33	12	3	88.68	95.23	-6.29	0.04

4.2 Individual Test Results

4.2.1 Test 1

Test 1 was carried out on Lias clay, of moisture content 29%, under an applied stress of 29 kPa.

The soil was placed directly into the permode, without being pre-frozen. Further details of apparatus and procedure development are given in Chapter 3, so will not be reiterated in full at this stage.

Temperature cycles comprised 5.5 hours freezing, (from both ends of the specimen), and 18.5 hours thawing (not assisted by warm water circulation). The permode stood in a normal temperature room, and the general temperature range achieved was from 18°C

to -12°C. The test comprised 7 freeze-thaw cycles and one 'rest' phase between the third and fourth cycles. Due to a power interruption, the disk recording device failed after time 190.90 hours. An auxiliary system continued to record data to printout, but at 1 hour intervals only.

Figure 4.1 shows summarised results, depicting high and low points of recorded pore water pressures. The maximum pore water pressure recorded was 10.25 kPa, at time 190.90 hours. This coincides with the start of freeze-thaw Cycle 6. The minimum value of pore water pressure recorded was –5.76 kPa, at time 31.83 hours, which coincided with the point in Cycle 2 where the average temperature thawed past 0°C. The average temperature was calculated from thermocouples situated at certain depths down the side of the barrel. These depths coincide with sample depths only at the start of the tests, prior to heaving/settlement occurring. Figure 4.2 gives the individual temperature profiles for each thermocouple during Cycle 1.

Examining the graphs in Figure 4.1 in more detail, the induced regime of freeze-thaw cycles are shown to have taken place by the rise and fall of the specimen average temperature. As the temperature drops below zero, the specimen starts to freeze and expands upwards (in the only possible direction of movement). This expansion can be seen in the displacement plot. On subsequent thawing, the specimen contracts, to a smaller volume than at the start of cycle each successive time. As the test models a 'closed system', where no drainage is permitted, no net change in volume would be anticipated. However, the permanent downwards displacement recorded indicates that leakage has occurred.

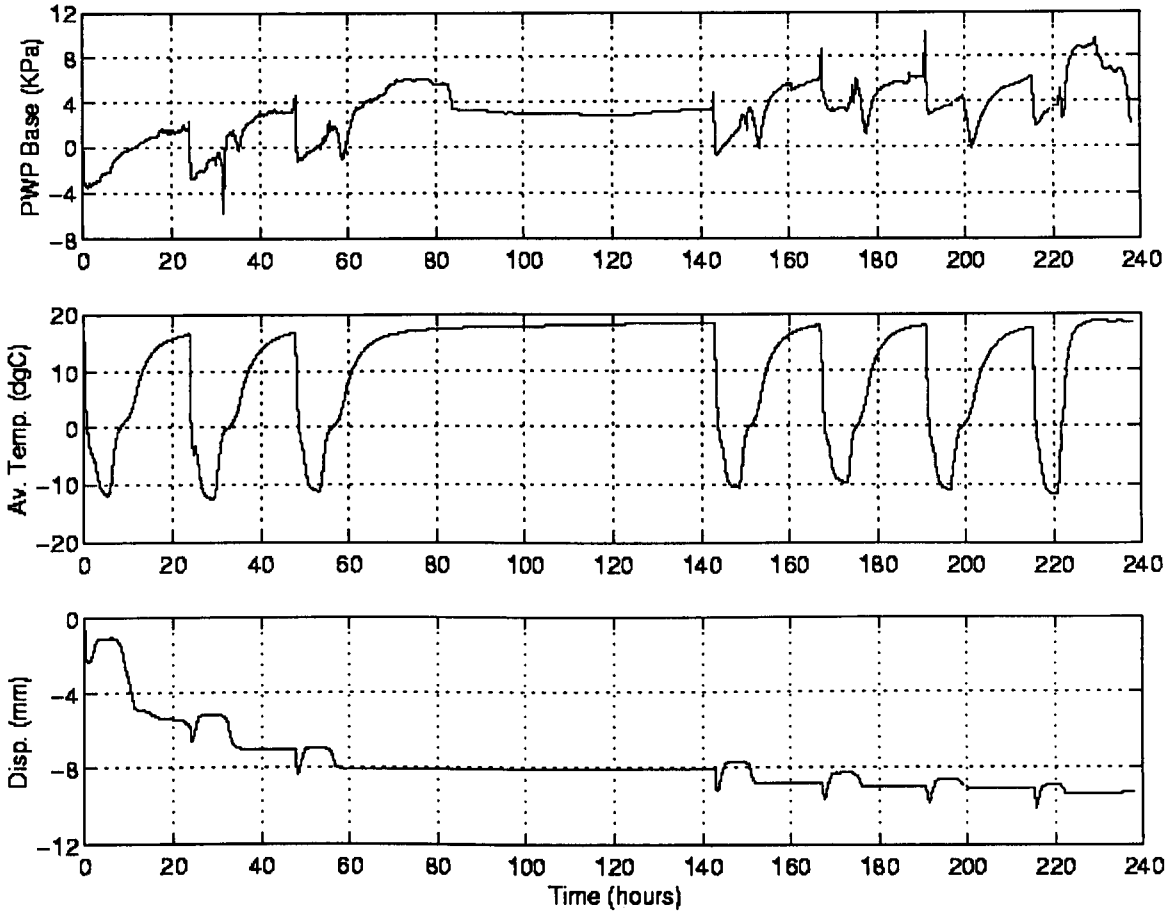

Figure 4.1 – Results for Test 1

Table 4.2 - Values of Pore Water Pressure Recorded at End of Cycle – Test 1

Cycle number:	Pore water Pressure (kPa)
1	1.66
2	3.34
3	5.88
4	6.30
5	6.16
6	6.28
7	6.87

It can be seen from the tabular results that the value of pore water pressure recorded at the end of each freeze-thaw cycle increases up until Cycle 4, after which a consistent value of around 6 kPa is returned at the end of each cycle. The graphical results in Figure 4.1 show that the maximum value gained in the test is a spiked increase from the surrounding values. Upward spikes were experienced at the onset of freezing in the majority of cycles.

As well as the upward spikes, downward spikes were also seen. In some cases these appeared to follow a pattern, happening in each cycle where average temperature was found to be crossing the 0°C threshold. However, other spikes were judged to be the result of sudden, 'breakthrough' leakage. This type of leakage was observed particularly in the thaw stage, as ice had previously formed a seal around the base for the freezing period.

Although the test was intended to be undrained, leakage occurred as discussed above, and demonstrated by the decrease in volume of the sample during the test. Measures to prevent leakage have been discussed previously in Section 3.2.5.1. The change in volume may also be attributed to other factors, which are discussed in Chapter 5.

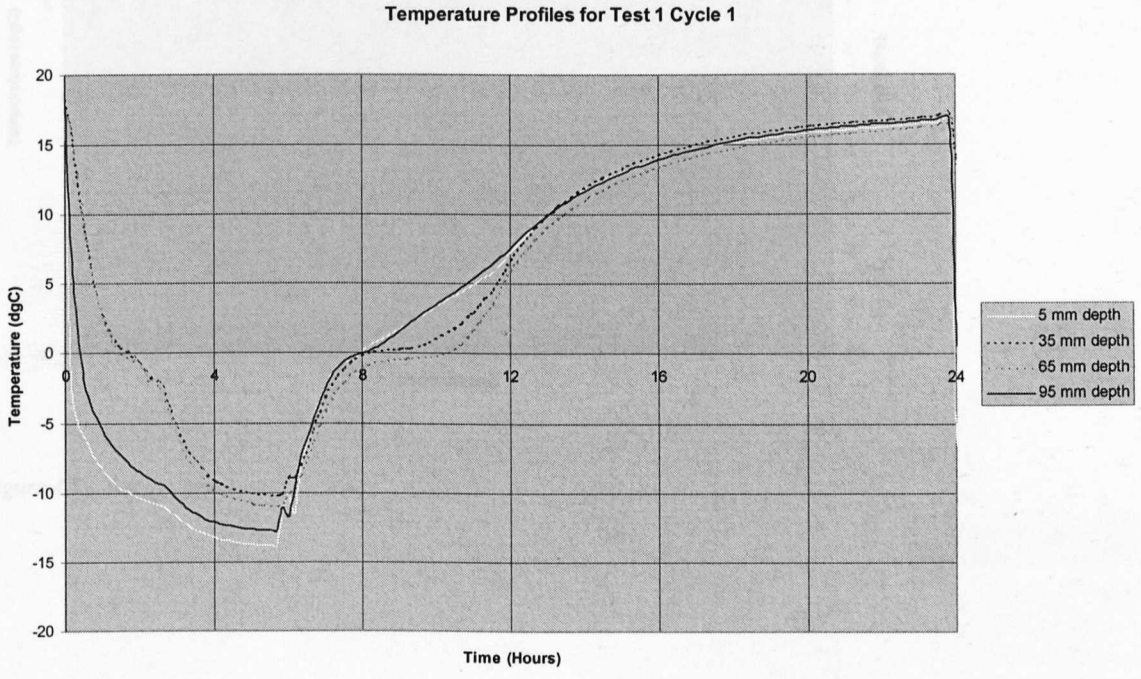

Figure 4.2 – Temperature Profiles for Test 1 Cycle 1

Figures 4.3-4.6 show in more detail the pore water pressure response recorded at the base of the specimen – PWP Base – plotted with the corresponding temperature at 95mm depth. Cycle 1 shows PWP Base dropping on freezing initially and then slowly increasing. Cycles 2, 5 and 6 show an initial drop followed by a steady increase as for Cycle 1, but then the response demonstrates the spiking behaviour noted above. The spike can be clearly seen to occur as the temperature approaches the 0°C threshold, thus improving on the data presented by the average temperature track in Figure 4.1. From this point forward, the average temperature can be considered as an *indicator* only of the temperature regime imposed for the purposes of giving summarised results.

Following the spike, the pore water pressure increases until the end of the temperatures representing the phase change period, (of ice to water within the soil), where a decrease in pore water pressure occurs, immediately followed by a convex curve increase.

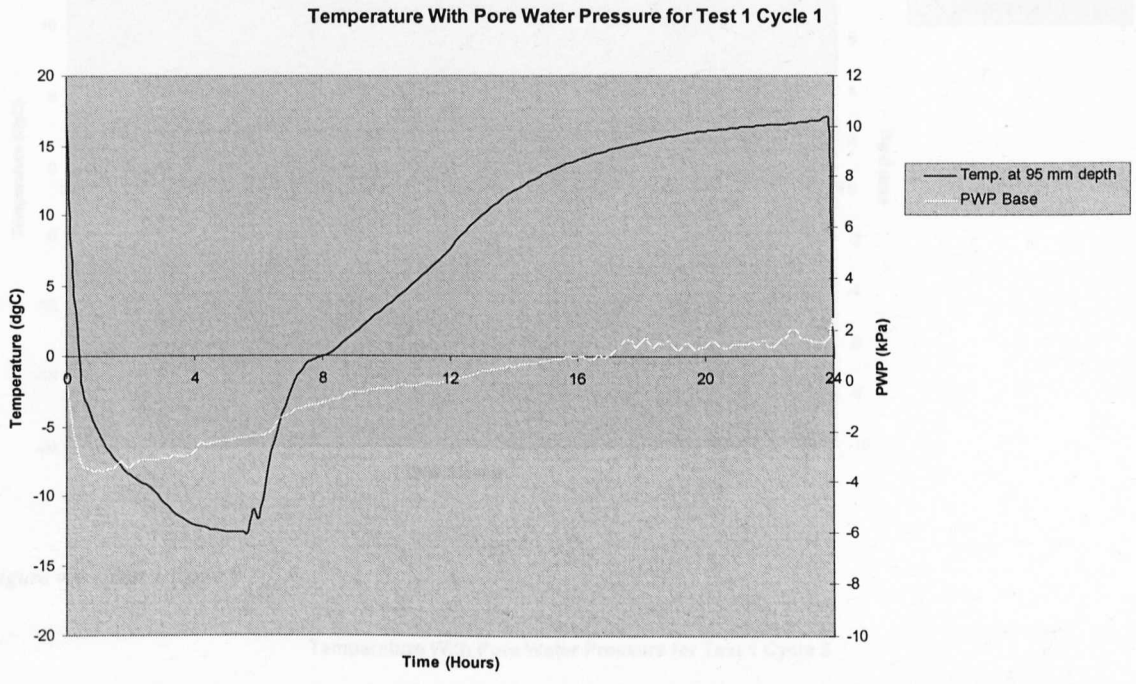

Figure 4.3 - Test 1 Cycle 1

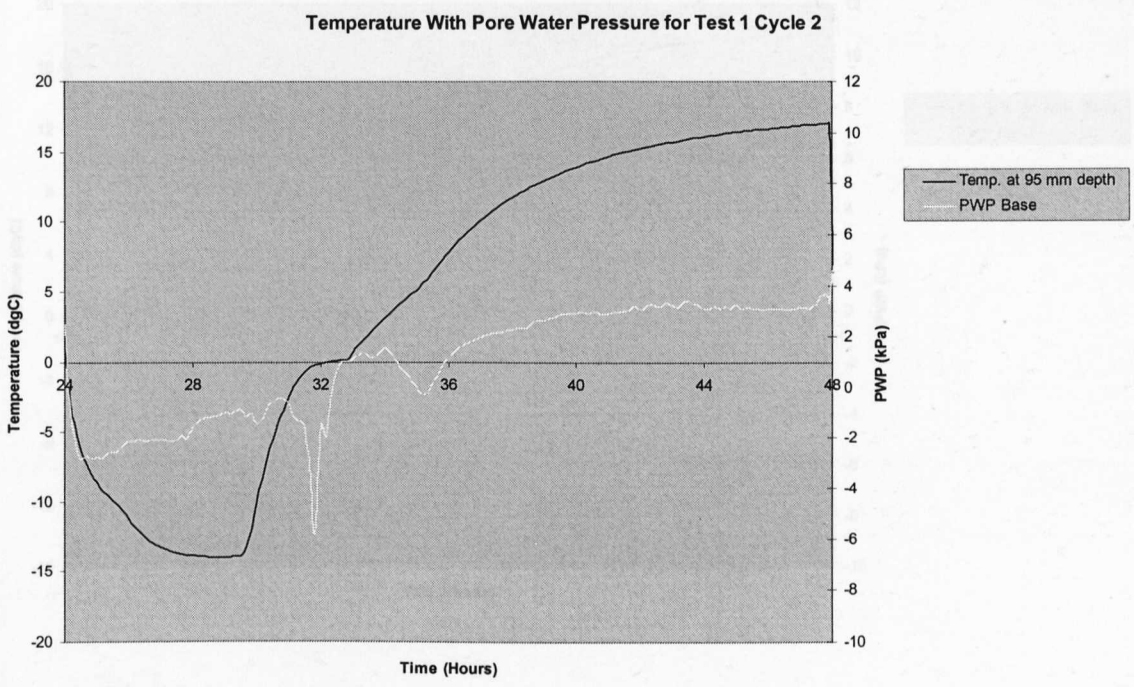

Figure 4.4 - Test 1 Cycle 2

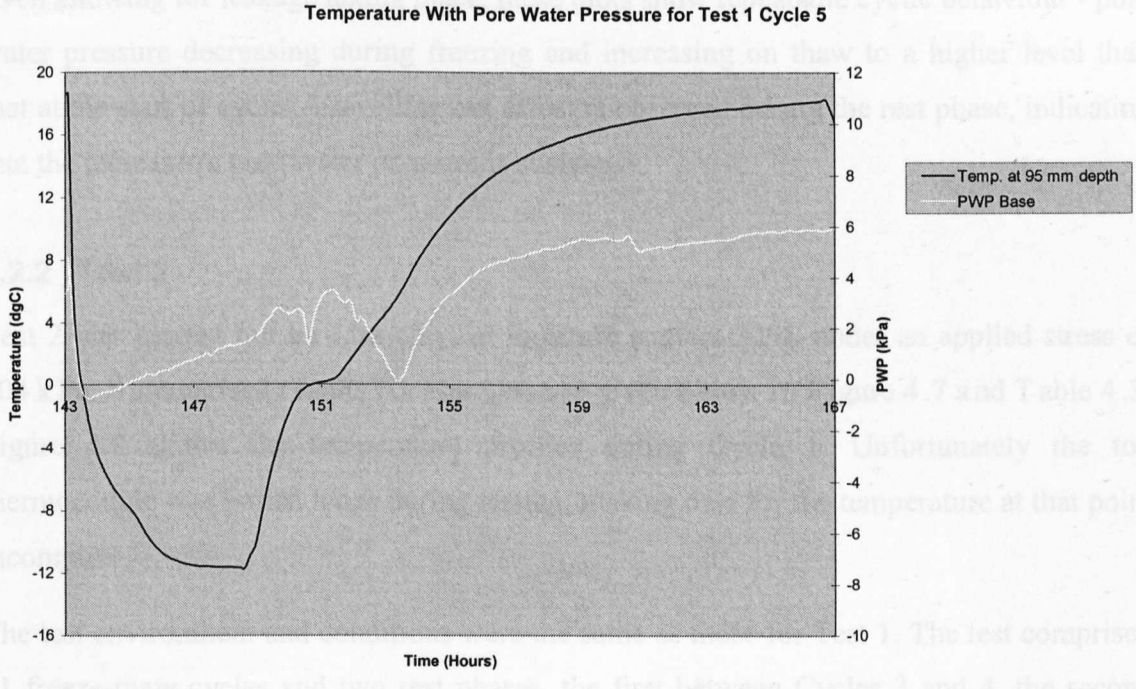

Figure 4.5 - Test 1 Cycle 5

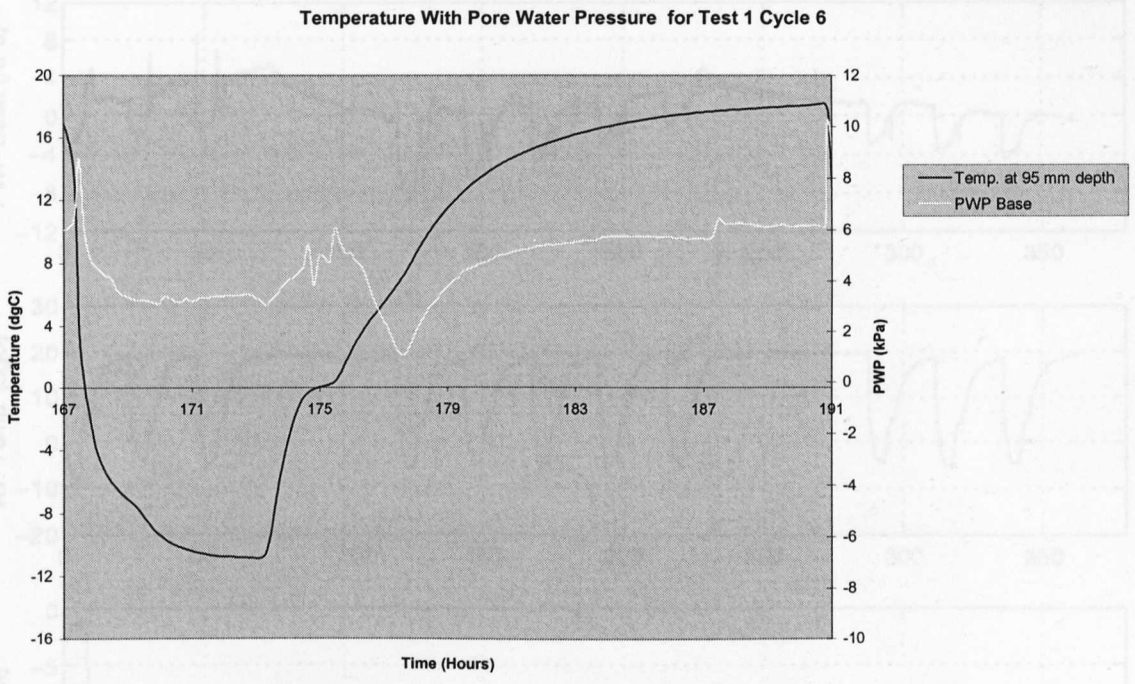

Figure 4.6 - Test 1 Cycle 6

Even allowing for leakage taking place, these plots show repeatable cyclic behaviour - pore water pressure decreasing during freezing and increasing on thaw to a higher level than that at the start of cycle. A levelling out effect is observed during the rest phase, indicating that the increase in pore water pressure is sustained.

4.2.2 Test 2

Test 2 was carried out on Lias clay, of moisture content 32%, under an applied stress of 104 kPa. Summarised results for this test are given below in Figure 4.7 and Table 4.3. Figure 4.8 shows the temperature profiles during Cycle 1. Unfortunately the top thermocouple was pulled loose during testing, making data for the temperature at that point incomplete.

The test environment and conditions were the same as those for Test 1. The test comprised 11 freeze-thaw cycles and two rest phases, the first between Cycles 3 and 4, the second between Cycles 8 and 9.

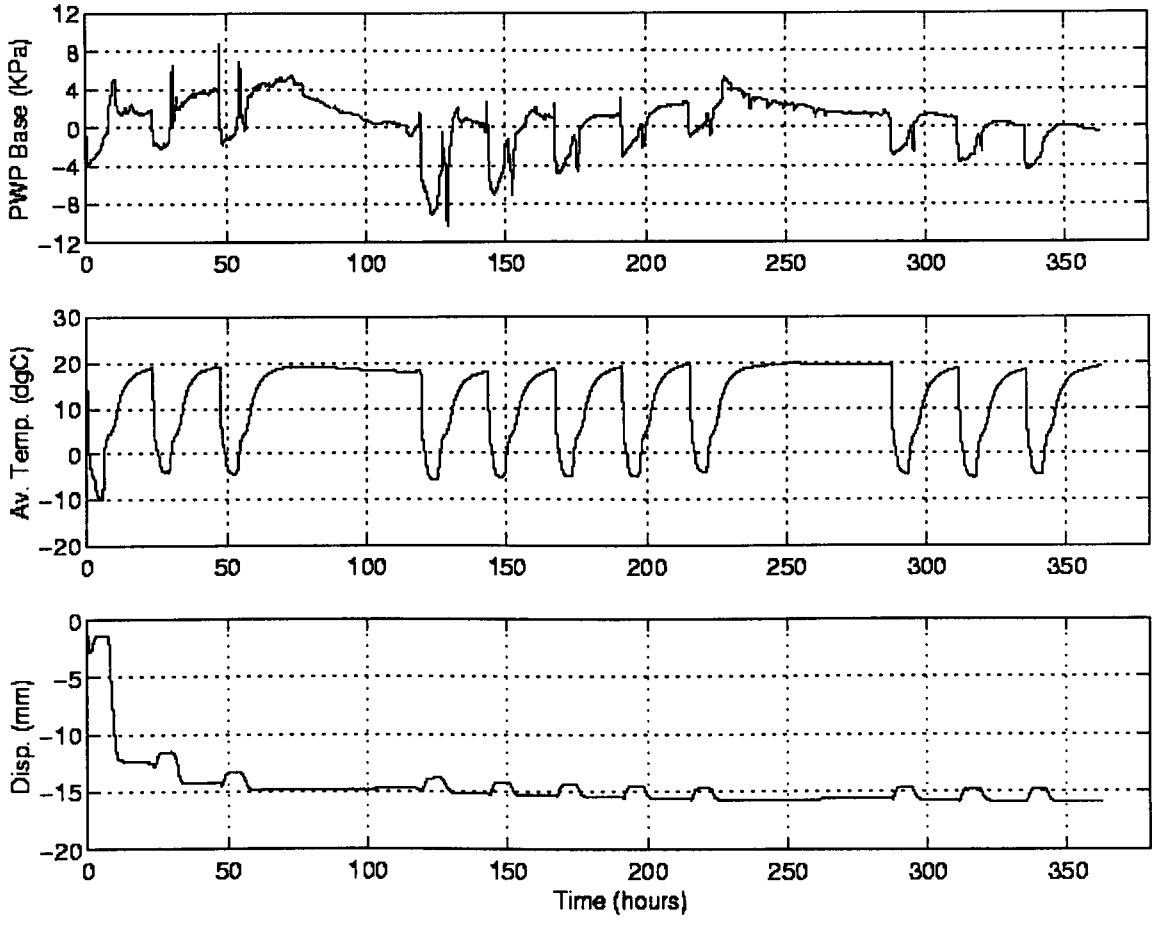

Figure 4.7 – Results for Test 2

Table 4.3 - Values of Pore Water Pressure Recorded at End of Cycle – Test 2

Cycle number:	Pore Water Pressure (kPa)
1	1.65
2	3.74
3	4.85
4	1.40
5	1.05
6	2.96
7	2.22
8	2.69
9	0.65
10	0.07
11	-0.36

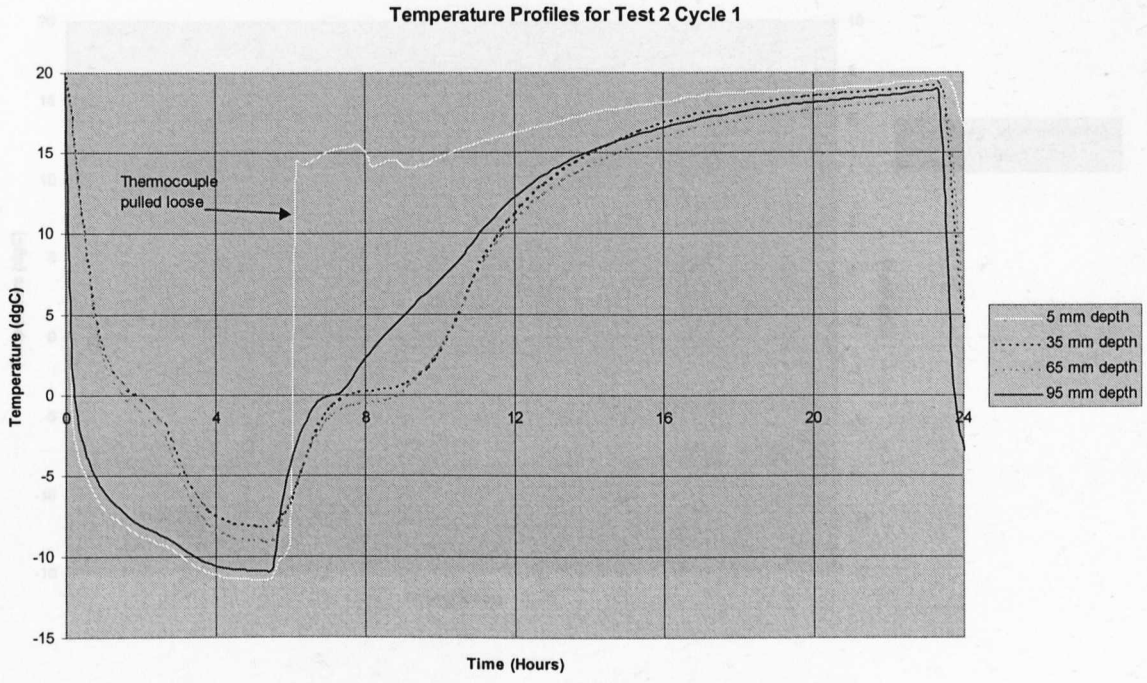

Figure 4.8 – Temperature Profiles for Test 2 Cycle 1

A drop in pore water pressure was experienced during both rest phases, (during which time average temperature was fairly level), due to leakage. This leakage effect was judged to be of a seeping nature, eventually lowering the pore water pressures to very low levels. After dismantlement of the apparatus at the end of the test, the final moisture content was found to be 22%, showing a loss of 10% of the specimen's water through leakage. However, some increase in pore water pressure values was recorded from end of Cycles 1 to 3, and also from Cycles 4 to 8.

Figures 4.9-4.12 show pore water pressure response and corresponding temperature with time for Cycles 1, 3, 4 and 8.

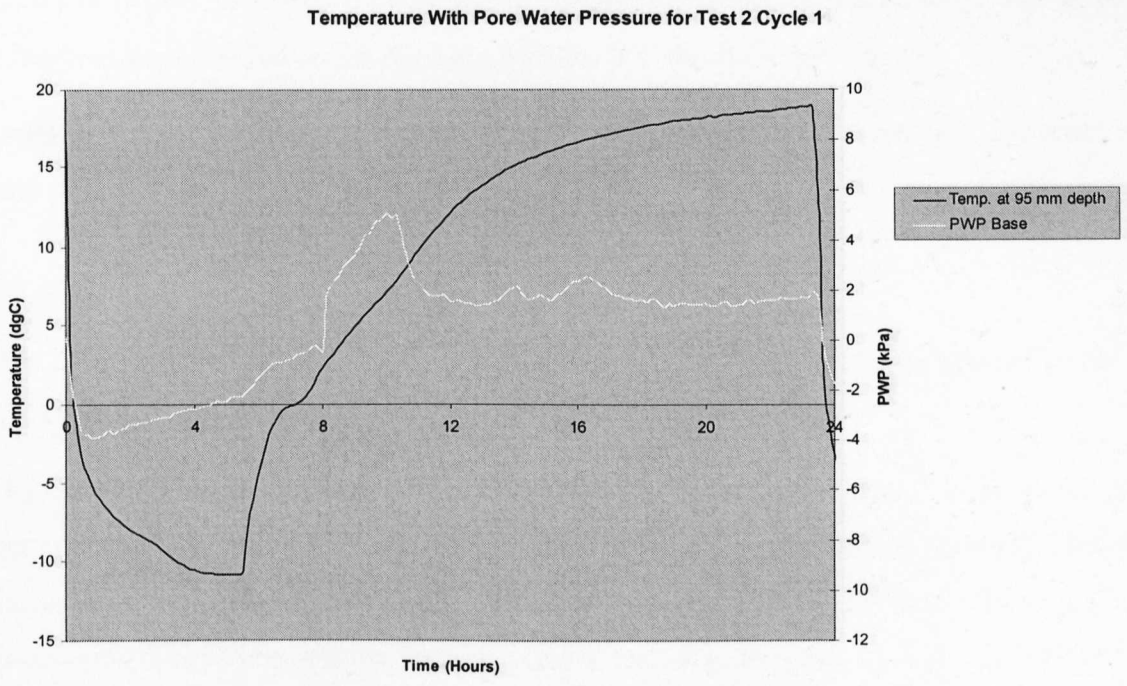

Figure 4.9 – Test 2 Cycle 2

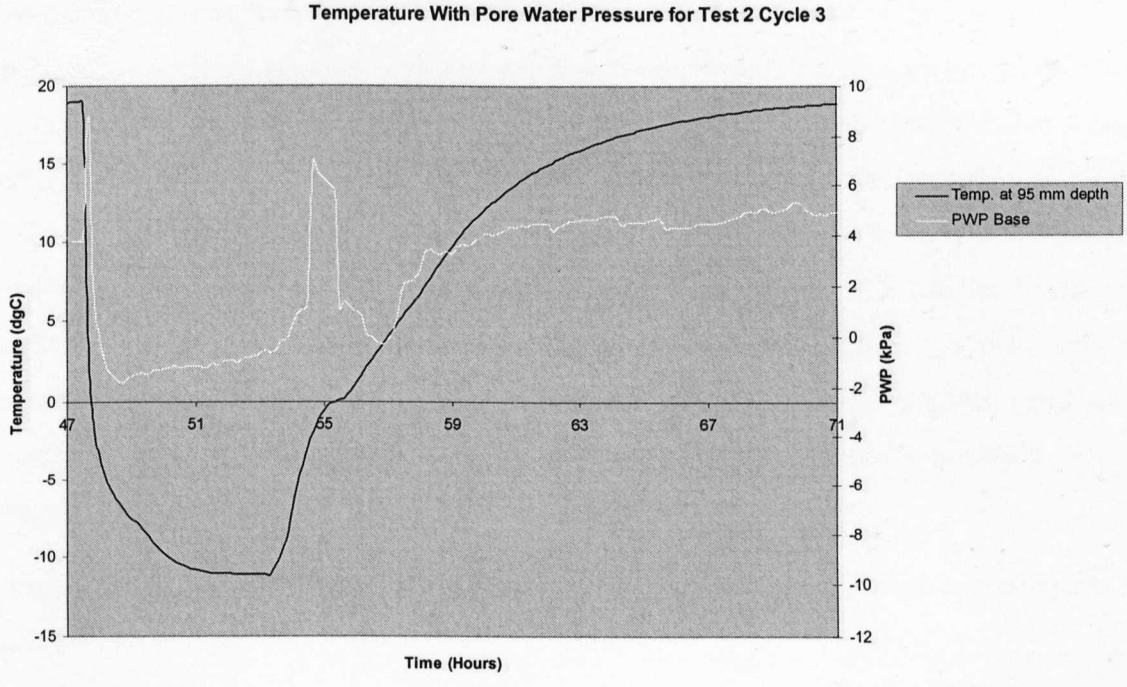

Figure 4.10 – Test 2 Cycle 3

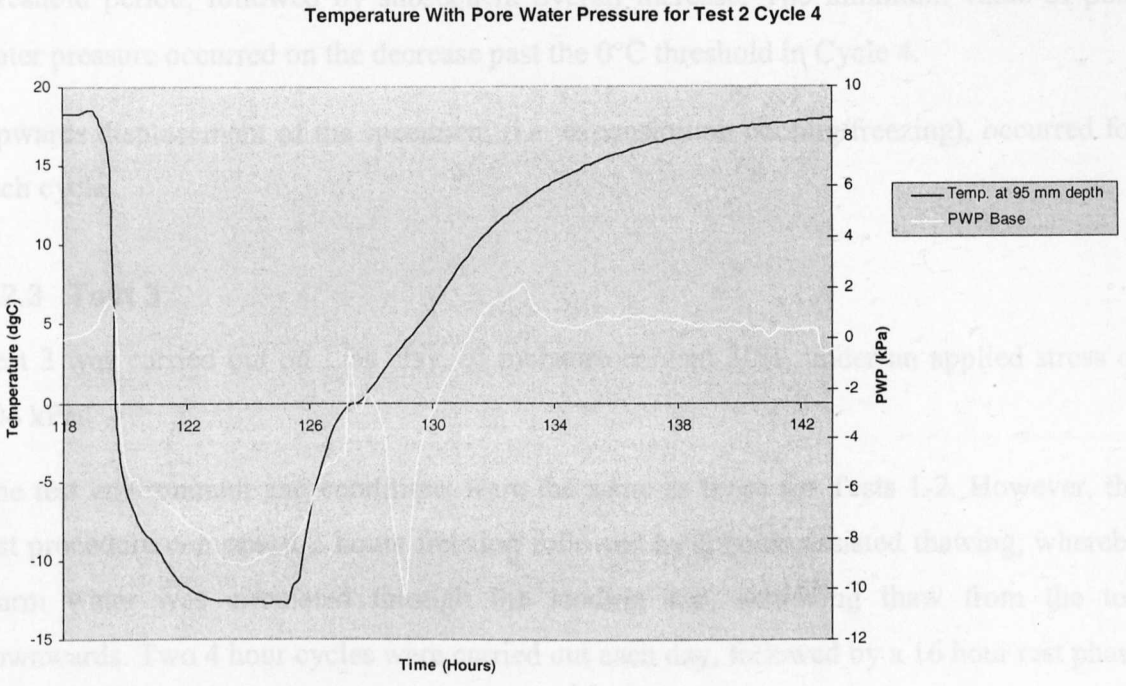

Figure 4.11 – Test 2 Cycle 4

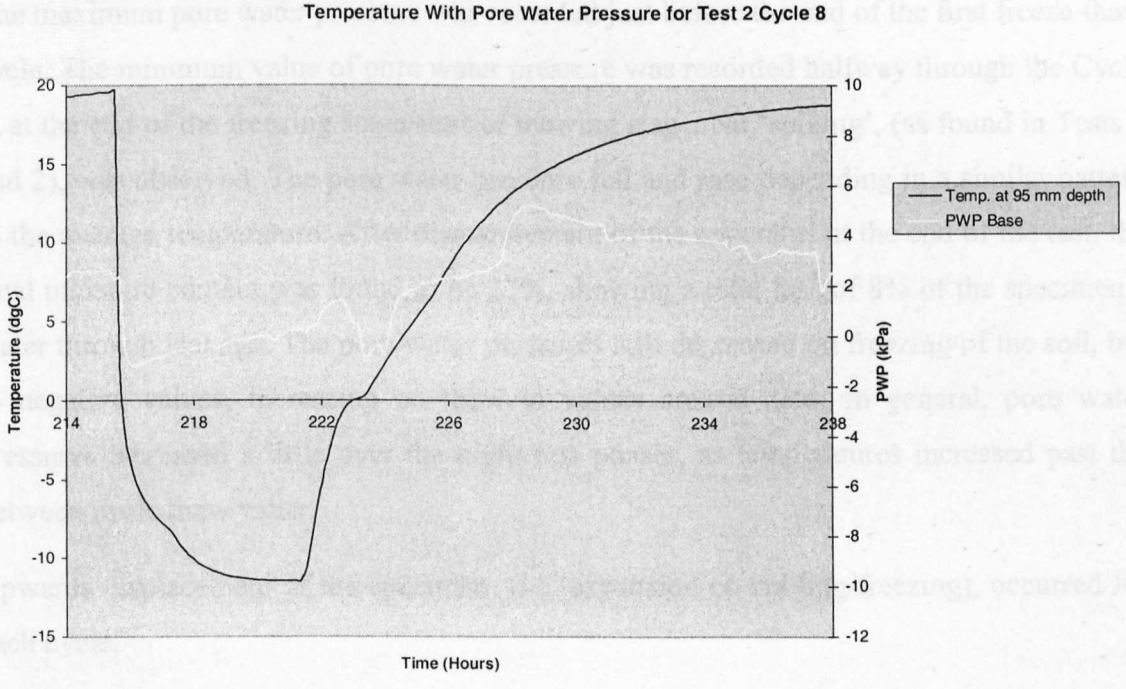

Figure 4.12 – Test 2 Cycle 8

The maximum value of pore water pressure recorded occurred at a spike at the beginning of Cycle 3, just as a freezing stage began. However, this sharp increase at the start of the freezing period was atypical. Apart from this peak, the pore water pressure generally followed a similar pattern to that in Test 1, i.e. increasing and decreasing during the 0°C

threshold period, followed by subsequent overall increase. The minimum value of pore water pressure occurred on the decrease past the 0°C threshold in Cycle 4.

Upwards displacement of the specimen, (i.e. expansion on cooling/freezing), occurred for each cycle.

4.2.3 Test 3

Test 3 was carried out on Lias clay, of moisture content 30%, under an applied stress of 104 kPa.

The test environment and conditions were the same as those for Tests 1-2. However, the test procedure comprised 2 hours freezing followed by 2 hours assisted thawing, whereby warm water was circulated through the loading cap, achieving thaw from the top downwards. Two 4 hour cycles were carried out each day, followed by a 16 hour rest phase whereby the permode returned to room temperature. The test comprised 8 freeze-thaw cycles and 4 rest phases, one after every 2 cycles.

The maximum pore water pressure was recorded just before the end of the first freeze-thaw cycle. The minimum value of pore water pressure was recorded halfway through the Cycle 7, at the end of the freezing stage/start of thawing stage. No 'spiking', (as found in Tests 1 and 2), was observed. The pore water pressure fell and rose depending in a similar pattern to the average temperature. After dismantlement of the apparatus at the end of the test, the final moisture content was found to be 22%, showing a total loss of 8% of the specimen's water through leakage. The pore water pressures still decreased on freezing of the soil, but to negative values, increasing on thaw to values around zero. In general, pore water pressures increased a little over the night rest phases, as temperatures increased past the between cycle thaw value.

Upwards displacement of the specimen, (i.e. expansion on cooling/freezing), occurred for each cycle.

4.2.4 Test 4

Test 4 was carried out on Lias clay, of moisture content 32%, under an applied stress of 104 kPa. Summarised results for this test are shown below in Figure 4.13.

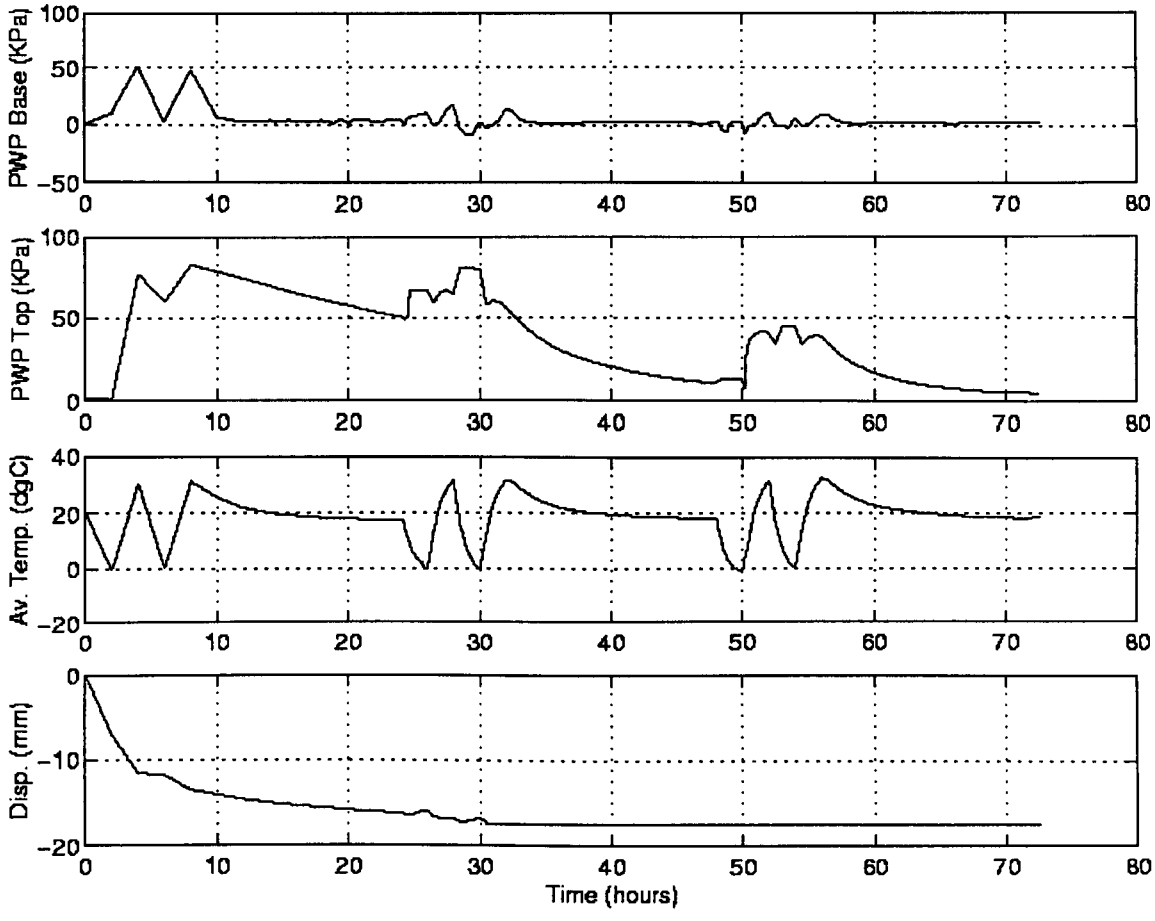

Figure 4.13 – Results for Test 4

The test environment and procedure were the same as for Test 3, except for three major differences.

1. Assisted thaw took place from both ends of the specimen.
2. A pressure transducer was installed at the top of the specimen as well as at the base.
3. The specimen was prepared by placing soil in a membrane held over a 100mm length mould, before placement in the permode.

The test comprised 6 freeze-thaw cycles and 3 rest phases. Figures 4.14 and 4.15 show temperature profiles generated under the changed thermal regime. Only the 95 mm thermocouple registered temperatures below 0°C, and then only for just over 1 hour. Therefore, temperature control difficulties were clearly demonstrated, as no overall freezing was achieved, and the specimen was subjected to overheating on thaw. The overnight rest phases started with a period of cooling down to room temperature conditions.

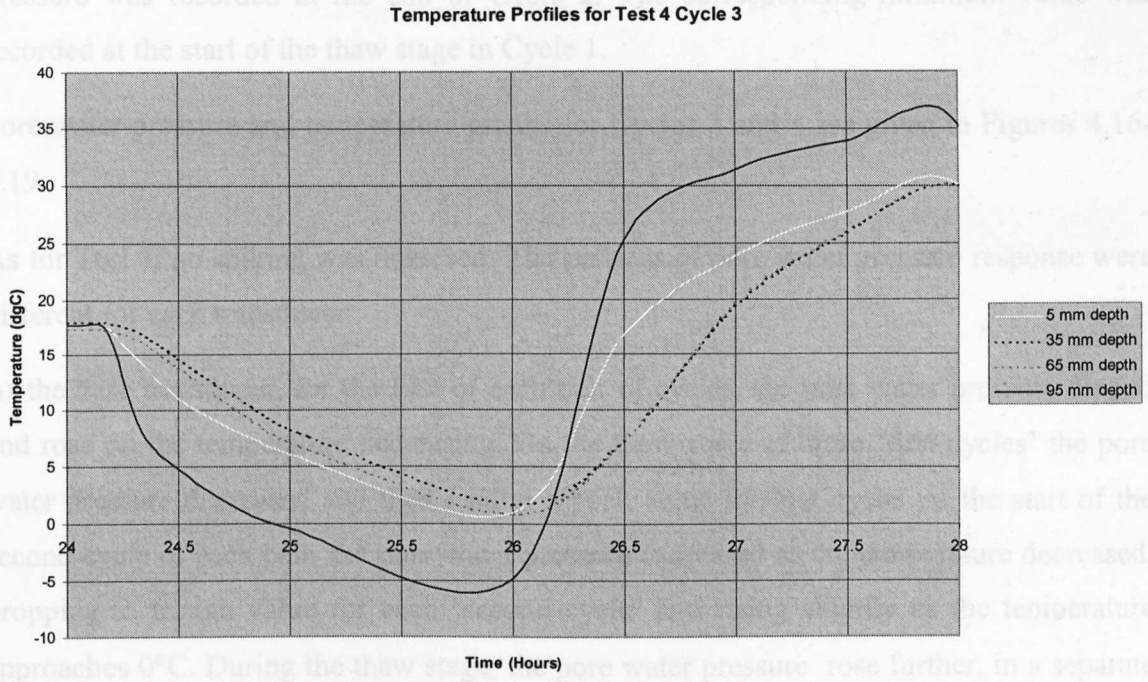

Figure 4.14 – Temperature Profiles for Test 4 Cycle 3

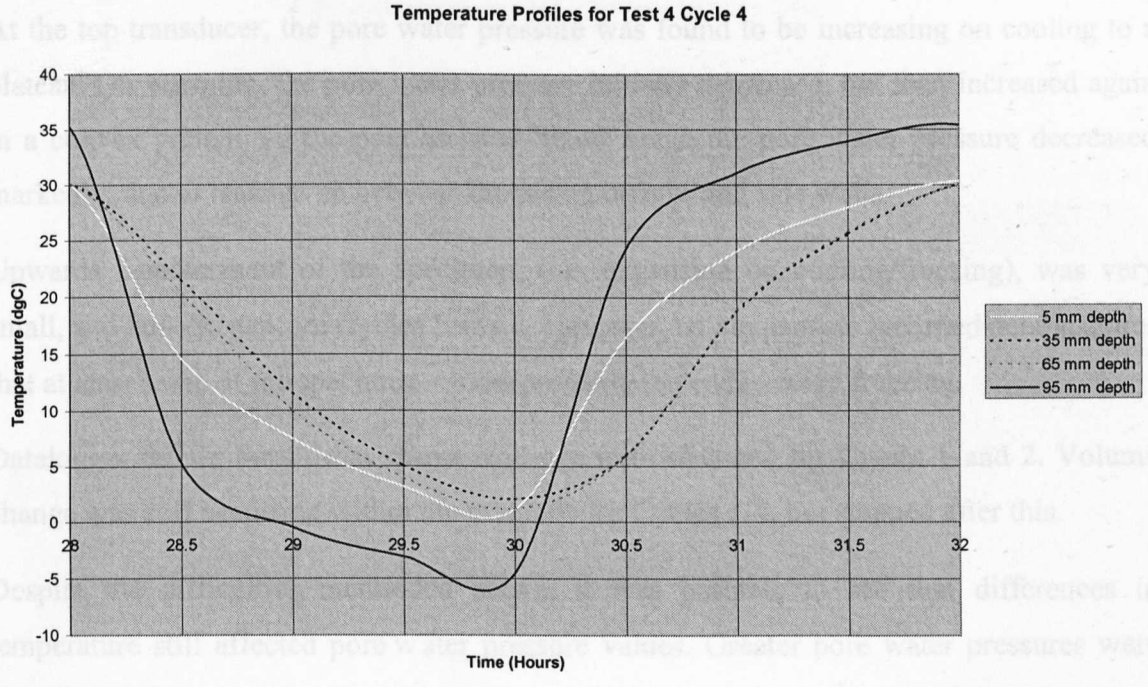

Figure 4.15– Temperature Profiles for Test 4 Cycle 4

At the base of the specimen, the maximum pore water pressure was recorded at the end of the first freeze-thaw cycle. The corresponding minimum value was recorded just after the start of the thaw stage in Cycle 5. At the top of the specimen, the maximum pore water

pressure was recorded at the end of Cycle 2. The corresponding minimum value was recorded at the start of the thaw stage in Cycle 1.

Pore water pressure and temperature graphs for Cycles 3 and 4 are given in Figures 4.16-4.19.

As for Test 3, no spiking was observed. The patterns of pore water pressure response were different for each transducer.

At the base transducer, for the first of each pair of cycles, the pore water pressure dipped and rose on the temperature decreasing. On the thaw stage of these 'first cycles' the pore water pressure decreased and then rose to a peak value for that cycle. At the start of the second cycle of each pair, the pore water pressure decreased as the temperature decreased, dropping to trough value for each 'second cycle' and rising slightly as the temperature approaches 0°C. During the thaw stage, the pore water pressure rose further, in a separate concave loop to the previous increase. In the post assisted thaw stage, (i.e. overnight), the pore water pressure settled to a steady residual level.

At the top transducer, the pore water pressure was found to be increasing on cooling to a plateau. On warming, the pore water pressure initially decreased, but then increased again in a convex pattern. In the post assisted 'thaw' stage the pore water pressure decreased markedly, due to leakage up between the piston o-rings and side walls.

Upwards displacement of the specimen, (i.e. expansion on cooling/freezing), was very small, and non-existent for Cycles 5 and 6. However, any expansion recorded demonstrates that at least some of the specimen – most probably the ends – were freezing.

Datalogger failure meant that sparse readings were obtained for Cycles 1 and 2. Volume change was still occurring within the permode for Cycles 1-4, but stopped after this.

Despite the difficulties mentioned above, it was possible to see that differences in temperature still affected pore water pressure values. Greater pore water pressures were recorded at the top pressure transducer than at the base.

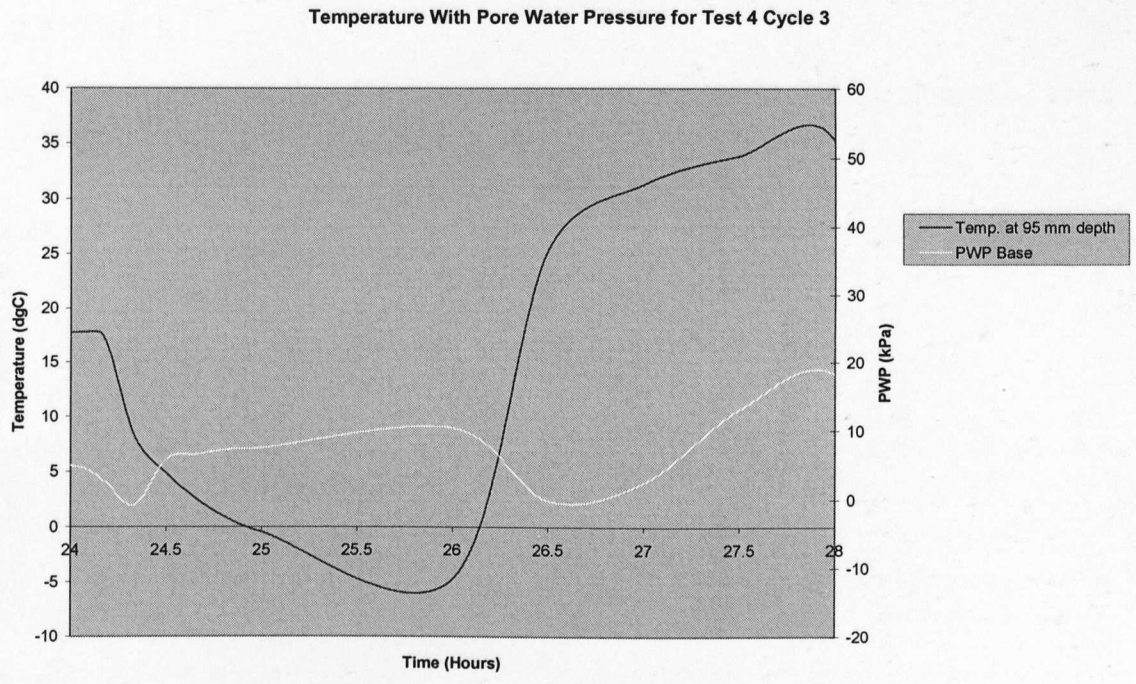

Figure 4.16 – Test 4 Cycle 3 Base

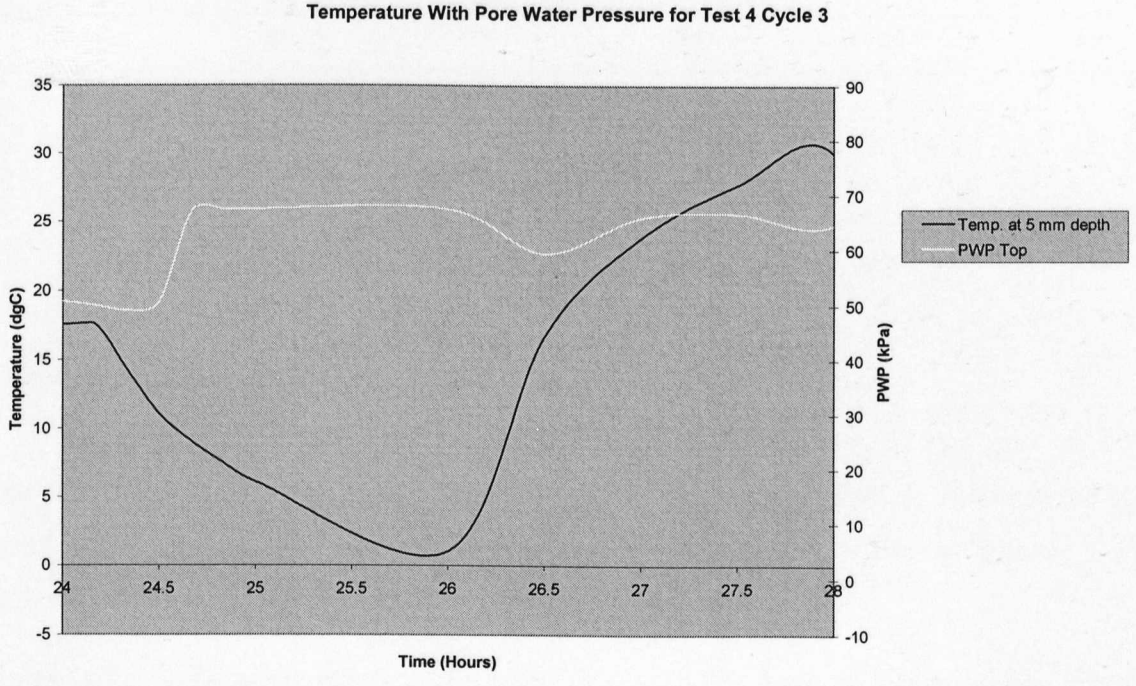

Figure 4.17 – Test 4 Cycle 3 Top

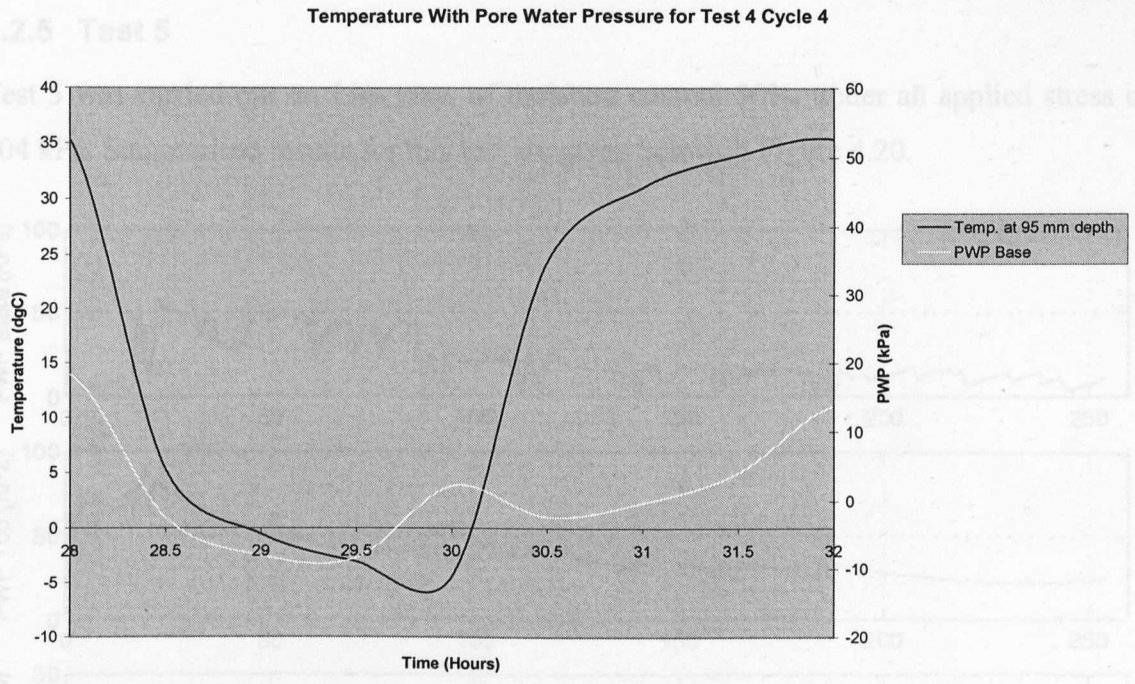

Figure 4.18 – Test 4 Cycle 4 Base

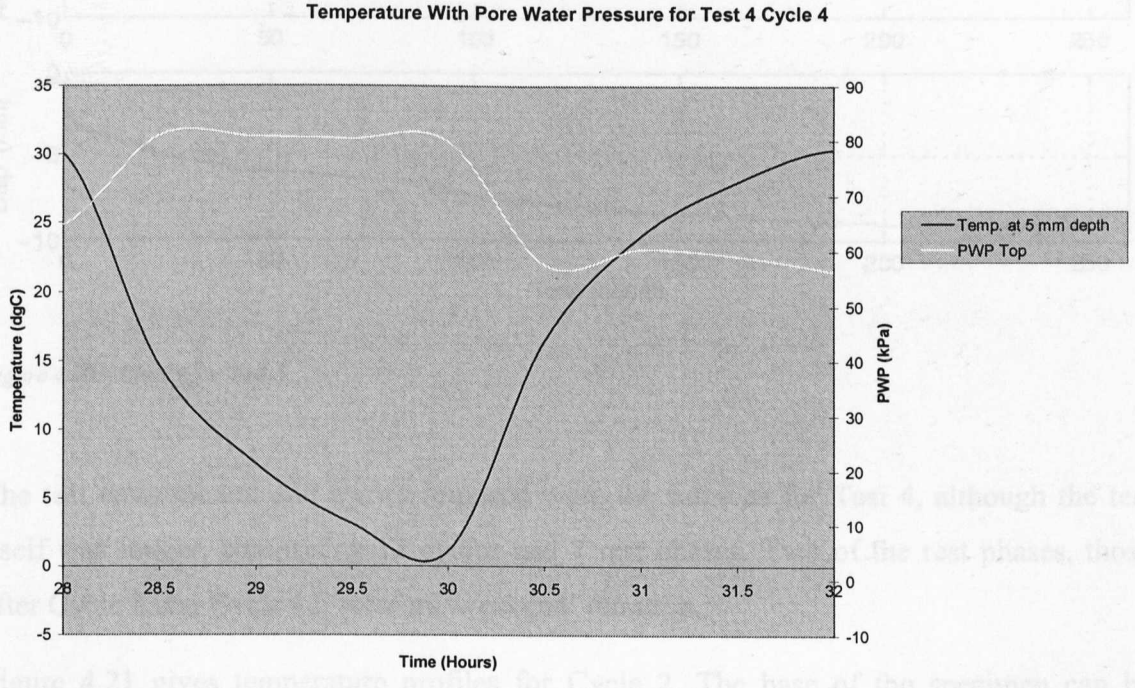

Figure 4.19 – Test 4 Cycle 4 Top

4.2.5 Test 5

Test 5 was carried out on Lias clay, of moisture content 30%, under an applied stress of 104 kPa. Summarised results for this test are given below in Figure 4.20.

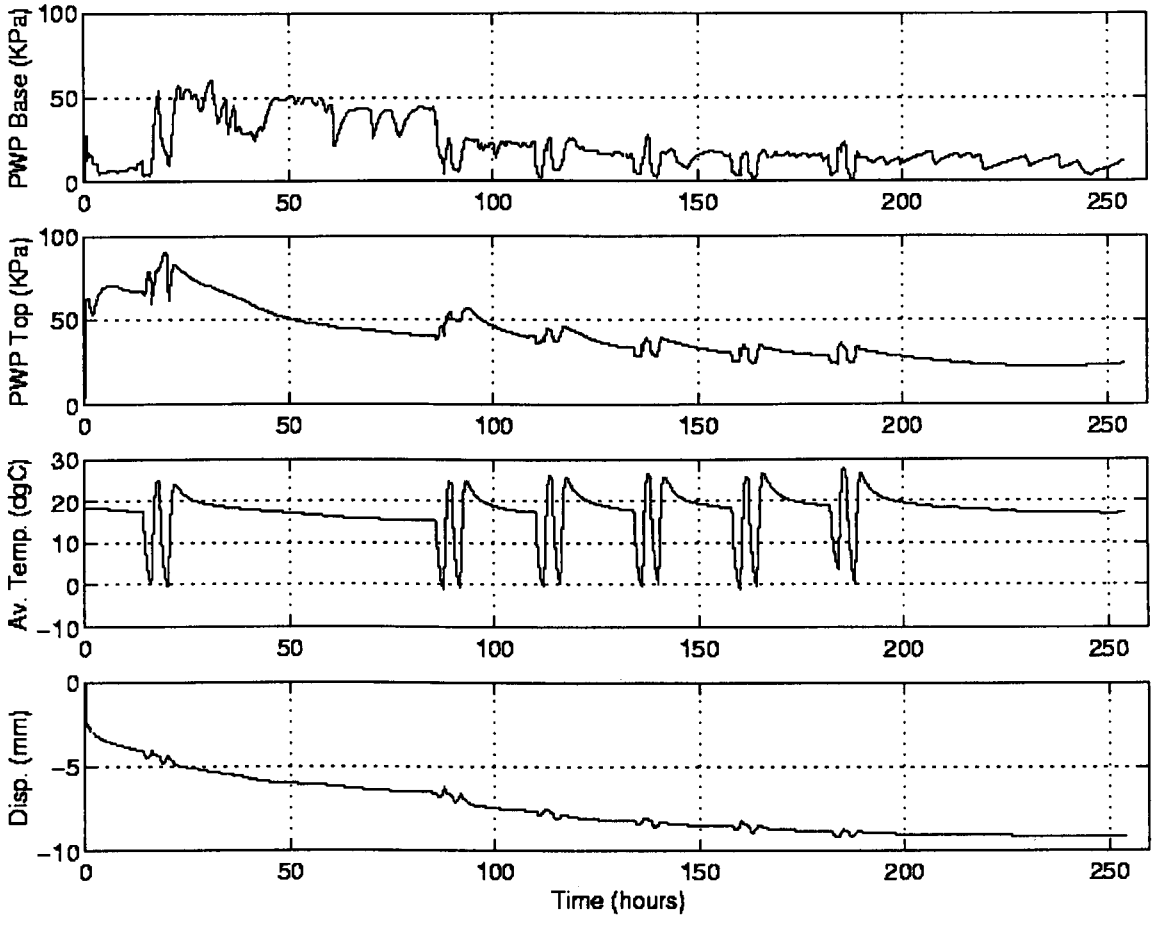

Figure 4.20 – Results for Test 5

The test environment and cycles imposed were the same as for Test 4, although the test itself was longer, comprising 12 cycles and 7 rest phases. Two of the rest phases, those after Cycle 2 and Cycle 12, were of 'weekend' duration.

Figure 4.21 gives temperature profiles for Cycle 2. The base of the specimen can be considered to be frozen for approximately 1.25 hours, and the top is briefly frozen, for approximately 0.25 hours. Freezing was not achieved over the whole depth of specimen.

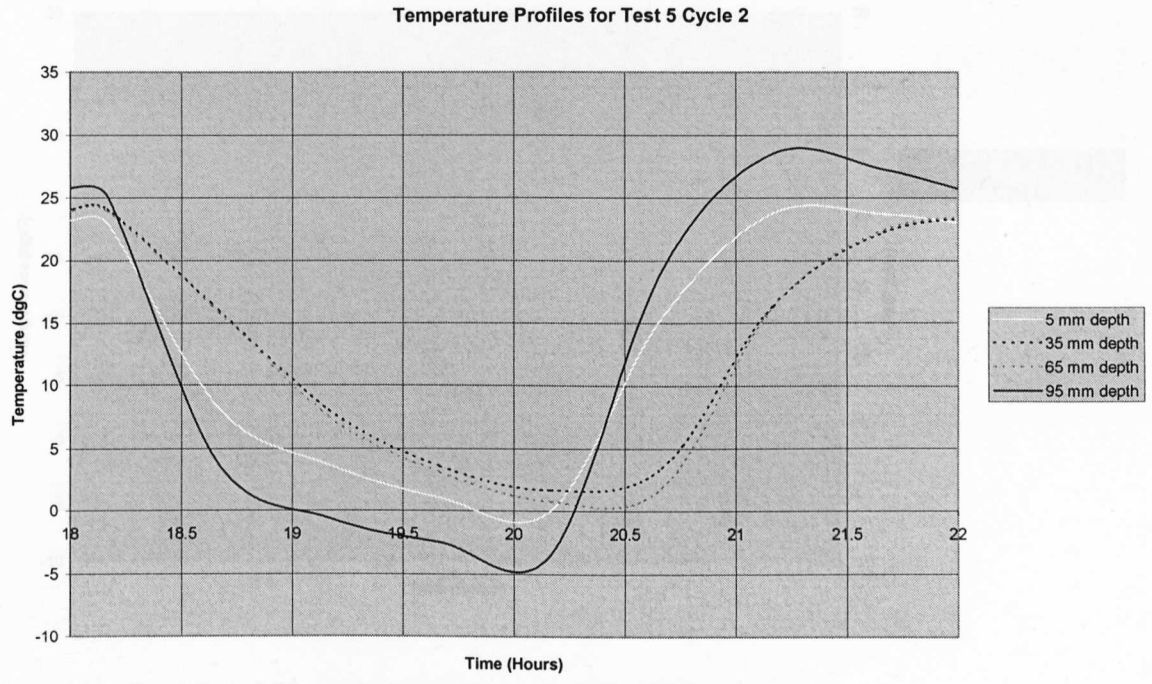

Figure 4.21 – Temperature Profiles for Test 5 Cycle 2

At the base of the specimen, the maximum pore water pressure was recorded about 10 hours after the end of Cycle 1, with the corresponding minimum value recorded at around the end of Cycle 10. At the top of the specimen, the maximum pore water pressure was recorded at the end of Cycle 2, and the corresponding minimum value was found to be that found at zero time.

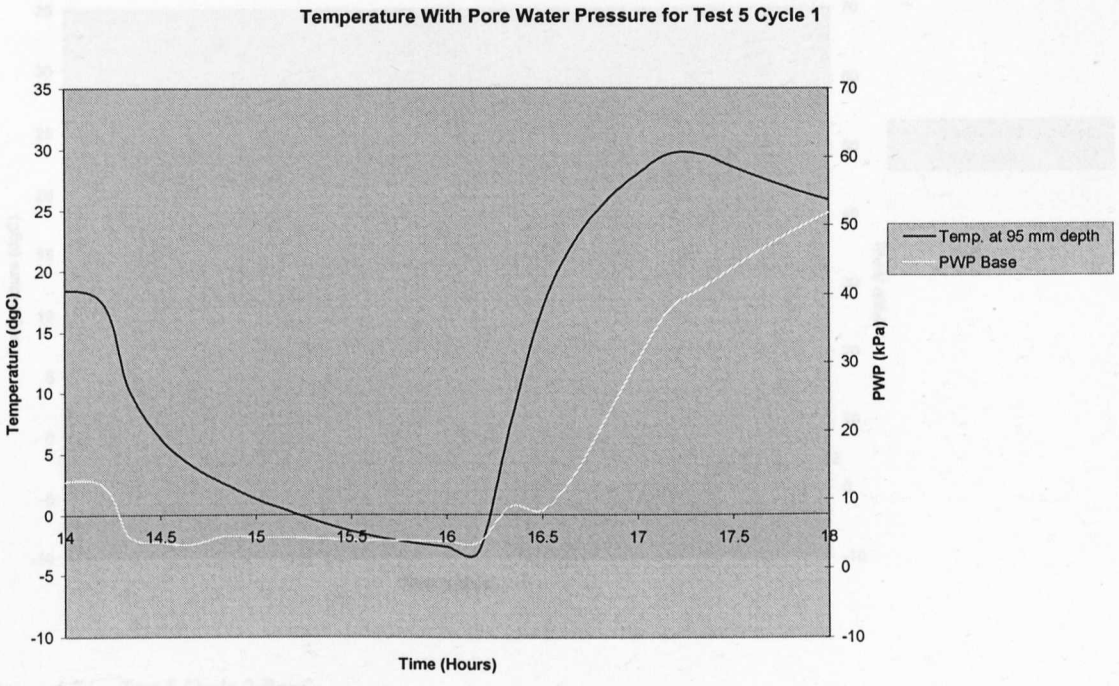

Figure 4.22 – Test 5 Cycle 1 Base

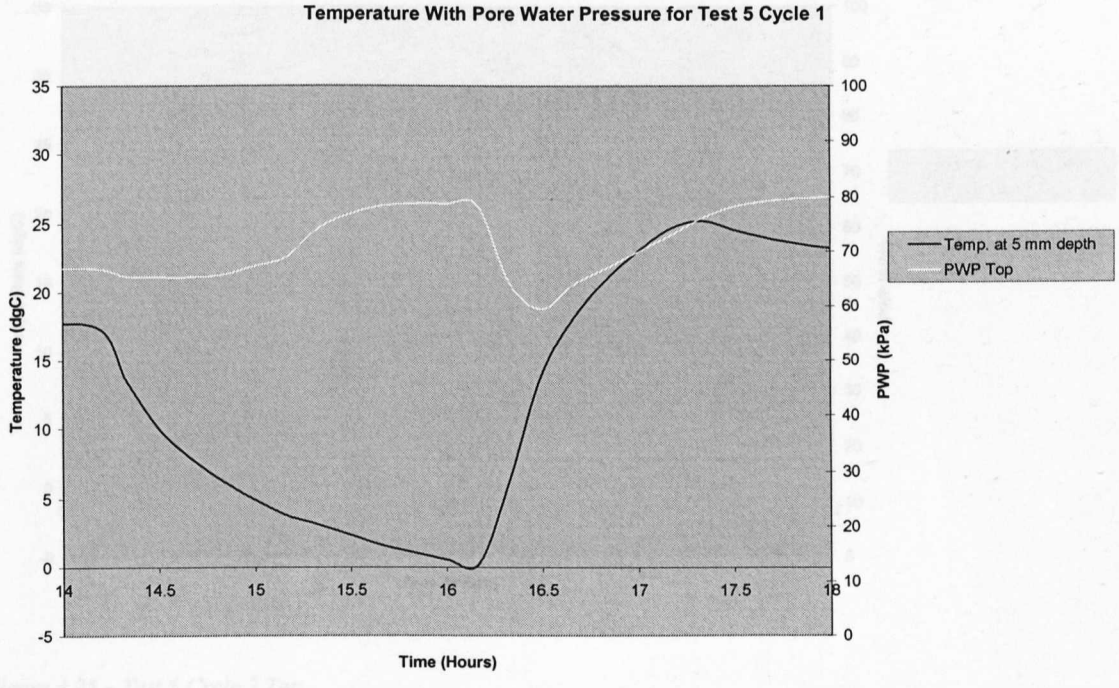

Figure 4.23 – Test 5 Cycle 1 Top

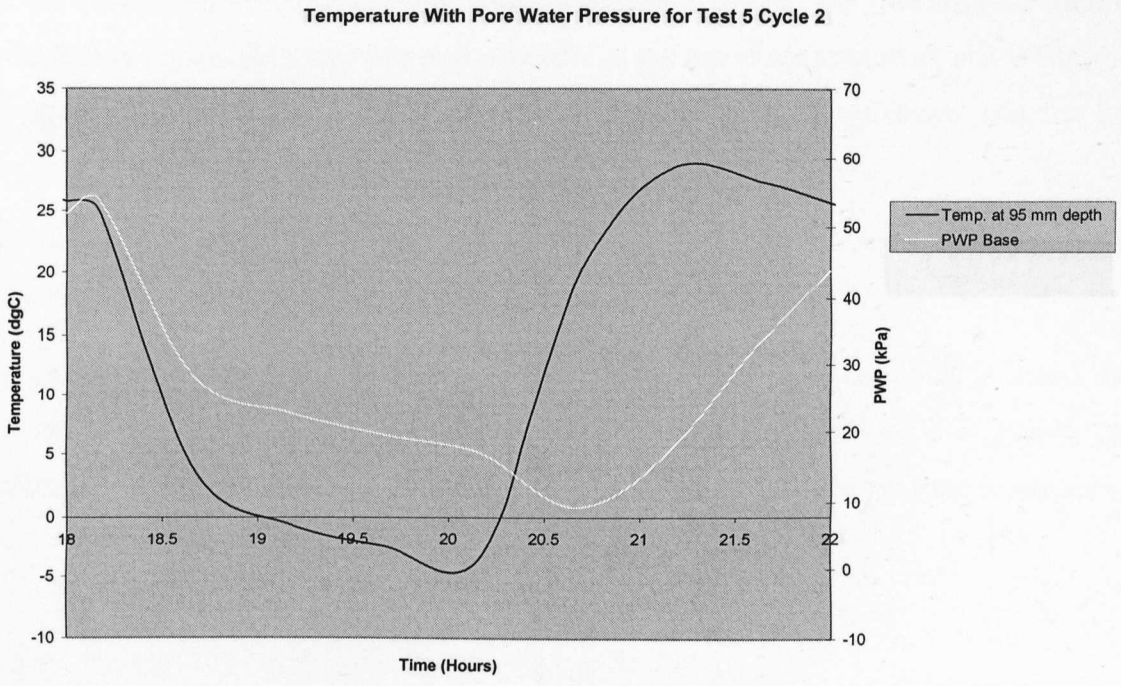

Figure 4.24 – Test 5 Cycle 2 Base

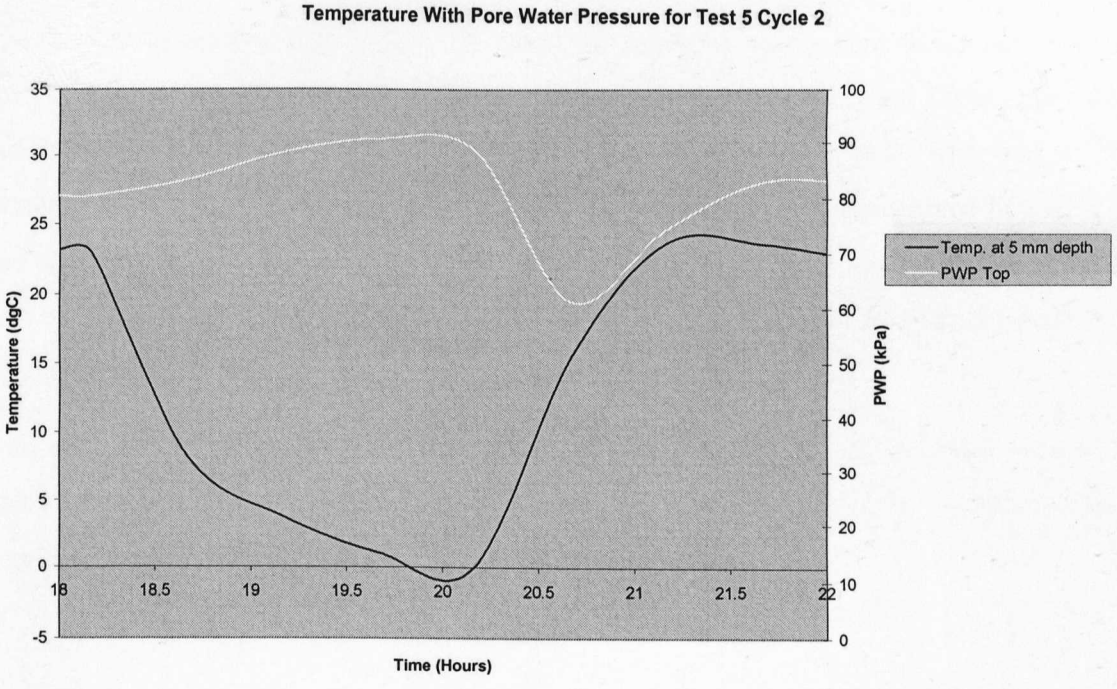

Figure 4.25 – Test 5 Cycle 2 Top

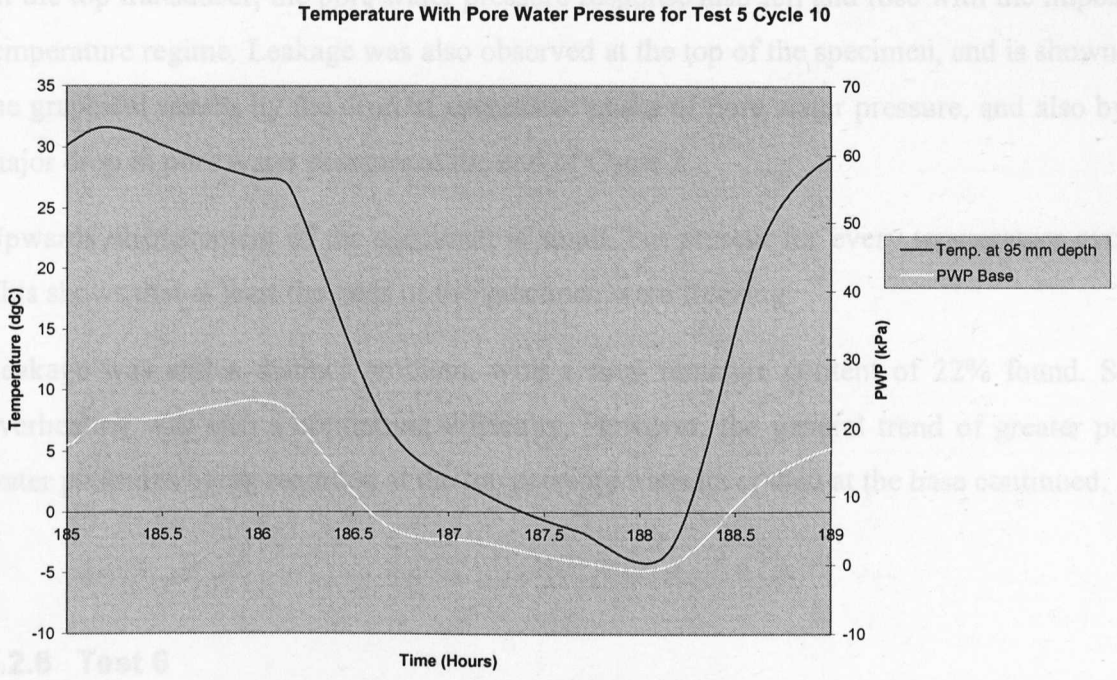

Figure 4.26 – Test 5 Cycle 10 Base

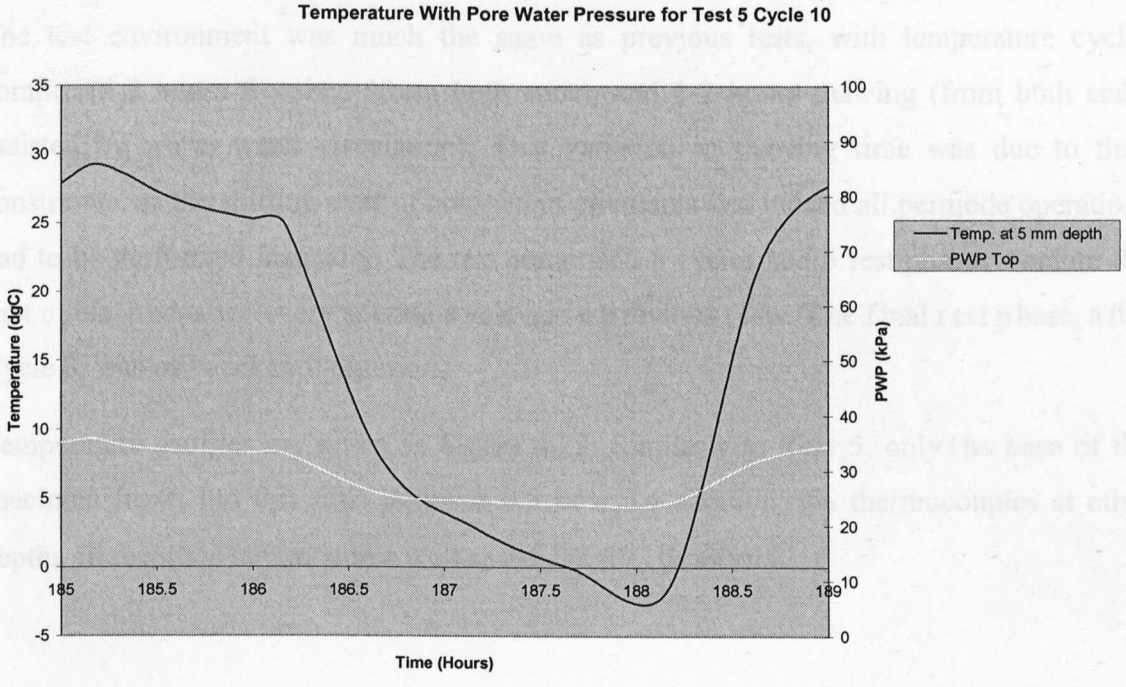

Figure 4.27 – Test 5 Cycle 10 Top

At the base transducer, a high amount of fluctuation was observed in the pore water pressure readings. This fluctuation took place while temperatures were fairly steady, and has been attributed to leakage. In general, the pore water pressure response fell and rose with the imposed temperature regime.

At the top transducer, the pore water pressure response also fell and rose with the imposed temperature regime. Leakage was also observed at the top of the specimen, and is shown in the graphical results by the drop in successive peaks of pore water pressure, and also by a major drop in pore water pressure at the end of Cycle 2.

Upwards displacement of the specimen is small, but present for every temperature cycle. This shows that at least the ends of the specimen were freezing.

Leakage was still a distinct problem, with a final moisture content of 22% found. Soil overheating was also a continuing difficulty. However, the general trend of greater pore water pressures being recorded at the top pressure transducer than at the base continued.

4.2.6 Test 6

Test 6 was carried out on Lias clay, of moisture content 35%, under an applied stress of 104 kPa. Figure 4.28 gives summarised results for Test 6.

The test environment was much the same as previous tests, with temperature cycles comprised 2 hours freezing, (from both ends), and 1-2 hours thawing (from both ends, assisted by warm water circulation). This variation in thawing time was due to time constraints, as the shifting over of cold/warm circulants and indeed all permode operations had to be performed manually. The test comprised 8 cycles and 5 rest phases - before the first cycle, and after every second cycle as in previous tests. The final rest phase, after Cycle 8, was of 'weekend' duration.

Temperature profiles are given in Figure 4.29. Similarly to Test 5, only the base of the specimen froze, but this time only for 0.5 hour. In addition, the thermocouples at other depths all recorded temperatures well above the 0°C threshold.

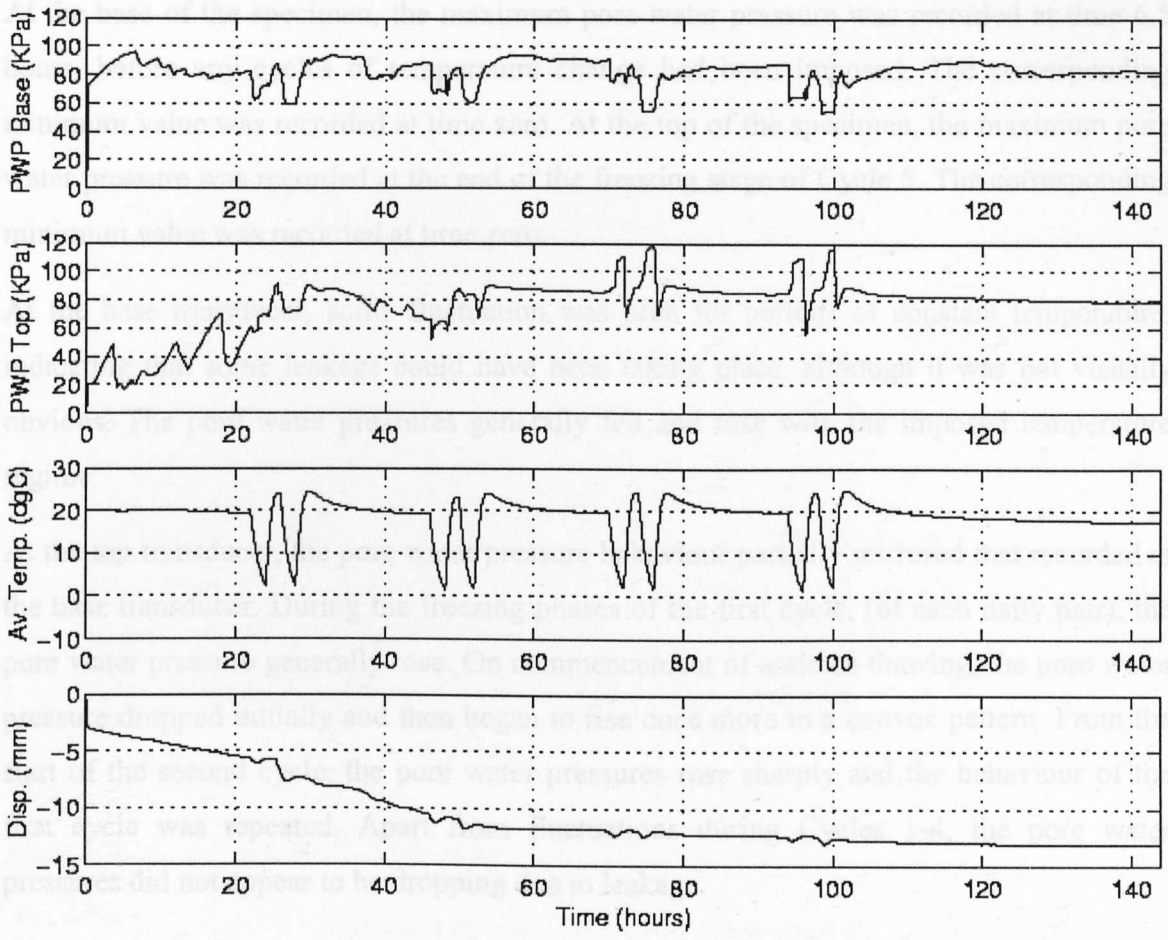

Figure 4.28 – Results for Test 6

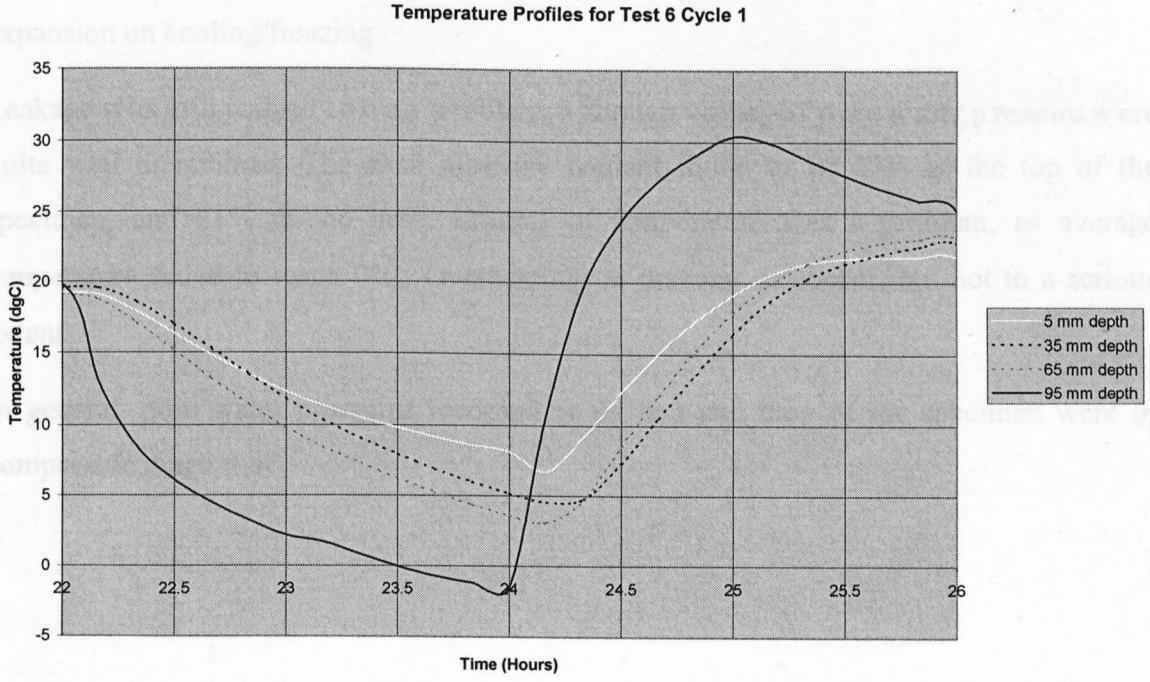

Figure 4.29 – Temperature Profiles for Test 6 Cycle 1

At the base of the specimen, the maximum pore water pressure was recorded at time 6.5 hours, before any cycles of temperature change had been imposed. The corresponding minimum value was recorded at time zero. At the top of the specimen, the maximum pore water pressure was recorded at the end of the freezing stage of Cycle 5. The corresponding minimum value was recorded at time zero.

At the base transducer, some fluctuation was seen for periods of constant temperature, indicating that some leakage could have been taking place, although it was not visually obvious. The pore water pressures generally fell and rose with the imposed temperature regime.

At the top transducer, the pore water pressure behaviour partially mirrored that recorded at the base transducer. During the freezing phases of the first cycle, (of each daily pair), the pore water pressure generally rose. On commencement of assisted thawing, the pore water pressure dropped initially and then began to rise once more in a convex pattern. From the start of the second cycle, the pore water pressures rose sharply and the behaviour of the first cycle was repeated. Apart from fluctuations during Cycles 1-4, the pore water pressures did not appear to be dropping due to leakage.

Figures 4.30-4.33 give pore water pressure responses with temperature for Cycles 1 and 2.

Upwards displacement of the specimen occurred for every cycle, therefore showing some expansion on cooling/freezing.

Leakage was still judged to be a problem, although values of pore water pressure were quite well maintained. The final moisture content found to be 32% at the top of the specimen, and 21% at the base. Control of temperature was a problem, as average temperature failed to reach 0°C. Overheating on thawing did occur, but not to a serious extent.

In general, pore water pressures recorded at the top and base of the specimen were of comparable magnitude.

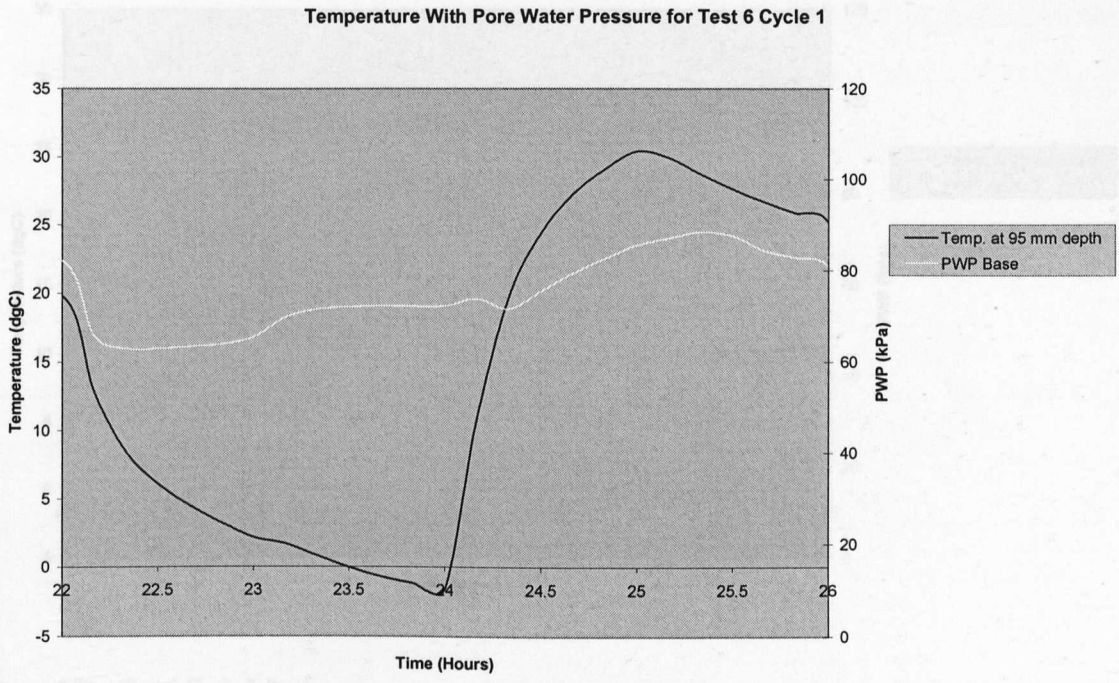

Figure 4.30 – Test 6 Cycle 1 Base

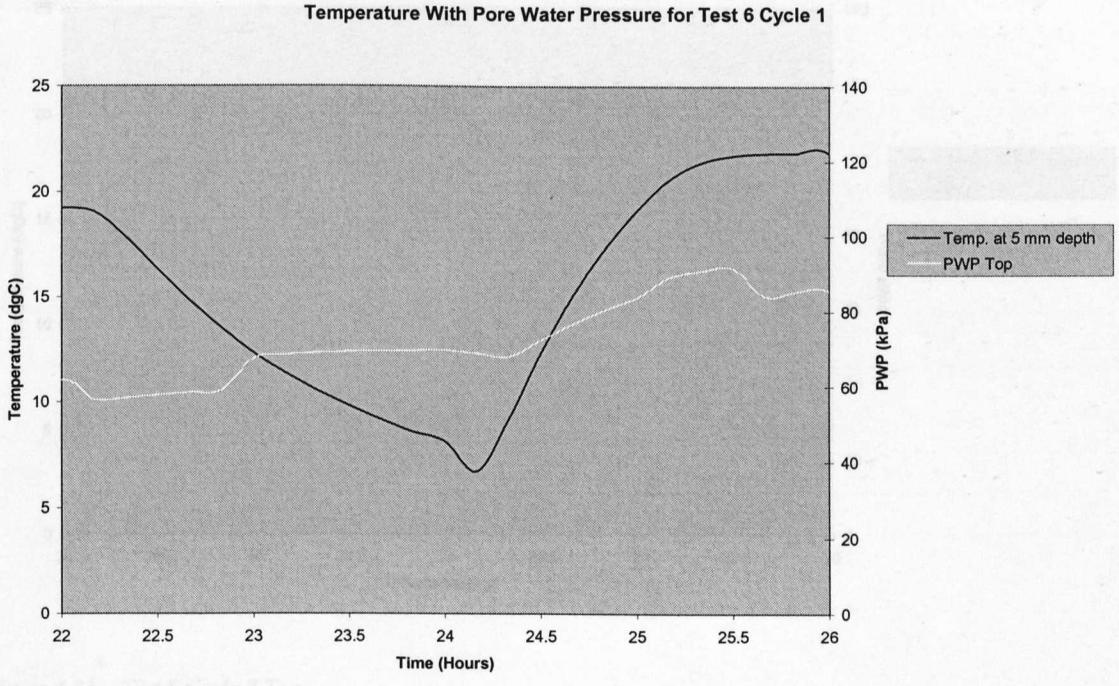

Figure 4.31 – Test 6 Cycle 1 Top

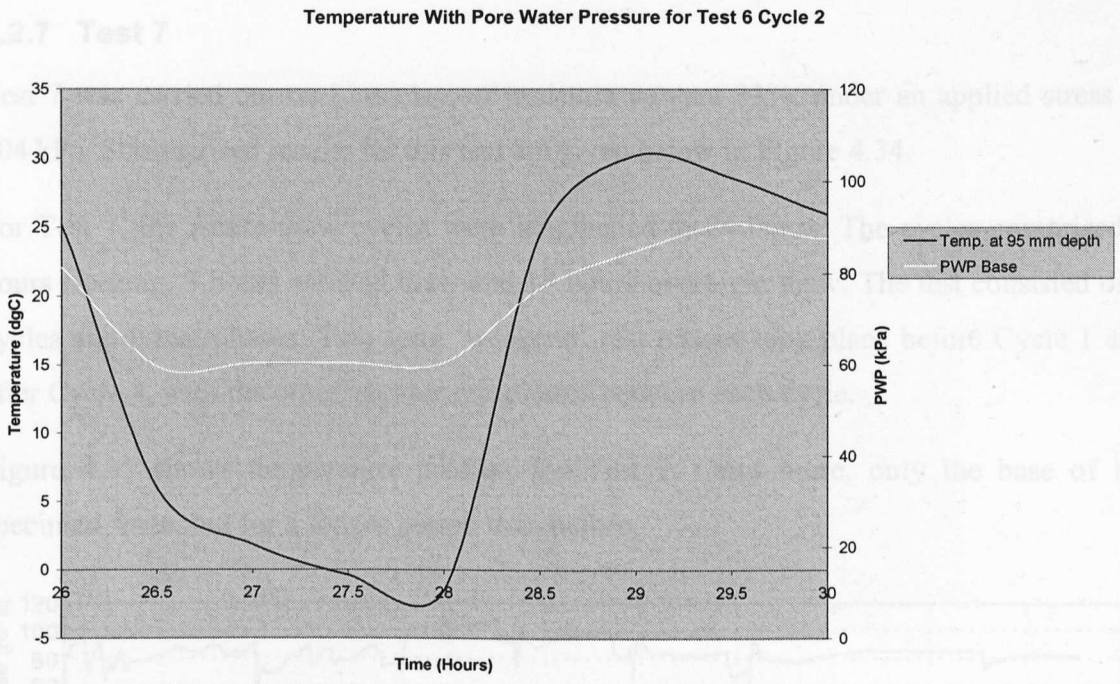

Figure 4.32 – Test 6 Cycle 2 Base

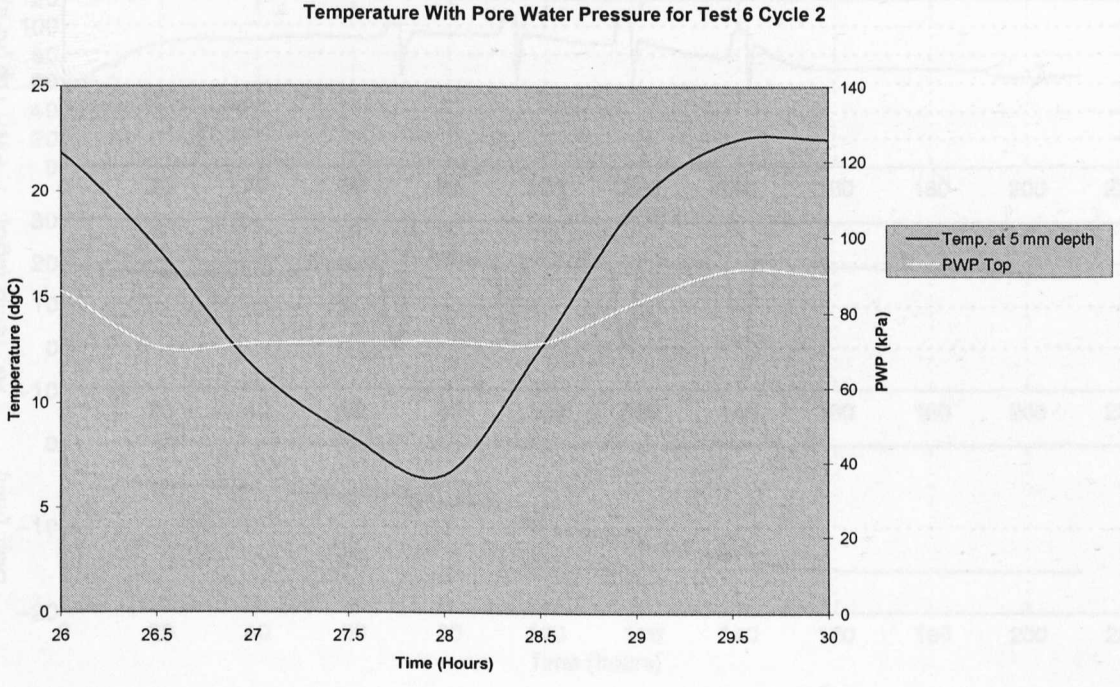

Figure 4.33 – Test 6 Cycle 2 Top

4.2.7 Test 7

Test 7 was carried out on Lias clay, of moisture content 33%, under an applied stress of 104 kPa. Summarised results for this test are given below in Figure 4.34.

For Test 7, the freeze-thaw cycles were lengthened to 24 hours. The cycles comprised 4 hours freezing, 3 hours assisted thaw and 17 hours overnight thaw. The test consisted of 4 cycles and 5 rest phases. Two long 'weekend' rest phases took place before Cycle 1 and after Cycle 4, with the other, shorter rest phases between each cycle.

Figure 4.35 shows temperature profiles for Test 7. Once more, only the base of the specimen froze, but for a longer period than before.

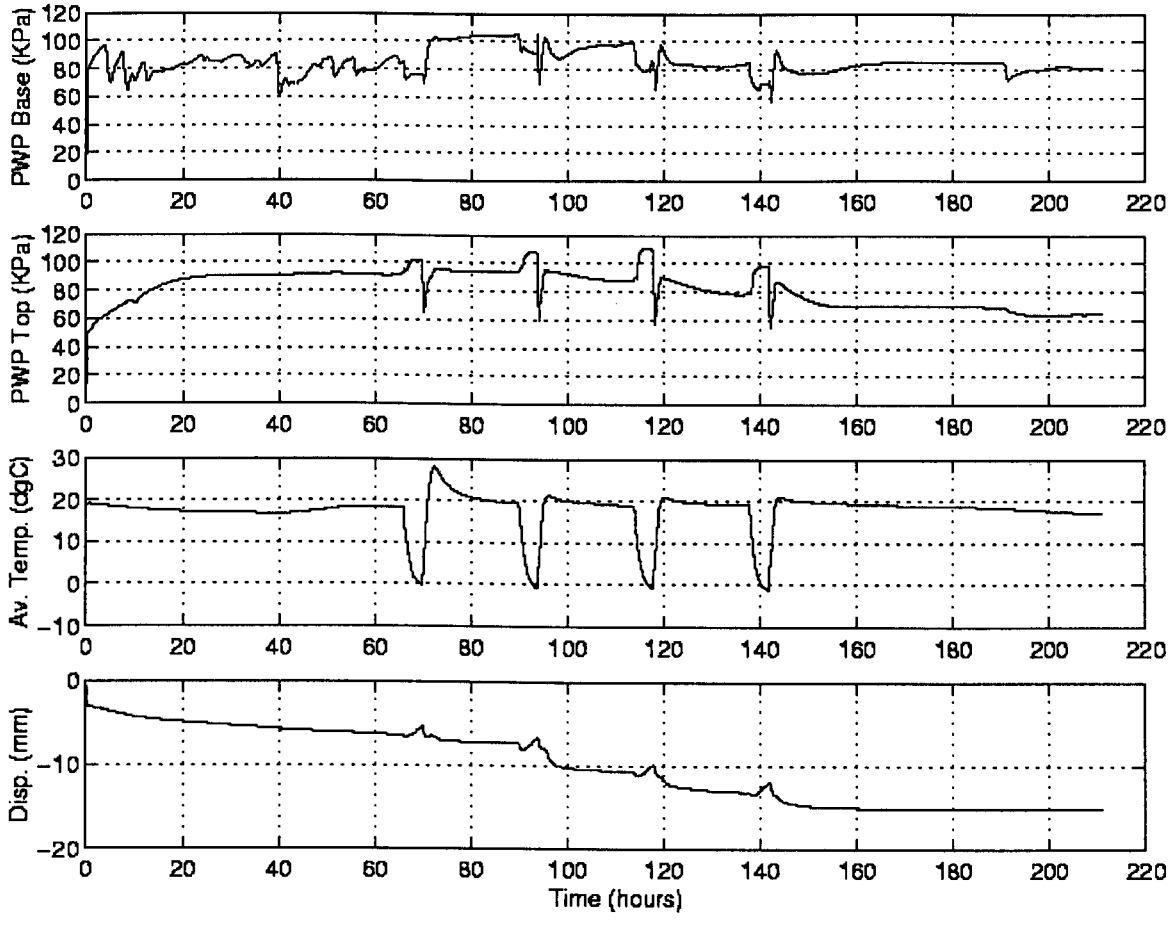

Figure 4.34 – Results for Test 7

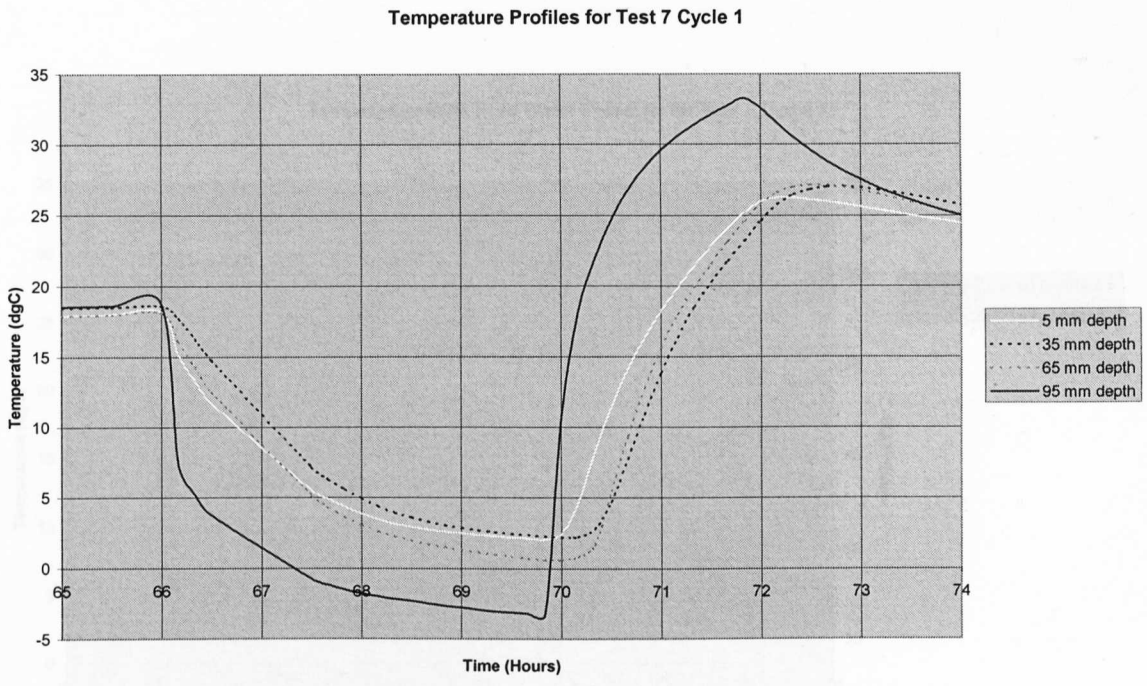

Figure 4.35 – Temperature Profiles for Test 7 Cycle 1

At the base of the specimen, the maximum pore water pressure was recorded at a high spike at the end of the freezing stage of Cycle 2. The corresponding minimum value occurred at time zero. At the top of the specimen, the maximum pore water pressure was recorded at the end of the freezing stage of Cycle 3. The corresponding minimum value occurred at time zero.

Figures 4.36-4.43 illustrate the basic repeatability of the pore water pressure response over Cycles 1-4.

At the base transducer, the pore water pressure underwent an initial drop at the start of freezing and then levelled out for the rest of the freezing stage before spiking and dropping sharply at the end of the freezing stage/beginning of the assisted thaw stage. At the start of the assisted thaw stage the pore water pressure increased at a steep gradient before dropping to a slightly lower, steady level overnight.

At the top transducer, the pore water pressure rose in a convex pattern to a plateau at the onset of cooling. At the end of the cooling stage, the pore water pressure dropped, and then increased during the assisted thaw period. The pore water pressure tended to drop slightly during the overnight thaw periods, perhaps a sign of leakage occurring.

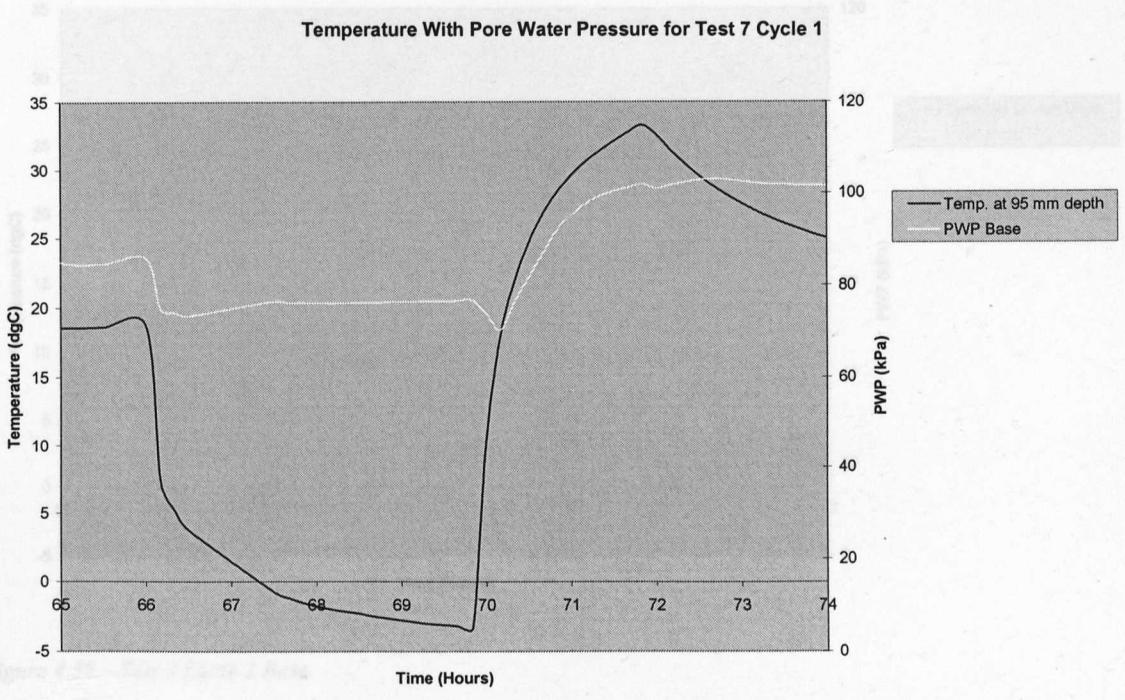

Figure 4.36 - Test 7 Cycle 1 Base

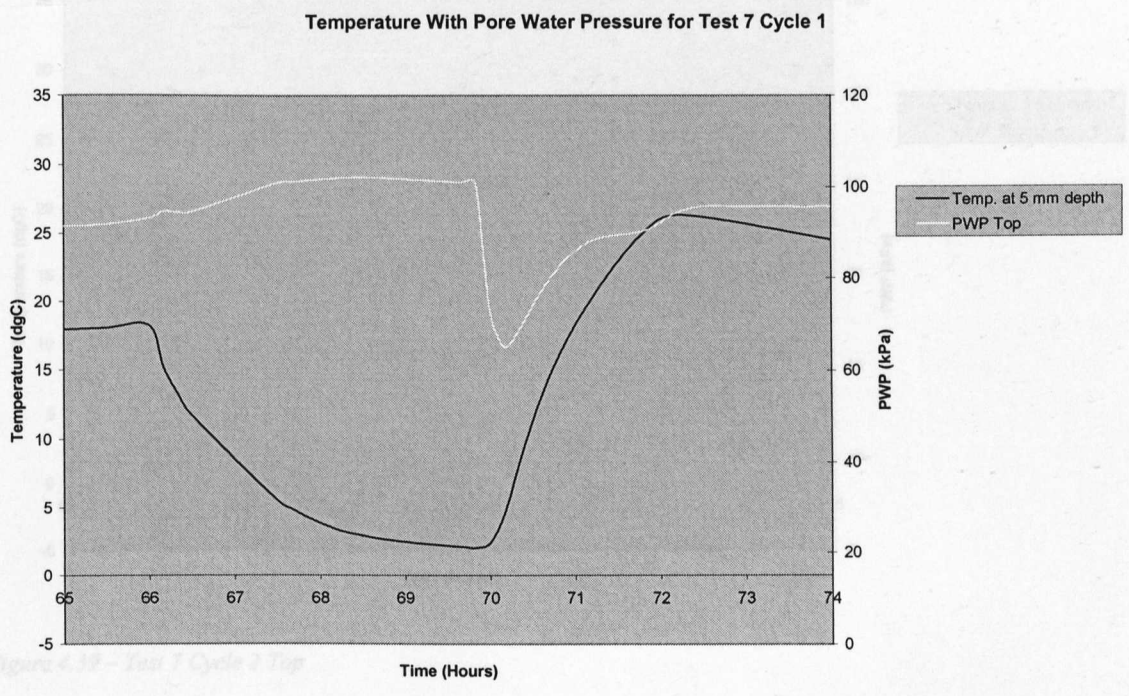

Figure 4.37 – Test 7 Cycle 1 Top

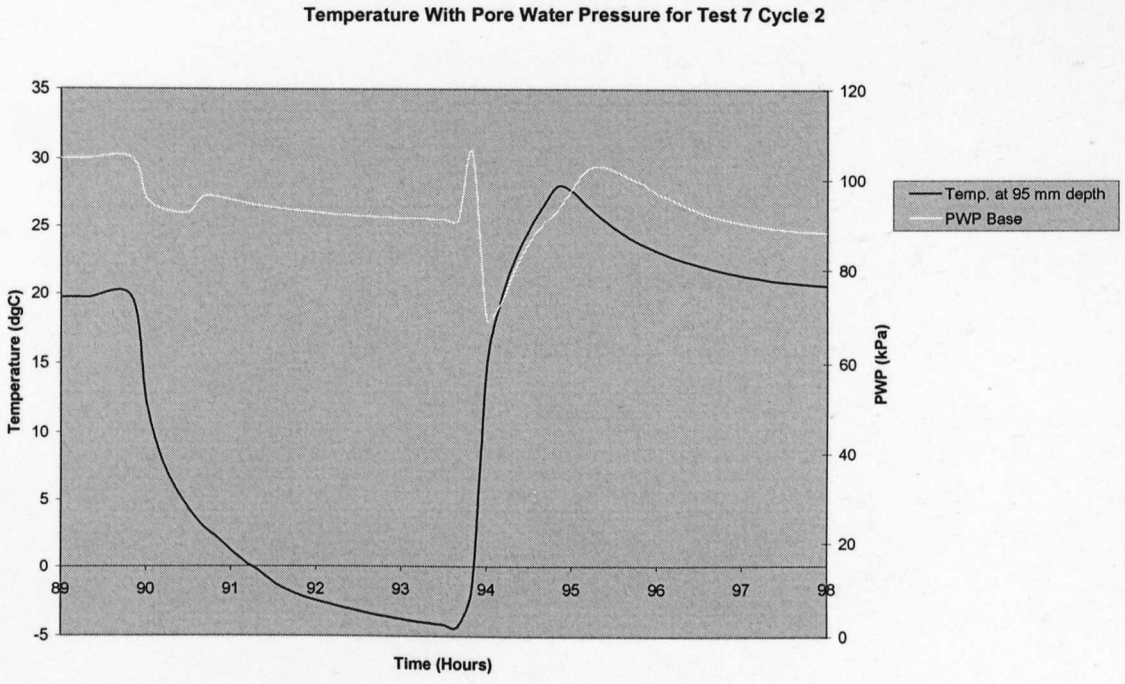

Figure 4.38 – Test 7 Cycle 2 Base

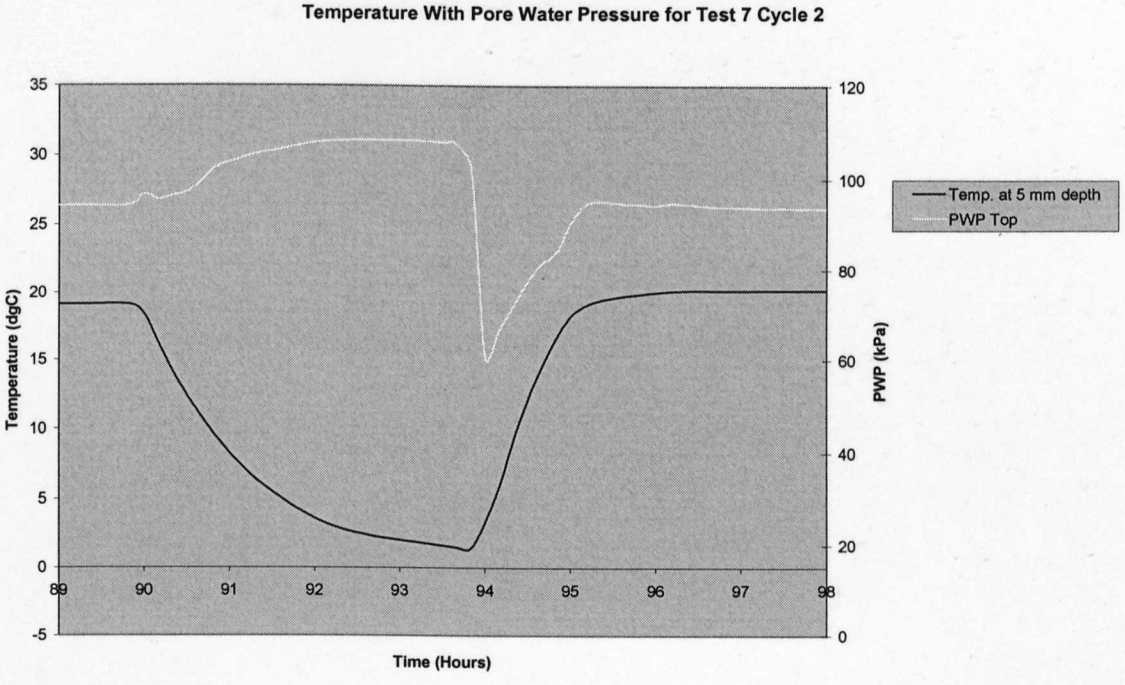

Figure 4.39 – Test 7 Cycle 2 Top

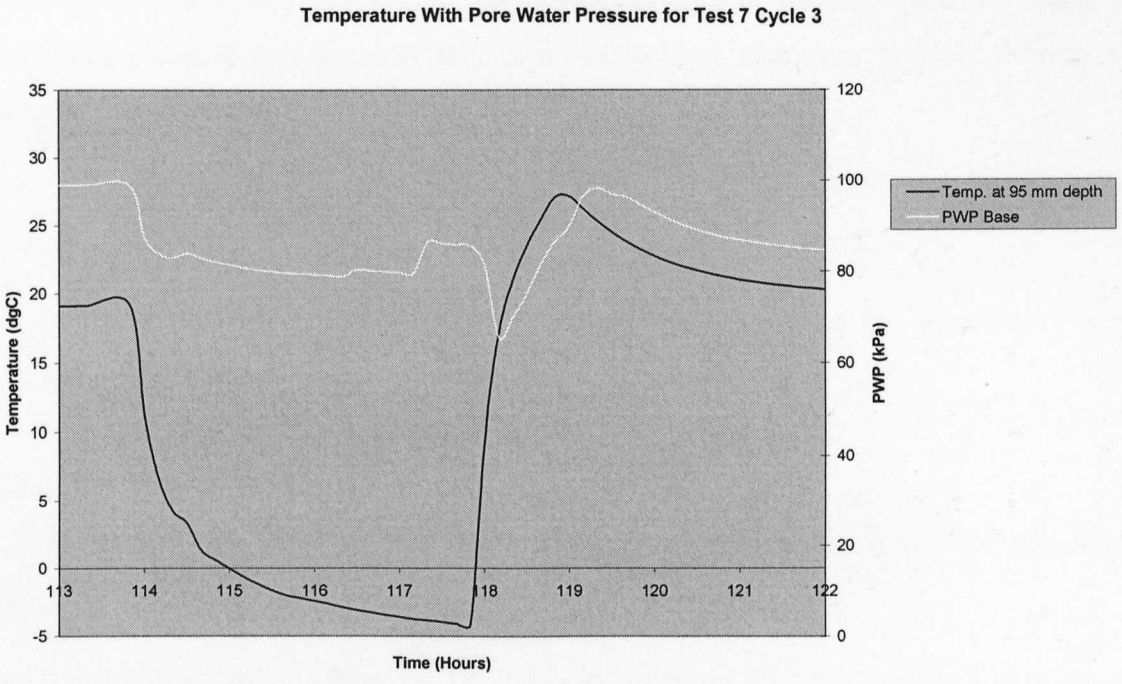

Figure 4.40 – Test 7 Cycle 3 Base

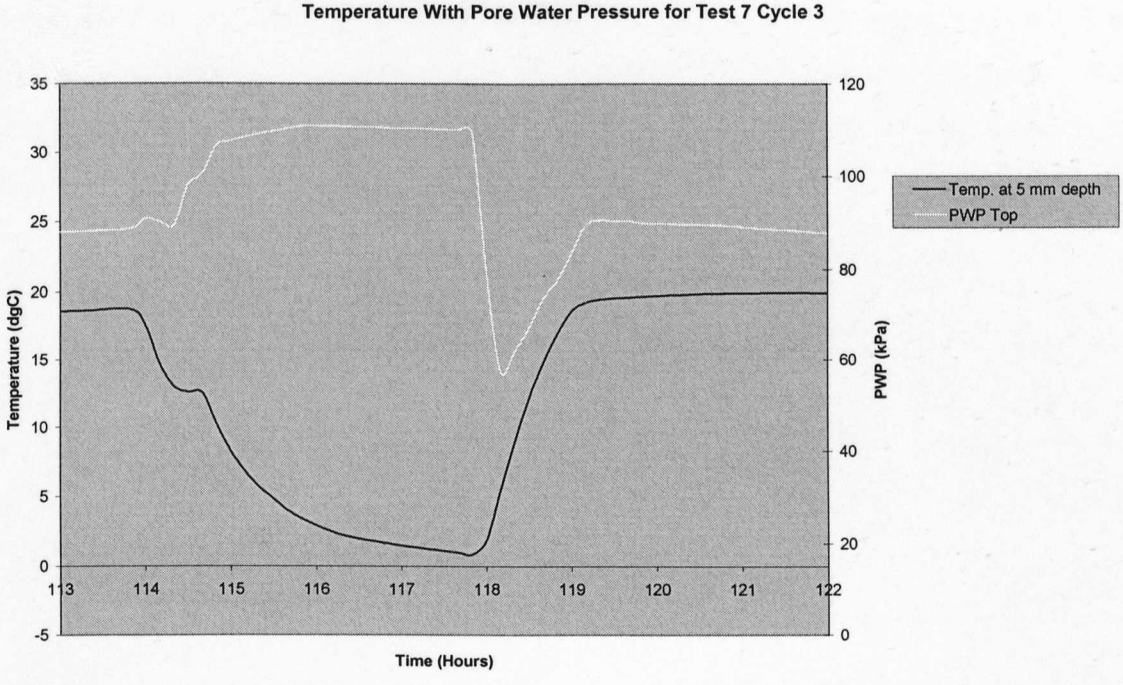

Figure 4.41 – Test 7 Cycle 3 Top

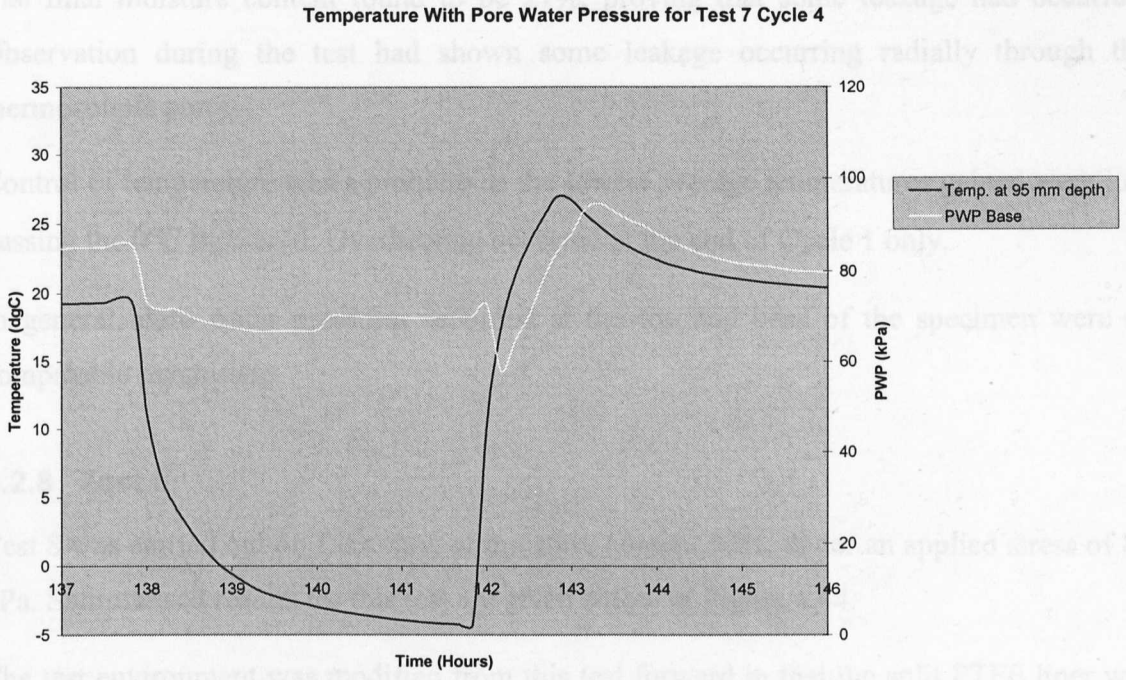

Figure 4.42 – Test 7 Cycle 4 Base

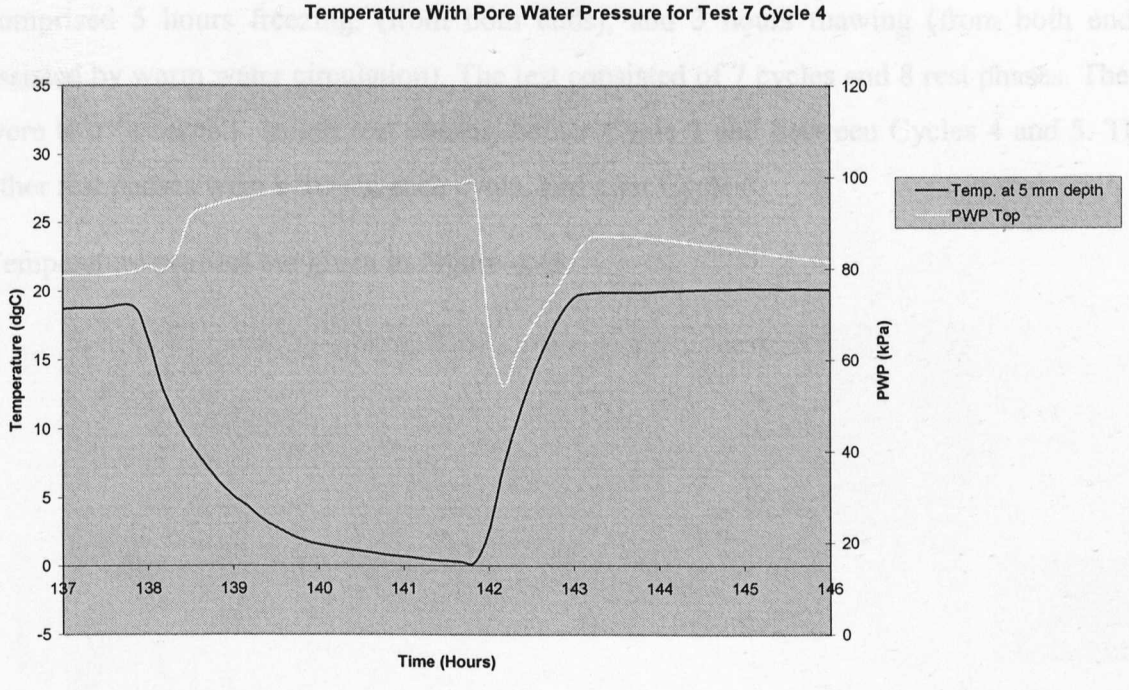

Figure 4.43 – Test 7 Cycle 4 Top

Upward displacement of the specimen occurred for each cycle, showing some expansion on cooling.

The final moisture content found to be 27%, proving that some leakage had occurred. Observation during the test had shown some leakage occurring radially through the thermocouple ports.

Control of temperature was a problem as the lowest average temperatures gained were just passing the 0°C threshold. Overheating occurred at the end of Cycle 1 only.

In general, pore water pressures recorded at the top and base of the specimen were of comparable magnitude.

4.2.8 Test 8

Test 8 was carried out on Lias clay, of moisture content 30%, under an applied stress of 80 kPa. Summarised results for this test are given below in Figure 4.44.

The test environment was modified from this test forward in that the split PTFE liner was replaced by a one-piece section in an effort to combat leakage. Also, extra o-rings were introduced at the base of the apparatus to provide a better seal. Temperature cycles comprised 5 hours freezing, (from both ends), and 3 hours thawing (from both ends, assisted by warm water circulation). The test consisted of 7 cycles and 8 rest phases. There were two 'weekend' length rest phases, before Cycle 1 and between Cycles 4 and 5. The other rest phases were between each cycle, and after Cycle 8.

Temperature profiles are given in Figure 4.45.

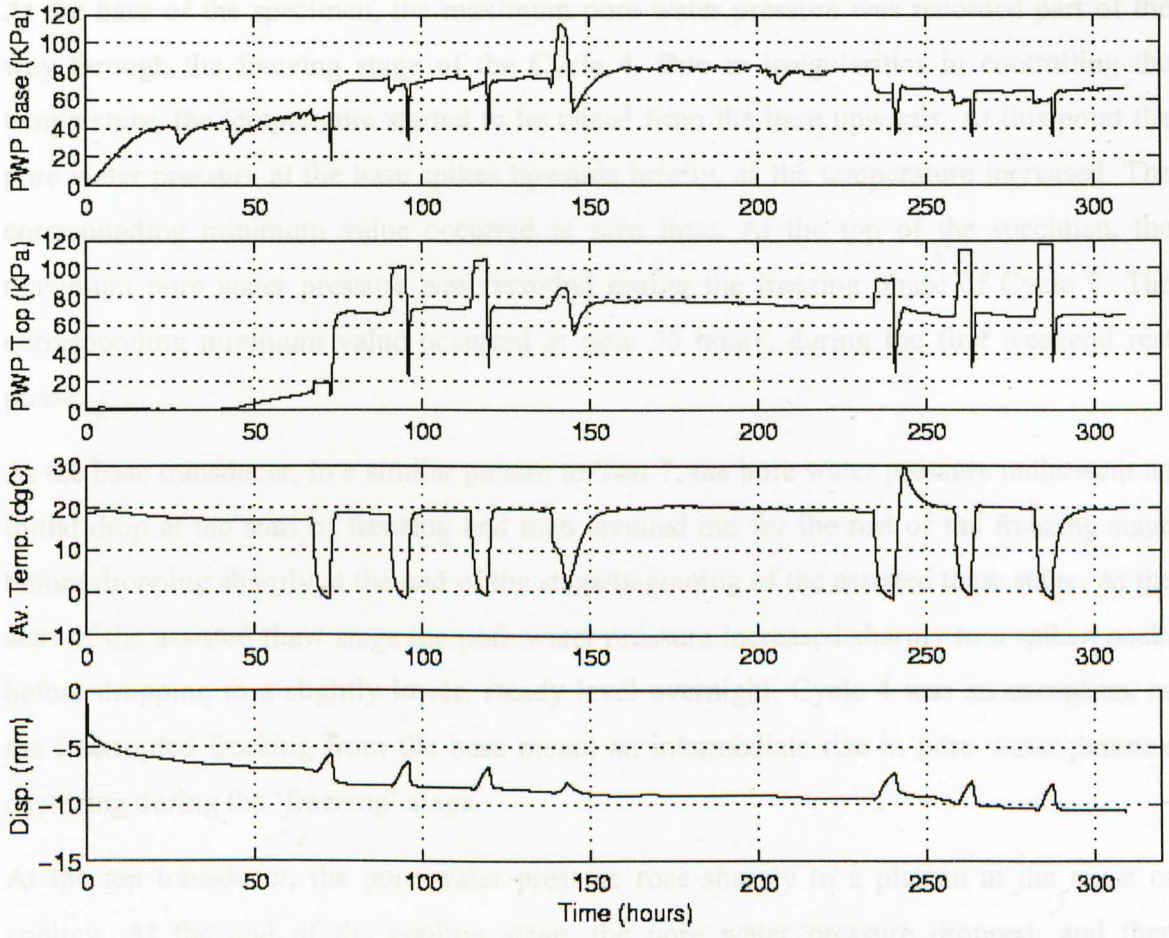

Figure 4.44 – Results for Test 8

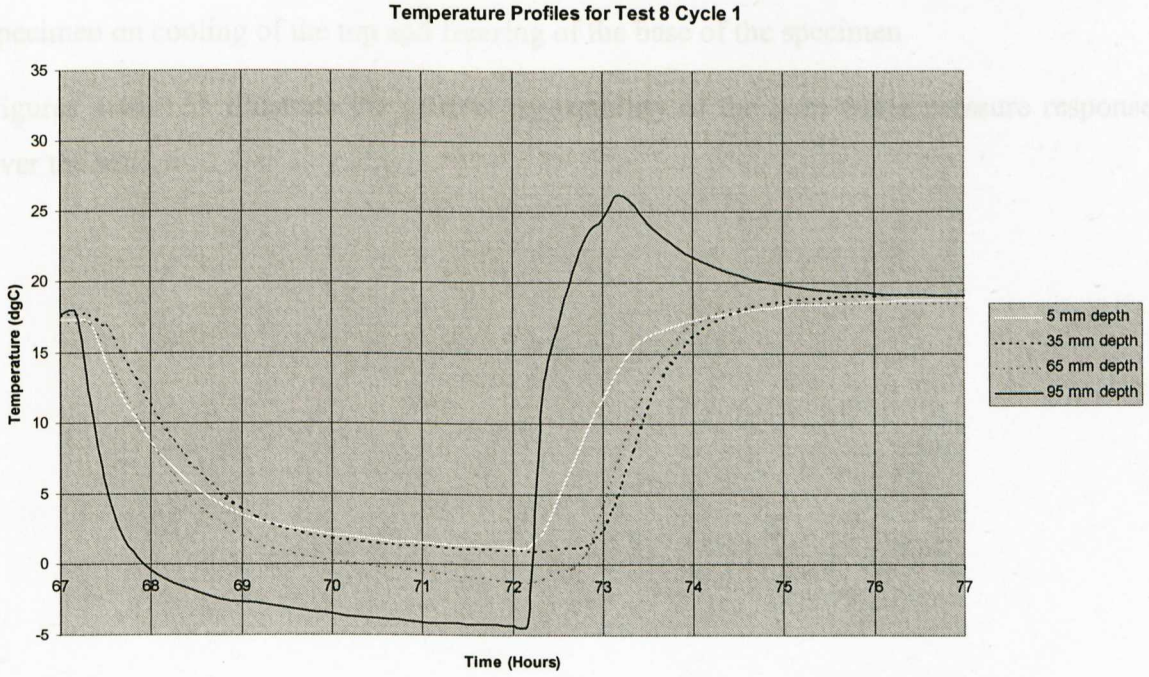

Figure 4.45 – Temperature Profiles for Test 8 Cycle 1

At the base of the specimen, the maximum pore water pressure was recorded part of the way through the freezing stage of the Cycle 4. Due to irregularities in controlling the temperature, the temperature started to be raised from the base upwards. At this point the pore water pressure at the base spikes upwards briefly, as the temperature increased. The corresponding minimum value occurred at zero time. At the top of the specimen, the maximum pore water pressure was recorded during the freezing phase of Cycle 7. The corresponding minimum value occurred at time 35 hours, during the first weekend rest phase.

At the base transducer, in a similar pattern to Test 7, the pore water pressure underwent an initial drop at the start of freezing and then levelled out for the rest of the freezing stage before dropping sharply at the end of the stage/beginning of the assisted thaw stage. At the start of the assisted thaw stage the pore water pressure increased sharply to a spiked peak, before dropping to a slightly lower, steady level overnight. Cycle 4 was an exception, as the interrupted freezing from the base meant an intermediate rise in pore water pressure occurring during the 'freezing' stage.

At the top transducer, the pore water pressure rose sharply to a plateau at the onset of cooling. At the end of the cooling stage, the pore water pressure dropped, and then increased once more during the assisted thaw period.

Upward displacement of the specimen occurred for each cycle, showing expansion of the specimen on cooling of the top and freezing of the base of the specimen.

Figures 4.46-4.55 illustrate the general repeatability of the pore water pressure response over the test.

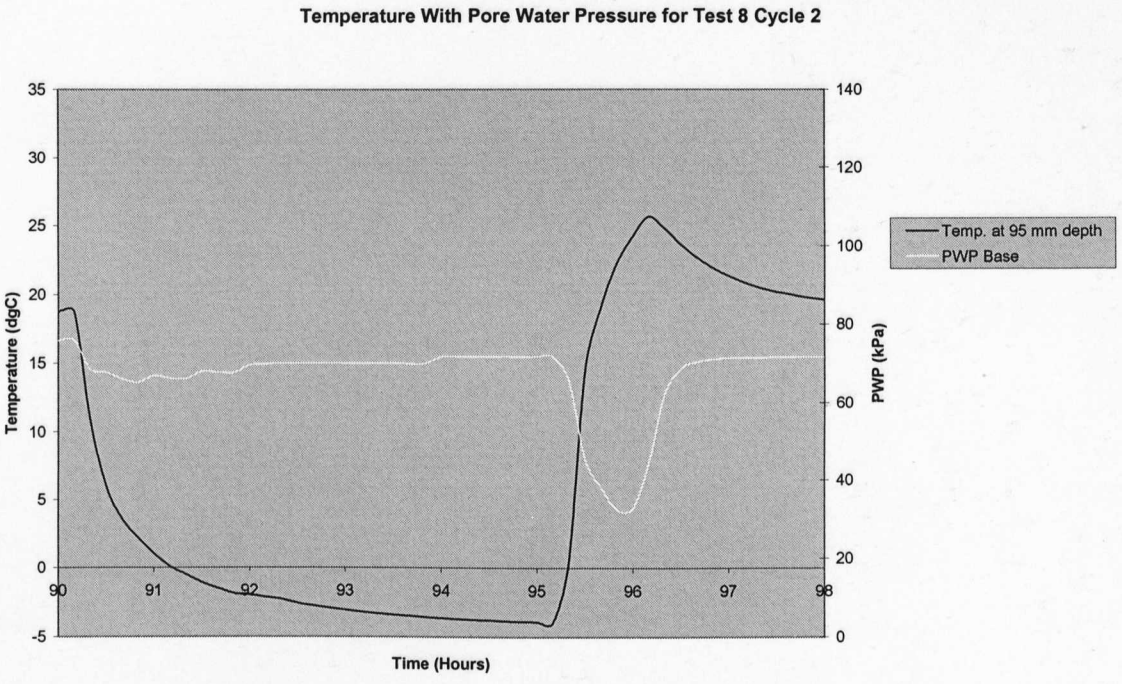

Figure 4.46 – Test 8 Cycle 2 Base

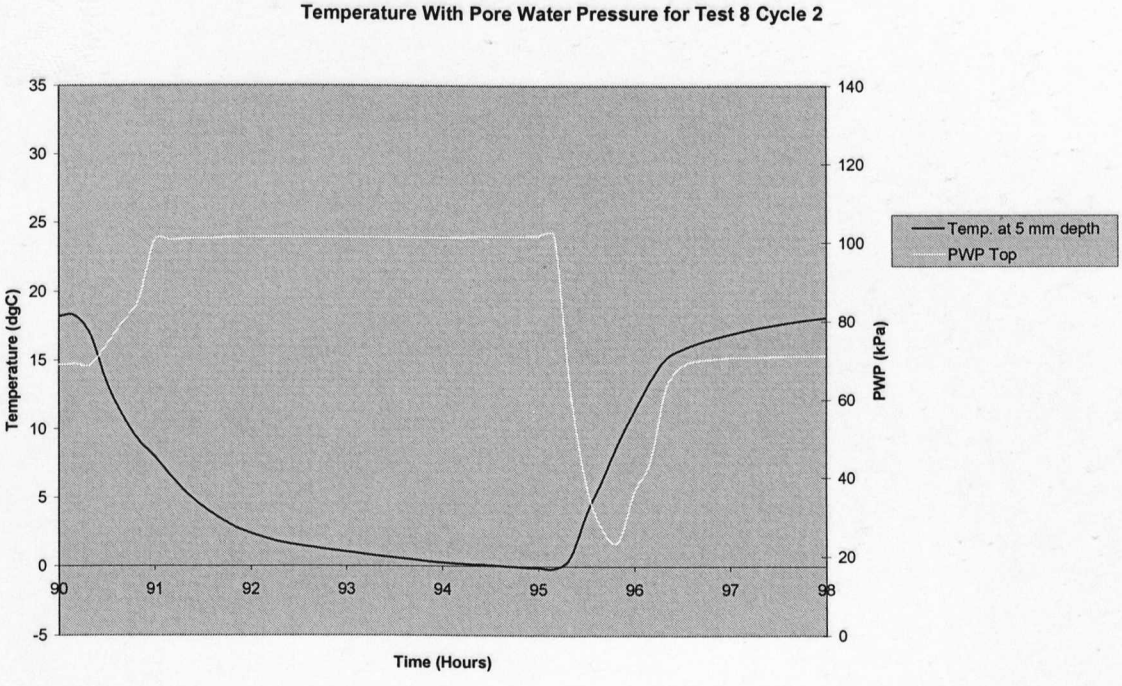

Figure 4.47 – Test 8 Cycle 2 Top

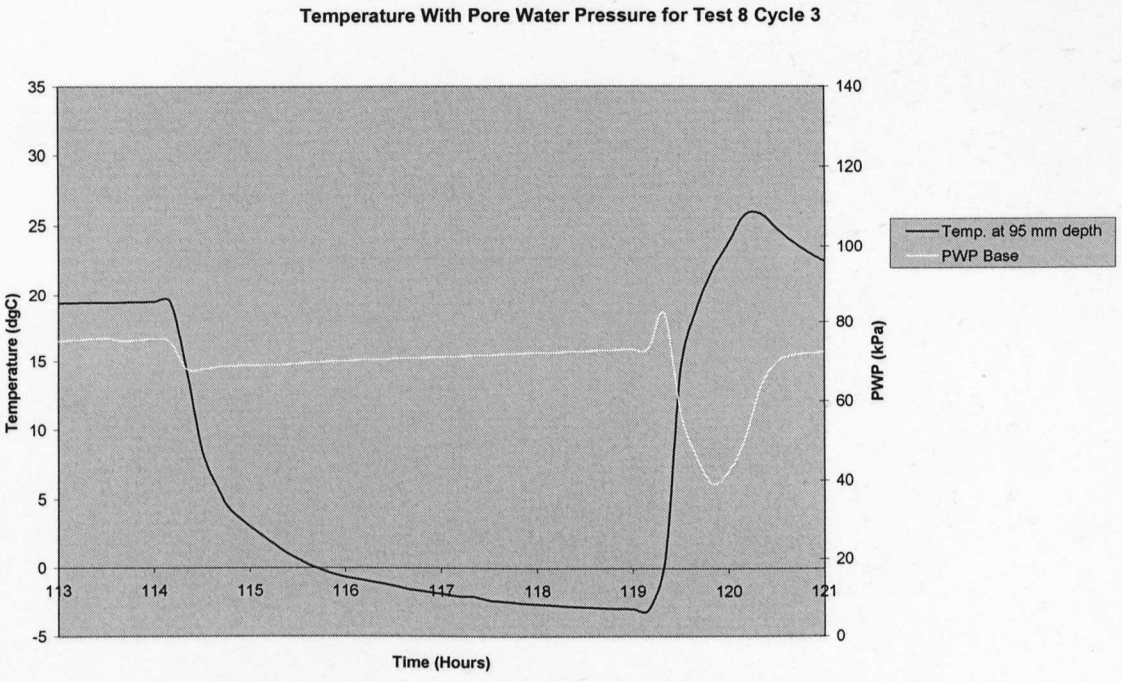

Figure 4.48 – Test 8 Cycle 3 Base

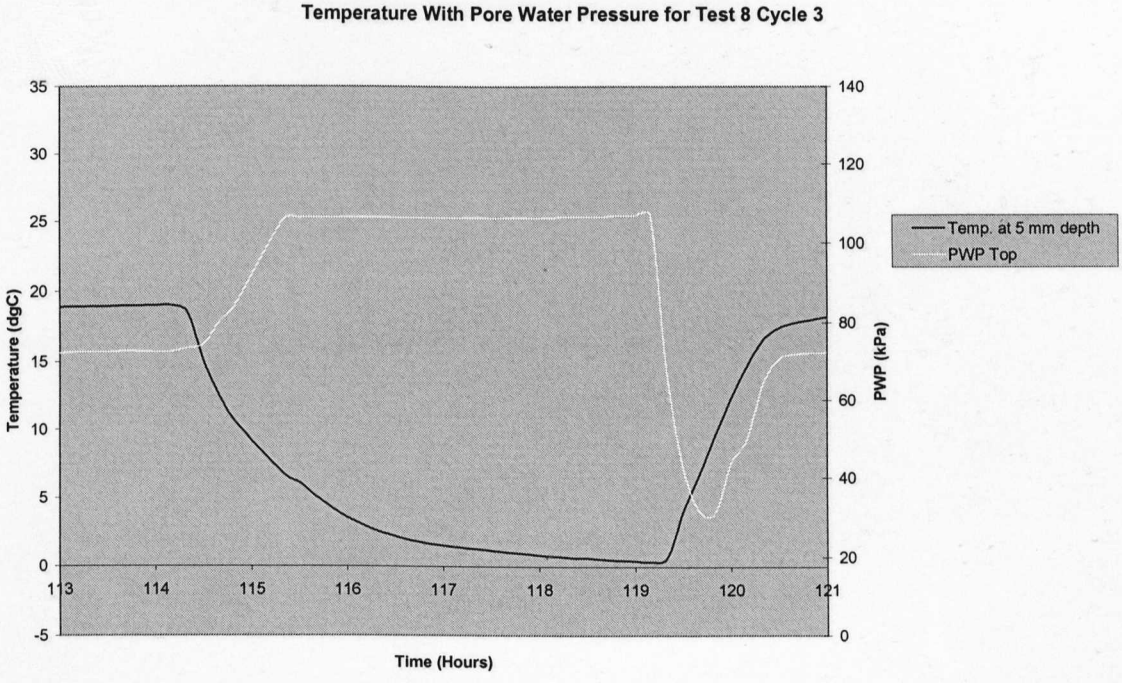

Figure 4.49 – Test 8 Cycle 3 Top

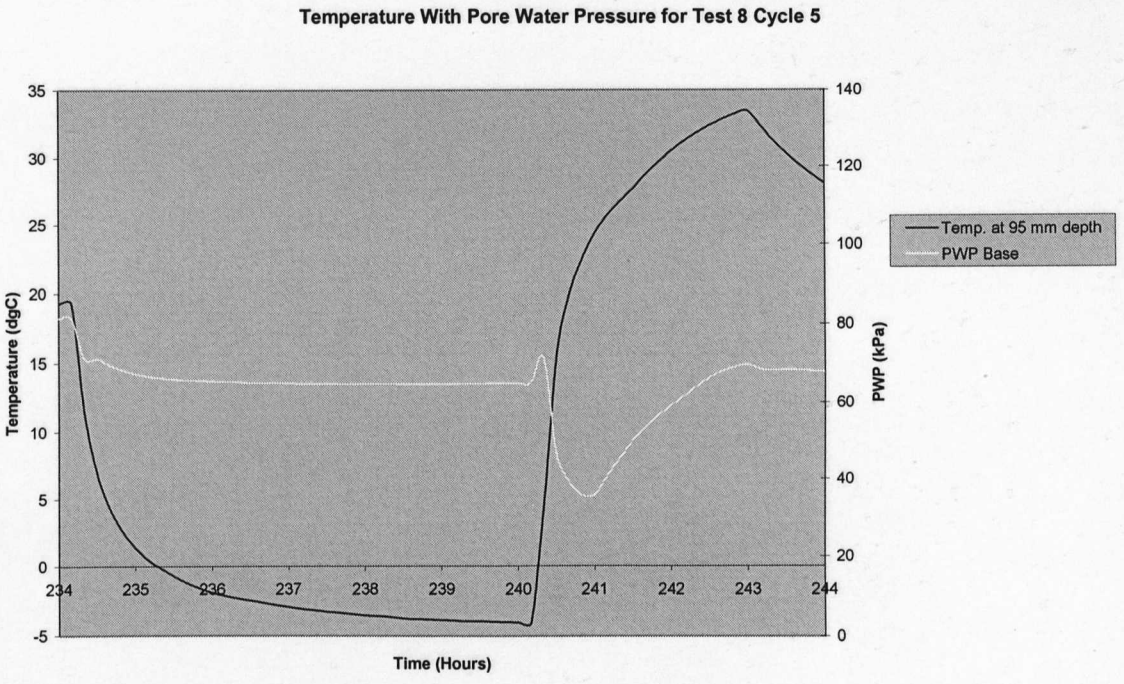

Figure 4.50 – Test 8 Cycle 5 Base

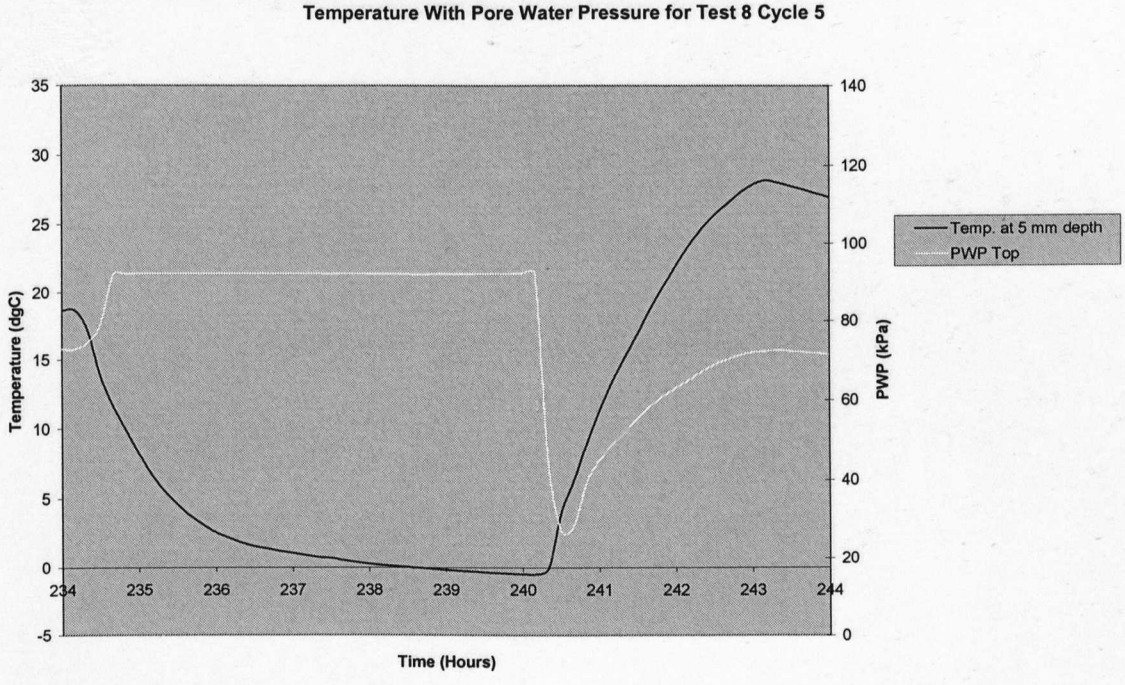

Figure 4.51 – Test 8 Cycle 5 Top

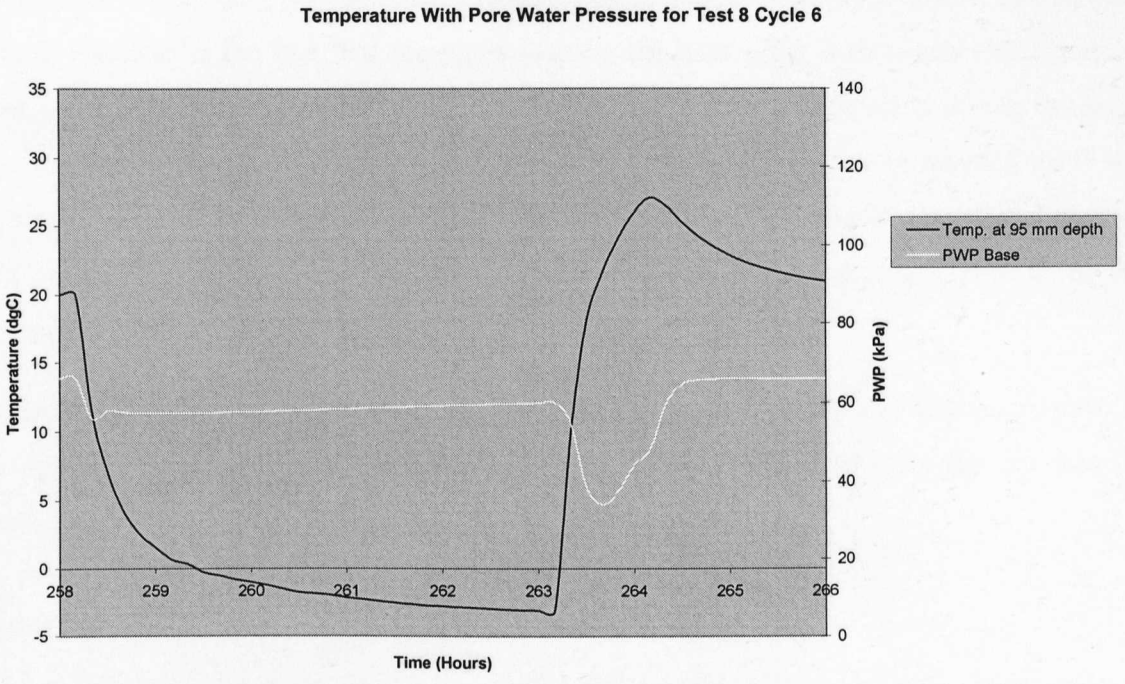

Figure 4.52 - Test 8 Cycle 6 Base

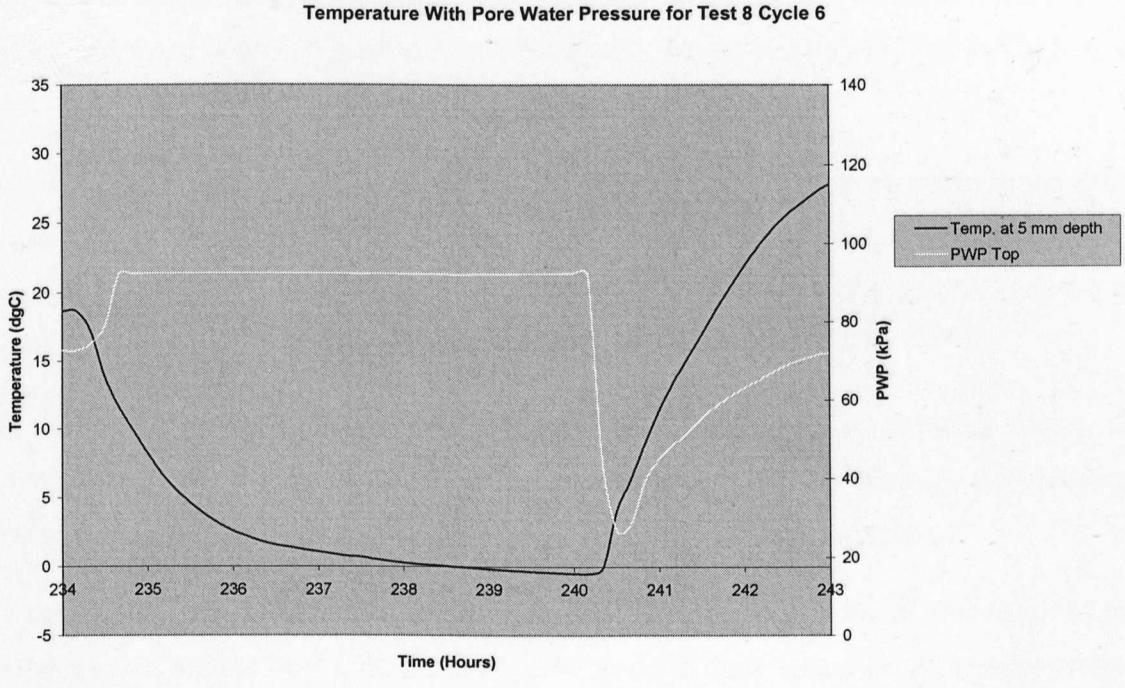

Figure 4.53 – Test 8 Cycle 6 Top

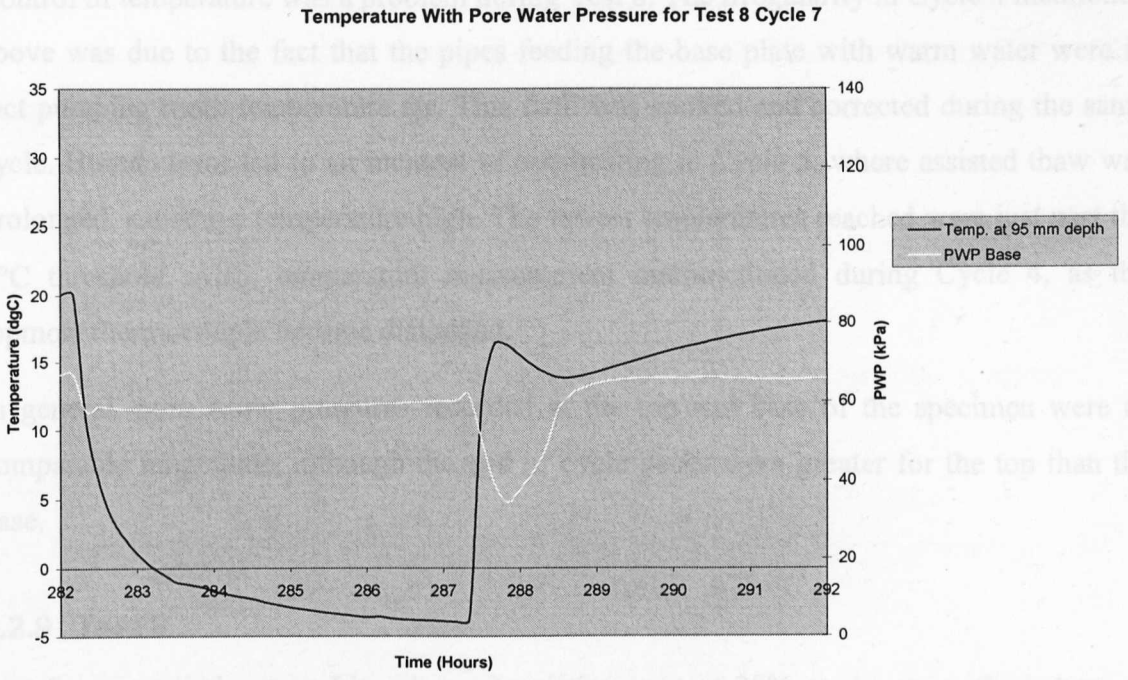

Figure 4.54 – Test 8 Cycle 7 Base

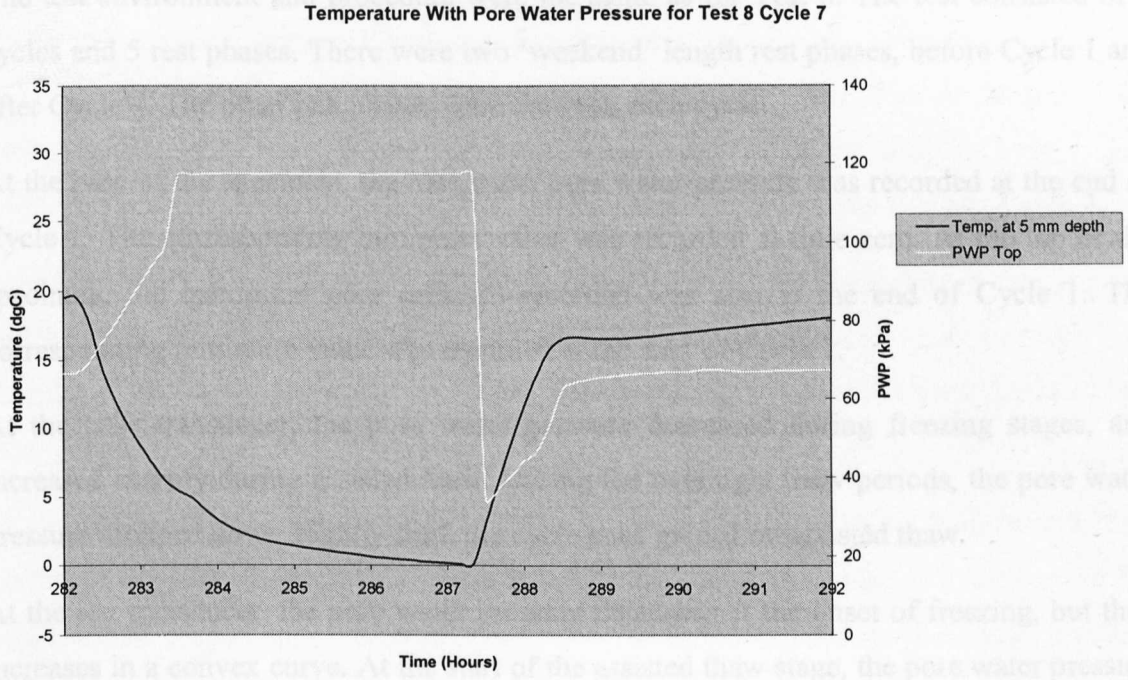

Figure 4.55 – Test 8 Cycle 7 Top

Leakage did not seem to be such a severe problem as in previous tests, with the final moisture content found to be 30% at the base and 36% at the top of the specimen, a distribution similar to that found in Test 6. However, the permanent downward settlement of the specimen revealed that leakage was still occurring.

Control of temperature was a problem during Test 8. The irregularity in Cycle 4 mentioned above was due to the fact that the pipes feeding the base plate with warm water were in fact pumping room temperature air. This fault was spotted and corrected during the same cycle. Human error led to an incident of overheating in Cycle 5, where assisted thaw was prolonged, causing a temperature high. The lowest temperatures reached were just past the 0°C threshold. Also, temperature measurement malfunctioned during Cycle 4, as the topmost thermocouple became dislodged.

In general, pore water pressures recorded at the top and base of the specimen were of comparable magnitude, although the end of cycle peaks were greater for the top than the base.

4.2.9 Test 9

Test 9 was carried out on Lias clay, of moisture content 29%, under an applied stress of 104 kPa.

The test environment and procedure were the same as for Test 8. The test consisted of 4 cycles and 5 rest phases. There were two 'weekend' length rest phases, before Cycle 1 and after Cycle 4. The other rest phases were between each cycle.

At the base of the specimen, the maximum pore water pressure was recorded at the end of Cycle 1. The corresponding minimum value was recorded at time zero. At the top of the specimen, the maximum pore pressure recorded was also at the end of Cycle 1. The corresponding minimum value was recorded at the start of Cycle 1.

At the base transducer, the pore water pressure decreased during freezing stages, and increased sharply during assisted thaw. During the overnight thaw periods, the pore water pressure dropped down slightly from the cycle peak gained on assisted thaw.

At the top transducer, the pore water pressure decreases at the onset of freezing, but then increases in a convex curve. At the start of the assisted thaw stage, the pore water pressure rises to a peak, (particularly in the case of Cycle 1, when the maximum value of pore water pressure was recorded), before settling to a residual level during the overnight thaw period.

Upward displacement of the specimen occurred for each cycle, showing expansion of the specimen on freezing.

Leakage was found to be a problem, despite the new one-piece liner. The final moisture content was found to be 21%. Leakage was observed particularly at the top, with water punching upwards between the piston and the side walls. The pore water pressures measured at the top of the specimen were very low, supporting the observation.

Control of temperature was acceptable, although the average temperatures were still fairly high, just reaching the 0°C threshold.

Pore water pressures recorded were greater at the base than at the top of the specimen.

4.2.10 Test 10

Test 10 was carried out on Lias clay, of moisture content 32%, under an applied stress of 80 kPa.

The test environment and procedure were the same as for Tests 8 and 9. The test consisted of 4 cycles and 5 rest phases. There were two 'weekend' length rest phases, before Cycle 1 and after Cycle 4. The other rest phases were between each cycle.

At the base of the specimen, the maximum pore water pressure was recorded at the end of Cycle 1. The corresponding minimum value was recorded at zero time. At the top of the specimen, the maximum pore water pressure was recorded at the end of Cycle 1. The corresponding minimum value was recorded at the end of the freezing stage of Cycle 4.

At the base transducer, the pore water pressure decreased at the onset of the freezing stages and levelled out. At the start of the assisted thaw stages, the pore water pressure rose sharply to a peak for that cycle, and then decreased to a lower level during the overnight thaw period.

At the top transducer, the pore water pressure varied in its pattern of behaviour, but in general, the pressure remained at a plateau during the freezing stages. At the start of the assisted thaw stages, the pore water pressure rose sharply to a peak for that cycle, and then decreased to a lower level during the overnight thaw period.

Upward displacement of the specimen occurred for each cycle, showing expansion of the specimen on freezing.

Leakage was still a problem, with the final moisture content found to be 24%. Both pressure transducers recorded fluctuations and decreases during periods of steady temperature, supporting the observed leakage.

Control of temperature was a problem, with the 0°C threshold not being met. The specimen was still achieving partial freezing however, as the specimen still expanded upwards during the freezing periods.

Pore water pressure values obtained from the top and the base transducers were of comparable magnitude.

4.2.11 Test 11

Test 11 was carried out on Lias clay, of moisture content 31%, under an applied stress of 80 kPa.

The test environment was substantially altered over the course of Tests 11-13, as

1. A shelter-box was constructed in order to maintain a constant temperature environment around the permode.
2. Freezing took place from the top downwards.
3. Assisted thaw was abandoned.

Temperature cycles comprised 6 hours freezing, and 18 hours thawing . The test consisted of 4 cycles and 5 rest phases. There was a long 'weekend' rest phase before the start of Cycle 1, and overnight rest phases, (which were really part of the thaw period), between each cycle and after Cycle 4.

At the base of the specimen, the maximum pore water pressure was recorded at the end of the freezing stage of Cycle 4. The corresponding minimum value was recorded at zero time. At the top of the specimen, the maximum pore water pressure was recorded just after the start of the freezing stage of Cycle 4. The corresponding minimum value was recorded at time zero.

At the base transducer, the pore water pressure varied in its pattern of behaviour. For Cycles 1 and 2, the pore water pressure decreased at the onset of the freezing stages. During the thaw stages, the pore water pressure rose in a convex curve. For Cycles 3 and 4,

the pore water pressure rose sharply to a peak during freezing, dropping to a lower value during thawing.

At the top transducer, the pore water pressure behaviour also varied, but not to such a great degree. The pore water pressure rose to a plateau during the freezing stages. At the start of the thaw stages, the pore water pressure decreased sharply, before increasing to a steady level.

Upward displacement of the specimen appeared to be fluctuating throughout the test, according to the datalogger, but this could not be observed as the permode was contained within the shelter box. After the test, the wiring to and from the datalogger was re-connected in case loose wires were causing 'odd' readings to be taken.

Leakage was not seen as a problem, with the final moisture content found to be 30%.

Control of temperature was a problem, with the 0°C threshold not being met. Difficulties were experienced particularly in the temperature control for Cycle 2.

Pore water pressure values obtained from the top and the base transducers were of comparable magnitude, excepting the peaks reached at the base transducer for Cycles 3 and 4.

4.2.12 Test 12

Test 12 was carried out on Lias clay, of moisture content 30%, under an applied stress of 80 kPa. Summarised results for this test are shown below in Figure 4.56.

As with Test 11, the test consisted of 4 cycles and 5 rest phases. There was a long 'weekend' rest phase before the start of cycle 1, and overnight rest phases between each cycle and after Cycle 4.

Figure 4.57 shows temperature profiles. It can be seen that freezing only occurred at the top of the specimen.

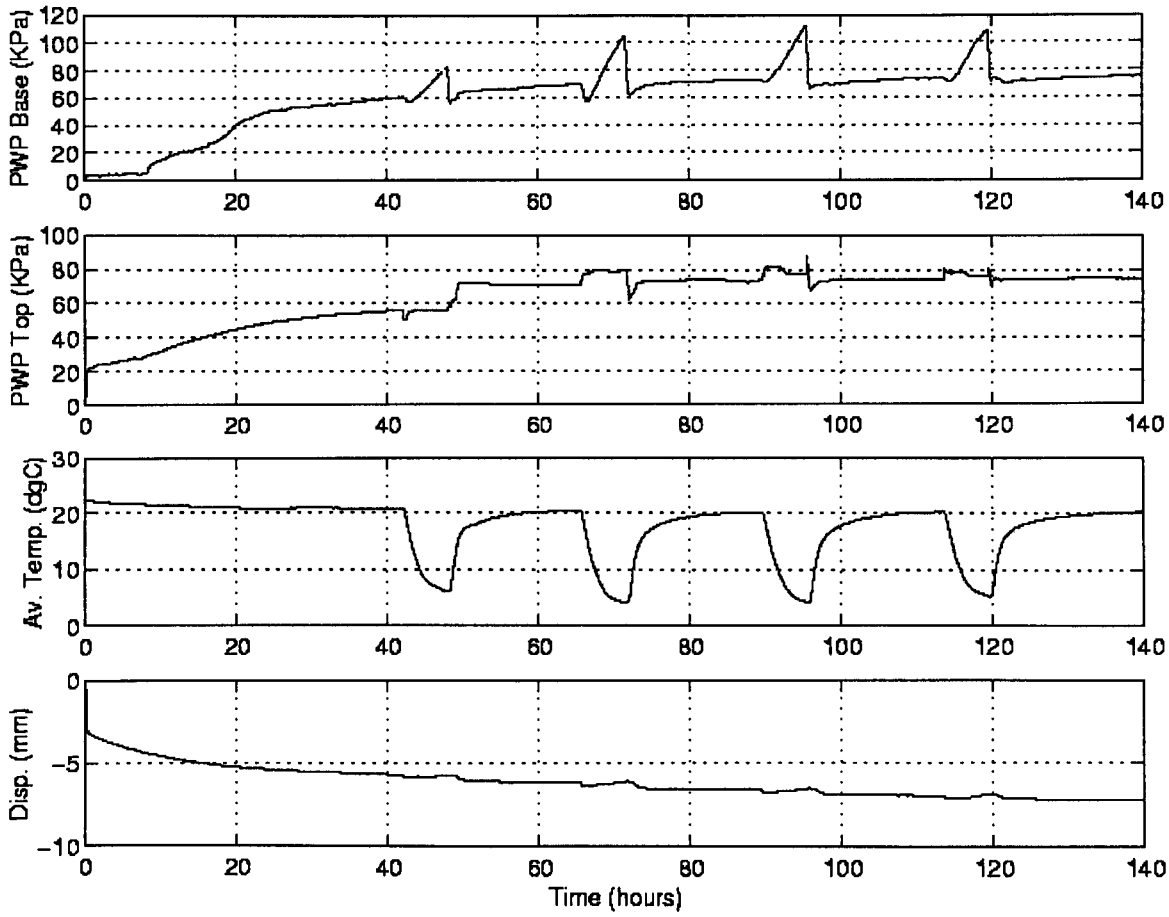

Figure 4.56 – Results for Test 12

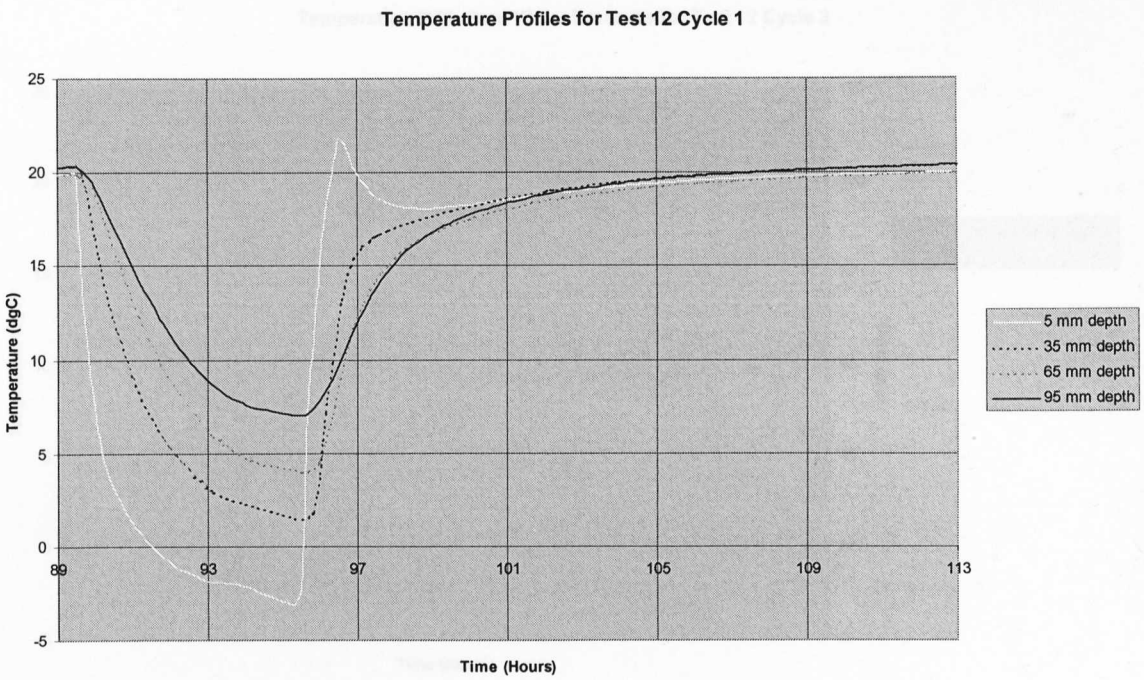

Figure 4.57 – Temperature Profiles for Test 12 Cycle 1

At the base of the specimen, the maximum pore water pressure was recorded at the end of the cooling stage of Cycle 3. The corresponding minimum value was recorded at zero time. At the top of the specimen, the maximum pore water pressure was also recorded at the end of the freezing stage of Cycle 3. The corresponding minimum value was also recorded at time zero.

Figures 4.58-4.61 show the pore water pressure response relative to the different temperatures achieved at the top and base of the specimen.

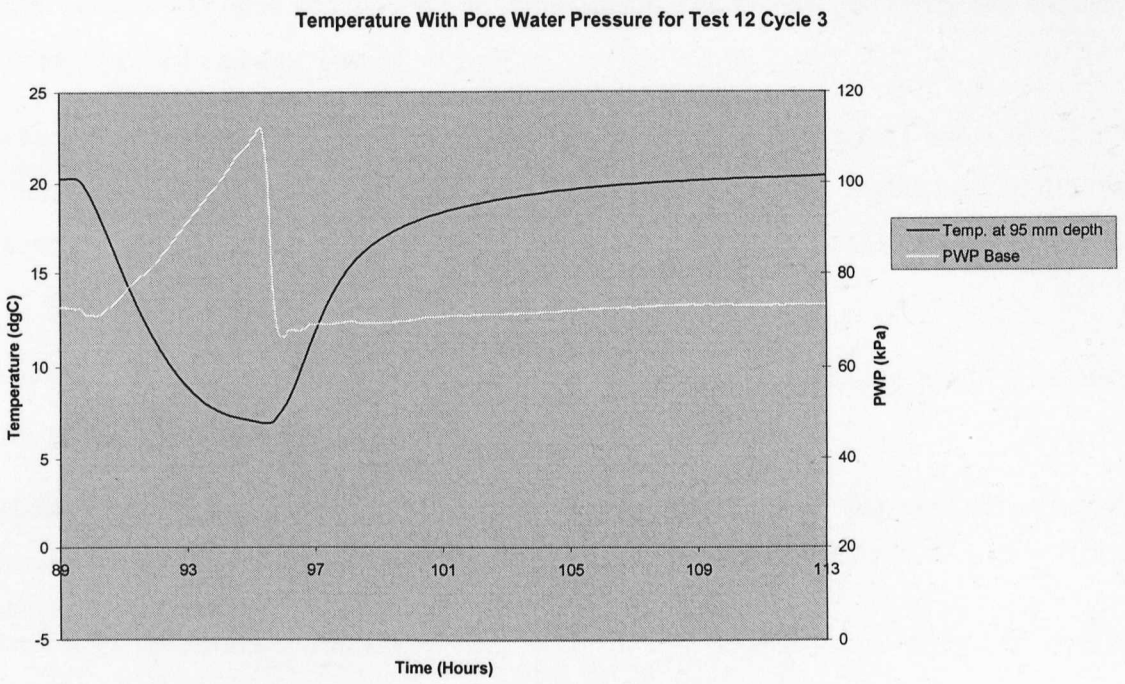

Figure 4.58 – Test 12 Cycle 3 Base

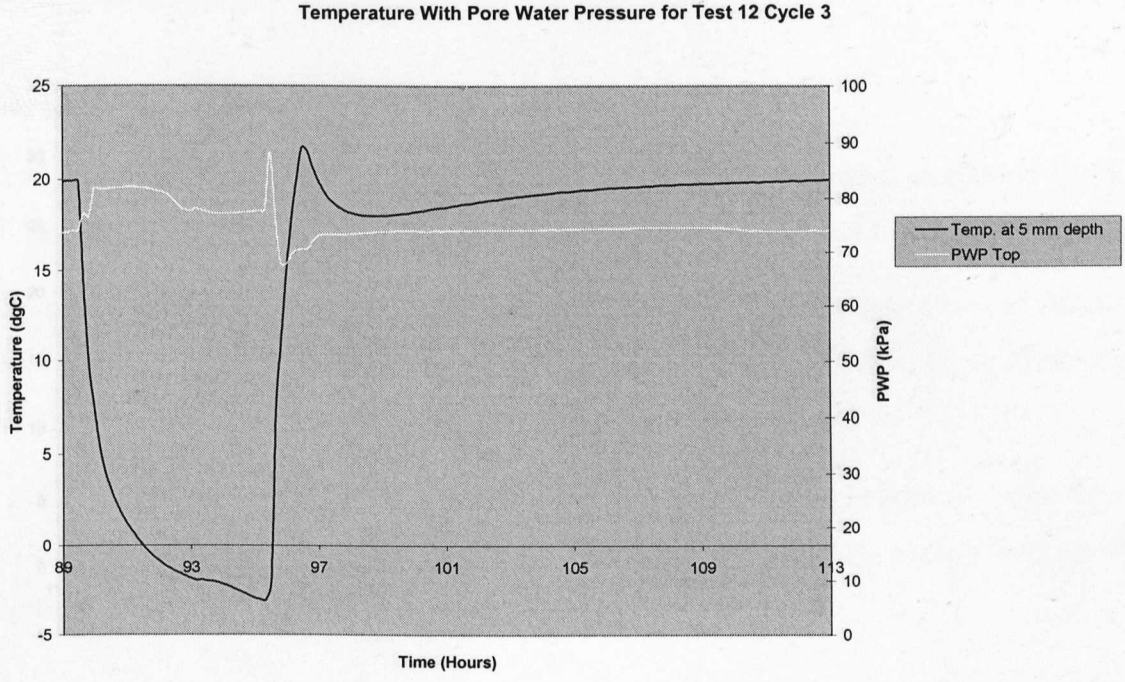

Figure 4.59 – Test 12 Cycle 3 Top

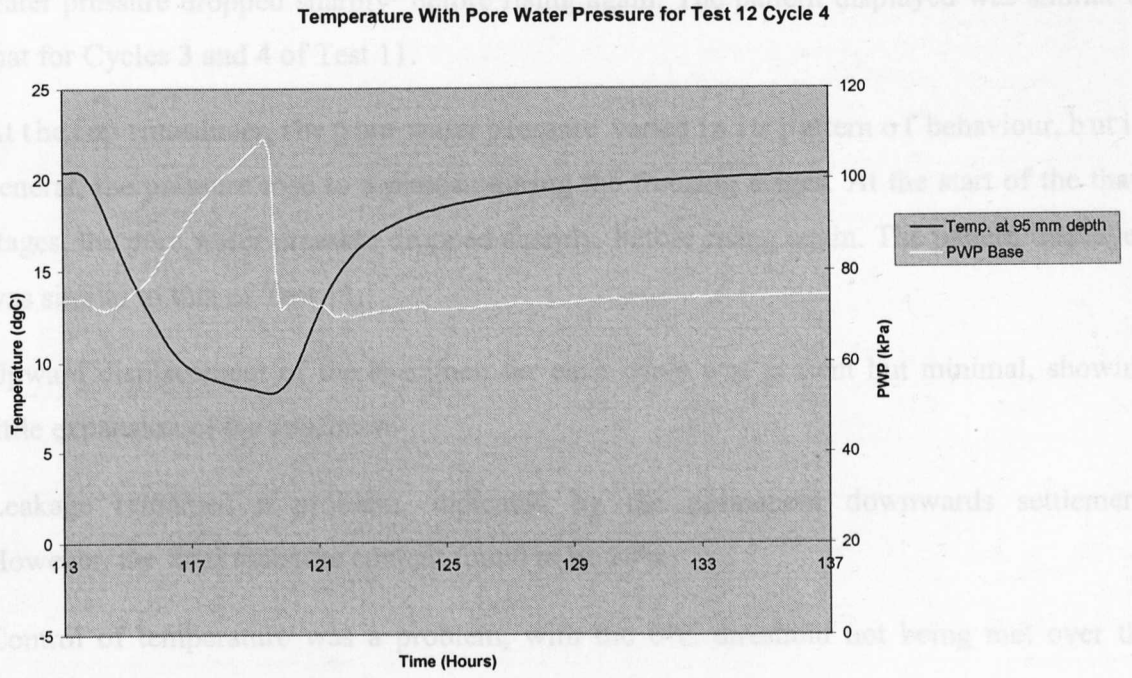

Figure 4.60 – Test 12 Cycle 4 Base

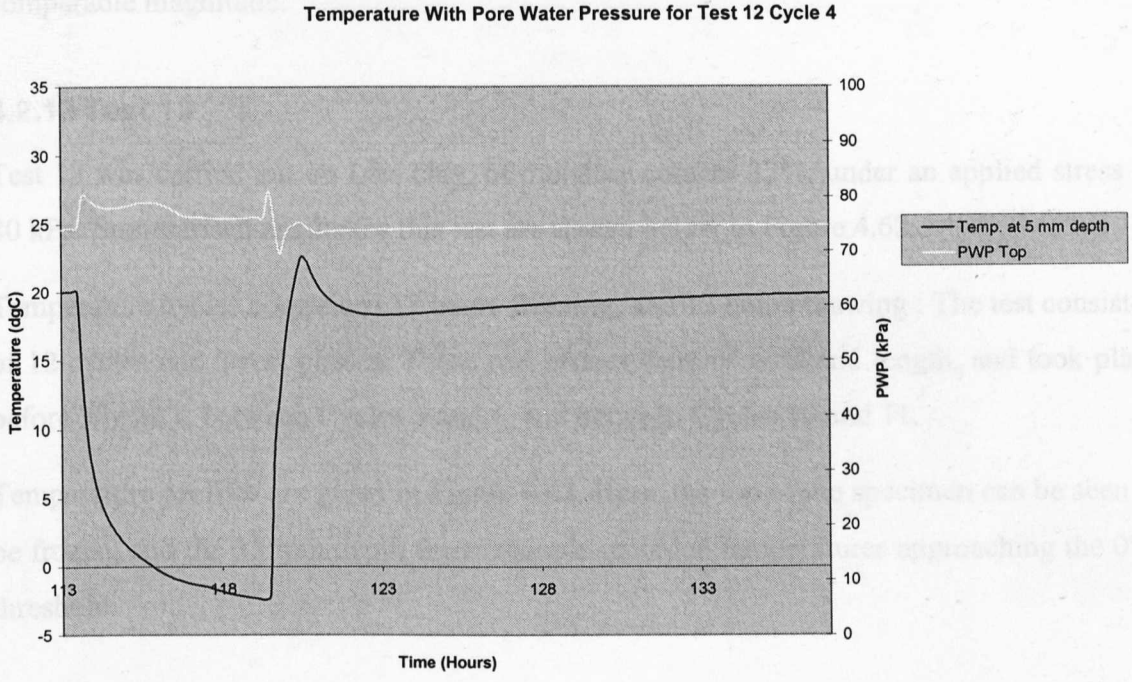

Figure 4.61 – Test 12 Cycle 4 Top

At the base transducer, the pore water pressure increased sharply at the onset of the cooling stages to reach a peak value for each cycle. At the start of the warming stages, the pore

water pressure dropped sharply before rising again. The pattern displayed was similar to that for Cycles 3 and 4 of Test 11.

At the top transducer, the pore water pressure varied in its pattern of behaviour, but in general, the pressure rose to a plateau during the freezing stages. At the start of the thaw stages, the pore water pressure dropped sharply, before rising again. The pattern displayed was similar to that of Test 11.

Upward displacement of the specimen for each cycle was present but minimal, showing little expansion of the specimen.

Leakage remained a problem, indicated by the permanent downwards settlement. However, the final moisture content found to be 29%.

Control of temperature was a problem, with the 0°C threshold not being met over the majority of the specimen.

Pore water pressure values obtained from the top and the base transducers were of comparable magnitude.

4.2.13 Test 13

Test 13 was carried out on Lias clay, of moisture content 32%, under an applied stress of 80 kPa. Summarised results for this test are shown below in Figure 4.62.

Temperature cycles comprised 12 hours freezing, and 12 hours thawing . The test consisted of 12 cycles and 3 rest phases. These rest phases were of weekend length, and took place before Cycle 1, between Cycles 5 and 6, and between Cycles 10 and 11.

Temperature profiles are given in Figure 4.63. Here, the top of the specimen can be seen to be frozen, and the 35 mm depth thermocouple recorded temperatures approaching the 0°C threshold.

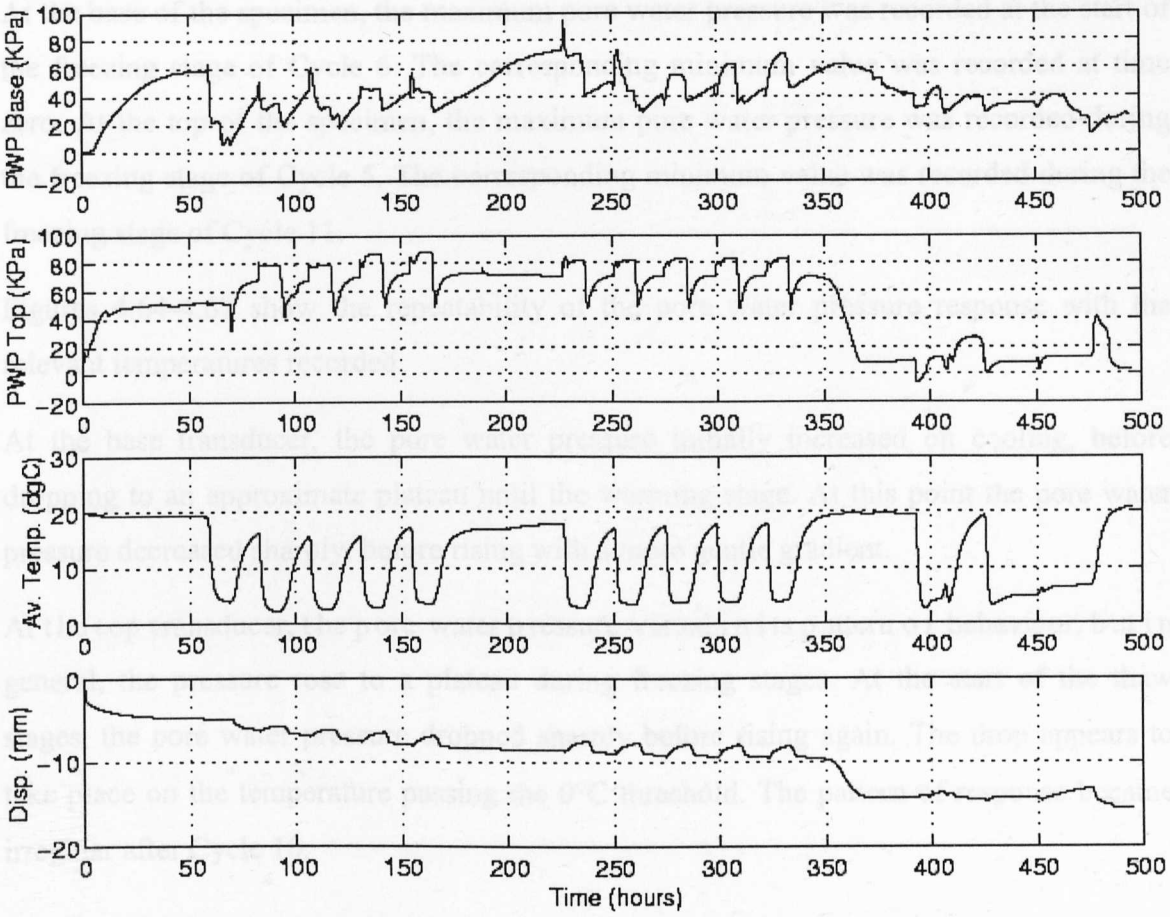

Figure 4.62 – Results for Test 13

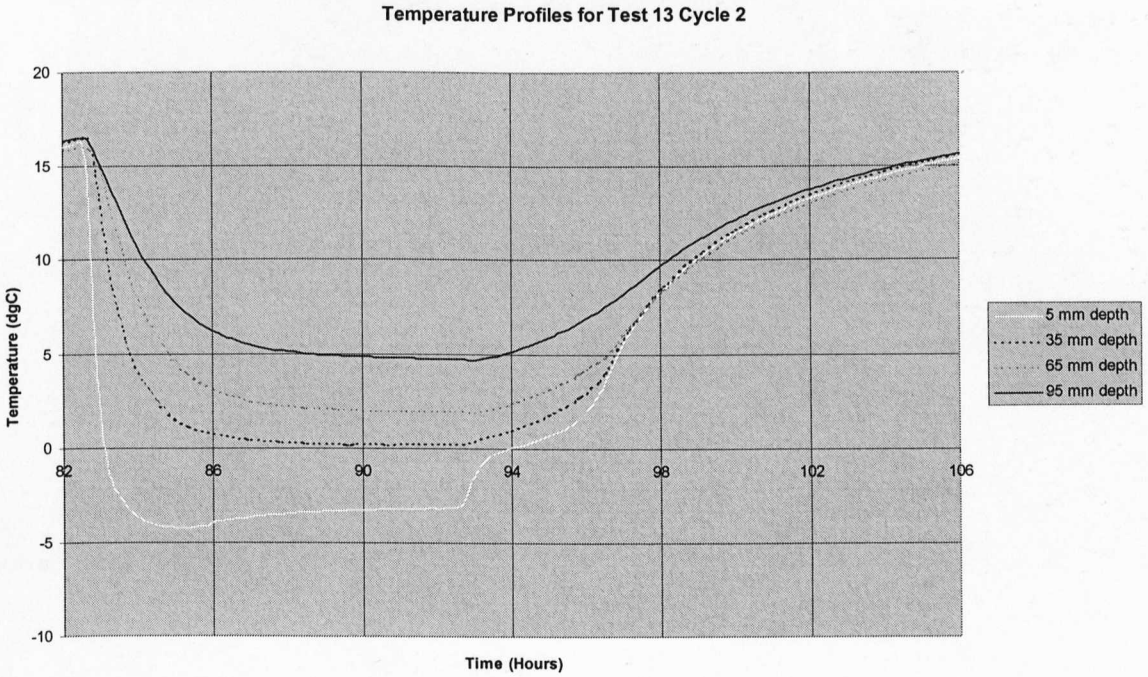

Figure 4.63 – Temperature Profiles for Test 13 Cycle 2

At the base of the specimen, the maximum pore water pressure was recorded at the start of the freezing stage of Cycle 6. The corresponding minimum value was recorded at time zero. At the top of the specimen, the maximum pore water pressure was recorded during the freezing stage of Cycle 5. The corresponding minimum value was recorded during the freezing stage of Cycle 11.

Figures 4.64-4.67 show the repeatability of the pore water pressure response with the relevant temperatures recorded.

At the base transducer, the pore water pressure initially increased on cooling, before dropping to an approximate plateau until the warming stage. At this point the pore water pressure decreased sharply, before rising with a more gentle gradient.

At the top transducer, the pore water pressure varied in its pattern of behaviour, but in general, the pressure rose to a plateau during freezing stages. At the start of the thaw stages, the pore water pressure dropped sharply before rising again. The drop appears to take place on the temperature passing the 0°C threshold. The pattern of response became irregular after Cycle 10.

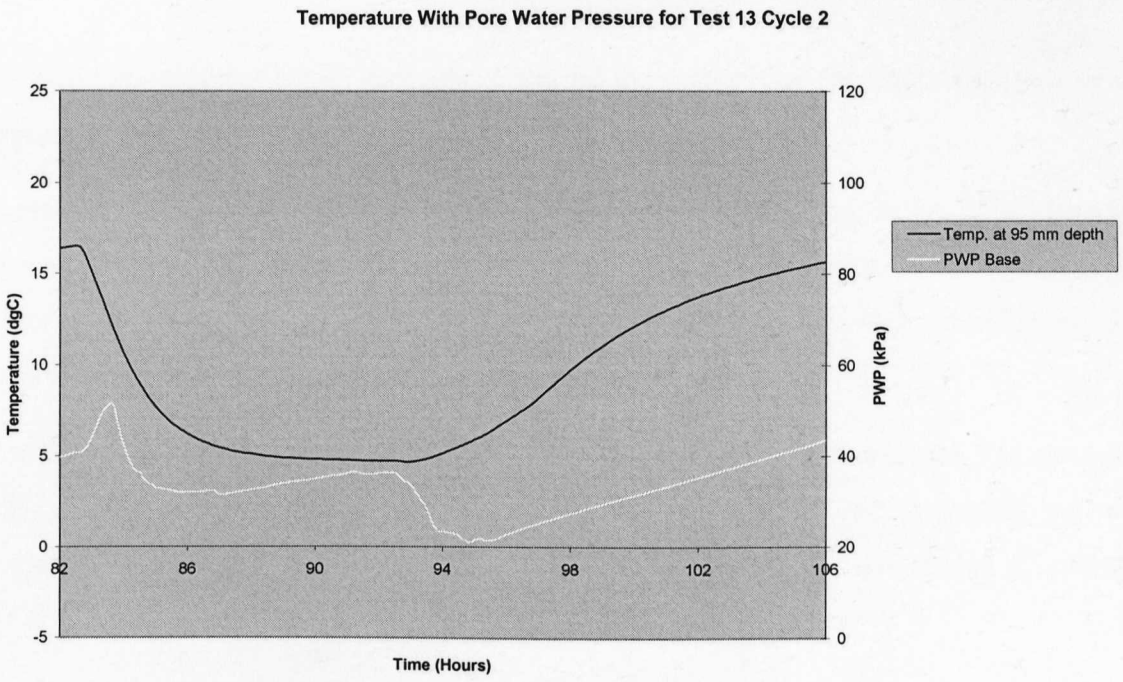

Figure 4.64 – Test 13 Cycle 2 Base

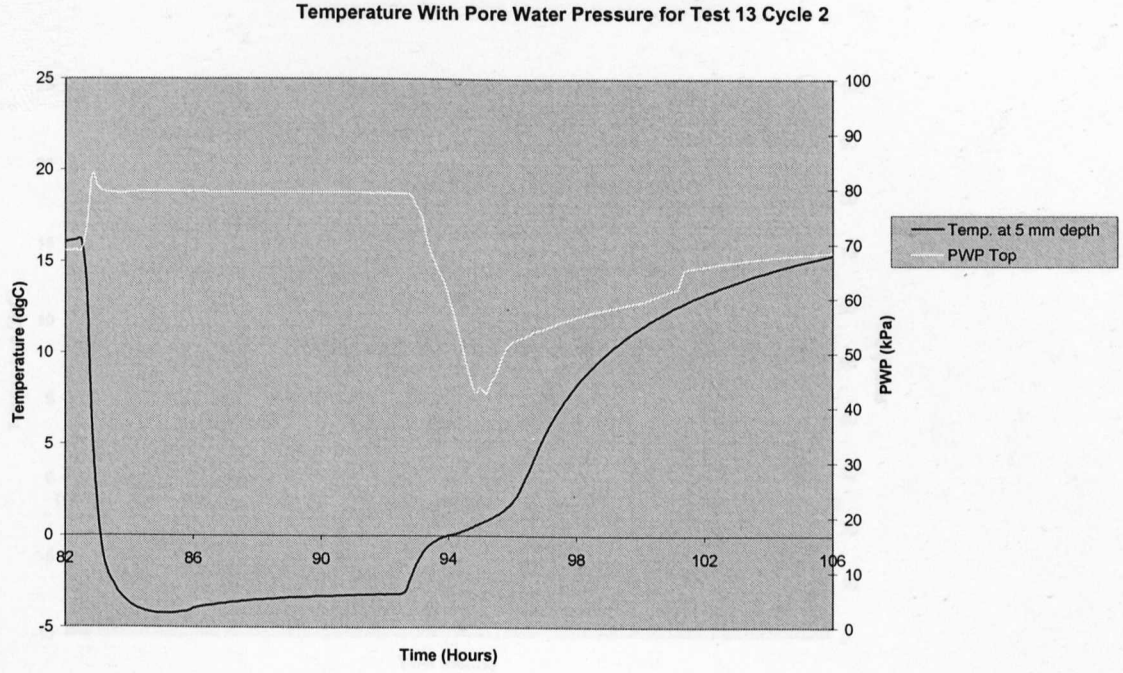

Figure 4.65 – Test 13 Cycle 2 Top

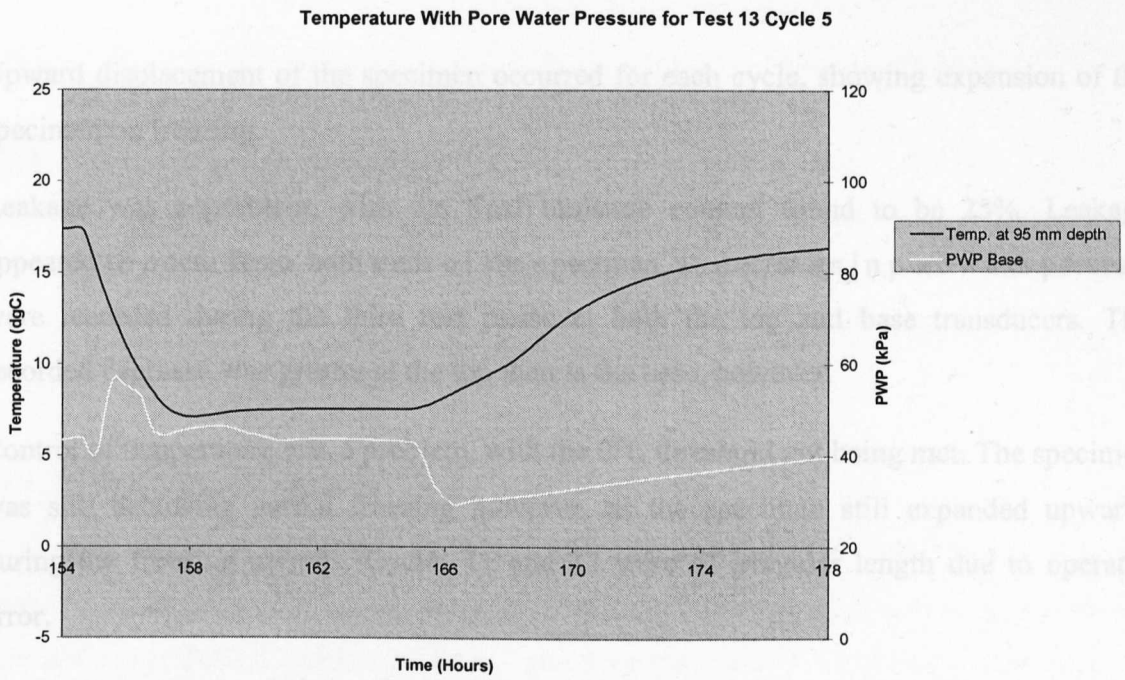

Figure 4.66 – Test 13 Cycle 5 Base

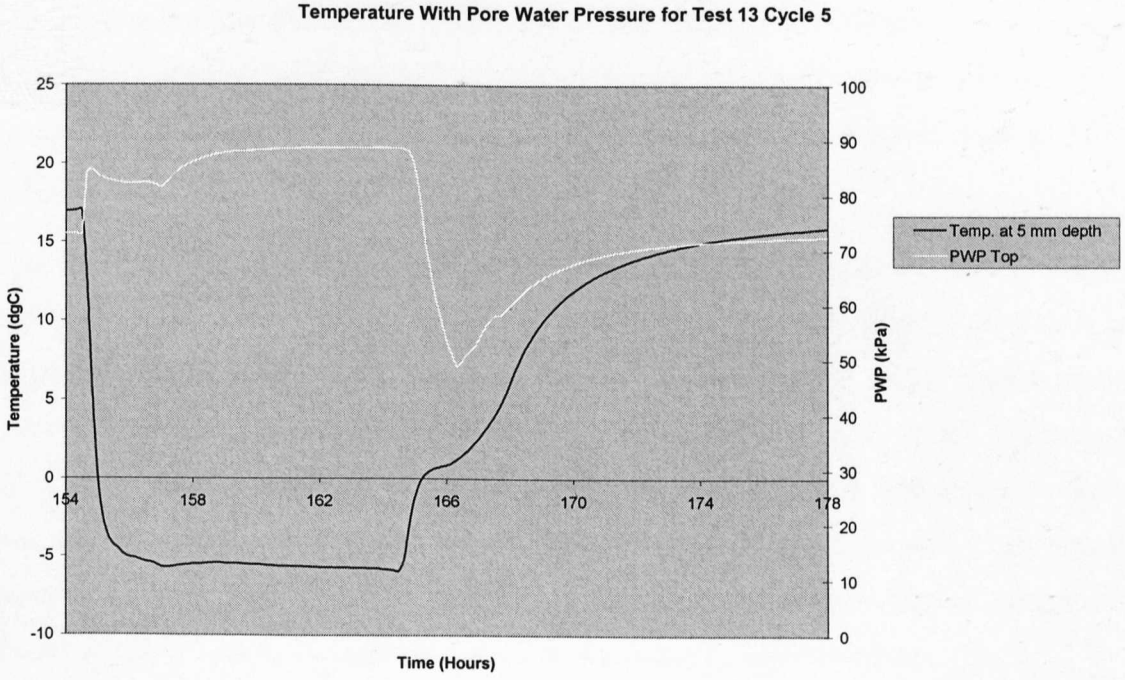

Figure 4.67 – Test 13 Cycle 5 Top

Upward displacement of the specimen occurred for each cycle, showing expansion of the specimen on freezing.

Leakage was a problem, with the final moisture content found to be 25%. Leakage appeared to occur from both ends of the specimen, as decreases in pore water pressure were recorded during the third rest phase at both the top and base transducers. The recorded decrease was greater at the top than at the base, however.

Control of temperature was a problem, with the 0°C threshold not being met. The specimen was still achieving partial freezing however, as the specimen still expanded upwards during the freezing periods. Cycles 11 and 12 were of irregular length due to operator error.

Pore water pressure values obtained from the top and the base transducers were of comparable magnitude, although the values recorded at the top transducer were generally higher. After Cycle 10, pore water pressure values decreased markedly, due to leakage.

Chapter 5 – Analysis of Results – Tests 1-13

5.1 Analysis of results

As these tests represent the commissioning period of both the apparatus and the testing procedure, it is not appropriate to form major research hypotheses based upon the results. However, the tests were vital to the development of the final test programme, apparatus and procedure. Areas of interest are outlined below.

5.1.1 Patterns of Results

Although the results for Tests 1–13 have already been discussed individually, it is also possible to note similarities or contrasts between the some of the sets of data obtained. Tests 4 and 5, Tests 8 and 12 and Tests 7 and 8 are particularly interesting in this respect.

Tests 4 and 5 were carried out under the same applied stress, but at different moisture contents. The results obtained for the two tests were found to be similar in terms of patterns displayed and values of pore water pressure measured. The increase to maximum pore water pressures recorded in Test 5 were approximately 10 kPa at both the top and base of the specimen. For both Tests 4 and 5, the maxima were obtained prior to the start of Cycle 3.

The 10 kPa increment higher pore water pressure values gained for Test 5 were not expected, as the initial moisture content was in fact lower than for Test 4. A greater pore water pressure response might have been expected to occur in the soil of higher moisture content. However, the difference in moisture content was only 2 %, which indicates that other factors could have caused the difference in values recorded. For example, leakage was noted as a particular problem in Test 5. The maximum/minimum pore water pressures recorded in Test 5 are therefore considered to be of a comparable order of magnitude to those gained in Test 4, thus demonstrating repeatability of soil behaviour.

In Test 8, a comparable magnitude of the pore water pressures was recorded at the base and top transducers in each test. The pattern of pore water pressure response was different

at the top and the base of the specimen, (see Chapter 4, Section 4.2.8), but reverted to a similar level during rest phases. The observed behaviour is in keeping with the double-sided freezing imposed, with water being attracted to the freezing fronts at both the top and the base of the specimen. This water migration would have produced roughly equal pore water pressures. This may not have been observed in other, similar tests due to leakage. However, additional evidence of moisture migration is still required, as similar behaviour was seen in Test 12, where freezing took place from the top downwards and only one freezing front was present.

Tests 7 and 8 could be considered as dissimilar tests, as both the applied stress and the initial moisture contents were different for each test. However, the results gained were similar in terms of the general patterns displayed. In terms of maximum pore water pressures recorded, maximum values recorded were approximately 7-8 kPa higher in Test 8 at both the top and base of the specimen. This was not expected, as both the applied stress and moisture content were lower than in Test 7. However, leakage was found to have occurred in Test 7, which may well have affected the results obtained. In addition, Test 8 was a longer test, with the maximum pore water pressures being recorded in Cycles 4 and 7, as opposed to Cycles 2 and 3 for Test 7. For both tests, the pore water pressures recorded at the top were generally higher than those recorded at the base, and followed a more consistent repeating pattern.

The pattern of results obtained from Tests 7 and 8 is discussed further in Section 5.1.1.

No correlation could be drawn between applied stress and pore water pressure response based on the results obtained. This is considered to be due to the development of the test apparatus and methodology, and is not felt to be critical for this point in the test programme.

5.1.2 Temperature Control

Tests 1-13 were carried out using initially unfrozen specimens.

For Tests 1 and 2, freezing was imposed from both ends of the permode, and thawing achieved by stopping the freezing action. In the case of Test 1, the amount of temperature loss was deemed to be excessive (reaching –10°C). Test 2, using the same cooling procedure, did not achieve such low average temperatures. This demonstrated that the freezing/thawing timetable was not reliable. The antifreeze reservoir was being filled and

cooled before the start of testing each day, rather than being maintained at constant temperature. This was due to safety concerns, as the methanol-based product originally available gave off vapour to the surrounding area. The antifreeze was then replaced with an ethylene glycol-based product, allowing the reservoir to be kept full and cooled at all times.

For Test 3, assisted thaw was introduced from the top of the permode downwards, in an attempt to limit the temperature range and allow two freeze-thaw cycles to be carried out per day. This was partially successful, although the second cycle of each day returned the temperature to a higher level on thaw than that of the first cycle, this being due to the additional overnight thaw.

For Tests 4 - 10 the assisted thaw method was revised to give thaw from both ends of the permode. At the time, this was intended to give a more uniform method of freezing and thawing. However, in retrospect, thawing from both ends did not simulate a natural procedure. Also, the extent of overheating meant that the pore water pressure response was suspect, as again it did not simulate natural conditions.

For Test 7, the number of freeze-thaw cycles reverted to one per 24 hours, with a complete cycle comprising 4 hours freezing, 3 hours assisted thawing and 17 hours overnight thawing. Temperature control was a problem in that the average temperatures only just passed the 0°C threshold on freezing.

For Tests 8–10, an extra hour of freezing was introduced, but, the same difficulties were encountered as in Test 7.

In all tests where high temperatures were generated by thawing, (or rather warming), the specimen, thermal expansion must be considered to have occurred. This expansion within a closed specimen, instead of expulsion through drainage ports, would cause the high values of pore water pressure to be recorded.

For Tests 11–13, it was decided that freezing from both ends and assisted thaw should be abandoned, as the pore water pressure response could not be considered to be likely to have occurred under the natural conditions considered – i.e. frost penetration from the ground surface downwards. Specimens were now frozen from the top downwards only. The construction of the shelter-box was the first attempt to provide a dedicated cold environment for the test apparatus. However, the system was not effective for two reasons.

Firstly, the box itself was not sealed, allowing warm air to intrude. Secondly, the attempts at cooling the interior via a cooling element were counter-productive. The antifreeze entering the element increased in temperature, raising the temperature of the reservoir and hence the element and the permode.

Following on from Tests 11-13, the shelter-box was replaced by a refrigerator. This meant that the test environment temperature could be maintained independently of the antifreeze reservoir. Also, the antifreeze was gaining less heat during its circulation through the permode. Overall, the introduction of the refrigerator provided a stable test environment and allowed more precise temperature regimes to be imposed on the specimens. As a result of this new capability, it was decided to change the temperature range to that of 'just frozen' to 'just thawed', as opposed to the original room temperature cycles.

5.1.2 The Consideration of Moisture Migration

Patterns of moisture migration were observed most clearly in Tests 6 and 8, where higher final moisture contents were recorded at the top of the specimen than at the base.

In Test 6, the final moisture content found to be 32 % at the top of the specimen, and 21 % at the base, compared with an original moisture content of 35 %. This suggests that either water migration through the sample, or greater leakage at the base than the top. It was felt in this case that the moisture contents were due to the latter situation, as freezing and thawing had been proceeding from both ends of the specimen and not setting up a unique frozen front.

In Test 8, leakage did not seem to be a problem, with the final moisture content found to be 36 % at the top of the specimen and 30 % at the base, compared with an original moisture content of 30 %. In this case, the suggestion of differential leakage is not supported. However, redistribution of water in the specimen is also not supported as end of cycle pore water pressures were found to be roughly the same for top and base transducers, in keeping with the freezing and thawing from both ends imposed. One possibility is that the uncontrolled, overnight thaw period has allowed more thawing to proceed from the top down, as a greater surface area of conductive metal, (i.e. the piston assembly), is available than at the base, (where only the radial portion of the metal baseplate is on contact with room temperature). This would lead to downwards percolation of meltwater being impeded by frozen/partially frozen soil below.

For Tests 11-13, moisture migration towards the top was not observed. This was to have been expected, as although the thermal changes were imposed from one direction only, freezing did not take place.

With regards to future tests carried out under improved temperature conditions, it was decided to monitor moisture migration closely, particularly when using one-directional freezing only.

5.2 Consideration of Zero Curtain Behaviour

Harris *et al*, (1995), and Harris & Davies, (1998), presented results from a full-scale model slope experiment. The experiment and results are outlined in Chapter 2, Section 2.5. Although the permode test conditions are substantially different, Tests 7 and 8 have been found to display pore water pressure responses similar to that recorded in by Harris & Davies, (1998), in the thawing zero curtain period.

Cycle by cycle results for Test 7 and selected cycles for Test 8 are given below in Figures 5.1-5.16. Each results set comprises 2 subplots:

1. Temperature Profiles for a 10 hour period representing the imposed thermal regime, with Pore Water Pressure recorded at the top and base of the specimen.

2. Pore Water Pressure measured relative to appropriate temperature reading, over a length of time including both zero curtain periods.

Freezing and thawing took place rapidly due to cooling and warming taking place from both the top and the base of the apparatus. This is the most significant difference between the model slope and permafrost approaches at this point in the testing programme. Harris *et al*, (1997), had defined the model slope simulations as equivalent to deep seasonal frost penetration, with surface downwards freezing only. The case of two-sided freezing was considered to be analogous with soil being subject to ground freezing from above and an underlying cold permafrost layer being present. Therefore, the method employed for the permode Tests 7 and 8 could be considered to be an example of two sided freezing, and thus having little in common with the model slope simulations. However, Harris *et al*, (1997), noted that the processes causing thaw-induced soil strain would be likely to occur in any case of ice-rich soil thawing, irrespective of the initial pre-thaw ice distribution. By implication, the results gained in Tests 7 and 8 can therefore be compared to the model slope simulation findings in this context.

Due to the fast implementation and short timescale of the freeze-thaw regime imposed, lengthy 'freezing' and 'thawing' zero curtain periods were not experienced. As mentioned previously in Sections 4.2.7 and 4.2.8, temperature control was not ideal and led to overheating of the specimen in some cases.

Considering Test 7 first, Figures 5.1, 5.3, 5.5 and 5.7 all show that while the temperature recorded at 5 mm depth, (i.e. nearest to the top of the specimen), approaches 0°C but does not pass it. Therefore there is no zero curtain behaviour at the top of the specimen. In Cycle 1 the 0°C isotherm did not progress from the base as far as the 65 mm depth thermocouple, meaning that less than a third of depth of specimen was frozen. In Cycles 2-4 the 0°C isotherm did reach the 65 mm depth thermocouple, and in Cycle 4, the temperature at the top of the specimen also approached 0°C.

The higher pore water pressures were recorded at the top of the specimen, but as freezing did not occur in this region this was perhaps due to thermal expansion and feedback of free water between the transducer sites in the closed test environment.

Considering zero curtain period behaviour, the pore water pressure response at the base transducer was not uniform. This may have been due to radial leakage which was observed during the test. In Cycle 1, the pore water pressure response rose to a plateau shortly after the freezing 0°C threshold. At the point of the thaw 0°C threshold, the pore water pressure rose slightly before dropping sharply. In Cycles 2-4 the pore water pressure response generally fluctuated during the period between the two 0°C thresholds, but rose and dropped sharply after the thaw 0°C threshold.

Now considering Test 8, an extra hour longer was added to the freezing stage of each cycle, giving longer periods of ~0°C temperatures, but again for the lower half of the specimen only. The temperature at 5 mm depth briefly dipped below 0°C in Cycle 2 however. The pattern of pore water pressure response is similar to that of Test 7, being mainly fluctuating but with the repeating rise and sharp dip at the thaw 0°C threshold. Moisture content values found at the end of the test were considered to be reliable, partly due to the one-piece liner being incorporated for first time.

No initial drop to negative pressure values during freezing, as reported by Harris & Davies, (1998), occurred. This is most likely to be due to the fact that freezing did not take place over the whole depth of the specimen due to poor temperature control. Instead pressures

rose immediately, but did drop during the nominal thawing zero curtain period, before rising once more in keeping with the Harris & Davies, (1998), results. It must be noted, however, that the pressures did not drop to negative values at this point either.

The maximum pore water pressures induced in the specimens, of order 100-120 kPa, were higher than those recorded in the model slope, which were quoted as 15-40 kPa (Harris & Davies, 1998). This can be accounted for by the overburden pressure on the specimens, not present on the model slope, and also by the elevated soil temperatures experienced by the specimens. For example, the fast transition to the thawed state would prevent the suction condition from arising.

The principal disadvantage of the thawing method employed in Tests 7 and 8 is that it induces too fast a temperature change, and breaks down the soil-ice structure with little regard for natural processes. The zero curtain periods on freezing and thawing were made much shorter. Later test methodology was adapted to rectify this issue, (see Chapter 3).

Despite the drawbacks mentioned above, Tests 7 and 8 yielded interesting results, as:

1. A repeatable pattern of pore water pressure was recorded.
2. Zero curtain phase change behaviour was observed.
3. Comparison to earlier research (Harris & Davies, 1998), was possible.

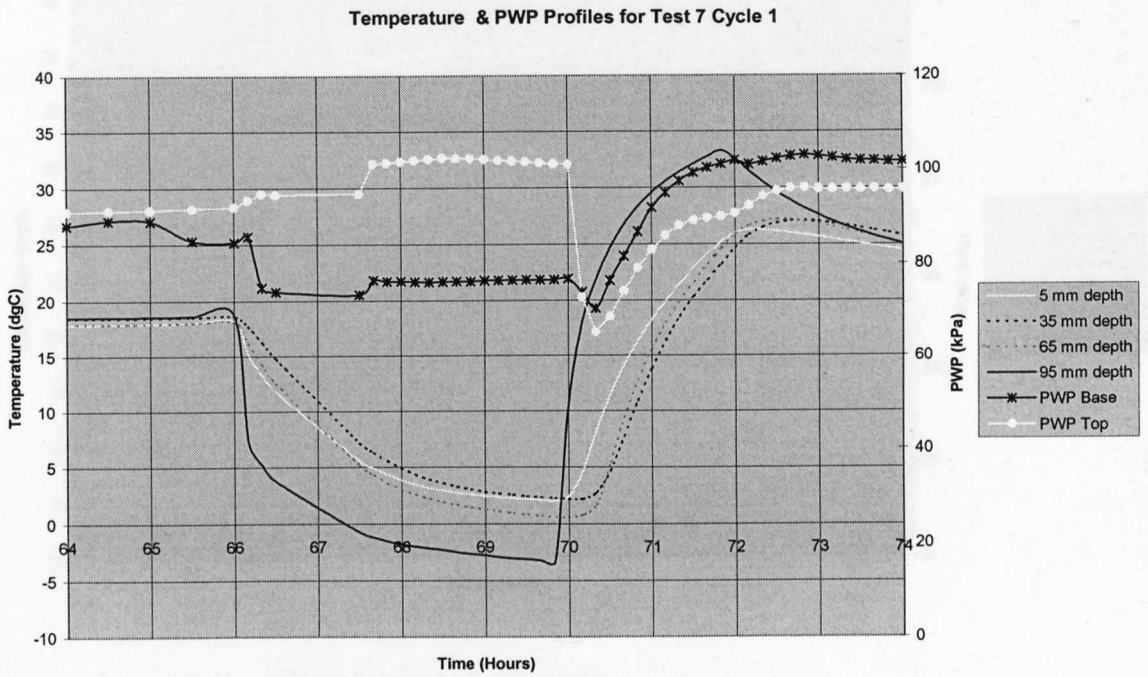

Figure 5.1 – Test 7 Cycle 1 Pore Water Pressure & Temperatures

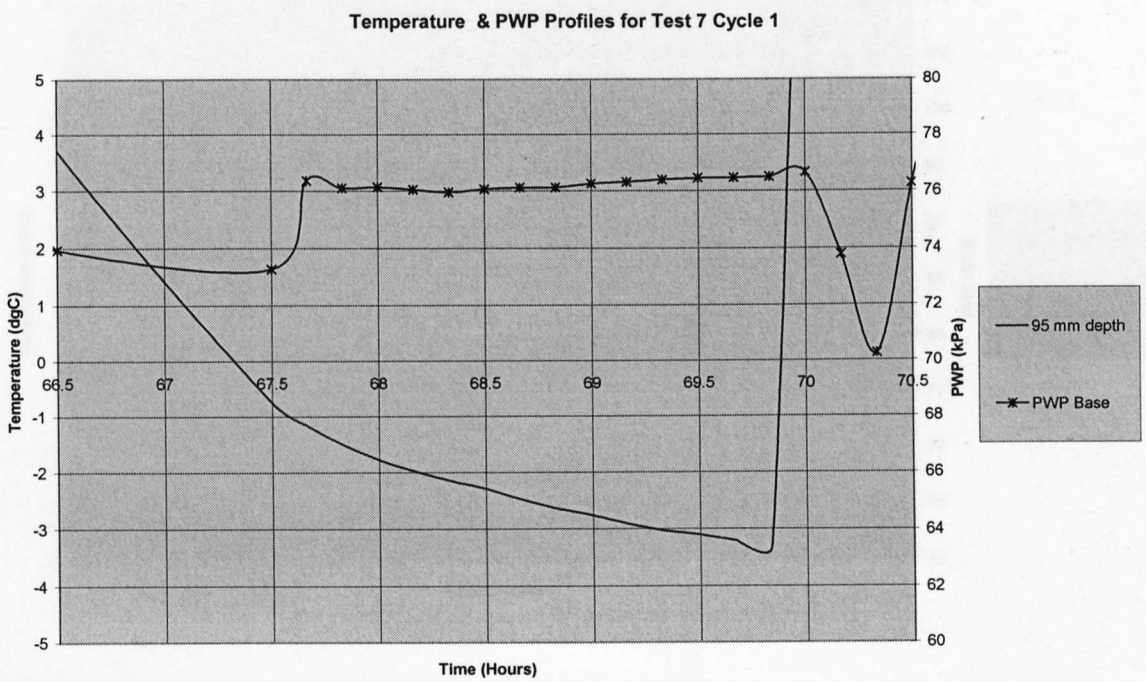

Figure 5.2 - Test 7 Cycle 1 Pore Water Pressure & Temperature at Base

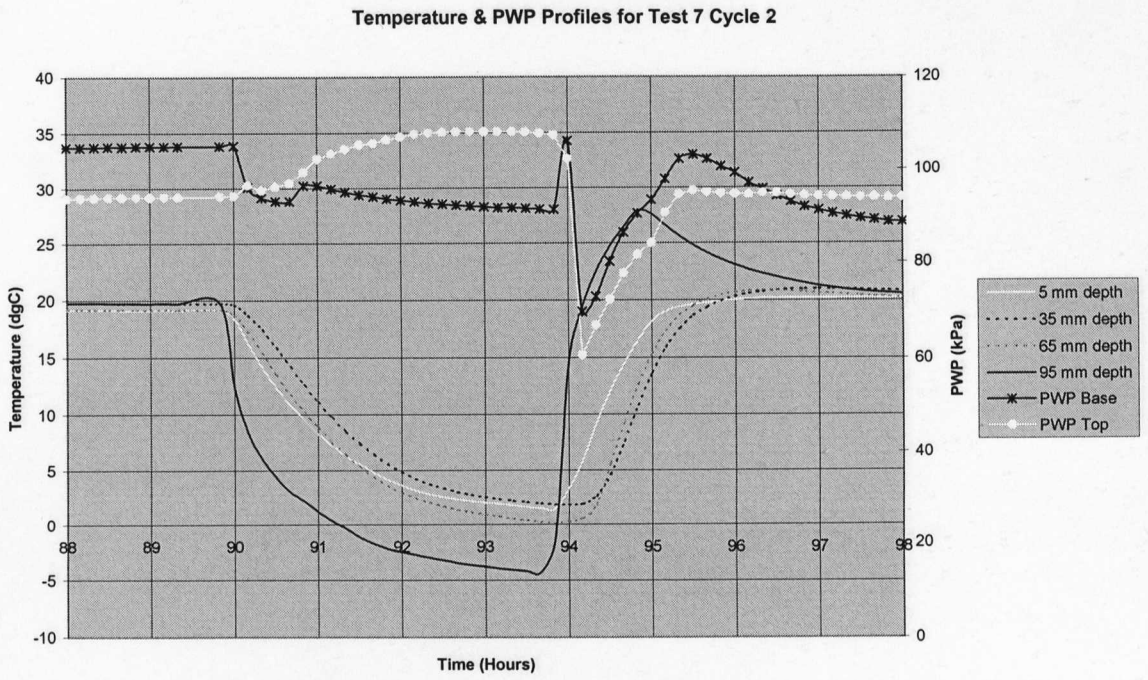

Figure 5.3 – Test 7 Cycle 2 Pore Water Pressure & Temperatures

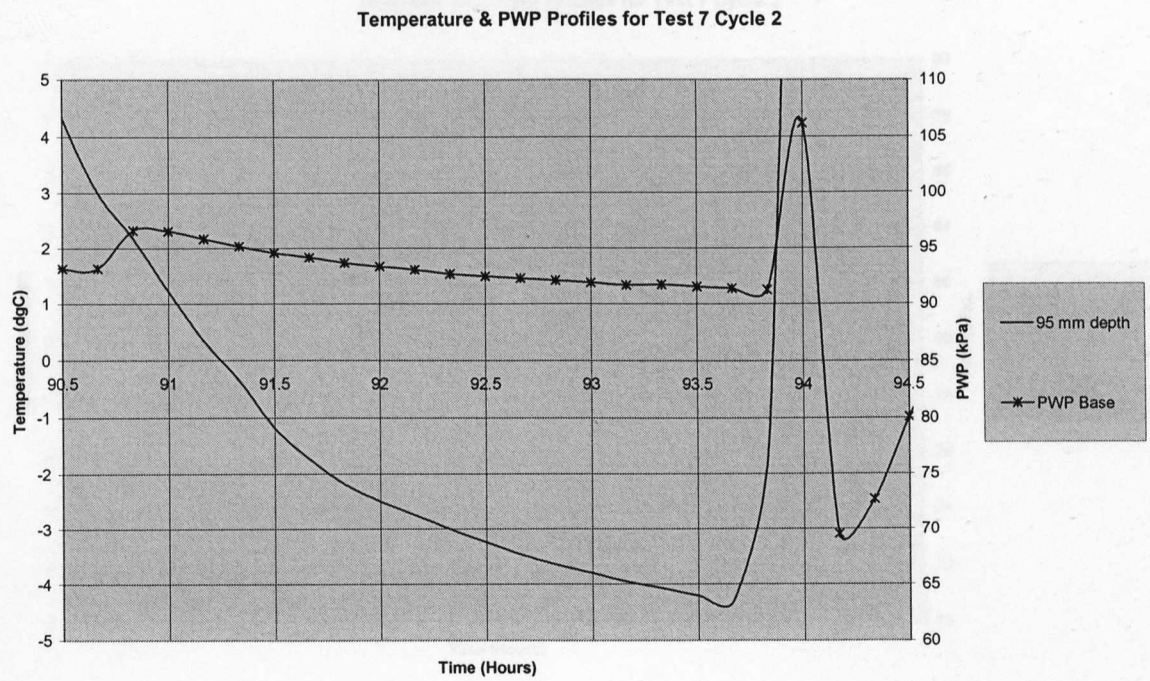

Figure 5.4 – Test 7 Cycle 2 Pore Water Pressure & Temperature at Base

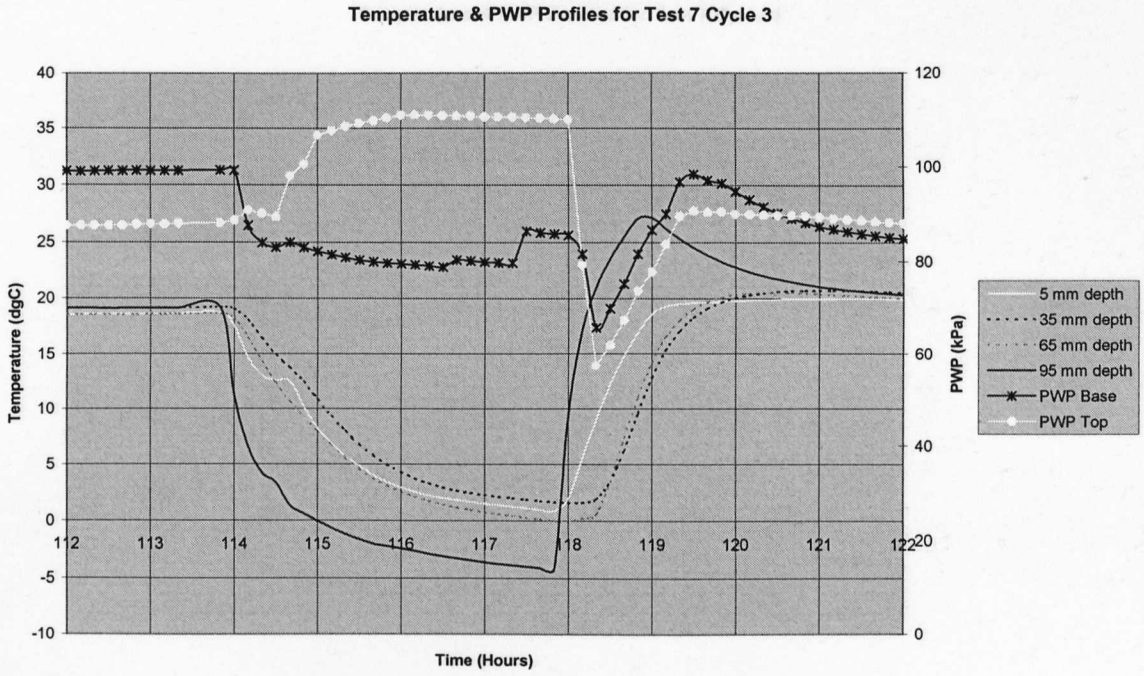

Figure 5.5 – Test 7 Cycle 3 Pore Water Pressure & Temperatures

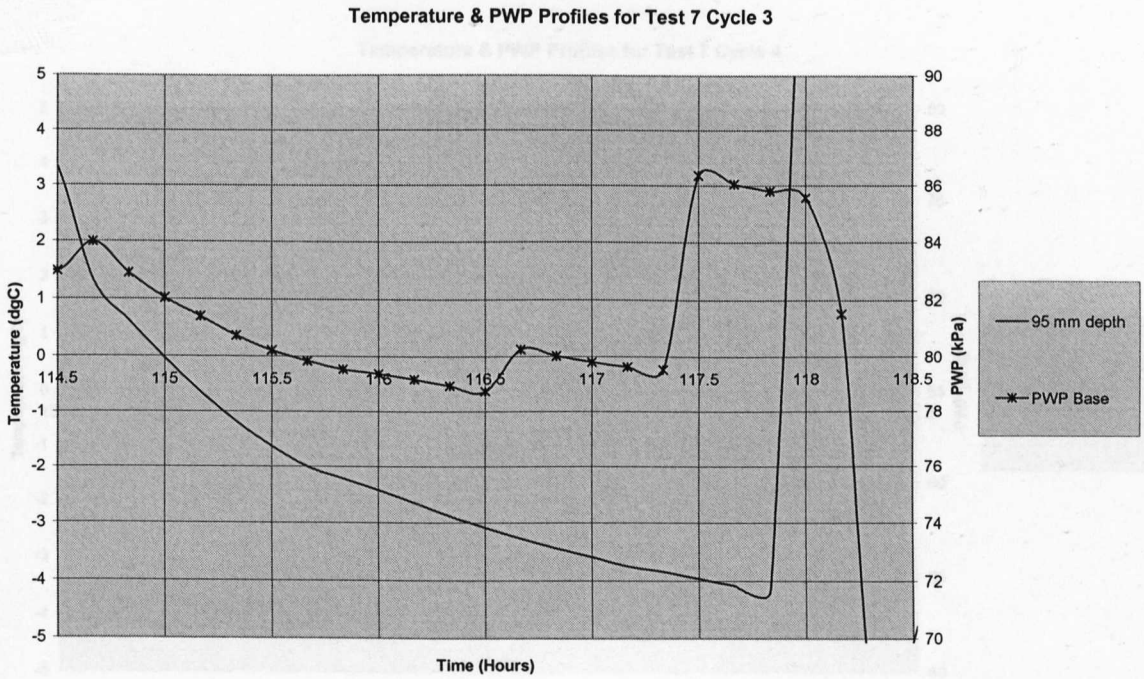

Figure 5.6 – Test 7 Cycle 3 Pore Water Pressure & Temperature at Base

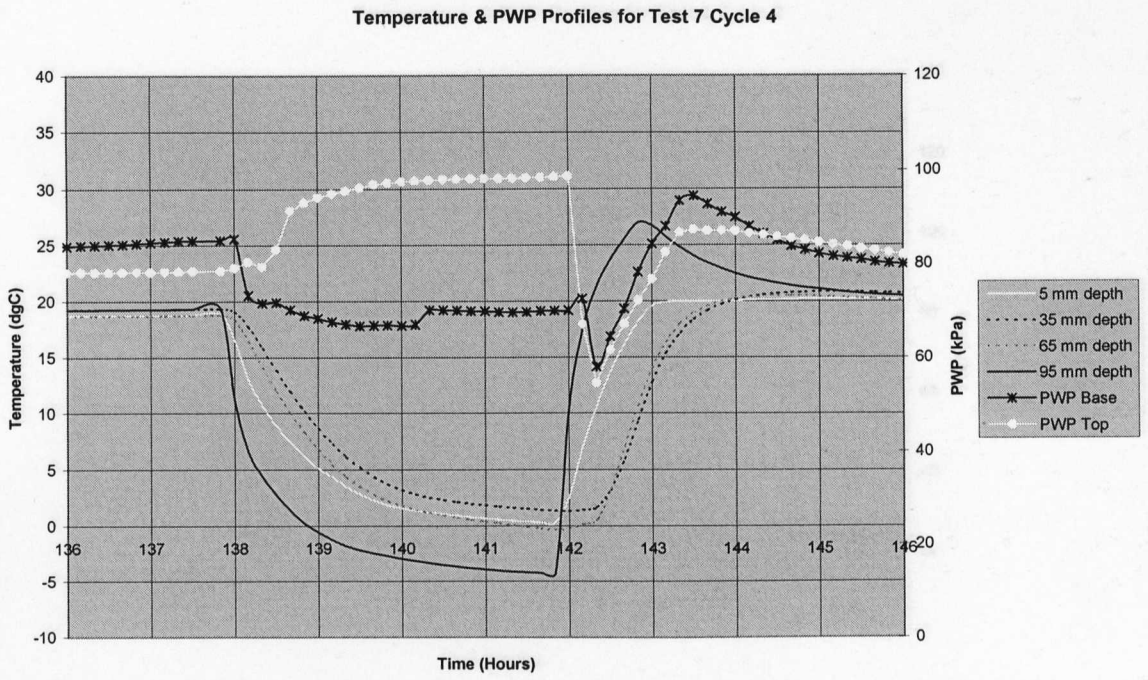

Figure 5.7 – Test 7 Cycle 4 Pore Water Pressure & Temperatures

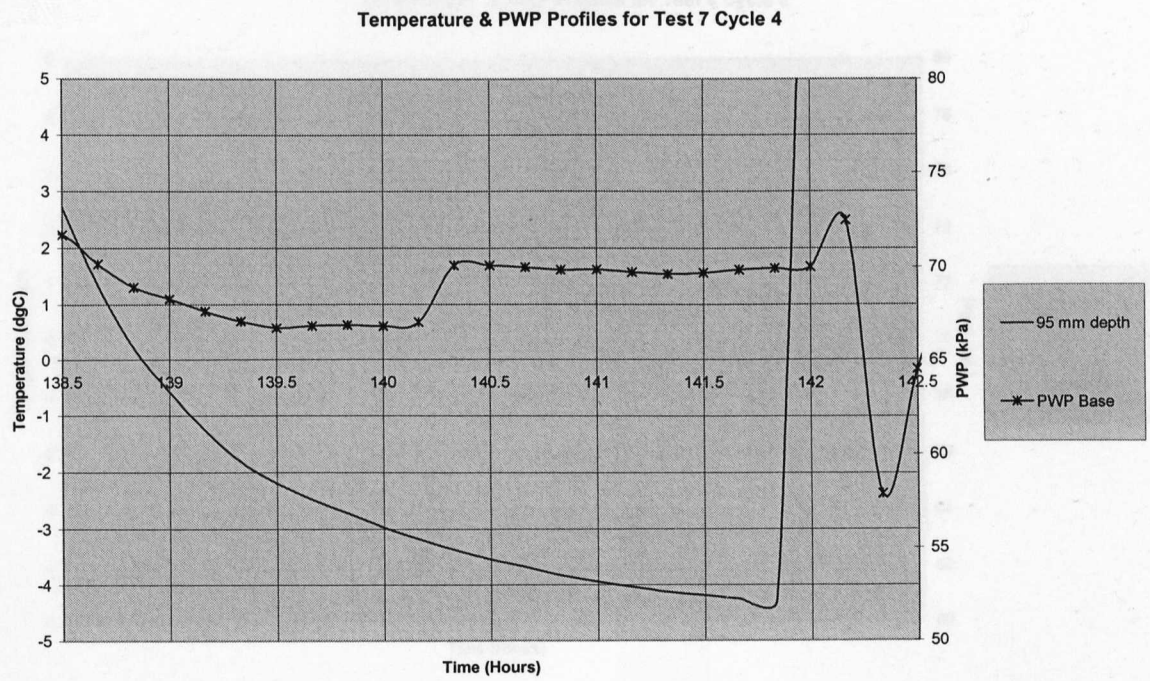

Figure 5.8 – Test 7 Cycle 4 Pore Water Pressure & Temperature at Base

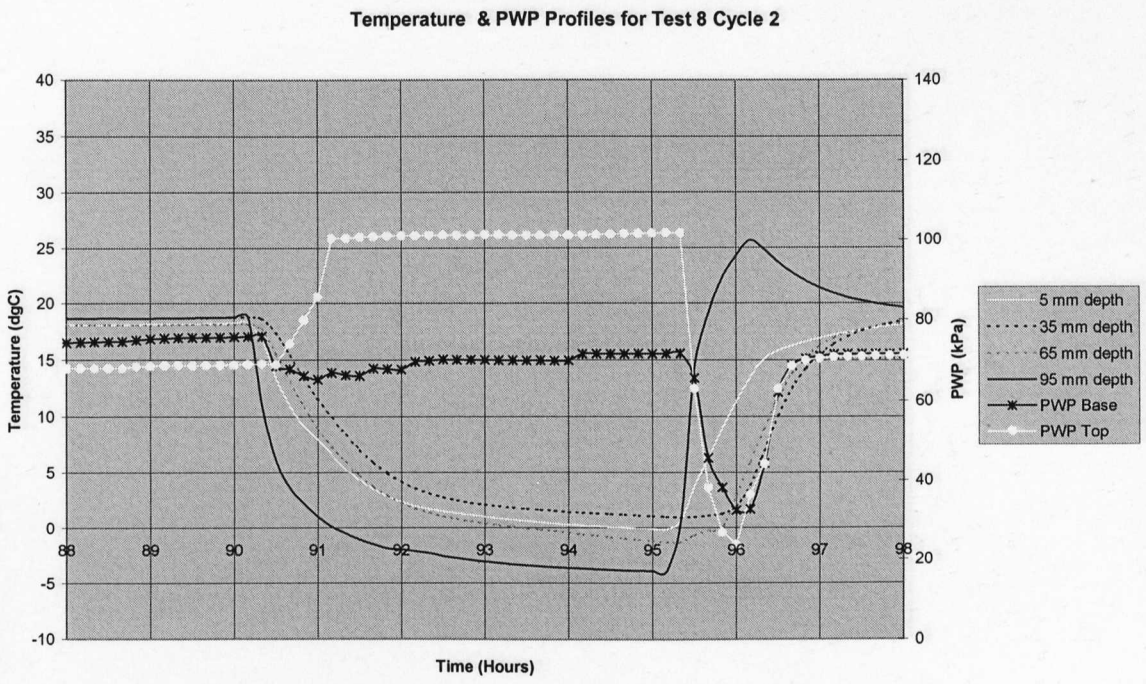

Figure 5.9 – Test 8 Cycle 2 Pore Water Pressure & Temperatures

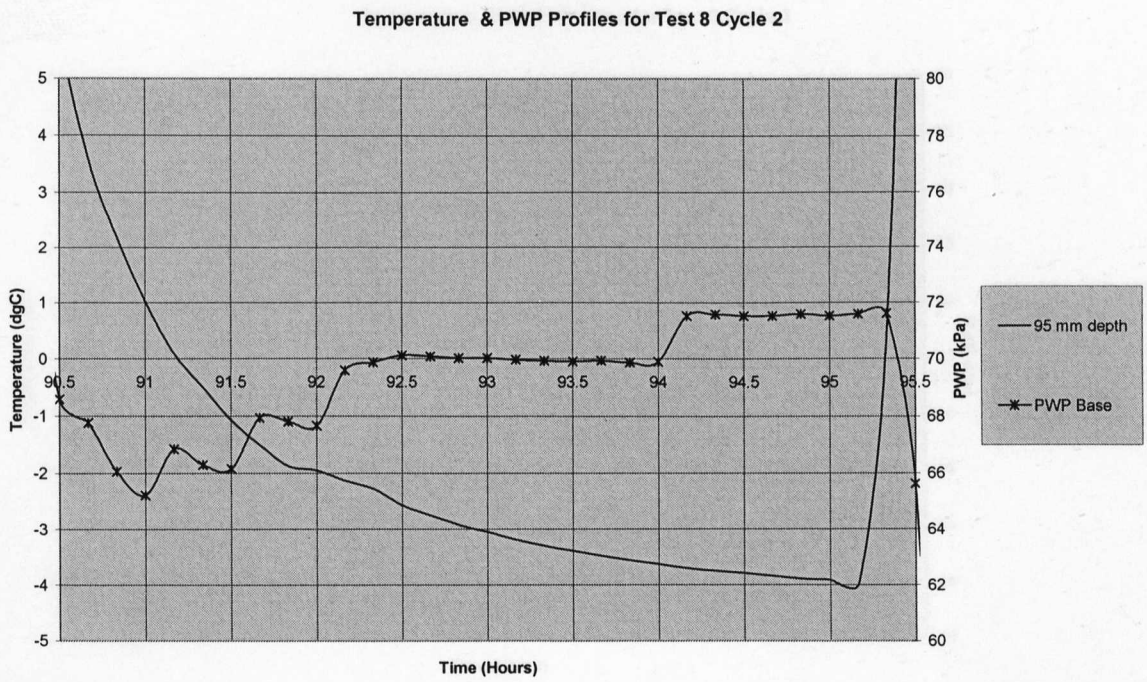

Figure 5.10 – Test 8 Cycle 2 Pore Water Pressure & Temperature at Base

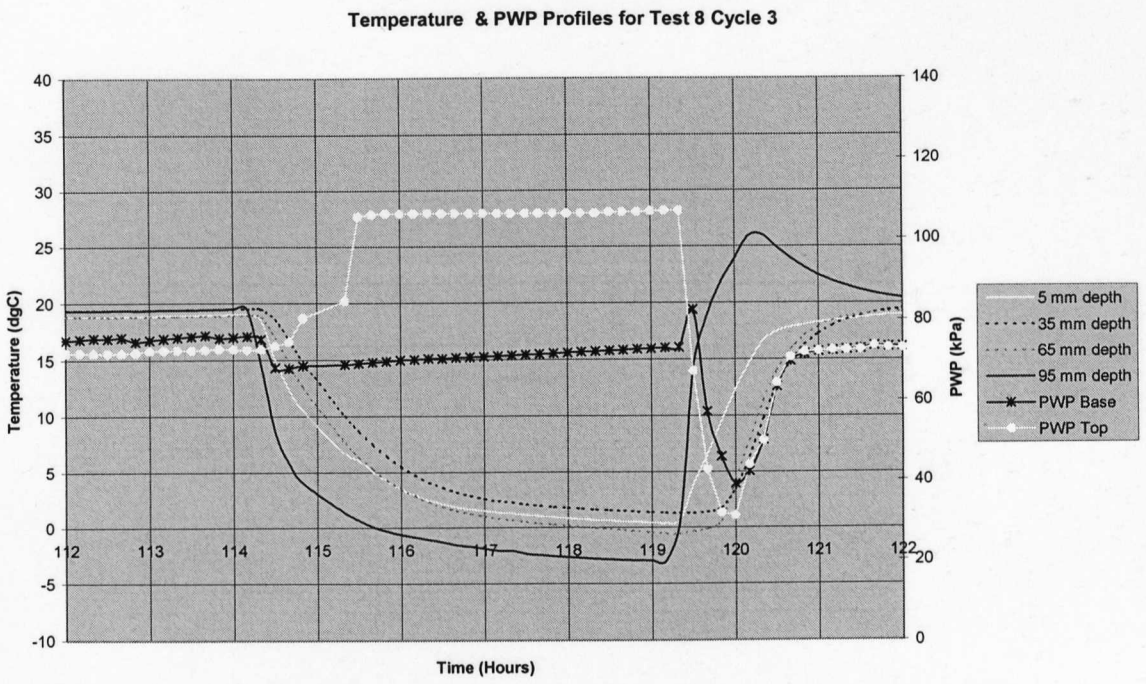

Figure 5.11 – Test 8 Cycle 3 Pore Water Pressure & Temperatures

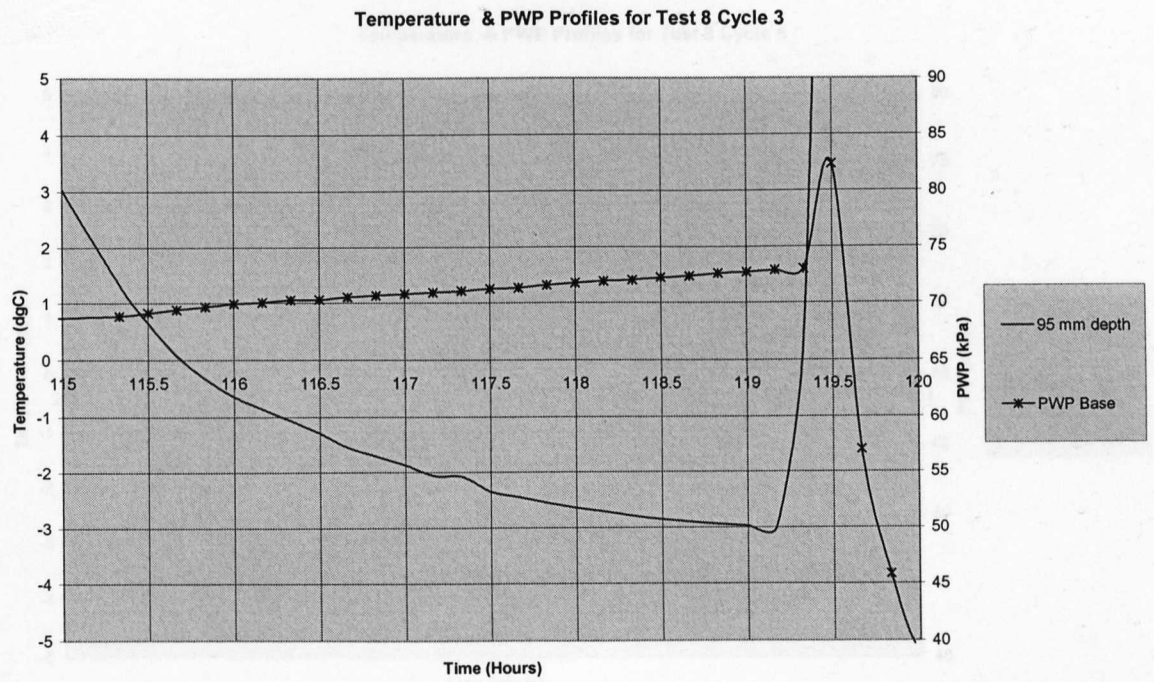

Figure 5.12 – Test 8 Cycle 3 Pore Water Pressure & Temperature at Base

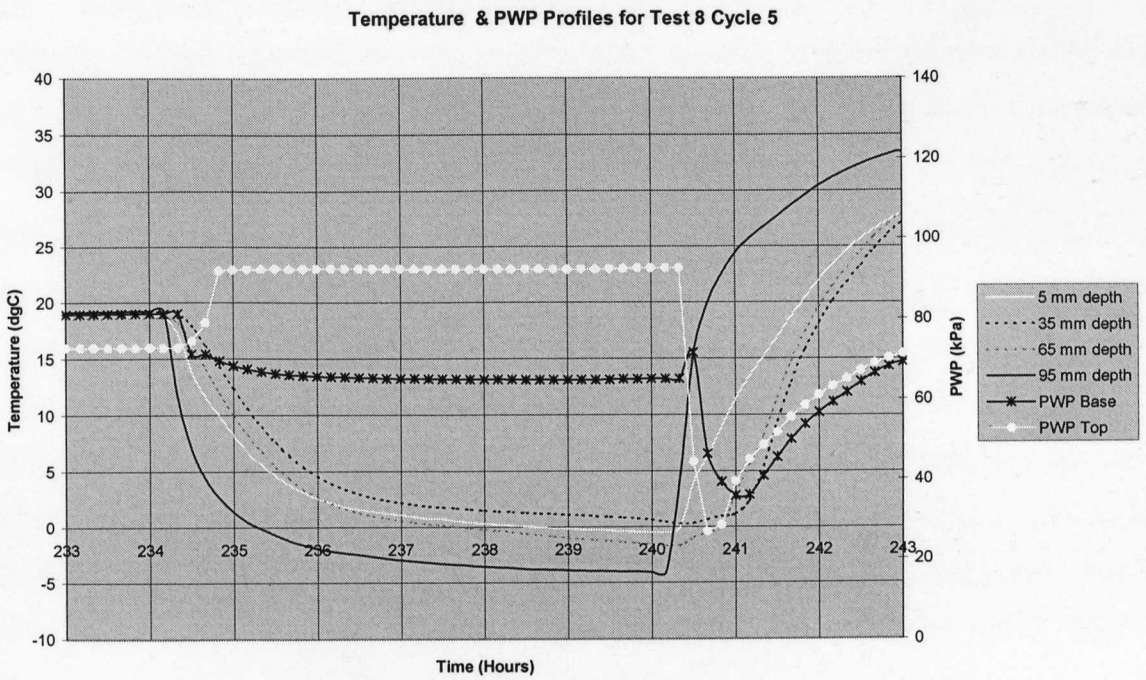

Figure 5.13 – Test 8 Cycle 5 Pore Water Pressure & Temperatures

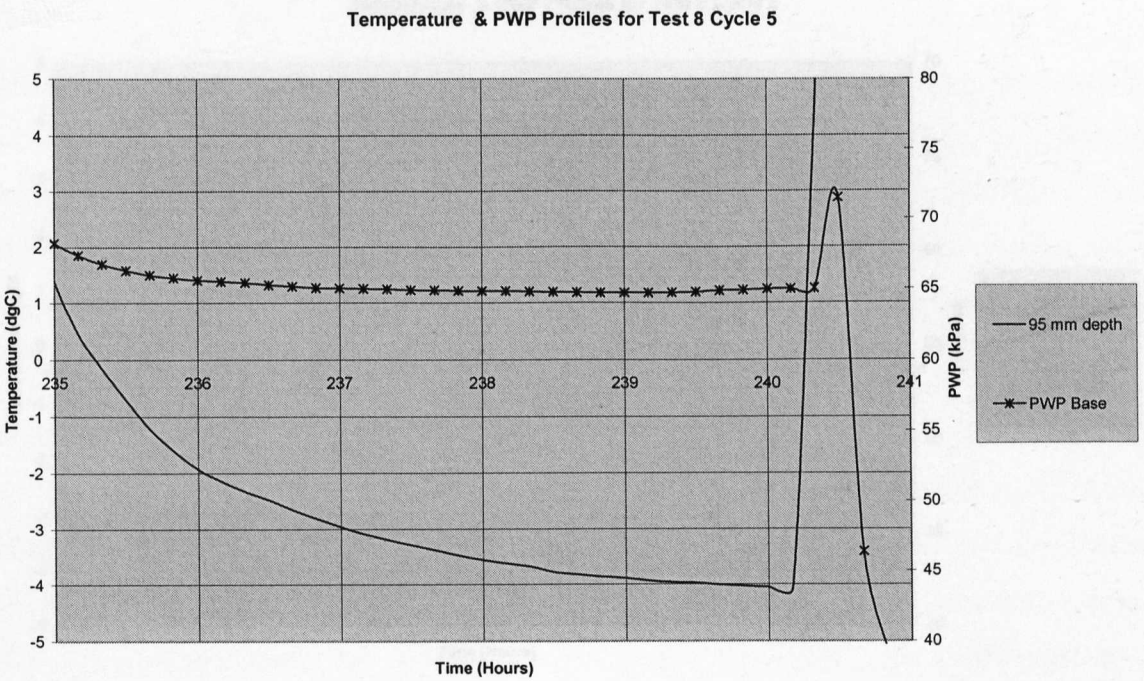

Figure 5.14 – Test 8 Cycle 5 Pore Water Pressure & Temperature at Base

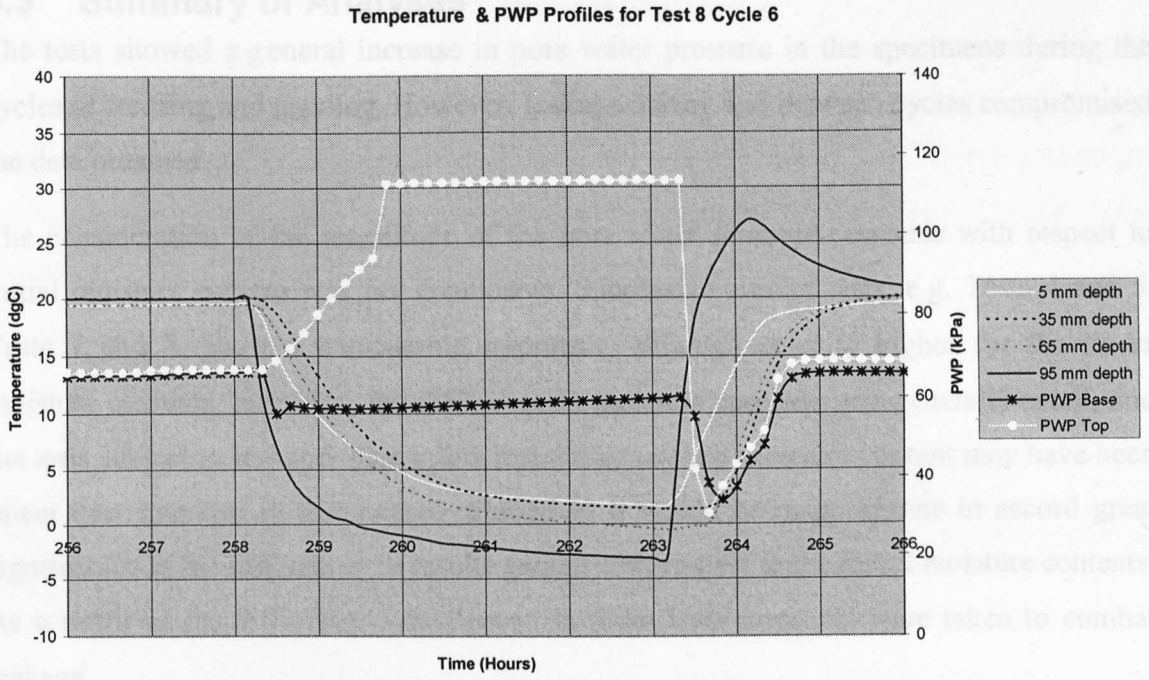

Figure 5.15 – Test 8 Cycle 6 Pore Water Pressure & Temperatures

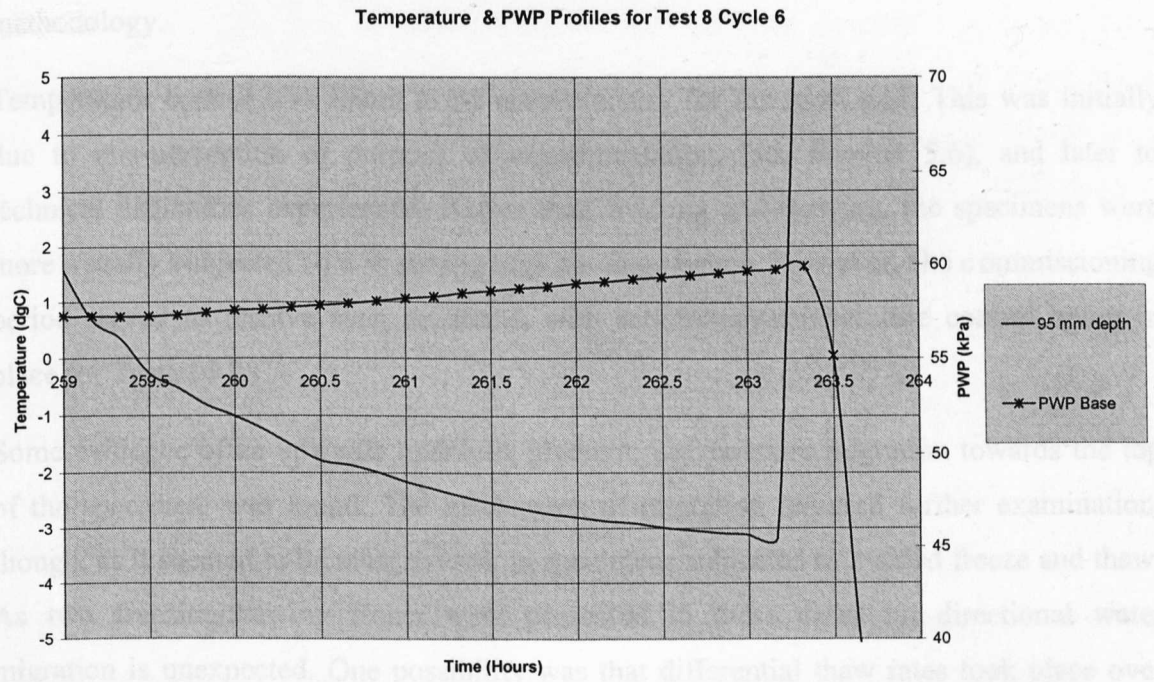

Figure 5.16 – Test 8 Cycle 6 Pore Water Pressure & Temperature at Base

5.3 Summary of Analyses

The tests showed a general increase in pore water pressure in the specimens during the cycles of freezing and thawing. However, leakage during and between cycles compromised the data obtained.

The consideration of the magnitude of the pore water pressure response with respect to initial moisture content was not conclusive. Successive similar tests, e.g. Tests 4 and 5, Tests 7 and 8, showed comparable responses, although actually higher for the lower moisture contents. However, the difference in moisture contents was generally small, and the tests subject to leakage. This infers that the *actual* test moisture content may have been lower than intended in some cases. Therefore, it would be inappropriate to accord great significance to the differences in results gained with respect to the initial moisture contents. As a result of the difficulties experienced in these tests measures were taken to combat leakage.

No link was found between applied stress and pore water pressure response, based on the results obtained to this point in the test programme. However, this aspect is considered further in Chapter 7, with respect to the fully commissioned test apparatus and improved methodology.

Temperature control was found to be unsatisfactory for the most part. This was initially due to mis-perception of purpose of experimentation, (see Section 5.6), and later to technical difficulties experienced. Rather than freezing and thawing, the specimens were more usually subjected to a warming and cooling regime. However, the commissioning period served to resolve such problems, with satisfactory temperature control being in place for Tests 14-28.

Some evidence of an upwards hydraulic gradient, i.e. moisture migration towards the top of the specimen, was found. The mechanism of migration required further examination, though, as it seemed to be most evident in specimens subjected to 2-sided freeze and thaw. As two freezing/thawing fronts were presented in these cases uni-directional water migration is unexpected. One possibility was that differential thaw rates took place over the night 'rest' phase. Alternatively, the pore water pressure transducers may have experienced a feedback exchange due to the lack of drainage from the specimen. Further investigation into moisture migration is carried out in Chapter 7.

5.4 Revised Purpose of Experimentation

As well as improvements to apparatus and procedure, the commissioning period highlighted the need to be clear as to what was being modelled. The basic purpose of experimentation was to subject soil specimens to cycles of freezing and thawing under an applied stress, monitoring pore water pressure response and volume change. This definition, while still true, was felt to be in need of refinement.

Each specimen tested was now to represent an element of soil at a depth below the ground surface, equivalent to the stress applied. Freezing would take place from the top downwards, simulating the advance of frost penetration through the active layer. Upwards freezing, (from the permafrost layer), was not induced as this would have caused rapid, uncontrolled freezing due to the small size of the specimen, not allowing any understanding of soil behaviour to be achieved. It was assumed that the base plate would remain at a roughly constant temperature throughout the test, as the radial portion would be exposed to the controlled temperature environment within the refrigerator.

In terms of temperature control, the objective was revised to cover the range of 'just frozen' to 'just thawed'. In practice, this meant a range of average temperature of approximately -5°C to +5°C. This was to ensure that all the specimen reached the frozen state. Previously, specimens were either only partially frozen, or subject to overheating. Considering the objective of simulation, the room temperature to frozen cycles were considered invalid, as during periods of intense cold ambient temperatures of above 20°C would have been highly improbable.

In terms of saturation, specimens were required to be consolidated to (as near as possible) saturation, and subsequently pre-frozen, from Test 14 onwards. This would enable the stress history of the specimen to be assumed to be zero at the start of test, and ensure uniformity of the specimen. Also, each test specimen would now commence from a temperature within the new operating range.

Therefore, the revised purpose of experimentation was to physically model a cylindrical element of saturated, frozen soil, with respect to the pore water pressure response. This element was considered to be at a depth, z m, below the ground surface within a low-angled slope. The element was represented by a remoulded specimen, (100 mm tall by 100 mm diameter), taken from a sample from a known soliflucted/periglacially affected area. The depth, z, was represented by a stress applied to the top of the element via a loading

piston. The specimen was subjected to cycles of freezing from the top of the specimen downwards and thawing over the general range of -5°C to +5°C. The ambient temperature was maintained at approximately 7°C. Pore water pressures and volume changes were monitored throughout the tests.

The test results may not be directly comparable to conditions in the field due to

- The pore water pressure in the middle of the sample not being measured due to practical instrumentation difficulties.
- One-Dimensional freezing not allowing for *in situ* temperatures of ground.
- A closed system being adopted, rather than an open, (i.e. drained), system, which would allow water to enter and leave the specimen.

Concerning the first two points, these are due to practical constraints in the laboratory, and care has to be taken when examining the test results. Pore water pressure readings must be considered in relation to the appropriate temperature readings, although readings along the depth of the specimen can give a good indication of the progression of the °C isotherm. The design and construction of the permode system aimed to afford as much insulation to the specimen as possible, so that the impact of the freezing/thawing regime would be clearly visible.

Concerning the last point, due to the low permeability of the clay soils tested, drainage of excess pore water was considered to be negligible. Therefore, in the experimental model, drainage was not permitted. This assumption has been considered earlier in Section 3.3, with respect to the rate of consolidation that could be expected in the field. In addition, it was considered beneficial to the efficiency of the experimental model to minimise the variables involved.

Tests 14-28 were carried out according to the revised purpose of experimentation. The results of these tests are presented in Chapter 6 and discussed in Chapter 7.

5

Freeze-Thaw Experiments on Some British Soils

Volume 2 of 2

By

Fiona Mhairi Thomson

A thesis submitted to the University of Warwick

for the degree of Doctor of Philosophy

School of Engineering, University of Warwick

December 2002

Table of Contents

List of Figures iv

List of Tables vii

List of Equations viii

Chapter 6 – Presentation of Results – Tests 14-28 171

6.1 Results of Consolidation Tests 171

6.2 Summary of Results for Tests 14-28 171

6.3 Individual Test Results 172
6.3.1 Test 14 172
6.3.2 Test 15 179
6.3.3 Test 16 180
6.3.4 Test 17 181
6.3.5 Test 18 186
6.3.6 Test 19 191
6.3.7 Test 20 192
6.3.8 Test 21 193
6.3.9 Test 22 198
6.3.10 Test 23 203
6.3.11 Test 24 207
6.3.12 Test 25 208
6.3.13 Test 26 209
6.3.14 Test 27 213
6.3.15 Test 28 213

Chapter 7 – Analysis of Results – Tests 14-28 219

7.1 General Points 219

7.2 Application of the Semi-Infinite Slope Model 219
7.2.1 Model Definition 219
7.2.2 Consideration of Permode Test Results 225
7.2.3 Reference to Existing Knowledge Base 229

7.3 The Consideration of Moisture Migration 232
7.3.1 Moisture Migration Observed 232
7.3.2 The Significance of Leakage 233
7.3.3 Reference to Existing Knowledge Base 234

7.4 Frost Heave 235
7.4.1 Observed Frost Heave 235
7.4.2 Predicting Frost Heave 238
7.4.3 Frost Heave and the 0°C Isotherm 244
7.4.4 Possible Effects of a Closed System 255

7.5 The Consideration of Zero Curtain Behaviour 256
7.5.1 Comparison of Permode Testing to Model Slope Simulation 256
7.5.2 Initial Indications of Zero Curtain Behaviour 257
7.5.3 Examples of Zero Curtain Behaviour 260
7.5.3.1 Lias Clay 260
7.5.3.2 Weald Clay 261
7.5.3.3 Oxford Clay 261
7.5.4 Summary 261

7.6 Initial Decreases in Pore Water Pressure with Temperature 268

7.7 Summary of Analyses 273

Chapter 8 – Conclusions 274

8.1 Increases in Pore Water Pressure due to Freezing and Thawing 274

8.2 Slope Failure Due to Increases in Pore Water Pressure 274

8.3 Patterns of Moisture Migration 275

8.4 Frost Heave 276

8.5 Zero Curtain Behaviour 276

8.6 The Efficiency of the Test Methodology 277
8.6.1 Validity of the Test Set-Up 277
8.6.2 Prevention of Leakage 278
8.6.3 Initial Drop in Pore Water Pressure with Temperature 278
8.6.4 Direction of Thaw 278
8.6.5 Overall Performance of the Apparatus 279

8.7 Implications for Theory and Practice 279

Chapter 9 – Scope for Further Work **280**

9.1 Scope for Further Modifications to the Apparatus **280**
9.1.1 Upgrading of Temperature Sensors 280
9.1.2 Increased Number and Optimisation of Temperature Sensors 281
9.1.3 Provision of Large-Scale Controlled Temperature Environment 282
9.1.4 Upgrading of Pressure Transducers 282
9.1.5 Optimisation of Permode Cell Construction 282
9.1.6 Development of an Integrated Data-Logging and Post-Processing System 283

9.2 Scope for Further Research **284**
9.2.1 Investigation of Different Soil Types 284
9.2.2 Investigation of Moisture Migration and Frost Heave 284
9.2.3 Introduction of a Freezing Zero Curtain 284
9.2.4 Investigation of Drained tests and In-Cell Consolidation 285
9.2.5 Investigation of Varying Levels of Saturation 285
9.2.6 Consideration of Varying Modes of Slope Failure 285

References **287**

Bibliography **294**

Appendix A – Photographs of Apparatus **296**

Appendix B – Instrumentation Calibration Data **300**

B.1 The Instrumentation to be Calibrated **300**

B.2 The 'Least Squares' Method of Regression Analysis **300**

B.3 Summary of Calibrations **301**

Appendix C – Computer Analysis Techniques **311**

C.1 Turbo-Pascal Program **311**

C.2 The Use of Microsoft Excel **313**

C.3 The Use of Matlab **314**

Appendix D – Permode Test Results – All Tests 315

List of Figures

Figure 6.1 - Results for Test 14 173
Figure 6.2 - Temperature Profiles for Test 14 Cycle 1 174
Figure 6.3 - Temperature Profiles for Test 14 Cycle 5 174
Figure 6.4 - Temperature Profiles for Test 14 Cycle 7 175
Figure 6.5 - Test 14 Cycle 1 Pore Water Pressure & Temperature at Base 176
Figure 6.6 - Test 14 Cycle 1 Pore Water Pressure & Temperature at Top 176
Figure 6.7 - Test 14 Cycle 5 Pore Water Pressure & Temperature at Base 177
Figure 6.8 - Test 14 Cycle 5 Pore Water Pressure & Temperature at Top 177
Figure 6.9 - Test 14 Cycle 7 Pore Water Pressure & Temperature at Base 178
Figure 6.10 - Test 14 Cycle 7 Pore Water Pressure & Temperature at Top 178
Figure 6.11 - Results for Test 17 181
Figure 6.12 - Temperature Profiles for Test 17 Cycle 1 182
Figure 6.13 - Test 17 Cycle 1 Pore Water Pressure & Temperature at Base 183
Figure 6.14 - Test 17 Cycle 1 Pore Water Pressure & Temperature at Top 183
Figure 6.15 - Test 17 Cycle 2 Pore Water Pressure & Temperature at Base 184
Figure 6.16 - Test 17 Cycle 2 Pore Water Pressure & Temperature at Top 184
Figure 6.17 - Test 17 Cycle 3 Pore Water Pressure & Temperature at Base 185
Figure 6.18 - Test 17 Cycle 3 Pore Water Pressure & Temperature at Top 185
Figure 6.19 - Test 17 Cycle 4 Pore Water Pressure & Temperature at Base 186
Figure 6.20 - Test 17 Cycle 4 Pore Water Pressure & Temperature at Top 186
Figure 6.21 - Results for Test 18 187
Figure 6.22 - Temperature Profiles for Test 18 Cycle 1 188
Figure 6.23 - Test 18 Cycle 1 Pore Water Pressure & Temperature at Base 189
Figure 6.24 - Test 18 Cycle 1 Pore Water Pressure & Temperature at Top 189
Figure 6.25 - Test 18 Cycle 2 Pore Water Pressure & Temperature at Base 190
Figure 6.26 - Test 18 Cycle 2 Pore Water Pressure & Temperature at Top 190
Figure 6.27 - Results for Test 21 193
Figure 6.28 - Temperature Profiles for Test 21 Cycle 1 194
Figure 6.29 - Test 21 Cycle 1 Pore Water Pressure & Temperature at Base 195
Figure 6.30 - Test 21 Cycle 1 Pore Water Pressure & Temperature at Top 195
Figure 6.31 - Test 21 Cycle 2 Pore Water Pressure & Temperature at Base 196
Figure 6.32 - Test 21 Cycle 2 Pore Water Pressure & Temperature at Top 196
Figure 6.33 - Test 21 Cycle 3 Pore Water Pressure & Temperature at Base 197
Figure 6.34 - Test 21 Cycle 3 Pore Water Pressure & Temperature at Top 197
Figure 6.35 - Results for Test 22 198
Figure 6.36 - Temperature Profiles for Test 22 Cycle 1 199
Figure 6.37 - Test 22 Cycle 1 Pore Water Pressure & Temperature at Base 200
Figure 6.38 - Test 22 Cycle 1 Pore Water Pressure & Temperature at Top 200
Figure 6.39 - Test 22 Cycle 2 Pore Water Pressure & Temperature at Base 201
Figure 6.40 - Test 22 Cycle 2 Pore Water Pressure & Temperature at Top 201
Figure 6.41 - Test 22 Cycle 3 Pore Water Pressure & Temperature at Base 202
Figure 6.42 - Test 22 Cycle 3 Pore Water Pressure & Temperature at Top 202
Figure 6.43 - Results for Test 23 203
Figure 6.44 - Temperature Profiles for Test 23 Cycle 1 204

Figure 6.45 - Test 23 Cycle 1 Pore Water Pressure & Temperature at Base 205
Figure 6.46 - Test 23 Cycle 1 Pore Water Pressure & Temperature at Top 205
Figure 6.47 - Test 23 Cycle 2 Pore Water Pressure & Temperature at Base 206
Figure 6.48 - Test 23 Cycle 2 Pore Water Pressure & Temperature at Top 206
Figure 6.49 - Results for Test 26 209
Figure 6.50 - Temperature Profiles for Test 26 Cycle 2 210
Figure 6.51 - Test 26 Cycle 2 Pore Water Pressure & Temperature at Base 211
Figure 6.52 - Test 26 Cycle 2 Pore Water Pressure & Temperature at Top 211
Figure 6.53 - Test 26 Cycle 5 Pore Water Pressure & Temperature at Base 212
Figure 6.54 - Test 26 Cycle 5 Pore Water Pressure & Temperature at Top 212
Figure 6.55 - Results for Test 28 214
Figure 6.56 - Temperature Profiles for Test 28 Cycle 1 215
Figure 6.57 - Test 28 Cycle 1 Pore Water Pressure & Temperature at Base 216
Figure 6.58 - Test 28 Cycle 1 Pore Water Pressure & Temperature at Top 216
Figure 6.59 - Test 28 Cycle 2 Pore Water Pressure & Temperature at Base 217
Figure 6.60 - Test 28 Cycle 2 Pore Water Pressure & Temperature at Top 217
Figure 6.61 - Test 28 Cycle 3 Pore Water Pressure & Temperature at Base 218
Figure 6.62 - Test 28 Cycle 3 Pore Water Pressure & Temperature at Top 218

Figure 7.1 - The Effect of $+\Delta u$ on the Stability of Slopes 224
Figure 7.2 - Numerical Solution for R and r_u, after Morgenstern & Nixon, (1971); Nixon, (1973). 231
Figure 7.3 - Measured Frost Heave 236
Figure 7.4 - Percentage Increase in Volume for Different Saturation Levels 243
Figure 7.5 - Plotting the Zero Isotherm for Freeze Phase of Test 14 Cycle 5 246
Figure 7.6 - Plotting the Zero Isotherm for Thaw Phase of Test 14 Cycle 5 247
Figure 7.7 - Comparing Heave with Progression of Zero Isotherm for Test 14 Cycle 5 248
Figure 7.8 - Plotting the Zero Isotherm for Freeze Phase of Test 25 Cycle 5 249
Figure 7.9 - Plotting the Zero Isotherm for Thaw Phase of Test 25 Cycle 5 250
Figure 7.10 - Comparing Heave with Progression of Zero Isotherm for Test 25 Cycle 5 251
Figure 7.11 - Plotting the Zero Isotherm for Freeze Phase of Test 20 Cycle 5 252
Figure 7.12 - Plotting the Zero Isotherm for Thaw Phase of Test 20 Cycle 5 253
Figure 7.13 - Comparing Heave with Progression of Zero Isotherm for Test 20 Cycle 5 254
Figure 7.14 - Position of Minimum Pore Water Pressure – Top 258
Figure 7.15 - Position of Minimum Pore Water Pressure – Base 258
Figure 7.16 - Test 15 Cycle 1 262
Figure 7.17 - Test 15 Cycle 2 262
Figure 7.18 - Test 15 Cycle 3 263
Figure 7.19 - Test 15 Cycle 4 263
Figure 7.20 - Test 17 Cycle 1 264
Figure 7.21 - Test 17 Cycle 2 264
Figure 7.22 - Test 17 Cycle 3 265
Figure 7.23 - Test 17 Cycle 4 265
Figure 7.24 - Test 26 Cycle 2 266
Figure 7.25 - Test 26 Cycle 5 266
Figure 7.26 - Test 19 Cycle 2 267
Figure 7.27 - Test 19 Cycle 5 267
Figure 7.28 - Pressure Transducer Behaviour 270

Figure 7.29 - Pressure Transducer Behaviour for Time Period 25 – 90.5 Hours 271

Figure 9.1 - Retrogressive Slope Failure, after Petley & Hutchinson, (2001) 286

Figure A.1 - The Permode Cell (usually inside refrigerated cabinet) 296
Figure A.2 - Permode Barrel and Liner 297
Figure A.3 - Thermocouple and Washer Assembly 297
Figure A.4 - Pressure and Displacement Transducers 298
Figure A.5 - Baseplate Assembly 298
Figure A.6 - Piston and Porous Plate 299

Figure B.1 - Excel Regression Analysis for SGDT Displacement Transducer – 1 308
Figure B.2 - Excel Regression Analysis for SGDT Displacement Transducer – 2 308
Figure B.3 - Excel regression Analysis for PWP Base Transducer - 1 309
Figure B.4 - Excel Regression Analysis for PWP Base Transducer – 2 309
Figure B.5 - Excel Regression Analysis for PWP Top Transducer - 1 310
Figure B.6 - Excel Regression Analysis for PWP Top Transducer – 2 310

Figure D.1 - Test 1 - Lias clay - σ = 29 kPa, m.c. = 29% 315
Figure D.2 - Test 2 - Lias clay - σ = 104 kPa, m.c. = 32% 316
Figure D.3 - Test 3 - Lias clay - σ = 104 kPa, m.c. = 30% 316
Figure D.4 - Test 4 - Lias clay - σ = 104 kPa, m.c. = 32% 317
Figure D.5 - Test 5 - Lias clay - σ = 104 kPa, m.c. = 30% 317
Figure D.6 - Test 6 - Lias clay - σ = 104 kPa, m.c. = 35% 318
Figure D.7 - Test 7 - Lias clay - σ = 104 kPa, m.c. = 33% 318
Figure D.8 - Test 8 - Lias clay - σ = 80 kPa, m.c. = 30% 319
Figure D.9 - Test 9 - Lias clay - σ = 104 kPa, m.c. = 29% 319
Figure D.10 - Test 10 - Lias clay - σ = 80 kPa, m.c. = 32% 320
Figure D.11 - Test 11 - Lias clay - σ = 80 kPa, m.c. = 31% 320
Figure D.12 - Test 12 - Lias clay - σ = 80 kPa, m.c. = 30% 321
Figure D.13 - Test 13 - Lias clay - σ = 80 kPa, m.c. = 32% 321
Figure D.14 - Test 14 - Lias clay - σ = 80 kPa, m.c. = 27% 322
Figure D.15 - Test 15 - Lias clay - σ = 55 kPa, m.c. = 27% 322
Figure D.16 - Test 16 - Lias clay - σ = 80 kPa, m.c. = 31% 323
Figure D.17 - Test 17 - Lias clay - σ = 55 kPa, m.c. = 31% 323
Figure D.18 - Test 18 - Lias clay - σ = 120 kPa, m.c. = 31% 324
Figure D.19 - Test 19 - Oxford clay - σ = 55 kPa, m.c. = 49% 324
Figure D.20 - Test 20 - Oxford clay - σ = 80 kPa, m.c. = 49% 325
Figure D.21 - Test 21 - Oxford clay - σ = 55 kPa, m.c. = 50% 325
Figure D.22 - Test 22 - Oxford clay - σ = 55 kPa, m.c. = 50%, Freezing from base upwards 326
Figure D.23 - Test 23 - Oxford clay - σ = 80 kPa, m.c. = 50%, Freezing from base upwards 326
Figure D.24 - Test 24 - Weald clay - σ = 55 kPa, m.c. = 39% 327
Figure D.25 - Test 25 - Weald clay - σ = 80 kPa, m.c. = 39% 327
Figure D.26 - Test 26 - Weald clay - σ = 55 kPa, m.c. = 38% 328
Figure D.27 - Test 27 - Weald clay - σ = 80 kPa, m.c. = 38% 328
Figure D.28 - Test 28 - Weald clay - σ = 67.5 kPa, m.c. = 38% 329

List of Tables

Table 6.1 - Consolidation Characteristics and Permeability Coefficients 171
Table 6.2 - Summary of Results for Tests 14-28 172

Table 7.1 - Comparisons Between the Soil Types 220
Table 7.2 - Values of z Corresponding to the Various Applied Stresses 221
Table 7.3 - Values of β Found using Conventional Analysis, ($r_u = 0.5$) 223
Table 7.4 - The Effect on Slope Stability of $+\Delta u$ Found in Permode Tests – Top of Specimen 225
Table 7.5 - The Effect on Slope Stability of $+\Delta u$ Found in Permode Tests – Base of Specimen 226
Table 7.6 - Summary of Minimum Values of β Found 228
Table 7.7 - Values of R for Each Soil Type 230
Table 7.8 - Values of r_u found from Nixon & Morgenstern, (1971), Solution. 231
Table 7.9 - Moisture Migration in Tests 14-28 232
Table 7.10 - Mean Values of Frost Heave for Cycles 1-5, $\sigma = 80$ kPa 237
Table 7.11 - Lias Clay Test 14 Expected and Actual Heave 241
Table 7.12 - Weald Clay Test 25 Expected and Actual Heave 241
Table 7.13 - Oxford Clay Test 20 Expected and Actual Heave 242
Table 7.14 - Position of Minimum Pore Water Pressures Recorded at the Top of the Specimen 257
Table 7.15 - Position of Minimum Pore Water Pressures Recorded at the Base of the Specimen 257

Table 8.1 - Comparison of Rates of Thaw, (using Equations 2.1 & 2.2 and Figure 7.2) 277

Table B.1 - Summary of Calibrations 301
Table B.2 - Calibration Table for SGDT Displacement Transducer – 1 302
Table B.3 - Calibration Table for SGDT Displacement Transducer – 2 303
Table B.4 - Calibration Table for PWP Base Transducer – 1 304
Table B.5 - Calibration Table for PWP Base Transducer - 2 305
Table B.6 - Calibration Table for PWP Top Transducer - 1 306
Table B.7 - Calibration Table for PWP Top Transducer - 2 307

List of Equations

Equation 7.1 - $r_{u(1)}$, the Full Hydrostatic Component of r_u 221
Equation 7.2 - $r_{u(2)}$, the Additional Pore Water Pressure Component of r_u 221
Equation 7.3 - The Combined Value of r_u 222
Equation 7.4 - An Equation to Find β Using the Combined Value of r_u 222
Equation 7.5 - The Limiting Value of $+\Delta u$ 222
Equation 7.6 - Void Ratio 238
Equation 7.7 - Water Content 238
Equation 7.8 - Density Relationships 239
Equation 7.9 - Volume of Solids 239
Equation 7.10 - Volume of Water 239
Equation 7.11 - Volume of Specimen After Freezing 239
Equation 7.12 - Percentage Increase in Volume from Freezing 240
Equation 7.13 - Moving Average Calculation performed by Microsoft Excel 268

Equation B.1 - x against y 300
Equation B.2 - m found using the 'Least Squares' method 300
Equation B.3 - Conversion factor for datalogger 300
Equation B.4 - Correlation coefficient, r 301

Chapter 6 – Presentation of Results – Tests 14-28

6.1 Results of Consolidation Tests

Table 6.1 below shows the consolidation characteristics determined through the preparative Rowe Cell tests. The tests were carried out over one pressure increment, of 50 kPa. The permeability coefficients found from Terzaghi's theory of one-dimensional consolidation are also given.

Table 6.1 – Consolidation Characteristics and Permeability Coefficients

Soil	c_v (m^2/year)	m_v (m^2/MN)	k (m/s)
Lias Clay	6.31	1.76	3.0×10^{-9}
Weald Clay	0.61	5.21	9.8×10^{-10}
Oxford Clay	0.37	5.32	6.0×10^{-10}

6.2 Summary of Results for Tests 14-28

Table 6.2 summarises the results for Tests 14-28. Values are given for the maximum and minimum pore water pressure recorded at the top and base of the specimen for each test, and also the 'baseline' pressures recorded before the start of the freeze-thaw cycles. Differences between the various pore water pressures are determined. An individual description of each test follows in Section 6.3.

Each test was carried out in accordance with the definitive test procedure as outlined in Chapter 3, Section 3.4.3.5.

A summarised set of results is not provided within the chapter for every test, but is available in Appendix D.

Table 6.2 – Summary of Results for Tests 14-28

Test No.	σ (kPa)	m.c. (%)	No. of Cycles	No. of Rest Phases	PWP before Start of Cycles (s.o.c.) (kPa)		Max. PWP during Cycles (kPa)		Increase in PWP from s.o.c. to Max. during Cycles (kPa)	
					Top	Base	Top	Base	Top	Base
14	80	27	11	3	-0.33	-4.56	10.94	3.74	11.27	8.30
15	55	27	4	1	-2.24	-8.00	0.62	-1.47	2.86	6.53
16	80	31	4	1	-2.90	-4.50	0.99	-2.24	3.89	2.26
17	55	31	4	2	-1.64	-7.17	1.38	-0.50	3.02	6.67
18	120	31	5	2	1.47	-7.22	5.75	1.22	4.28	8.44
19	55	49	7	2	-7.15	-6.63	9.97	-5.08	17.12	1.55
20	80	49	5	1	8.76	-6.20	50.44	-5.35	41.68	0.85
21	55	50	3	1	10.45	6.20	15.32	7.91	4.87	1.71
22	55	50	3	1	16.35	3.20	94.16	8.35	77.81	5.15
23	80	50	5	2	56.00	4.00	131.28	6.34	75.28	2.34
24	55	39	5	2	6.46	2.70	34.76	4.80	28.30	2.10
25	80	39	9	3	34.65	17.00	72.76	52.52	38.11	35.52
26	55	38	7	3	-2.12	0.00	3.76	4.49	5.88	4.49
27	80	38	7	3	4.80	1.38	62.96	19.62	58.16	18.24
28	67.5	38	7	3	28.60	28.72	44.00	41.22	15.40	12.50

6.3 Individual Test Results

6.3.1 Test 14

Test 14 was carried out on Lias Clay, of moisture content 27 %, under an applied stress of 80 kPa.

The test consisted of 11 cycles and 3 rest phases. There were 3 'weekend' length rest phases, after Cycles 1, 6 and 11.

Figure 6.1 below shows the summarised results for Test 14.

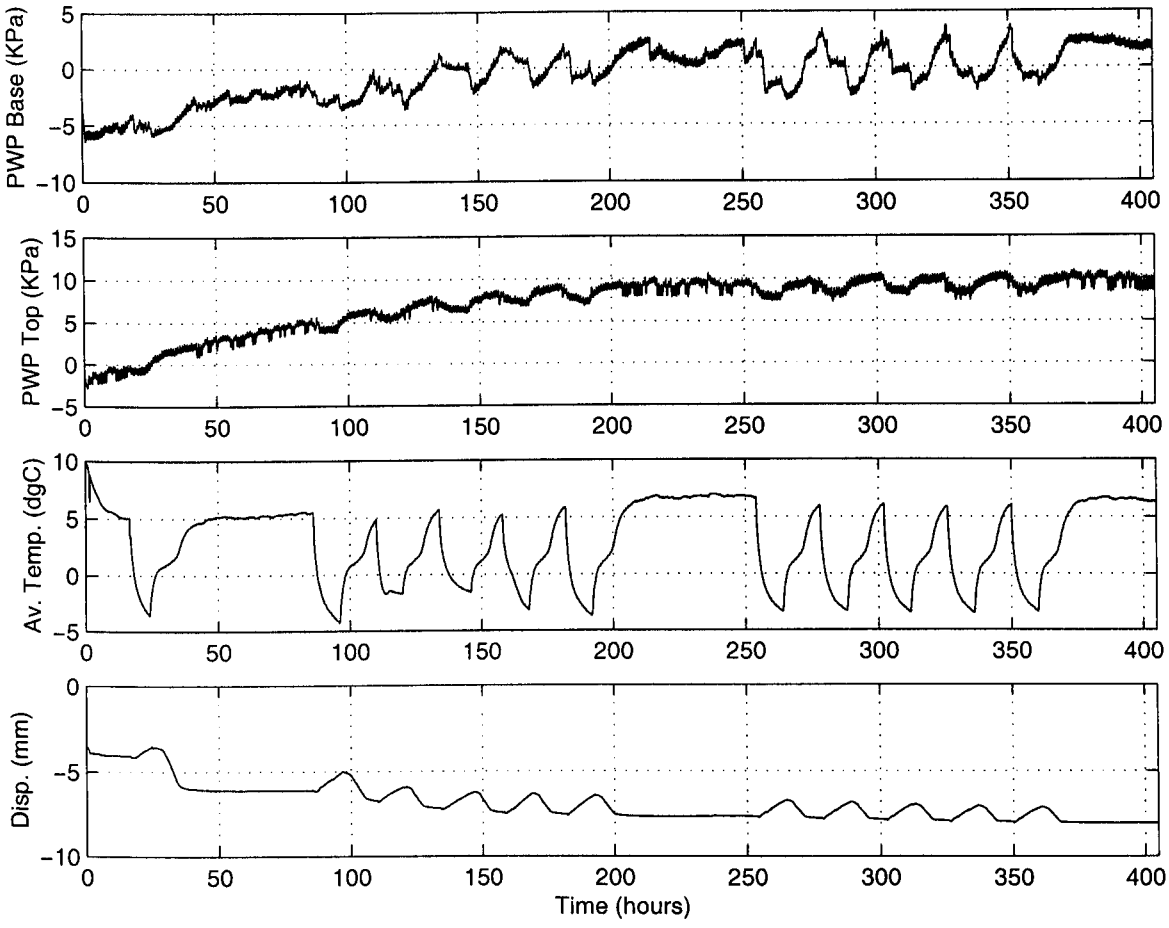

Figure 6.1 – Results for Test 14

Upward displacement of the specimen occurred for each cycle, showing expansion of the specimen on freezing. However, the subsequent drops denote leakage. In addition, the actual increase of +2 mm is somewhat low for a 100 mm high specimen. This is considered to be due to leakage, and could also be due to the specimen perhaps not being 100 % saturated at the start of the test.

Figures 6.2-6.4 show detailed temperature profiles for selected cycles.

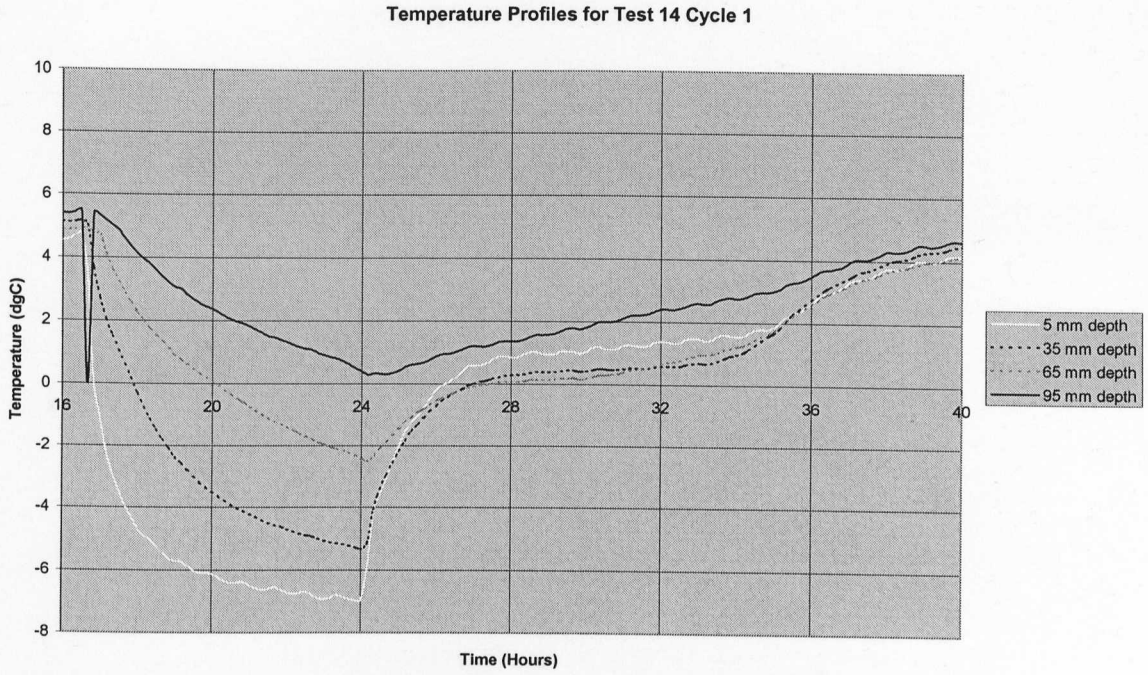

Figure 6.2 – Temperature Profiles for Test 14 Cycle 1

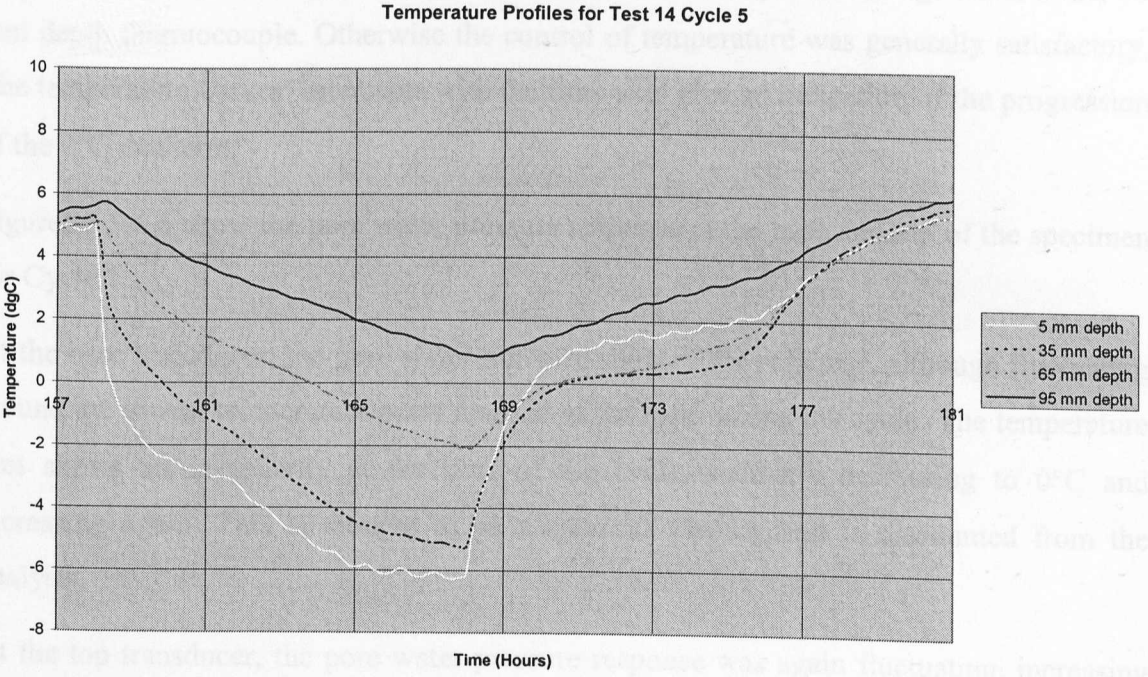

Figure 6.3 – Temperature Profiles for Test 14 Cycle 5

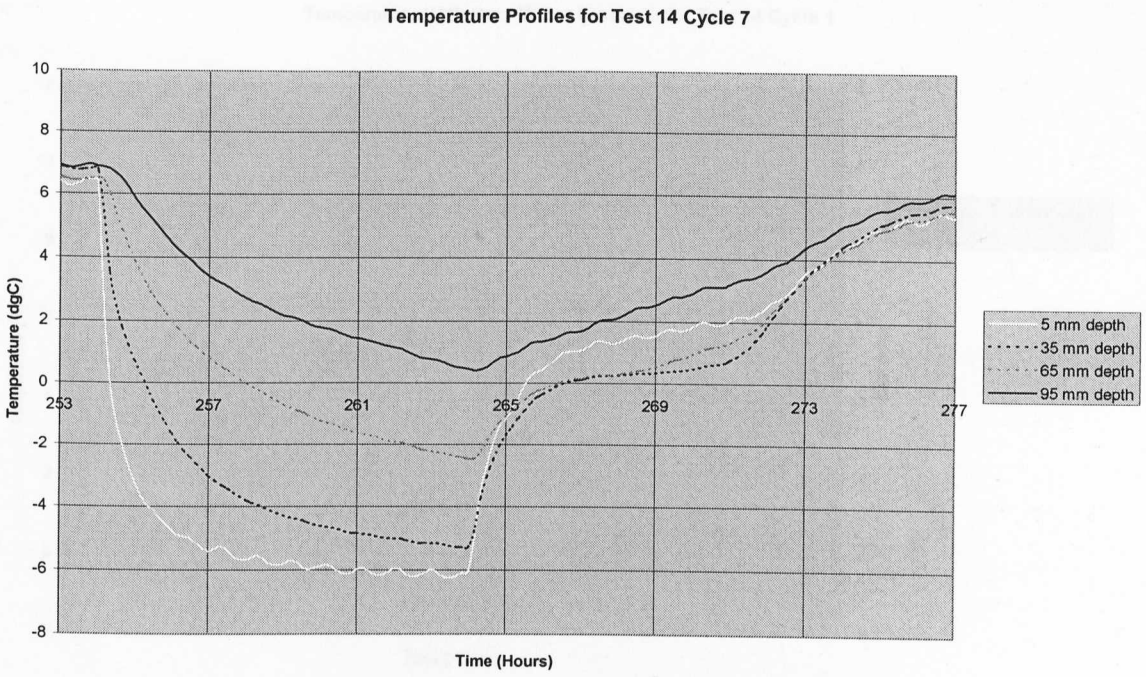

Figure 6.4 – Temperature Profiles for Test 14 Cycle 7

The very base of the specimen failed to freeze, as shown by the readings taken at the 95 mm depth thermocouple. Otherwise the control of temperature was generally satisfactory. The temperature curves' intercepts with the time axis give an indication of the progression of the 0°C isotherm.

Figures 6.5-6.6 show the pore water pressure response at the base and top of the specimen for Cycle 1.

At the base transducer, the pore water pressure shows little response, although fluctuating around the lowest temperature point reached at the base during the cycle. The temperature plot shows an irregularity at the start of the cycle, suddenly decreasing to 0°C and increasing again. This is thought to be a spurious reading and is discounted from the analysis.

At the top transducer, the pore water pressure response was again fluctuating, increasing on thawing of the specimen at that depth.

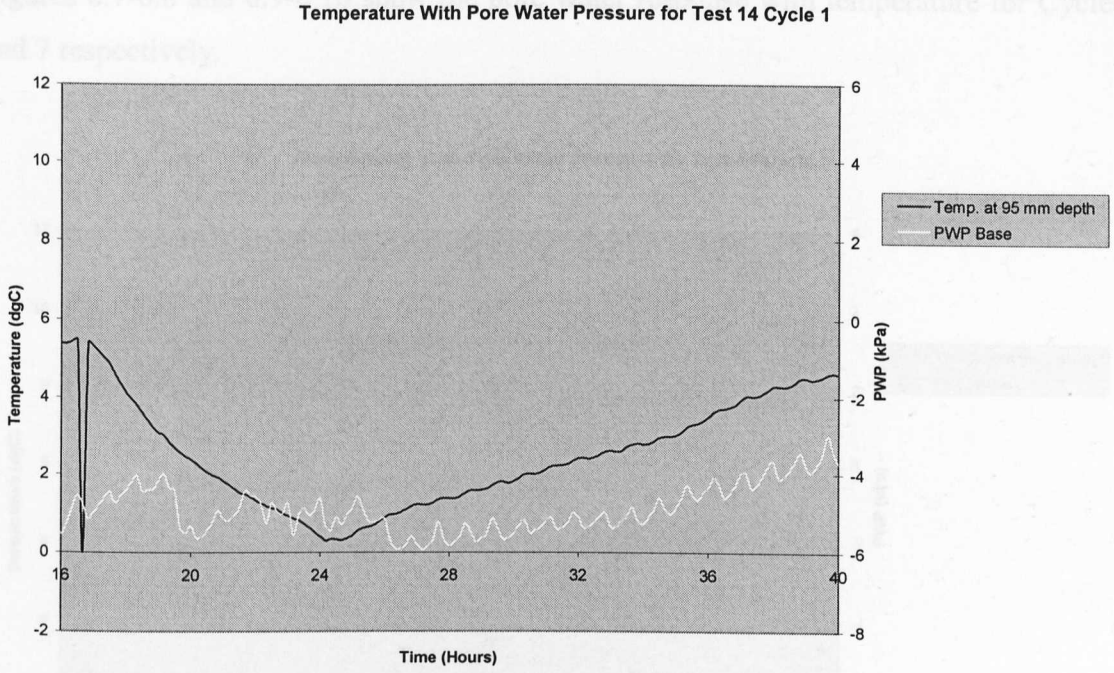

Figure 6.5 – Test 14 Cycle 1 Pore Water Pressure & Temperature at Base

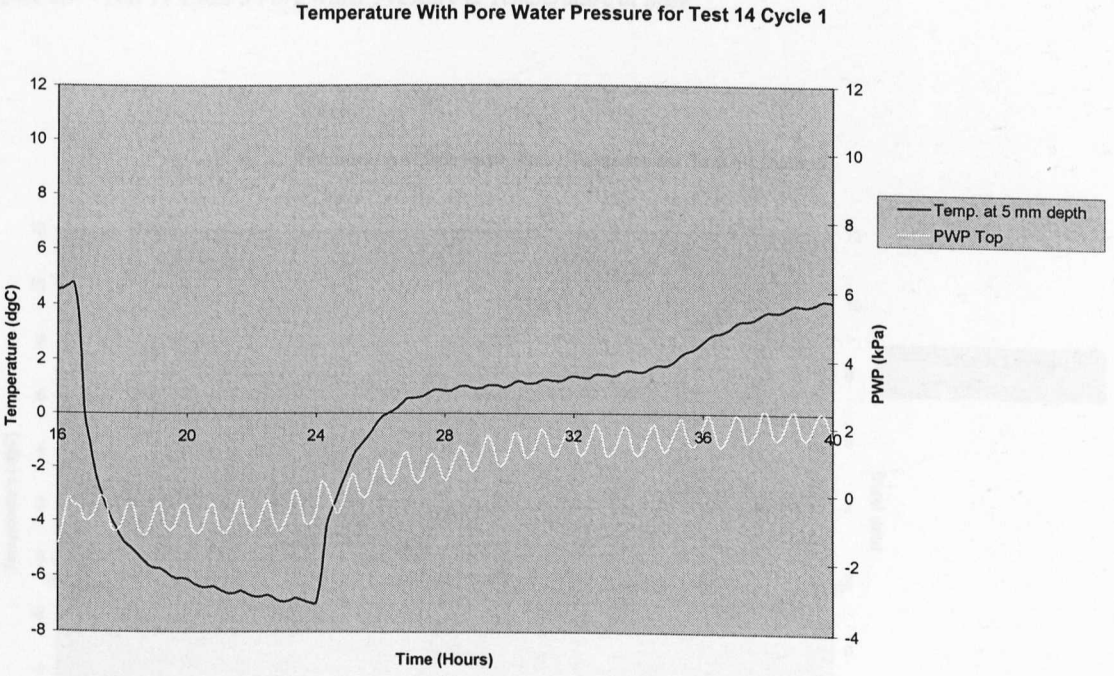

Figure 6.6 – Test 14 Cycle 1 Pore Water Pressure & Temperature at Top

Figures 6.7-6.8 and 6.9-6.10 show the pore water response with temperature for Cycles 5 and 7 respectively.

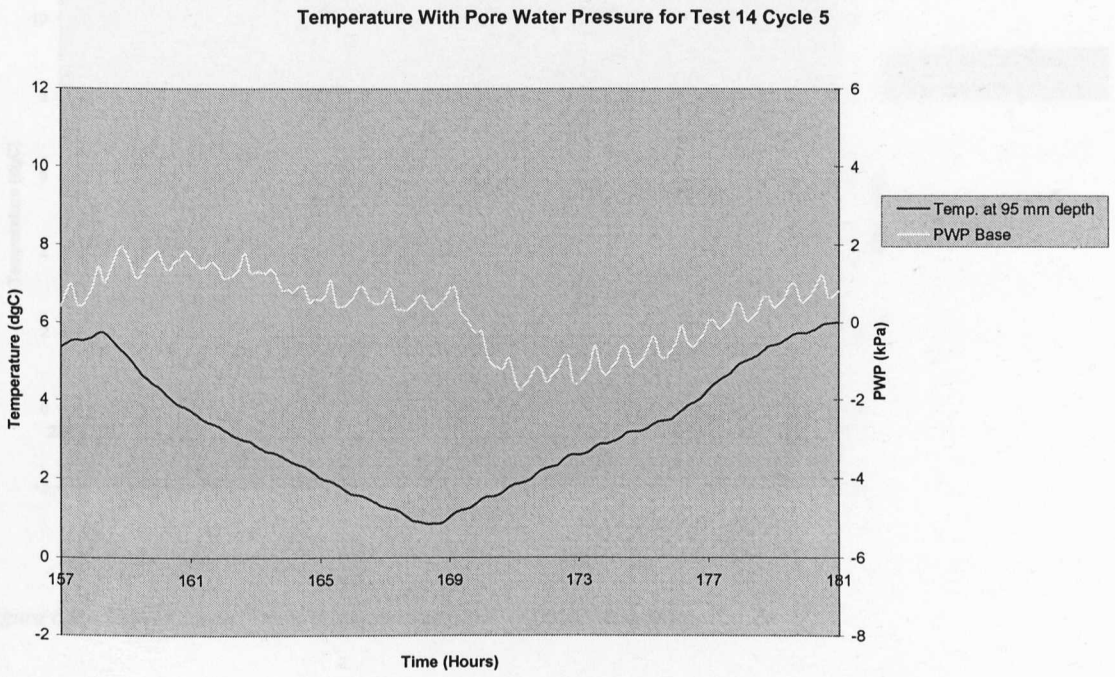

Figure 6.7 – Test 14 Cycle 5 Pore Water Pressure & Temperature at Base

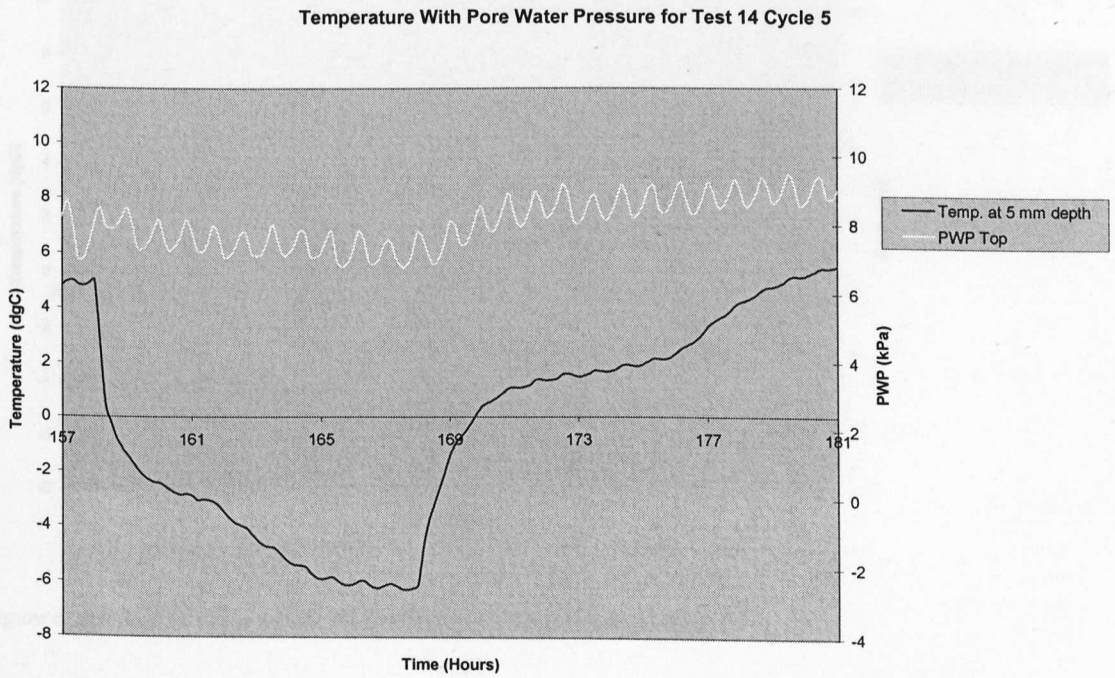

Figure 6.8 – Test 14 Cycle 5 Pore Water Pressure & Temperature at Top

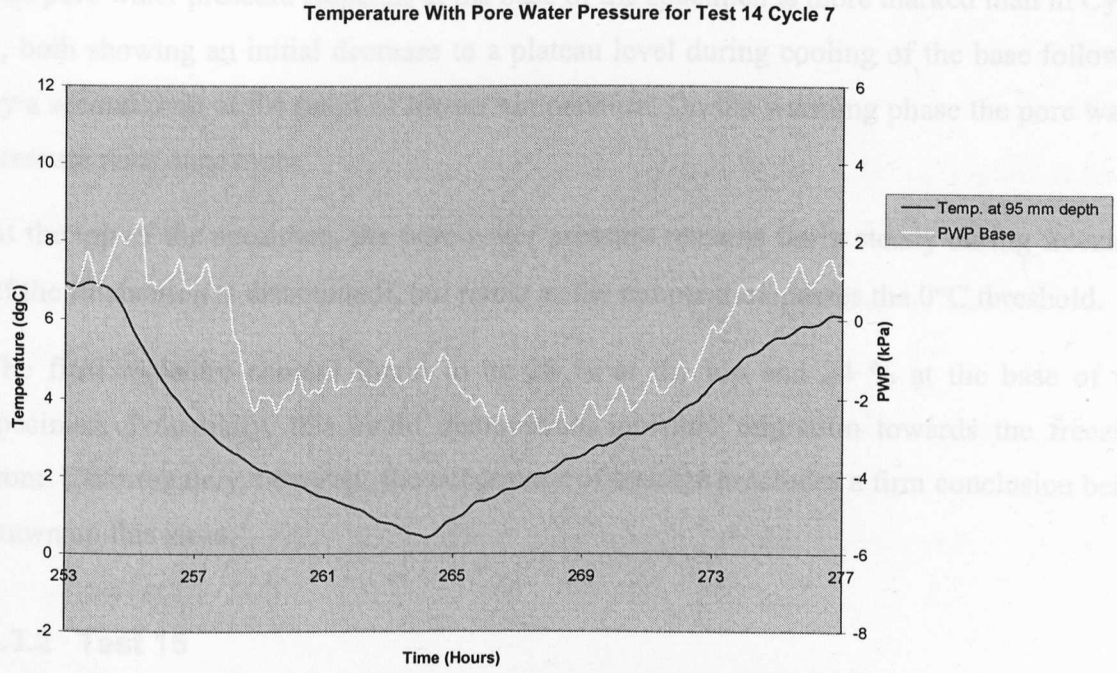

Figure 6.9 – Test 14 Cycle 7 Pore Water Pressure & Temperature at Base

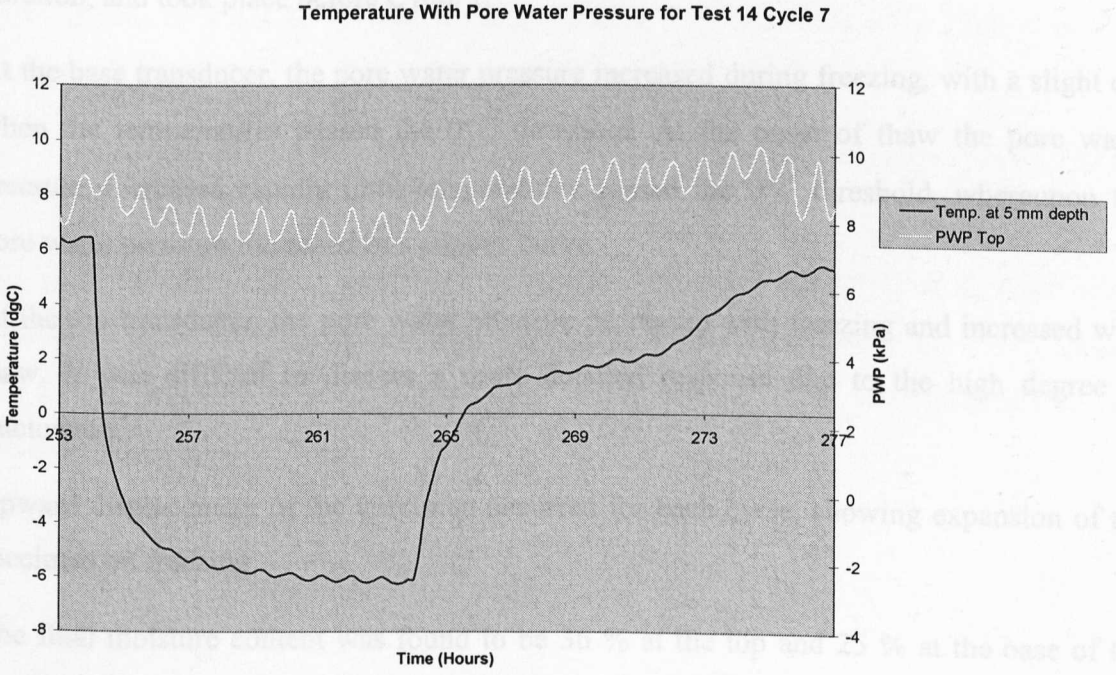

Figure 6.10 – Test 14 Cycle 7 Pore Water Pressure & Temperature at Top

The pore water pressure response at the base of the specimen is more marked than in Cycle 1, both showing an initial decrease to a plateau level during cooling of the base followed by a second drop at the point of lowest temperature. On the warming phase the pore water pressure rises once more.

At the top of the specimen, the pore water pressure remains fairly steady during freezing, (if the fluctuation is discounted), but rising as the temperature passes the 0°C threshold.

The final moisture content found to be 28 % at the top and 24 % at the base of the specimen. Potentially, this could demonstrate moisture migration towards the freezing front. Unfortunately, however, the occurrence of leakage precludes a firm conclusion being drawn on this issue.

6.3.2 Test 15

Test 15 was carried out on Lias Clay, of moisture content 27 %, under an applied stress of 55 kPa.

The test consisted of 4 cycles and 1 rest phase. The rest phase was of long, 'weekend' duration, and took place before Cycle 1.

At the base transducer, the pore water pressure increased during freezing, with a slight dip when the temperatures passed the 0°C threshold. At the onset of thaw the pore water pressure decreased rapidly until temperatures passed the 0°C threshold, whereupon the pore water pressure increased in a convex curve.

At the top transducer, the pore water pressure decreased with freezing and increased with thaw. It was difficult to discern a more detailed response due to the high degree of fluctuation.

Upward displacement of the specimen occurred for each cycle, showing expansion of the specimen on freezing.

The final moisture content was found to be 36 % at the top and 25 % at the base of the specimen, demonstrating moisture migration towards the freezing front.

6.3.3 Test 16

Test 16 was carried out on Lias Clay, of moisture content 27 %, under an applied stress of 55 kPa.

The test consisted of 4 cycles and 1 rest phase. The rest phase was of long, 'weekend' duration, and took place before Cycle 1.

A power-cut occurred at Time 100 hours. Although the freeze-thaw process re-started, the data-logger malfunctioned. This prevented readings being taken until Time 120 hours when the fault was detected. Consequently, the recording of measurements in Cycles 2 and 3 was disrupted.

At the base transducer, the pore water pressure decreased with freezing and increased with thawing, although with a sharp drop and rise in pore water pressure at about the 0°C threshold in the thaw stage.

At the top transducer, the pore water pressure decreased with freezing and increased with thaw. It was difficult to discern a more detailed response due to the high degree of fluctuation.

Upward displacement of the specimen occurred for each cycle, showing expansion of the specimen on freezing.

The final moisture content was found to be 30 % at the top and 24 % at the base of the specimen, demonstrating moisture migration towards the freezing front. However, leakage was found to have occurred during the test, which detracts from the significance of the moisture migration.

6.3.4 Test 17

Test 17 was carried out on Lias Clay, of moisture content 31 %, under an applied stress of 80 kPa.

The test consisted of 4 cycles and 2 rest phases. The rest phases were of long, 'weekend' duration, and took place before Cycle 1 and after Cycle 4.

Figure 6.11 shows summarised results for Test 17.

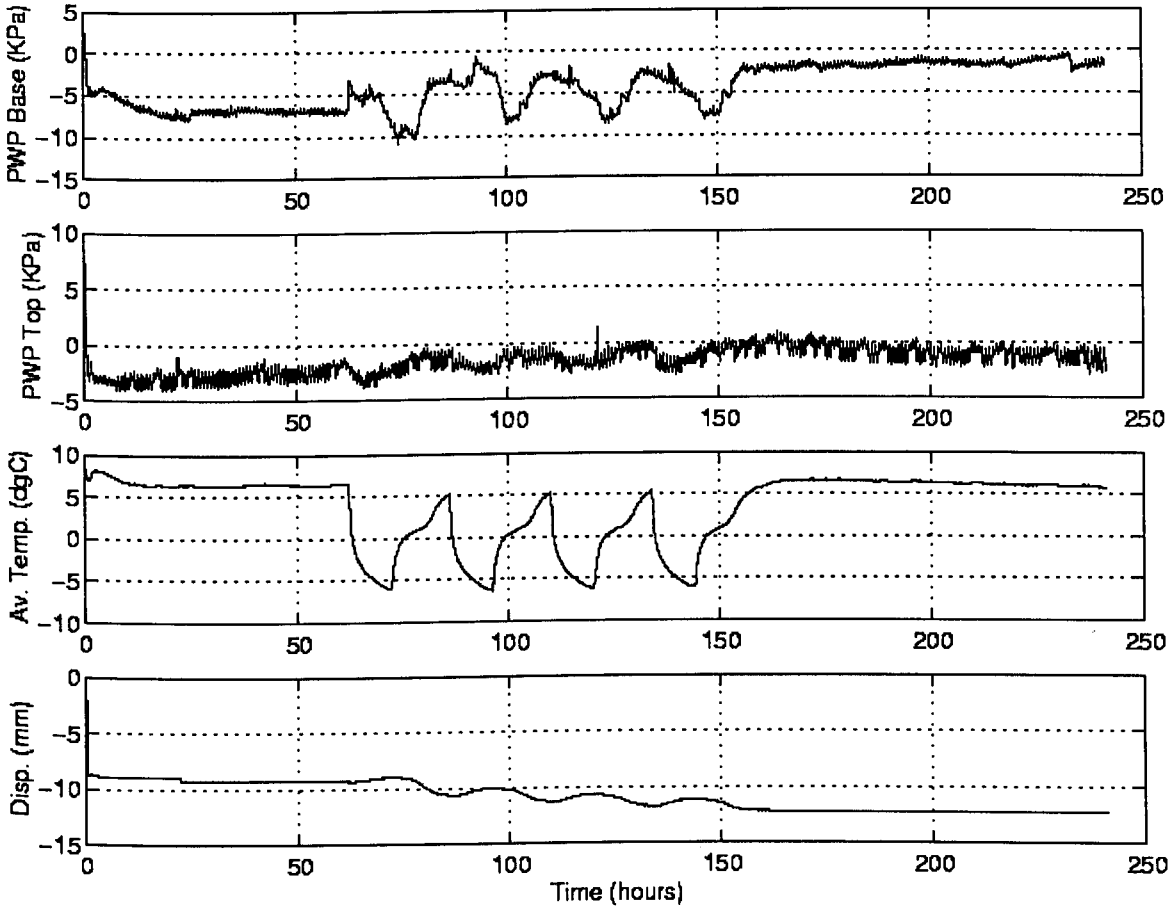

Figure 6.11 – Results for Test 17

Upward displacement of the specimen occurred for each cycle, showing expansion of the specimen on freezing.

The final moisture content was found to be 31 % at the top and 24 % at the base of the specimen, demonstrating moisture migration towards the freezing front. However, leakage also occurred.

Figure 6.12 below shows typical temperature profiles.

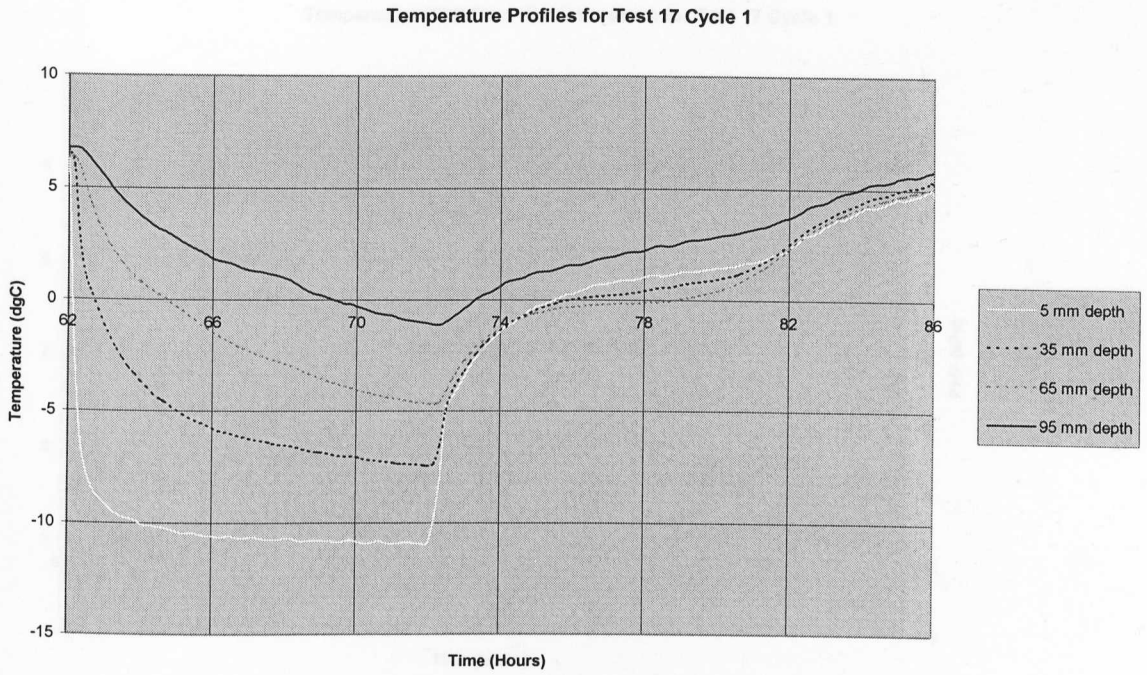

Figure 6.12 - Temperature Profiles for Test 17 Cycle 1

Figures 6.13-6.20 show the pore water pressure response at the base and top of the specimen for Cycles 1-4.

At the base transducer, during Cycle 1, the pore water pressure initially increased to a peak and then dropped to a rough, fluctuating level. As the temperature dropped below the 0°C threshold the pore water pressure decreased markedly. At the onset of thaw, the pore water pressure continued to decrease for approximately 1 hour, then fluctuating until increasing past the pre-freeze level. The onset of this increase was approximately 6 hours into the thaw period.

At the top transducer, the pore water pressure fluctuated during the freeze phase, increasing on the thaw phase.

Cycles 2-4 exhibit a similar pore water pressure response to that in Cycle 1. At the base transducer the pore water pressure rises during the freeze phase, although it is difficult to discern a detailed picture of the response due to fluctuation.

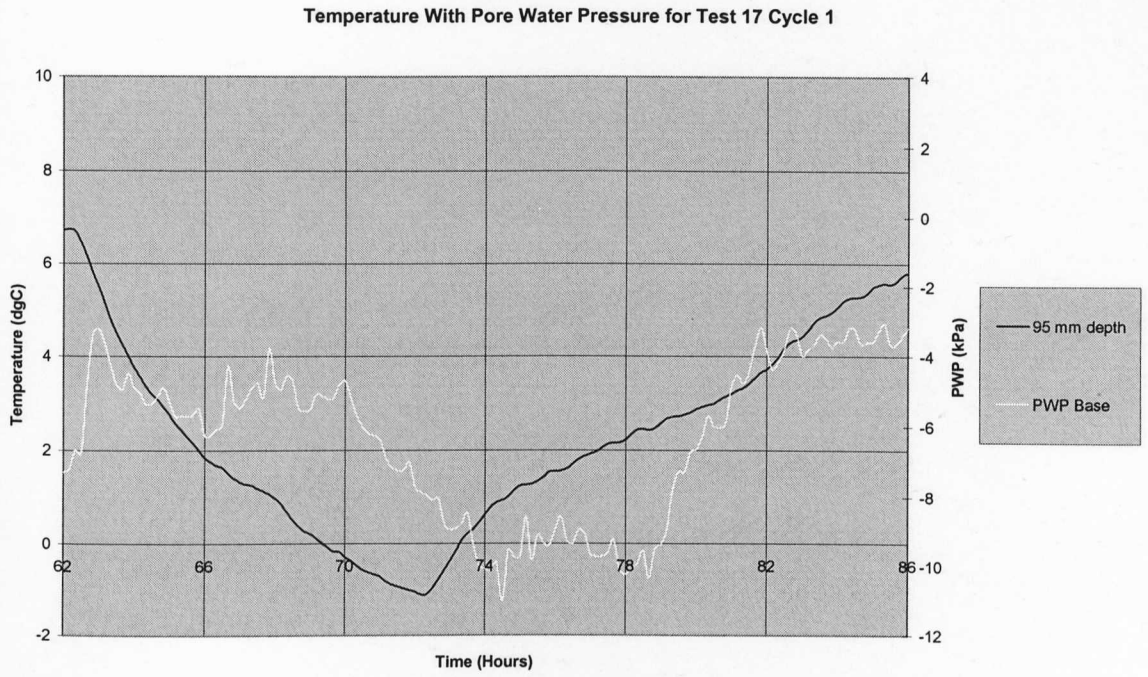

Figure 6.13 – Test 17 Cycle 1 Pore Water Pressure & Temperature at Base

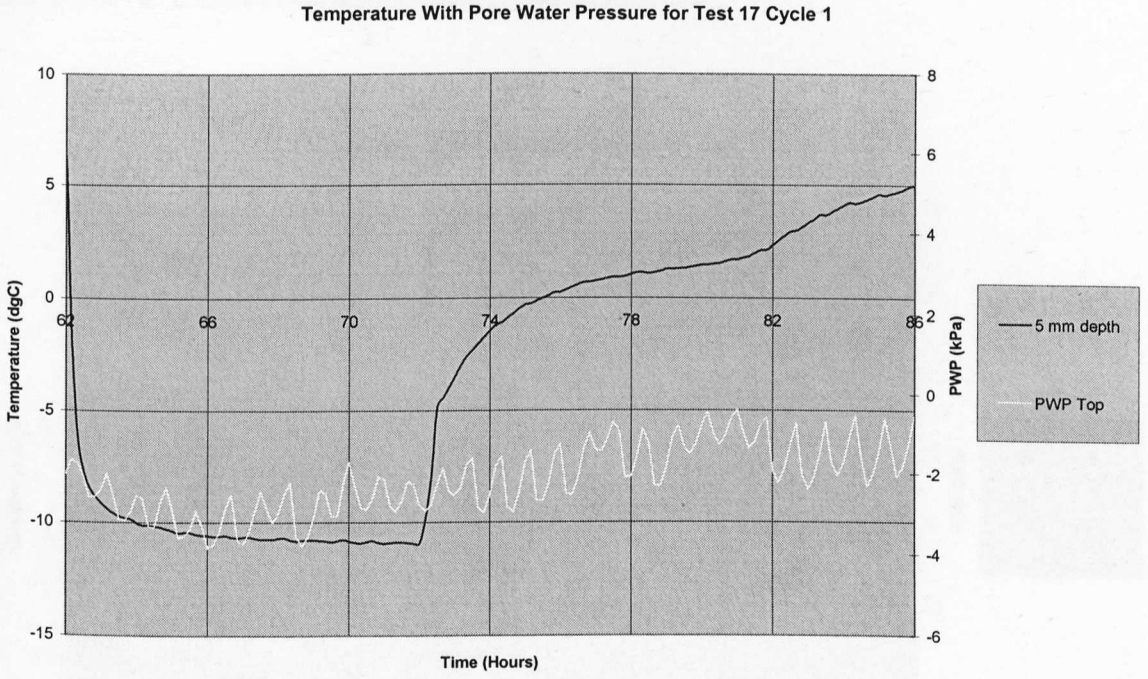

Figure 6.14 – Test 17 Cycle 1 Pore Water Pressure & Temperature at Top

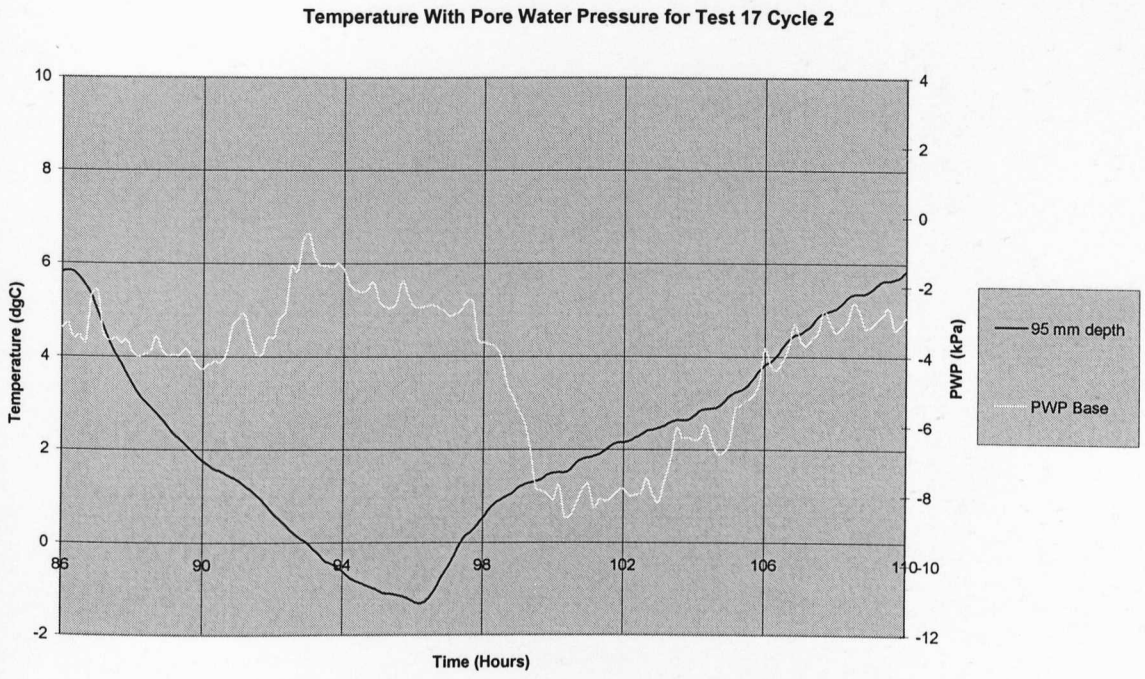

Figure 6.15 – Test 17 Cycle 2 Pore Water Pressure & Temperature at Base

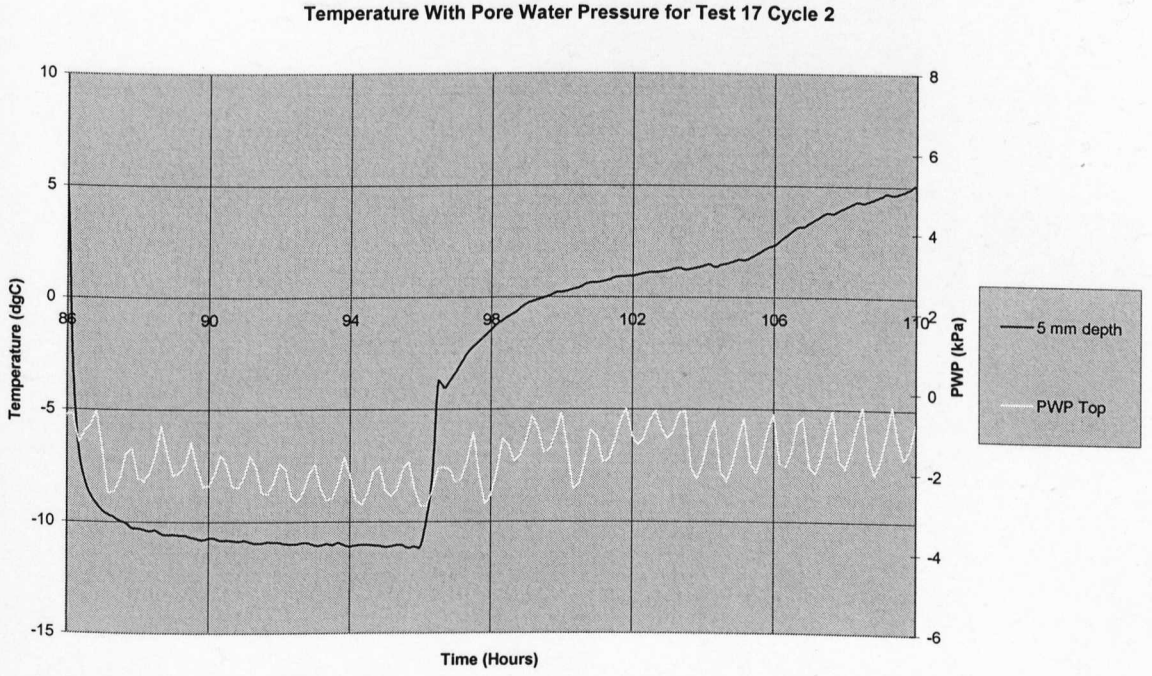

Figure 6.16 – Test 17 Cycle 2 Pore Water Pressure & Temperature at Top

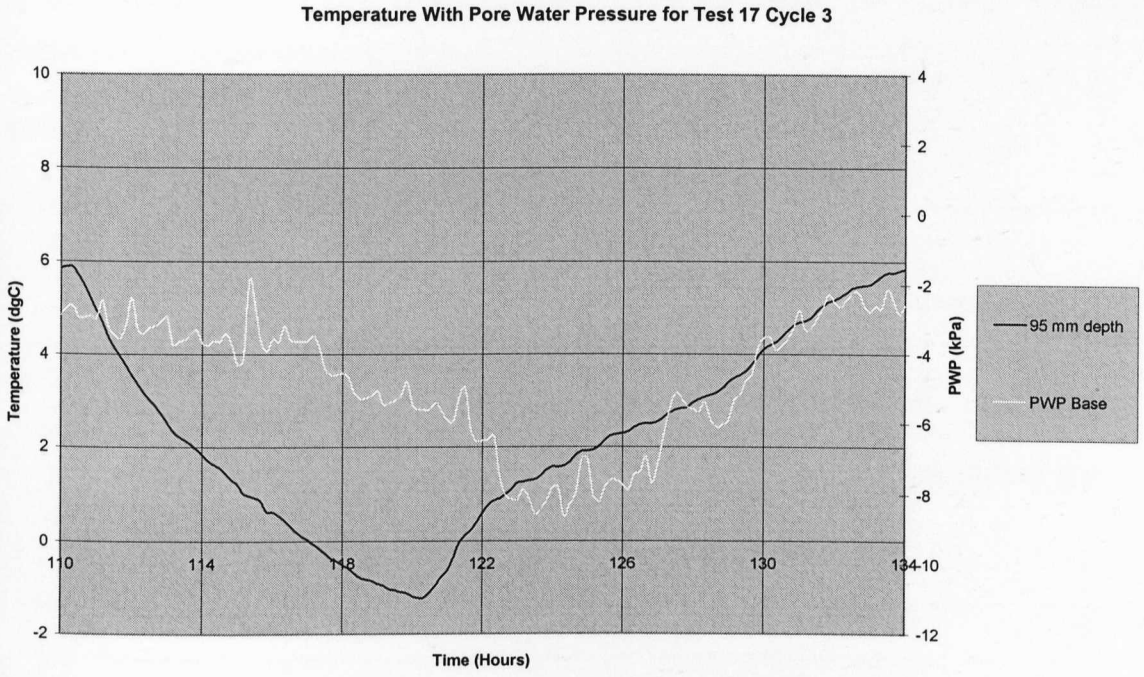

Figure 6.17 – Test 17 Cycle 3 Pore Water Pressure & Temperature at Base

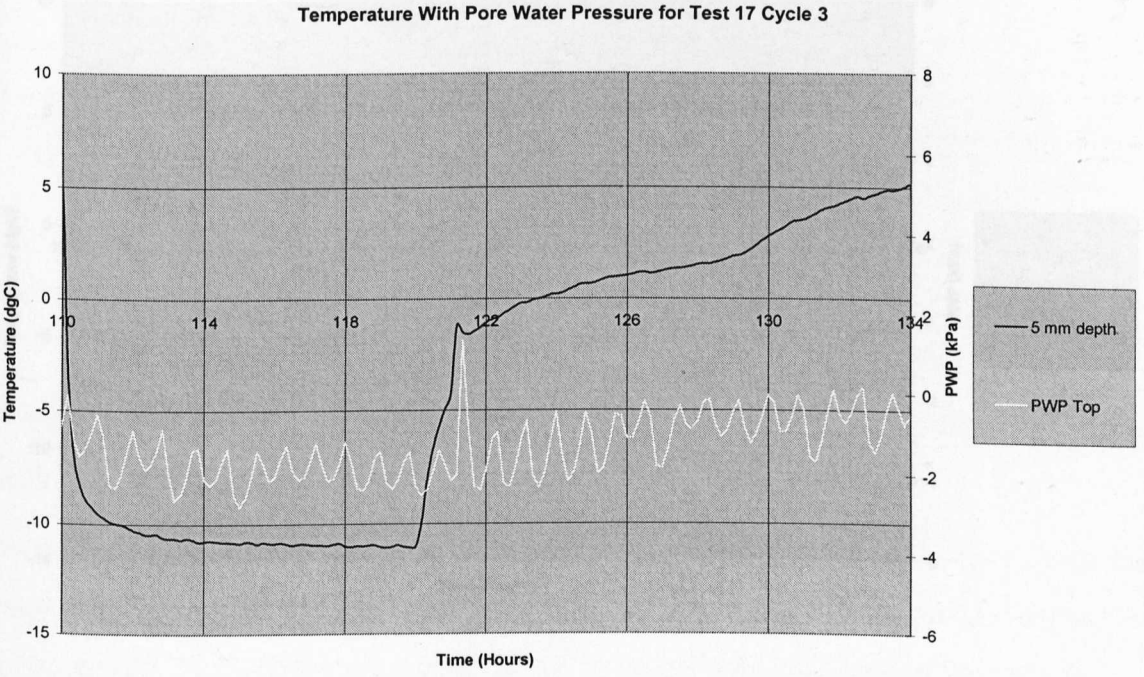

Figure 6.18 – Test 17 Cycle 3 Pore Water Pressure & Temperature at Top

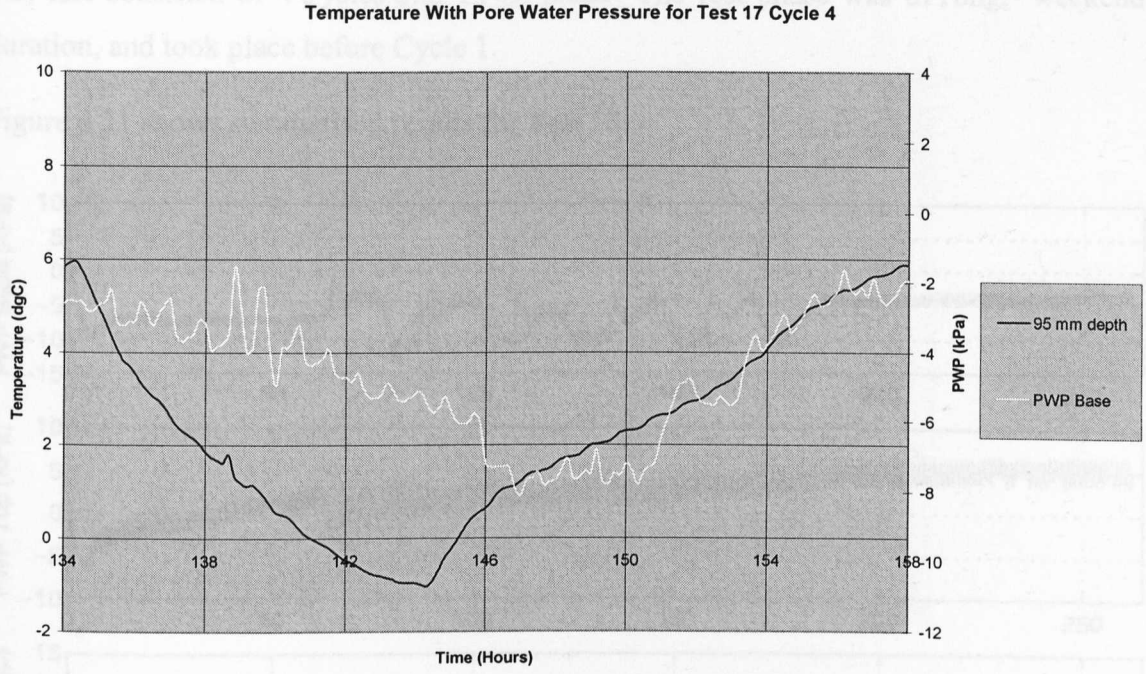

Figure 6.19 – Test 17 Cycle 4 Pore Water Pressure & Temperature at Base

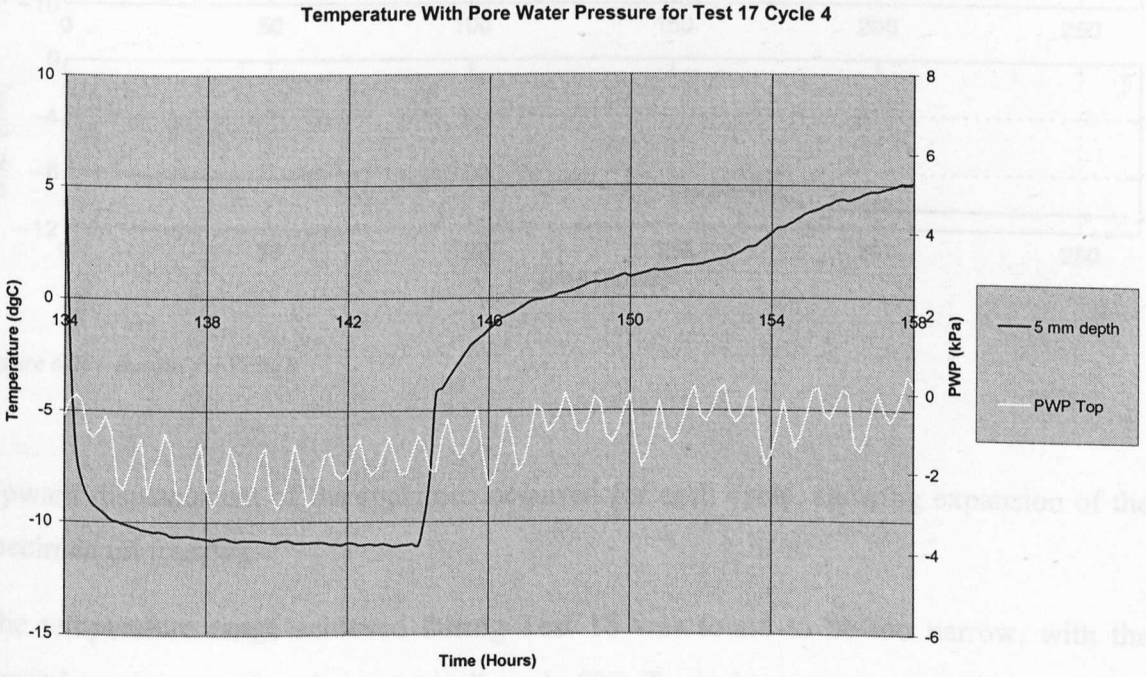

Figure 6.20 – Test 17 Cycle 4 Pore Water Pressure & Temperature at Top

6.3.5 Test 18

Test 18 was carried out on Lias Clay, of moisture content 31 %, under an applied stress of 55 kPa.

The test consisted of 4 cycles and 1 rest phase. The rest phase was of long, 'weekend' duration, and took place before Cycle 1.

Figure 6.21 shows summarised results for Test 18.

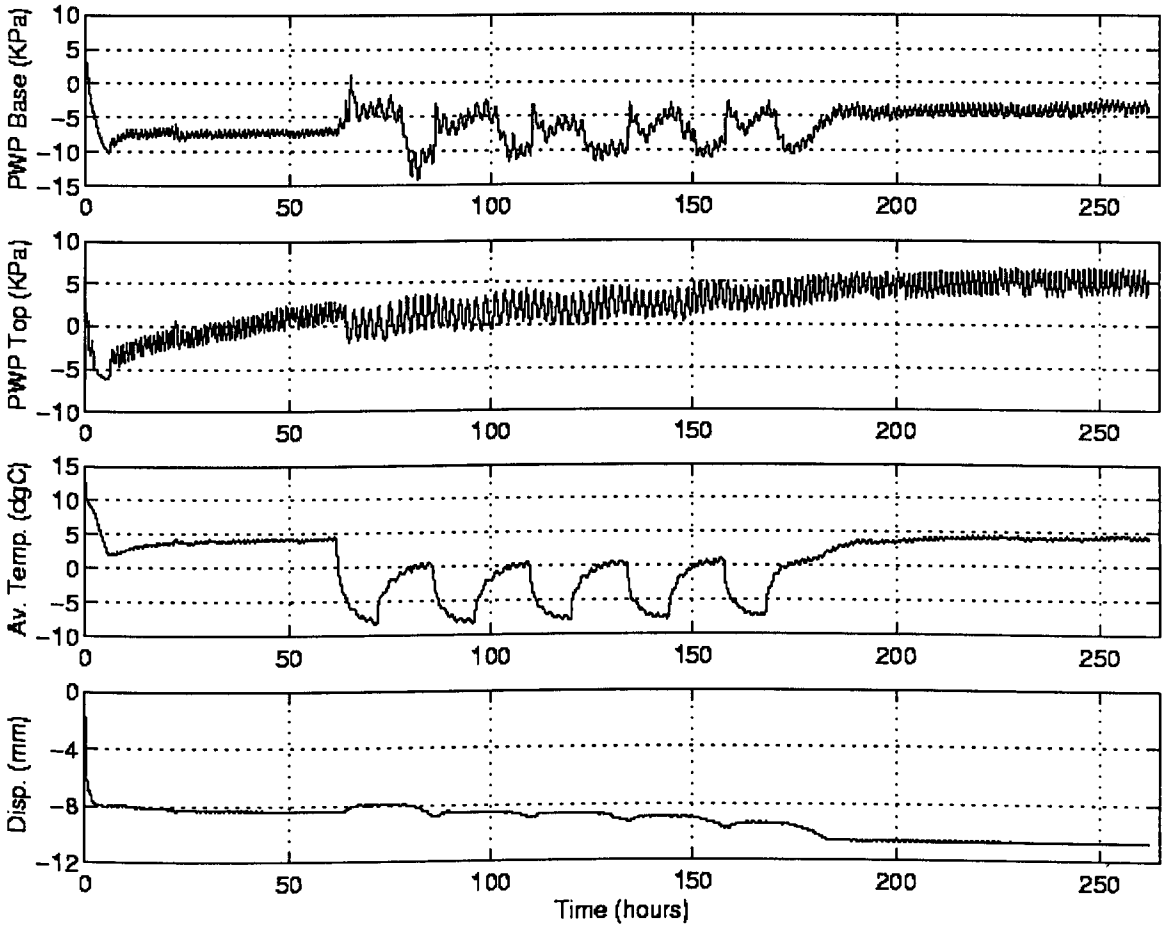

Figure 6.21 – Results for Test 18

Upward displacement of the specimen occurred for each cycle, showing expansion of the specimen on freezing.

The temperature range achieved during Test 18 was found to be too narrow, with the upper-bound temperature being typically only 0°C. Typical temperature profiles are shown in Figure 6.22. The temperature curves show a comparatively high level of fluctuation.

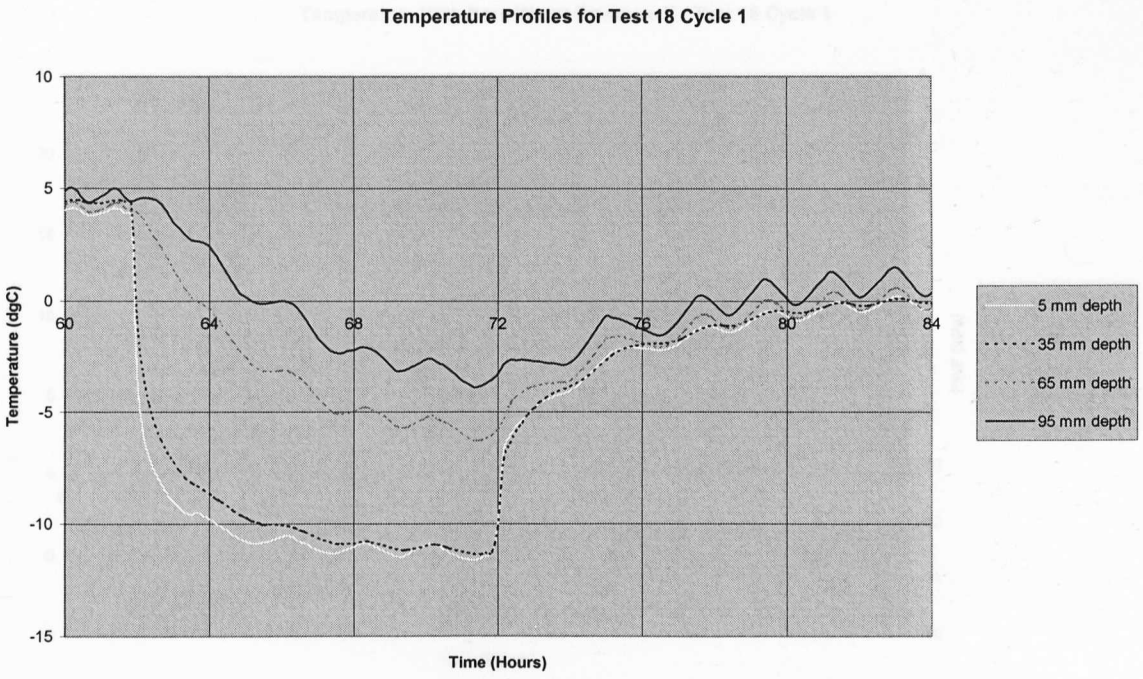

Figure 6.22 – Temperature Profiles for Test 18 Cycle 1

Figures 6.23-6.26 show the pore water pressure response at the base and top of the specimen for Cycles 1 and 2.

At the base transducer, the pore water pressure increased with freezing to reach a fluctuating plateau. This level was maintained during thawing until the 0°C threshold was approached, at which point a sharp decrease in pore water pressure occurred.

At the top transducer, there was very little discernible pore water pressure response, although the pressure was seen to increase slightly over the whole test.

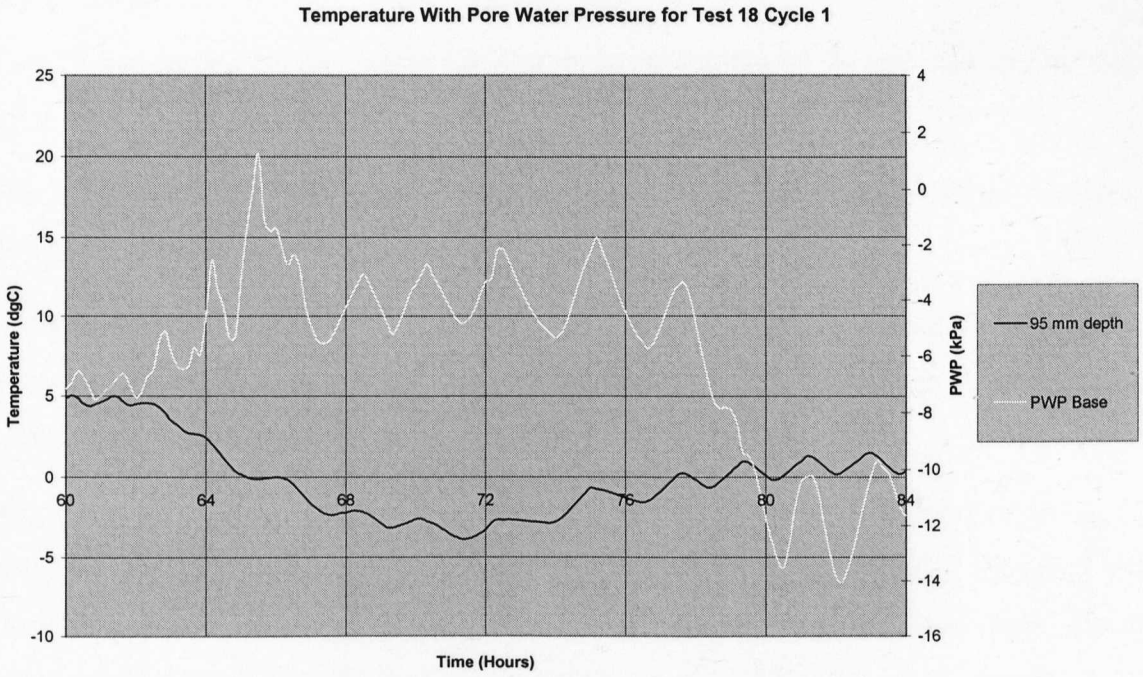

Figure 6.23 – Test 18 Cycle 1 Pore Water Pressure & Temperature at Base

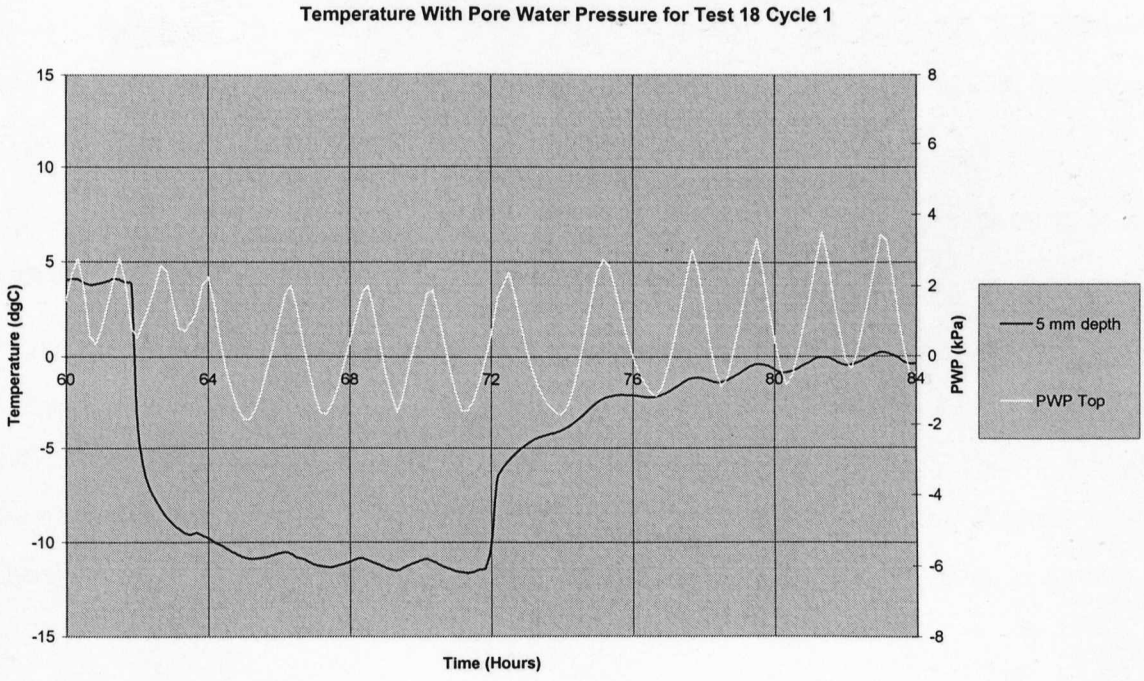

Figure 6.24 – Test 18 Cycle 1 Pore Water Pressure & Temperature at Top

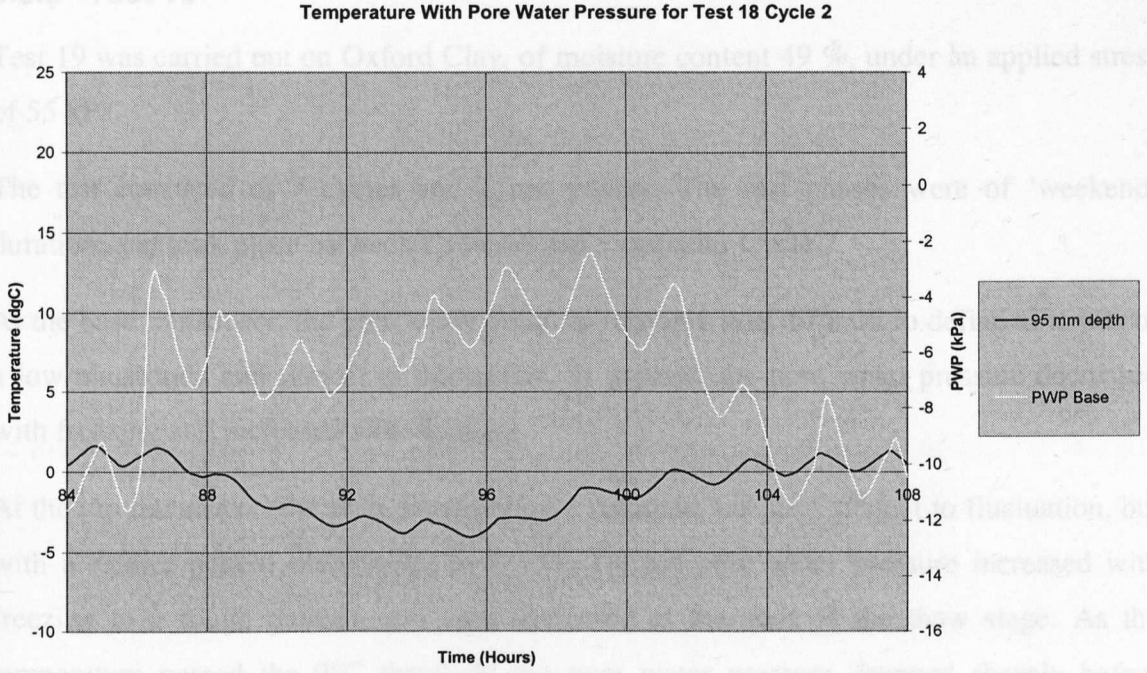

Figure 6.25 – Test 18 Cycle 2 Pore Water Pressure & Temperature at Base

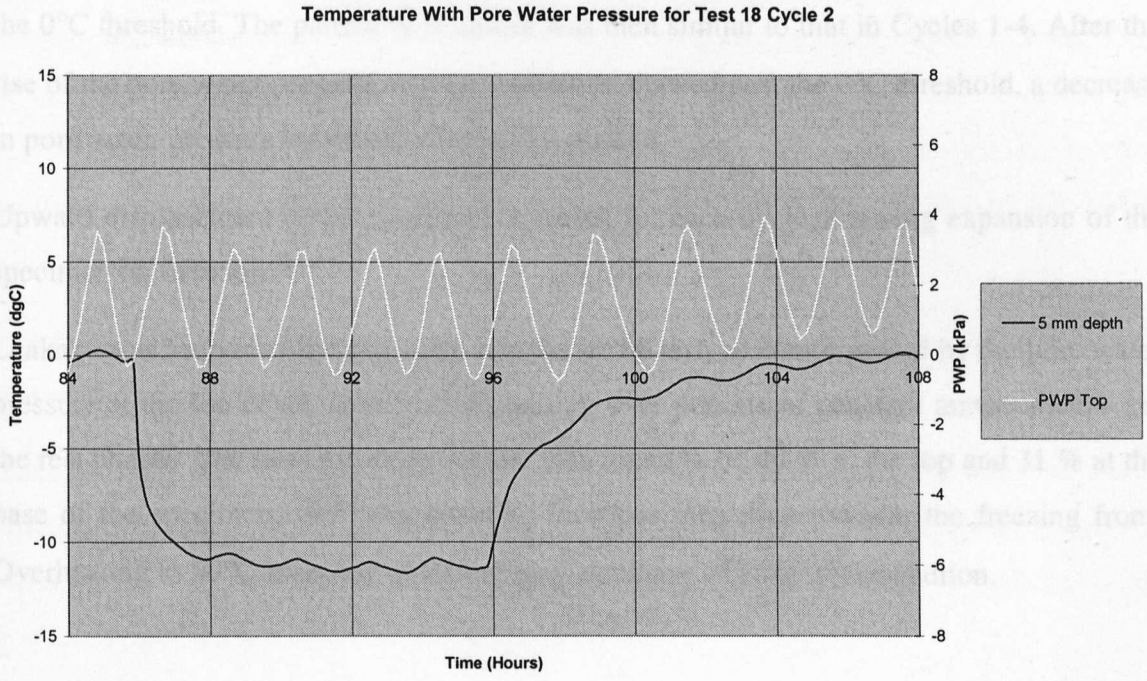

Figure 6.26 – Test 18 Cycle 2 Pore Water Pressure & Temperature at Top

The final moisture content found to be 29 % at the top and 24 % at the base of the specimen, demonstrating moisture migration towards the freezing front. However, leakage was found to have occurred.

6.3.6 Test 19

Test 19 was carried out on Oxford Clay, of moisture content 49 %, under an applied stress of 55 kPa.

The test consisted of 7 cycles and 2 rest phases. The rest phases were of 'weekend' duration, and took place between Cycles 4 and 5 and after Cycle 7.

At the base transducer, the pore water pressure response was difficult to define as it was of a low magnitude and subject to fluctuation. In general, the pore water pressure decreased with freezing and increased with thawing.

At the top transducer, the pore water pressure response was also subject to fluctuation, but with a clearer pattern observable. In Cycles 1-4 the pore water pressure increased with freezing to a rough plateau, and then decreased at the start of the thaw stage. As the temperature passed the 0°C threshold the pore water pressure dropped sharply before increasing for the rest of the thaw period. In Cycles 5-7 the pore water pressure rose to a peak at the onset of the freezing stage, but then decreased as the temperature dropped past the 0°C threshold. The pattern of response was then similar to that in Cycles 1-4. After the rise of the pore water pressure as the temperature thawed past the 0°C threshold, a decrease in pore water pressure occurred, settling to a plateau.

Upward displacement of the specimen occurred for each cycle, showing expansion of the specimen on freezing.

Leakage was found to have occurred at times in the test, as demonstrated by the pore water pressure at the top of the specimen decreasing over periods of constant temperature – i.e. the rest phases. The final moisture content was found to be 40 % at the top and 31 % at the base of the specimen, still demonstrating moisture migration towards the freezing front. Overheating to 20°C after end of testing may also have affected redistribution.

6.3.7 Test 20

Test 20 was carried out on Oxford Clay, of moisture content 49 %, under an applied stress of 80 kPa.

The test consisted of 5 cycles and 1 rest phase. The rest phase was of short duration and took place before Cycle 1.

At the base transducer, there was very little discernible pore water pressure response, although the pore water pressure could be seen to be decreasing with freezing and increasing on thaw.

At the top transducer, in Cycles 1 and 2 the pore water pressure remained roughly level during freezing and decreased from the onset of the thaw stage, following a convex shape. After the temperature rose past the 0°C threshold, the pore water pressure increased. In Cycle 3, the pore water pressure decreased during freezing, rapidly at first and then levelling out. At the onset of the thaw stage, the pore water pressure remained level until the temperature passed the 0°C threshold, whereupon it dipped and rose for the rest of the thaw stage. In Cycles 4 and 5, the pore water pressure response was similar to that observed in Cycles 1 and 2, but with a slight rise in Pore water pressure to the initial plateau during the freezing stage.

Upward displacement of the specimen occurred for each cycle, showing expansion of the specimen on freezing.

Leakage was found to have occurred, although this was not evidenced in the pore water pressure response during the cycles, or by visual observation. The final moisture content was found to be 35 % at the top and 28 % at the base of the specimen, still demonstrating moisture migration towards the freezing front.

6.3.8 Test 21

Test 21 was carried out on Oxford Clay, of moisture content 50 %, under an applied stress of 55 kPa. Summarised results are given in Figure 6.27.

The test consisted of 3 cycles and 1 rest phase. The rest phase was of long, 'weekend' duration, and took place before Cycle 1.

Upward displacement of the specimen occurred for each cycle, showing expansion of the specimen on freezing. At the start of the test, the displacement transducer was not sufficiently free to move. This was corrected, leading to a 'stepped' downwards displacement being recorded. This accentuates the problem of non-recovered downwards movement – i.e. indication of leakage occurring.

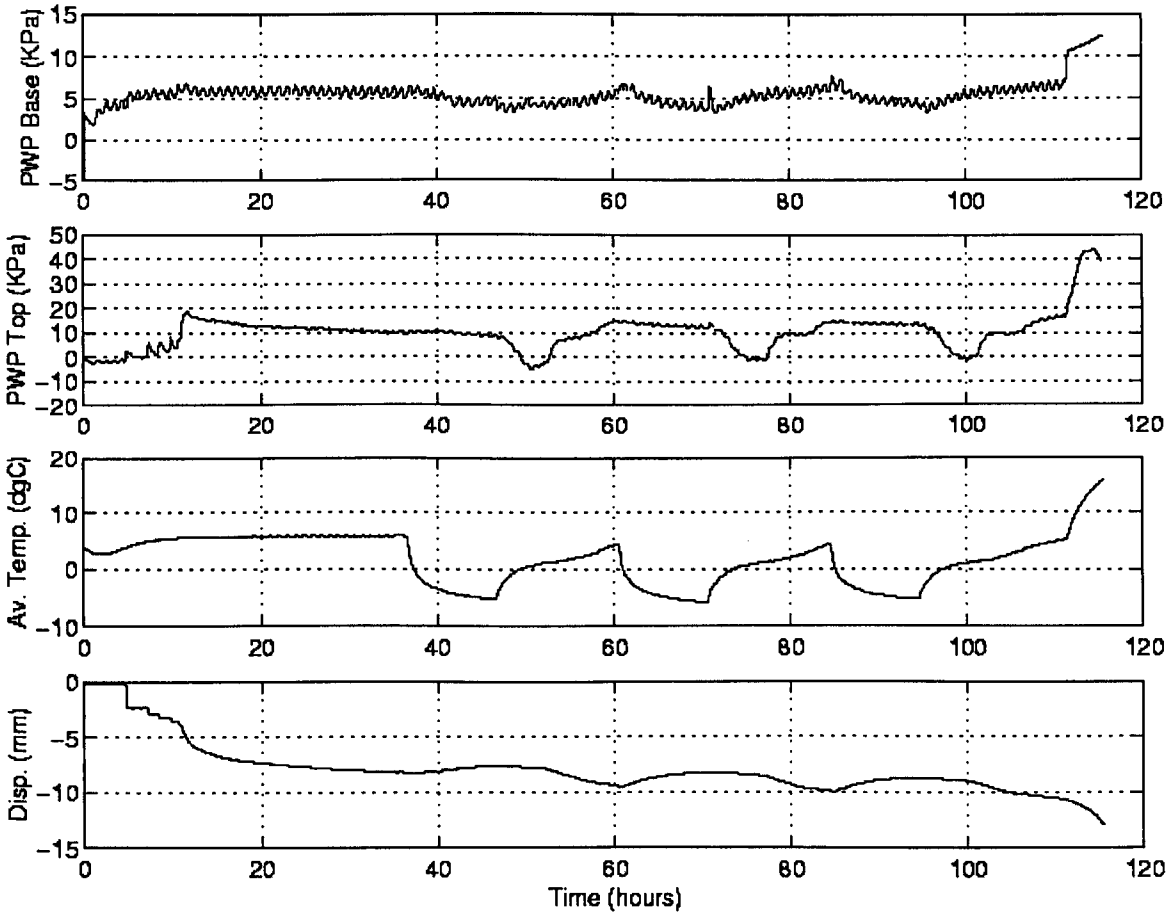

Figure 6.27 – Results for Test 21

Figure 6.28 shows typical temperature profiles. Unfortunately, the very base of the specimen is shown not to freeze.

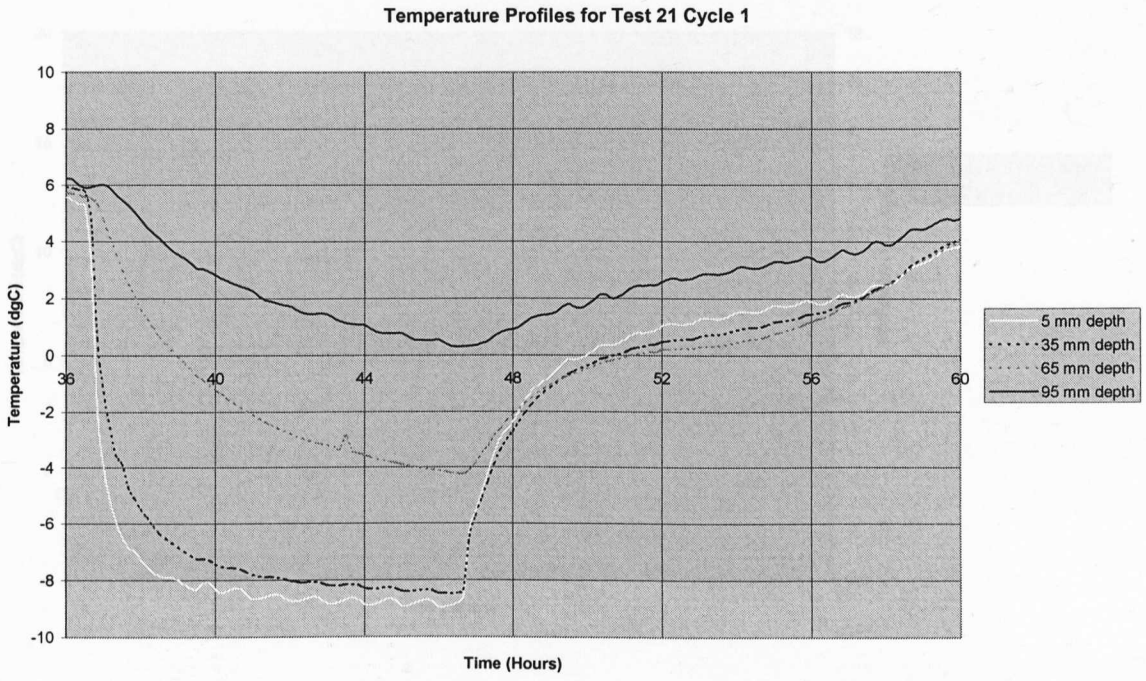

Figure 6.28 – Temperature Profiles for Test 21 Cycle 1

Figures 6.29-6.34 show the pore water pressure response at the base and top of the specimen for Cycles 1-3.

At the base transducer, a fluctuating pore water pressure response is seen for all cycles. However, the pore water pressure is generally seen to drop on cooling and rise on warming.

At the top transducer, in Cycle 1 the pore water pressure remained roughly level during freezing and decreased sharply from the onset of the thaw stage. The pore water pressure remained in a trough for 2.5-3 hours past the 0°C threshold. At this time, the temperature was ~1°C, and the pore water pressure began to rise at this point, but then levelling off as the thaw curve flattened out. Following this, at ~2.5°C, the pore water pressure began to rise once more.

A similar response was seen in Cycles 2 and 3.

The final moisture content found to be 47 % at the top and 34 % at the base of the specimen, demonstrating moisture migration towards the freezing front. Leakage occurred during the test, shown by the downwards displacement recorded.

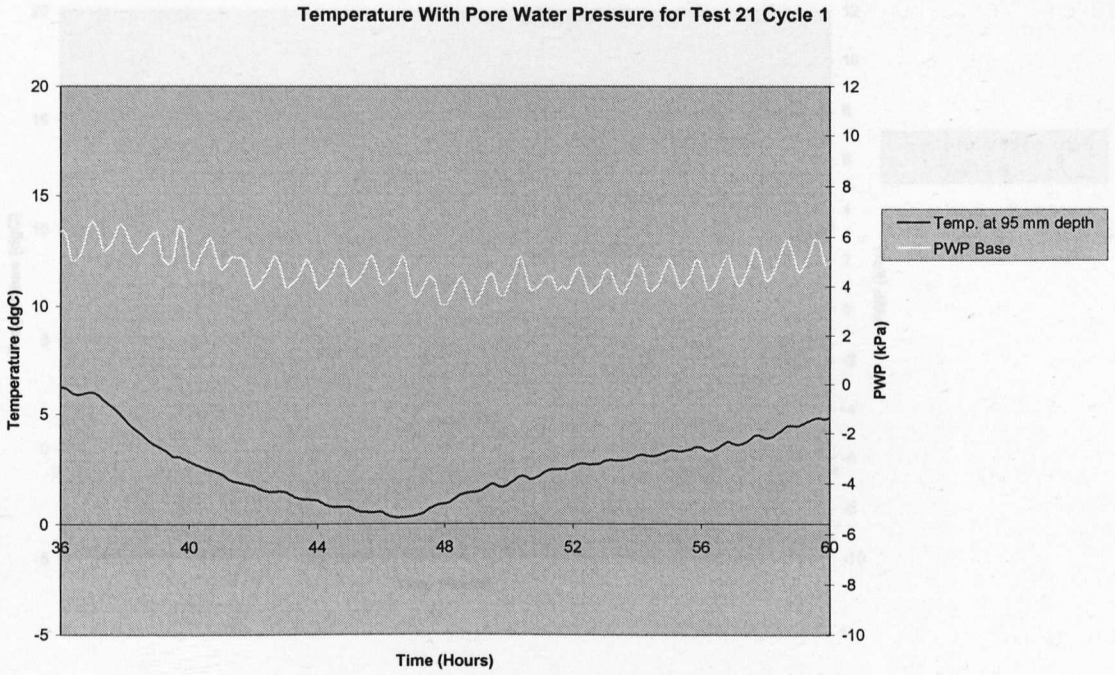

Figure 6.29 – Test 21 Cycle 1 Pore Water Pressure & Temperature at Base

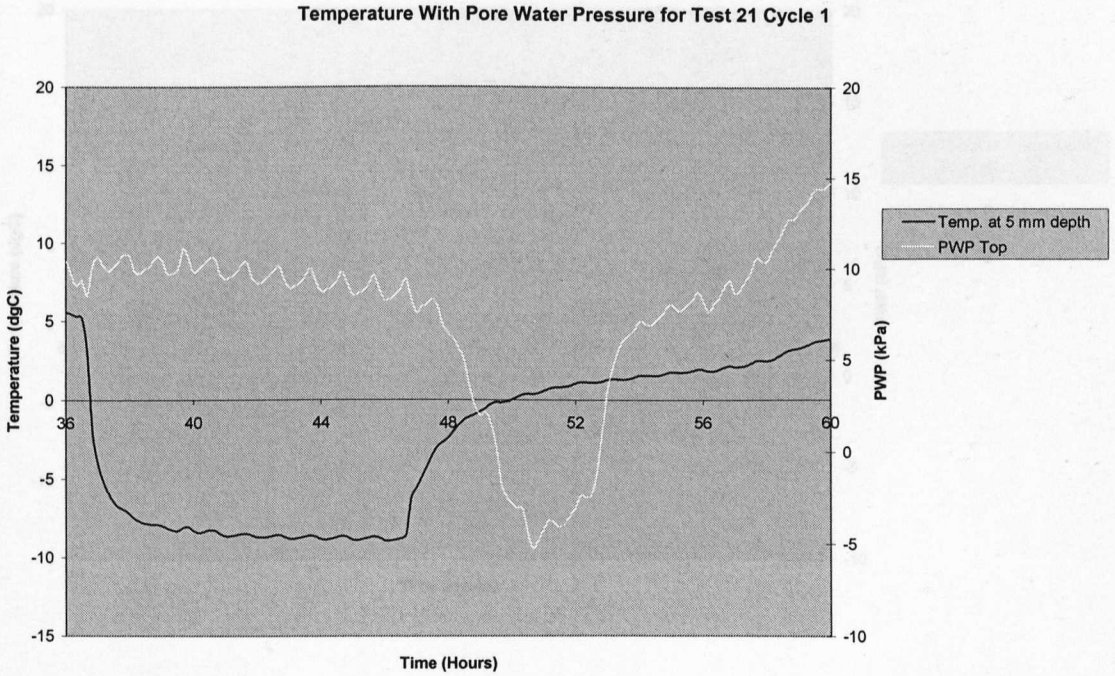

Figure 6.30 – Test 21 Cycle 1 Pore Water Pressure & Temperature at Top

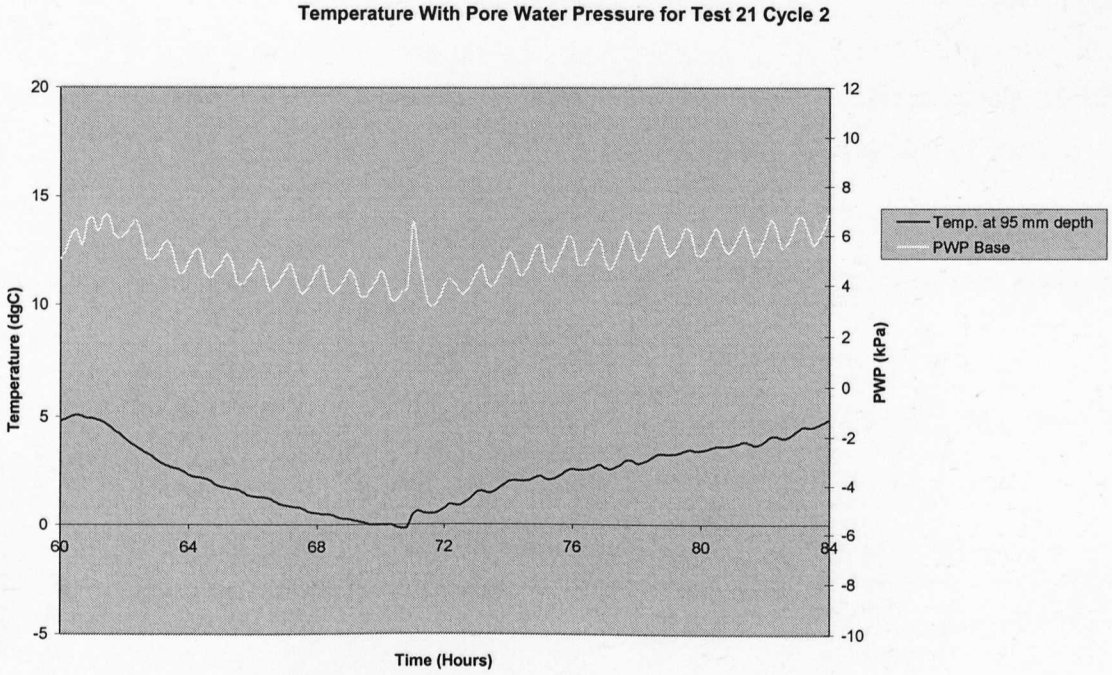

Figure 6.31 – Test 21 Cycle 2 Pore Water Pressure & Temperature at Base

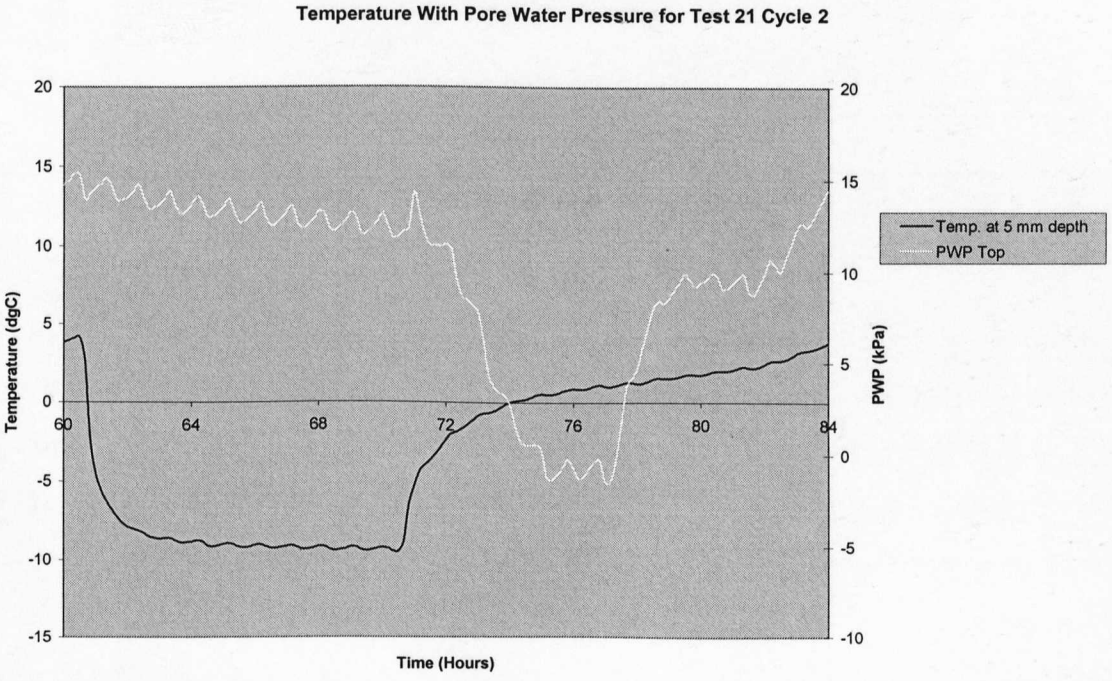

Figure 6.32 – Test 21 Cycle 2 Pore Water Pressure & Temperature at Top

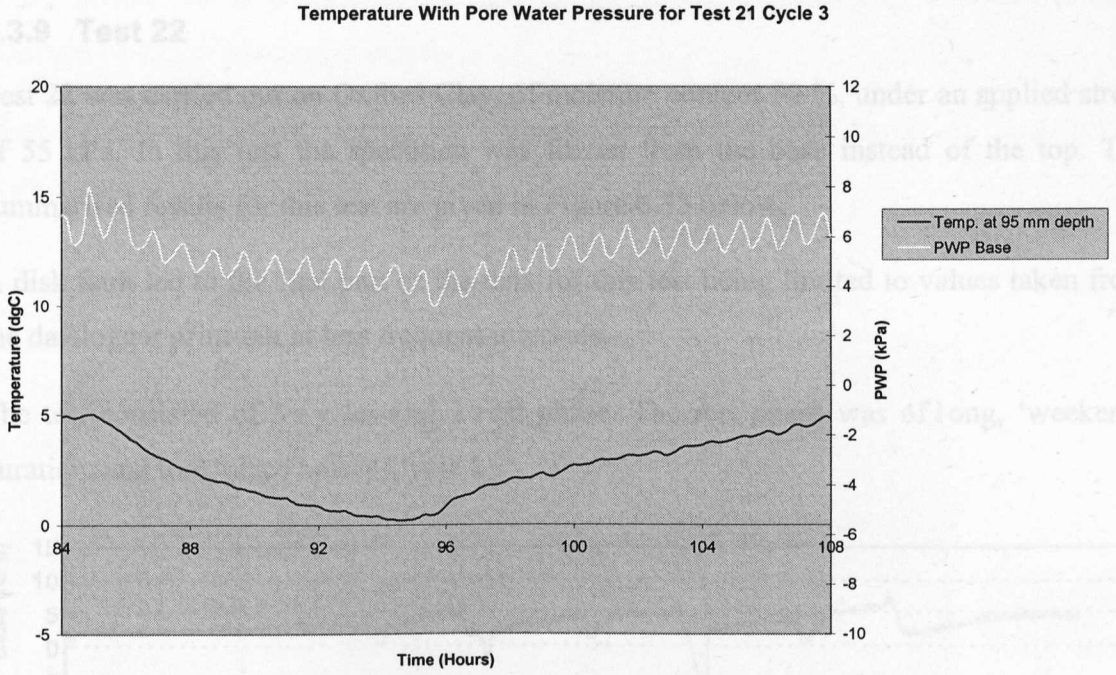

Figure 6.33 – Test 21 Cycle 3 Pore Water Pressure & Temperature at Base

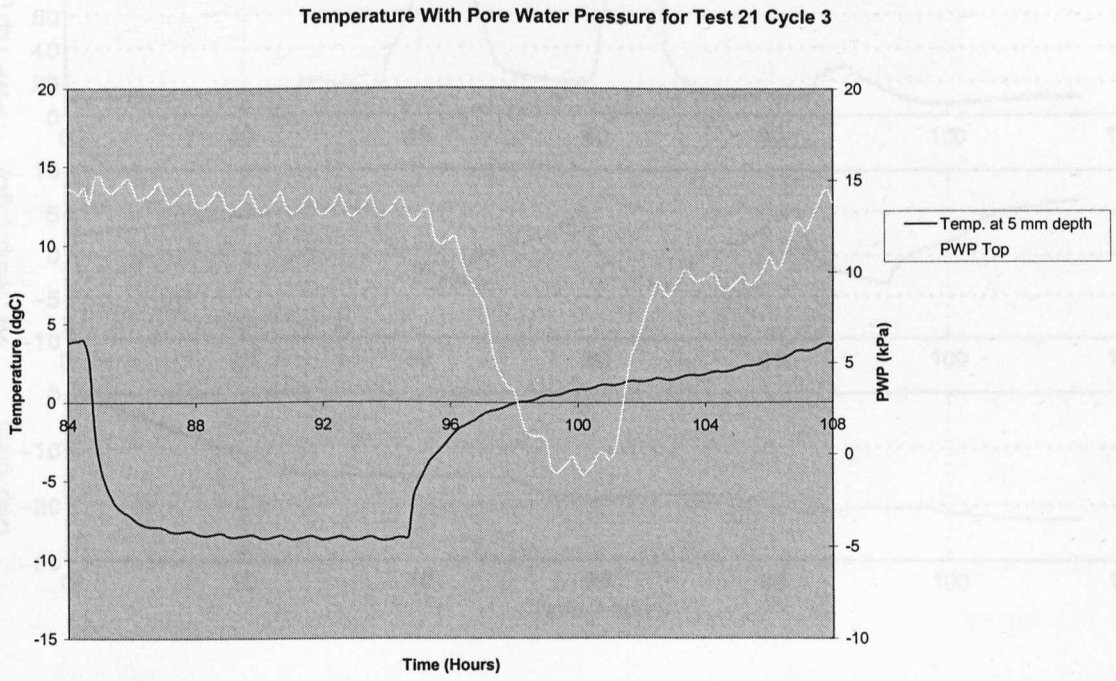

Figure 6.34 – Test 21 Cycle 3 Pore Water Pressure & Temperature at Top

6.3.9 Test 22

Test 22 was carried out on Oxford Clay, of moisture content 50 %, under an applied stress of 55 kPa. In this test the specimen was frozen from the base instead of the top. The summarised results for this test are given in Figure 6.35 below.

A disk fault led to the first part of the data for this test being limited to values taken from the datalogger print-out at less frequent intervals.

The test consisted of 3 cycles and 1 rest phase. The rest phase was of long, 'weekend' duration, and took place before Cycle 1.

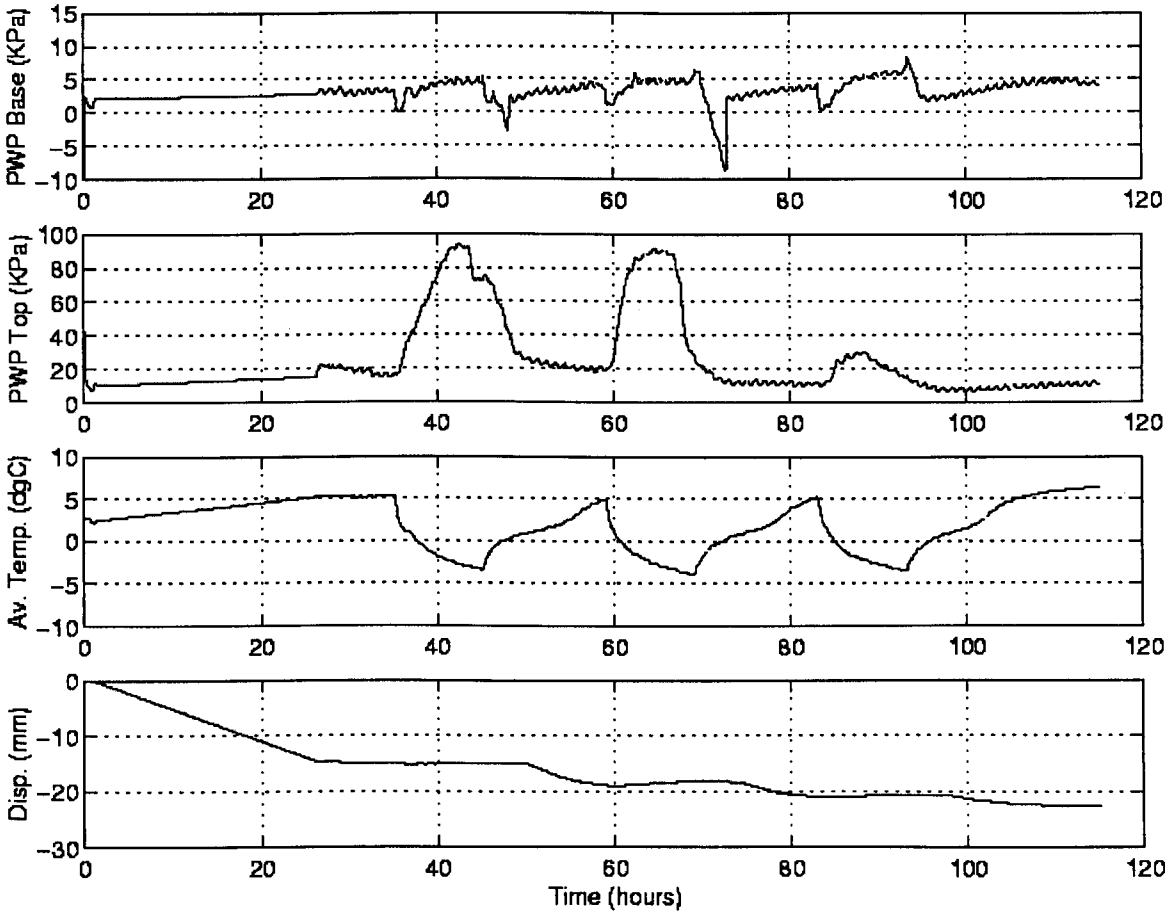

Figure 6.35 – Results for Test 22

Upward displacement of the specimen occurred for each cycle, showing expansion of the specimen on freezing.

The final moisture content found to be 36 % at the top and 40 % at the base of the specimen. However, this still indicates moisture migration towards the freezing front,

which in this test is situated at the base of the permode. Leakage is indicated to have occurred by the displacement graph.

Figure 6.36 shows typical temperature profiles. A relatively high degree of fluctuation is shown, and the top of the specimen did not freeze.

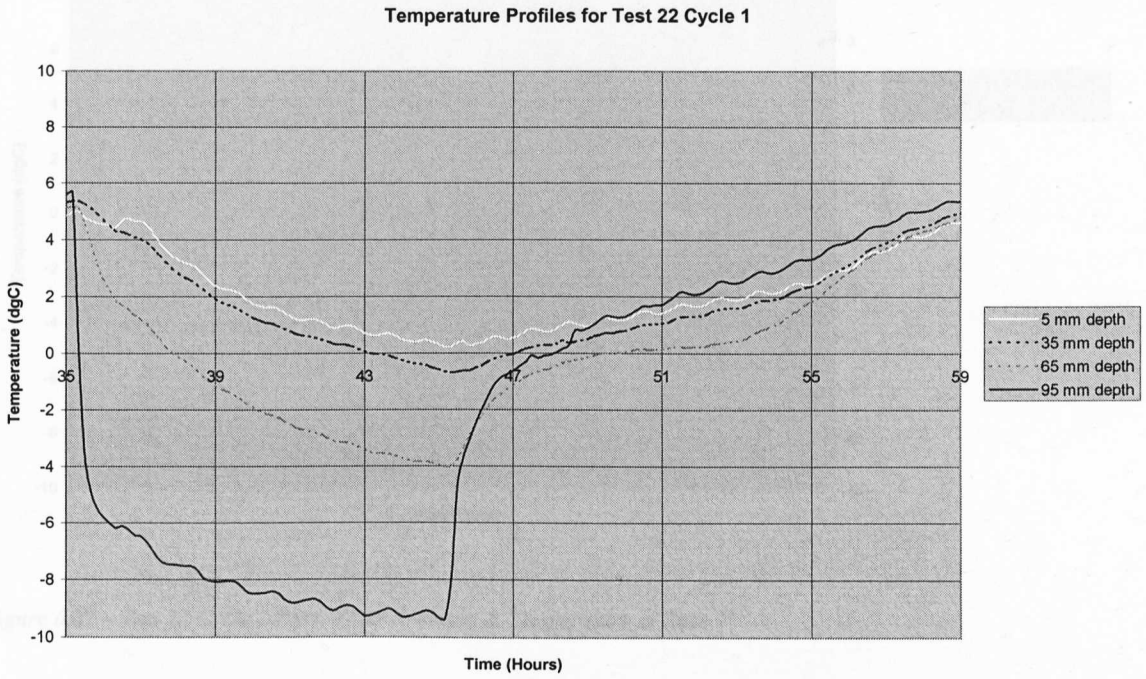

Figure 6.36 – Temperature Profiles for Test 22 Cycle 1

Figures 6.37-6.42 show the pore water pressure response at the base and top of the specimen for Cycles 1-3.

At the base transducer, in Cycle 1, the pore water pressure decreased slightly, (~2-3 kPa), at the beginning of the freezing stage before increasing back to its former value. At the onset of the thaw stage the pore water pressure decreased. As the temperature approached the 0°C threshold, the pore water pressure dropped and rose sharply, and continued to increase at a slower rate for the rest of the thaw stage. In Cycle 2 a similar pattern was observed, but with a very deep dip at the 0°C threshold of the thaw stage. In Cycle 3 no dip is observed, with a gentle increase in pore water pressure from the 0°C threshold seen instead.

At the top transducer, in Cycle 1, the pore water pressure experienced a massive increase during the cooling stage. At the onset of the warming stage the pore water pressure decreased rapidly for ~2 hours, after which the decrease proceeded at a more gentle rate. In

Cycle 2, the pore water pressure also experienced a massive increase, but dropped as the temperatures just passed below the 0°C threshold during the cooling/freezing stage.

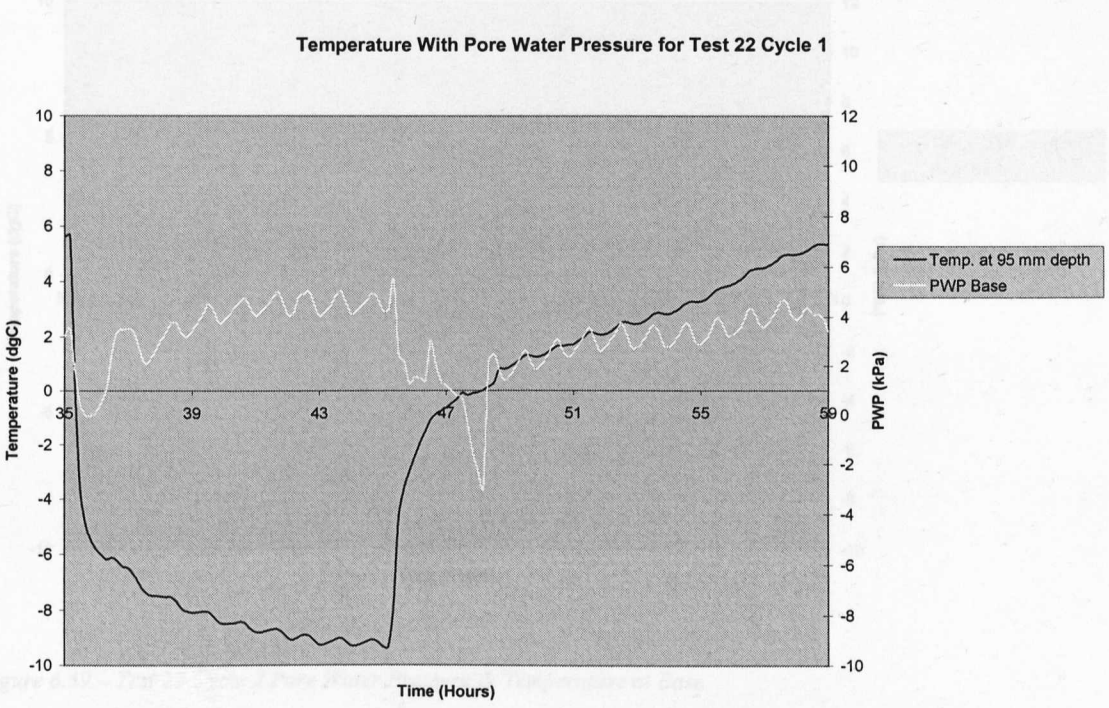

Figure 6.37 – Test 22 Cycle 1 Pore Water Pressure & Temperature at Base

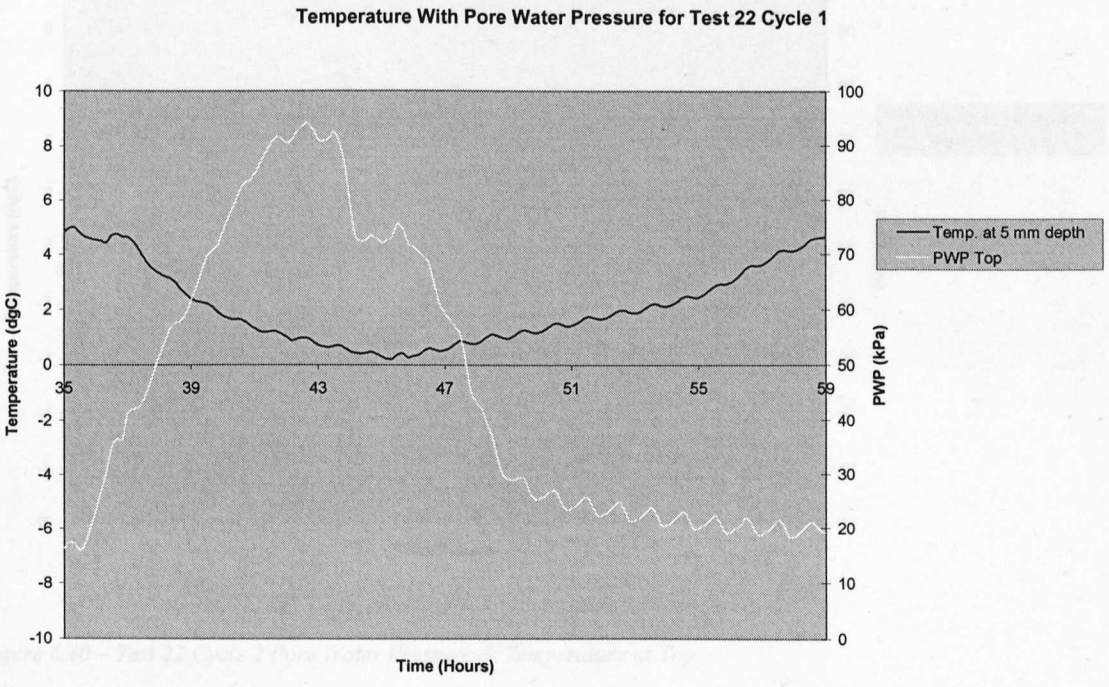

Figure 6.38 – Test 22 Cycle 1 Pore Water Pressure & Temperature at Top

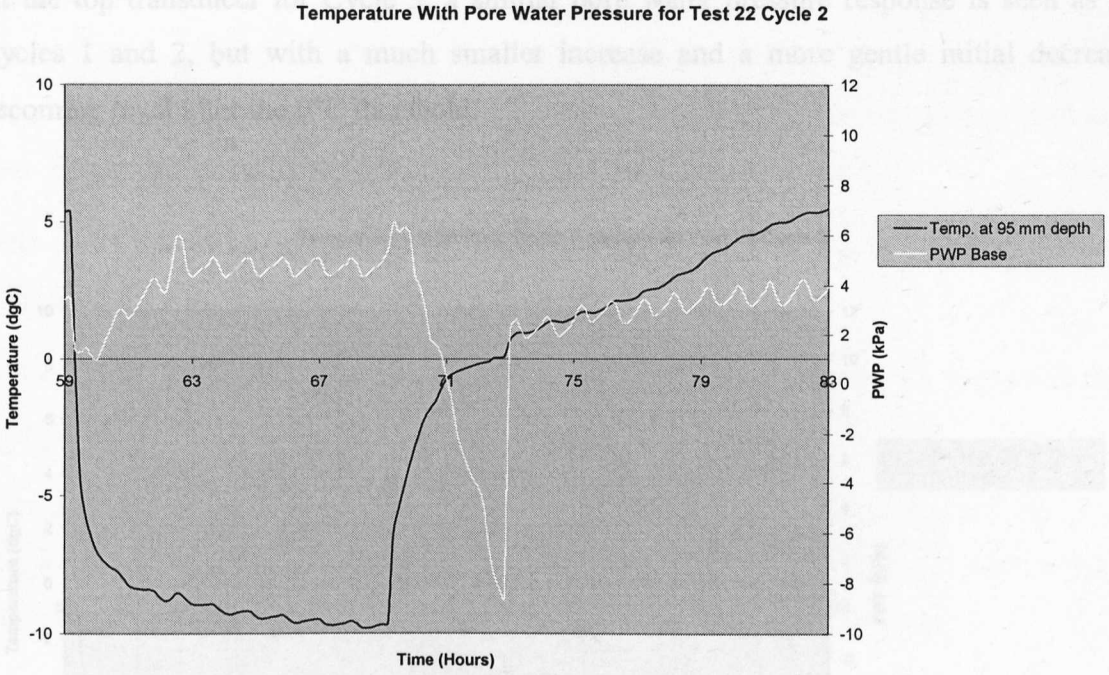

Figure 6.39 – Test 22 Cycle 2 Pore Water Pressure & Temperature at Base

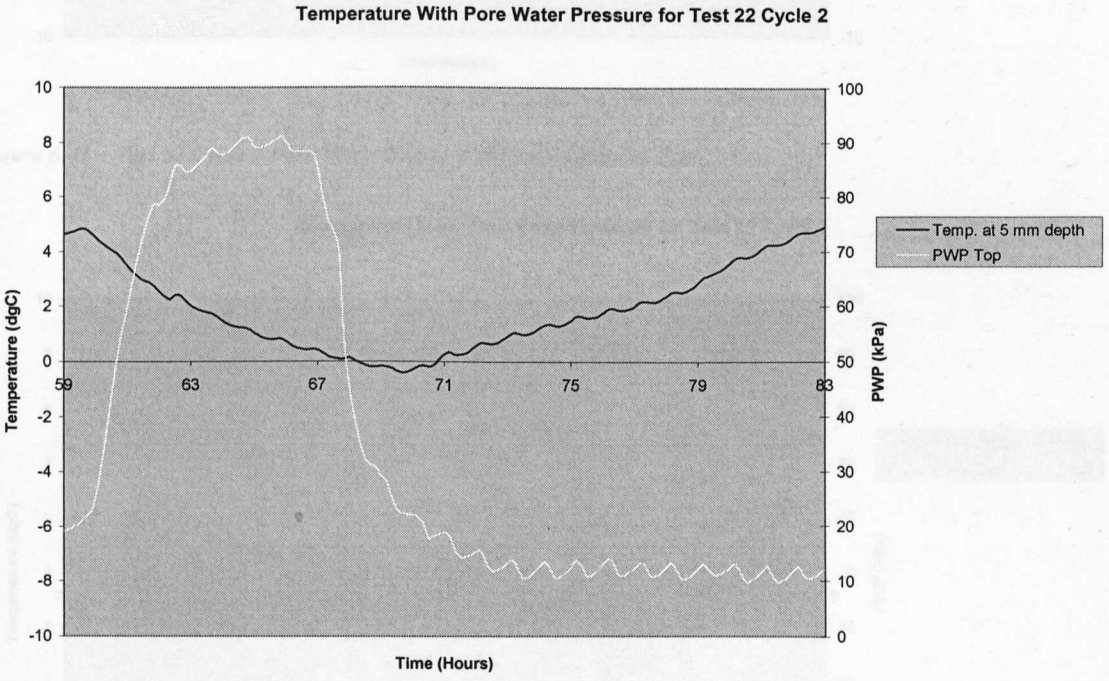

Figure 6.40 – Test 22 Cycle 2 Pore Water Pressure & Temperature at Top

At the top transducer for Cycle 3, a similar pore water pressure response is seen as for Cycles 1 and 2, but with a much smaller increase and a more gentle initial decrease, becoming level after the 0°C threshold.

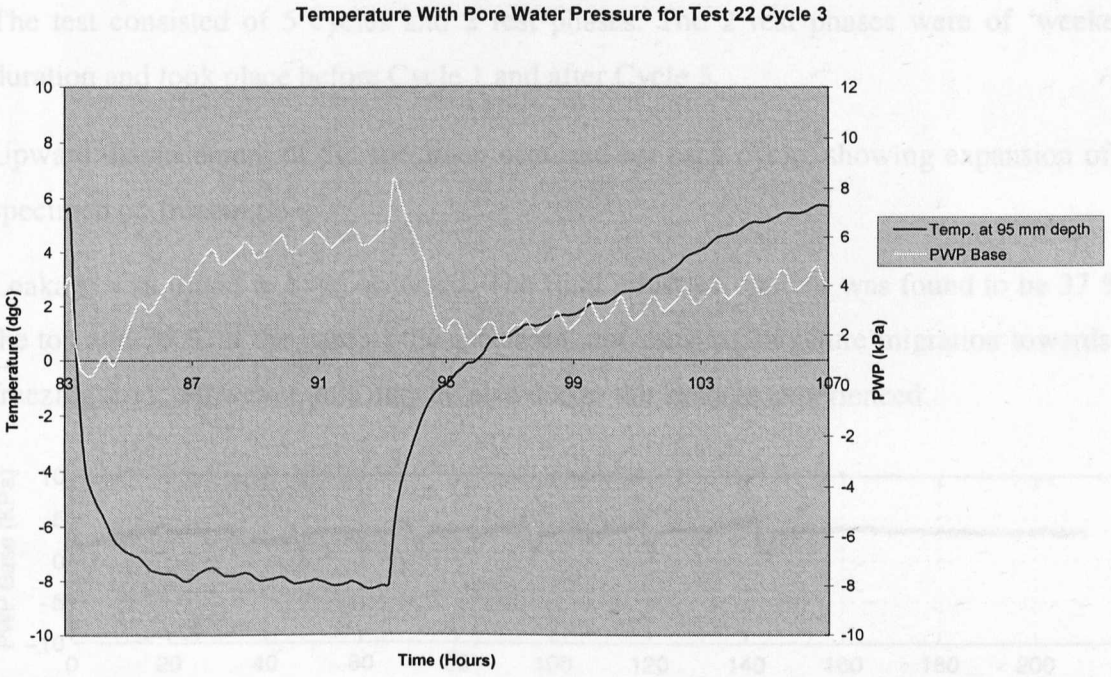

Figure 6.41 – Test 22 Cycle 3 Pore Water Pressure & Temperature at Base

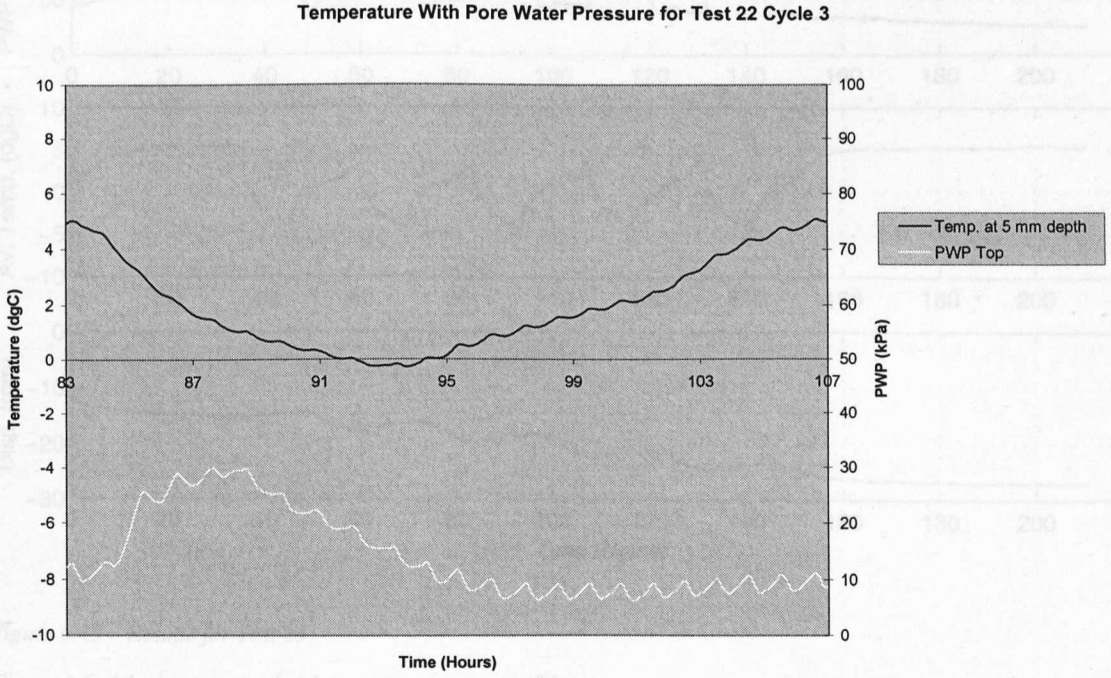

Figure 6.42 – Test 22 Cycle 3 Pore Water Pressure & Temperature at Top

6.3.10 Test 23

Test 23 was carried out on Oxford Clay, of moisture content 50%, under an applied stress of 80 kPa. In Test 23, as in Test 22, the specimen was frozen from the base instead of the top. Summarised results for Test 23 are given in Figure 6.43 below.

The test consisted of 5 cycles and 2 rest phases. The 2 rest phases were of 'weekend' duration and took place before Cycle 1 and after Cycle 5.

Upward displacement of the specimen occurred for each cycle, showing expansion of the specimen on freezing.

Leakage was found to have occurred. The final moisture content was found to be 37 % at the top and 36 % at the base of the specimen, not showing moisture migration towards the freezing front. However, this may be also due to the leakage experienced.

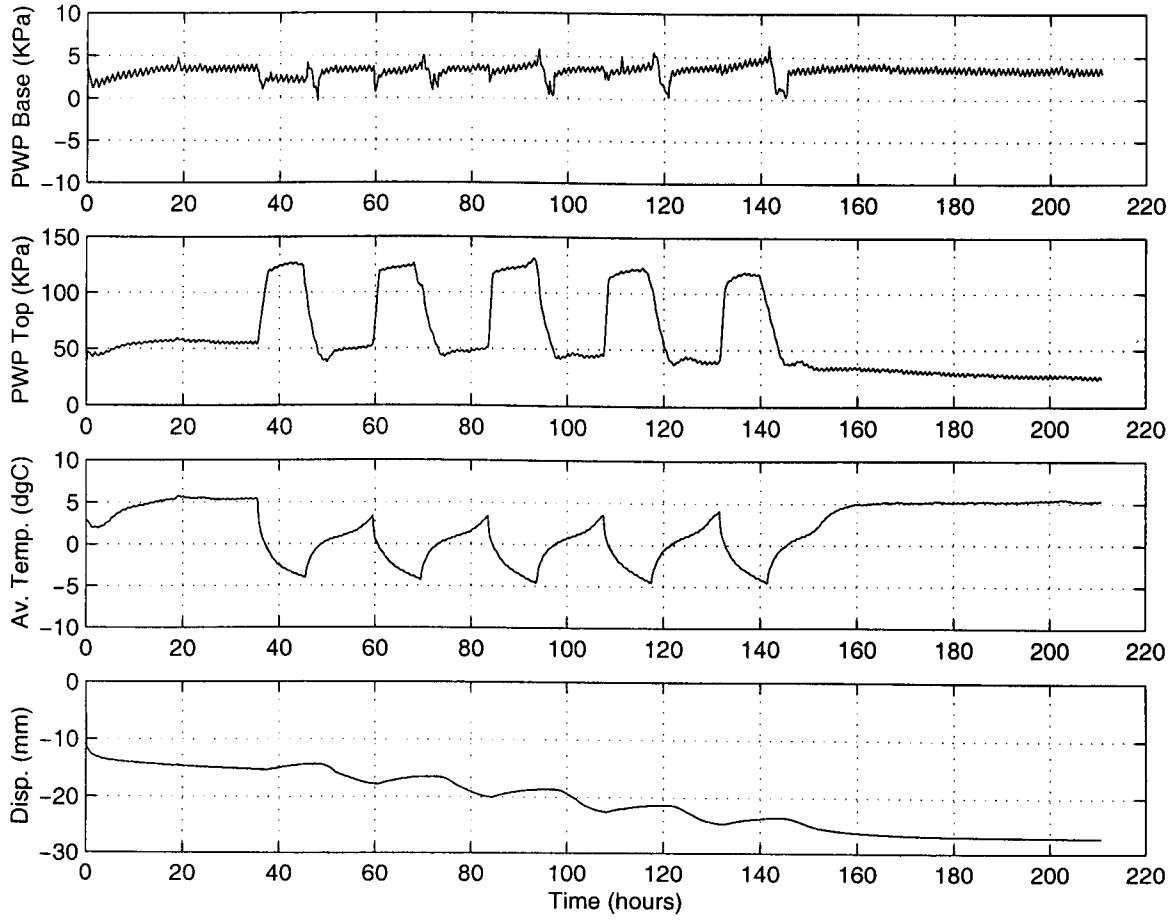

Figure 6.43 – Results for Test 23

Figure 6.44 shows typical temperature profiles.

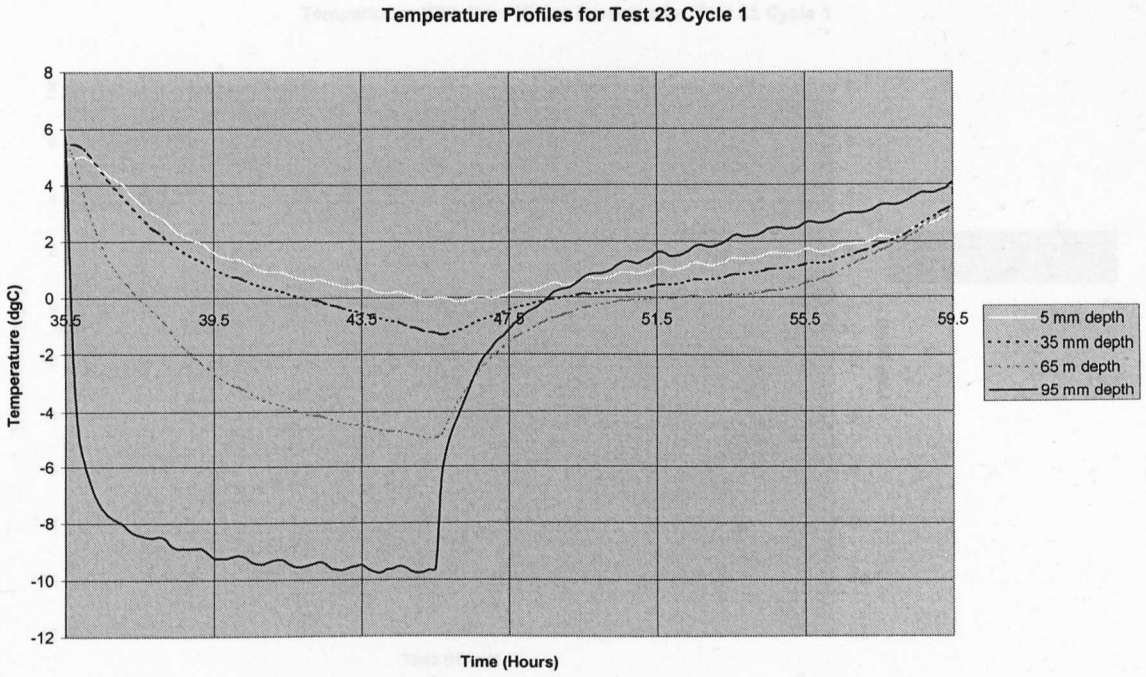

Figure 6.44 – Temperature Profiles for Test 23 Cycle 1

The pore water response was seen to be highly regular.

Figures 6.45-6.48 show the pore water pressure response at the base and top of the specimen for Cycles 1 and 2.

At the base transducer, the pore water pressure response was of a low magnitude. The pore water pressure remained fairly level during the freezing stage. A slight increase was observed at the onset of the thaw stage, followed by a dip and rise as the temperature passed the 0°C threshold on thawing.

At the top transducer, the pore water pressure experienced a massive increase during the cooling/freezing stage. As can be seen from the temperature curves for both cycles selected, temperatures only just reach the 0°C threshold. The pore water pressure appears to begin its decline from the point of that freezing 0°C threshold. At ~ 4 hours into the thaw/warming stage, the pore water pressure increases slightly to a plateau level.

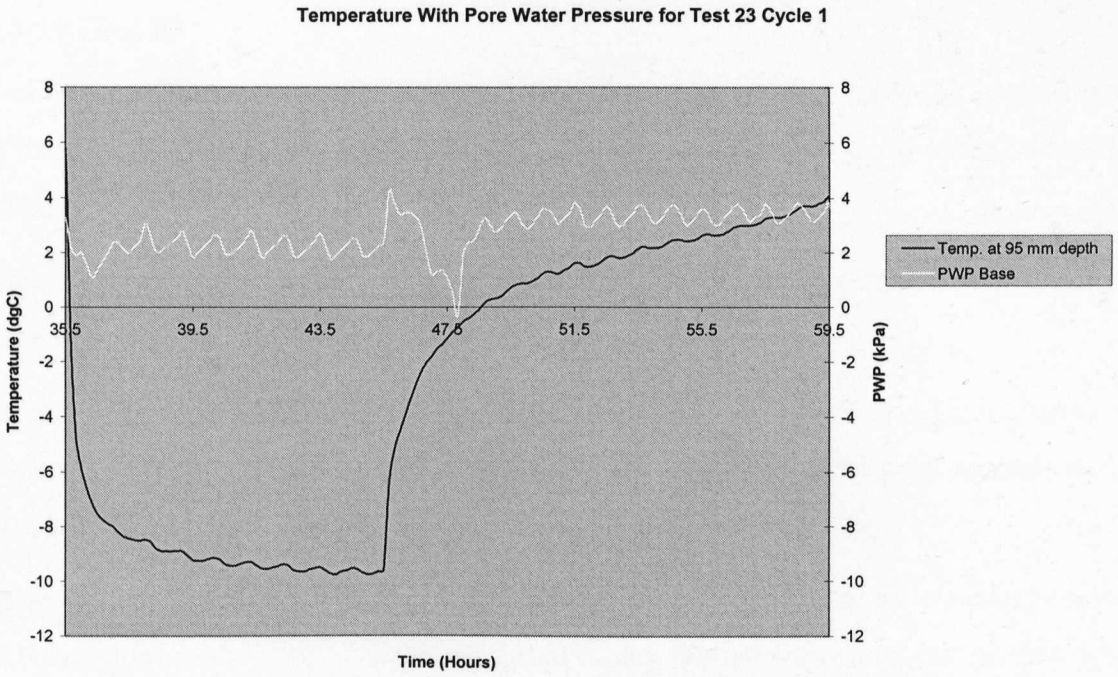

Figure 6.45 – Test 23 Cycle 1 Pore Water Pressure & Temperature at Base

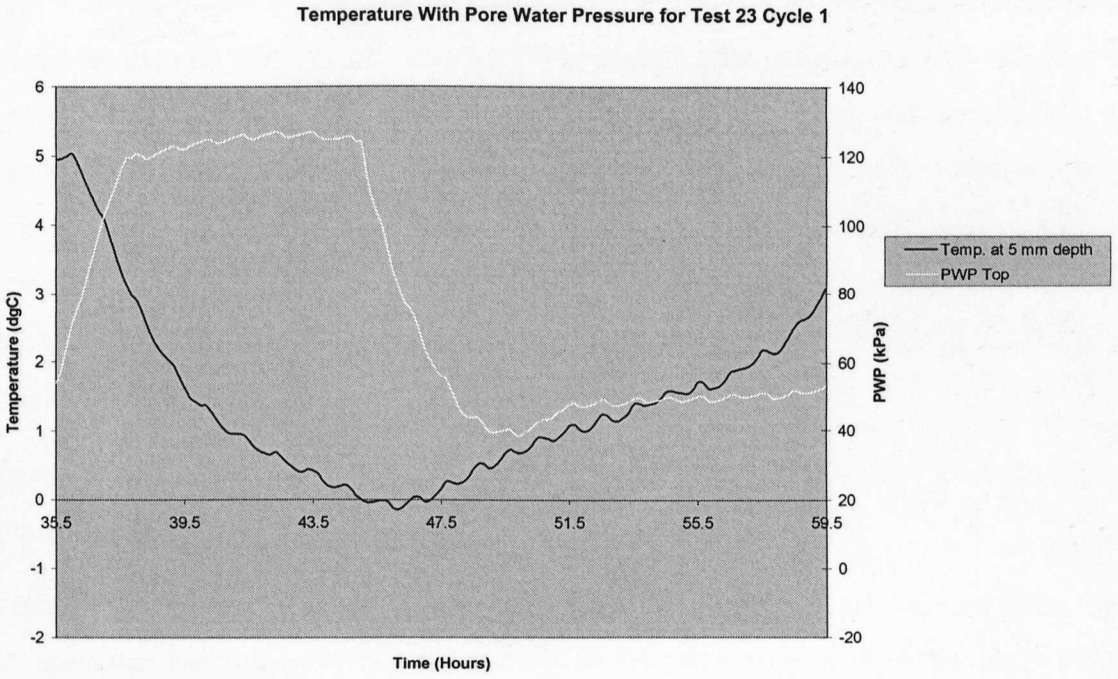

Figure 6.46 – Test 23 Cycle 1 Pore Water Pressure & Temperature at Top

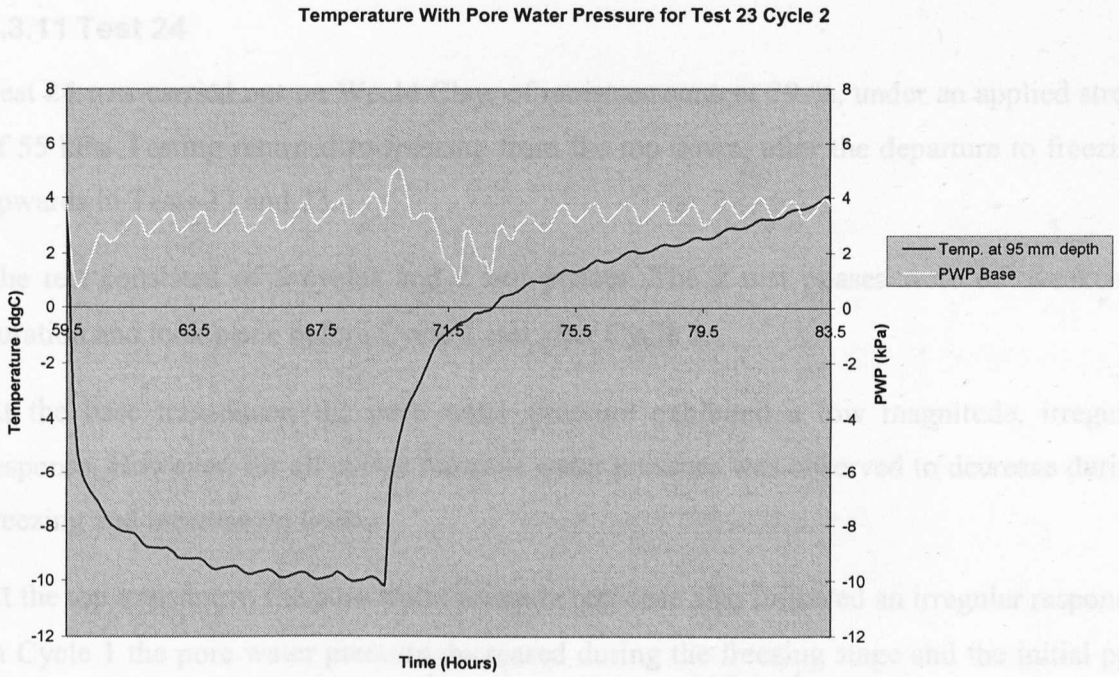

Figure 6.47 – Test 23 Cycle 2 Pore Water Pressure & Temperature at Base

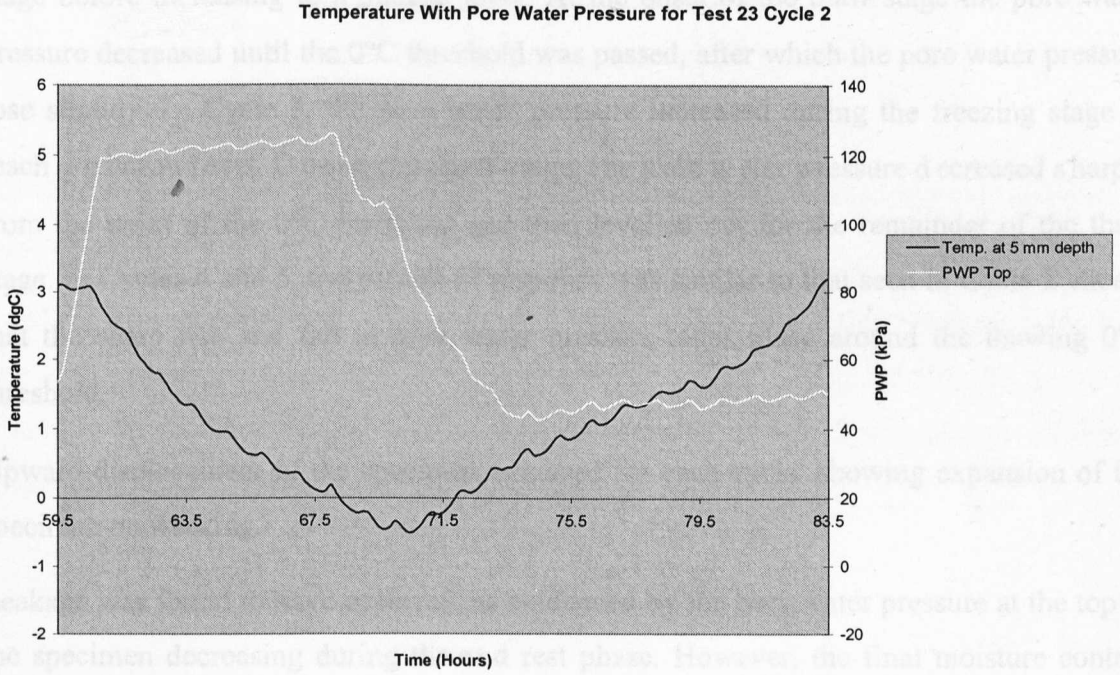

Figure 6.48 – Test 23 Cycle 2 Pore Water Pressure & Temperature at Top

6.3.11 Test 24

Test 24 was carried out on Weald Clay, of moisture content 39 %, under an applied stress of 55 kPa. Testing returned to freezing from the top down, after the departure to freezing upwards in Tests 22 and 23.

The test consisted of 5 cycles and 2 rest phases. The 2 rest phases were of 'weekend' duration and took place before Cycle 1 and after Cycle 5.

At the base transducer, the pore water pressure exhibited a low magnitude, irregular response. However, for all cycles the pore water pressure was observed to decrease during freezing and increase on thaw.

At the top transducer, the pore water pressure response also followed an irregular response. In Cycle 1 the pore water pressure decreased during the freezing stage and the initial part of the thaw stage. The pore water pressure did not increase until temperatures passed the 0°C threshold. In Cycle 2 the pore water pressure remained level for part of the freezing stage before increasing to a plateau level. At the onset of the thaw stage the pore water pressure decreased until the 0°C threshold was passed, after which the pore water pressure rose slightly. In Cycle 3, the pore water pressure increased during the freezing stage to reach a plateau level. During the thaw stage, the pore water pressure decreased sharply from the point of the 0°C threshold and then levelled out for the remainder of the thaw stage. In Cycles 4 and 5, the pattern of response was similar to that seen in Cycle 2 except that the sharp rise and fall in pore water pressure takes place around the thawing 0°C threshold.

Upward displacement of the specimen occurred for each cycle, showing expansion of the specimen on freezing.

Leakage was found to have occurred, as evidenced by the pore water pressure at the top of the specimen decreasing during the end rest phase. However, the final moisture content was found to be 35 % at the top and 25 % at the base of the specimen, still demonstrating moisture migration towards the freezing front.

6.3.12 Test 25

Test 25 was carried out on Weald Clay, of moisture content 39 %, under an applied stress of 80 kPa.

The test consisted of 9 cycles and 3 rest phases. The rest phases were of 'weekend' duration, and took place before Cycle 1, between Cycles 5 and 6, and after Cycle 9.

At the base transducer, the pore water pressure increased sharply during the freezing stage to a peak value before decreasing once more. At the start of the thaw stage, the pore water pressure decreased a little more. As the temperature approached the 0°C threshold, the pore water pressure increased, (at a slower rate than in the freezing stage).

At the top transducer, in Cycles 1-5 the pore water pressure rose slightly to a plateau level during the freezing stage. At the onset of the thawing stage the pore water pressure decreased sharply, before increasing again as the 0°C threshold was passed. In Cycles 6-8, the pore water pressure increased to a peak value at the end of the thaw stage and decreasing slightly before the start of the next freezing stage. In Cycle 9, the pore water pressure response followed a similar pattern to that of the previous cycles, but reaching a lower level of pore water pressure on thaw.

Upward displacement of the specimen occurred for each cycle, showing expansion of the specimen on freezing.

Leakage was found to have occurred, as evidenced by the pore water pressure at the top of the specimen decreasing during the rest phases. However, the final moisture content was found to be 31 % at the top and 24 % at the base of the specimen, still demonstrating moisture migration towards the freezing front.

6.3.13 Test 26

Test 26 was carried out on Weald Clay, of moisture content 38 %, under an applied stress of 55 kPa. Summarised test results are given in Figure 6.49 below.

The test consisted of 7 cycles and 3 rest phases. The rest phases were of 'weekend' duration, and took place before Cycle 1, between Cycles 5 and 6, and after Cycle 7.

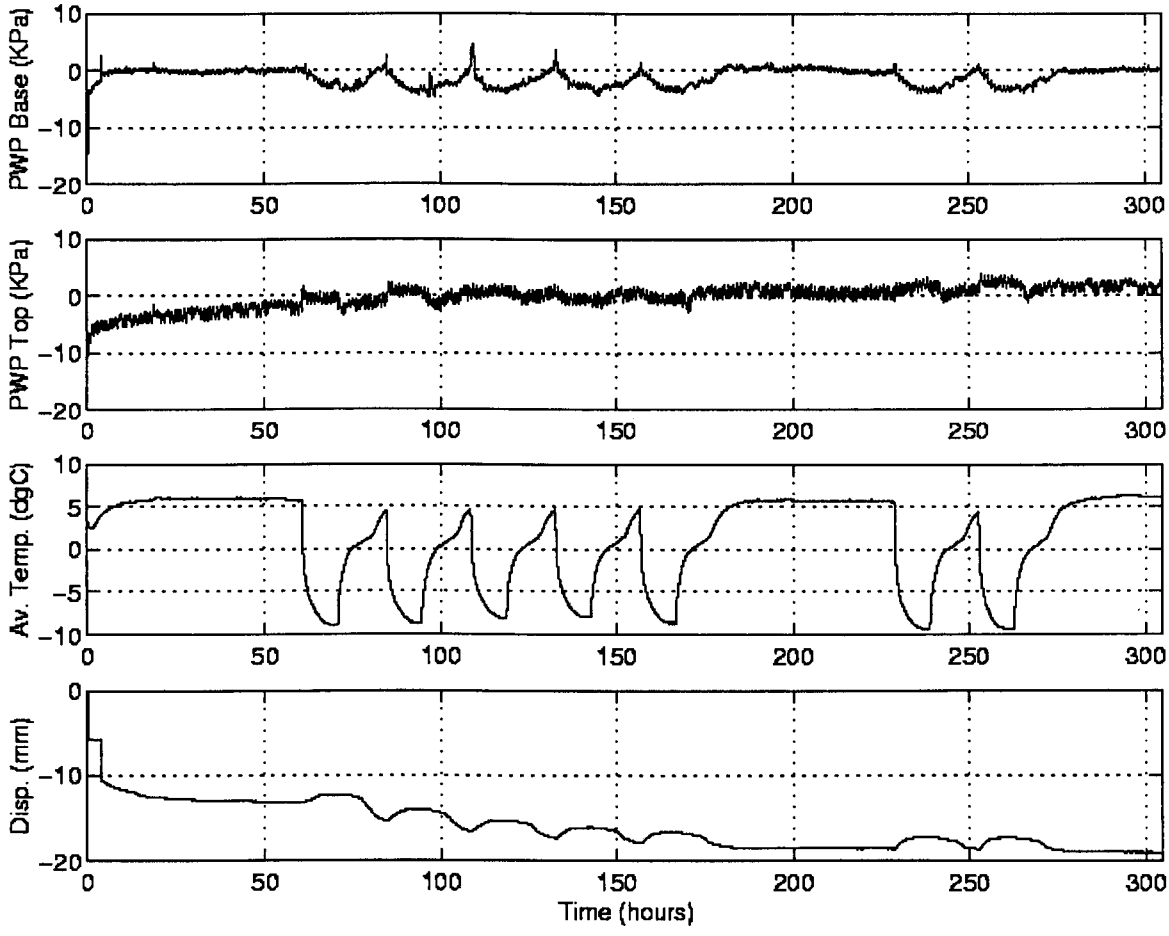

Figure 6.49 – Results for Test 26

Upward displacement of the specimen occurred for each cycle, showing expansion of the specimen on freezing.

The final moisture content was found to be 35 % at the top and 24 % at the base of the specimen, demonstrating moisture migration towards the freezing front. Leakage is indicated by the displacement graph.

Figure 6.50 shows typical temperature profiles.

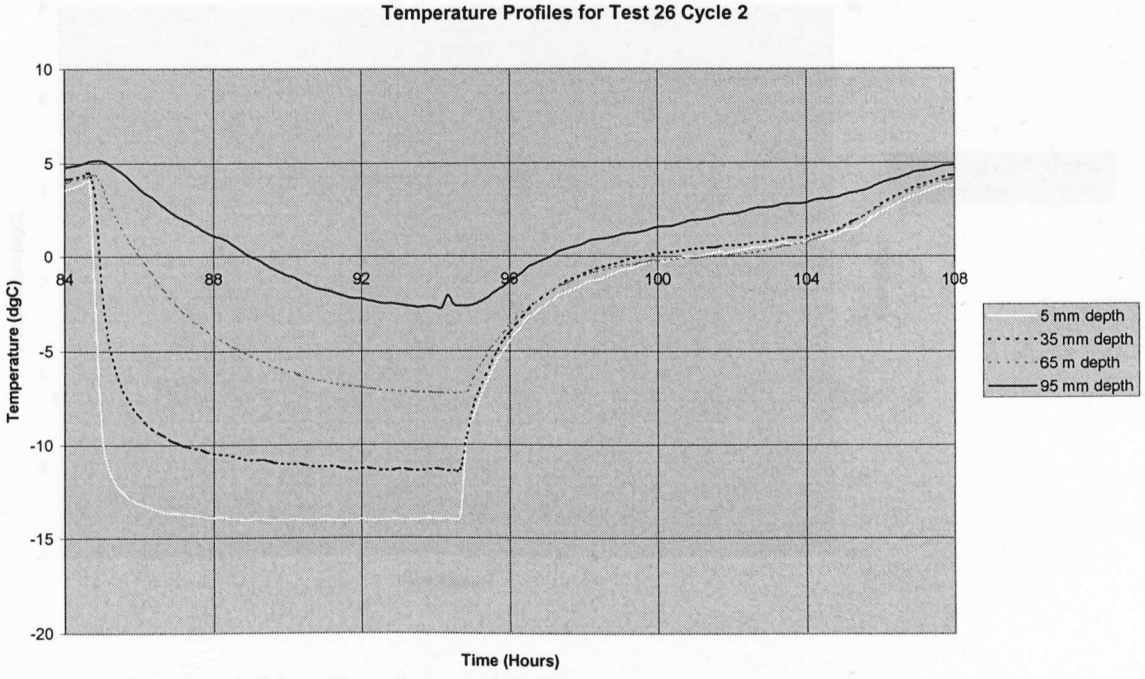

Figure 6.50 – Temperature Profiles for Test 26 Cycle 2

Figures 6.51-6.54 show the pore water pressure response at the base and top of the specimen for Cycles 2 and 5.

At the base transducer, in Cycle 2 the pore water pressure decreased during the freezing stage and increased during the thaw stage. A slight spike was observed as the temperatures passed the 0°C threshold on thawing. In Cycle 5 the pattern is similar, but no spike occurred.

At the top transducer, fluctuation made it harder to discern the pattern of pore water pressure. In Cycle 2 the pore water pressure remained approximately level during freezing, dipped at the onset of thaw and then increased as temperatures passed the 0°C threshold on thawing. In Cycle 5 the response was similar.

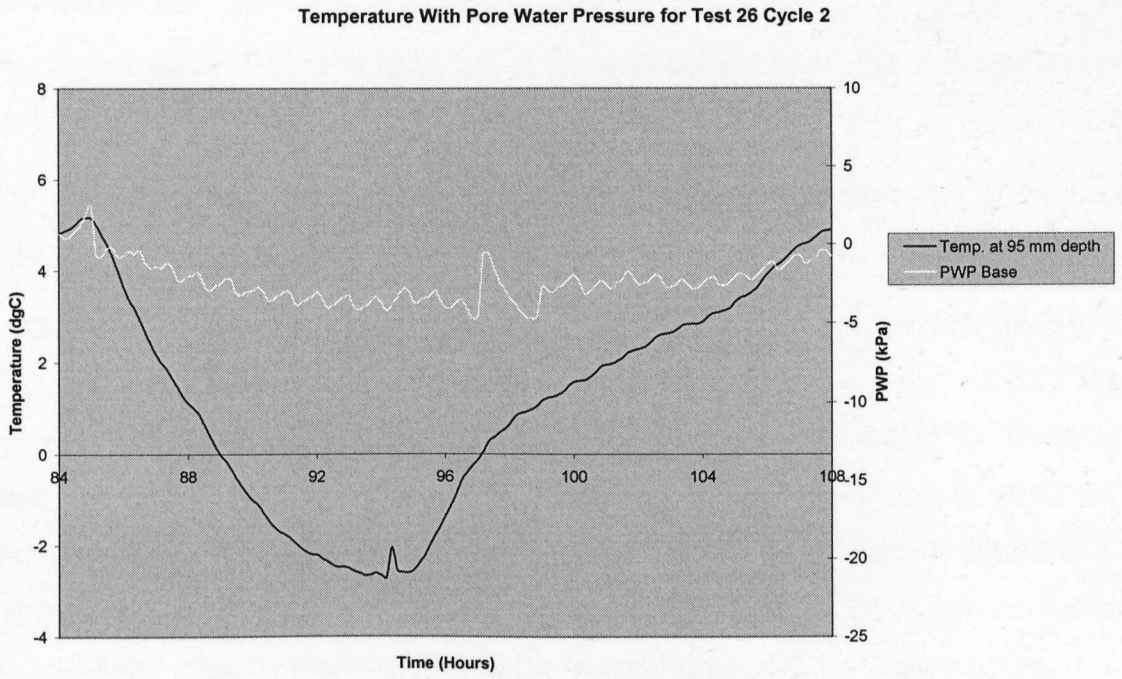

Figure 6.51 – Test 26 Cycle 2 Pore Water Pressure & Temperature at Base

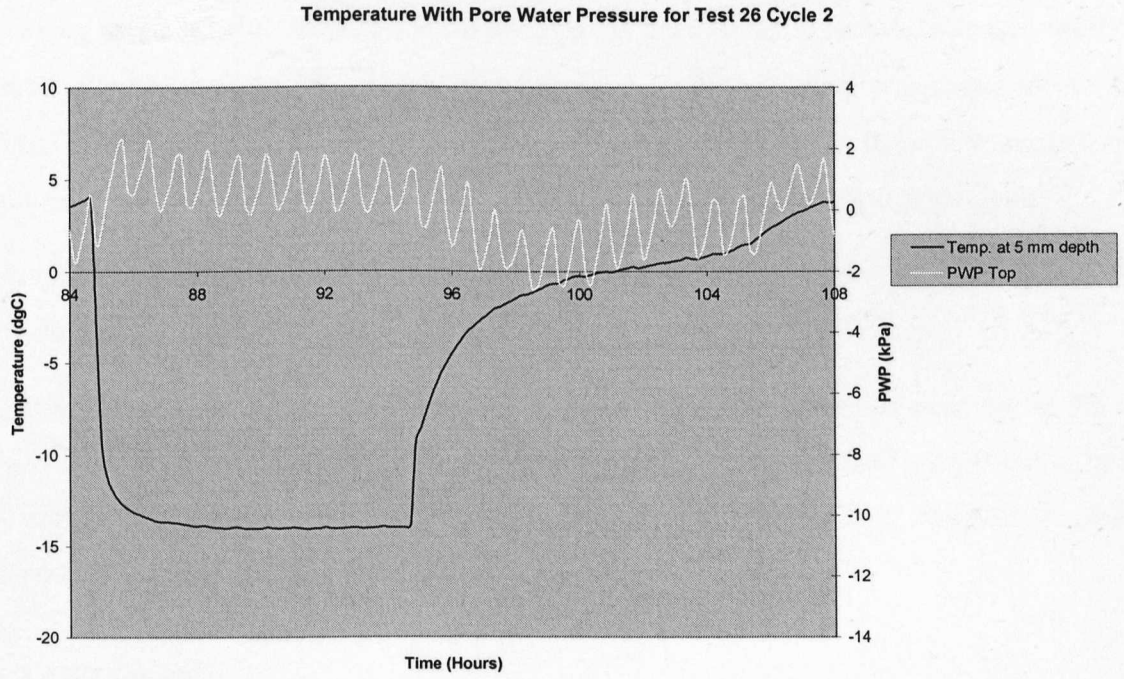

Figure 6.52 – Test 26 Cycle 2 Pore Water Pressure & Temperature at Top

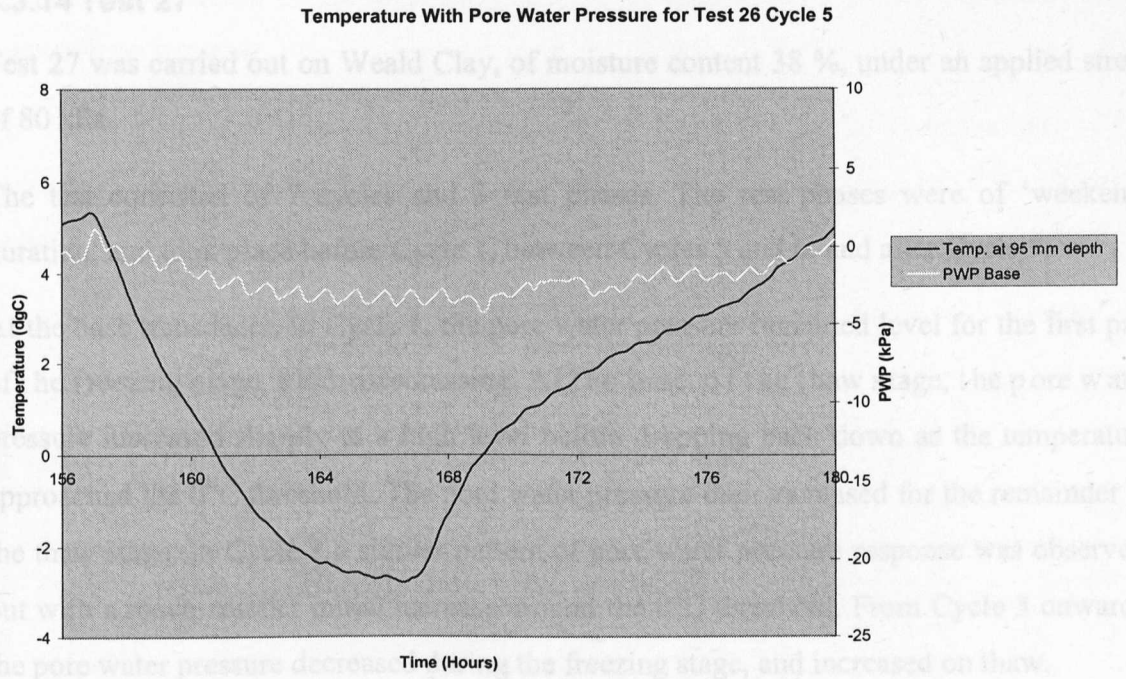

Figure 6.53 – Test 26 Cycle 5 Pore Water Pressure & Temperature at Base

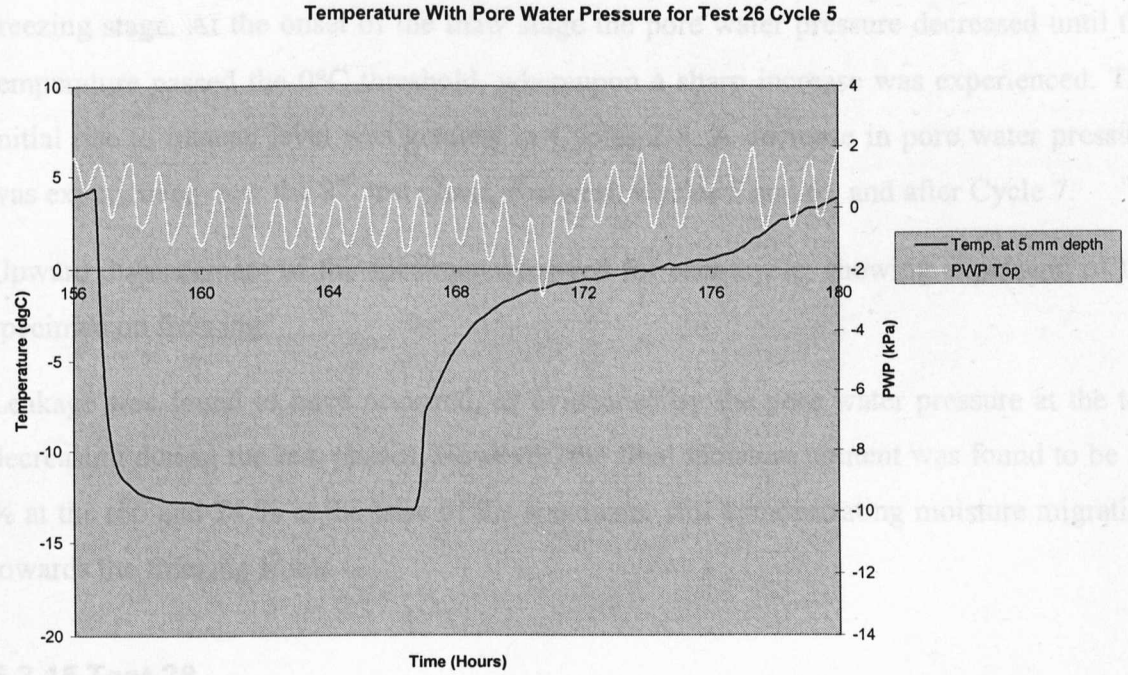

Figure 6.54 – Test 26 Cycle 5 Pore Water Pressure & Temperature at Top

6.3.14 Test 27

Test 27 was carried out on Weald Clay, of moisture content 38 %, under an applied stress of 80 kPa.

The test consisted of 7 cycles and 3 rest phases. The rest phases were of 'weekend' duration, and took place before Cycle 1, between Cycles 5 and 6, and after Cycle 7.

At the base transducer, in Cycle 1, the pore water pressure remained level for the first part of the freezing stage, before decreasing. At the onset of the thaw stage, the pore water pressure increased sharply to a high level before dropping back down as the temperature approached the 0°C threshold. The pore water pressure then increased for the remainder of the thaw stage. In Cycle 2 a similar pattern of pore water pressure response was observed, but with a much smaller initial increase around the 0°C threshold. From Cycle 3 onwards, the pore water pressure decreased during the freezing stage, and increased on thaw.

At the top transducer, the pore water pressure response followed a fairly regular pattern. In general, the pore water pressure initially increased to reach a plateau level during the freezing stage. At the onset of the thaw stage the pore water pressure decreased until the temperature passed the 0°C threshold, whereupon a sharp increase was experienced. The initial rise to plateau level was greatest in Cycles 2-5. A decrease in pore water pressure was experienced over the 2nd rest phase, (between Cycles 5 and 6), and after Cycle 7.

Upward displacement of the specimen occurred for each cycle, showing expansion of the specimen on freezing.

Leakage was found to have occurred, as evidenced by the pore water pressure at the top decreasing during the rest phases. However, the final moisture content was found to be 30 % at the top and 24 % at the base of the specimen, still demonstrating moisture migration towards the freezing front.

6.3.15 Test 28

Test 28 was carried out on Weald Clay, of moisture content 38 %, under an applied stress of 67.5 kPa. The summarised results for this test are given in Figure 6.55 below.

The test consisted of 7 cycles and 3 rest phases. The rest phases were of 'weekend' duration, and took place before Cycle 1, between Cycles 5 and 6, and after Cycle 7.

Upward displacement of the specimen occurred for each cycle, showing expansion of the specimen on freezing.

The final moisture content was found to be 40 % at the top and 24 % at the base of the specimen, demonstrating moisture migration towards the freezing front. Leakage is indicated by the displacement graph.

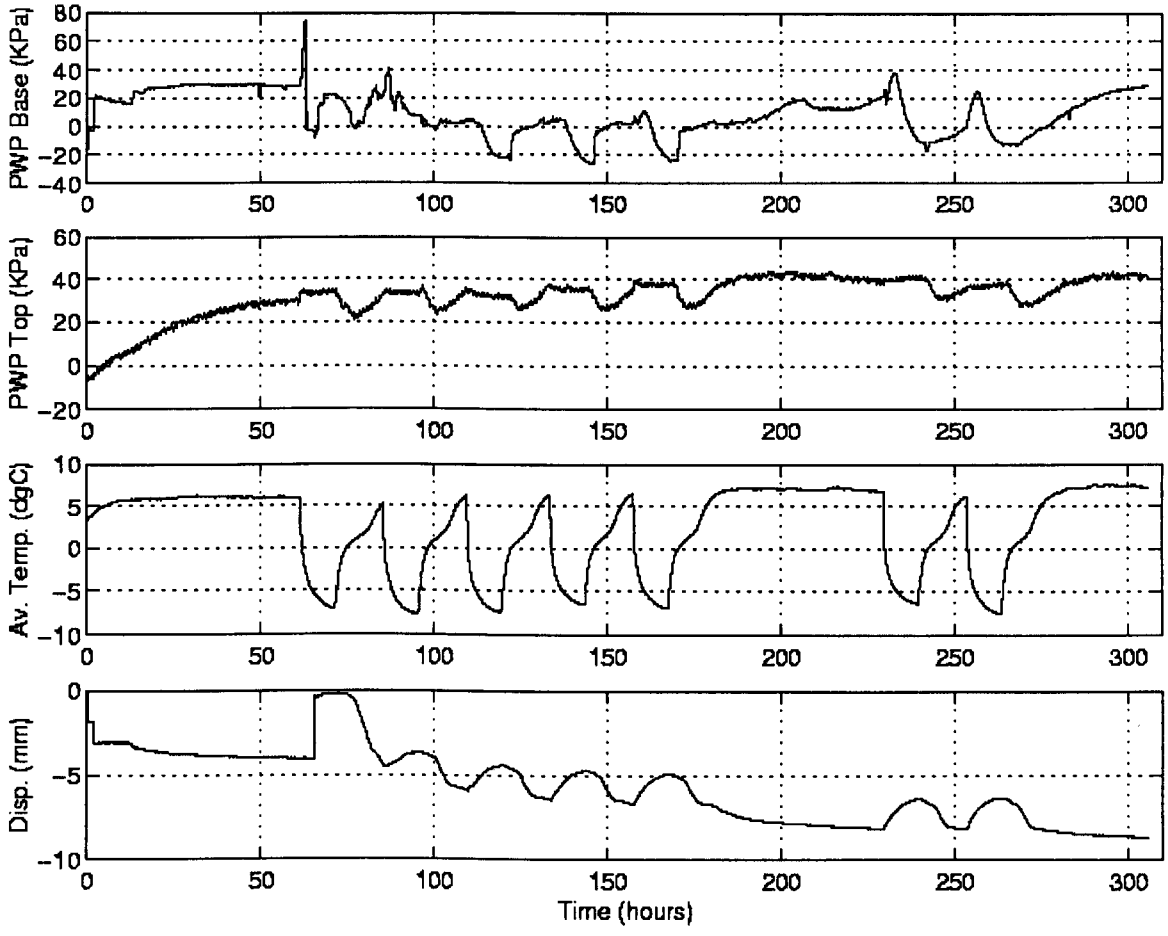

Figure 6.55– Results for Test 28

Figure 6.56 shows typical temperature profiles.

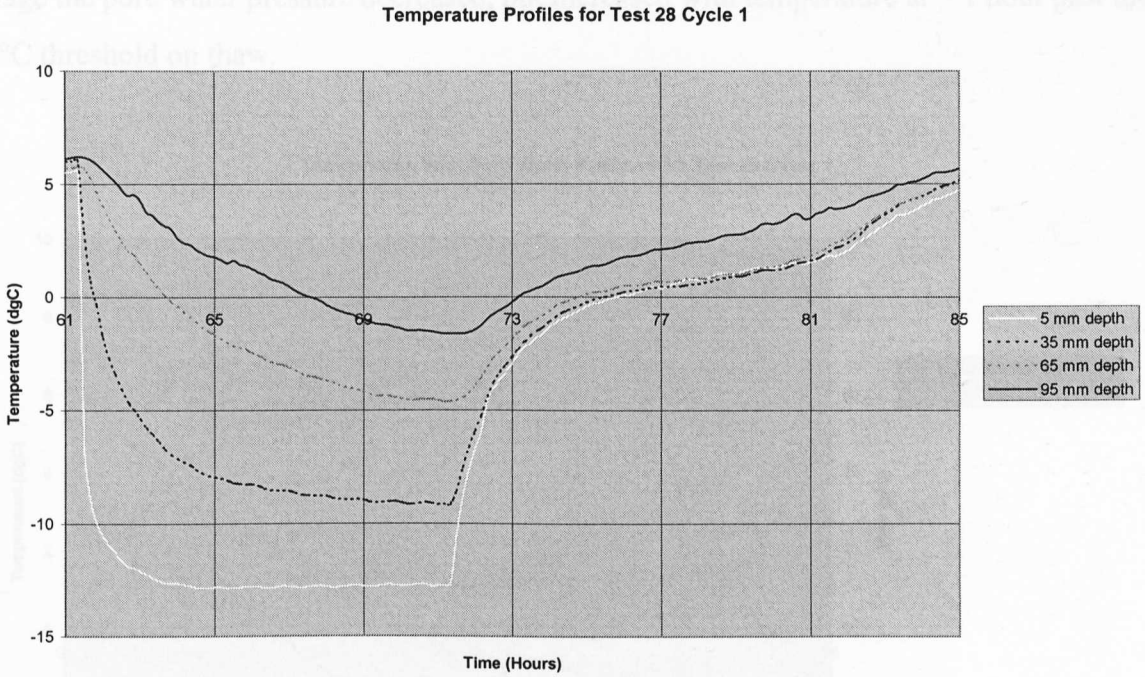

Figure 6.56 – Temperature Profiles for Test 28 Cycle 1

Figures 6.57-6.62 show the pore water pressure response at the base and top of the specimen for Cycles 1-3.

At the base transducer, in Cycle 1, the pore water pressure initially increased to a spiked high value at the start of the freezing stage, then decreasing to a lower level. The highest pore water pressure value of the test, 74.16 kPa, was recorded at this point. Further examination showed the initial rise in pore water pressure to be very brief, and the high value was considered atypical and thus discounted from Table 6.2. Following the atypical value, the pore water pressure rose again for the period of time that temperatures were below the 0°C threshold. Following the thaw 0°C threshold the pore water pressure dips and then increases with temperature. In Cycle 2, the pore water pressure experienced a small initial increase and then subsequently decreased, in a similar pattern to Cycle 1. At the onset of thaw, the pore water pressure was still decreasing, until the 0°C threshold was passed. After this point the pore water pressure increased to a plateau level. In Cycle 3, the pore water pressure decreased during the freezing stage. At the onset of the thaw stage, the pore water pressure remained level, but increased as the temperature passed the 0°C threshold.

At the top transducer, the pore water pressure response was fairly regular. The pore water pressure remained at a plateau level during the freezing stage. At the onset of the thaw

stage the pore water pressure decreased, but increased with temperature at ~ 1 hour past the 0°C threshold on thaw.

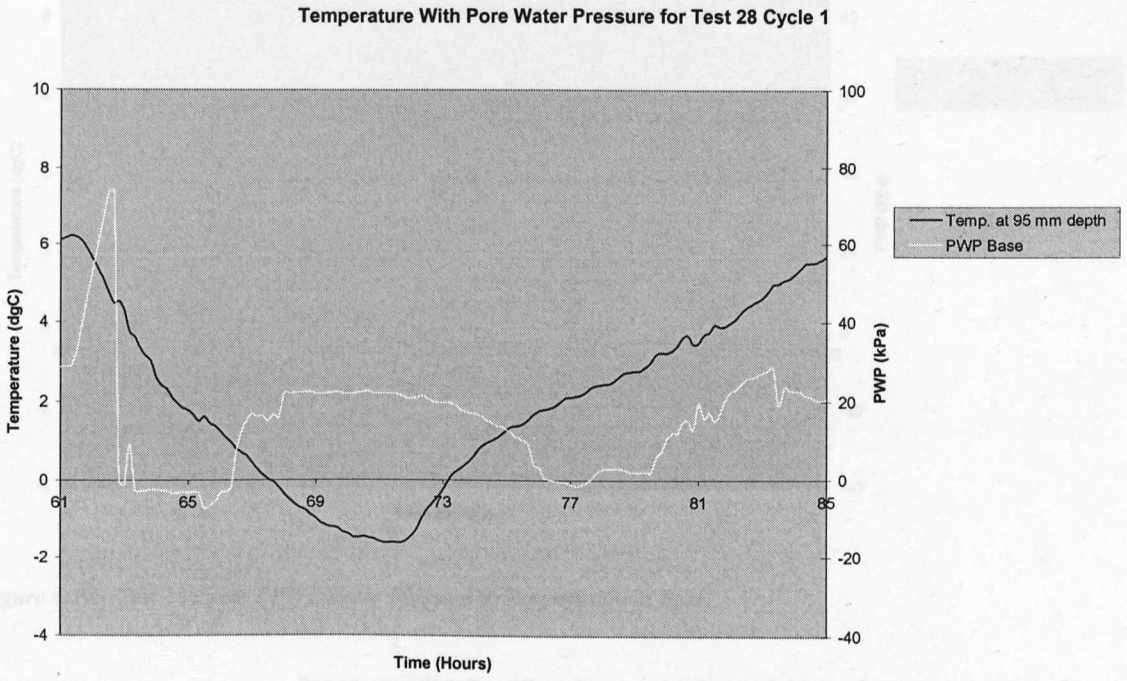

Figure 6.57 – Test 28 Cycle 1 Pore Water Pressure & Temperature at Base

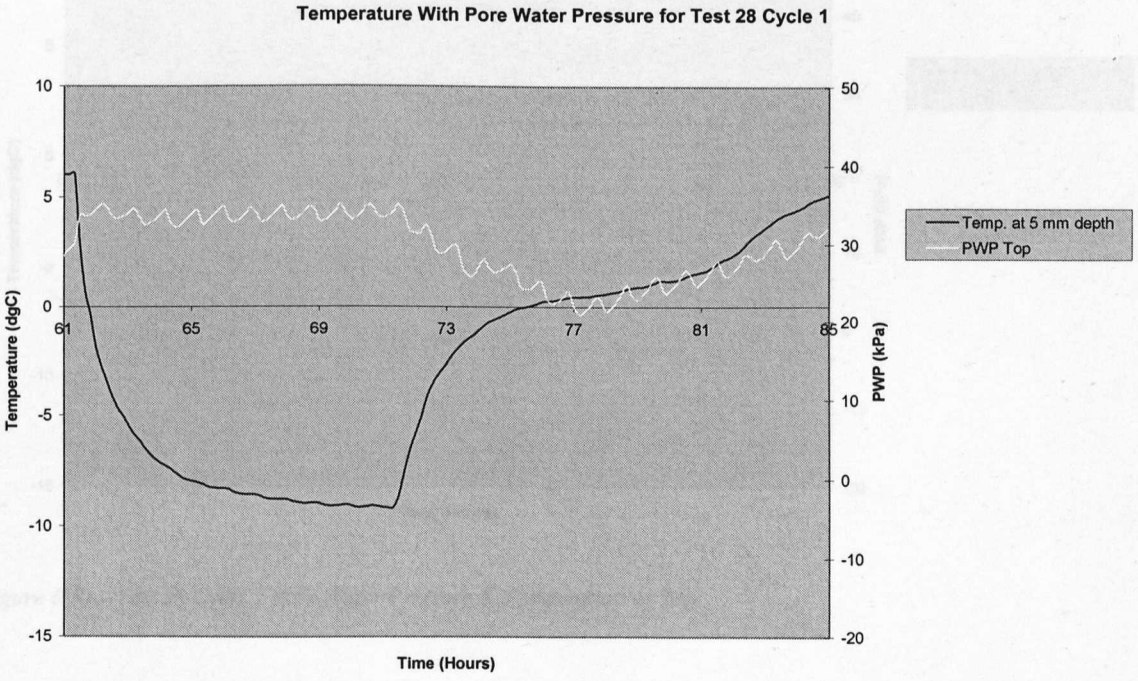

Figure 6.58 – Test 28 Cycle 1 Pore Water Pressure & Temperature at Top

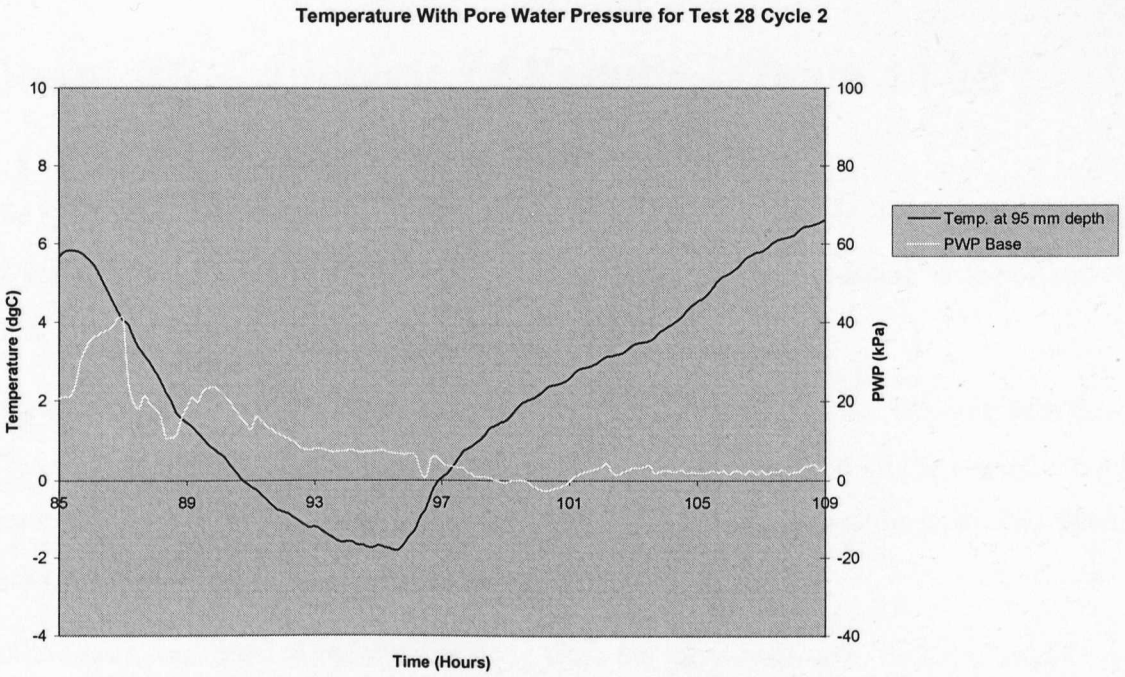

Figure 6.59 – Test 28 Cycle 2 Pore Water Pressure & Temperature at Base

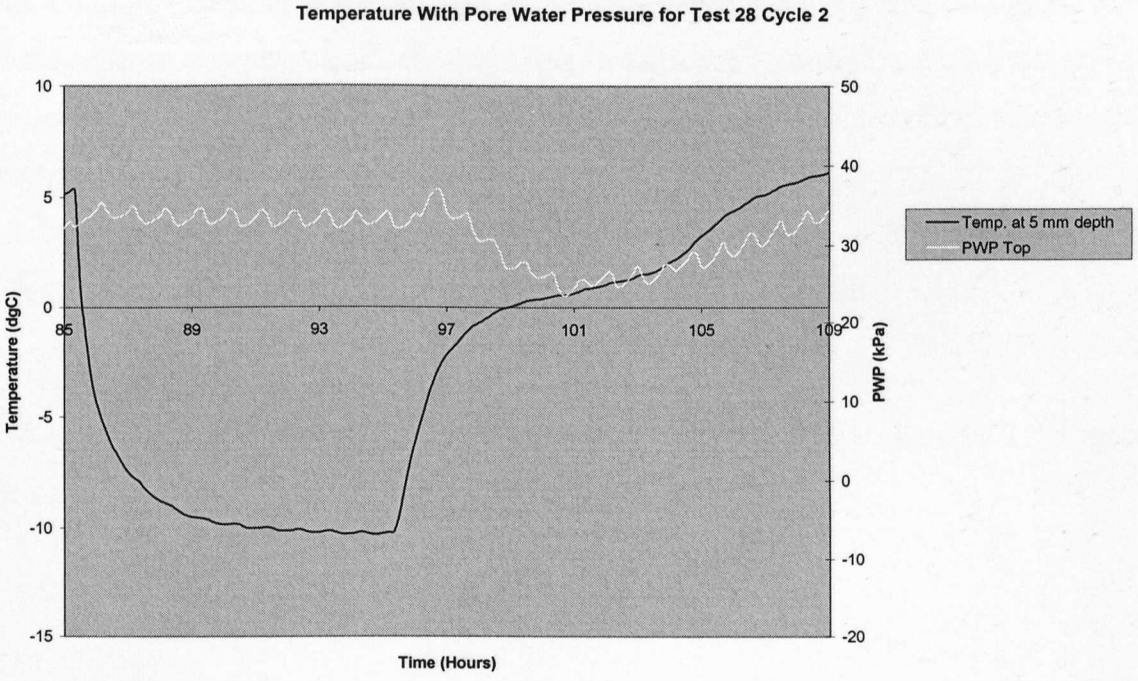

Figure 6.60 – Test 28 Cycle 2 Pore Water Pressure & Temperature at Top

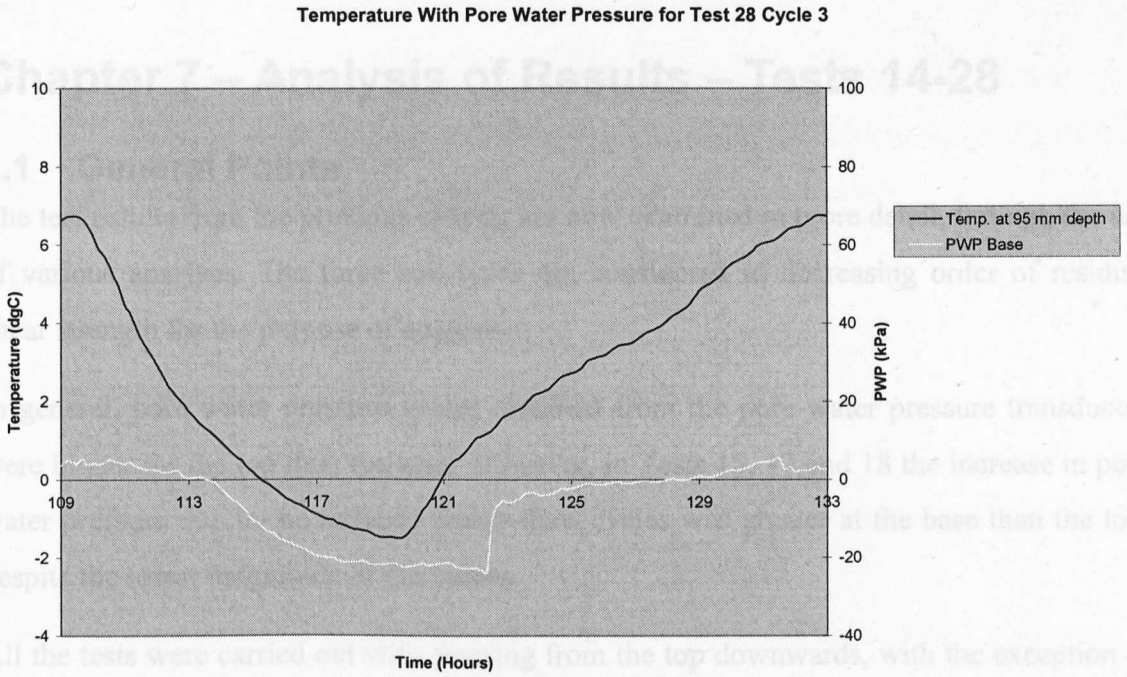

Figure 6.61 – Test 28 Cycle 3 Pore Water Pressure & Temperature at Base

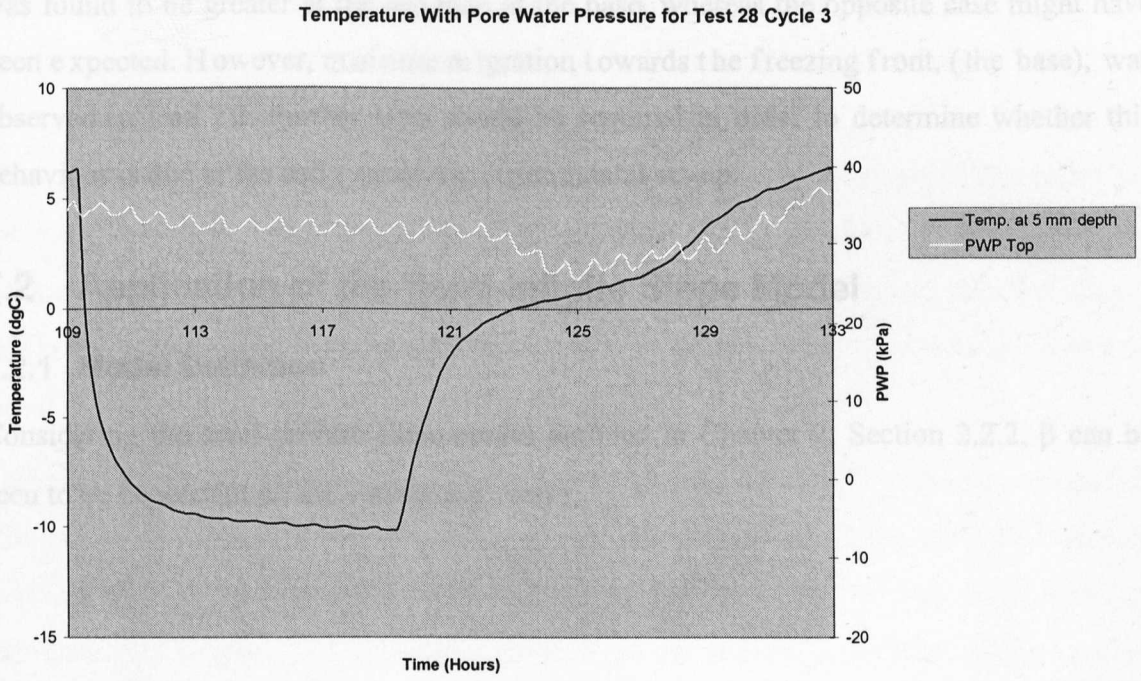

Figure 6.62 – Test 28 Cycle 3 Pore Water Pressure & Temperature at Top

Chapter 7 – Analysis of Results – Tests 14-28

7.1 General Points

The test results from the previous chapter are now examined in more detail, through the use of various analyses. The three soil types are considered in decreasing order of residual shear strength for the purpose of analysis.

In general, pore water pressure values obtained from the pore water pressure transducers were higher for the top than the base. However, in Tests 15, 17 and 18 the increase in pore water pressure due to the induced freeze-thaw cycles was greater at the base than the top, despite the lower magnitude of the values.

All the tests were carried out with freezing from the top downwards, with the exception of Tests 22 and 23, which were carried out with freezing from the base upwards. The results obtained from these two tests were inconclusive. During the tests the pore water pressure was found to be greater at the top than at the base, whereas the opposite case might have been expected. However, moisture migration towards the freezing front, (the base), was observed in Test 22. Further tests would be required in order to determine whether this behaviour is due to the soil type or the experimental set-up.

7.2 Application of the Semi-Infinite Slope Model

7.2.1 Model Definition

Considering the semi-infinite slope model outlined in Chapter 2, Section 2.2.2, β can be seen to be dependant on the variables ϕ'_r and r_u.

The residual shear strength parameter, ϕ'_r, has been considered in Chapter 2, Section 2.2.1. The three clay soils tested can be considered in terms of clay fraction. Referring back to Table 3.3, (Index Properties), the following comparisons can be made:

Table 7.1 – Comparisons Between the Soil Types

Soil	PI	% Clay Size Particles	ϕ'_r (°)
Lias Clay	15	16	24
Weald Clay	22	39	18
Oxford Clay	40	41	17

A single value of ϕ'_r is used, as found from ring shear tests. The single value is appropriate for the range of applied stresses considered.

As found by Skempton, (1964), residual shear strength decreases as the clay fraction increases. The soil types identified above can be considered with reference to Skempton's results, as reproduced in Figure 2.5, (Chapter 2, Section 2.2.1). The Oxford Clay plots close to the value provided by Skempton. The Weald Clay plots adjacent to the Oxford Clay. Both fall within the envelope of clayey soils identified by Skempton. The Lias Clay plots to the left of the Wiener Tegel soil, but outside the envelope. This is due to its comparatively low clay fraction. Despite the low clay fraction, however, the Lias Clay is still considered a clayey soil for the purposes of the research, as index tests placed it as a CI soil (BS 5930: Part 8: 1981).

Lupini *et al.*, (1981), warned against generalised correlation of soil properties to residual strength, restricting their use to studies of individual variable soil deposits. The detailed investigation of mineralogy and residual shear strength necessary to draw conclusions on the matter lies beyond the scope of the research, so the implications of the varying residual shear strengths is considered instead.

For a given value of r_u, soils with a lower value of ϕ'_r will fail at a lower value of β. Therefore, the Weald Clay and Oxford Clay can be expected to fail at similar values of β for the same value of r_u, (their differing plasticity being irrelevant). The Lias Clay can be expected to fail at a value of β higher than that of the Weald Clay and Oxford Clay, for the

same value of r_u. This relationship between β and ϕ'_r has been presented in Chapter 2, Section 2.2.2 for the full hydrostatic case, when $r_u \approx 0.5$, i.e. $\tan\beta \approx 0.5\tan\phi'_r$.

The pore water pressure ratio, r_u, has been considered in Chapter 2, Section 2.2.2. For the purposes of the research, r_u is split into two component parts. The first part is the r_u developed in the full hydrostatic case. This value is taken as 0.5, and is dependant on the assumptions that:

- The water table lies at the ground surface.
- The soil is considered saturated throughout.
- The soil specimen lies at a depth, z below the ground surface.
- The ratio of $\gamma_w/\gamma \approx 0.5$.

$$r_{u(1)} = 0.5$$

Equation 7.1 – $r_{u(1)}$, the Full Hydrostatic Component of r_u

The second component of r_u is determined from the additional pore water pressures developed as a result of induced cycles of freezing and thawing. This increase in pore water pressure is termed $+\Delta u$, and is defined as the increase in pore water pressure from the start of the freeze-thaw cycles to the maximum value of pore water pressure recorded during the cycles.

$$r_{u(2)} = \frac{+\Delta u}{\gamma z}$$

Equation 7.2 – $r_{u(2)}$, the Additional Pore Water Pressure Component of r_u

For the purpose of the research, γ, the saturated density of the soil specimens, is taken as 20 kN/m^3. (This value was adopted as it was previously used by Chandler, 1972). This in turn means that γz is equal to the applied stress. The values of z corresponding to applied stress are as follows:

Table 7.2 – Values of z Corresponding to the Various Applied Stresses

σ (kPa)	z (m)
55	2.750
67.5	3.375
80	4.000
120	6.000

Therefore, the combined value of r_u is equal to the full hydrostatic case plus an extra term produced by any additional pore water pressure generated by cyclic freezing and thawing.

$$r_u = 0.5 + \frac{+\Delta u}{\gamma z}$$

Equation 7.3 – The Combined Value of r_u

In order to determine values of β, the combined value of r_u should be less than or equal to the geostatic condition, $r_u = 1.0$. At values of r_u above the geostatic, liquefaction can be assumed to have taken place.

At the failure condition, substitution of the combined value of r_u gives an equation for β as follows:

$$\beta = \tan^{-1}[(1 - r_u)\tan\phi'_r] = \tan^{-1}\left[\left(1 - \left[0.5 + \frac{+\Delta u}{\gamma z}\right]\right)\tan\phi'_r\right]$$

or

$$\beta = \tan^{-1}\left[\left(0.5 - \frac{+\Delta u}{\gamma z}\right)\tan\phi'_r\right]$$

Equation 7.4 – An Equation to Find β Using the Combined Value of r_u

Therefore, the condition $+\Delta u/\gamma z < 0.5$ is necessary for values of β to be determined. If this value of $r_{u(2)}$ is equal to or greater than 0.5, then the combined value of r_u will cause the geostatic condition to be reached.

Whether or not a soil specimen can be considered using the semi-infinite slope model will therefore depend on the magnitude of $+\Delta u$. Considering Equation 5.2, $r_{u(2)}$ would have to equal 0.5. Therefore, the limiting value of $+\Delta u$ can be expressed as:

$$+\Delta u_L = \frac{\sigma}{2} = 10z \qquad (\text{assuming } \gamma = 20\text{kN/m}^3)$$

Equation 7.5 – The Limiting Value of $+\Delta u$

Considering the combined value of r_u, it can be seen that as it increases, β decreases. As the initial value of r_u is assumed to be 0.5, then β decreases with increasing values of $+\Delta u$. During the permode tests, greater values of $+\Delta u$, for a given applied stress, tended to be recorded for the Weald Clay and Oxford Clay than for the Lias Clay. This means

that slopes in the Weald Clay and Oxford Clay are liable to fail at lower values of β due to the double effect of having a lower angle of residual shear strength and a tendency to generate higher values of $+\Delta u$.

Figure 7.1 demonstrates the effect of $+\Delta u/z$ on β for the three soils tested. The point where $+\Delta u/z = 0$ represents the value of β determined assuming the full hydrostatic case, i.e. the minimum value of β found using conventional analysis.

Table 7.3 – Values of β Found using Conventional Analysis, (r_u = 0.5)

β(°)		
Lias Clay	Weald Clay	Oxford Clay
12.6	9.2	8.7

The β axis has not been extended back to 0° as this implies liquefaction rather than the development of slip surfaces. The actual lower limit of 2° was selected as it was deemed feasible during periglacial conditions by Skempton & Weeks, (1976). It can be seen that the greater the value of z for each soil, the greater the amount of $+\Delta u$ required to cause failure at a given value of β.

Figure 7.1 gives a comparison of the effects of $+\Delta u$ on β for all three soils when normalised for z. It can be seen that a higher value of $+\Delta u$ is required in the Lias Clay to induce failure, at a given β, than in the Weald Clay and Oxford Clay. A slightly higher value of $+\Delta u$ is required in the Weald Clay to induce failure, at a given β, than in the Oxford Clay.

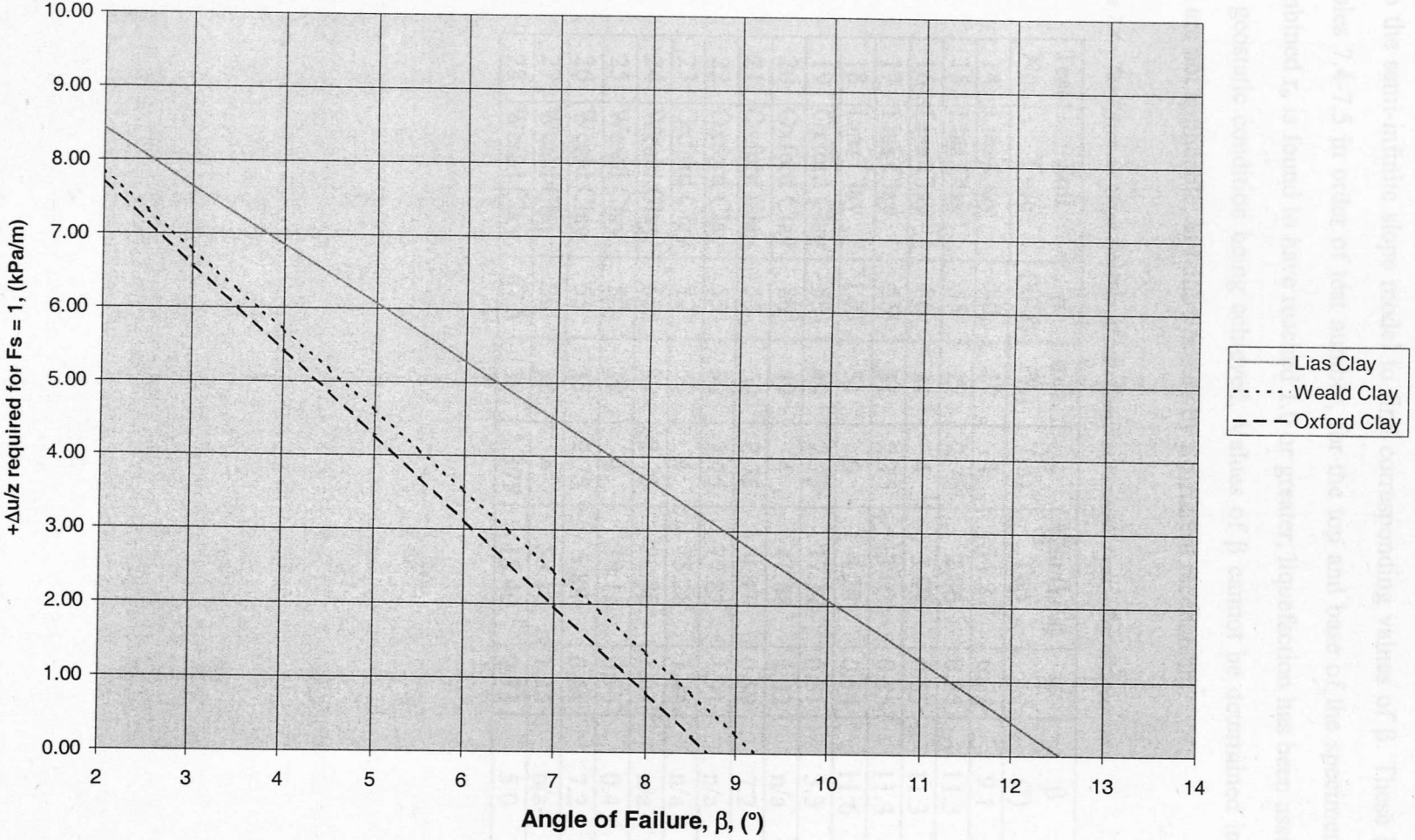

Figure 7.1 - The Effect of +Δu on the Stability of Slopes

7.2.2 Consideration of Permode Test Results

The increases in pore water pressure recorded during the permode tests can be substituted into the semi-infinite slope model to find corresponding values of β. These are shown in Tables 7.4-7.5 in order of test number, for the top and base of the specimen. Where the combined r_u is found to have reached 1.0 or greater, liquefaction has been assumed, due to the geostatic condition being achieved. Values of β cannot be determined in such cases, and are not applicable, as failure occurs by a different mechanism.

Table 7.4 – The Effect on Slope Stability of +Δu Found in Permode Tests – Top of Specimen

Test No.	Soil Type	σ (kPa)	m.c. (%)	*z* (m)	+Δu (kPa) Top	r_u	β (°)
14	Lias Clay	80	27	4	11.27	0.64	9.1
15	Lias Clay	55	27	2.75	2.86	0.55	11.3
16	Lias Clay	80	31	4	3.89	0.55	11.3
17	Lias Clay	55	31	2.75	3.02	0.55	11.3
18	Lias Clay	120	31	6	4.28	0.54	11.6
19	Oxford Clay	55	49	2.75	17.12	0.81	3.3
20	Oxford Clay	80	49	4	41.68	1.02	n/a
21	Oxford Clay	55	50	2.75	4.87	0.59	7.2
22	Oxford Clay	55	50	2.75	77.81	1.91	n/a
23	Oxford Clay	80	50	4	75.28	1.44	n/a
24	Weald Clay	55	39	2.75	28.30	1.01	n/a
25	Weald Clay	80	39	4	38.11	0.98	0.4
26	Weald Clay	55	38	2.75	5.88	0.61	7.2
27	Weald Clay	80	38	4	58.16	1.23	n/a
28	Weald Clay	67.5	38	3.375	15.40	0.73	5.0

Table 7.5 - The Effect on Slope Stability of +Δu Found in Permode Tests – Base of Specimen

Test No.	Soil Type	σ (kPa)	m.c. (%)	z (m)	+Δu (kPa) Base	r_u	β (°)
14	Lias Clay	80	27	4	8.30	0.60	10.1
15	Lias Clay	55	27	2.75	6.53	0.62	9.6
16	Lias Clay	80	31	4	2.26	0.53	11.8
17	Lias Clay	55	31	2.75	6.67	0.62	9.6
18	Lias Clay	120	31	6	8.44	0.57	10.8
19	Oxford Clay	55	49	2.75	1.55	0.53	8.2
20	Oxford Clay	80	49	4	0.85	0.51	8.5
21	Oxford Clay	55	50	2.75	1.71	0.53	8.2
22	Oxford Clay	55	50	2.75	5.15	0.59	7.2
23	Oxford Clay	80	50	4	2.34	0.53	8.2
24	Weald Clay	55	39	2.75	2.10	0.54	8.5
25	Weald Clay	80	39	4	35.52	0.94	1.1
26	Weald Clay	55	38	2.75	4.49	0.58	7.8
27	Weald Clay	80	38	4	18.24	0.73	5.0
28	Weald Clay	67.5	38	3.375	12.50	0.69	5.8

The three soils are now considered individually, and in order of decreasing residual shear strength, i.e. Lias Clay, Weald Clay, Oxford Clay.

For the Lias Clay, the magnitude of +Δu recorded at the top of the specimen in Test 14 was sufficient to raise the value of r_u to 0.64, thus causing a significant decrease in β from that predicted using $r_u = 0.5$. In Tests 15-18 the magnitude of +Δu recorded at the top of the specimen was greater at greater values of *z*. However, the difference in +Δu is not great enough to give different values of r_u, so similar values of β are obtained. In addition the general value of r_u gained, 0.55, reduces β by only 1.3° from β = 12.6° obtained for the full hydrostatic condition, (see Table 7.3).

At the base of the specimen, the magnitude of +Δu was greater than at the top for Tests 15, 17 and 18, leading to lower values of β. Otherwise, higher values of β were obtained.

For the Weald Clay, at the top of the specimen, Tests 24 and 27 recorded values of +Δu causing the geostatic condition to be reached. Test 25 shows an r_u value very close to geostatic. As mentioned above, permode tests on both the Weald Clay and Oxford Clay tended to produce greater values of +Δu than the Lias Clay, as is shown by the generally greater values of r_u determined. In Tests 25, 26 and 27, where values of β were obtained, the amount of +Δu generated was greater at greater values of *z*. In contrast to the Lias Clay,

(Tests 15-18), the difference in $+\Delta u$ was great enough to give likewise increasing values of r_u, and so an decrease in β was obtained.

At the base of the specimen, the magnitude of $+\Delta u$ was consistently lower than at the top, although fairly close in the case of Tests 25, 26 and 28. In these tests a similar pattern to the top was observed, with decrease in β with increase in z.

For the Oxford Clay, at the top of the specimen, Tests 20, 22 and 23 recorded values of $+\Delta u$ causing the geostatic condition to be reached. Tests 22 and 23 have been considered previously, in terms of their different test method, (freezing from base upwards). Tests 19 and 21 produced values of β of a comparable order of magnitude to those gained for the Weald Clay. In Test 21 particularly, the value of $\beta = 7.2°$ obtained is the same as that found for Test 26 in the Weald Clay. Both tests were carried out under the same applied stress, 55 kPa. The level of plasticity was similar. The r_u values were 0.59 and 0.61 respectively.

At the base of the specimen, the magnitude of $+\Delta u$ was consistently lower than at the top, leading to higher values of β.

On the basis of the results gained, additional pore water pressures have been found to be generated during freeze-thaw cycles. This additional quantity, termed $+\Delta u$, appears to be greater in the Weald Clay and Oxford Clay than in the Lias Clay. Therefore, as the residual shear strength decreases, $+\Delta u$ increases. ϕ'_r can in turn be related to the clay fraction. To better quantify this relationship, more soil types of differing clay fractions would need to be tested.

All three soil types were intended to have been tested at comparable levels of consistency, rather than moisture content. In general, the soils were tested at moisture contents 50-60 % between the plastic and liquid limits. Tests 14 and 15 in the Lias Clay were exceptions, with a moisture content only 27% between the plastic and liquid limits. The Lias Clay had the lowest plasticity index, so changes in consistency occurred over lower moisture content ranges, leading to a greater possibility of error when setting up the tests. In overview, however, the general similarity of plasticity across the three soils was intended to provide a common benchmark for testing three soils of varying plasticity. It should therefore be noted that the Weald Clay and Oxford Clay, which appear to behave similarly during the permode tests are only doing so at similar consistency. For example, if the two soils were

both tested at a moisture content of 49 %, the Oxford Clay would be half-way between its plastic and liquid limit, but the Weald Clay would be behaving as a liquid and thus could not constitute a stable slope in any case.

The range of moisture contents tested within each soil type was intentionally limited, and on the basis of the results gained is not considered as a variable.

The tests on the Weald Clay and Oxford Clay showed a tendency to geostatic conditions at the top of the specimens. This is due to values of $+\Delta u$ greater than $+\Delta u_L$ being generated. The geostatic condition was not observed in the tests on the Lias Clay. Where $+\Delta u$ is large enough to cause the geostatic condition, a liquefaction effect will occur. This fluidisation can be considered to be similar to the 'viscous flow' effect considered by Ballantyne & Harris, (1994); Gallop, (1991). Therefore, on the basis of the test results gained, it is considered that some soils fail in different modes, depending on whether the amount of $+\Delta u$ generated exceeds $+\Delta u_L$. However, in this research the semi-infinite slope model is of primary interest.

Table 7.6 gives the minimum value of β found at varying z for each soil type. This value represents the worst case for each soil type, on the basis of the results gained. It can be seen that β can be significantly reduced from its predicted value by the action of cyclic freeze-thaw activity.

Table 7.6 – Summary of Minimum Values of β Found

z (m)	Minimum β (°)		
	Lias Clay	Weald Clay	Oxford Clay
2.75	9.6	7.2	3.3
3.375	-	5.0	-
4	9.1	0.4	8.2
6	10.8	-	-

From the test results obtained there is no unique, proportional relationship between applied stress, i.e. z, and $+\Delta u$ generated. This could be due to differences in moisture content, (either initial or due to leakage), or minor procedural differences, e.g. positioning and length of rest phases. However, referring to Tables 7.4-7.5, in Tests 26-28, $+\Delta u$ is seen to increase with applied stress, albeit non-linearly.

7.2.3 Reference to Existing Knowledge Base

The range of values of β given above in Table 7.6 are comparable to those discovered in the field for clayey soils. For example, the Wellingborough and Isham failures (Chandler, 1970b); the slip surface of 4° located in Weald Clay at Sevenoaks (Skempton & Weeks, 1976); the low angle slope failures viewed at Daventry (Biczysko & Starzewski, 1977a).

The range of values of r_u generated as a result of the permode tests include some of similar magnitude to those calculated from thaw consolidation theory by Skempton & Weeks, (1976). Similar ranges of r_u were also considered by Chandler, (1972), who used a semi-infinite slope model to determine values of r_u required for mudslides to be initiated at Vestspitsbergen. The values of r_u calculated were significantly greater than the hydrostatic case. This was supported by values observed in situ. These findings strongly contribute to the validation of the permode test as a method of investigating the effects of periglacial freeze-thaw cycles on slope stability.

In Chapter 3, it was determined that for cyclical freezing modelled on an annual pattern, the consolidation parameter t_{90} showed that the decision not to allow drainage was acceptable for all three soil types under one-way drainage, and for two-way drainage it was acceptable for Weald Clay and Oxford Clay, but only under high values of applied pressure for Lias Clay.

If this line of reasoning is accepted, the specimens can be considered in terms of R, the thaw-consolidation ratio, (Morgenstern & Smith, 1971), determined using the test rate of thaw and values of c_v presented in Chapter 3.

Therefore, for a specimen 100 mm high being thawed in 12 hours, using Equations 2.1 and 2.2 presented in Chapter 2:

$$R = \frac{1}{2}\alpha c_v^{-\frac{1}{2}}$$

Where:

$$\alpha = Xt^{-\frac{1}{2}}$$

$$= 0.1 \text{ m x } (0.5 \text{ days})^{-1/2}$$

$= 0.1 \times (1/730 \text{ year})^{-1/2}$

$= 2.70$

Therefore,

$R = 0.5 \times 2.70 \times c_v^{-1/2}$

As shown below:

Table 7.7 – Values of R for Each Soil Type

	c_v (m^2/year)	R
Lias Clay	6.31	0.54
Weald Clay	0.61	1.73
Oxford Clay	0.37	2.22

Morgenstern & Nixon, (1971), stated that if R exceeded unity, then excess pore water pressures at the thaw plane would be at their maximum values and effective stresses would tend to zero. This would therefore increase the chances of slope instability. The high values of R gained for the Weald Clay and Oxford Clay correspond to the geostatic conditions found from r_u recorded during the tests.

Skempton & Weeks, (1976), used data gained from their investigations at Sevenoaks, Kent, to find a value of R of 1.3 for brecciated Weald Clay. Depth of thaw was 2 m, time of thawing 3 months, and c_v taken as 2.5 m^2/year. Skempton & Weeks than utilised the Morgenstern & Nixon, (1971), graphical solution to achieve an r_u value of 0.89. this is of a similar magnitude to the values determined for Weald Clay as part of the permode tests, (see Section 7.2.2).

From inspection of Skempton & Weeks, (1976), it would appear that the 'applied pressure' version of the numerical solution was used, as given in Figure 7.2. 'P_o' refers to applied pressure, but it is assumed that Skempton & Weeks, (1976), took this as γz, thus giving a value of r_u, at a full depth Z.

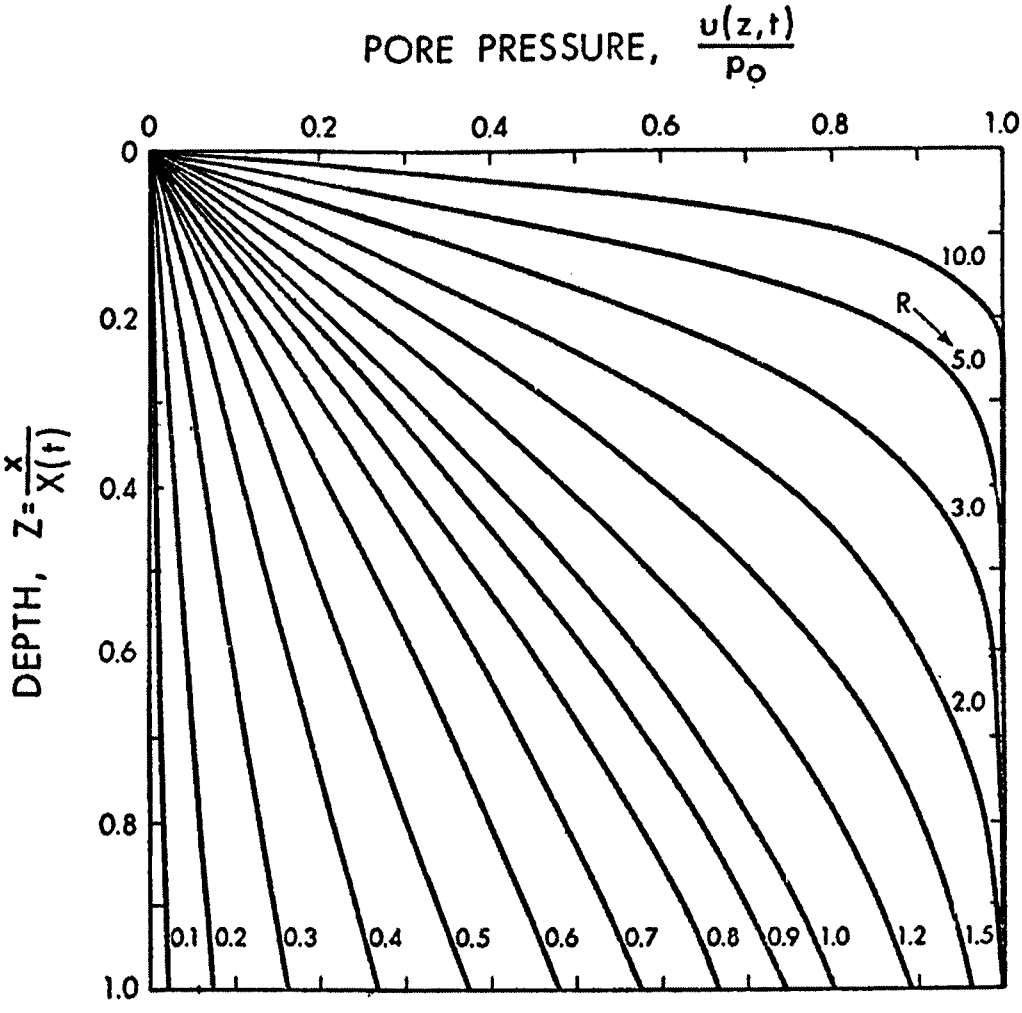

Figure 7.2 – Numerical Solution for R and r_u, after Morgenstern & Nixon, (1971); Nixon, (1973).

Using this for the permode tests would yield:

Table 7.8 – Values of r_u found from Nixon & Morgenstern, (1971), Solution.

	c_v (m^2/year)	R	r_u
Lias Clay	6.31	0.54	0.42
Weald Clay	0.61	1.73	0.98
Oxford Clay	0.37	2.22	1.00

The value of r_u determined for Lias Clay is lower than that found through the permode tests, (see Section 7.2.2), but this may be due to the rate of thaw being too fast to permit the Morgenstern & Nixon theory to apply accurately. For the Weald Clay and Oxford Clay

high values of r_u were determined at the top of the specimen as part of the permode tests in any case.

7.3 The Consideration of Moisture Migration

7.3.1 Moisture Migration Observed

Table 7.9 below shows the initial moisture content for each test, together with the final moisture content recorded at the top and base of the specimen.

Table 7.9 – Moisture Migration in Tests 14-28

Test	Soil	σ (kPa)	m.c. (%)	End of test m.c. (%)	
				Top	Base
14	Lias Clay	80	27	28	24
15	Lias Clay	55	27	36	25
16	Lias Clay	80	31	30	24
17	Lias Clay	55	31	31	24
18	Lias Clay	120	31	29	24
19	Oxford Clay	55	49	40	31
20	Oxford Clay	80	49	35	28
21	Oxford Clay	55	50	47	34
22	Oxford Clay	55	50	36	40
23	Oxford Clay	80	50	37	36
24	Weald Clay	55	39	35	25
25	Weald Clay	80	39	31	24
26	Weald Clay	55	38	35	24
27	Weald Clay	80	38	30	24
28	Weald Clay	67.5	38	40	24

The final moisture content at the top of the specimen tends to be greater than at the base, in keeping with principle of water migrating towards the frozen front in a closed system, (Mageau & Morgenstern, 1979).

As discussed in Chapter 2 Sections 2.1.2 and 2.5, a frozen fringe is set up behind the progressing freezing front, namely the 0°C isotherm. The frozen fringe consists of unfrozen soil water occupying smaller pores surrounding larger ice-filled pores, (Miller, 1980). Water migrates towards the 0°C isotherm due to the condition of freezing point depression as considered by Williams & Smith, (1989). The soil medium causes the soil water to contain impurities, giving it a lower Gibbs free energy than pure water. For ice to be

formed from this solution a lower free energy is also needed. The frozen fringe exists at state of lower free energy, and so the soil water migrates upwards through the 0°C isotherm in order to become frozen also. Such migration accounts for the higher pore water pressures measured at the top of the specimens during the freeze-thaw cycles.

The greater increases in pore water pressure at the top of the specimens experienced in the Weald Clay and Oxford Clay than in the Lias Clay would seem to indicate that more water migration took place in these soil types. This is of particular interest as clay-rich soils generally have lower permeability, which is thought to restrict water migration (Ballantyne & Harris, 1994). However, this does not appear to be the case with the Weald Clay and Oxford Clay tested.

In Tests 22 and 23, the specimen was frozen from the base upwards. In Test 22, moisture migration towards the base is indicated, but not in Test 23 where there is no conclusive evidence of moisture migration, based upon the initial and final moisture contents.

Despite the trends shown above, it is necessary to consider the leakage factor. Due to leakage, the permode tests cannot be treated as closed, un-drained tests. This means that moisture migration cannot be fully quantified in this analysis, particularly for those tests where both the top and base end-of-test moisture contents are lower than the starting value.

7.3.2 The Significance of Leakage

Leakage occurred in all of the tests to varying degrees, as detailed in Chapter 6, Section 6.3.

The statistical sample size of tests carried out, i.e. 15, is relatively small, and therefore not necessarily representative of permode behaviour. Observation of the test results showed drops in pore water pressure at the top of the specimen during rest phases. This indicates leakage through/around the piston. However, pore water pressures generally remained higher at the top than the base, indicating a pattern of moisture migration towards the freezing front. If Tests 22 and 23 are discounted, all other tests show distinct moisture migration towards the top of the specimen.

As leakage was taking place, the tests cannot be considered as completely 'closed' or 'un-drained' in the fashion intended. However, a standard drained test would also allow influx of water, allowing ice lensing and greater frost heave to take place.

Visual examination of specimens post-testing generally showed softer, more plastic consistency of soil at the top, in keeping with moisture migration to this region. Significant ice lensing was not observed, although thin freezing planes were visible in specimens removed from the permode frozen, (due to tests having to be aborted/stopped early).

Therefore, despite top leakage, the action of moisture migration and patterns of pore water pressure are still generally observable. In the interests of optimising the test apparatus, further measures against leakage are outlined in Chapter 9, Section 9.1.5.

7.3.3 Reference to Existing Knowledge Base

Although the detailed consideration of moisture migration lies beyond the scope of the research, the test method could be adapted to allow drained conditions in order to investigate the shut-off pressure concept outlined by Arvidson & Morgenstern, (1977). In addition, halting the tests during a freezing stage would allow examination of ice lens formation.

Drained tests are considered further in Chapter 9, Section 9.2.4.

7.4 Frost Heave

7.4.1 Observed Frost Heave

Frost heave can be observed in all the permode tests and is recorded in the graphs of displacement against time. A test from each soil type was selected, with the applied stress being 80 kPa. As the Oxford Clay test took place for five freeze-thaw cycles only, data has only been abstracted for the first five cycles of the Weald Clay and Lias Clay tests, in order to allow direct comparison of the different soil types.

Figure 7.3 shows the amount of heave experienced during the freezing stages of Cycles 1-5. The Weald Clay is shown to have undergone the greatest amount of frost heave, with the Oxford Clay and Lias Clay experiencing similar, lower levels of heave. Across the cycles examined, the Lias Clay generally experienced slightly greater frost heave than the Oxford Clay.

Figure 7.3 can also be interpreted to read the rate of heave in mm/hr. As the freezing stages were 10 hours long, the actual heave measured can be taken as 10 x the rate of heave.

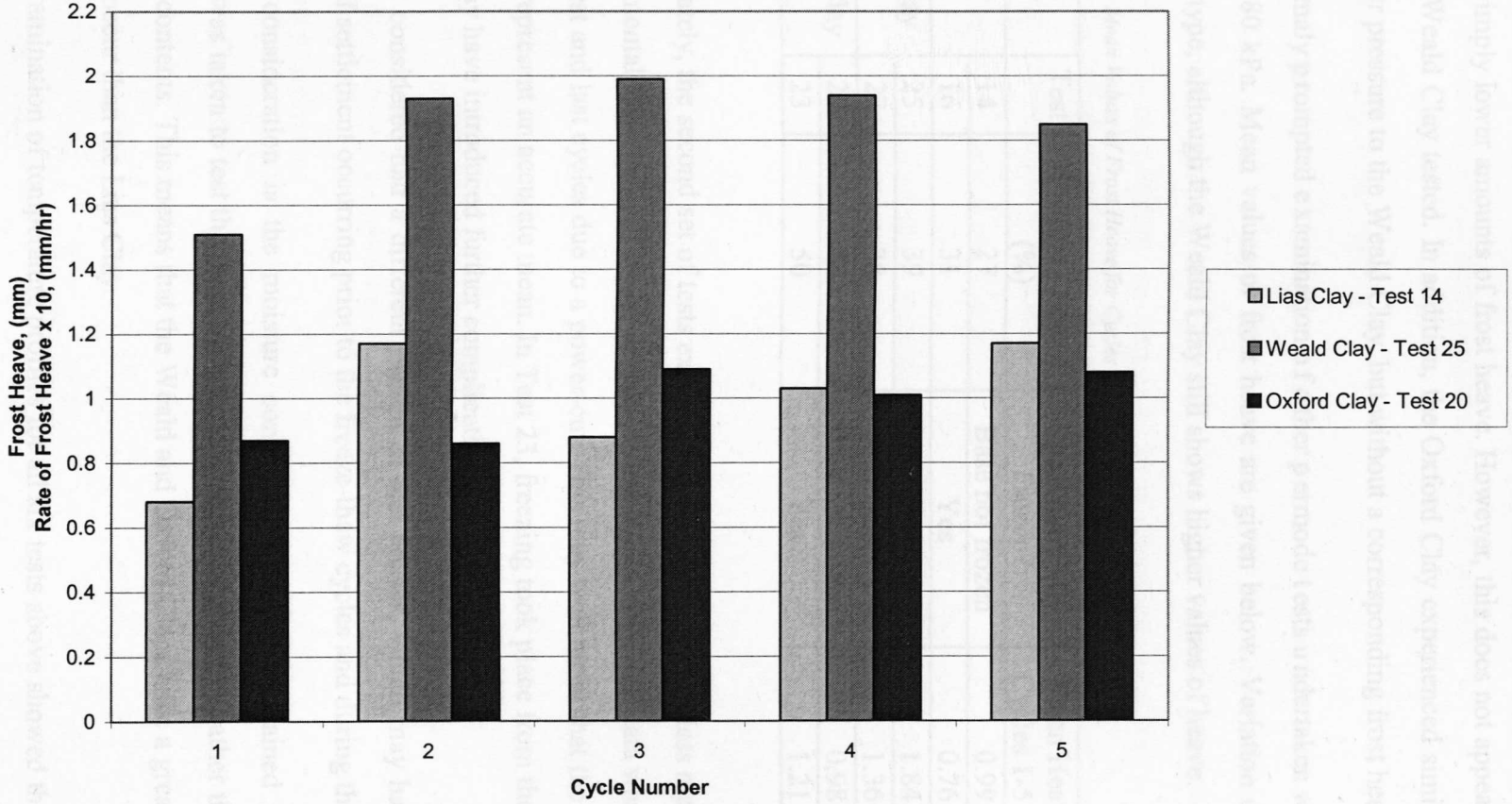

Figure 7.3 – Measured Frost Heave

The results are a little unexpected, as the Lias Clay could generally be expected to be the most frost susceptible due to its higher silt content (Hutchinson, 1991; Harris *et al.*, 1995). As mentioned in Section 7.3.1, the lower permeability of clay-rich soils is thought to restrict water migration and ice-lens growth (Ballantyne & Harris, 1994), which would therefore imply lower amounts of frost heave. However, this does not appear to be the case with the Weald Clay tested. In addition, the Oxford Clay experienced similar increases in pore water pressure to the Weald Clay, but without a corresponding frost heave.

This anomaly prompted examination of other permode tests undertaken with an applied stress of 80 kPa. Mean values of frost heave are given below. Variation can be seen for each soil type, although the Weald Clay still shows higher values of heave.

Table 7.10 – Mean Values of Frost Heave for Cycles 1-5, σ = 80 kPa

Soil	Test	Moisture Content (%)	Specimen Fully Frozen?	Mean Heave for Cycles 1-5 (mm)
Lias Clay	14	27	Base not frozen	0.99
	16	31	Yes	0.76
Weald Clay	25	39	Yes	1.84
	27	38	Yes	1.36
Oxford Clay	20	49	Base not frozen	0.98
	23	50	Yes	1.21

Unfortunately, the second set of tests examined are considered to be less representative due to experimental uncertainty. Test 16 lasted for four cycles only, and data was only available for the first and last cycles due to a power-cut. This may well mean that the average gained may not represent an accurate mean. In Test 23, freezing took place from the base upwards, which may have introduced further complications.

Each test considered had a different pattern of rest phases, which may have affected the amount of settlement occurring prior to the freeze-thaw cycles and during the thaw stages.

Another consideration is the moisture content adopted. As explained previously, the decision was taken to test the three soils at comparable consistency rather than comparable moisture contents. This means that the Weald and Oxford Clays have a greater resource for heave to occur than the Lias Clay.

Closer examination of temperature profiles for all six tests above showed that the specimen was not fully frozen in each case. This may suggest why the Weald Clay experienced most

heave, as there was more water available to freeze, and the temperature regime allowed more freezing to take place.

A larger set of data, (all at a common applied stress), is needed in order to draw firm conclusions, but an attempt is made in the next section to review findings for Tests 14, 20 and 25 by considering approximate predicted values of heave.

7.4.2 Predicting Frost Heave

In terms of expected frost heave, it is important to note the effect of the intended un-drained test set-up. As no water was allowed to enter the specimen during testing, the maximum volume increase obtainable in frost heave will be governed by the ~9% expansion of water content on freezing. It is therefore possible to determine the approximate expected value of closed system frost heave by considering soil phase relationships. The equations used are given below, and tabulated results are given in Table 7.2 for expected and actual heave achieved.

For simplicity, units of g and cm were adopted and entered into a spreadsheet.

For a cylindrical specimen 10 cm high by 10 cm diameter, volume is known, $V = 314.159\ cm^3$.

$$e = \frac{wG_s}{S_r}$$

Equation 7.6 – Void Ratio

Where:

e = void ratio

G_s = specific gravity = 2.7 assumed

S_r = degree of saturation

w = water content, here expressed as a decimal ratio:

$$w = \frac{M_w}{M_s}$$

Equation 7.7 – Water Content

Where:

M_w = Mass of water, (g)

M_s = Mass of solids, (g)

With e determined,

$$\rho = \left[\frac{G_s + S_r e}{1 + e} \rho_w \right] = \frac{M}{V}$$

Equation 7.8 – Density Relationships

Where:

ρ = bulk density, (g/cm^3)

ρ_w = density of water = 1.0 g/cm^3 assumed

M = Total Mass, (g)

V = Volume, (cm^3)

From this, when the bulk density is known, total mass M can be found. As both the ratio of M_w to M_s and the sum of M_w and M_s are known, both quantities can be determined. Now:

$$V_s = \frac{M_s}{G_s \rho_w}$$

Equation 7.9 – Volume of Solids

$$V_w = \frac{M_w}{\rho_w}$$

Equation 7.10 – Volume of Water

The volume of water will expand on freezing by say 9 %. Therefore, total volume after freezing will be:

$$V_f = 1.09 V_w + V_s$$

Equation 7.11 - Volume of Specimen After Freezing

The percentage volume increase is found as:

$$\% \text{ Increase in V} = \left[\frac{V_f - V}{V}\right] x\, 100$$

Equation 7.12 – Percentage Increase in Volume from Freezing

As the specimen is 100 mm high, the percentage increase in volume may also be thought of as the increase in height of mm.

Tables 7.11-7.13 give the edited spreadsheet output for each test. The spreadsheet has been used to interrogate the formulae to find a degree of saturation that would account for actual heave being lower than predicted.

Figure 7.4 gives a set of predicted curves derived from the equations above, showing the change in percentage increase in volume with water content for different degrees of saturation.

It can be seen below that for a comparatively small reduction in degree of saturation the amount of heave experienced can be severely limited. The degree of saturation may be lower than 1.0 due to leakage during the tests, or as a function of the pre-test consolidation process. These are both aspects of experimental set-up and procedure, for example if an open system were designed then leakage might not be so critical, and consolidation within the permode itself could be investigated. This latter option would reduce any discrepancies arising from 'bad fit' of specimen to cylinder, e.g. cavities at the top, base or side walls, and also reduce air intrusion from extra handling stages. Disadvantages would be the longer turn-around in testing time, and loss of homogeneity of specimen length.

Table 7.11 – Lias Clay Test 14 Expected and Actual Heave

Cycle	w	S_r	e	ρ (g/cm^3)	M (g)	M_w (g)	M_s (g)	V_w (cm^3)	V_s (cm^3)	V_f (cm^3)	% Incr. in V	Expected Incr. in h (mm)	Actual Incr. in h (mm)	Actual S_r required
1	0.27	1.000	0.729	1.983	623.049	132.459	490.590	132.459	181.700	326.081	3.795	3.795	0.680	0.932
2	0.27	1.000	0.729	1.983	623.049	132.459	490.590	132.459	181.700	326.081	3.795	3.795	1.170	0.942
3	0.27	1.000	0.729	1.983	623.049	132.459	490.590	132.459	181.700	326.081	3.795	3.795	0.880	0.936
4	0.27	1.000	0.729	1.983	623.049	132.459	490.590	132.459	181.700	326.081	3.795	3.795	1.030	0.939
5	0.27	1.000	0.729	1.983	623.049	132.459	490.590	132.459	181.700	326.081	3.795	3.795	1.170	0.942

Table 7.12 – Weald Clay Test 25 Expected and Actual Heave

Cycle	w	S_r	e	ρ (g/cm^3)	M (g)	M_w (g)	M_s (g)	V_w (cm^3)	V_s (cm^3)	V_f (cm^3)	% Incr. in V	Expected Incr. in h (mm)	Actual Incr. in h (mm)	Actual S_r required
1	0.39	1.000	1.053	1.828	574.301	161.135	413.166	161.135	153.024	328.661	4.616	4.616	1.510	0.944
2	0.39	1.000	1.053	1.828	574.301	161.135	413.166	161.135	153.024	328.661	4.616	4.616	1.930	0.951
3	0.39	1.000	1.053	1.828	574.301	161.135	413.166	161.135	153.024	328.661	4.616	4.616	1.990	0.952
4	0.39	1.000	1.053	1.828	574.301	161.135	413.166	161.135	153.024	328.661	4.616	4.616	1.940	0.951
5	0.39	1.000	1.053	1.828	574.301	161.135	413.166	161.135	153.024	328.661	4.616	4.616	1.850	0.950

Table 7.13 – Oxford Clay Test 20 Expected and Actual Heave

Cycle	w	S_r	e	ρ (g/cm^3)	M (g)	M_w (g)	M_s (g)	V_w (cm^3)	V_s (cm^3)	V_f (cm^3)	% Incr. in V	Expected	Actual	
												Incr. in h (mm)	Incr. in h (mm)	S_r required
1	0.49	1.000	1.323	1.732	544.065	178.921	365.144	178.921	135.239	330.262	5.126	5.126	0.870	0.931
2	0.49	1.000	1.323	1.732	544.065	178.921	365.144	178.921	135.239	330.262	5.126	5.126	0.860	0.931
3	0.49	1.000	1.323	1.732	544.065	178.921	365.144	178.921	135.239	330.262	5.126	5.126	1.090	0.934
4	0.49	1.000	1.323	1.732	544.065	178.921	365.144	178.921	135.239	330.262	5.126	5.126	1.010	0.933
5	0.49	1.000	1.323	1.732	544.065	178.921	365.144	178.921	135.239	330.262	5.126	5.126	1.080	0.934

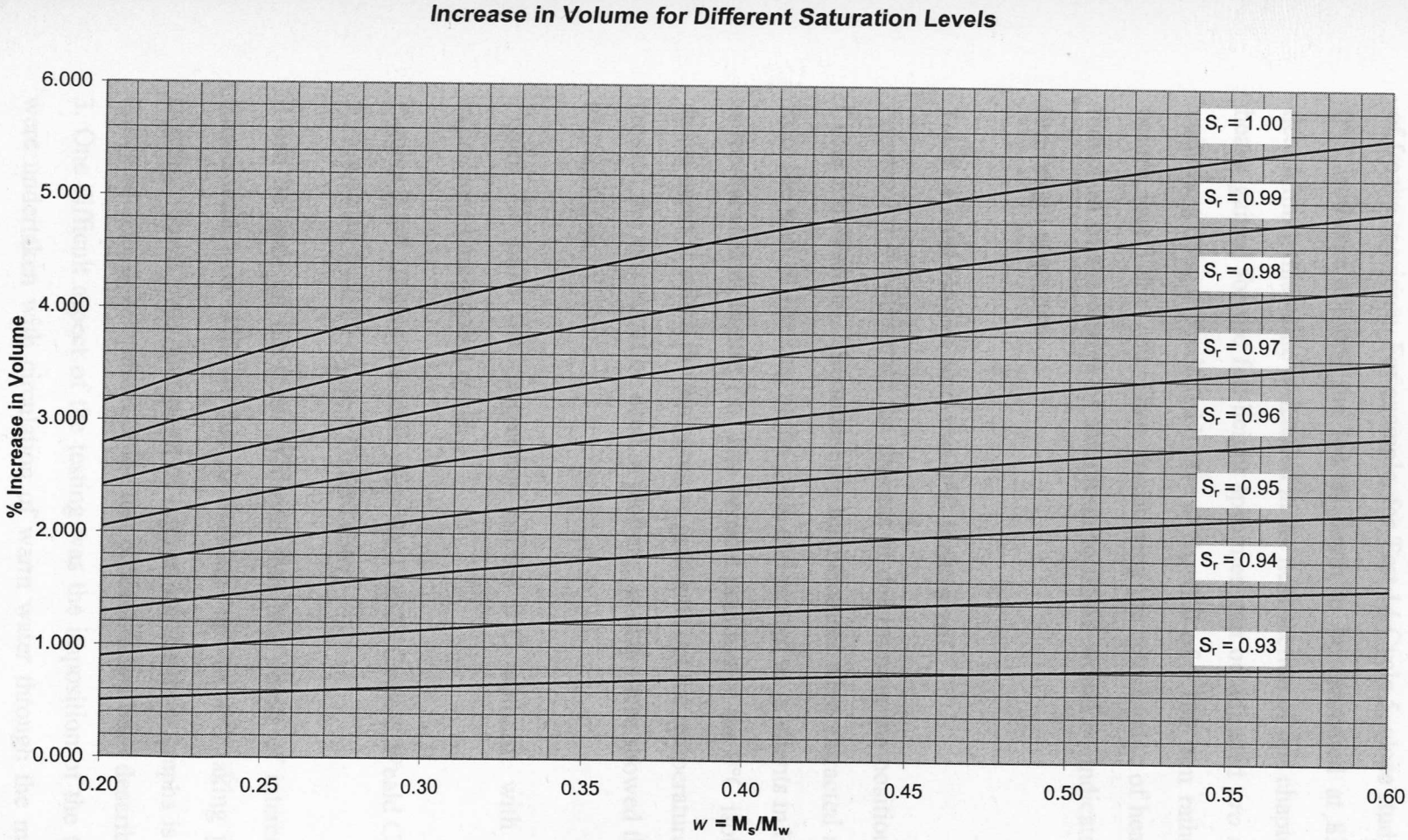

Figure 7.4 – Percentage Increase in Volume for Different Saturation Levels

Another consideration is the extent of freezing of the specimen. For example, in the case of Tests 14 and 20 the specimen did not experience full freezing, (i.e. to the depth of the base thermocouple). Where this is the case, a tentative reduction in frost heave potential might be considered by repeating the calculation procedure outlined above for a modified depth of frozen specimen. For example, for Test 14 Cycle 5, close study of the progression of the 0°C isotherm allowed the lowest depth to be estimated at 83.5 mm. (The process of determining this value is detailed in the next section of this chapter). The value of predicted heave gained for the full-height specimen can be adjusted *pro rata* to reflect the smaller volume, giving a predicted heave at S_r =1.0 of 3.169 mm rather than 3.795 mm gained before, (see Table 7.9). Then, considering the actual value of heave recorded, 1.170 mm, a reduction of the degree of saturation to 0.947 would be indicated rather than 0.942 for a full-height specimen.

7.4.3 Frost Heave and the 0°C Isotherm

Figures 7.5–7.6 illustrate the process of determining the position of the 0°C isotherm for Cycle 5 of Test 14. Thermocouple temperatures were extracted at intervals of 30 minutes from the start of freezing in the cycle and plotted as gradients in Figure 7.5. The thaw stage is represented in Figure 7.6. The vertical position of the 0°C isotherm was then estimated as the point at which the temperature gradients cut the temperature axis. Only gradients that crossed the axis could be used in plotting, as only these showed the relative position of the 0°C isotherm.

Figure 7.7 plots the progression of the 0°C isotherm with time against the heave experienced during that cycle.

Figures 7.8-7.10 give the same plots for Test 25 Cycle 5 Weald Clay, and similarly Figures 7.11-7.13 for Test 20 Cycle 5 Oxford Clay.

It can be seen on the thaw gradients that less points of intercept were found with the temperature axis. This is due to thawing 'up' to 0°C taking place more quickly than freezing 'down'. Another point of interest on the thaw graphs is the direction of thawing indicated. The development of the test procedure has been described previously in Chapter 3. One difficult aspect of the testing was the imposition of the thaw phase. Experiments were undertaken with circulation of warm water through the metal plates at top and/or

base, but these were abandoned due to the steep ramping up of temperatures in the specimen and the physical difficulty of changing over the circulation supply. Instead, it was decided that by stopping freezing, thawing would occur through the now-warmer top metal contact plate. However, Figures 7.6, 7.9 and 7.12 demonstrate the actual resultant situation to be different. The metal plate at the base of the permode was insufficiently insulated to prevent conduction of heat into the permode. Therefore, the specimens tended to thaw non-directionally, as can be seen from the general upwards transposition of the thawing temperature gradients.

Figures 7.7, 7.10 and 7.13 demonstrate the extent of heaving occurring as the 0°C isotherm progresses downwards through the specimen. Due to the uncertainty in thawing patterns indicated above, the comparison of thawing isotherm and heave is less reliable, but the points are included for interest.

In the Lias Clay, (Test 14), heave does not appear to start until the 0°C isotherm reaches a depth of 6-8 mm. In the Weald Clay, (Test 25), and Oxford Clay, (Test 20), expansion starts from the onset of freezing, with the heave following a convex curve pattern rather than the single-gradient increase observed in the Lias Clay. Approximately 44 % of the total heave in the Lias Clay occurs after the 0°C isotherm reaches a depth of 50 mm. For the same depth in the Weald Clay and Oxford Clay, approximately 43 % and 26 % of the total heave occurs respectively.

Therefore, in the Lias Clay, for heave to occur, the 0°C isotherm has to reach greater depths than in the Weald Clay and Oxford Clay, perhaps indicating that water is not being attracted towards the frozen fringe in sufficient quantities to demonstrate heave. Instead, the water is frozen *in situ* and expands as the greater depth of soil is frozen. Also, a longer time is taken for the 0°C isotherm to progress to its half-way depth than for the Weald Clay or Oxford Clay. For example, although the Weald Clay exhibits roughly the same percentage as the Lias Clay of total heave as the 0°C isotherm reaches 50 mm depth, when time is taken into account the Weald Clay is achieving its heave more quickly. The Oxford Clay only achieves a quarter of its total heave resultant from the 50 mm depth of the 0°C isotherm being achieved, but the heave curve also shows a more stepped increase pattern.

In fact, these findings serve more to prompt further work than to resolve frost heave queries. As noted above, the choice of testing at similar plasticity rather than similar

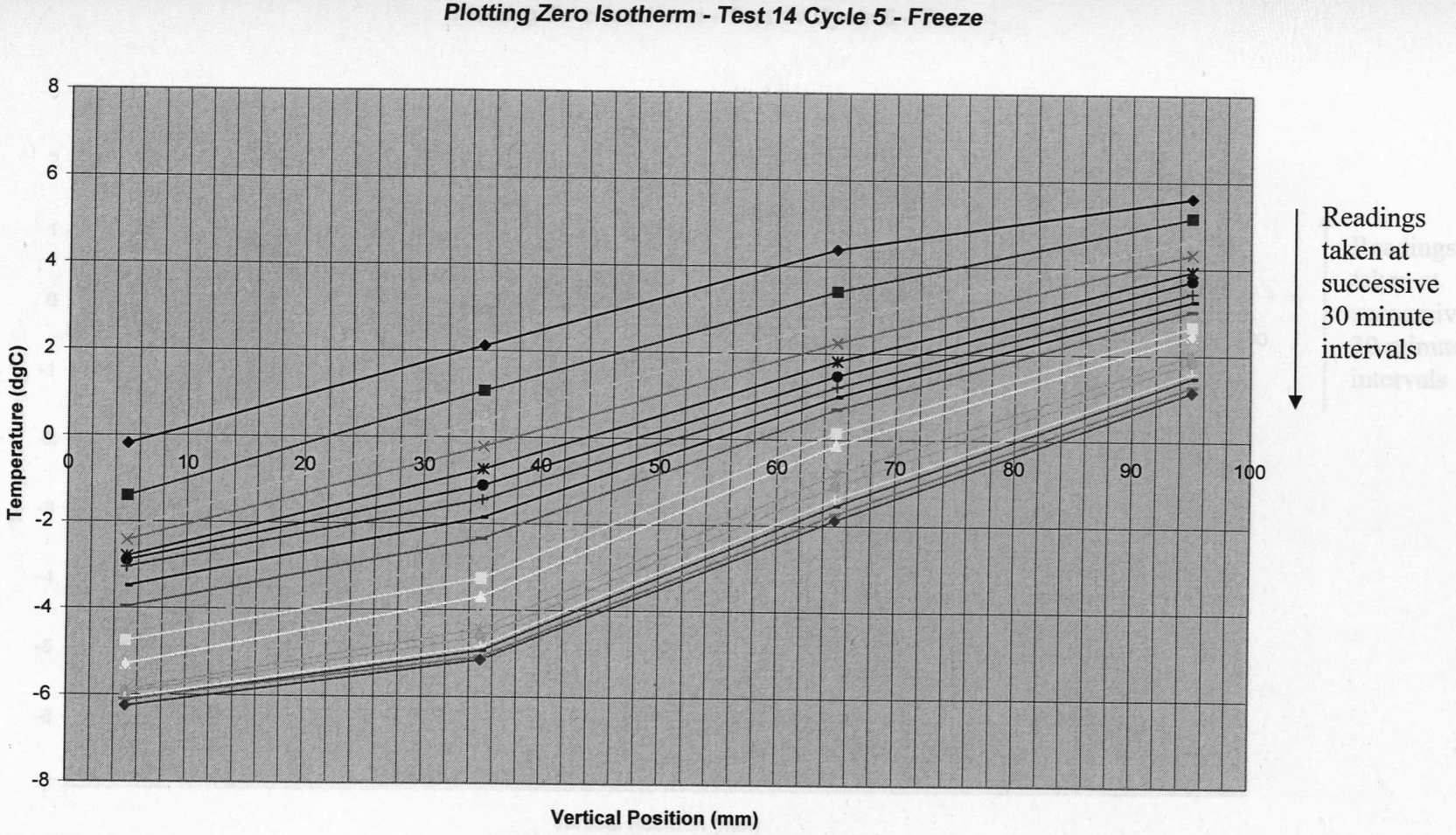

Figure 7.5 – Plotting the Zero Isotherm for Freeze Phase of Test 14 Cycle 5

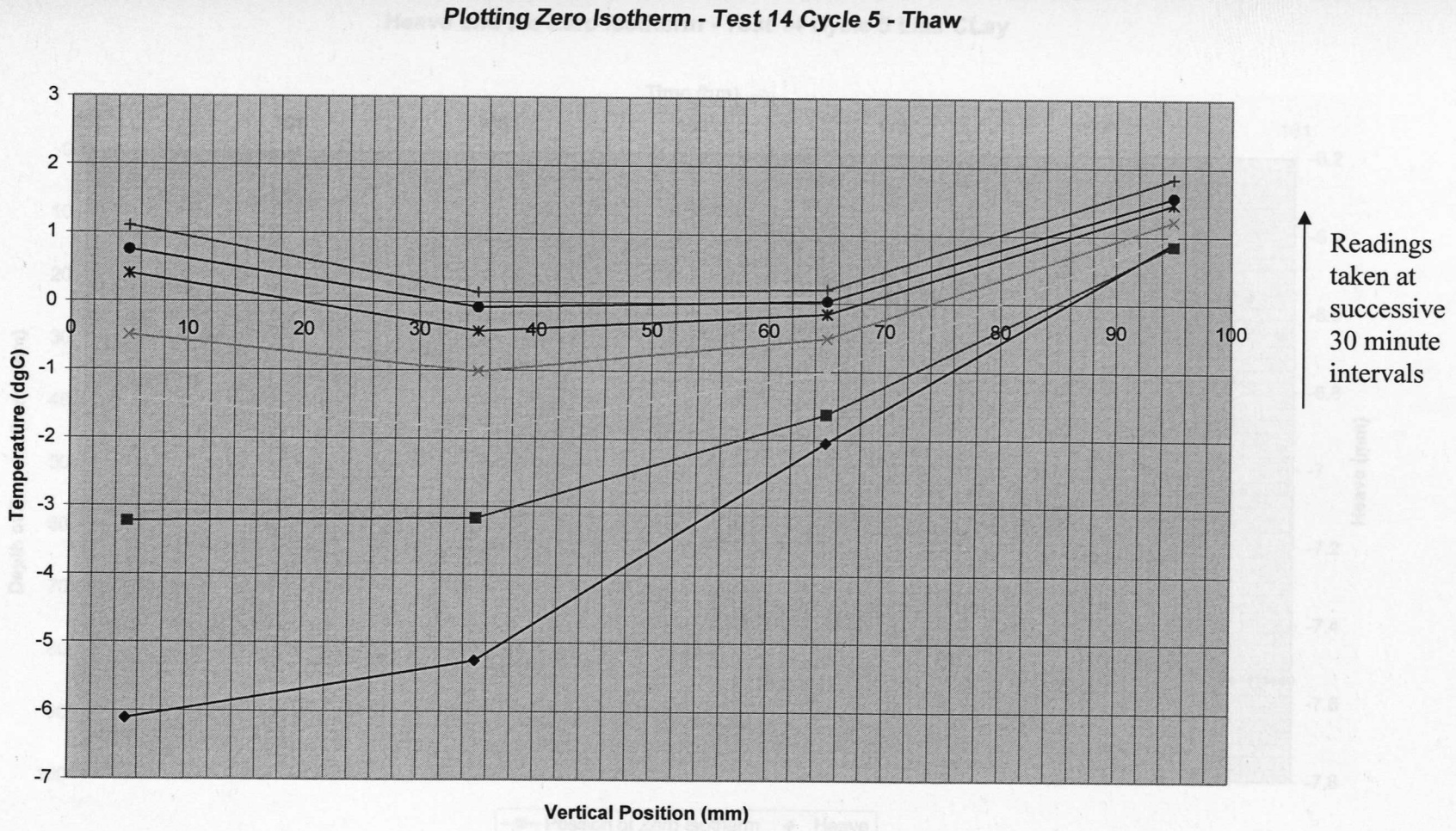

Figure 7.6 – Plotting the Zero Isotherm for Thaw Phase of Test 14 Cycle 5

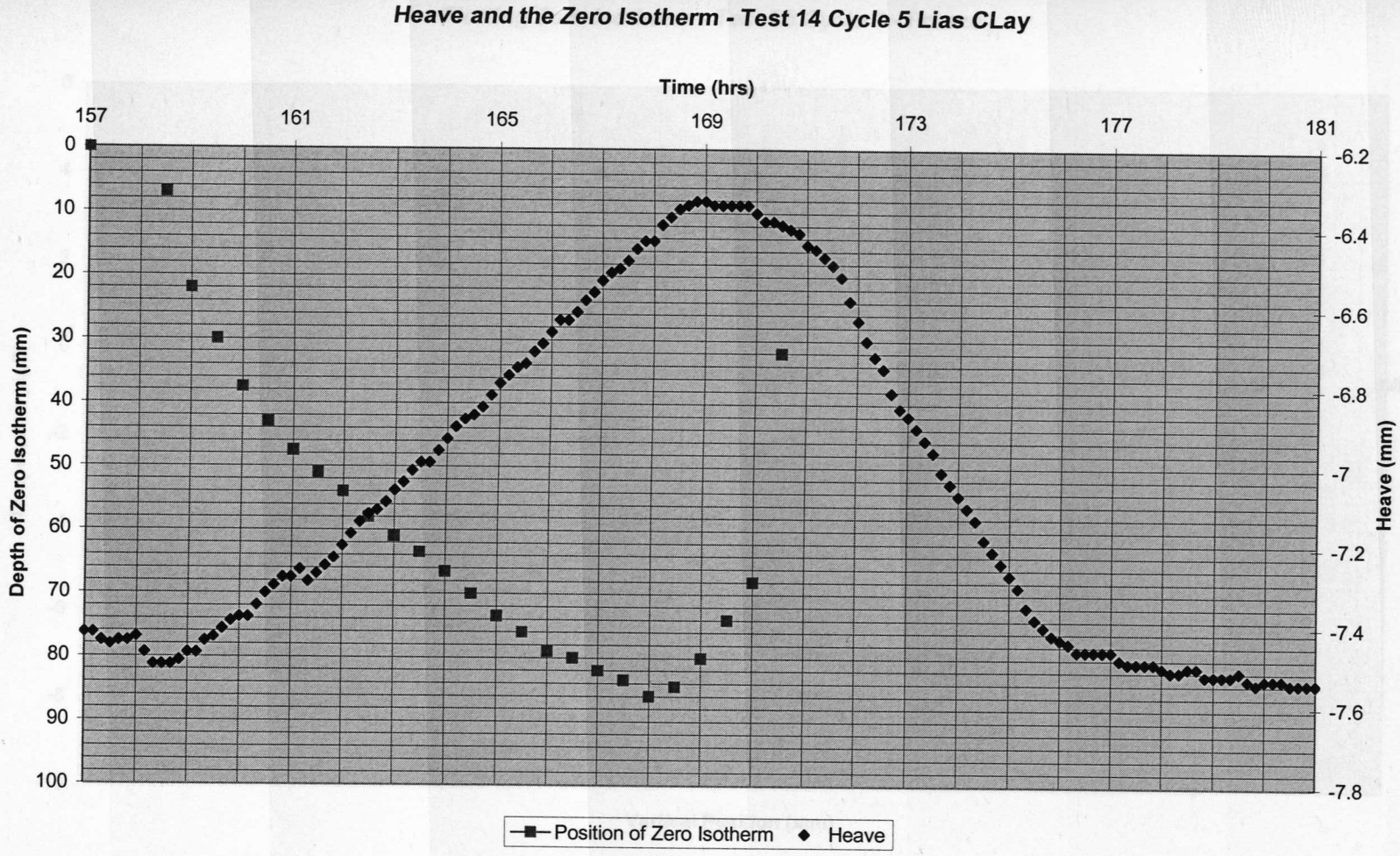

Figure 7.7 - Comparing Heave with Progression of Zero Isotherm for Test 14 Cycle 5

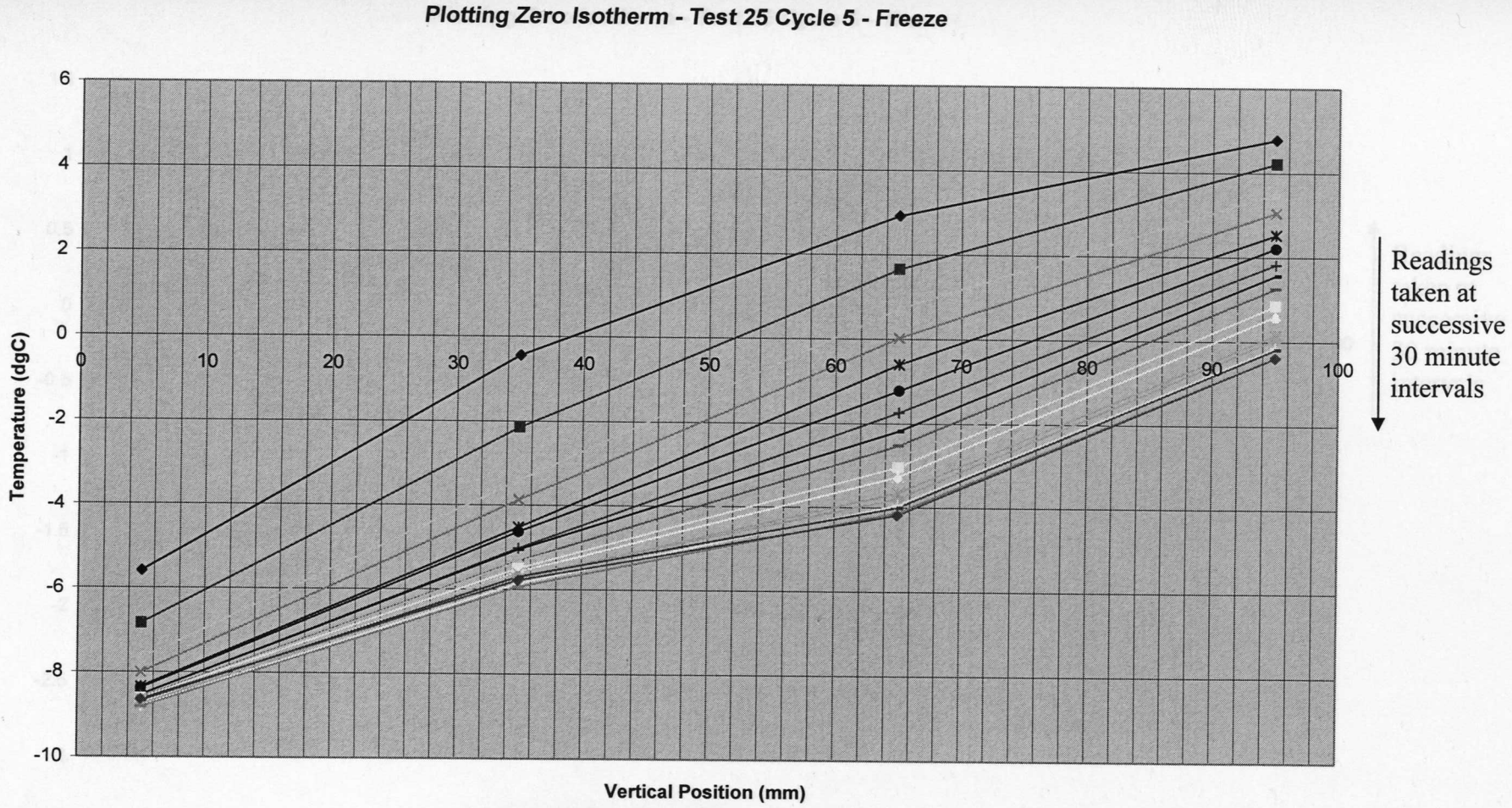

Figure 7.8 – Plotting the Zero Isotherm for Freeze Phase of Test 25 Cycle 5

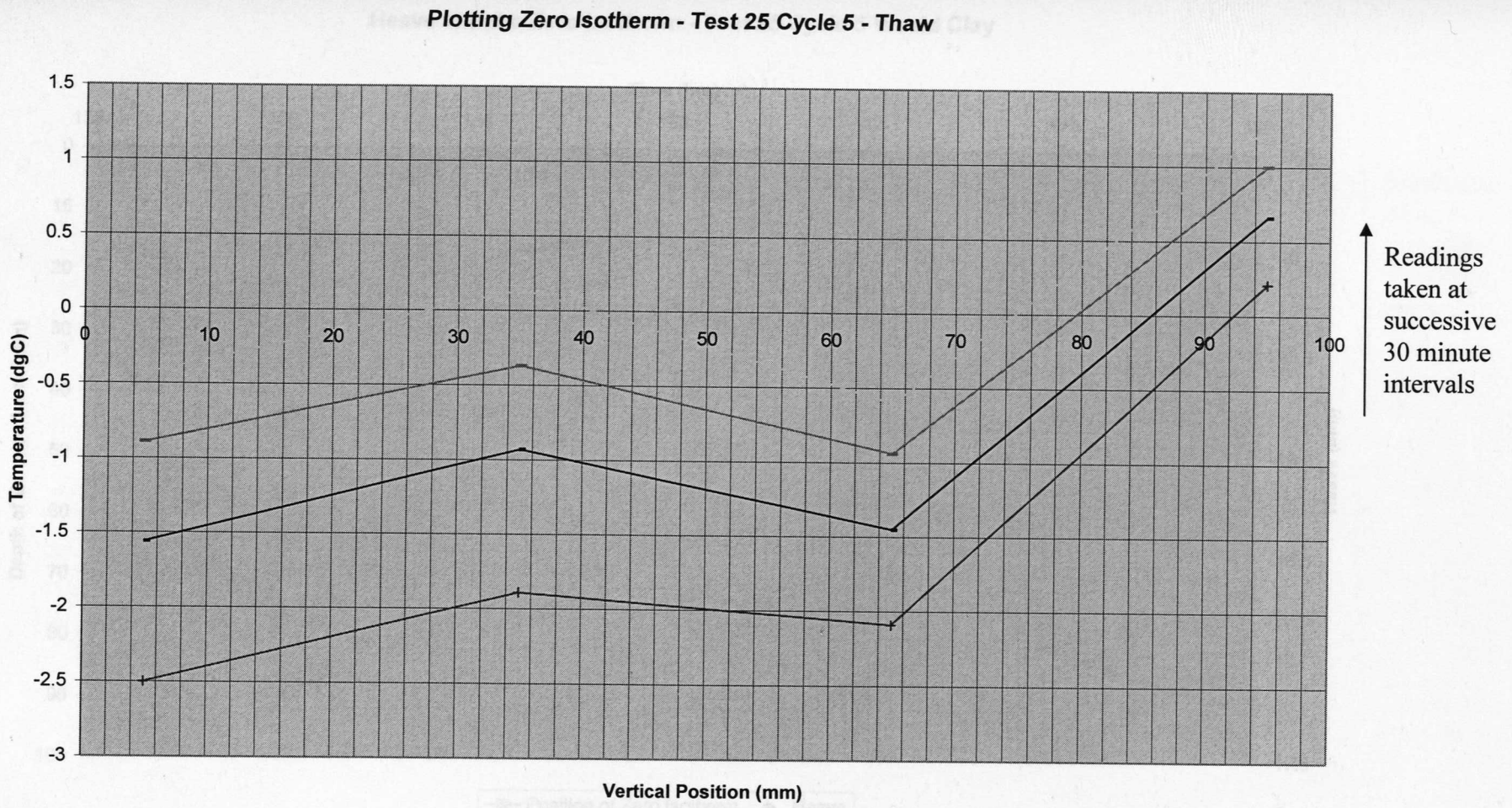

Figure 7.9 – Plotting the Zero Isotherm for Thaw Phase of Test 25 Cycle 5

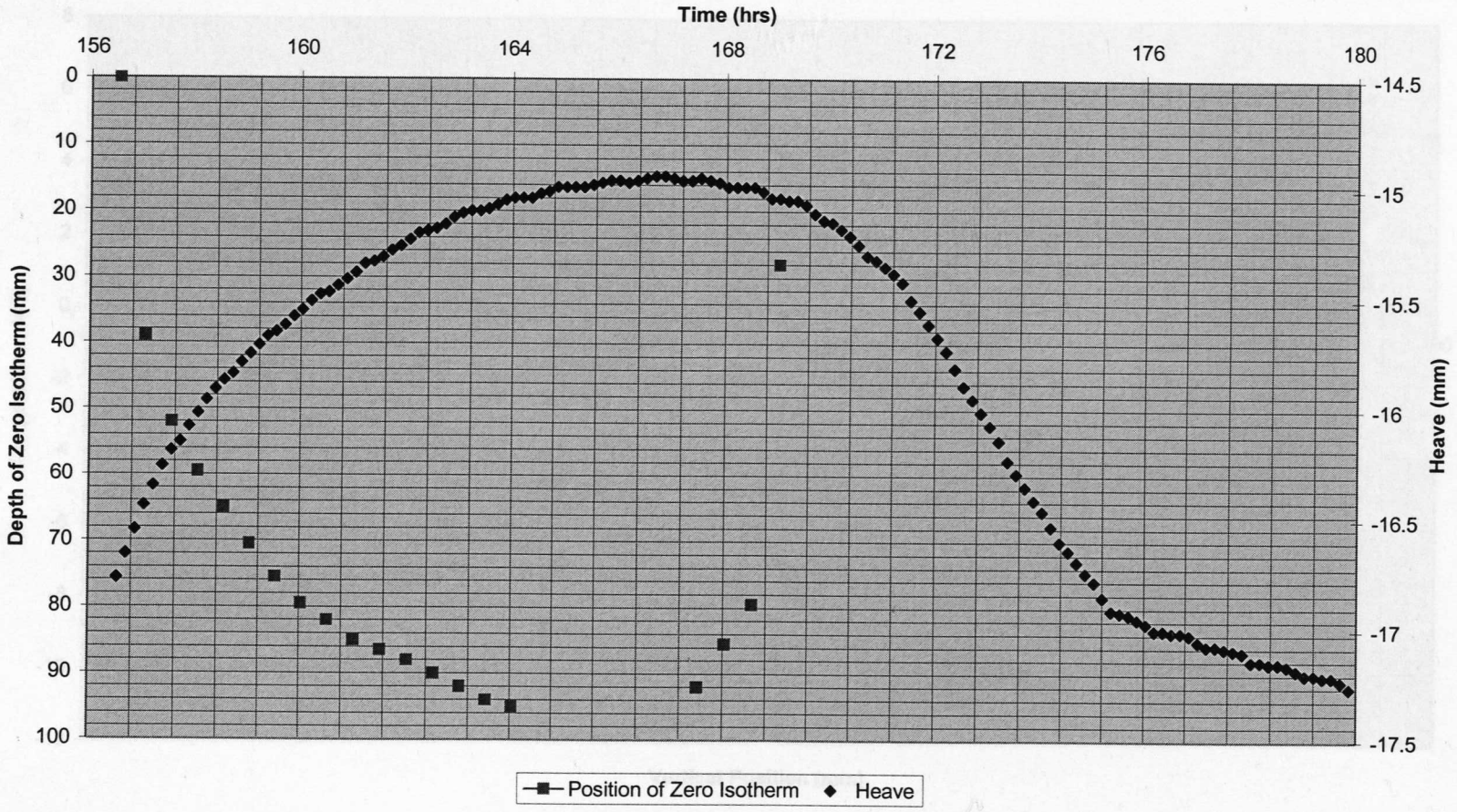

Figure 7.10 - Comparing Heave with Progression of Zero Isotherm for Test 25 Cycle 5

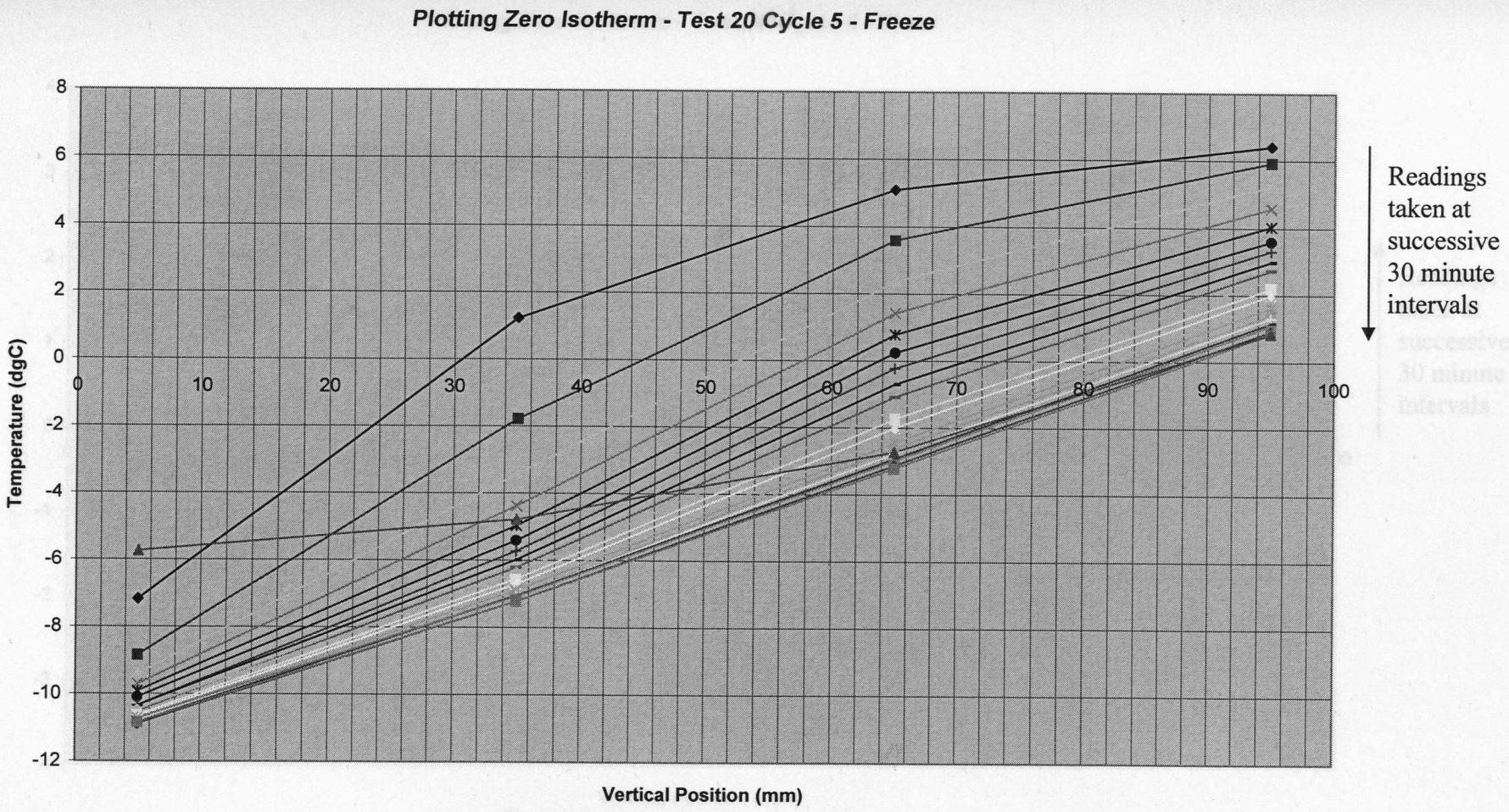

Figure 7.11 – Plotting the Zero Isotherm for Freeze Phase of Test 20 Cycle 5

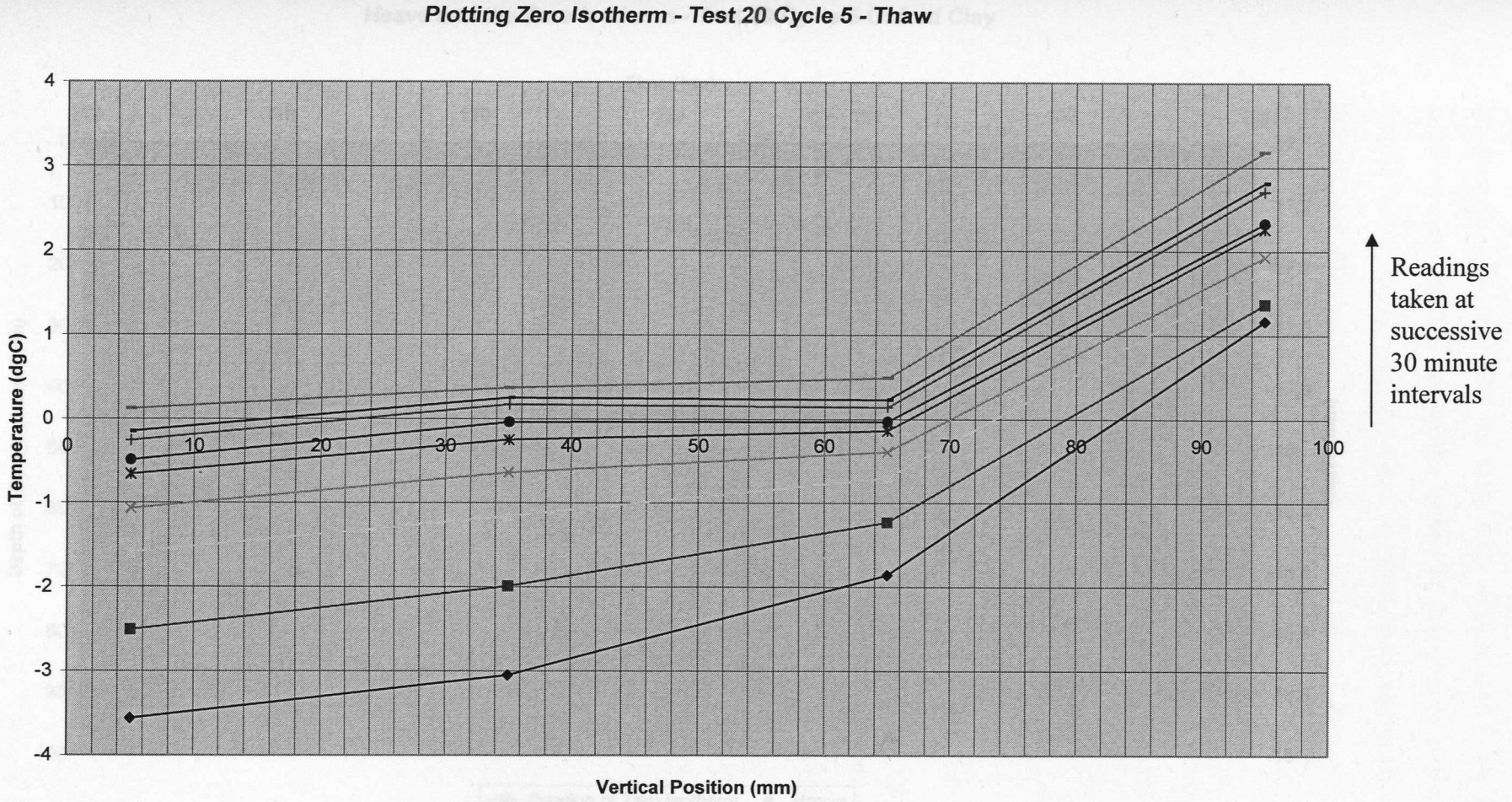

Figure 7.12 – Plotting the Zero Isotherm for Thaw Phase of Test 20 Cycle 5

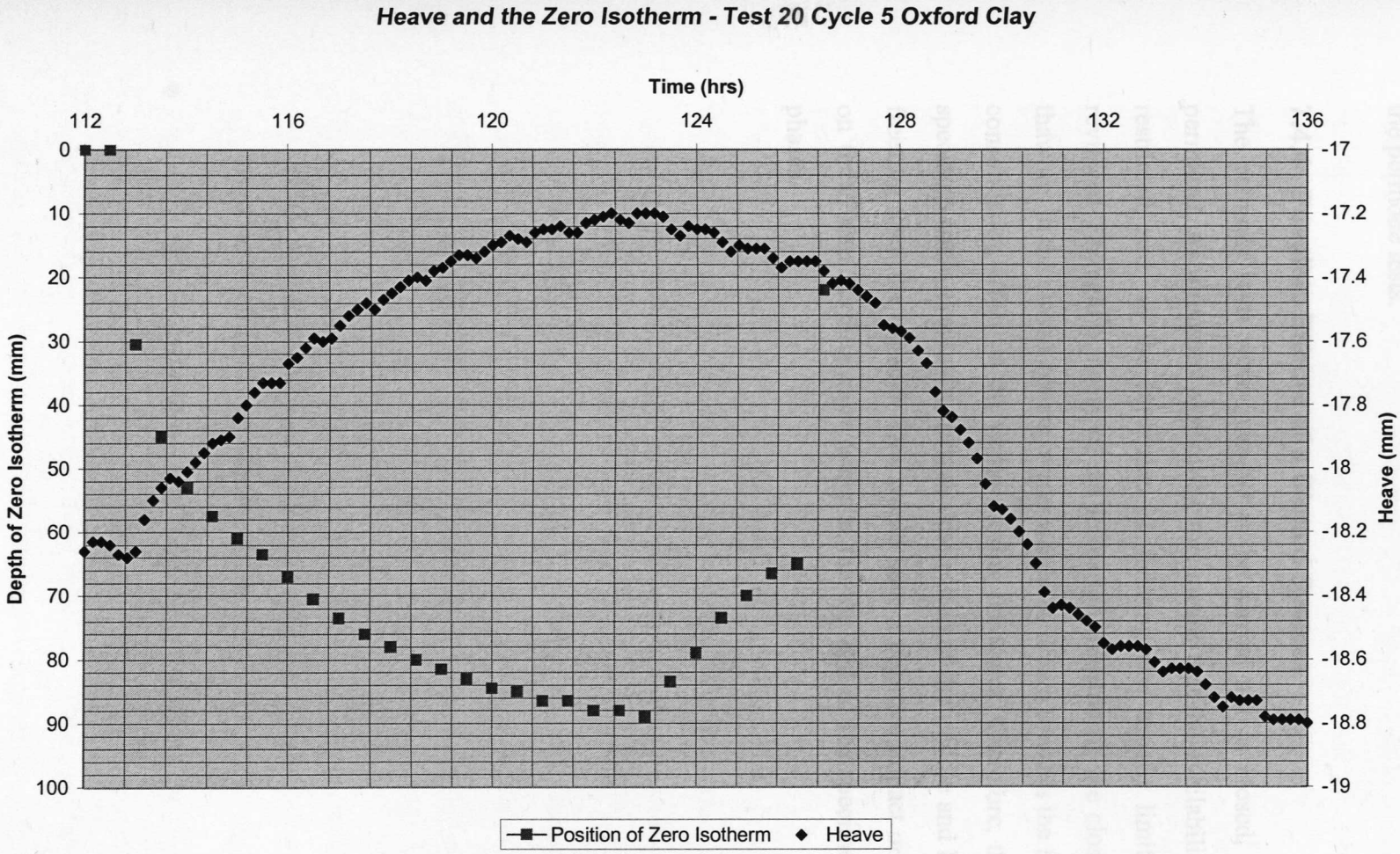

Figure 7.13 - Comparing Heave with Progression of Zero Isotherm for Test 20 Cycle 5

moisture content may distort the results somewhat. Tests with all three soils at high moisture contents, and with the total depth of specimen being frozen would be needed to draw detailed conclusions on the nature of frost heave in the permode tests. However, despite these uncertainties, it is clear that frost heave occurred in all three soil types during the permode tests.

7.4.4 Possible Effects of a Closed System

The permode tests were intended to be carried out as closed, with no entry of water permitted. As discussed previously, this means that the availability of water in the soil is restricted, and so the expansion on freezing was equally limited. Andersland, (1987), reviewed Terzaghi's theory of ice formation, illustrating the closed and open systems of thawing. In the closed system, water would be drawn towards the freezing front, effecting a consolidation effect on the section losing the water. Therefore, the final condition of the specimen could eventually include dessication of the middle and lower sections, assuming freezing from the top end. This would have a negative impact on downwards percolation on thaw, thus keeping more water at the top end of the specimen for subsequent freeze phases.

7.5 The Consideration of Zero Curtain Behaviour

7.5.1 Comparison of Permode Testing to Model Slope Simulation

The zero curtain phenomenon (Harris *et al.*, 1995; Harris & Davies, 1996), has already been described in Chapter 2, Section 2.5. Its application to permode test results has been considered in Chapter 5, Section 5.2. The definitive test procedure used in Tests 14-28, however, has produced results that require separate attention.

During this second tranche of tests, freezing has been one-directional only, as with the model slope experiments outlined by Harris *et al.*, (1995); Harris *et al.*, (1997); Harris & Davies, (1998). Freezing took place from the top downwards, (with the exception of Tests 22 and 23, which are not considered in this section). Substantial differences in the two experiments still exist, however. For example, the permode tests were carried out undrained, unlike the model slope simulation. The freeze-thaw cycles induced in the permode were far shorter than those induced in the model slope, and the temperature range far smaller. Also, as mentioned previously, one-directional thaw was not fully ralised in the permode.

The situations modelled were also different, however. Harris *et al*, (1997), determined that the profiles of soil movement found through the experiments were similar to those found in mountainous regions subjected to periglacial activity. This contrasts with the low-angle slopes considered in conjunction with the permode tests. The slope model experiments were constructed at full scale, and so dealt with slope movement over a relatively short distance. The soils examined in the model slope experiments and the permode tests were different. The model slope experiments were carried out using sandy and silty soils, whilst the permode tests concerned clayey soils, although one silty clay was investigated.

However, the basic soil mechanics observed will not change, so one possible correlation of the two experiments would be to consider the soil element modelled in the permode as part of a longer slope, suitable for analysis using the semi-infinite slope model of analysis.

The wet, viscous thaw-strain type movement observed by Harris *et al*, (1995), is not completely applicable to the author's research. There is some similarity, namely the liquefaction-type behaviour understood to occur at and above the geostatic condition in the permode, which could be related to viscous movements. Also, Harris *et al.*, (1995),

suggested that thawing soil displayed both viscous and frictional properties, the relative importance of which would change through time and drainage. This provides a framework which could include both viscous flow theory and semi-infinite slope analysis.

7.5.2 Initial Indications of Zero Curtain Behaviour

Tables 7.14 and 7.15 below show the position of the minimum pore water pressures recorded at the top and base of the specimen respectively.

Table 7.14 – Position of Minimum Pore Water Pressures Recorded at the Top of the Specimen

Test No.	PWP (kPa) Top - Min	Time (hours)	Point reached in the test cycles
14	-1.22	18.7	20% into freeze stage of Cycle 1
15	-4.20	64.0	40% into freeze stage of Cycle 1
16	-4.21	62.2	22% into freeze stage of Cycle 1
17	-3.83	65.9	39% into freeze stage of Cycle 1
18	-1.83	65.0	40% into freeze stage of Cycle 1
19	-10.32	31.2	26% into thaw stage of Cycle 1
20	-7.09	32.2	41% into thaw stage of Cycle 1
21	-5.20	50.7	34% into thaw stage of Cycle 1
22	6.14	100.9	56% into thaw stage of Cycle 3
23	32.50	152.0	75% into thaw stage of Cycle 5
24	0.84	47.4	17% into thaw stage of Cycle 1
25	15.89	315.5	39% into thaw stage of Cycle 9
26	-3.28	72.9	21% into thaw stage of Cycle 1
27	-1.23	79.0	50% into thaw stage of Cycle 1
28	20.98	77.2	44% into thaw stage of Cycle 1

Table 7.15 - Position of Minimum Pore Water Pressures Recorded at the Base of the Specimen

Test No.	PWP (kPa) Base - Min	Time (hours)	Point reached in the test cycles
14	-5.94	27.2	5% into thaw stage of Cycle 1
15	-16.35	79.5	68% into thaw stage of Cycle 1
16	-6.83	76.5	46% into thaw stage of Cycle 1
17	-11.00	74.4	17% into thaw stage of Cycle 1
18	-14.05	82.0	79% into thaw stage of Cycle 1
19	-8.74	169.2	77% into freeze stage of Cycle 5
20	-8.65	53.2	21% into thaw stage of Cycle 2
21	3.20	71.5	18% into thaw stage of Cycle 2
22	-8.62	72.8	24% into thaw stage of Cycle 2
23	-0.33	47.9	17% into thaw stage of Cycle 1
24	-1.32	49.2	30% into thaw stage of Cycle 1
25	4.66	314.7	34% into thaw stage of Cycle 9
26	-4.72	98.7	34% into thaw stage of Cycle 2
27	-5.47	122.2	16% into thaw stage of Cycle 3
28	-25.82	145.8	20% into thaw stage of Cycle 4

Figures 7.14 and 7.15 show that the majority of minimum values of pore water pressure occur during the thawing stage of the freeze-thaw cycles. The thawing stage can then be split into two halves, with most minimum values being recorded in the first half. These minimum points may indicate pressure drops due to the onset of the thaw, but before the zero curtain period.

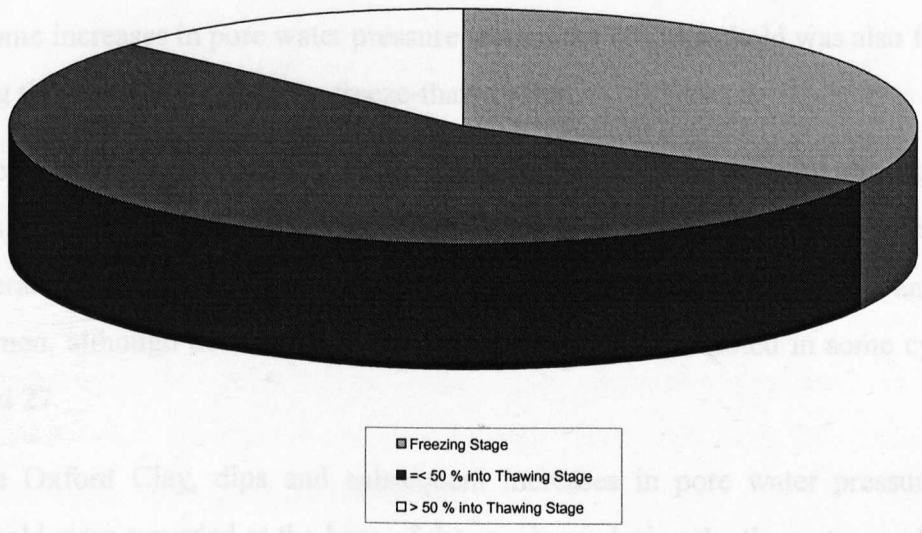

Figure 7.14 – Position of Minimum Pore Water Pressure - Top

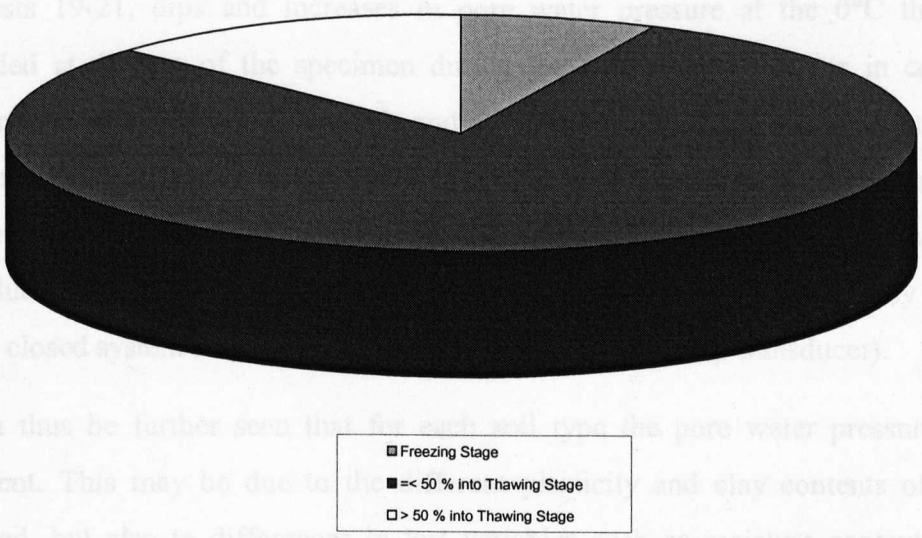

Figure 7.15 - Position of Minimum Pore Water Pressure – Base

In addition to the information quantified above, individual test data from Chapter 6, Section 6.3 also records evidence of a pore water pressure response due to soil temperatures passing the 0°C threshold.

Patterns of pore water pressure response in the Lias Clay generally show a good deal of fluctuation at the top transducer. At the base transducer, in general increases in pore water pressure were found to occur as the temperatures passed the 0°C threshold. In Tests 14 and 15, some increases in pore water pressure around the 0°C threshold was also found to occur during the freezing stage of the freeze-thaw cycles.

In the Weald Clay, no indication of the zero curtain was apparent during the freezing stages. Generally, during the thaw stages, dips and increases in pore water pressures as temperatures passed through the 0°C threshold were recorded at the top and base of the specimen, although decreases in pore water pressures were noted in some cycles of Tests 24 and 27.

In the Oxford Clay, dips and subsequent increases in pore water pressure at the 0°C threshold were recorded at the base of the specimen during the thaw stages of Tests 22 and 23. Also in Test 22, at the top of the specimen during the freezing stages, some of the cycles showed a change to a slower rate of decrease in pore water pressure as temperatures decreased past the 0°C threshold. This is the only test in which this response was observed. In Tests 19-21, dips and increases in pore water pressure at the 0°C threshold were recorded at the top of the specimen during the thaw stages. This is in contrast to the response shown in Tests 22 and 23, and is considered to be due to the fact that freezing took place from the base upwards in these two tests. (These tests were also anomalous due to the lack of suction and steep ramping up of pore water pressures observed at the top transducer during freezing. It is possible that the high values were induced by ice expansion in the closed system acting with unfrozen water against the top transducer).

It can thus be further seen that for each soil type the pore water pressure response is different. This may be due to the different plasticity and clay contents of the samples selected, but also to differences in test variables such as moisture content as discussed earlier in relation to frost heave.

7.5.3 Examples of Zero Curtain Behaviour

Various tests have been considered cycle by cycle in order to view any zero curtain behaviour. The value of applied stress for the tests considered was 55 kPa.

More test results are given for the Lias Clay, as its silty composition affords more possibility of comparison to Harris & Davies, (1998), and also due to he high amounts of fluctuation experienced in the Weald Clay and Oxford Clay tests.

The zero curtain period is clearly visible during the thawing stages of the tests as a 'flattening' of the temperature plots. The freezing stage of the permode tests may be imposed too rapidly to achieve the curtain effect. It is considered that the zero curtain periods are less pronounced than in Harris & Davies, (1998), due to the relatively short length of cycle and smaller amount of soil involved. The end of the zero curtain period is considered to be where all temperatures increase from 0°C, although in some cases the base of the specimen failed to freeze. Unfortunately, the thermocouple depths can only be approximate, as they refer to the initial depths along the specimen. As the specimen expands/contracts, the relative position of the thermocouples along the specimen change, as they are held in place along the barrel wall.

7.5.3.1 Lias Clay

Tests 15 and 17 are considered in Figures 7.16-7.23.

Considering Test 15 first:

The base of the specimen has failed to freeze.

The pore water pressure at the top of the specimen does not appear to exhibit a significant response to the freezing and thawing operations.

The pore water pressure at the base of the specimen is seen to increase during the freezing stage, remaining roughly level until the start of the thaw stage. On closer examination, the increase does not commence immediately on cooling, but 1-2 hours afterwards. However, a true curtain period is not shown by the temperature profiles. The initial drop in pore water pressures reported by Harris & Davies, (1998), was not observed. At the onset of the thawing stage, the pore water pressure starts to decrease, flattening out during the clearer thawing zero curtain. As temperatures rise out of the zero curtain period, the pore water pressure begins to increase once more. The pore water pressure decrease from the start of

the zero curtain period reported by Harris & Davies, (1998), was not observed. The increase in pore water pressure following the zero curtain period was in keeping with that seen by Harris & Davies, (1998).

In Test 17, similar patterns to Test 15 are observed. The base of the specimen was observed to freeze, although only in the last 3 hours before the thawing stage commenced. More fluctuation in pore water pressure was experienced than before, obscuring the response in places. The increase in pore water pressure during the freezing stage is not evident except in Cycle 2. The thawing zero curtain period is longer, due to the fact that greater cooling was achieved overall than in Test 15. The decrease in pore water pressure on thaw appears to occur at the start of the zero curtain rather than the start of thaw.

7.5.3.2 Weald Clay

Test 26 is considered in Figures 7.24-7.25.

A great deal of fluctuation was experienced at both transducers, with only very general patterns to be seen. A decrease in pore water pressure is seen from the onset of thaw, although a further dip around the thawing zero curtain can be seen in Cycle 5.

7.5.3.3 Oxford Clay

Test 19 is considered in Figures 7.26-7.27.

The base pore water pressure transducer did not record a significant response. At the top transducer, a slight rise and fall was observed during the freezing stage of Cycle 5. In both cycles shown, the pore water pressure decreases at the onset of thaw, but then increases sharply as the temperatures enter the zero curtain period, in contrast to the other test results examined. The pore water pressure decreases after this sharp rise.

7.5.4 Summary

Due to the rate of freezing imposed, the permode tests do not allow a freezing zero curtain period to develop. A thawing zero curtain period does occur, however. The effects of this zero curtain period appear most clearly in the test results from the Lias Clay. Some similarity of response to that seen by Harris & Davies, (1998), was observed. Due to the different natures of the test systems it is not appropriate to read too much into this, without a detailed comparative study being undertaken.

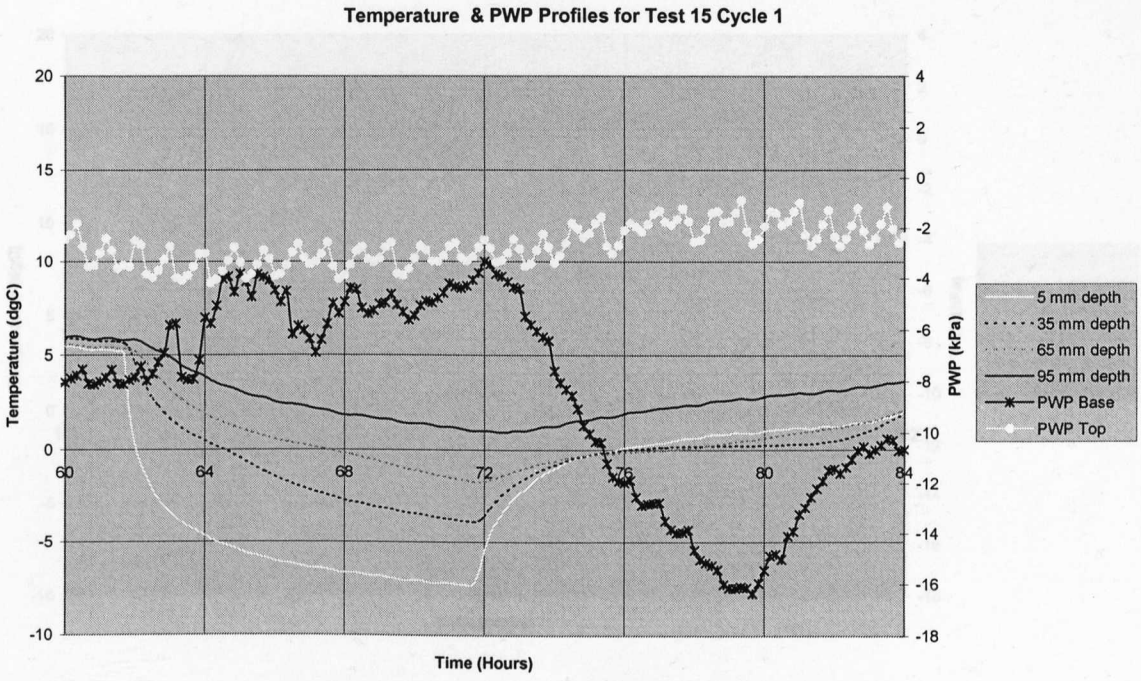

Figure 7.16 – Test 15 Cycle 1

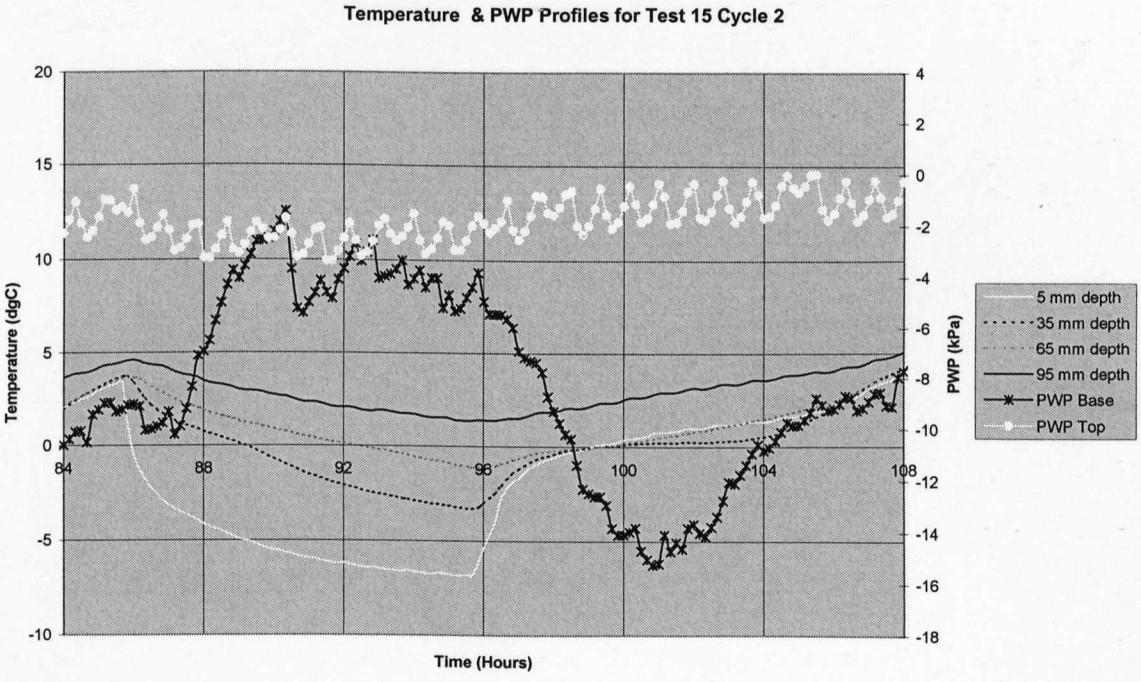

Figure 7.17 – Test 15 Cycle 2

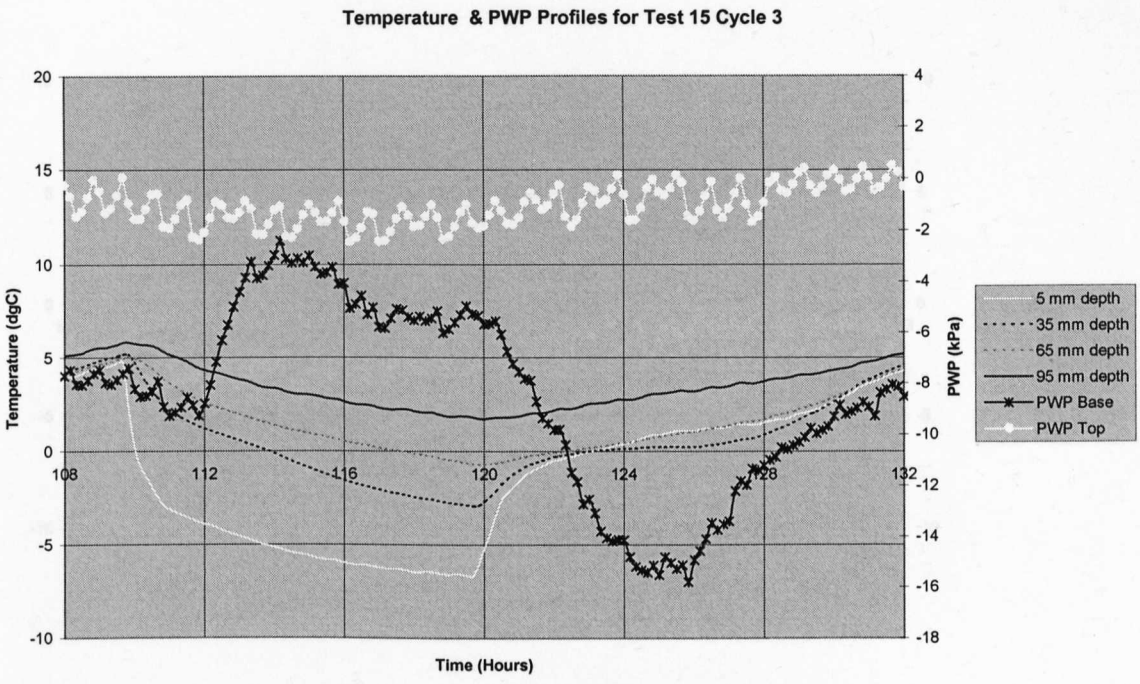

Figure 7.18 – Test 15 Cycle 3

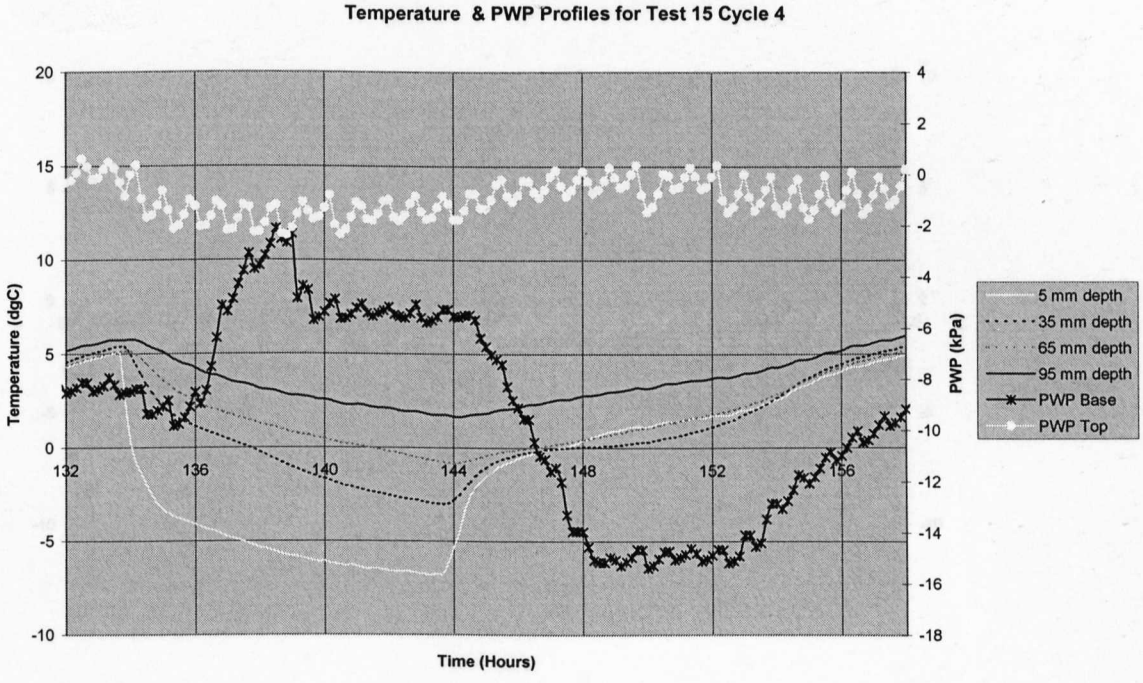

Figure 7.19 – Test 15 Cycle 4

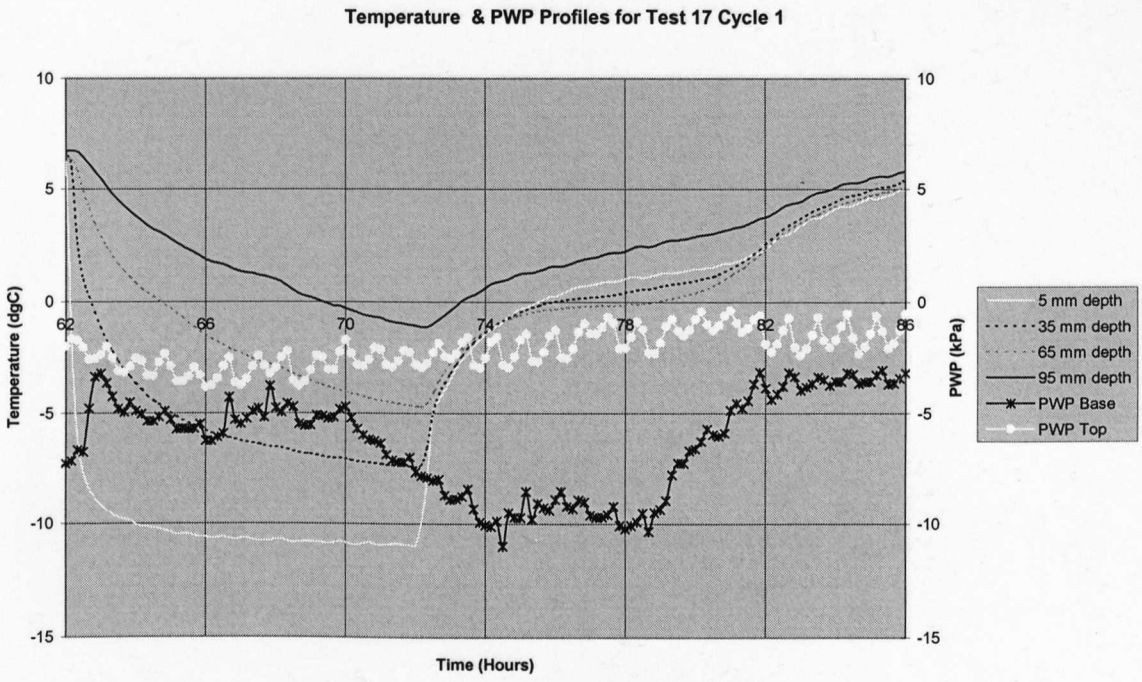

Figure 7.20 – Test 17 Cycle 1

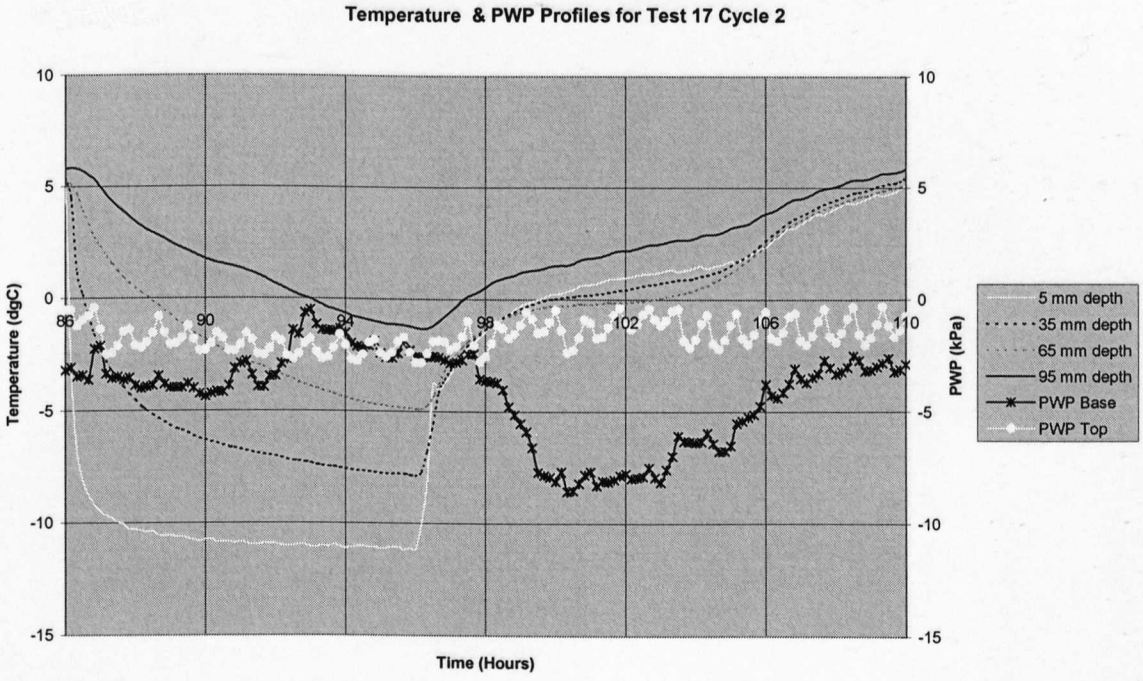

Figure 7.21 – Test 17 Cycle 2

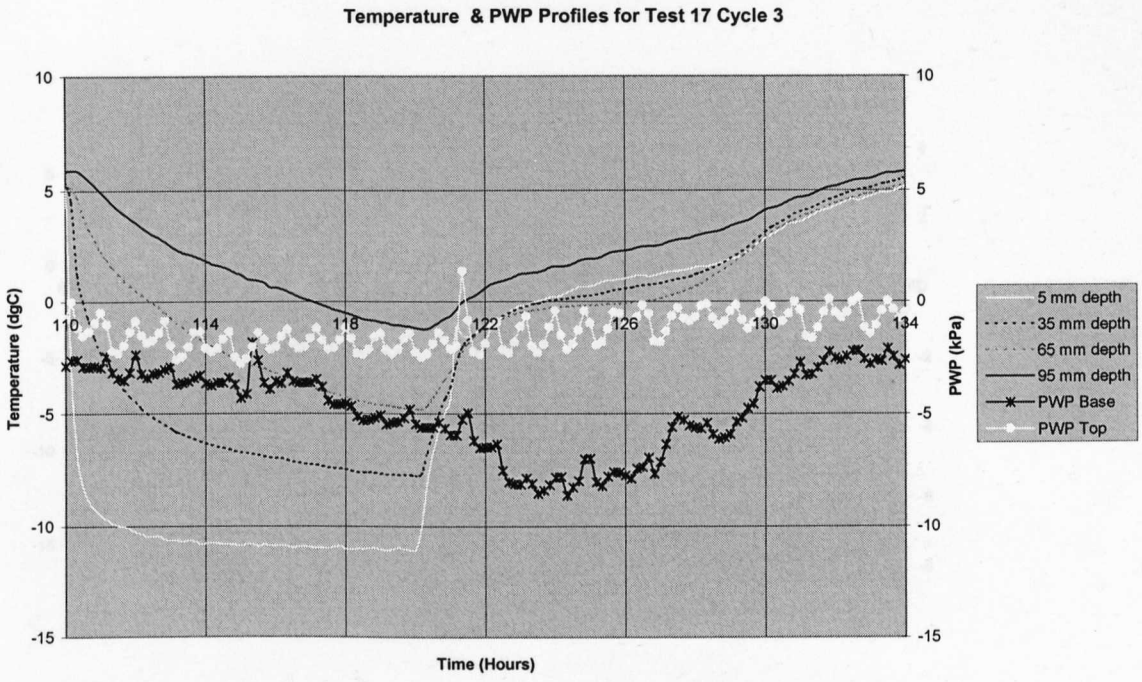

Figure 7.22 – Test 17 Cycle 3

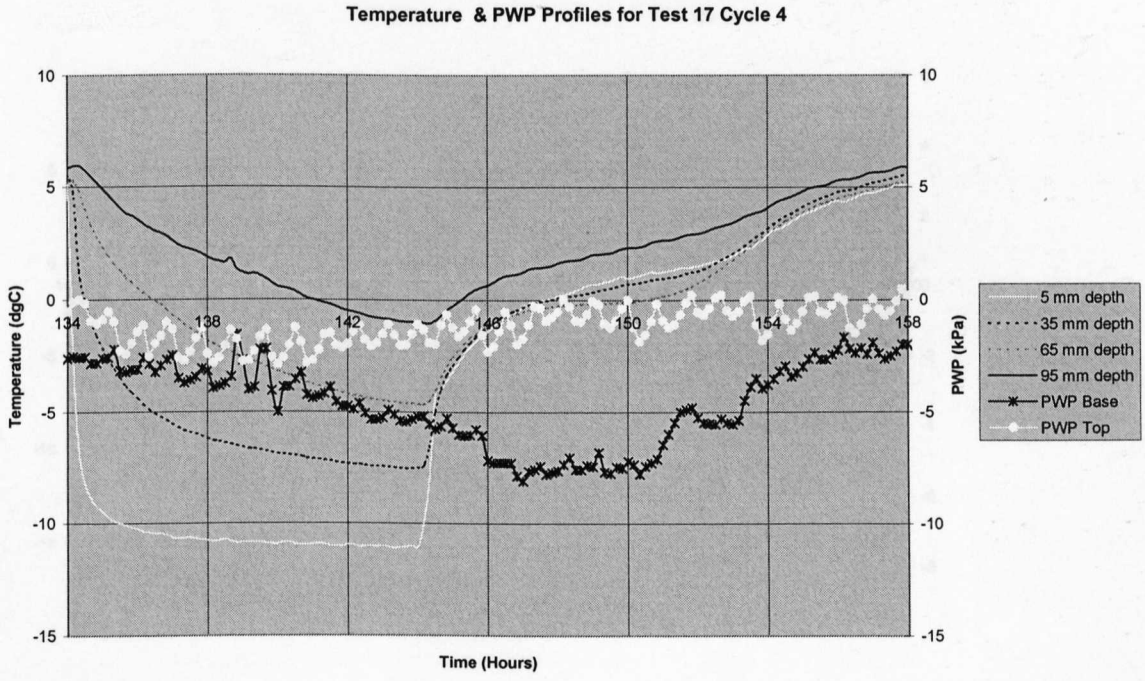

Figure 7.23 – Test 17 Cycle 4

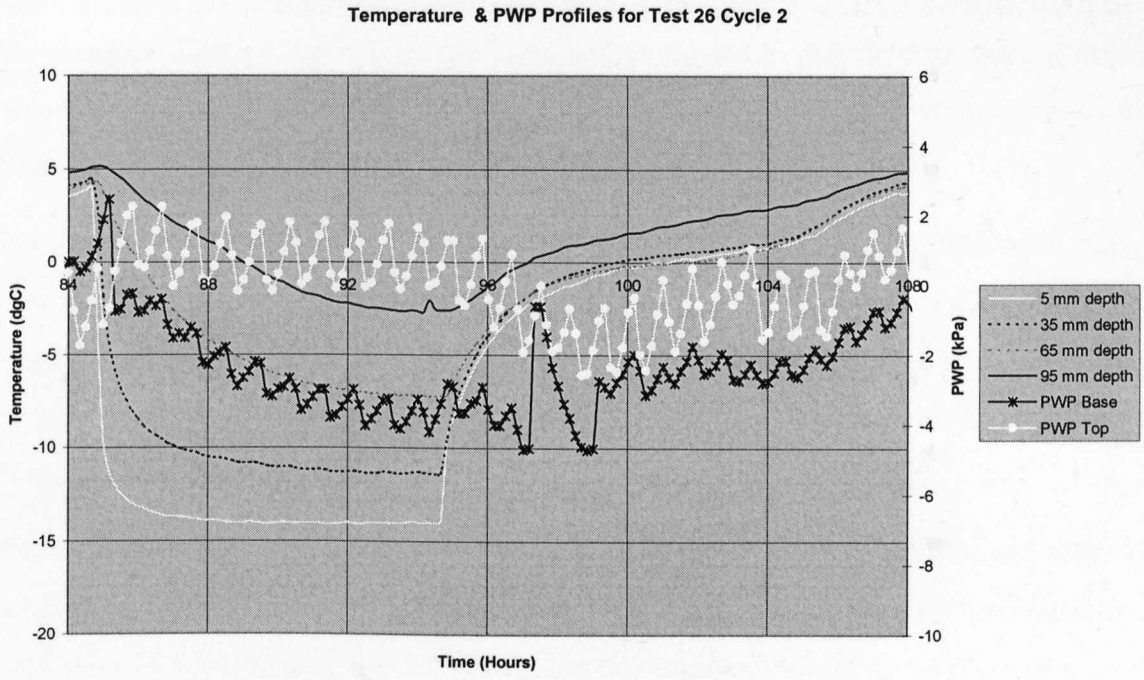

Figure 7.24 – Test 26 Cycle 2

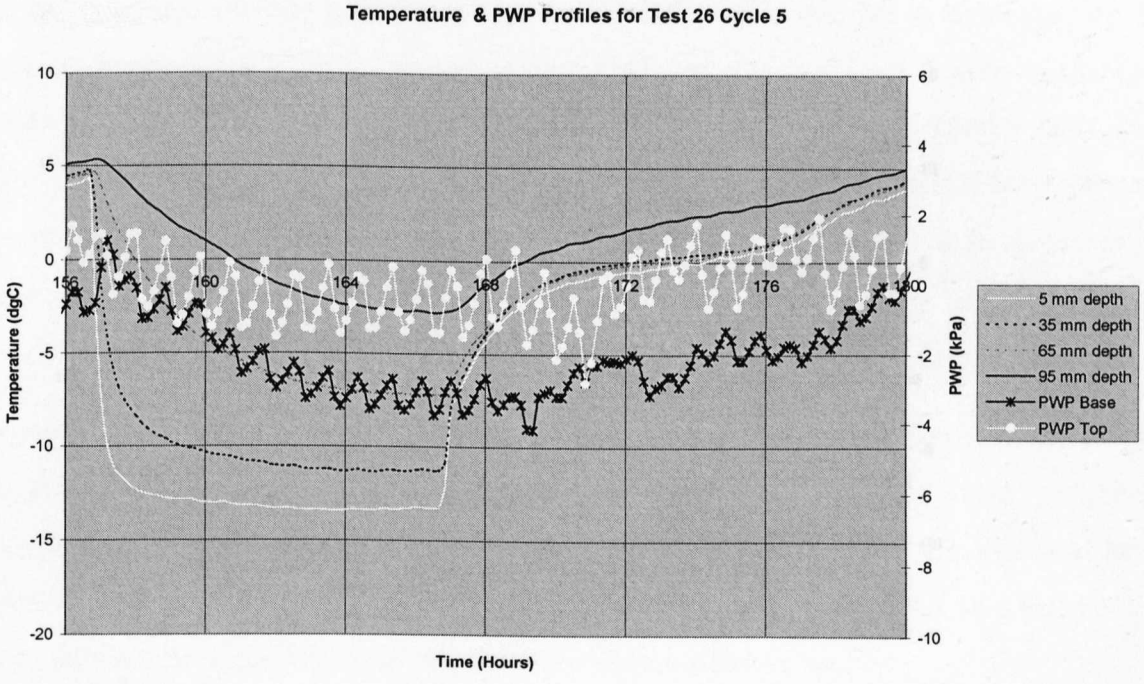

Figure 7.25 – Test 26 Cycle 5

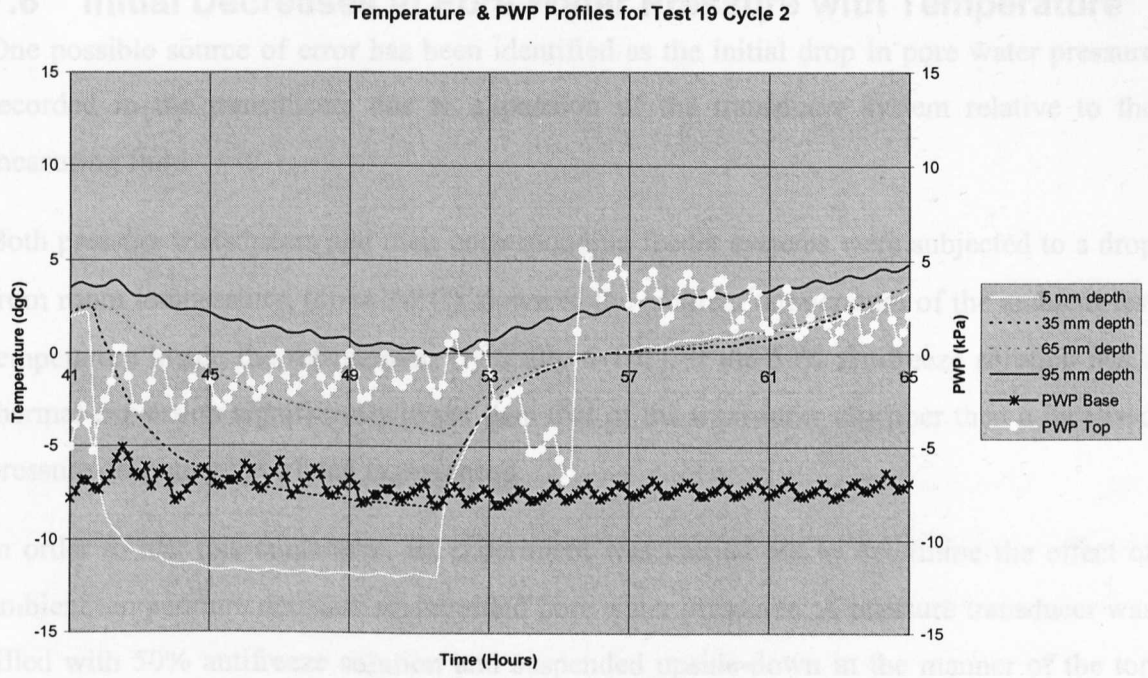

Figure 7.26 – Test 19 Cycle 2

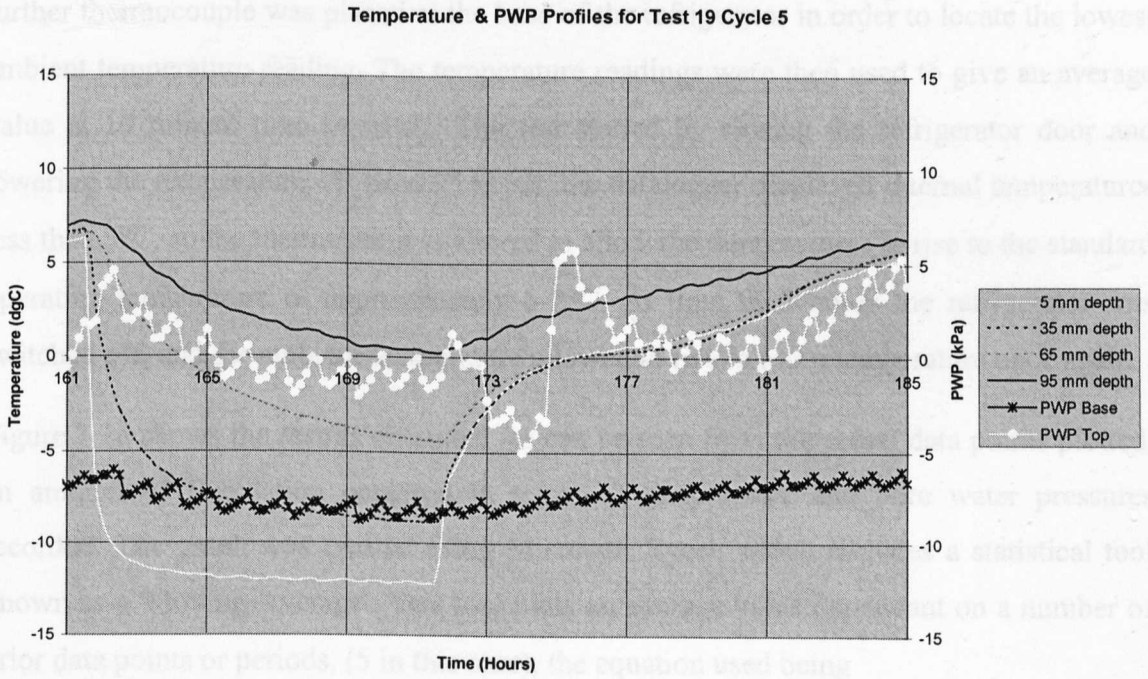

Figure 7.27 – Test 19 Cycle 5

7.6 Initial Decreases in Pore Water Pressure with Temperature

One possible source of error has been identified as the initial drop in pore water pressure recorded in the transducers due to expansion of the transducer system relative to the measuring fluid.

Both pressure transducers and their corresponding feeder systems were subjected to a drop from room temperature, (circa 20°C), down to the ambient temperature of the ambient test temperature inside the refrigerator, (typically 6-7°C). If the 50% antifreeze solution has a thermal expansion significantly lower than that of the transducer chamber then a localised pressure drop may have been experienced.

In order to test this conjecture, an experiment was carried out to determine the effect of ambient temperature decrease on recorded pore water pressures. A pressure transducer was filled with 50% antifreeze solution and suspended upside-down in the manner of the top transducer under test conditions. Four thermocouples were laid in a radial pattern on a pedestal inside the refrigerator where the permode is situated under test conditions. A further thermocouple was placed at the base of the refrigerator in order to locate the lowest ambient temperature reading. The temperature readings were then used to give an average value at 10 minute time intervals. The test started by closing the refrigerator door and lowering the temperature. At time 25 hours, the datalogger displayed internal temperatures less than 5°C, so the thermostat was altered to allow the temperatures to rise to the standard operating temperature of approximately 6-7°C. At time 90.5 hours the refrigerator was switched off, and the ambient temperature allowed to rise to room temperature once again.

Figure 7.28 shows the results obtained. As can be seen from the actual data points plotted, an amount of fluctuation occurred in terms of temperature and pore water pressures recorded. The graph was created using Microsoft Excel, which includes a statistical tool known as a 'Moving Average'. This tool plots an average value dependant on a number of prior data points or periods, (5 in this case), the equation used being

$$F_{(t+1)} = \frac{1}{N} \sum_{j=1}^{N} A_{t-j+1}$$

Equation 7.13 – Moving Average Calculation performed by Microsoft Excel

where

N is the number of prior periods to include in the moving average

Aj is the actual value at time j

Fj is the forecasted value at time j

The average values gained can be considered to form a smoothed line for analysis purposes. As the imposed ambient temperature drops from ~20°C to 4°C, the pore water pressure recorded drops from ~0 kPa to –16 kPa. At this point, the thermostat was altered to give the desired ambient temperature. A period of fluctuation follows, with the pore water pressure rising with the temperature. From time 25 hours to 90.5 hours, a steady state is achieved. After this period, the ambient temperature was allowed to rise to room temperature by shutting down the refrigerator and opening the door to atmosphere. Pore water pressure rises sharply, before roughly levelling out at ~2 kPa.

The time period of most interest is that from 25-90.5 hours. Figure 7.29 shows a plot of imposed ambient temperature against pore water pressure recorded for this time period only. The most common value, or 'mode', of average temperature achieved was 6.91°C. If all the paired data with temperature around this mode value is considered, the minimum value of pore water pressure recorded was –8.71 kPa. This minimum value could be considered the maximum discrepancy found when ambient temperature is at its desired level.

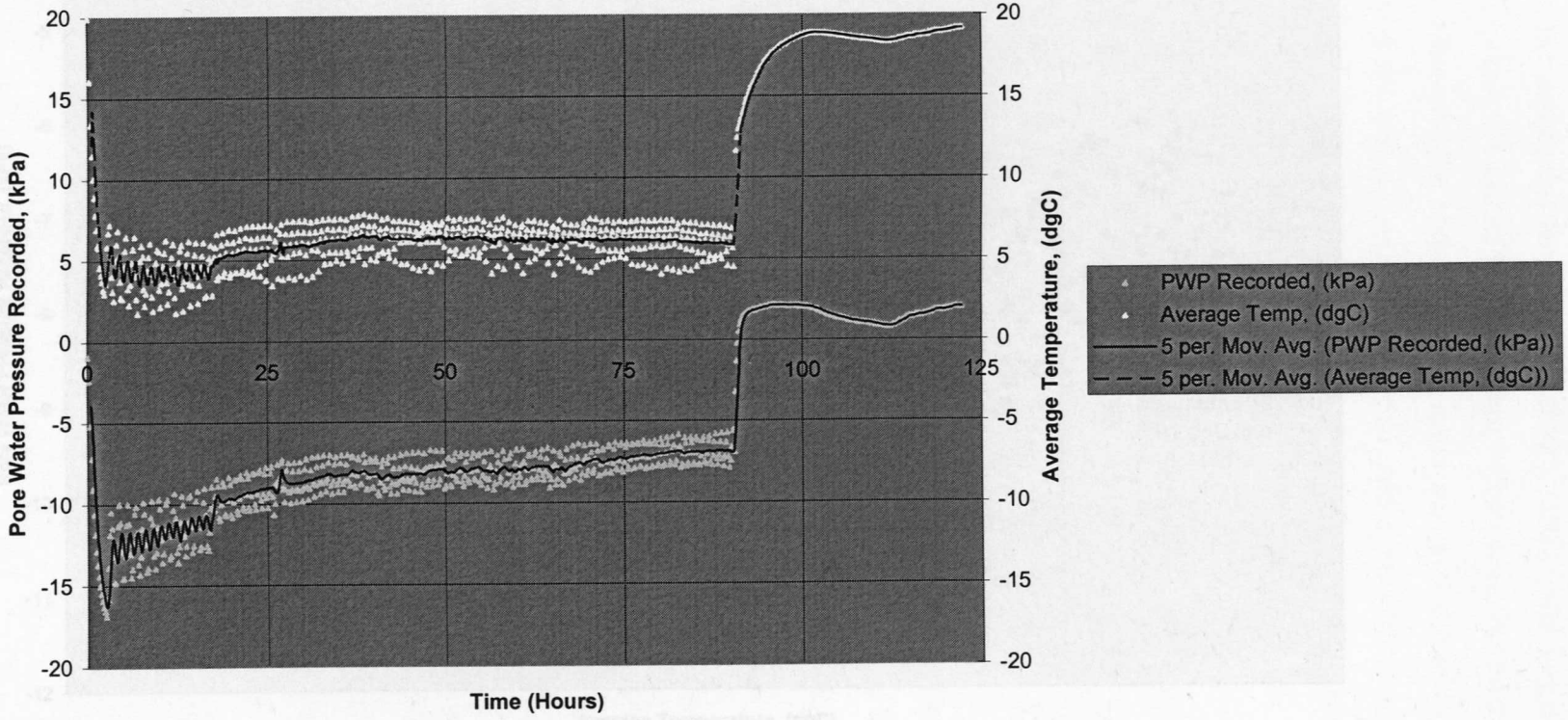

Figure 7.28 – Pressure Transducer Behaviour

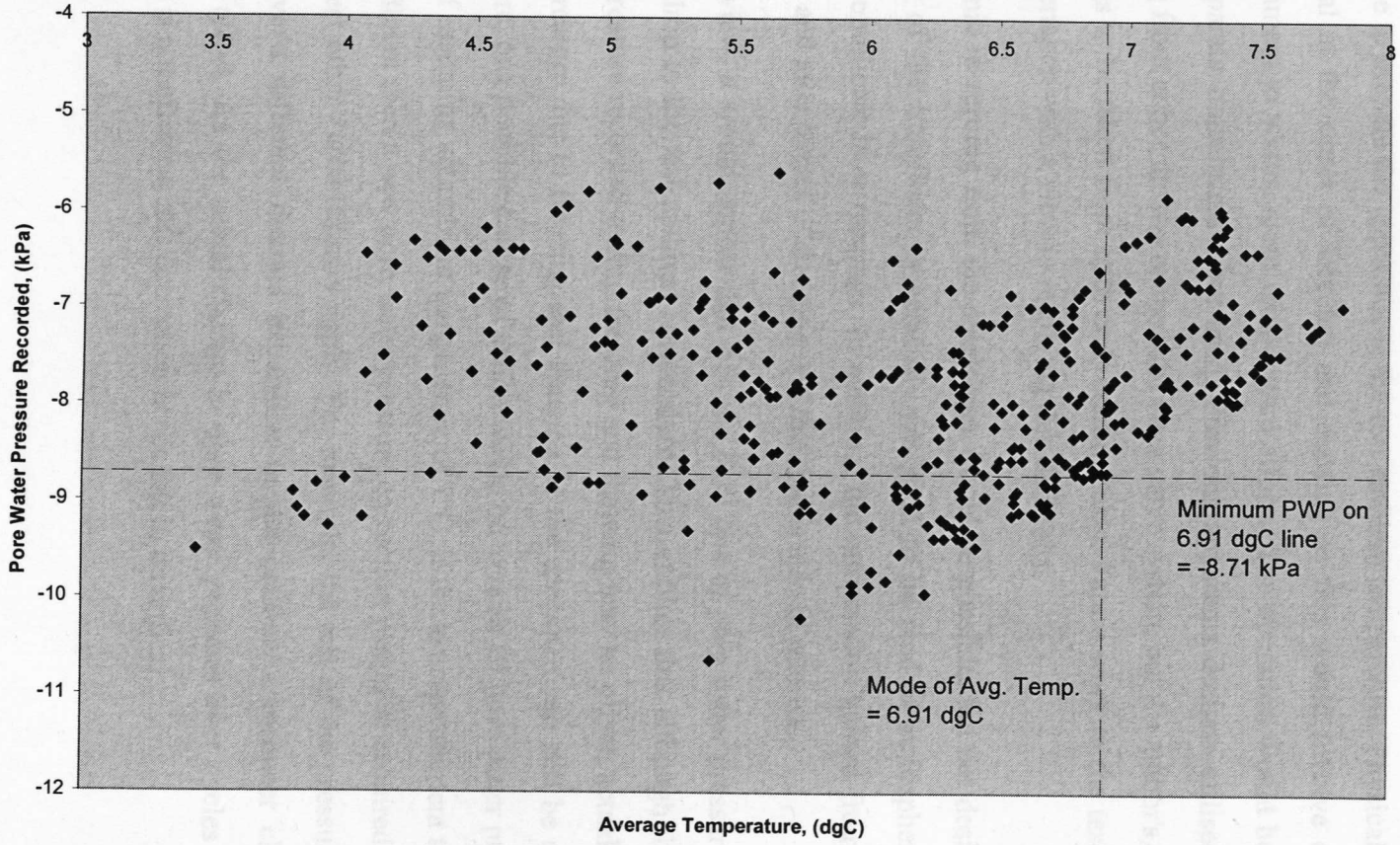

Figure 7.29 – Pressure Transducer Behaviour for Time Period 25 – 90.5 Hours

In the interest of preventing this problem, both Smith, (1972), and Roggensack, (1977), re-zeroed permode pressure systems to atmosphere before commencement of freezing and thawing cycles. However, the author's experimental set-up is substantially different. The permode apparatus sits within a refrigerator, rather than a dedicated cold room, so it is not possible to prepare the apparatus at the test ambient temperature. Physical re-zeroing is not practical at the onset of freezing and thawing as this would involve opening the cold environment to warm, room temperature effects. The operation would be complicated, as two separate transducers were used. Previous apparatus designs utilised one transducer reading from either the top or the base via a valve system, but the author's research required readings to be taken from both ends continuously. Future work to the test apparatus could be undertaken with a view to resolving this difficulty.

Electronic re-zeroing from the datalogger would be possible, but not desirable as the zero reading of the transducer is generally designed to be read at atmospheric pressure, and could complicate later readings. In addition, the information gained from the rest periods prior to and after cycles of freezing and thawing is also of interest.

In overview, it would appear that it is the *base line* of pore water pressure that is lowered by the drop to the test ambient temperature. This implies that although the values of pore water pressure recorded during freezing and thawing may be offset, actual *changes* in pore water pressure due to freezing and thawing of the specimen can still be considered valid. Therefore, one possible course of action would be to raise all pore water pressure values by 9 kPa, if assuming an ambient temperature of 7°C. If the average ambient temperature were very different then a new pore water pressure correction would be required. However, in an actual test other variables may apply. For example, the rest of the pressure feeder system may have a different thermal expansion to the pressure transducer chamber, causing another offset. As the actual change in pore water pressure over cycles of freezing and thawing is not affected, this correction is not felt to be critical.

7.7 Summary of Analyses

During the testing programme, it was observed that cycles of freezing and thawing acted to increase the pore water pressures in the specimens.

Larger values of increase in pore water pressure, $+\Delta u$, were typically obtained for the Weald Clay and Oxford Clay than the Lias Clay. This would suggest that as the shear strength, ϕ'_r, of the soil decreases, $+\Delta u$ increases. Examination of more soils of differing clay fraction, (related to ϕ'_r), would be required to further test this theory. The values of pore water pressure obtained were generally consistent with values suggested in the existing knowledge base.

Using the semi-infinite slope model, it was found a larger value of $+\Delta u$ was required to induce slope failure in the Lias Clay rather than the Weald Clay and Oxford Clay, for the same given value of angle of slope failure, β. A slightly higher value of $+\Delta u$ was required for failure at a given β in the Weald Clay than in the Oxford Clay. Of the three soils, the Lias Clay was determined to be most likely to fail in a planar slip mode, while the Weald Clay and Oxford Clay were considered to be more susceptible to liquefaction.

Leakage was experienced during the tests, but moisture migration and pore water pressure patterns were still detectable.

Frost heave was observed in all three soil types, although factors such as the closed test set-up, potential variation of initial degree of saturation, partial freezing of the specimen and leakage were all considered to have contributed to limiting the maximum heave achievable.

Zero curtain periods for the three soils were investigated, but the rate of freezing imposed did not allow a freezing curtain to develop. Of the thaw curtains, those of the Lias Clay were observed most clearly.

Initial decreases in pore water pressure as a result of the test set-up were considered, but were not judged to be critical in terms of actual changes in pore water pressure observed.

Chapter 8 – Conclusions

8.1 Increases in Pore Water Pressure due to Freezing and Thawing

Cycles of freezing and thawing served to increase pore water pressures.

Due to moisture migration towards the freezing front, pore water pressures were generally found to be greater at the top of the specimen rather than the base. This was generally due to the base freezing later than the top, (or in some cases not at all), so that free unfrozen water migrated upwards through the frozen fringe. However, the actual *increase* in pore water pressure could still be greater at the base than the top.

Greater increases in pore water pressure were observed in the Oxford Clay and Weald Clay than in the Lias Clay. The Oxford Clay and Weald Clay have higher plasticity indices and higher clay content than the Lias Clay. It would appear, therefore, that the pore water pressure response during freezing and thawing is related to the plasticity index and/or the clay content of the soil. However, this tentative conclusion requires further support in the shape of more permode tests on diverse soil types, and over a set range of moisture contents, as the permode tests so far have concentrated on comparing behaviour at similar plasticity.

8.2 Slope Failure Due to Increases in Pore Water Pressure

On the basis of the permode test results, two failure modes were suggested. Firstly, planar slip surfaces developed at a depth z below the ground surface, in accordance with the semi-infinite slope model. Secondly, a downslope 'flow' situation caused by the geostatic condition being developed.

Using semi-infinite slope analysis, the predicted angle of slope failure, β, was reduced significantly by relatively low increases in pore water pressure. This could be seen for all three soil types. Slopes in the Weald Clay and Oxford Clay were found to be liable to fail at lower values of β than the Lias Clay due to the effect of having lower values of ϕ'_r and greater increases in pore water pressure.

The Weald Clay and Oxford Clay showed a tendency towards liquefaction taking place. This was due to the high values of excess pore water pressure generated and water migration towards the freezing front, (liquefaction did not occur in any of the tests on Lias Clay). This fluidisation is considered to be similar to the viscous flow, thaw strain behaviour observed by Harris *et al.*, (1995); Harris & Davies, (1998), but was not investigated in this research.

The permode test results can be interpreted as supporting the suggestion made by Harris *et al.*, (1995), that thawing soil displayed both viscous and frictional properties.

8.3 Patterns of Moisture Migration

The moisture contents determined at the end of each test tended to be higher at the top of the specimen than at the base, as expected with moisture migration towards a frozen front in a closed system. Water migrated towards the 0°C isotherm due freezing point depression. The soil water contained impurities, giving it a lower Gibbs free energy than pure water. For ice to be formed from this solution a lower free energy was also needed. The frozen fringe exists at state of lower free energy, and so the soil water migrated upwards through the 0°C isotherm, becoming frozen in its turn.

This moisture migration resulted in greater pore water pressures being measured at the top of the specimens than at the base.

Greater moisture migration was found in the Weald Clay and Oxford Clay than in the Lias Clay. This was not expected as the clay-rich soils had lower permeability which could restrict migration of water. However, Chamberlain & Gow, (1979), found that freeze-thaw cycles caused structural changes leading to increased permeability. Similar behaviour may have been experienced in the permode tests, although the Chamberlain & Gow tests were carried out drained.

Returning to the permode tests, another factor to consider is initial moisture content. In order to test the soils at a baseline consistency, the initial moisture contents were higher for the Weald Clay and Oxford Clay than for the Lias Clay. Further testing, at a greater range of initial moisture contents, would therefore prove beneficial.

8.4 Frost Heave

Frost Heave was observed in all the permode tests. The Weald Clay appeared to experience most heave, followed by the Lias Clay and Oxford Clay.

As noted above, the decision was taken to test the three soils at comparable consistency rather than comparable moisture contents. This means that the Weald and Oxford Clays had a greater inherent ability to heave compared to the Lias Clay.

Prediction of frost heave in closed systems showed that even for small amounts of leakage and/or lowered initial saturation there could be a large reduction in potential heave heights. Also, for a specimen that did not freeze completely, a reduced *pro rata* frost heave value can be determined.

The limitations of the closed system for frost heave became apparent during the tests. Ice lense formation was not observed. However, specimens removed still frozen from the permode were noted to contain ice crystal structures, thus showing the possibility of heave at the micro-scale level.

Consideration of the progression of the 0°C isotherm showed that in the Lias Clay heave did not start until the 0°C isotherm reached a depth of 6-8 mm. In the Weald Clay and Oxford Clay heave started from the onset of freezing, but with the heave following a convex curve pattern rather than the slope increase observed in the Lias Clay, which was therefore heaving at a faster rate than the Weald Clay or Oxford Clay, albeit taking longer to achieve full heave due its slower start.

For the Lias Clay, it is suggested that water was not being attracted towards the frozen fringe in sufficient quantities to demonstrate heave initially. This could be due to there being less water available, demonstrating the incentive for testing at higher moisture content and under drained conditions.

8.5 Zero Curtain Behaviour

The mode of testing did not allow a significant freezing zero curtain to develop. A recognisable thawing zero curtain was developed, however. The most distinct changes in pore water pressure with temperature occurred in the silty Lias Clay.

8.6 The Efficiency of the Test Methodology

8.6.1 Validity of the Test Set-Up

Consideration of the test set-up in Chapter 3 found that for cyclical freezing modelled on an annual pattern, the consolidation parameter t_{90} showed the decision not to allow drainage to be acceptable for all three soil types under one-way drainage, and under two-way drainage for Weald Clay and Oxford Clay, and for Lias Clay under high values of applied pressure.

In Chapter 7, investigation using the thaw-consolidation ratio, R, (with values of c_v presented in Chapter 3), showed that comparably high values of r_u could be determined for the Weald Clay and Oxford Clay as from the permode test results, indicating liquefaction as the failure mode. However, the values of r_u for Lias Clay were lower than those found from the permode tests. The rate of thaw in the laboratory was far faster than in the field, as suggested by the rate of thaw put forward by Skempton & Weeks, (1976), of 2 m in 3 months for Weald Clay. In their case c_v was taken as 2.5 m^2/year, R was found as 1.3 and hence r_u was 0.89. For the permode Weald Clay tests, c_v was taken as 0.61 m^2/year, R found as 1.73 and r_u as 0.98. Therefore, if this rate of thaw was used for the permode tests, the following results are gained:

Table 8.1 – Comparison of Rates of Thaw, (using Equations 2.1 & 2.2 and Figure 7.2)

	R (Test Thaw Rate)	**r_u**	**R** (Assumed Thaw Rate)	**r_u**
Lias Clay	0.54	0.42	0.80	0.60
Weald Clay	1.73	0.98	2.56	1.00
Oxford Clay	2.22	>1.00	3.29	1.00

For Lias Clay, the value of r_u at 0.60 for the Skempton & Weeks, (1976), assumed thaw rate is comparable to the values gained from the permode tests. For the Weald Clay and Oxford Clay the values of R are so large that r_u tends to unity in the Morgenstern & Nixon, (1971), model depicted in Figure 7.2. This is in keeping with fluidisation being more likely to occur in these more plastic soils. However, in the permode tests a wider range of r_u values were recorded. This range demonstrated failures at slope angle β rather than simply through liquefaction, (see Chapter 6), in keeping with the findings of Skempton & Weeks, (1976).

It would appear that the rate of thaw used in the permode tests provides low values of R and hence r_u. Therefore, longer cycles might be considered for future testing. In addition, as the consolidation procedure was carried out independently of the permode test, there may be some scope for inaccuracy in the determination of c_v. However, in general, the permode test yield values of r_u comparable to those found through other methods.

8.6.2 Prevention of Leakage

The potentially most serious problem encountered during the test programme was leakage. Chapter 3, Sections 3.2.4.1 and 3.2.5.1 detailed the original difficulties experienced, and the measures taken to overcome them. These alterations were all in place by the start of Test 14. Their eventual efficiency in overcoming leakage was examined in Chapter 6, Section 6.3 and Chapter 7, Section 7.3.2.

Leakage was not fully eliminated, and so the tests cannot be considered as completely 'closed' or 'un-drained' as intended. However, despite this, the action of moisture migration and patterns of pore water pressure were still generally observable.

In the interests of optimising the test apparatus, further measures against leakage are outlined in Chapter 9, Section 9.1.5.

8.6.3 Initial Drop in Pore Water Pressure with Temperature

This phenomenon has been investigated and discussed in Chapter 7, Section 7.6. The initial drop in pore water pressure due to the decrease in ambient temperature was not felt to be significant for the tests carried out as the *change* in pore water pressure was critical, not the absolute value. However, the irregularity could be avoided by having a full cold-room assembly, with less temperature differentials. This solution would be costly, and highly dependant on space and services available. It is discussed further in Chapter 9, Section 9.1.3.

8.6.4 Direction of Thaw

The permode test results demonstrated that the direction of thaw of the frozen specimens was not fully one-directional due to insulation difficulties. This is an aspect of the permode construction that requires further work.

8.6.5 Overall Performance of the Apparatus

In overview, the test apparatus gave an adequate level of performance for the tests carried out. However, various refinements were identified as a result of Tests 14-28, and are detailed in Chapter 9, Section 9.1. Such modifications would optimise the performance of the apparatus in the current style of tests, and could also increase the range of activities that could be carried out.

8.7 Implications for Theory and Practice

Reference to the existing knowledge base supported the use of the semi-infinite slope model, and contributed to the validation of the permode test as a method of investigating the effects of freeze-thaw cycles on slope stability.

The angle of slope failure, β, was found to be significantly reduced from its predicted value as a result of cyclic freeze-thaw activity. The range of β values gained from the permode tests compared well with those found in the field for clayey soils.

A possible application of permode testing would be to use soil taken from a known depth below ground surface, and apply the test regime. The increase in pore water pressure achieved could then be input into a semi-infinite slope analysis, together with other known parameters, to obtain β. Alternatively, the existing slope angle could be used in order to find the factor of safety against sliding.

Further research is needed in order to determine how the pore water pressure response is affected by varying soil properties, test parameters and stress history. It can be seen that the generation of additional pore water pressure and corresponding decrease in residual effective strength have considerable implications for the stability of slopes previously exposed to periglacial conditions.

Chapter 9 – Scope for Further Work

9.1 Scope for Further Modifications to the Apparatus

Much useful information concerning the permode construction was gained during a visit to the Department of Geotechnical Engineering, University of Alberta, Canada, in June 1998. By that time the Warwick permode had been constructed and was in use, so it was not possible to implement all improvements noted.

9.1.1 Upgrading of Temperature Sensors

The Type K thermocouples used at Warwick were selected as they were judged to have the following advantages:

- Simple to use, interfacing well with the datalogger.
- Low cost.
- Durability.
- Wide operating temperature range.

Thermocouples are not the most accurate of temperature measuring devices, with a possible error of 0.0075 x T, where T is the measured temperature (RS Data Sheet 229-7559, 1996), but at sufficient accuracy for the tests carried out at Warwick. Type K thermocouples experience error at high temperature, outside the remit of the testing programme.

The disadvantages of using thermocouples in the testing programme were of a physical nature. It proved difficult at first to thread the thermocouples through the side walls without causing leakage, although this was largely remedied by using soft rubber washers to clamp the thermocouple points in place. Another problem encountered was the occasional thermocouple point pushing through the side wall and rupturing the membrane. While these problems were overcome by due care and attention, it would be more useful to improve the sensor make-up with regards to standardisation. One possible solution would be to have thermocouple points or patches permanently embedded flush with the side wall, and an intermediate junction to the datalogger. However, the thermocouple points/patches could still offer resistance to sample and membrane movement, and be difficult to replace if damaged.

At the University of Alberta, Platinum Thin Film Resistance Temperature Detectors, (RTDs) are used. The RTDs measure temperature in terms of change of resistance. Platinum is most commonly used as the conductor as it displays a stable and approximately linear temperature change with change of resistance. This linearity of response affords a greater accuracy than the thermocouples. The 'Thin Film' aspect refers to the platinum being deposited as a film and then encapsulated in ceramic, producing a small, (e.g. 4 mm x 4 mm), flat sensor. This sensor could then be recessed into the wall, leaving no path for leakage. The recessing technique could also allow for replacement. RTDs tend to be more expensive, in the region of £10-15 pounds each, rather than £5 for 4 in the case of thermocouples. However, the cost is not excessively high. As the current datalogger requires voltage input, some additional circuitry might be required to enter the resistance values gained. Thermocouples interface directly with the current datalogger, and therefore maintain this advantage over the RTDs.

In overview, the cost of replacing the thermocouples with RTDs is not prohibitive, but other factors should be considered. A recessed system of 'plug-in' sensors would be most attractive in terms of standardising the set-up and reducing time and effort. The increased accuracy would also be useful if temperatures were required to be tracked in more detail. Finally, provision would have to be made for interfacing with the data acquisition system employed.

9.1.2 Increased Number and Optimisation of Temperature Sensors

During the testing programme, thermocouples were only placed at 4 points down the barrel line. In addition, the top thermocouple point was situated at 5 mm down from the initial top of specimen. Therefore, at greater than 5 mm of downwards displacement this sensor was not in contact with the specimen. An increased number of sensors could be used in order to give a more detailed profile of temperature, (at different depths), with time.

The positioning of the sensors could also be improved. For example, a sensor could be embedded within the piston, so that a reading would always be taken at the top of the specimen irrespective of displacement. This would, however, require a modified piston and specially shaped porous disc to be manufactured. The side wall sensors could be spread around the barrel, thus measuring a more representative sample of the specimen.

9.1.3 Provision of Large-Scale Controlled Temperature Environment

At the University of Alberta, test laboratories are kept at low temperatures, (sometimes down to -20°C), by the user of compressor refrigeration pumps. This is certainly an ideal test environment, but one which clearly depends on the availability of dedicated space. Apart from temperature stabilisation during the test itself, advantages are also afforded in terms of sample preparation. Once specimens have been either sampled or remoulded they could be kept in a freezer until ready for use. Then, still within a cold area, the specimens could be saw-cut and then trimmed using a lathe to achieve the exact shape required (Roggensack, 1977).

The primary advantage of having a cold room, (instead of or together with a cold chamber), would be the reduction of temperature differentials experienced by the specimen and apparatus. During the tests at Warwick, specimens were subject to surface thawing when being emplaced in the permode for testing. This led to the possibility of pore water pressures being built up prior to the main test. Also the pressure transducers were found to experience expansion on drop of ambient temperature, (see Chapter 5, Section 5.5.3. and Chapter 6, Section 6.2.4.2), which would be avoided if the apparatus could be assembled closer to the testing temperature.

9.1.4 Upgrading of Pressure Transducers

The pressure transducers used in the test programme were certainly adequate, but consideration should be given to newer models, in order to compare accuracy levels. The pressure measurement path could be improved, with a de-airing block fixed to the top as well as the base transducer.

9.1.5 Optimisation of Permode Cell Construction

The split cylinder version of the PTFE liner was not found to be practicable for the Warwick permode due to leakage. However, the split cylinder is still used at the University of Alberta without difficulty, due to the use of longitudinal o-rings between the two halves of the liner. This area requires closer examination, as it is would be necessary to machine PTFE precisely to accommodate the o-rings and form a complete seal.

One other detail of construction seen at the University of Alberta concerned attachment of the membrane to the base and piston. The membrane was of a size large enough to act as

an inner sleeve to the liner. It was attached to the base and also the piston, with o-rings over the top. This meant that the piston and upstanding portion of the base must have been of slightly smaller diameter than previously understood. In the event of a new permode being constructed this approach could be attempted.

9.1.6 Development of an Integrated Data-Logging and Post-Processing System

The Orion 3531 D datalogger used for the test programme had 3 output devices – a disk drive, print roll and RS-232 PC interface. During the testing programme, the main output device used was the disk drive, with less frequent readings being sent to the print roll as a back-up device. The PC used during the test programme was not adjacent to the datalogger and therefore the RS-232 interface was not convenient. An interfaced PC could have allowed faster processing of results, perhaps with some automatic post-processing, or graphic display allowing real-time observation and decision-making. The time advantages gained result from reducing the number of stages required to disseminate the required information from the .dat files.

Dedicated hardware and software packages are available for turning a PC into a datalogger by the use of Analogue-To-Digital conversion boards or data acquisition boards through RS-232 port. With the relevant software installed, data can be collected and manipulated as required. Having a PC as a datalogger would be particularly useful if it were to form part of a dedicated laboratory suite. However, the Orion datalogger is highly reliable and easy to use. Also, the accuracy of readings taken is clearly of far greater importance than convenience. The Orion offers high accuracy as well as being robust. A PC Windows system would be less stable in terms of hardware and software crashes. Also, initial inquiries suggested that the system would have a slower response time from the instrumentation, (i.e. time required to take readings), than purpose-built datalogging systems, but this aspect would have to investigated further.

A lower-cost/high-reliability solution would be to retain the current data acquisition system and pay more attention to post-processing. For example, the reading of the .dat file and subsequent data analysis could be attempted via Microsoft Excel using a Visual Basic program.

9.2 Scope for Further Research

The permode tests apparatus and procedure can be adapted and extended to consider further research topics. Some possibilities are outlined below.

9.2.1 Investigation of Different Soil Types

More permode tests on varied soil types are required. The results of these tests could then be used to further investigate the relationship between plasticity, clay fraction and $+\Delta u$ generated during cycles of freezing and thawing.

9.2.2 Investigation of Moisture Migration and Frost Heave

The varying patterns of moisture migration shown by the three soil types require further investigation. As observed from the permode test results, the Weald Clay and Oxford Clay experienced greater moisture migration and frost heave than the Lias Clay. As the Lias Clay is silty and more permeable than the other soils, this was not initially expected. Permeability tests could be carried out using the permode and similar procedure to Chamberlain & Gow, (1979), who observed increases in permeability due to structural change during cycles of freeze-thaw. Alternatively, the effect of initial moisture content on migration could also be considered, by establishing a baseline for permode tests of moisture content rather than consistency.

The use of open system freezing would allow potential for continuous uptake of water by the specimen and expulsion during freezing and thawing. This would enable the growth of ice lenses and subsequently greater heave. Tests could be stopped during a freezing stage and the specimen examined to determine the extent of the lenses. This would require a dedicated cold room facility, split liner permode and cutting equipment for producing sections of the specimen.

9.2.3 Introduction of a Freezing Zero Curtain

The timeframe of freezing does not allow a significant zero curtain period to occur. Lengthening the freezing stage could rectify this.

The test timescale could be further altered to give longer periods of freezing and thawing, and perhaps with varying rates of freezing. This would introduce an additional test parameter.

9.2.4 Investigation of Drained tests and In-Cell Consolidation

Drained tests could be carried out in order to examine permeability, as carried out by Chamberlain & Gow, (1979). The change in permeability during permode tests could be related to potential for moisture migration, frost heave and generation of $+\Delta u$.

Another application of drained tests would be investigation of shut-off pressure, P_o, as defined by Arvidson & Morgenstern, (1977). If the value of P_o were known for a soil type, then a limiting applied pressure for moisture migration towards the freezing front could be established. In turn, this would mean that a limiting value of depth z could be determined, as the generation of $+\Delta u$ is at least partly due to the amount of moisture migration taking place.

Thaw consolidation of British soils could be examined using the permode in order to conduct similar experiments to Smith, (1972), i.e. considering consolidation over consecutive freeze-thaw cycles. The permode would therefore be used for its original purpose, with in-cell consolidation taking place.

9.2.5 Investigation of Varying Levels of Saturation

Tests 1-13 were carried out at unknown degrees of saturation, while Tests 14-28 were carried out at as near complete saturation as possible. Analysis in Chapter 7 demonstrated the sensitivity of frost heave to even small variations in degree of saturation. If the test specimens were to be consolidated within the permode, as per Smith, (1972), then control over the final degree of saturation could be exerted, providing an additional test parameter.

9.2.6 Consideration of Varying Modes of Slope Failure

The mode of slope failure considered in most detail has been that of slippage along shear surfaces parallel to the ground surface, using the semi-infinite slope model. The viscous, thaw-strain behaviour observed by Harris *et al.*, (1995); Harris & Davies, (1998), was mentioned in connection with flow failures in the Weald Clay and Oxford Clay, but not covered extensively. Harris *et al.*, (1995), suggested that thawing soils probably displayed both viscous and frictional properties. Further permode research, in conjunction with other freeze-thaw testing methods, could allow more insight into the relative importance of each set of properties.

An alternative mode of failure has recently been suggested by Petley & Hutchinson, (2001). It involves retrogressive circular failures along a slope, as shown in Figure 9.1 below:

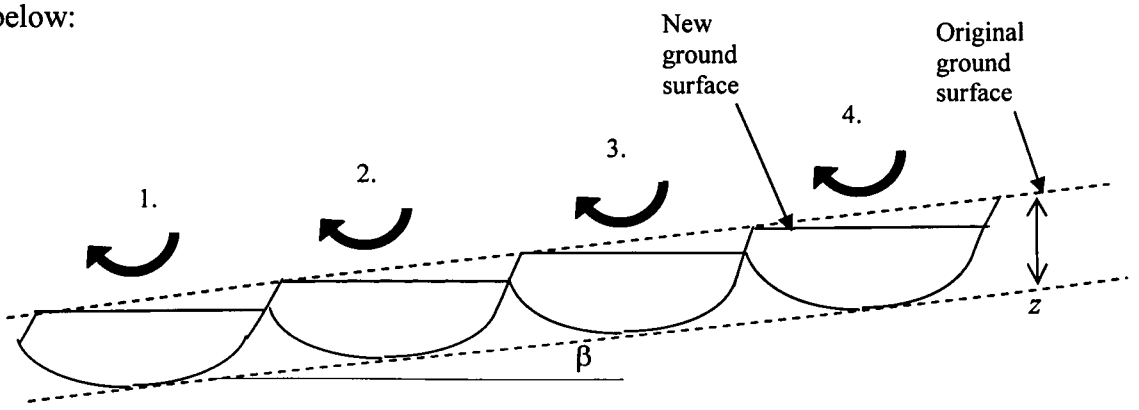

Figure 9.1 – Retrogressive Slope Failure, after Petley & Hutchinson, (2001)

This model represents the 'hummock' pattern of ground often seen in landslide areas, which is not compatible with the concept of parallel slippage (Petley & Hutchinson, 2000). The circular slip surfaces are considered to be tangential to a common depth below the ground surface. If this depth is taken to be z, then a limiting condition between whether the soil will fail along a parallel plane at depth z, or in a retrogressive series of circular slips. If τ developed along the circular surface at the toe of the slope is termed τ_c, and τ developed along the planar surface is at the toe of the slope is termed τ_p, then if $\tau_c > \tau_p$, the circular slip surface is the critical mode of failure.

The development of the retrogressive circular slip surfaces is still under investigation by Petley & Hutchinson, (2001). At present, the concept is of interest in providing an additional mode of failure for periglacially-affected soils, which could be of importance in the future.

References

Andersland, O.B., 1987. Frozen Ground Engineering. Ground Engineering Reference Book, ed. F.G. Bell, Butterworth, 8/1-8/24.

Arvidson, W.D. & Morgenstern, N.R., 1977. Water Flow Induced By Soil Freezing. Can. Geotech. J., 14, 237-245.

Atkinson, T.C., Briffa, K.R. & Coope, G.R., 1987. Seasonal Temperatures in Britain During the Past 22,000 Years, Reconstructed Using Beetle Remains. Nature, 325, 587-592.

Ballantyne, C.K. & Harris, C., 1994. The Periglaciation of Great Britain. Cambridge University Press, Cambridge, 113-140.

Benson, H., 1991. University Physics, John Wiley & Sons Inc.

Biczysko, S.J., 1976. East Midlands Jurassic Soils. Journal of the Institution of Highway Engineers, Nov., 21-32.

Biczysko, S.J., 1981. Relic Landslip in West Northamptonshire. Q. J. Eng. Geol., 14, 169-174.

Biczysko, S.J. & Starzewski, K., 1977a. Daventry Bypass Landslip - A Lesson for Road Engineers. Ground Engineering, Jan., 23-25.

Biczysko, S.J. & Starzewski, K., 1977b. Response to Chandler, R.J., 1977. Letter to Editor: Daventry Bypass Landslip. Ground Engineering, April, 8.

Bishop, A.W., Green, G.E., Garga, V.K., Andresen, A. & Brown, J.D., 1971. A New Ring Shear Apparatus and its Application to the Measurement of Residual Strength. Geotechnique, 21, 273-328.

Blyth, F.G.H. & De Freitas, M.H., 1984. A Geology for Engineers. Arnold, London.

Bowders, J.J. & McClelland, S., 1994. The Effects of Freeze/Thaw Cycles on the Permeability of Three Compacted Soils. Hydraulic Conductivity and Waste Contaminant Transport in Soil, ASTM STP 1142, Daniel, D.E. & Trautwein, S. (eds.), American Society for Testing and Materials, Philadelphia, 1994, 461-481.

Bowen, D.Q., Rose, J., McCabe, A.M. & Sutherland, D.G., 1986. Correlation of Quaternary Glaciations in England, Ireland, Scotland & Wales. Quaternary Science Reviews, 5, 299-340.

BS 1377: Part 2: 1990. British Standard Methods of tests for soils for Civil Engineering Purposes - Part 2 Classification Tests. BSI, London.

BS 1377: Part 7: 1990. British Standard Methods of tests for soils for Civil Engineering Purposes - Part 7 Shear Strength Tests (Total Stress). BSI, London.

BS 5930: Part 8: 1981. Code of Practice for Site Investigations. BSI, London.

Burt, T.P. & Williams, P.J., 1976. Hydraulic Conductivity in Frozen Soils. Earth Surface Processes, 1, 3, 349-60)

Chamberlain, E.J. & Blouin, S.E., 1977. Frost Action as a Factor in Enhancement of the Drainage and Consolidation of Fine-Grained Dredged Material. U.S. Army Eng. Waterw. Exp. Stn. Dredged Mater. Res. Program, Tech. Rep. D-77-16.

Chamberlain, E.J. & Gow, A.J., 1979. Effect of Freezing and Thawing on the Permeability and Structure of Soils. Engrg. Geology, 13, 73-92.

Chandler, R.J., 1970a. The Degradation of Lias Clay Slopes in an Area of the East Midlands. Q. Jl. Engng. Geol, 2, 161-181.

Chandler, R.J., 1970b. Solifluction on Low-Angled Slopes in Northamptonshire. Q.Jl. Engng. Geol., 3, 65-69.

Chandler, R.J., 1972. Periglacial Mudslides in Vestpitsbergen and Their Bearing on the Origin of Fossil 'Solifluction' Shears in Low Angled Clay Slopes. Q. Jl. Engng. Geol., 5, 223-242.

Chandler, R.J., 1977. Letter to Editor: Daventry Bypass Landslip. Ground Engineering, April, 6-7.

Chandler, R.J. & Skempton, A.W., 1974. Lias Clay – The Long Term Stability of Cutting Slopes. Geotechnique, 24, 21-38.

French, H.M., 1996. The Periglacial Environment, (2e), Longman, Harlow.

Gallop, M.C., 1991. Quaternary Slope Processes in South West England: Integrated Field and Laboratory Studies. Ph.D. Thesis, University of Wales, Cardiff.

Graham, J. & Au, V.C.S., 1985. Effects of Freeze-Thaw and Softening on A Natural Clay At Low Stresses. Can. Geotech. J., 22, 69-78.

Harris, C., 1987. Solifluction and Related periglacail Deposits in England and Wales. Periglacial Processes and Landforms in Britain and Ireland, Boardman, J., (ed.), Cambridge University Press, Cambridge.

Harris, C., 1996. Physical Modelling of Periglacial Solifluction: Review and Future Strategy. Permafrost and Periglacial Processes, 7, 349-360.

Harris, C. & Davies, M.C.R., 1996. Processes of Thaw-Induced Mass Movement in Non-Cohesive Soils: Results of an Instrumented Slope Simulation Experiment. Advances in Hillslope Processes, eds. Anderson, M.G. & Brooks, S.M., John Wiley & Sons Ltd., Vol. 2, 1153-1171.

Harris, C. & Davies, M.C.R., 1998. Pressures Recorded During Laboratory Freezing and Thawing of A Natural Silt-Rich Soil. Proceedings, Permafrost: 7th International Conference, Yellowknife, Canada, June 23-27, 433-439.

Harris, C., Davies, M.C.R. & Coutard, J-P, 1995. Laboratory Simulation of Periglacial Solifluction: Significance of Porewater Pressures, Moisture Contents and Undrained Shear Strengths During Soil Thawing. Permafrost and Periglacial Processes, 6, 293-311.

Harris, C., Davies, M.C.R. & Coutard, J-P., 1997. Rates and Processes of Periglacial Solifluction: An Experimental Approach. Earth Surface Processes and Landforms, 22, 849-868.

Harris, C., Davies, M.C.R. & Rea, B., 2000. Geotechnical Centrifuge Modelling of Mass Movement Processes Associated with Thawing Permafrost Soils. Landslides in Research, Theory and Practice, Bromhead, E., Dixon, W. & Ibsen, M-L. (eds), Thomas Telford, London, 2, 693-700.

Harris, C. & Lewkowicz, A.G., 1993. Form and Internal Structure of Active-Layer Detachment Slides, Fosheim Peninsula, Ellesmere Island, Northwest Territories, Canada. Can. J. Earth Sci., 30, 1708-1714.

Harris, S.A., French, H.M., Heginbottom, J.A., Johnston, G.H., Ladanyi, B., Sego, D.C. & van Everdingen, R.O., 1988. Glossary of Permafrost and Related Ground-Ice Terms. National Research Council of Canada Technical Memorandum 142, Ottawa, 156pp.

Hawkins, A.B. & Privett, K.D., 1986. Residual Strength: Does BS 5930 Help or Hinder? Geological Society, Engineering Geology Special Publication No. 2, 279-282.

Head, K.H., 1992. Manual of Soil Laboratory Testing, Vol. 1, Soil Classification and Compaction Tests (2nd ed.). Pentech Press Ltd., London.

Higginbottom, I.E. & Fookes, P.G., 1971. Engineering Aspects of Periglacial Features in Britain. Q. Jl. Engng. Geol., 3, 85-117.

Hutchinson, J.N., 1967. The Free Degradation of London Clay Cliffs. Proc. Geot. Conf. Oslo, Vol. 1, 113-118.

Hutchinson, J.N., 1974. Periglacial Solifluxion: An Approximate Mechanism for Clayey Soils. Geotechnique, 24, 443.

Hutchinson, J.N., 1991. Periglacial and Slope Processes, Quaternary Engineering Geology. Geol. Soc. Engng. Geol. Special Publication No. 7, 283-331.

Ingold, T.S., 1975. The Stability of Highways in Landslipped Areas. The Highway Engineer, May, 14-22.

Jones, P.F. & Derbyshire, E., 1983. Late Pleistocene Periglacial Degradation of Lowland Britain: Implications for Civil Engineering. Q. Jl. Engng. Geol., 16, 197-211.

Konrad, J.M. & Morgenstern, N.R., 1982. Prediction of Frost Heave in the Laboratory During Transient Freezing. Can. Geotech. J., 19, 250-259.

Lewkowicz, A.G., 1990. Morphology, Frequency and Magnitude of Active-Layer Detachment Slides, Fosheim Peninsula, Ellesmere Island, NWT. Proceedings of the 5th Canadian Permafrost Conference, eds. Burgess, M.M., Harry, D.G. & Sego, D.C., 111-118, Quebec: Universite Laval.

Lupini, J.F., Skinner, A.E. & Vaughan, P.R., 1981. The Drained Residual Strength of Cohesive Soils. Geotechnique 41, No. 2, 181-213.

Mageau, D. & Morgenstern, N.R., 1979. Observations on Moisture Migration in Frozen Soils. Can. Geotech. J., 17, 54-60.

McRoberts, E.C. & Morgenstern, N.R., 1974. The Stability of Thawing Slopes. Can. Geotech. J., 11, 447-469.

McRoberts, E.C. & Morgenstern, N.R., 1975. Pore Water Expulsion During Freezing. Can. Geotech. J., 12, 130-141.

McRoberts, E.C., 1973. Stability of Slopes in Permafrost. Ph.D. Thesis, University of Alberta, Edmonton.

Miller, R.D., 1980. Freezing Phenomena in Soils. Applications of Soil Physics, Hillel, R., (ed.), Academy Press, New York.

Morgenstern, N.R. & Nixon, J.F., 1971. One-Dimensional Consolidation of Thawing Soils. Can. Geotech. J., 8, 558-565

Morgenstern, N.R. & Smith, L.B., 1973. Thaw-Consolidation Tests on Remoulded Clays. Can. Geotech. J., 10, 25-40.

Nixon, J.F., 1973. The Consolidation of Thawing Soils. Ph.D. Thesis, University of Alberta, Edmonton.

Nixon, J.F. & McRoberts, E.C., 1973. A Study of Some of the Factors Affecting the Thawing of Frozen Soils. Can. Geotech. J., 10, 439-452.

Nixon, J.F. & Morgenstern, N.R., 1973a. Practical Extensions to A Theory of Consolidation for Thawing Soils. Proceedings, Permafrost: Second International Conference, Yakutsk, U.S.S.R., 369-377.

Nixon, J.F. & Morgenstern, N.R., 1973b. The Residual Stress in Thawing Soils. Can. Geotech. J., 10, 571-580.

Ono, T., & Mitachi, T., 1997. Computer Controlled Triaxial Freeze-Thaw-Shear Apparatus. Ground Freezing 97, Knutsson (ed.), Balkema, Rotterdam. 335-339.

Othman, M.A., Benson, C.H., Chamberlain, E.J. & Zimmie, T.F., 1994. Laboratory Testing to Evaluate Changes in Hydraulic Conductivity of Compacted Clays Caused By Freeze-Thaw: State-of-the-Art. Hydraulic Conductivity and Waste Contaminant Transport in Soil, ASTM STP 1142, Daniel, D.E. & Trautwein, S. (eds.), American Society for Testing and Materials, Philadelphia, 1994, 227-254.

Parks, C.D., 1991. A Review of the Possible Mechanisms of Cambering and Valley Bulging. Quaternary Engineering Geology. Geol. Soc. Engng. Geol. Special Publication No. 7, 373-380.

Penn, S., Royce, C.J. & Evans,C.J., 1983. The Periglacial Modification of the Lincoln Scarp. Q. Jl. Engng. Geol., 16, 309-318.

Petley, D.J. & Hutchinson, J.N., 2001. Personal communication.

Ray, M.S., 1988. Engineering Experimentation: Ideas, Techniques and Presentation. McGraw-Hill, London.

Roggensack, W.D., 1977. Geotechnical Properties of Fine-Grained Permafrost Soils. Ph.D. Thesis, University of Alberta, Edmonton.

Rowe, P.W. & Barden, L. 1966. A New Consolidation Cell. Geotechnique, 16, 162-170.

RS Data Sheet 229-7559, 1996. Thermocouples. RS Components U.K..

Skempton, A.W., 1964. Long-Term Stability of Clay Slopes. Geotechnique, 14, 77-101.

Skempton, A.W. & DeLory, F.A., 1957. Stability of Natural Slopes in London Clay. Proc. 4th Int. Conf. on Soil Mechanics and Foundation Engineering, London, Vol. 2, 378-381.

Skempton, A.W. & Hutchinson, J.N., 1969. Stability of Natural Slopes and Embankment Foundations. Proc. 7th Int. Conf. Soil Mech., Mexico, State-of-Art, 291-340.

Skempton, A.W. & Petley, D.J., 1967. The Strength Along Structural Discontinuities in Stiff Clays. Proc. Geot. Conf. Oslo, Vol. 2, 29-46.

Skempton, A.W. & Weeks, A.G., 1976. The Quaternary History of the Lower Greensand Escarpment and Weald Clay Vale Near Sevenoaks, Kent. Phil. Trans. R. Soc., Series A, 283, 493-526.

Smith, L.B., 1972. Thaw Consolidation Tests on Remoulded Clay. MSc. Thesis, University of Alberta, Edmonton.

Sparks, B.W. & West, R.G., 1972. The Ice Age in Britain. Methuen & Co. Ltd., U.S.A.

Symons, I.F. & Booth, A.I., 1971. Investigation of the Stability of Earthwork Construction on the Original Line Sevenoaks Bypass, Kent. TRRL LR 393, D.O.E.

Vaughan, P.R., 1976. The deformation of the Empingham Valley Slope. Appendix to Horswill, P. & Horton, A., 1976. Cambering and Valley Bulging in the Gwash Valley at Emphigam, Rutland. Philosophical Transactions of the Royal Society, A, 283, 451-462.

Weeks, A.G., 1969. The Stability of Natural Slopes in South-East England as affected by Periglacial Activity. Q. Jl. Engng. Geol., 2, 49-61.

Williams, M.A.J., Dunkerly, D.L., De Deckker, P., Kershaw, A.P. & Stokes, T., 1993. Quaternary Environments. Edward Arnold, London.

Williams, P.J. & Smith, M.W., 1989. The Frozen Earth: Fundamentals of Geocryology. Cambridge University Press, Cambridge.

Wong, L.C. & Haug, M.D., 1991. Cyclical Closed-System Freeze-Thaw Permeability Testing of Soil Liner and Cover Materials. Can. Geotech. J., 28, 784-793.

Bibliography

Akroyd, T.N.W., 1957. Laboratory Testing in Soil Engineering. Soil Mechanics Ltd., London.

Andersland, O.B. & Anderson, D.M. (eds.), 1978. Geotechnical Engineering for Cold Regions. McGraw-Hill, New York.

ASHRAE, 1993. Handbook of Fundamentals, American Technical Publishers Ltd..

ASHRAE, 1994. Handbook of Refrigeration, American Technical Publishers Ltd..

Benson, C.H. & Othman, M.A., 1993. Hydraulic Conductivity of Compacted Clay Frozen and Thawed In Situ. Journal of Geotechnical Engineering, American Society of Civil Engineers, 119, 2, 276-294.

Bishop, A.W. & Henkel, D.J., 1962. The Measurement of Soil Properties in the Triaxial Test (2nd ed.). William Clowes and Sons Ltd., London and Beccles.

Bishop, J., 1992. Turbo Pascal Precisely. Addison-Wesley.

Bolton, W., 1996. Measurement and Instrumentation Systems. Newnes, Oxford.

Craig, R.F., 1997. Soil Mechanics (6th ed.). Chapman & Hall, London.

Dally, W., Riley, W.F. & McConnel, K.G., 1993. Instrumentation for Engineering Measurements (2nd ed.). John Wiley & Sons Inc.

Das, B.M., 1990. Principles of Geotechnical Engineering. PWS-Kent Publishing Co., Boston, 505-512.

Early, K.R. & Skempton, A.W., 1972. Investigations of the Landslide at Walton's Wood, Staffordshire. Q. Jl Geol., 5, 19-41.

Embleton, C. & King, C.A.M., 1975. Periglacial Geomorphology. Arnold, London, 96-105.

Hall, A.M. & Bent, A.J.A., 1990. The Limits of the Last British Ice Sheet in Northern Scotland and the Adjacent Shelf. Quaternary Newsletter, 61, 2-12.

Hausmann, M.R., 1990. Engineering Principles of Ground Modification. McGraw-Hill, U.S.A.

Holman, J.P., 1992. Heat Transfer (7th ed.). McGraw-Hill International, U.K.

Kotz, J.C. & Treichel, P., 1996. Chemistry and Chemical Reactivity (3rd ed.). Saunders College Publishing, U.S.A.

Polak, T.A. & Pande, C., 1999. Engineering Measurements: Methods and Intrinsic Errors. Professional Engineering Publishing Limited, London & Bury St. Edmunds.

Ramsay, D.C., 1996. Principles of Engineering Instrumentation. Arnold, London.

Scott, R.F., 1965. Principles of Soil Mechanics. Wiley International.

Vickers, B., 1978. Laboratory Work in Soil Mechanics (2nd ed.). Granada, London.

Washburn, A.L., 1973. Periglacial Processes and Environments. Arnold, London, 1-2, 163-189.

Appendix A – Photographs of Apparatus

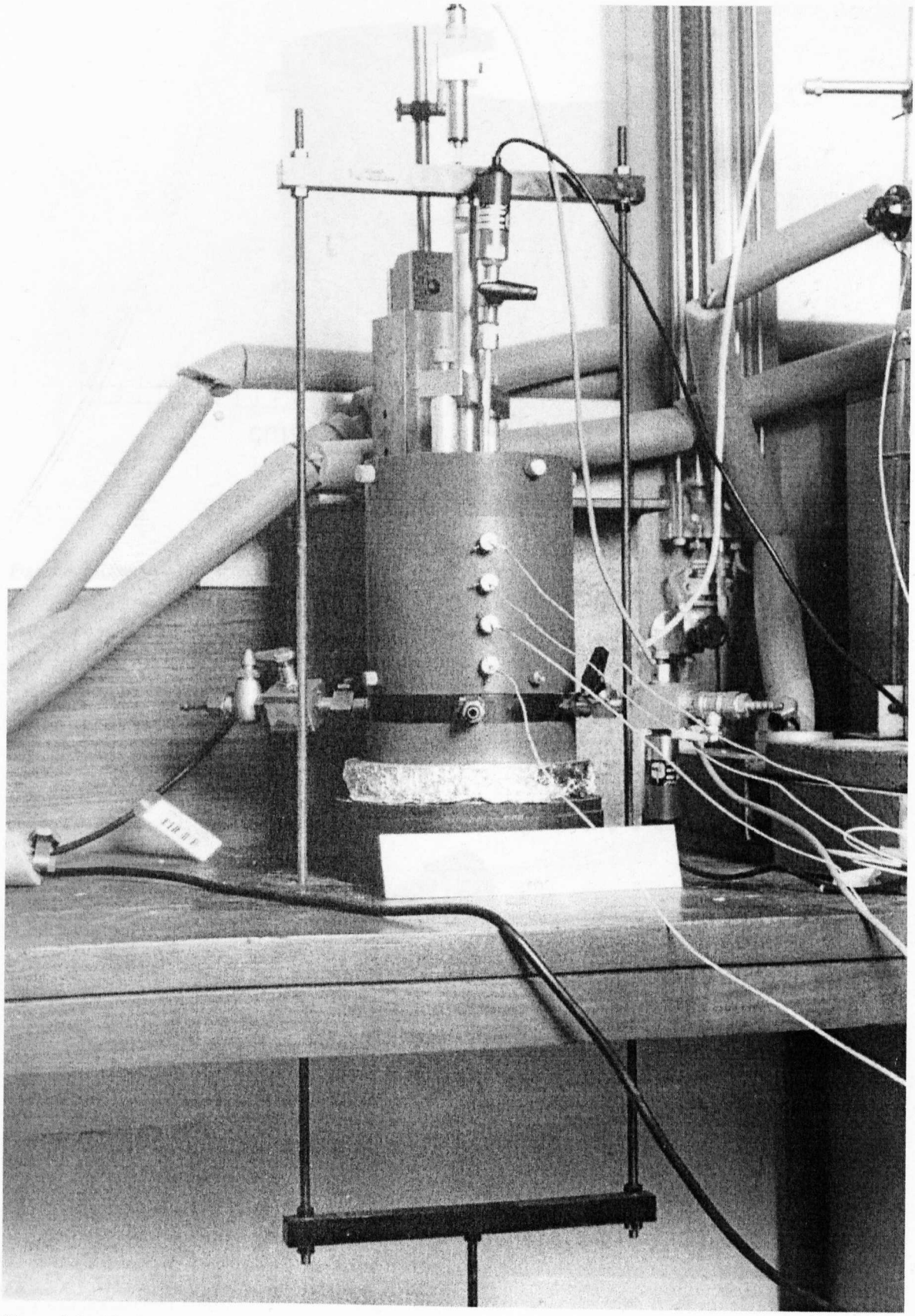

Figure A.1 – The Permode Cell (usually inside refrigerated cabinet)

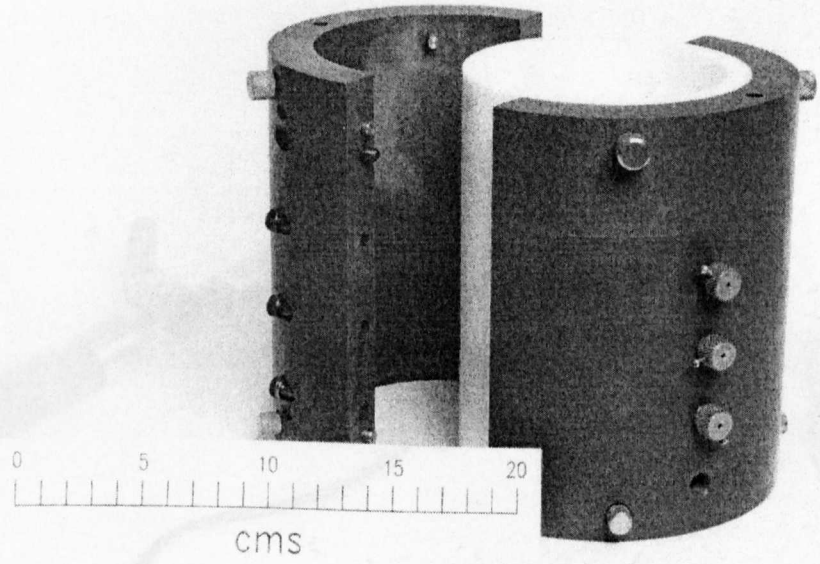

Figure A.2 – Permode Barrel and Liner

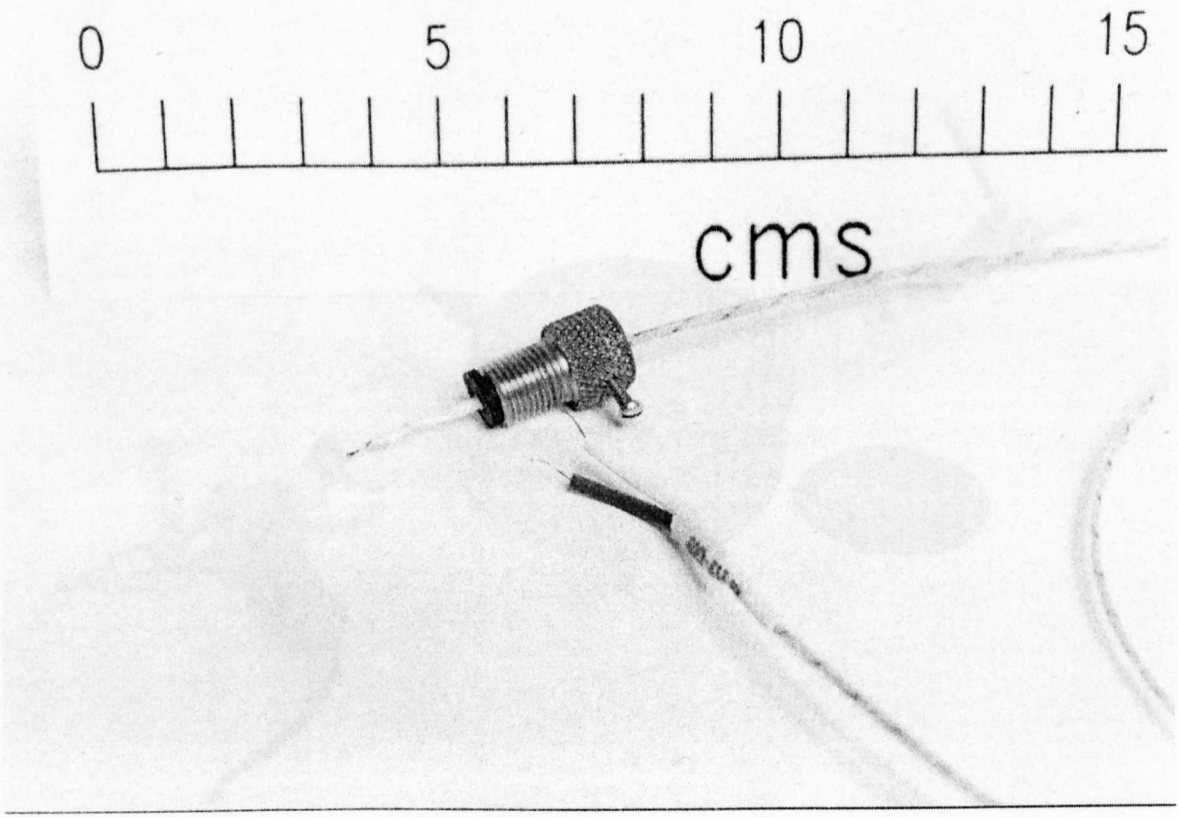

Figure A.3 – Thermocouple and Washer Assembly

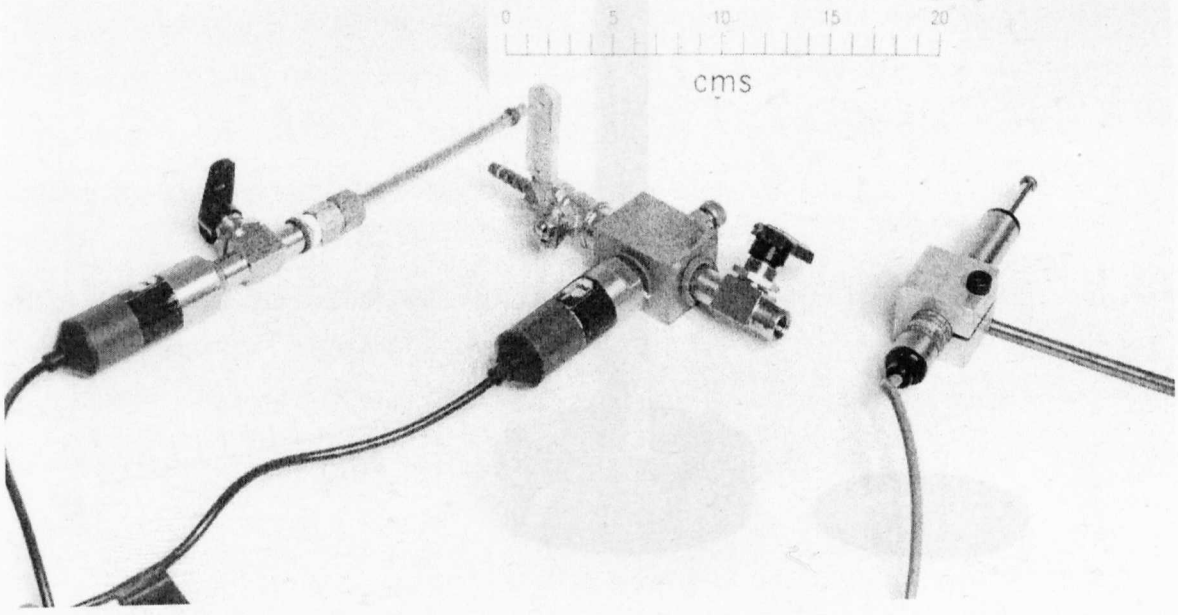

Figure A.4 – Pressure and Displacement Transducers

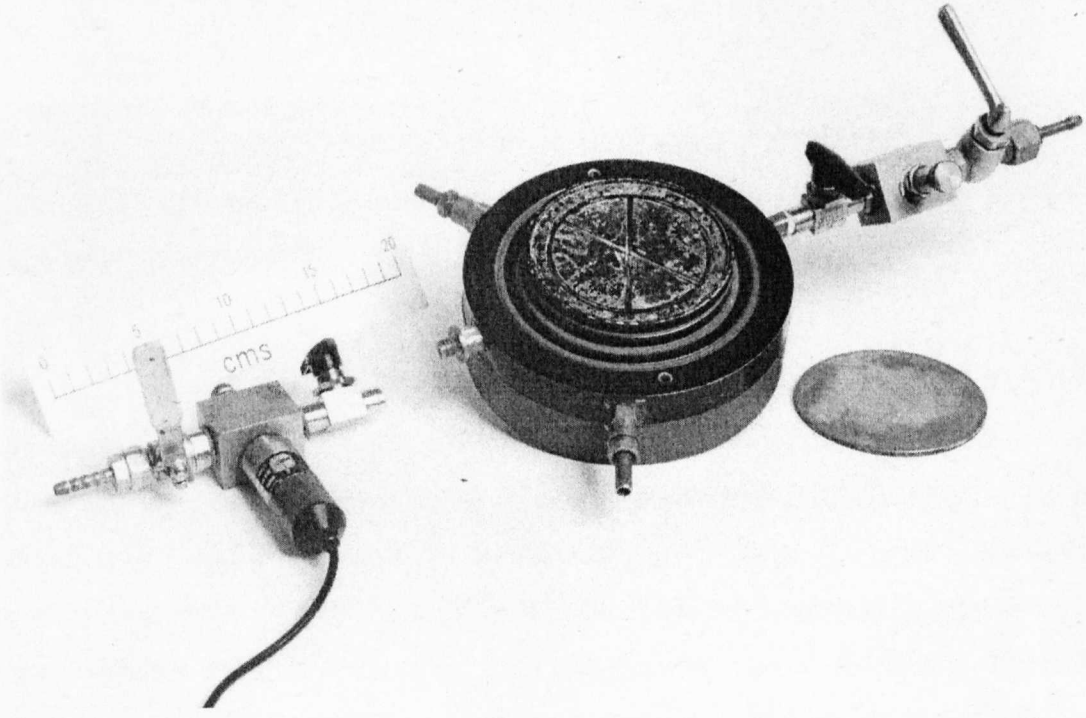

Figure A.5 – Baseplate Assembly

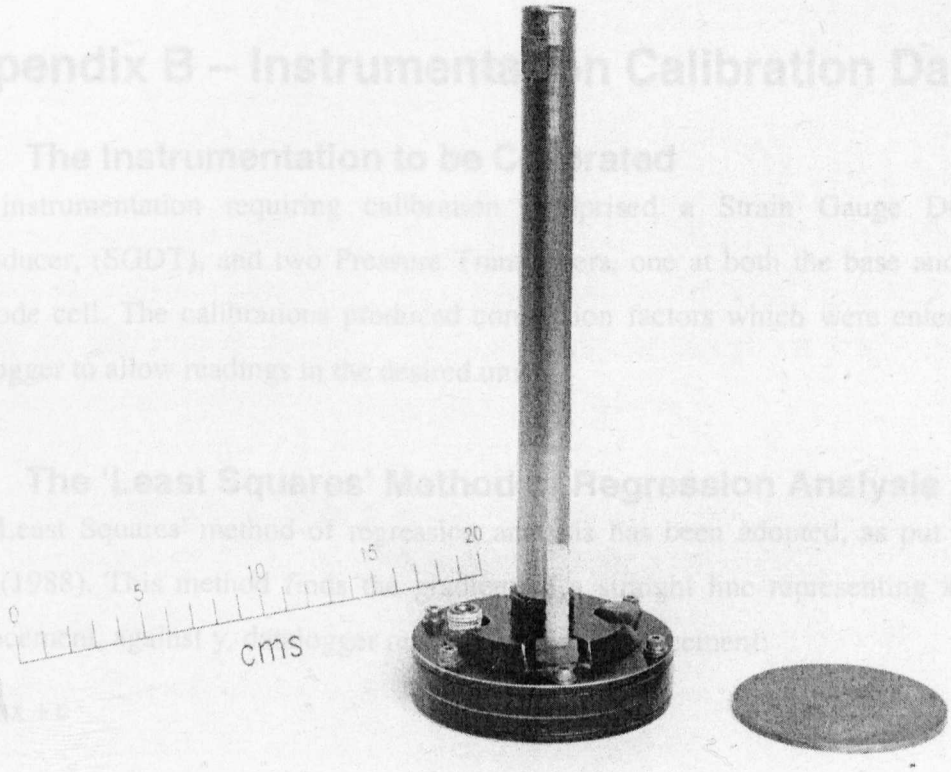

Figure A.6 – Piston and Porous Plate

Appendix B – Instrumentation Calibration Data

B.1 The Instrumentation to be Calibrated

The instrumentation requiring calibration comprised a Strain Gauge Displacement Transducer, (SGDT), and two Pressure Transducers, one at both the base and top of the permode cell. The calibrations produced conversion factors which were entered into the datalogger to allow readings in the desired units.

B.2 The 'Least Squares' Method of Regression Analysis

The 'Least Squares' method of regression analysis has been adopted, as put forward by Ray, (1988). This method finds the gradient of a straight line representing x, e.g. a set displacement, against y, datalogger reading for that displacement:

$$y = mx + c$$

Equation B.1 – x against y

For the calibrations carried out, c was set to zero for entering into the datalogger. The gradient m was found by:

$$m = \frac{n\sum xy - \sum x \sum y}{n\sum x^2 - \left(\sum x\right)^2}$$

where n = no. of data points

Equation B.2 – m found using the 'Least Squares' method

The conversion required by the datalogger is

$$1/m$$

Equation B.3 – Conversion factor for datalogger

As a straight line is achieved irrespective of where the individual points lie, a check is required to evaluate how well the line actually fits the data. A correlation coefficient, r, can be determined by measuring the dispersion of paired data from the regression line. For a set of data x and y, two regression lines are possible, 'y on x' and 'x on y'. If the slopes of these are equal, then r becomes 1. If the two lines are perpendicular, then r = 0. Therefore, r is required to be near 1.

$$r = \frac{n\sum xy - \sum x \sum y}{\sqrt{\left(n\sum x^2 - \left(\sum x\right)^2\right)}\sqrt{\left(n\sum y^2 - \left(\sum y\right)^2\right)}}$$

Equation B.4 – Correlation coefficient, r

For each calibration, values of 1/m and r were found and checked using Microsoft Excel. Within the spreadsheet, results of the automatic regression analysis were expressed graphically using a 'predicted y' and actual y set of values.

B.3 Summary of Calibrations

The 1st calibration took place on initialising the test apparatus.

The 2nd calibration took place following the introduction of extension wiring to the three transducers. This calibration was carried out in order to eliminate the possibility of spurious errors due to the altered wiring condition. Tabulated data and calculated values of m, 1/m and r are given below, together with the graphical check.

Table B.1 – Summary of Calibrations

Calibration / conversion	SGDT - 1	SGDT - 2	PWP Base - 1	PWP Base - 2	PWP Top - 1	PWP Top - 2
m	503.939	502.687	42.486	42.274	40.532	40.806
1/m	0.001984	0.001989	0.023537	0.023655	0.024672	0.024506
r	0.999999	0.991879	0.999983	0.999750	0.999360	0.999941

The pressure transducers, (here noted as 'PWP Base/Top Transducers'), proved harder to calibrate than the displacement transducers. This was due to the variability encountered when setting up known pressures on the Bourdon Gauge.

Table B.2 – Calibration Table for SGDT Displacement Transducer – 1

	Disp.	Microstrain									
	(mm)	Run 1		Run 2		Run 3		Avg. y	xy	x^2	y^2
	0	0	-1.9	0	-0.4	0	1.7	-0.1	0	0	0.01
	1	499.7	496.2	495.2	500.5	499	505.8	499.4	499.4	1	249400.4
	2	1001.7	1001.9	1002.7	1006.2	1004	1009.5	1004.333	2008.667	4	1008685
	3	1501.5	1506.6	1504.4	1508.5	1505.6	1513.2	1506.633	4519.9	9	2269944
	4	2008.5	2008.1	2010.9	2010.1	2009.9	2016	2010.583	8042.333	16	4042445
	5	2515.4	2510.5	2517.5	2514	2515.6	2522.6	2515.933	12579.67	25	6329921
	6	3014.4	3014.4	3016.5	3018.9	3019.9	3021	3017.517	18105.1	36	9105407
	8	4034.7	4022	4036.5	4024.4	4030.2	4032	4029.967	32239.73	64	16240631
	10	5039.1	5031.3	5036.2	5037.3	5037.3	5038.7	5036.65	50366.5	100	25367843
	12	6058	6054.3	6065.7	6047.5	6045.7	6048.7	6053.317	72639.8	144	36642643
	14	7056.4	7046.2	7074.3	7048.6	7061.1	7055	7056.933	98797.07	196	49800308
	16	8062	8058.2	8060	8059.8	8063.3	8066.4	8061.617	128985.9	256	64989663
	18	9072.8	9061.6	9068.9	9086.8	9077.1	9069.5	9072.783	163310.1	324	82315397
	20	10073.5	10067.8	10073.5	10070.5	10075.3	10073.1	10072.28	201445.7	400	1.01E+08
	25	12584.5	12589.8	12589.1	12591.8	12591.9	12592.3	12589.9	314747.5	625	1.59E+08
Σ	**144**						Σ	**72527.8**	**1108287**	**2200**	**5.6E+08**
Σ^2	**20736**						Σ^2	**5.3E+09**			

Table B.3 – Calibration Table for SGDT Displacement Transducer – 2

Disp.	Microstrain									
(mm)	Run 1		Run 2		Run 3		Avg. y	xy	x^2	y^2
0	0	-0.7	0	-0.2	0	0.4	-0.083333	0	0	0.006944
1	503.7	490.2	491.9	434.9	434.3	365.4	453.4	453.4	1	205571.6
2	1002.1	991.6	993.7	934.3	935.5	866	953.8667	1907.733	4	909861.6
3	1506.4	1494.7	1495.2	1437.2	1436.7	1370.8	1456.833	4370.5	9	2122363
4	2012.5	1998.6	1994.9	1944.8	1942.2	1877.8	1961.8	7847.2	16	3848659
5	2510.9	2499.4	2494.7	2439.3	2445	2377.2	2461.083	12305.42	25	6056931
6	3012.5	3000.2	2996.4	2926.4	2945.2	2878.4	2959.85	17759.1	36	8760712
8	4020.1	4007.2	4004.6	3932.1	3955.6	3883	3967.1	31736.8	64	15737882
10	5025.1	5012.4	5009	4934.8	4959.1	4888.2	4971.433	49714.33	100	24715149
12	6030.2	6019.4	6015.9	5953.7	5964.3	5921.1	5984.1	71809.2	144	35809453
14	7035.5	7029.1	7023.4	6969.8	6969.2	6931.7	6993.117	97903.63	196	48903681
16	8036.6	8036.4	8026.8	7973.9	7974.1	7973.9	8003.617	128057.9	256	64057880
18	9044.5	9043.7	9030.4	9015.9	8969	8955.4	9009.817	162176.7	324	81176796
20	10051	10047.6	10036.3	10019.5	9967.4	9960.4	10013.7	200274	400	1E+08
25	12569.4	12565.8	12539.6	12537.4	12472.8	12471.8	12526.13	313153.3	625	1.57E+08
Σ 144						**Σ**	**71715.8**	**1099469**	**2200**	**5.5E+08**
Σ^2 20736						**Σ^2**	**5.1E+09**			

Table B.4 – Calibration Table for PWP Base Transducer – 1

Pressure, x		Microstrain									
Bar	**kPa**	**Run 1**		**Run 2**		**Run 3**		**Avg. y**	**xy**	**x^2**	**y^2**
0	0	0	0	0	0	0	0	0	0	0	0
0.5	50	2112.6	2011.8	2321.6	2182.8	2053.6	1930.5	2102.15	105107.5	2500	4419035
1	100	4244	4197.6	4462.1	4392.5	4257.1	4215.3	4294.767	429476.7	10000	18445024
1.5	150	6189.4	6199.4	6567.3	6328	6363.6	6333.1	6330.133	949519.95	22500	40070584
2	200	8487.6	8432.6	8627.6	8617.3	8487.1	8318.3	8495.083	1699016.6	40000	72166435
2.5	250	10530.6	10557.3	10800.3	10918.3	10418.2	10511	10622.617	2655654.25	62500	1.13E+08
3	300	12792.8	12684.3	12845.8	12849.4	12683.8	12621.7	12746.3	3823890	90000	1.62E+08
Σ	**1050**						**Σ**	**44591.1**	**9662665**	**227500**	**4.1E+08**
Σ^2	**1102500**						**Σ^2**	**2E+09**			

Table B.5 – Calibration Table for PWP Base Transducer - 2

Pressure, x		Microstrain									
Bar	**kPa**	**Run 1**		**Run 2**		**Run 3**		**Avg. y**	**xy**	**x^2**	**y^2**
0	0	0	0	0	0	0	0	0	0	0	0
0.5	50	1961.4	1811.5	1730.1	1612.9	1916.5	1834.4	1811.133	90556.67	2500	3280204
1	100	4158.5	3994.7	3892.1	3801.5	4110.1	4019.9	3996.133	399613.3	10000	15969082
1.5	150	6184.7	6005.9	6120	5917.5	6264.4	6112.8	6100.883	915132.5	22500	37220777
2	200	8368.4	8243.2	8133.4	8122.7	8343.5	8300.3	8251.917	1650383	40000	68094129
2.5	250	10382.2	10399.9	10331.5	10234.8	10495.7	10466.3	10385.07	2596267	62500	1.08E+08
3	300	12648.9	12678.6	12475.1	12446	12680.3	12629.7	12593.1	3777930	90000	1.59E+08
Σ	**1050**						**Σ**	**43138.2**	**9429883**	**227500**	**3.9E+08**
$Σ^2$	**1102500**						**$Σ^2$**	**1.9E+09**			

Table B.6 – Calibration Table for PWP Top Transducer - 1

Pressure, x		Microstrain									
Bar	**kPa**	**Run 1**		**Run 2**		**Run 3**		**Avg. y**	**xy**	**x^2**	**y^2**
0	0	0	0	0	0	0	0	0	0	0	0
0.5	50	1615.2	1475	1634.5	1561.3	1612.4	1435.1	1555.5833	77779.1667	2500	2419840
1	100	3697.9	3579.7	3737.5	3646	3698	3698.8	3676.3167	367631.667	10000	13515304
1.5	150	5713.9	5629.6	5753.8	5679.6	5811	5614.6	5700.4167	855062.5	22500	32494750
2	200	7818.5	7744.6	7920.3	7794.7	7747.6	7751.8	7796.25	1559250	40000	60781514
2.5	250	9920.4	9828.5	10001	9828.6	9948	9843.5	9895	2473750	62500	97911025
3	300	11991.4	11982	11994.4	11993.8	11968.3	11963.1	11982.167	3594650	90000	1.44E+08
Σ	**1050**						**Σ**	**40605.7**	**8928123**	**227500**	**3.5E+08**
Σ^2	**1102500**						**Σ^2**	**1.6E+09**			

Table B.7 – Calibration Table for PWP Top Transducer - 2

Pressure, x		Microstrain									
Bar	kPa	Run 1		Run 2		Run 3		Avg. y	xy	x^2	y^2
0	0	0	0	0	0	0	0	0	0	0	0
0.5	50	1942.4	1816.6	1957.3	1845.4	1972.1	1868.6	1900.4	95020	2500	3611520
1	100	4017	3937.6	4062.2	3946.8	4032.7	3973.6	3994.983	399498.3	10000	15959892
1.5	150	6092.9	5924.7	6042.8	5929.5	6115.2	5973.6	6013.117	901967.5	22500	36157572
2	200	8019.3	8034.3	8140.5	8024.3	8028.6	8062.5	8051.583	1610317	40000	64827994
2.5	250	10119.4	10089.1	10113.8	10110.3	10210.8	10100.4	10123.97	2530992	62500	1.02E+08
3	300	12174.9	12114.9	12267.7	12187.1	12264.4	12241	12208.33	3662500	90000	1.49E+08
Σ	**1050**						Σ	**42292.4**	**9200294**	**227500**	**3.7E+08**
Σ^2	**1102500**						Σ^2	**1.8E+09**			

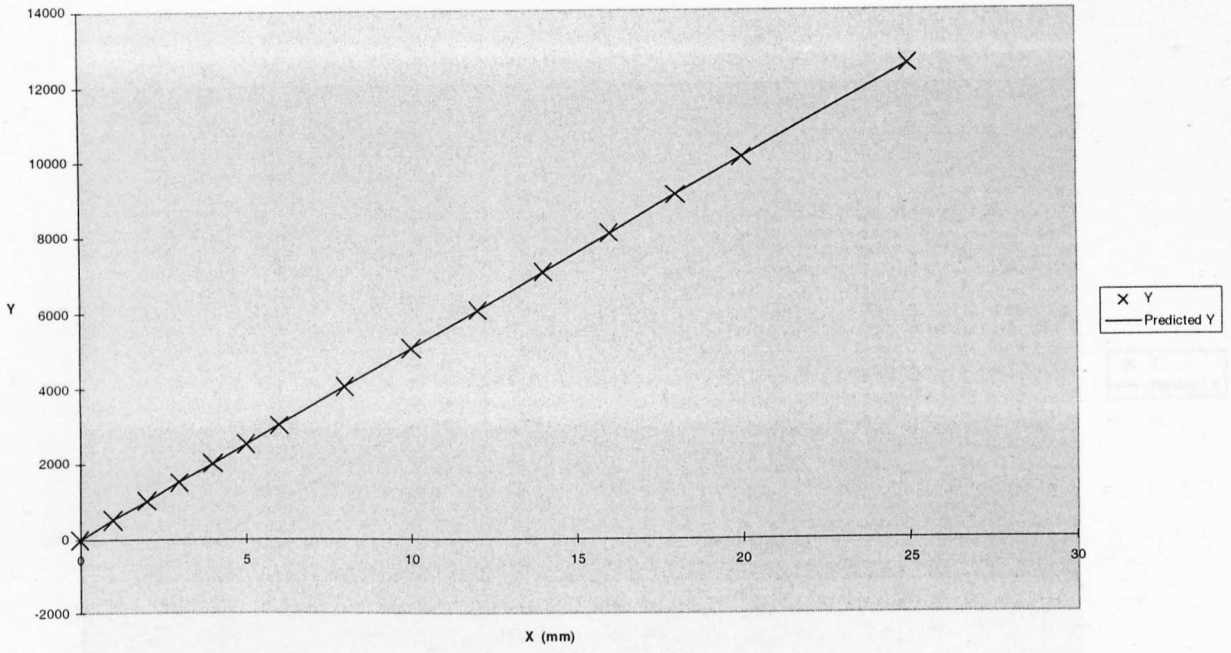

Figure B.1 – Excel Regression Analysis for SGDT Displacement Transducer – 1

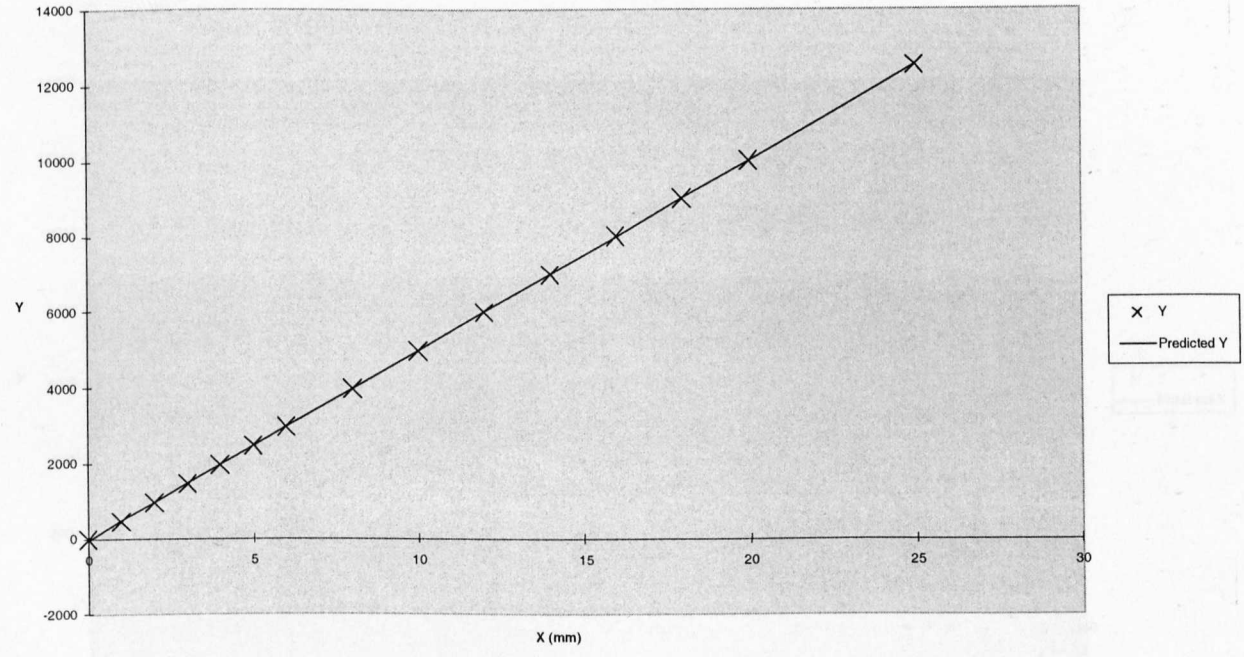

Figure B.2 – Excel Regression Analysis for SGDT Displacement Transducer – 2

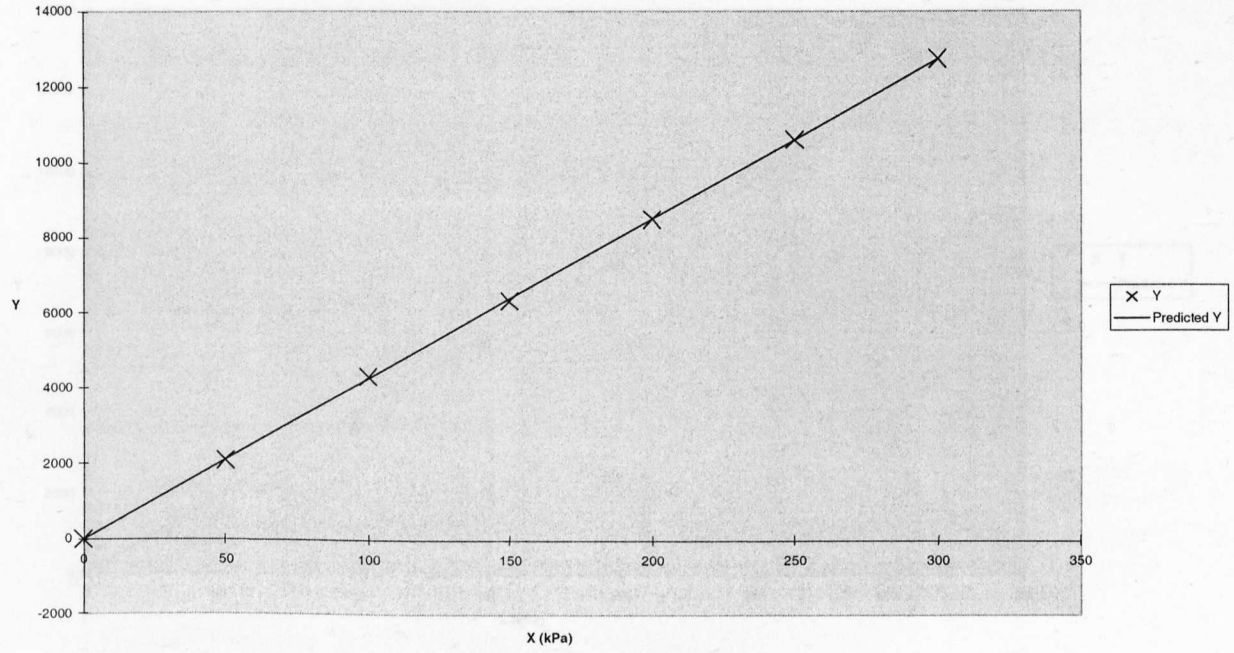

Figure B.3 – Excel regression Analysis for PWP Base Transducer - 1

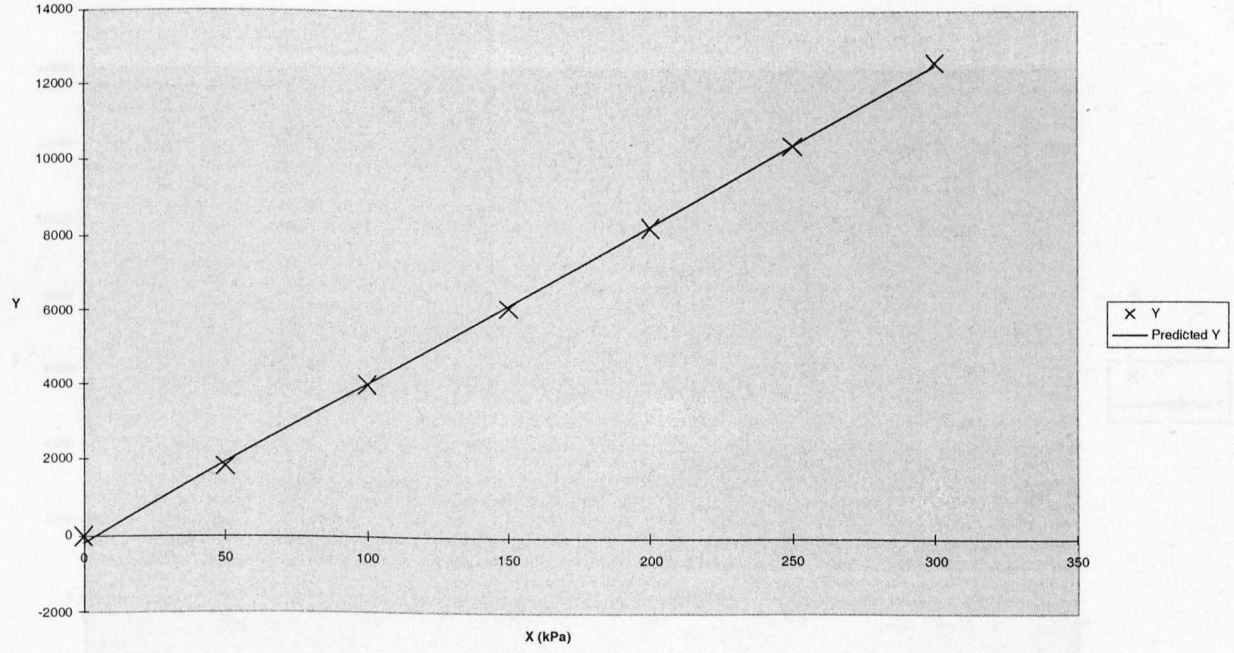

Figure B.4 – Excel Regression Analysis for PWP Base Transducer – 2

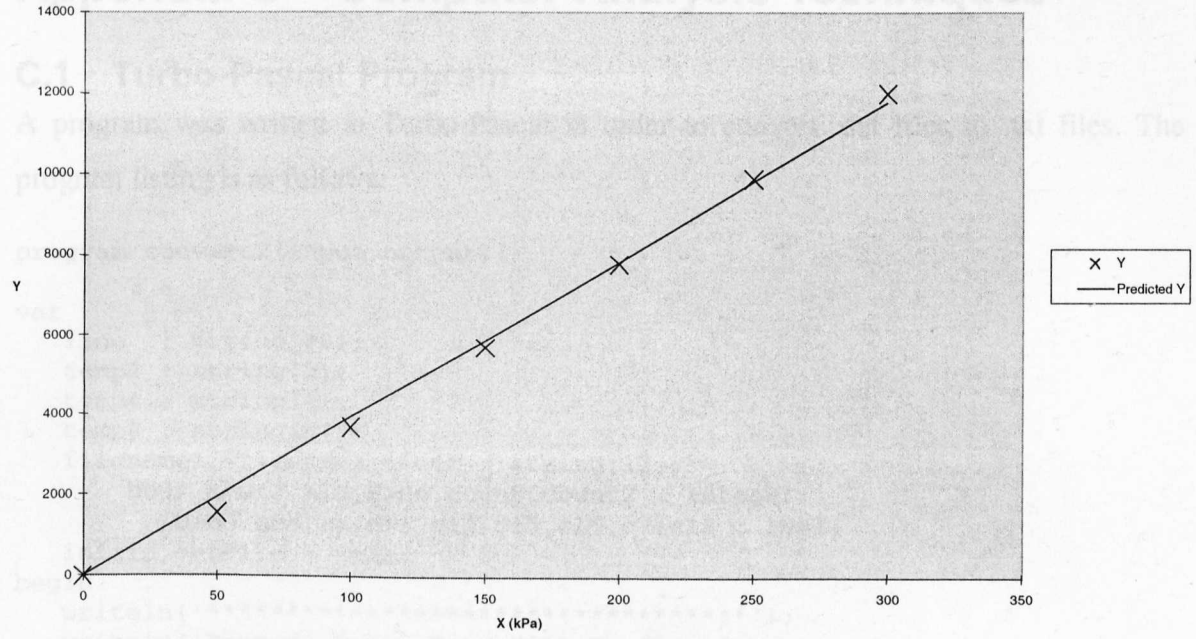

Figure B.5 – Excel Regression Analysis for PWP Top Transducer - 1

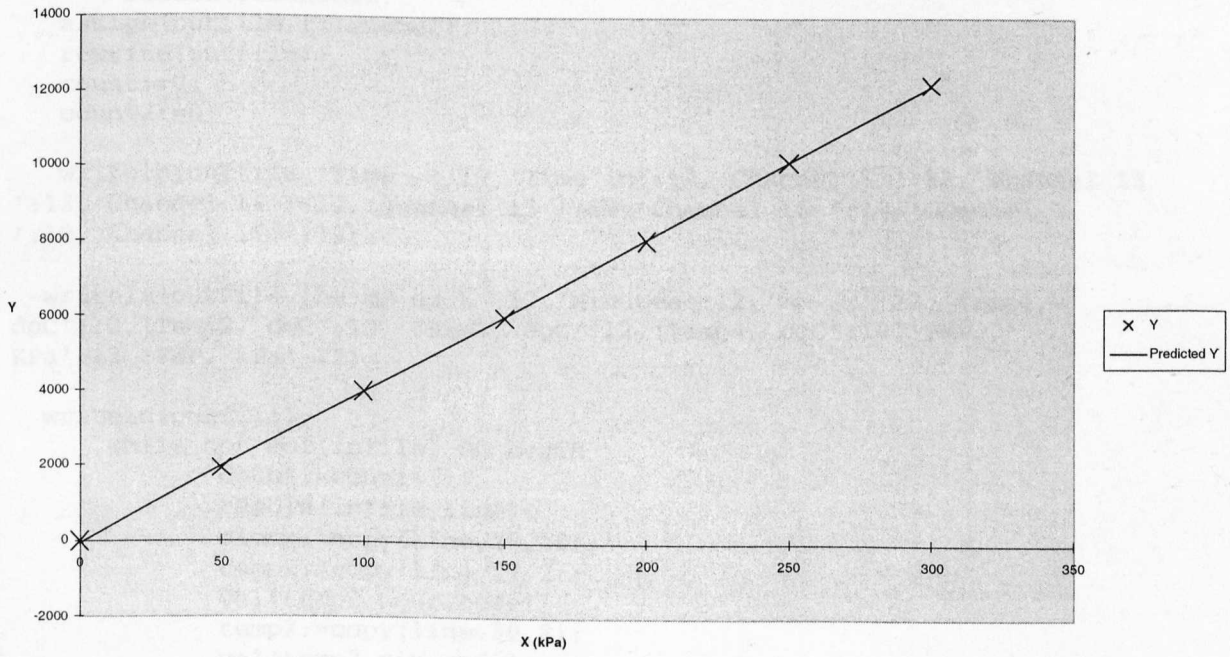

Figure B.6 – Excel Regression Analysis for PWP Top Transducer – 2

Appendix C – Computer Analysis Techniques

C.1 Turbo-Pascal Program

A program was written in Turbo-Pascal in order to convert .dat files to .txt files. The program listing is as follows:

```
program convert2(input,output);

var
   line  : string[80];
   temp2 : string[2];
   temp4 : string[4];
   temp8 : string[8];
   filename1,filename2,clock : string[12];
       hour,hour2,min,code,count,count2 : integer;
          time,sec,c1,c13,c14,c15,c16,c7,c11 : real;
   infile,outfile : text;
begin
   writeln('**********************************');
   writeln('Permode Test, Data File Handler');
   writeln('**********************************');
   writeln;
   writeln;
   write('Please enter name of input file:');
       readln(filename1);
   assign(infile,filename1);
   reset(infile);
   write('Please enter name for output file:');
       readln(filename2);
   assign(outfile,filename2);
   rewrite(outfile);
   count:=0;
   count2:=0;

   writeln(outfile,'Time  ':12,'Time in':12,'Channel 1 ':12,'Channel 13
':12,'Channel 14 ':12,'Channel 15 ':12,'Channel 16 ':12,'Channel 7
':12,'Channel 11 ':12);

  writeln(outfile,'hh:mm:ss.t':12,'Minutes':12,'mm   ':12,'Temp1,
dgC':12,'Temp2, dgC':12,'Temp3, dgC':12,'Temp4, dgC':12,'PWP,
KPa':12,'PWP, KPa':12);

  writeln(outfile);
      while not eof(infile) do begin
             count:=count+1;
             readln(infile,line);
             clock:=copy(line,27,10);
             temp2:=copy(line,27,2);
             val(temp2,hour,code);
             temp2:=copy(line,30,2);
             val(temp2,min,code);
             temp4:=copy(line,33,4);
             val(temp4,sec,code);
```

```
            readln(infile,line);
            temp8:=copy(line,26,8);
            val(temp8,c1,code);
            temp8:=copy(line,66,8);
            val(temp8,c13,code);

                readln(infile,line);
                temp8:=copy(line,26,8);
                val(temp8,c14,code);
                temp8:=copy(line,66,8);
                val(temp8,c15,code);

            readln(infile,line);
            temp8:=copy(line,26,8);
            val(temp8,c16,code);
            temp8:=copy(line,66,8);
            val(temp8,c7,code);

            readln(infile,line);
            temp8:=copy(line,26,8);
            val(temp8,c11,code);

          readln(infile,line);

writeln(outfile,clock:12,time:12:3,c1:12:2,c13:12:2,c14:12:2,c15:12:4,c16
:12:4,c7:12:4,c11:12:4);
   end;
   close(infile);
   close(outfile);

end.
```

The program's function was to read the .dat file produced by the datalogger and abstract recorded values, arranging them in tabular format. An attempt was also made to change the time-values into number of minutes from start of test, (as opposed to clock times), but this was unsuccessful. However, the full original listing has been provided in the interests of completeness. The time counting difficulty was resolved in the next stage of post-processing, where the .txt files were exported to Microsoft Excel.

C.2 The Use of Microsoft Excel

Microsoft Excel is a spreadsheet application, ideal for dealing with tabular data. The major use of Excel during the research was to continue the post-processing of the test results. Text files were opened within a spreadsheet and then processed as required.

Extra columns could be easily inserted, e.g. for 'Average temperature' and 'Time in hours', or replaced, e.g. for 'Time in minutes'. Spreadsheets are also useful for repetitive calculations, where an equation can be entered to find values for one line and then copied down the table. An example of this would be to find the time in minutes from the start of the test, t_n, as $t_{n-1} + 10$, where readings were taken at 10 minute intervals.

Where more than one file required the same processing, a series of actions could be recorded as a macro within one file and then replayed in another, thus saving time and effort.

Graphs were created from the data tables, but were not always precise enough for analysis and presentation purposes. In these cases, the improved tabular data was saved as .txt and used with Matlab, a mathematical analysis application.

Excel was also used for regression analysis of the instrumentation calibration data. Other statistical and logical analyses proved of use when examining the permode test results.

C.3 The Use of Matlab

The Matlab software was used to construct graphs of the permode test results. Using this application proved to be faster and easier than using Excel in some cases, as less memory was required to perform operations, and more versatility could be achieved in terms of output.

Matlab has its own programming language controlling its operations. Instructions can either be entered individually through a command window, or assembled as a batch in a pre-written .m file as shown below:

```
load test26

clf

subplot (4,1,1) , plot (test26(:,3),test26(:,11))
grid

ylabel ('PWP Base (KPa)')
axis ([0 220 -20 10])

subplot (4,1,2) , plot (test26(:,3),test26(:,12))
grid
ylabel ('PWP Top (KPa)')
axis ([0 220 -20 160])

subplot (4,1,3) , plot (test26(:,3) ,test26(:,10))
grid
ylabel ('Av. Temp. (dgC)')
axis ([0 220 -10 10])

subplot (4,1,4) , plot (test26(:,3) ,test26(:,5))
grid
xlabel ('Time (hours)')
ylabel ('Disp. (mm)')
axis ([0 220 -30 0])
```

In the above example a data file is loaded, and columns of data plotted against each other in a column of four 'subplots' with various specified axes limits and titles.

Appendix D – Permode Test Results – All Tests

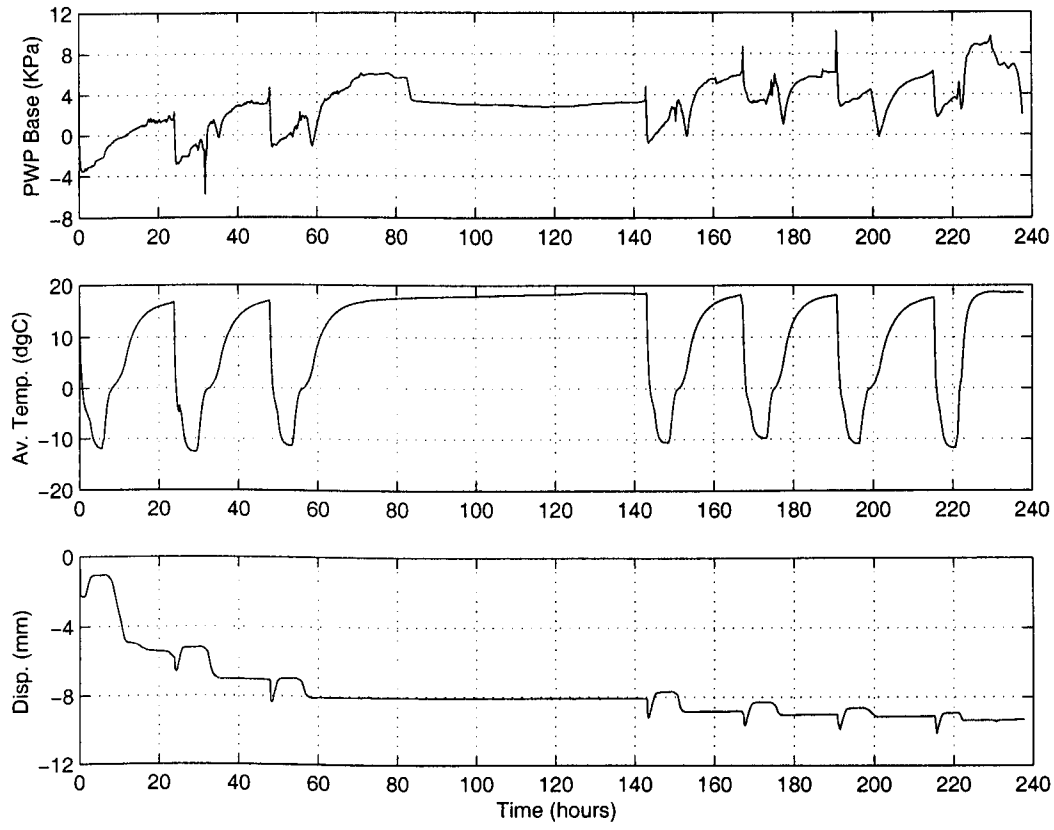

Figure D.1 – Test 1 - Lias Clay - σ = 29 kPa, m.c. = 29%

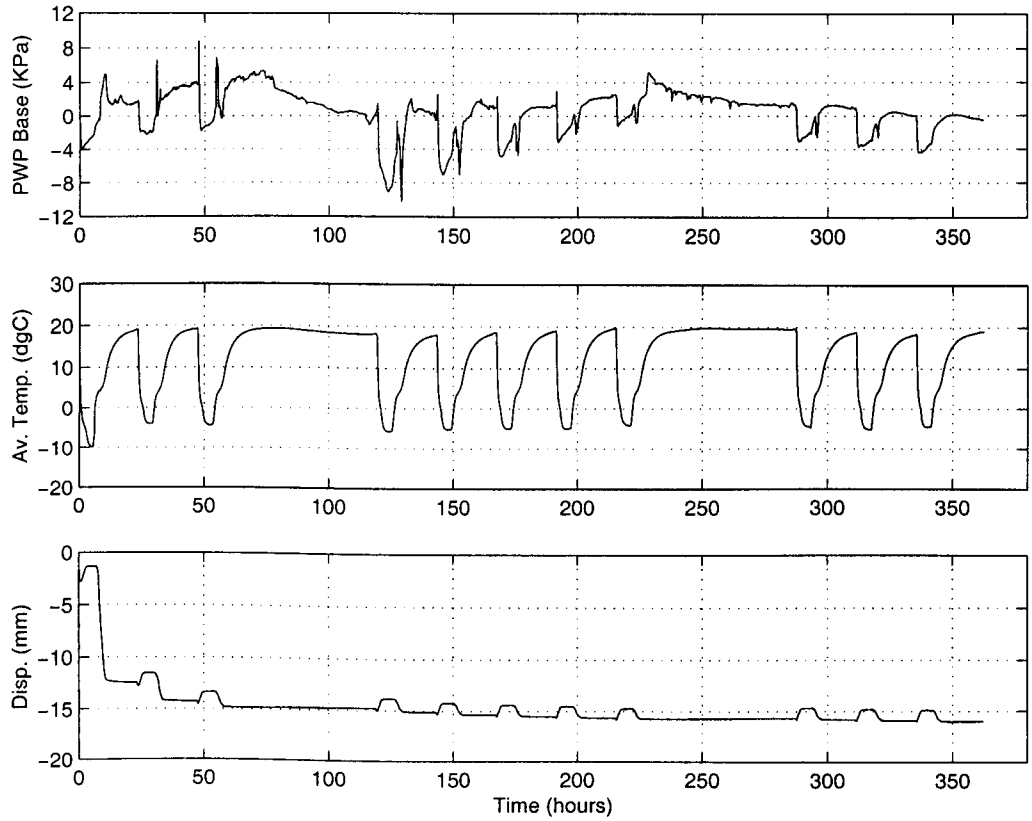

Figure D.2 - Test 2 - Lias Clay - σ = 104 kPa, m.c. = 32%

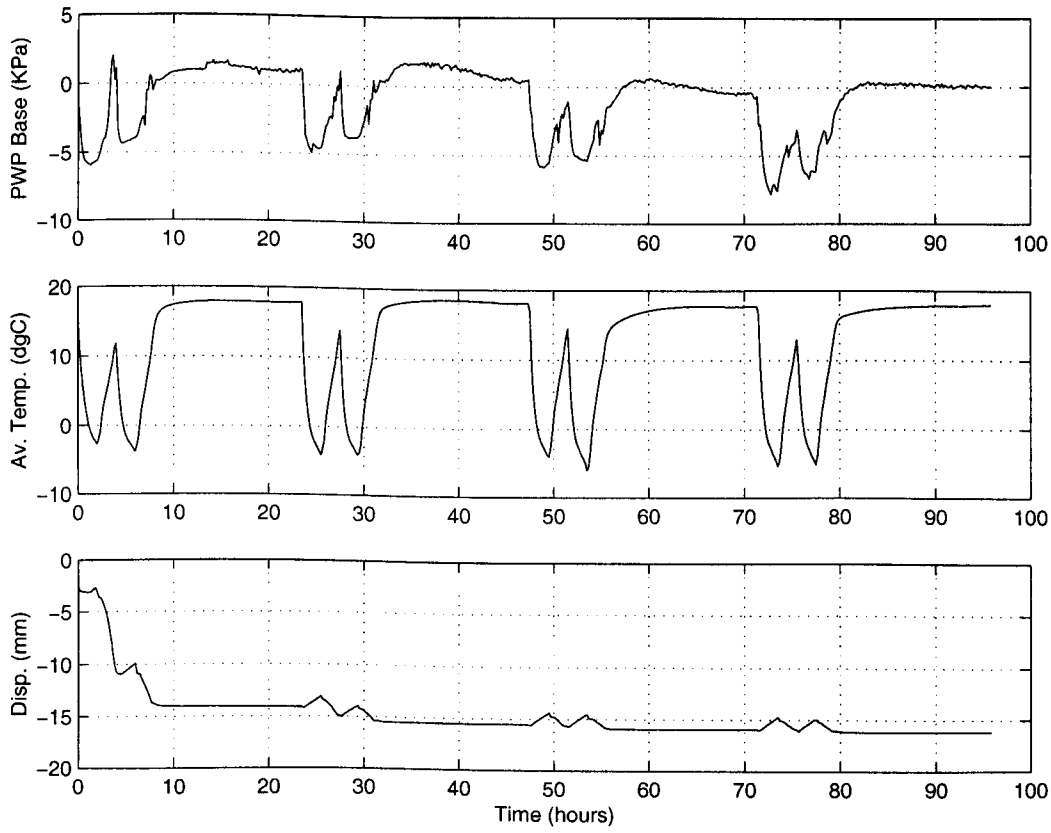

Figure D.3 – Test 3 - Lias Clay - σ = 104 kPa, m.c. = 30%

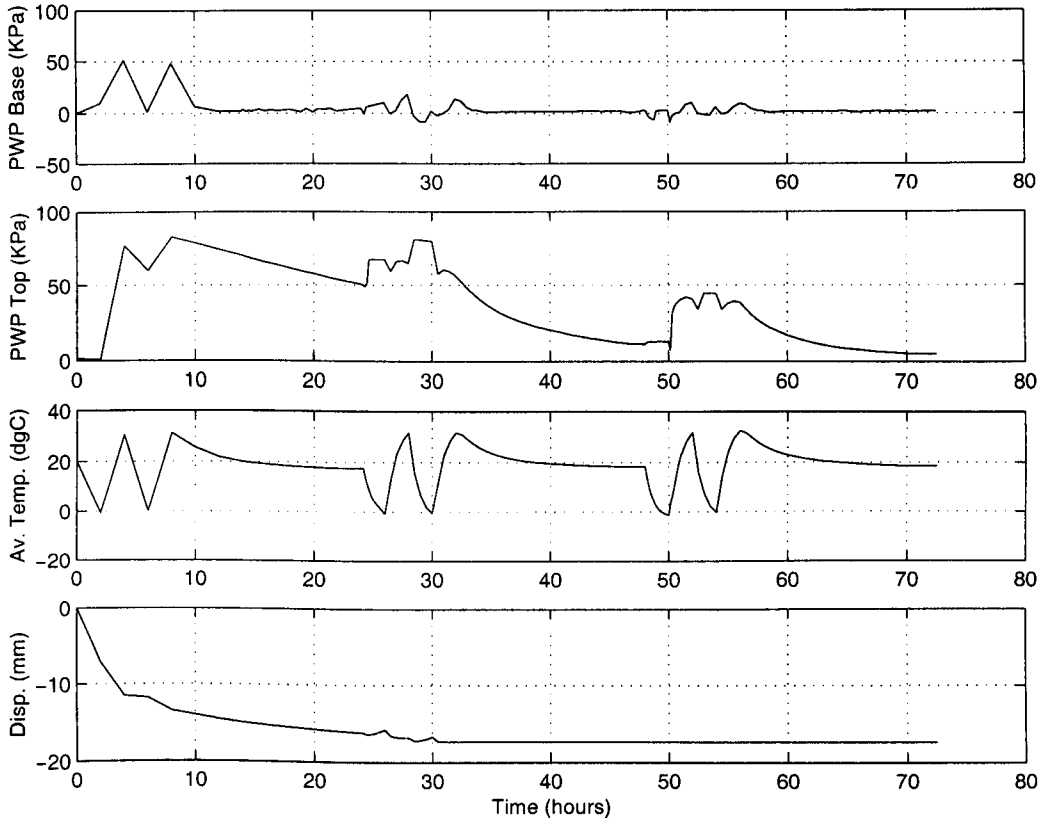

Figure D.4 – Test 4 - Lias Clay - σ = 104 kPa, m.c. = 32%

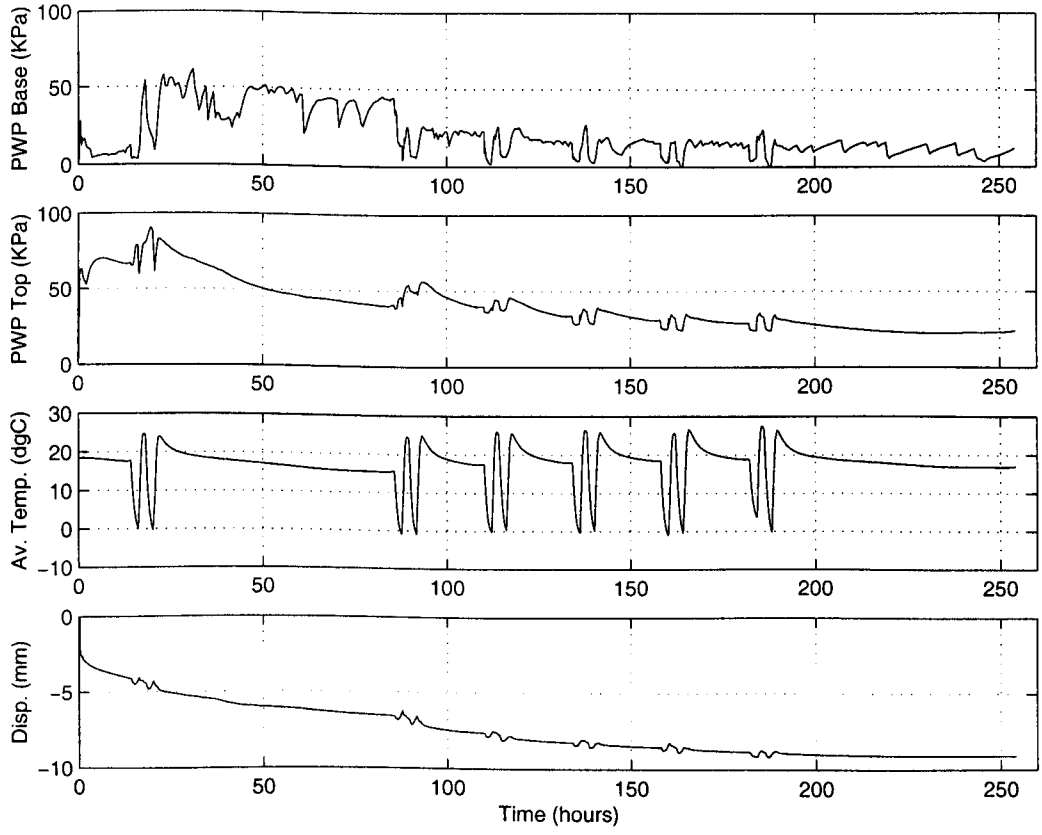

Figure D.5 – Test 5 - Lias Clay - σ = 104 kPa, m.c. = 30%

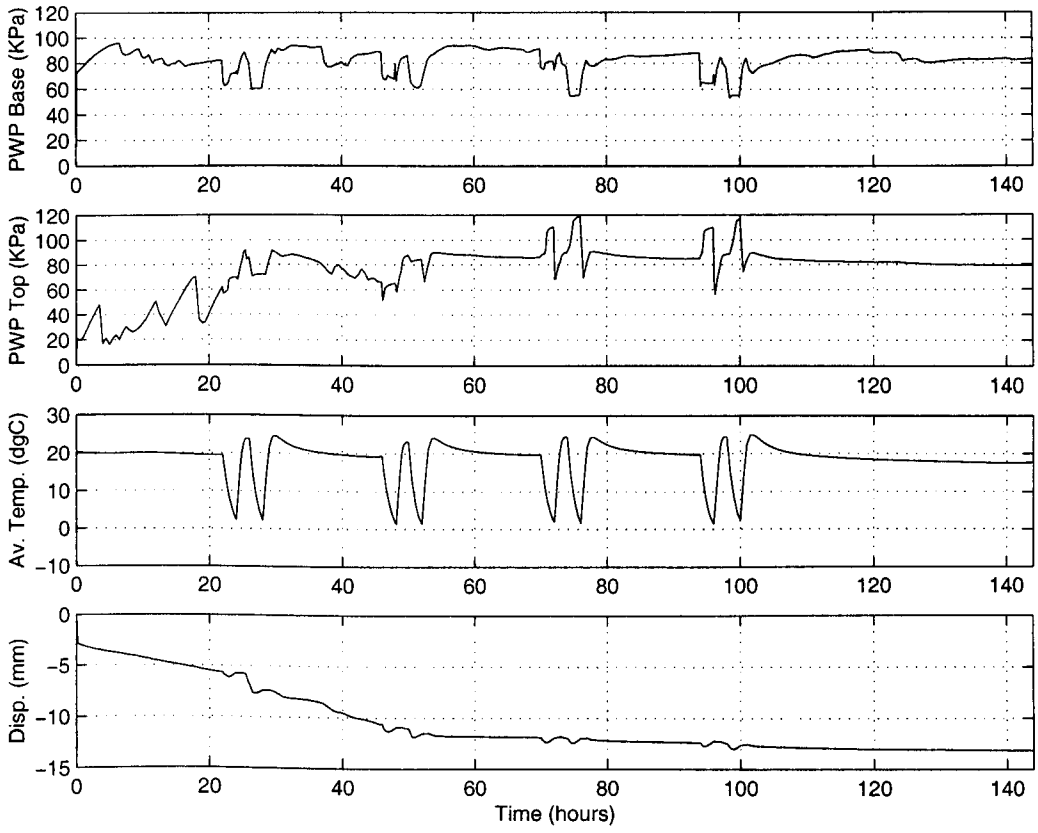

Figure D.6 – Test 6 - Lias Clay - σ = 104 kPa, m.c. = 35%

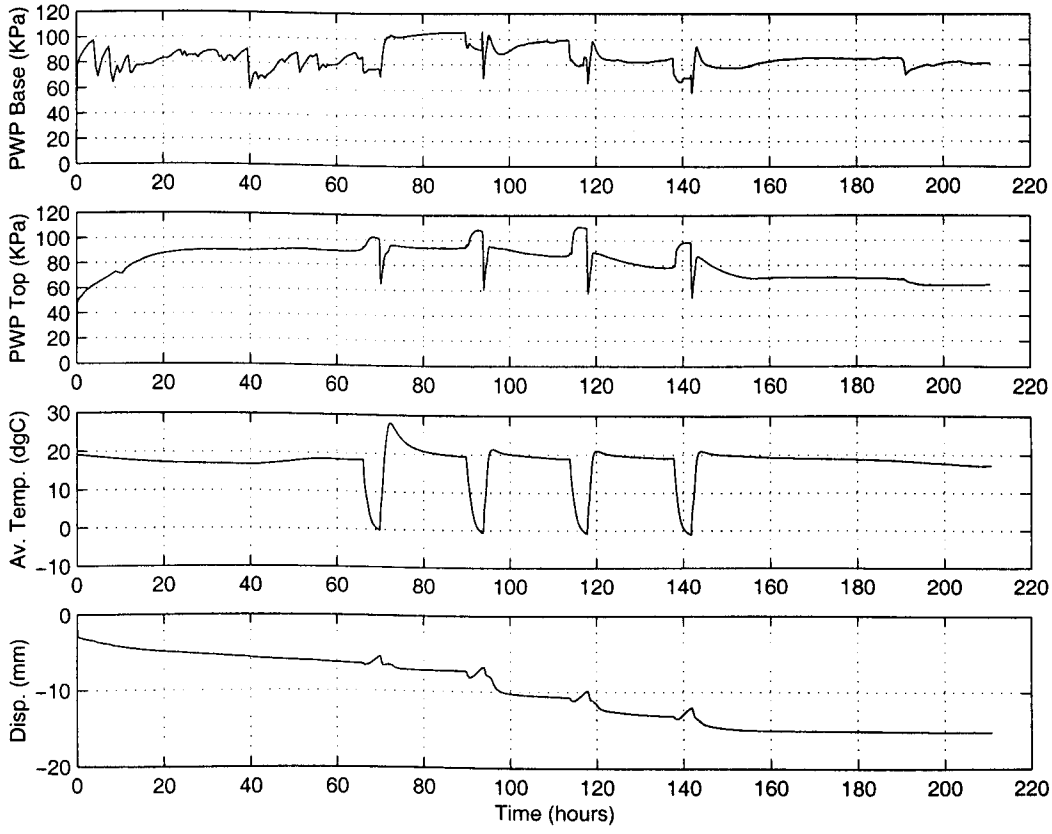

Figure D.7 – Test 7 - Lias Clay - σ = 104 kPa, m.c. = 33%

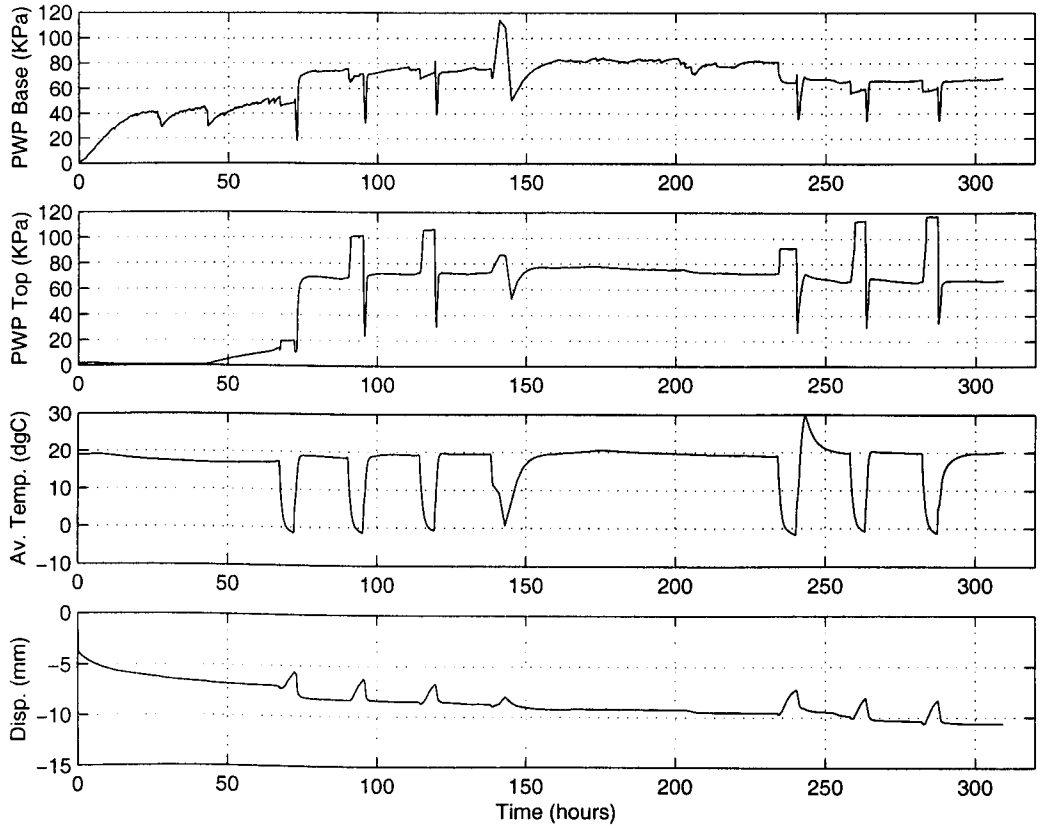

Figure D.8 – Test 8 - Lias Clay - σ = 80 kPa, m.c. = 30%

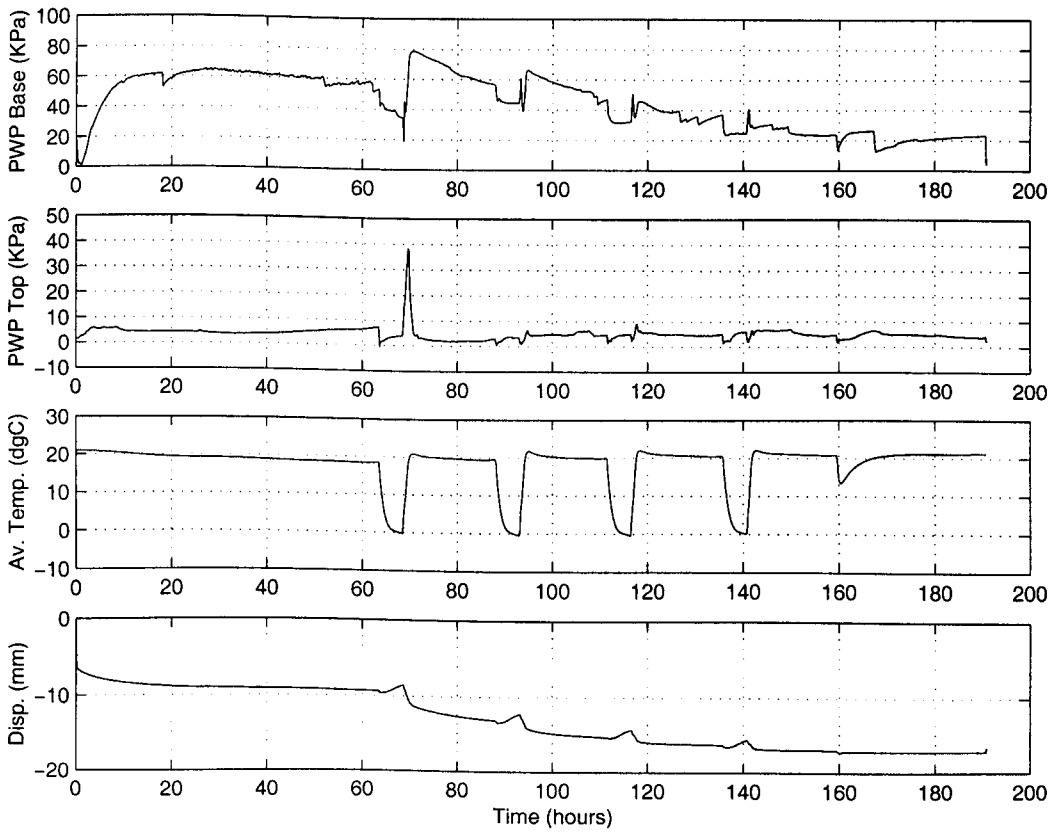

Figure D.9 - Test 9 - Lias Clay - σ = 104 kPa, m.c. = 29%

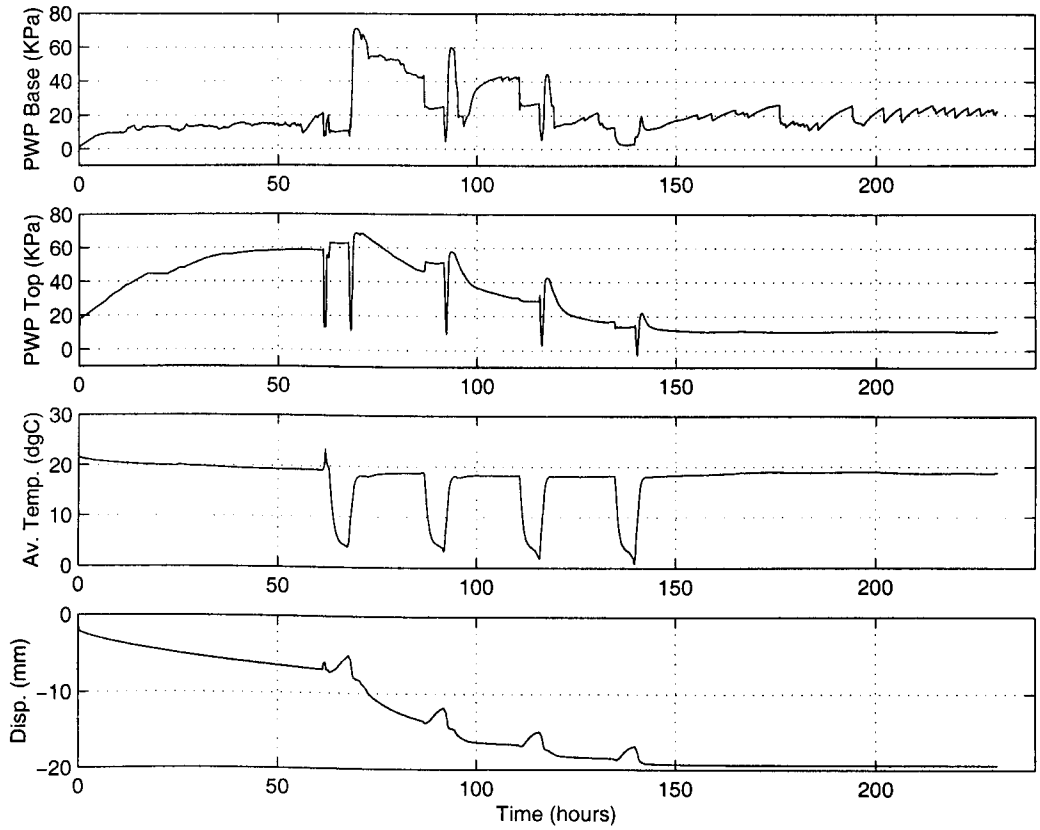

Figure D.10 - Test 10 - Lias Clay - σ = 80 kPa, m.c. = 32%

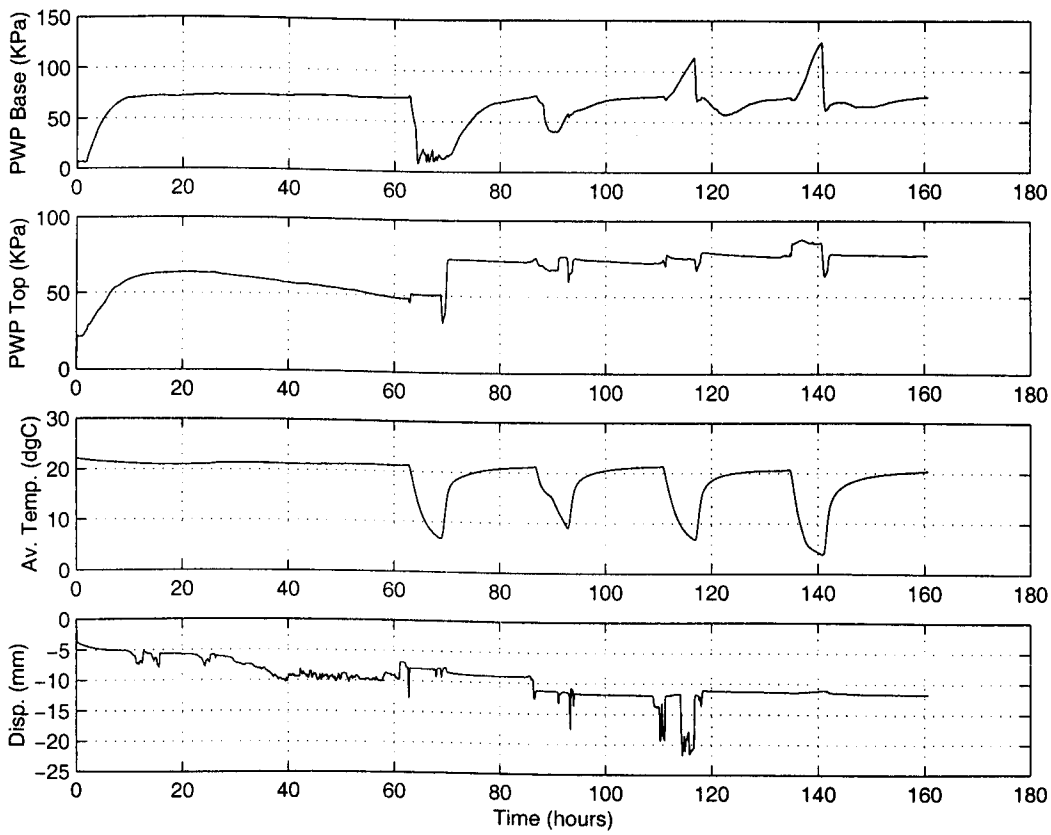

Figure D.11 – Test 11 - Lias Clay - σ = 80 kPa, m.c. = 31%

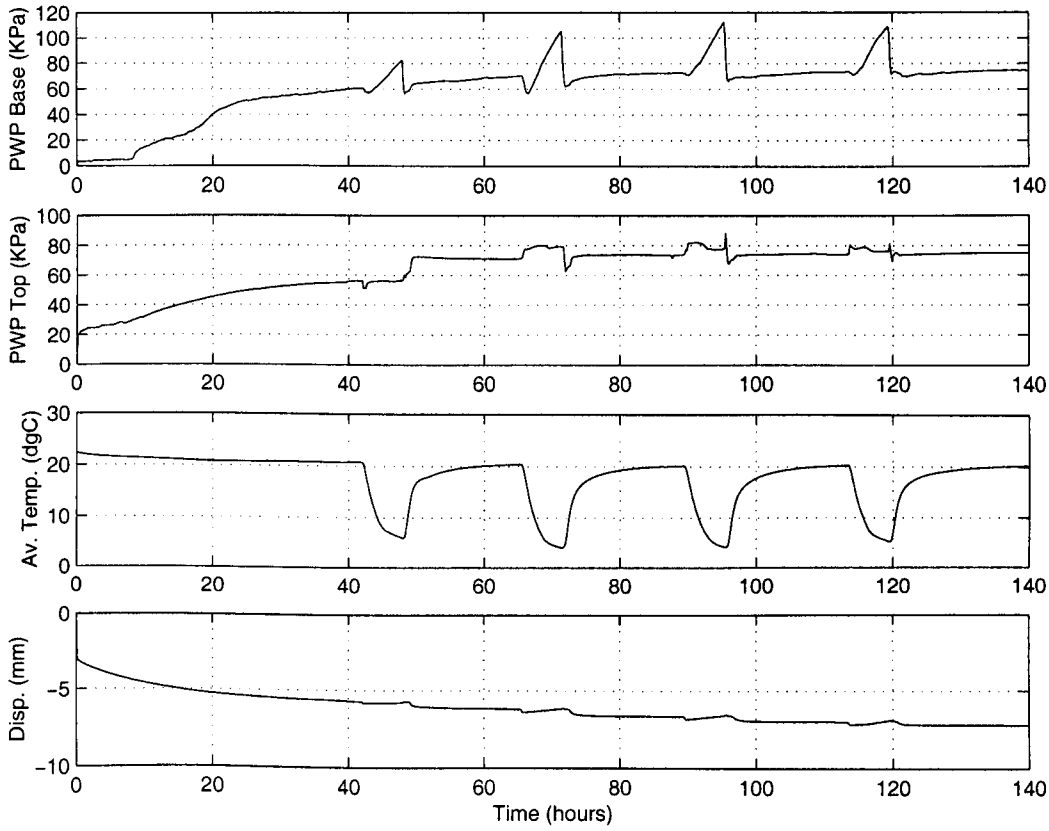

Figure D.12 – Test 12 - Lias Clay - σ = 80 kPa, m.c. = 30%

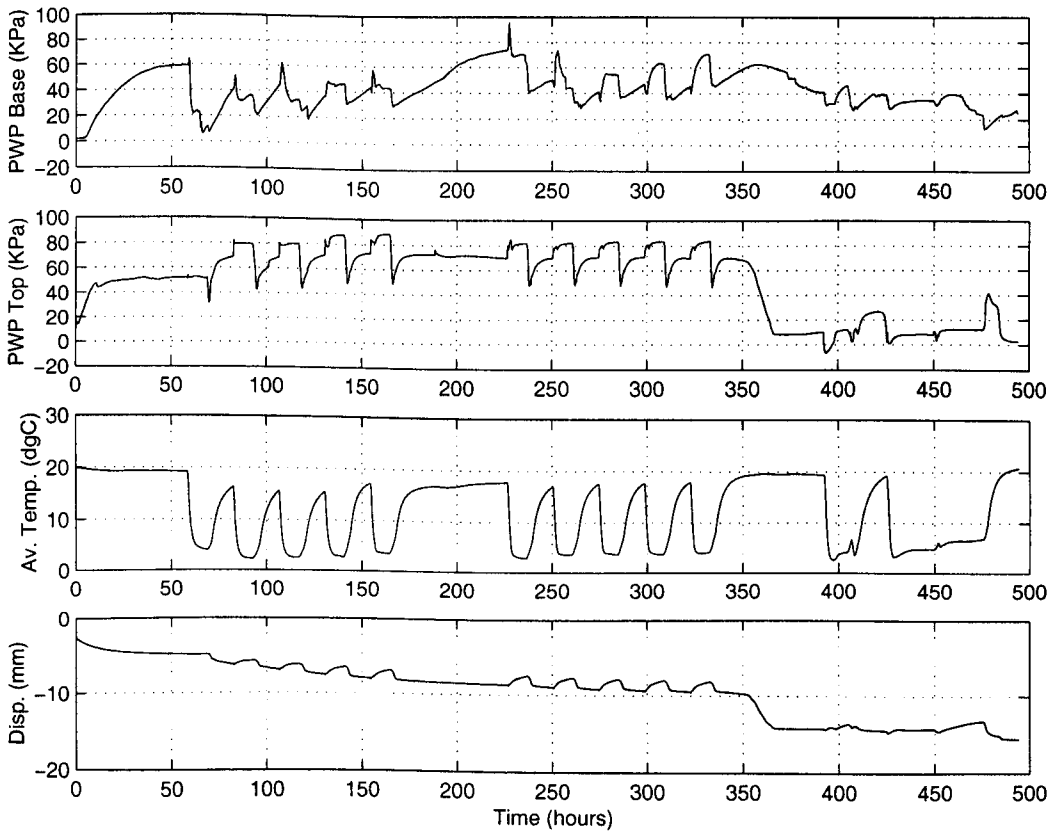

Figure D.13 – Test 13 - Lias Clay - σ = 80 kPa, m.c. = 32%

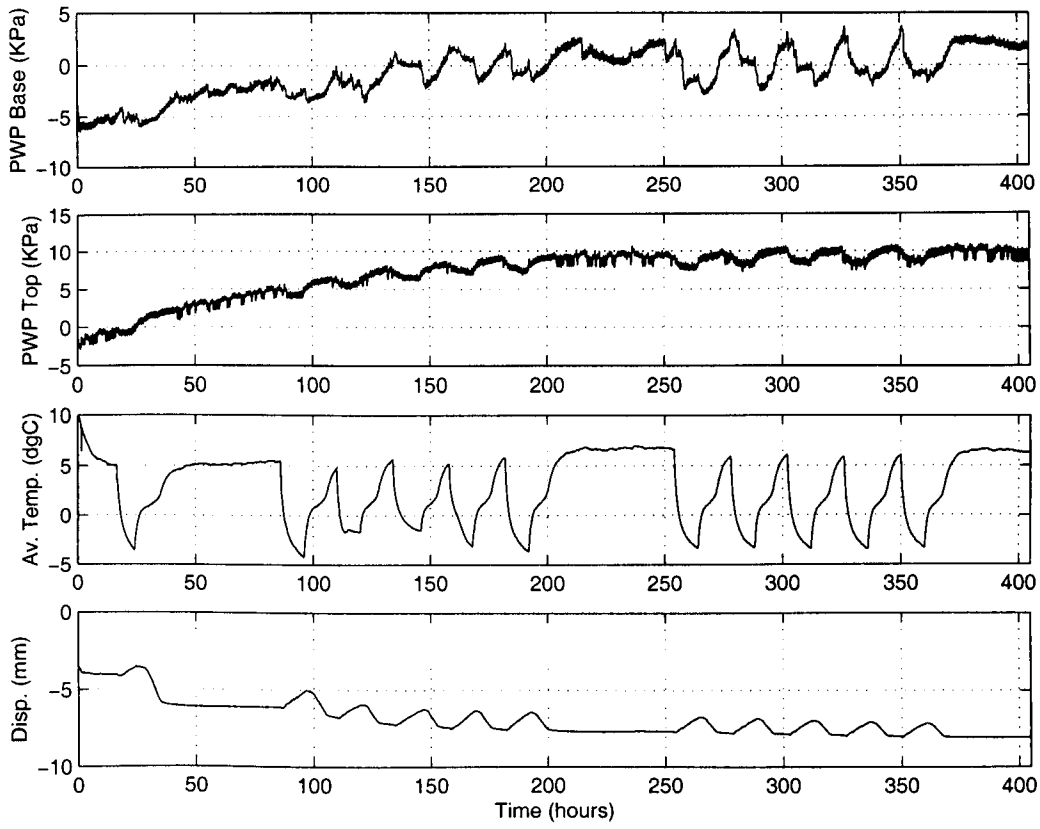

Figure D.14 – Test 14 - Lias Clay - σ = 80 kPa, m.c. = 27%

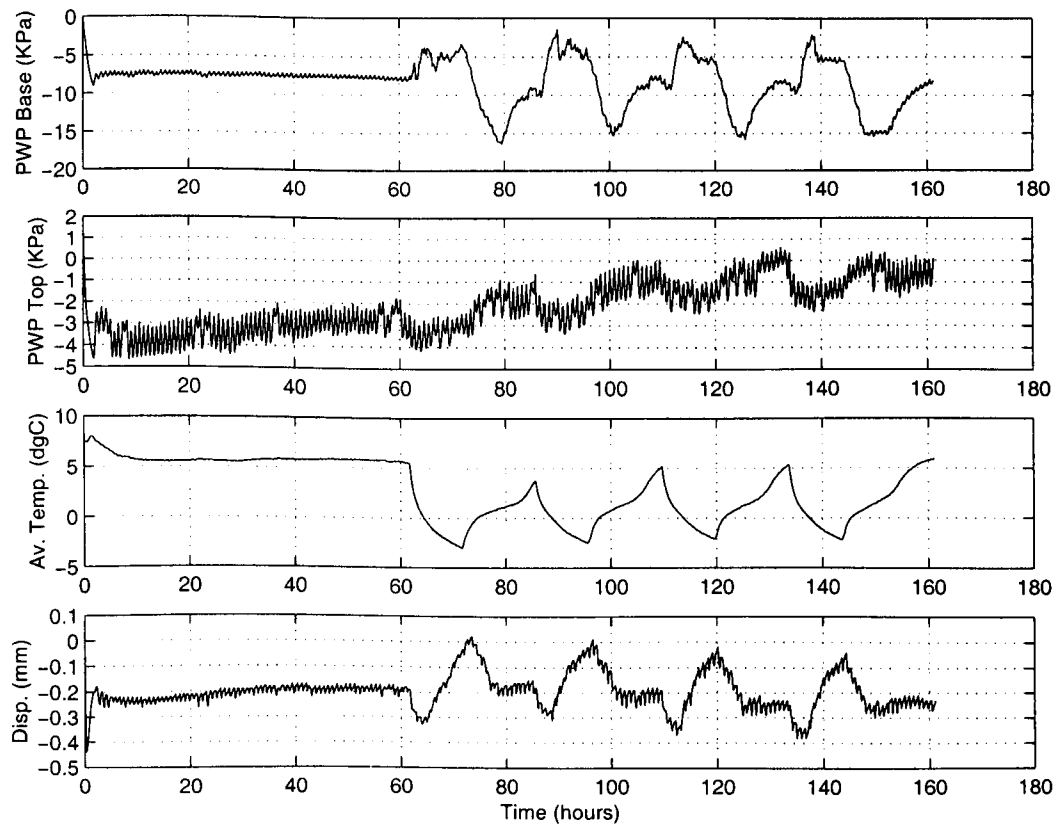

Figure D.15 – Test 15 - Lias Clay - σ = 55 kPa, m.c. = 27%

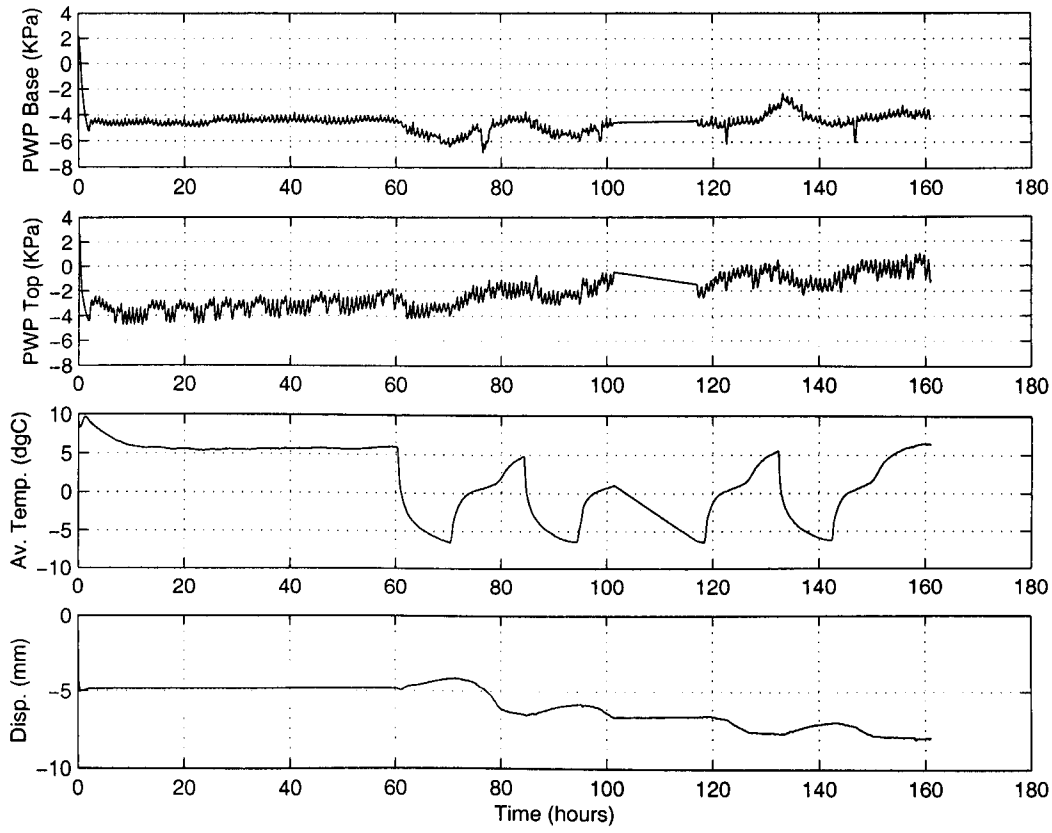

Figure D.16 – Test 16 - Lias Clay - σ = 80 kPa, m.c. = 31%

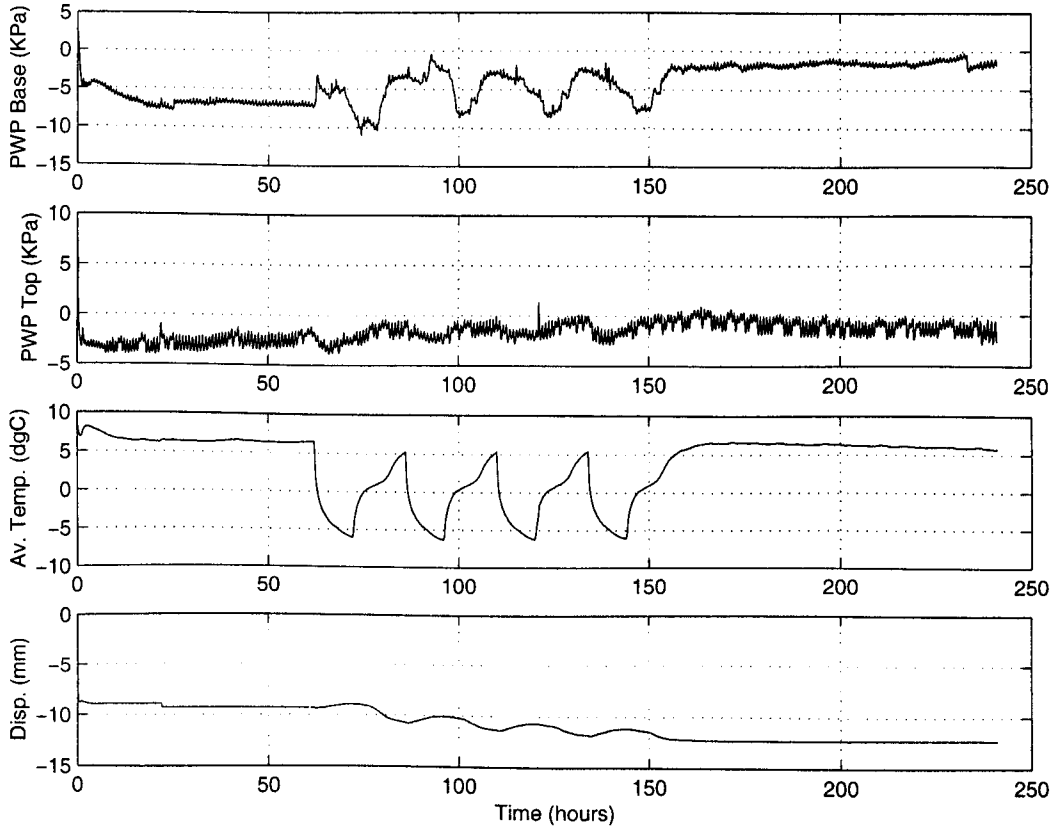

Figure D.17 – Test 17 - Lias Clay - σ = 55 kPa, m.c. = 31%

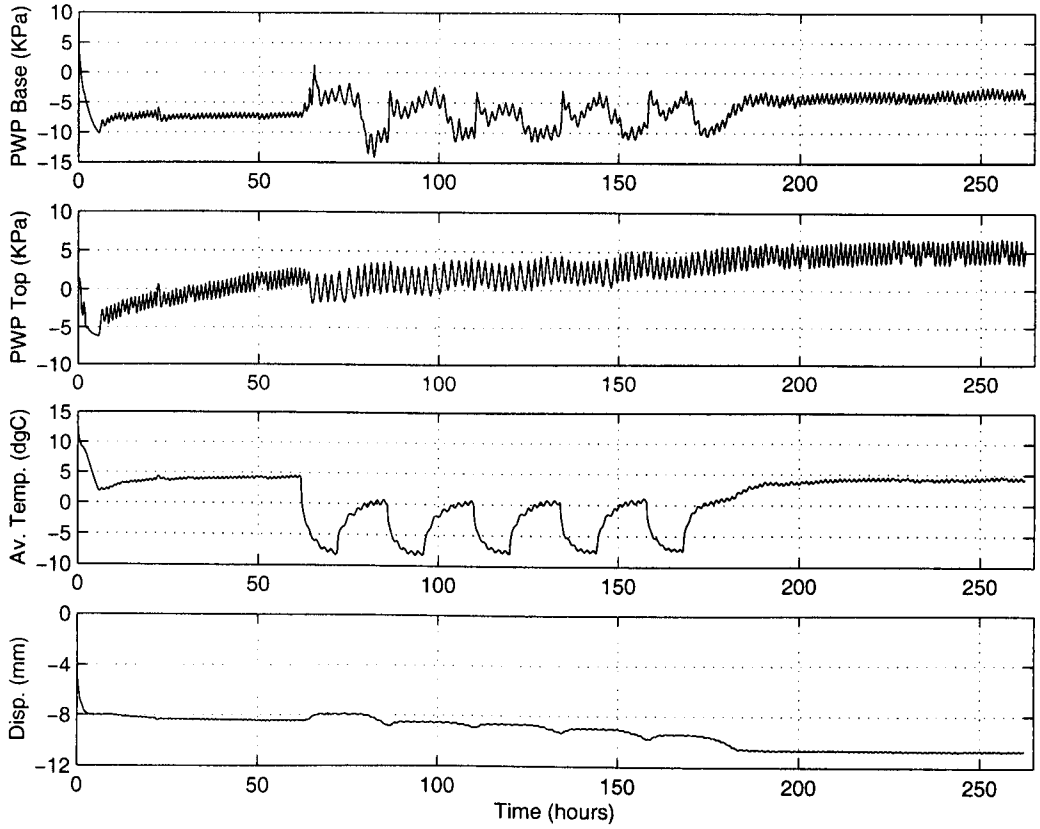

Figure D.18 – Test 18 - Lias Clay - σ = 120 kPa, m.c. = 31%

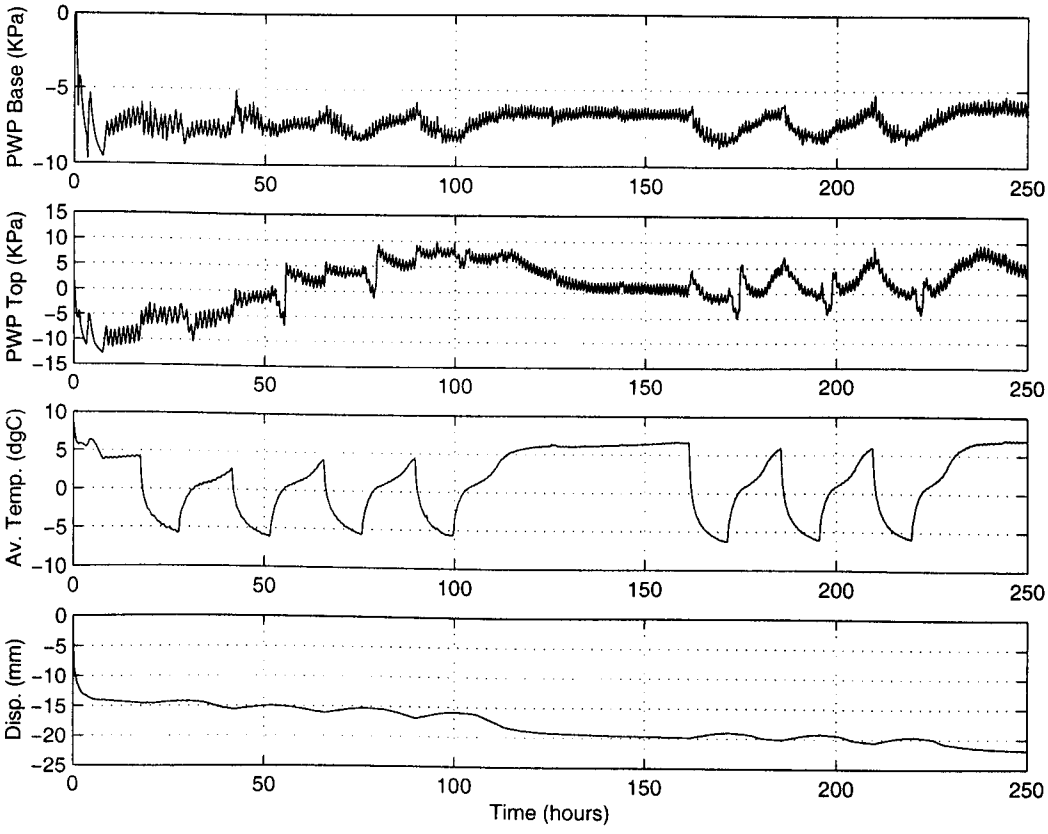

Figure D.19 – Test 19 - Oxford Clay - σ = 55 kPa, m.c. = 49%

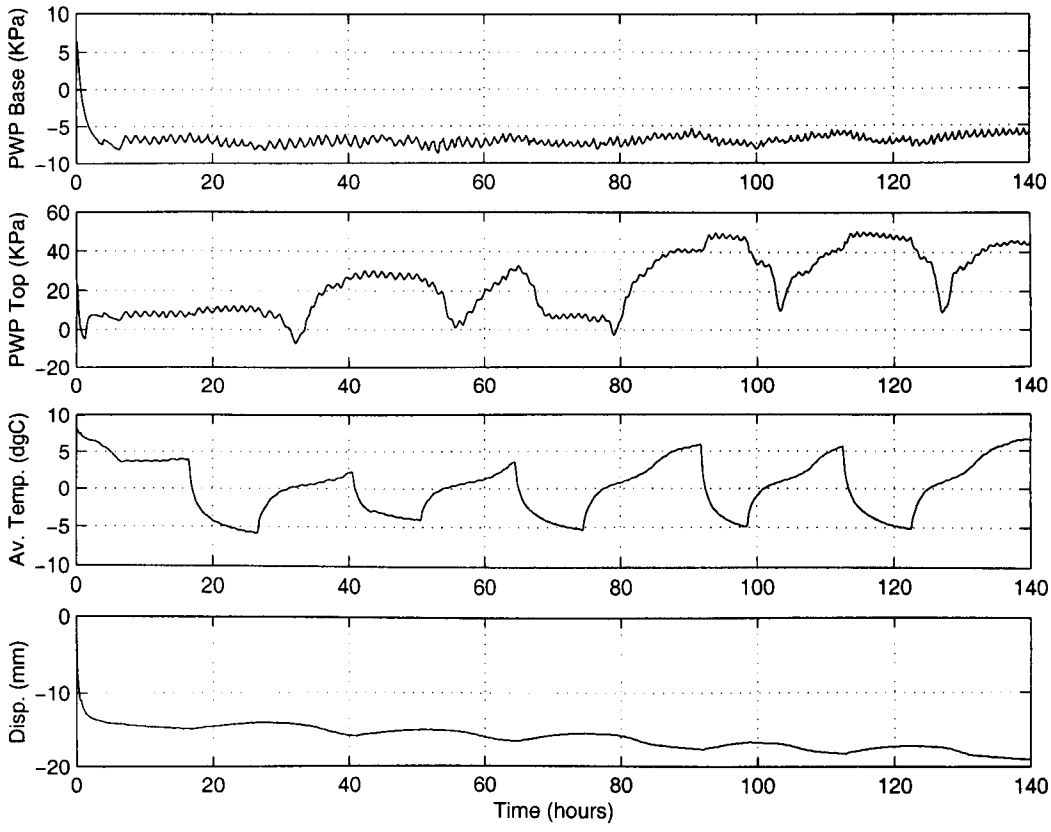

Figure D.20 – Test 20 - Oxford Clay - σ = 80 kPa, m.c. = 49%

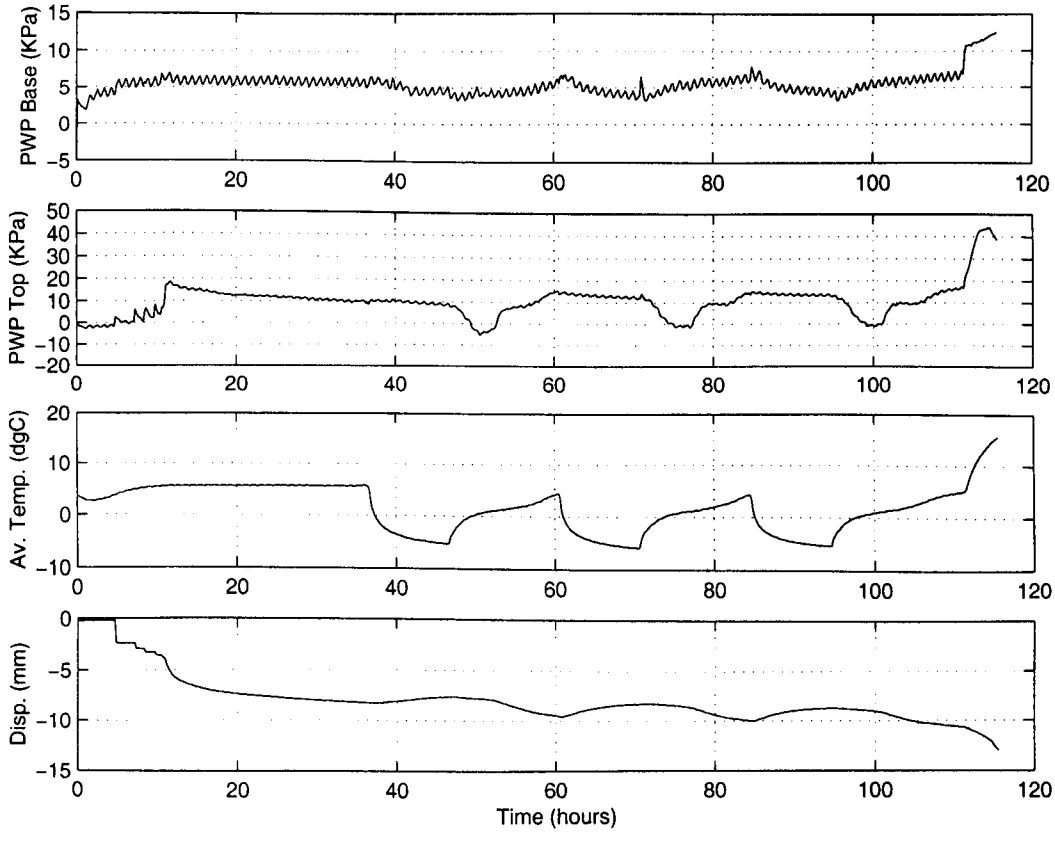

Figure D.21 – Test 21 - Oxford Clay - σ = 55 kPa, m.c. = 50%

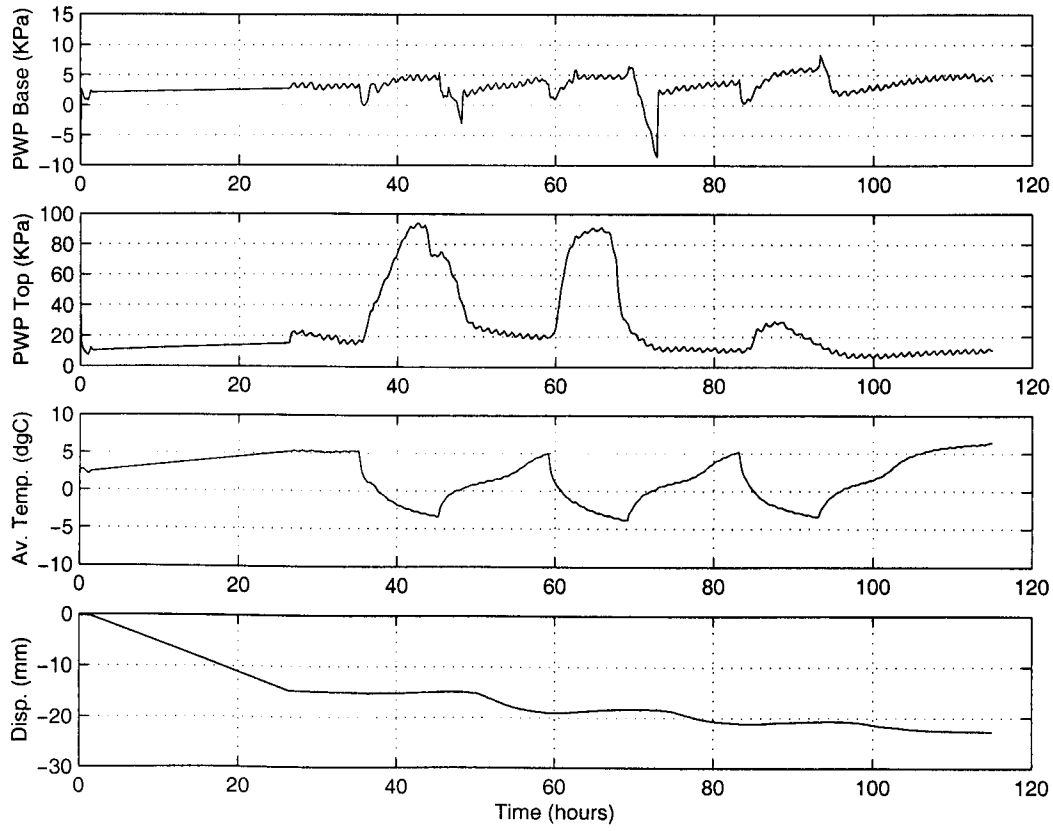

Figure D.22 – Test 22 - Oxford Clay - σ = 55 kPa, m.c. = 50%, Freezing from base upwards

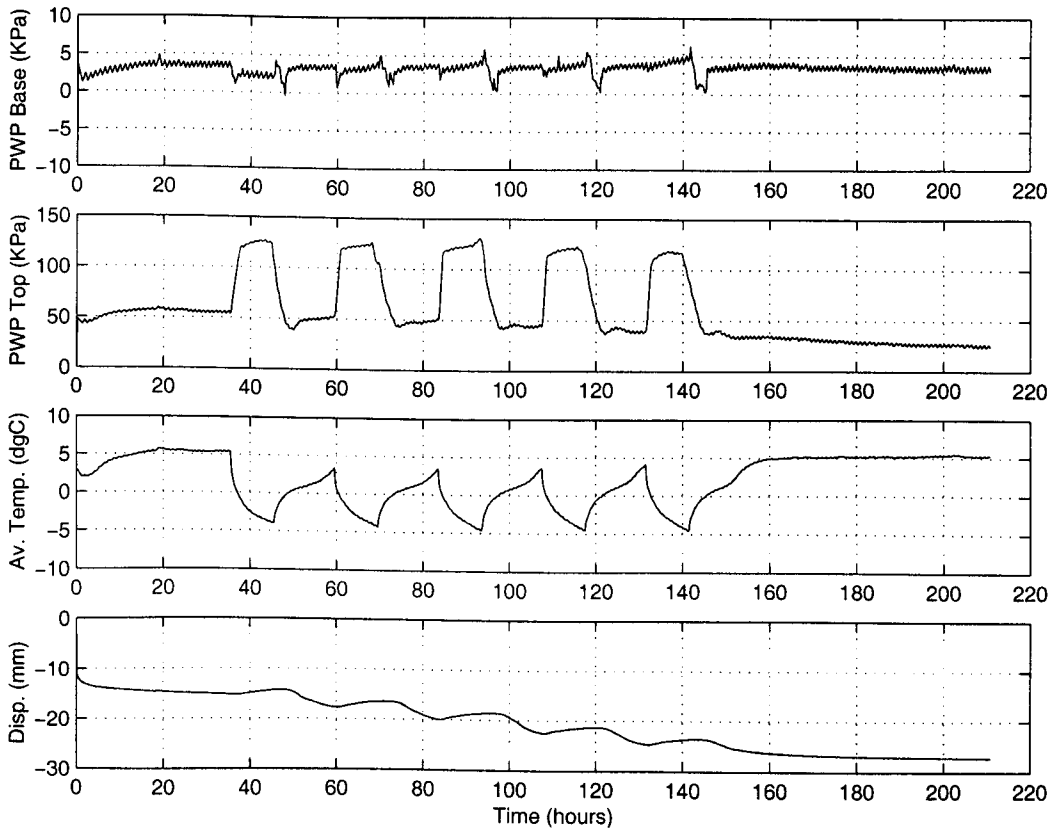

Figure D.23 – Test 23 - Oxford Clay - σ = 80 kPa, m.c. = 50%, Freezing from base upwards

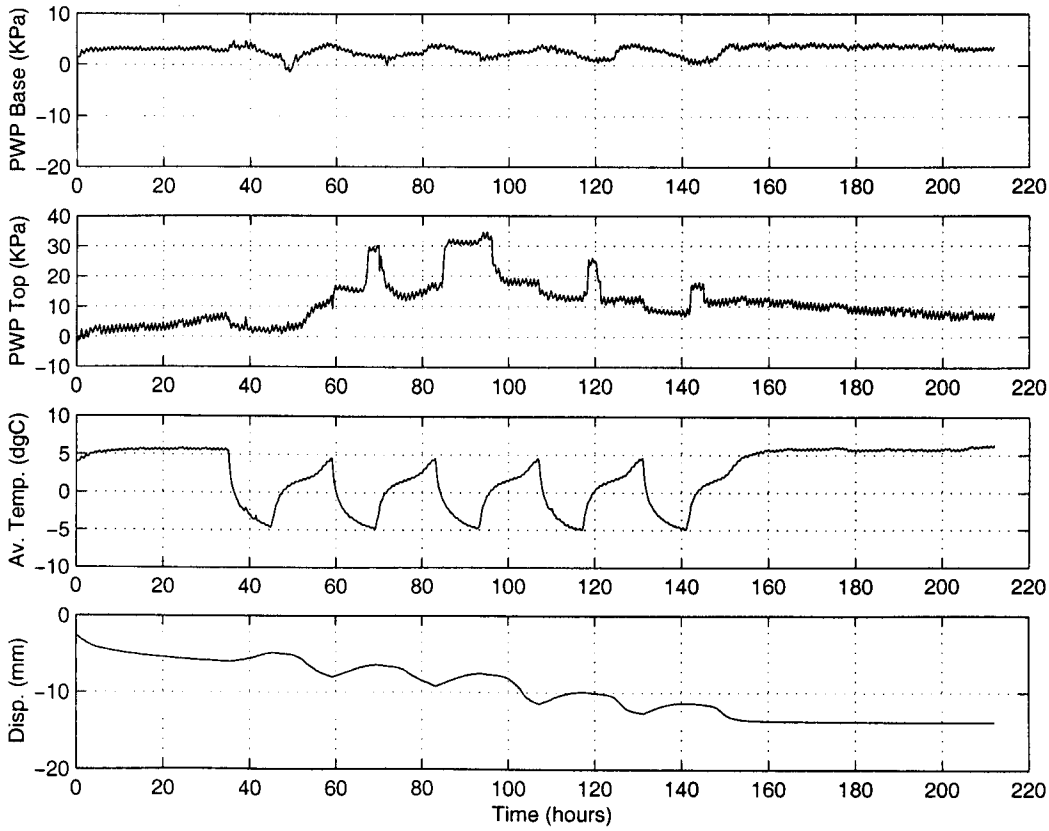

Figure D.24 – Test 24 - Weald Clay - σ = 55 kPa, m.c. = 39%

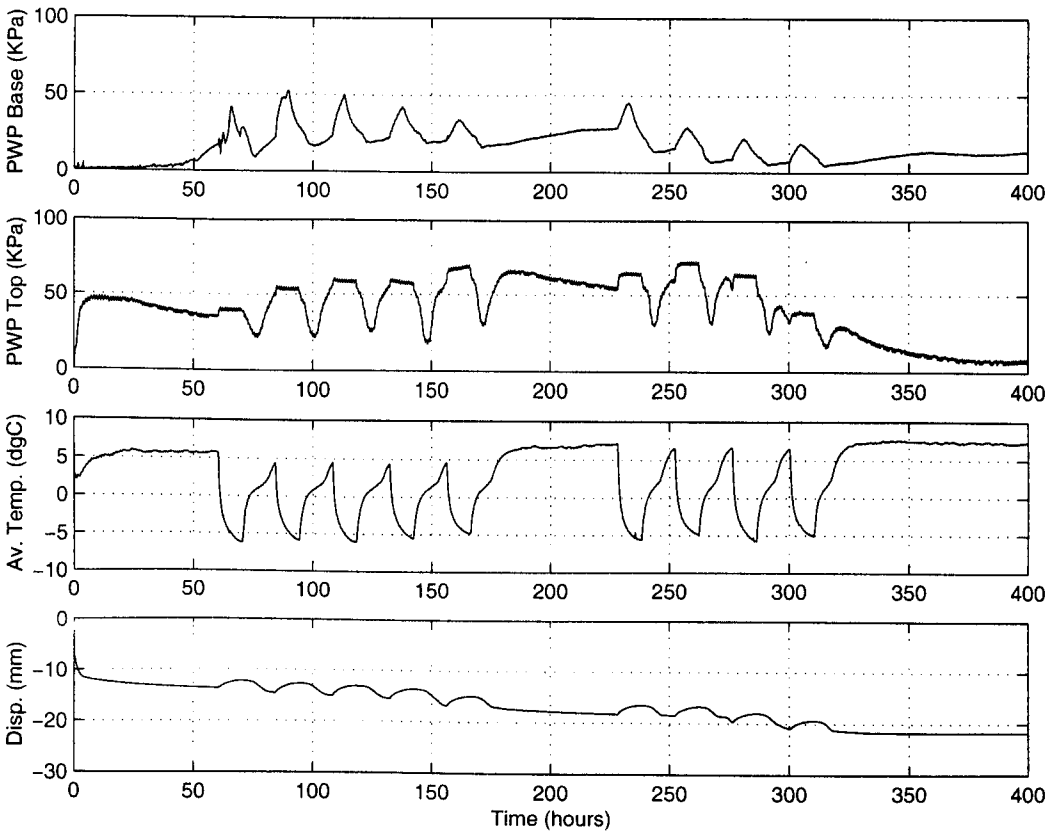

Figure D.25 – Test 25 - Weald Clay - σ = 80 kPa, m.c. = 39%

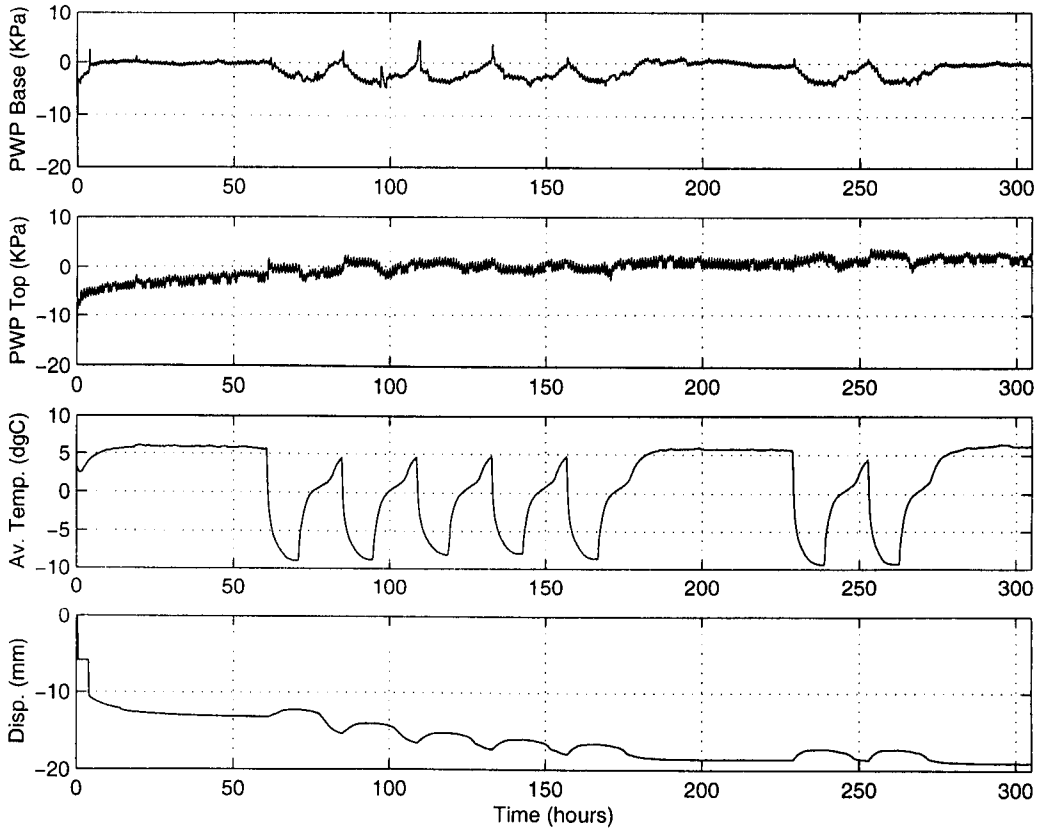

Figure D.26 – Test 26 - Weald Clay - σ = 55 kPa, m.c. = 38%

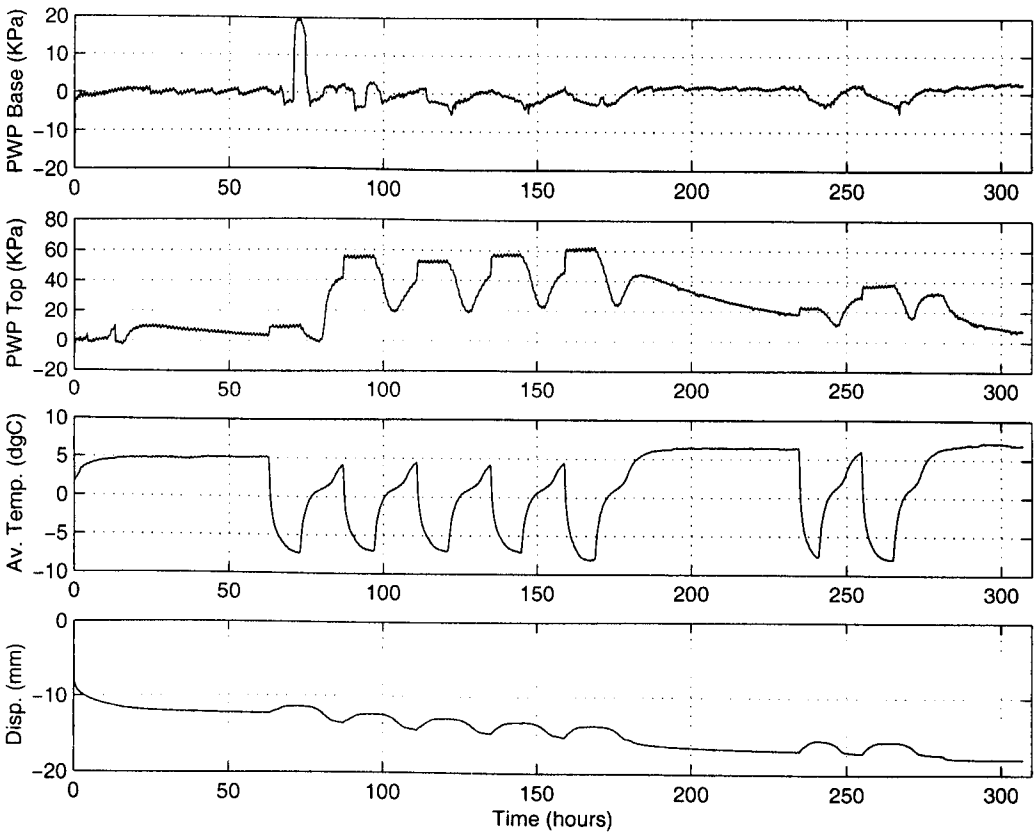

Figure D.27 – Test 27 - Weald Clay - σ = 80 kPa, m.c. = 38%

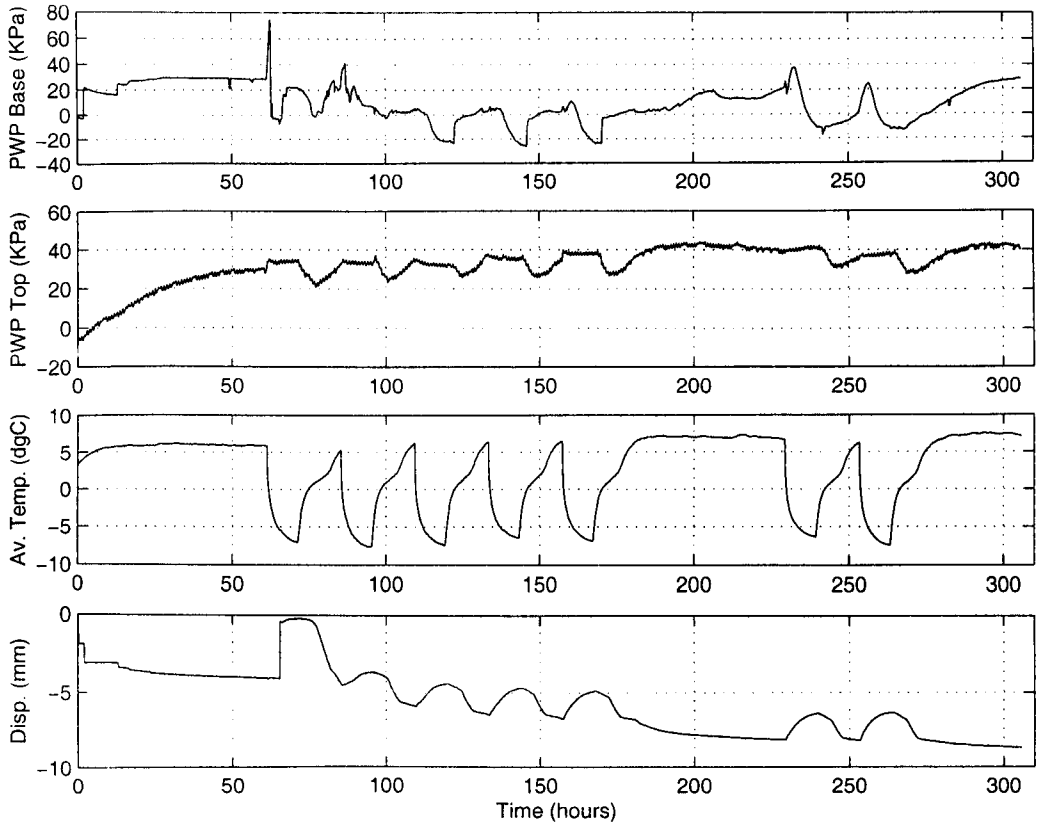

Figure D.28 – Test 28 - Weald Clay - σ = 67.5 kPa, m.c. = 38%